THE JOURNAL OF
PHYSICAL CHEMISTRY

VOLUME 72, NUMBER 11 OCTOBER 25, 1968

Symposium on

Photochemistry and Radiation Chemistry

U. S. Army Natick Laboratories, Natick, Massachusetts

April 22–24, 1968

Introductory Remarks

by Elie Hayon

Pioneering Research Laboratory, U. S. Army Natick Laboratories, Natick, Massachusetts, and Chemistry Department, Brandeis University, Waltham, Massachusetts

No more than two conferences appear to have been held within the past 2 or 3 decades with the intended purpose of bringing together scientists working in the fields of photochemistry and radiation chemistry. To an unduly large degree, photochemists and radiation chemists appear to be divided by a common interest and goal. It was the purpose of this conference to bridge this gap by attracting distinguished research workers active in the field and to provide a program which would highlight the common interests underlying both fields.

A number of papers presented at this meeting used the fast-reaction technique of kinetic absorption spectroscopy. It is indeed appropriate that this meeting was held the year following the Nobel Prize award in Chemistry to M. Eigen, R. G. W. Norrish, and G. Porter for their work on fast-reaction methods in chemical kinetics.

This symposium was sponsored by the National Academy of Sciences–National Research Council and the U. S. Army Natick Laboratories. A NAS–NRC Program Committee consisting of H. Linschitz, Chairman (Brandeis University), A. O. Allen (Brookhaven National Laboratory), E. Hayon (U. S. Army Natick Laboratories), and E. C. Pollard (Pennsylvania State University) organized the scientific content of the conference. About 230 persons attended the meeting, of whom over 50 persons came for this conference from outside the U. S. A. Nineteen different nationalities with representatives from five continents were present. A list of the persons attending this meeting follows these Introductory Remarks.

The papers published in this volume appear in the order in which they were presented during the full three-day meeting. The following persons were chairmen of the sessions: R. G. W. Norrish (Cambridge), M. Burton (Notre Dame), L. J. Heidt (M.I.T.),

J. J. Weiss (Newcastle-upon-Tyne), G. S. Hammond (Cal. Tech.), E. J. Hart (Argonne), and G. B. Kistiakowsky (Harvard). One of the sessions of this symposium was held at Brandeis University.

Finally, one cannot close these remarks without acknowledging gratitude to those who contributed to the planning and organization of this conference: Dr. S. David Bailey and Dr. Dale H. Sieling of the Natick Laboratories for their support and help; Dr. Frank R. Fisher of NAS–NRC, sponsors of this symposium, for organizing and attending to the innumerable details associated with an international conference of this type. To Dr. Henry Linschitz and the NAS–NRC Program Committee, to the session chairmen, to Dr. Frederick T. Wall, Editor of the Journal of Physical Chemistry, and last, but not least, to the authors of the papers presented and to all those who participated in the conference, I express my sincere thanks. The interest, help, and effort of all these scientists has led to the success of this symposium.

ATTENDANCE LIST

Abell, P. (Kingston, R. I.)
Adams, G. (Northwood, England)
Adamson, A. W. (Los Angeles, Calif.)
Alabran, D. M. (Natick, Mass.)
Allen, A. O. (Brookhaven, N. Y.)
Anbar, M. (Moffett Field, Calif.)
Appleby, A. (New Brunswick, N. J.)
Armstrong, D. A. (Calgary, Ala.)
Armstrong, W. (Ottawa, Ont.)
Ausloos, P. J. (Washington, D. C.)
Bailey, S. D. (Natick, Mass.)
Baxendale, J. H. (Manchester, England)
Bensasson, R. (Orsay, France)
Bernhard, W. A. (University Park, Pa.)
Bertelson, R. C. (Dayton, Ohio)
Bielski, B. H. J. (Brookhaven, N. Y.)
Black, E. D. (Natick, Mass.)
Bluhm, A. L. (Natick, Mass.)
Boag, J. W. (Surrey, England)
Bowers, P. G. (Boston, Mass.)
Breccia, A. (Bologna, Italy)
Bronskill, M. J. (Toronto, Ont.)
Brown, A. K. (Dow Chemical, Colo.)
Brynsolfsson, A. (Natick, Mass.)
Bulusu, S. N. (Picatinny, N. J.)
Burger, L. L. (Battelle, Wash.)
Burton, M. (Notre Dame, Ind.)
Buxton, G. V. (Leeds, England)
Carapellucci, P. A. (Boston, Mass.)
Caspari, G. (Boston, Mass.)
Caspersen, J. M. (Natick, Mass.)
Castorina, T. C. (Picatinny, N. J.)
Cercek, B. (Manchester, England)
Charbonnier, F. M. (McMinnville, Ore.)
Charlesby, A. (Shrivenham, U. K.)
Chen, Tung-Ho (Picatinny, N. J.)
Chollar, B. H. (Dayton, Ohio)
Clapp, R. C. (Natick, Mass.)
Cohen, S. G. (Brandeis, Mass.)
Compton, D. M. J. (San Diego, Calif.)
Cooper, R. D. (Natick, Mass.)
Cramer, W. A. (Delft, The Netherlands)
Cundall, R. B. (Nottingham, England)
Cziesla, M. J. (Naval Ordnance, Md.)
Danziger, R. M. (Natick, Mass.)
Davies, J. M. (Natick, Mass.)
DeBoer, C. (Eastman Kodak, Rochester, N. Y.)
Devillers, C. R. (Saclay, France)
Dogliotti, L. M. (Natick, Mass.)
Driscoll, J. N. (Bedford, Mass.)
Endicott, J. F. (Boston, Mass.)
Fajer, J. (Brookhaven, N. Y.)
Feit, E. D. (Bell Telephone, N. J.)
Fisher, F. R. (Washington, D. C.)
Fujimori, E. (Bedford, Mass.)
Gerace, F. J. (Natick, Mass.)
Giffee, J. W. (Natick, Mass.)
Goldfinger, P. (Bruxelles, Belgium)
Goodfriend, P. L. (Orono, Me.)
Gordon, S. (Argonne, Ill.)
Gottschall, W. C., Jr. (Denver, Colo.)
Granzow, A. (Boston, Mass.)
Greenstock, C. L. (Toronto, Ont.)
Groth, W. E. (Bonn, Germany)
Guarino, J. P. (Princeton, N. J.)
Gunthard, Hs. H. (Zurich, Switzerland)
Guttenplan, J. (Brandeis, Mass.)
Haebig, J. E. (Gulf Res., Pittsburgh, Pa.)
Halpern, A. M. (Boston, Mass.)
Hamill, W. H. (Notre Dame, Ind.)
Hammond, G. S. (Pasadena, Calif.)
Hart, E. J. (Argonne, Ill.)
Harteck, P. (Troy, N. Y.)
Hayon, E. (Natick, Mass.)
Heidt, L. J. (M.I.T., Cambridge, Mass.)
Henick, A. S. (Natick, Mass.)
Herkstroeter, W. G. (Eastman Kodak, Rochester, N. Y.)
Herz, M. L. (Kingston, R. I.)
Hirayama, F. (Minneapolis, Minn.)
Hoffman, M. Z. (Boston, Mass.)
Huber, J. R. (Natick, Mass.)
Hunt, J. W. (Toronto, Ont.)
Jarrett, R. D. (Natick, Mass.)
Johnson, G. R. A. (Argonne, Ill.)
Kalb, J. W. (General Mills, Minneapolis, Minn.)
Kalkwarf, D. R. (Battelle, Wash.)
Kanepejs, J. (Terre Haute, Ind.)
Kaplan, A. M. (Natick, Mass.)
Kapsalis, J. G. (Natick, Mass.)
Kaufman, J. V. (Picatinny, N. J.)
Kavarnos (Kingston, R. I.)
Keene, J. P. (Manchester, England)
Kellmann, A. (Paris, France)
Kevan, L. (Lawrence, Kan.)
Kistiakowsky, G. B. (Harvard, Cambridge, Mass.)
Klein, N. (Edgewood Arsenal, Md.)
Knoll, J. E. (Boston, Mass.)
Koob, R. D. (Fargo, N. D.)
Kronman, M. J. (Natick, Mass.)
Kuhn, L. P. (Aberdeen Proving Grd, Md.)
Kuppermann, A. (Pasadena, Calif.)
Lamb, F. A. (Kingston, R. I.)
Lamola, A. A. (Bell Telephone, N. J.)
Langmuir, M. E. (Natick, Mass.)
Lanzerotti, M. Y. D. (Picatinny, N. J.)
Leermakers, P. A. (Middletown, Conn.)
Lehmann, H. P. (Notre Dame, Ind.)
Lias, S. G. (Gaithersburg, Md.)
Lichtin, N. N. (Boston, Mass.)
Linschitz, H. (Brandeis, Mass.)
Lipsky, S. (Minneapolis, Minn.)
Liuti, G. (Goddard Center, Md.)
Louwrier, P. W. F. (Notre Dame, Ind.)
Ludwig, P. K. (Notre Dame, Ind.)
Mabrouk, A. F. (Natick, Mass.)
MacKenzie, D. R. (Brookhaven, N. Y.)
MacLachlan, A. (E. I. du Pont de Nemours, Del.)
Macnair, R. N. (Natick, Mass.)
Mahoney, F. J. (Natick, Mass.)
Mazza, C. (M.I.T., Cambridge, Mass.)
Mazumdar, A. S. G. (Argonne, Ill.)
McBride, E. (Natick, Mass.)
McGarvey, J. J. (Belfast, Ireland)
McLaughlin, W. L. (Washington, D. C.)
Meaburn, G. M. (Bethesda, Md.)
Meisels, G. G. (Houston, Texas)
Menczel, J. (Little Falls, N. J.)
Merritt, C., Jr. (Natick, Mass.)
Milne (Brandeis, Mass.)
Mittal, J. P. (Los Angeles, Calif.)
Munday, C. S. (Moffett Field, Calif.)
Nielsen, S. O. (Riso, Denmark)
Niemann, E. G. (Hannover, Germany)
Norland, K. (Polaroid, Cambridge, Mass.)
Norrish, R. G. W. (Cambridge, England)
Novack, R. L (Prototech, Mass.)
Ottolenghi, M. (Jerusalem, Israel)
Parrish, C. F. (Terre Haute, Ind.)
Pearce, C. K. (Fort Monmouth, N. J.)
Peng, Chin-Tzu (San Francisco, Calif.)

Pertel, R. (Chicago, Ill.)
Phillips, G. O. (Salford, England)
Pilette, Y. P. (Boston, Mass.)
Pirog, J. A. (Endicott, N. Y.)
Platt, J. R. (Ann Arbor, Mich.)
Polanyi, J. C. (Toronto, Ont.)
Porter, W. L. (Natick, Mass.)
Rees, C. W. (Natick, Mass.)
Reeves, R. R. Jr. (Troy, N. Y.)
Ronayne, M. R. (Boston, Mass.)
Ruigh, W. L. (Arlington, Va.)
Safrany, D. R. (Avco-Everett, Mass.)
Sandner, M. R. (Natick, Mass.)
Sauer, M. C., Jr. (Argonne, Ill.)
Schenck, G. O. (Muelheim-Ruhr, Germany)
Schlochauer, M. (South Hadley, Mass.)
Schmidt, W. F. (Brookhaven, N. Y.)
Schneider, C. (Koln, Germany)
Schofield, K. (Buffalo, N. Y.)
Scholes, G. (Newcastle-upon-Tyne, England)
Schuler, R. H. (Pittsburgh, Pa.)
Schwarz, H. A. (Brookhaven, N. Y.)
Sears, J. T. (Brookhaven, N. Y.)
Serauskas, R. W. (Chicago, Ill.)
Seris, J. L. (Pau, France)
Shapiro, J. S. (Brookhaven, N. Y.)
Skutnik, B. (Brandeis, Mass.)
Sieling, D. H. (Natick, Mass.)
Simic, M. (Natick, Mass.)
Simpson, W. H. (Philadelphia, Pa.)
Slagg, N. (Picatinny, N. J.)
Smith, K. E. (Rutherford, N. J.)
Snipes, W. (University Park, Pa.)
Sousa, J. A. (Natick, Mass.)
Steel, C. (Brandeis, Mass.)
Stevens, B. (Tampa, Fla.)
Suryanarayanan, K. (Boston, Mass.)
Sutherland, J. W. (Brookhaven, N. Y.)
Swallow, A. J. (Manchester, England)
Taylor, W. D. (University Park, Pa.)
Thrush, B. A. (Cambridge, England)
Tiernan, T. O. (Wright-Patterson, Ohio)
Tomlinson, M. (Pinawa, Manitoba)
Treinin, A. (Jerusalem, Israel)
Tsuji, K. (Knoxville, Tenn.)
Vecchi, E. (Bologna, Italy)
Vermeil, C. (Paris, France)
Vittimberga, B. M. (Kingston, R. I.)
Walter, D. C. (Vancouver, Canada)
Walker, J. E. (Natick, Mass.)
Warneck, P. (Bedford, Mass.)
Wason, S. K. (E. I. du Pont de Nemours, Del.)
Weinstein, J. (Natick, Mass.)
Weiss, J. J. (Newcastle-upon-Tyne, England)
Weiss, K. (Boston, Mass.)
Wettermark, G. (Uppsala, Sweden)
Wharton, D. R. A. (Natick, Mass.)
Wierbicki, E. (Natick, Mass.)
Wijnen, M. H. J. (Hunter College, N. Y.)
Wild, U. P. (Zurich, Switzerland)
Wilkinson, F. (Leeds, England)
Williams, F. (Knoxville, Tenn.)
Willis, C. (Chalk River, Ont.)
Woods, R. J. (Saskatoon, Sask.)
Wrigley, A. S. (Natick, Mass.)
Wyman, G. M. (Durham, N. C.)
Yamanashi, B. S. (M.I.T., Cambridge, Mass.)
Yelland, W. E. C. (Natick, Mass.)
Yip, R. W. (Ottawa, Ont.)
Zwolenik, J. J. (Washington, D. C.)

Chemiluminescence in Gases: Reactions Yielding Electronically Excited Sulfur Dioxide[1]

by B. A. Thrush, C. J. Halstead, and A. McKenzie

Department of Physical Chemistry, University of Cambridge, Cambridge, England *(Received May 7, 1968)*

The mechanism of formation of electronically excited molecules in transfer reactions is discussed briefly. New data are presented on the energy distribution of excited SO_2 molecules formed in the transfer reaction, $SO + O_3 = SO_2 + O_2$. This reaction is shown to be somewhat similar to the formation of electronically excited SO_2 by the reaction of SO with chemisorbed oxygen atoms on the walls of low-pressure flow systems.

Introduction

Many gaseous recombination reactions involving atoms and simple molecules are known to yield electronically excited products which chemiluminesce.[2] The majority are three-body processes and in most cases the radiating state does not correlate directly with the species from which it is formed. In some such cases, a high proportion of recombinations populate the excited state, but little is known about the detailed mechanism of crossing between states. The pressures at which such processes are studied often make it difficult to eliminate or identify the effects of collisional processes subsequent to stabilization.

By comparison, few transfer reactions yielding electronically excited molecules are known. This arises partly because few such reactions are exothermic enough to populate excited electronic states of their products and partly from correlation rules. This communication discusses factors which govern the formation of electronically excited molecules in transfer reactions; the formation of excited atoms[3] is not considered specifically here.

New data on the formation of electronically excited

(1) Presented at the Conference on Photochemistry and Radiation Chemistry, Natick, Mass., April 22–24, 1968.

(2) B. A. Thrush, *Ann. Rev. Phys. Chem.*, in press.

SO_2 in the reaction of sulfur monoxide (SO) with ozone are presented and discussed.

General

A transfer reaction can yield electronically excited products in three basic ways: (a) if a potential surface leads directly from the reactants to electronically excited products; (b) if a radiationless transition to the potential surface yielding electronically excited products occurs in the region of the transition state; and (c) if a highly vibrationally excited product is converted into an electronically excited one by a radiationless transition (which is the reverse of internal conversion).

Mechanism a is governed by correlation rules.[4] These show that this process will be largely confined to systems where one reactant is an atom or linear molecule, for which the possible presence of degeneracy associated with orbital angular momentum means that the reactants can correlate with more than one potential surface having a particular resultant spin. The high multiplicities of the ground states of some atoms and linear diatomics associated with partly filled degenerate orbitals also raise the possibility of reactions in which the formation of ground-state products is spin forbidden.

Nonlinear molecules have lower symmetry, few of their point groups allow degenerate molecular orbitals, and such orbitals are normally full or empty in the ground states of gaseous nonlinear species. Separate potential surfaces connecting nonlinear reactants with products therefore only arise due to difference in spin coupling between the reactants which will normally have singlet or doublet ground states. Mechanism a is therefore rare in transfer reactions between nonlinear species.

Where these rules allow reactants to correlate both with ground state and electronically excited states of a product, the formation of both states should involve similar frequency factors. The separation of the potential surfaces in the transition state will generally give different activation energies for the two processes: that for the formation of electronically excited products should be higher by an obvious extension of Polanyi's rules.[5] The chemiluminescent bimolecular reaction of nitric oxide with ozone

$$NO + O_3 = NO_2 + O_2 \qquad (1)$$

is probably the clearest example of mechanism a, where the formation of ground state ($^2A_1$) and electronically excited ($^2B_1$) NO_2 both have frequency factors of $(6 \pm 2) \times 10^{11}$ cm^3 mol^{-1} sec^{-1} and activation energies of 2.3 and 4.2 kcal/mol, respectively.[6]

Several processes appear to be responsible for CN chemiluminescence in the reactions of active nitrogen, but the best investigated process probably involves mechanism a. This is the strong orange-yellow flame reaction between halomethanes and active nitrogen, where Broida and coworkers[7] have shown that levels $v' = 4$–10 of the $A^2\Pi$ state of CN are populated in this reaction in preference to isoenergetic levels of the ground state ($X^2\Sigma^+$) or of the $B^2\Sigma^+$ state. This excitation is almost certainly due to the very exothermic transfer reactions

$$N(^4S) + CCl(^2\Pi) = CN(A^2\Pi) + Cl(^2P) \qquad (2)$$

and

$$N(^4S) + CH(^2\Pi) = CN(A^2\Pi) + H(^2S) \qquad (3)$$

For reaction 3, the formation of $CN(A^2\Pi)$ cannot be regarded as an example of the selection involving conservation of orbital angular momentum in linear systems as its transition state would correspond essentially to a triplet state of HCN which would be nonlinear in its equilibrium configuration. This excitation is an example of mechanism a but only in a limited sense, because the $A^2\Pi$ state is the lowest lying state of CN for $r(C–N) > 1.5$ Å, and is therefore the "ground state" of CN in the region of the transition state.[8] The crossing of the $X^2\Sigma$ and $A^2\Pi$ states at $r(C–N) \simeq 1.5$ Å is unusual and arises from the decreased bonding of $\pi_u 2p$ orbitals relative to $\sigma_g 2p$ with increasing internuclear distance.

In contrast to mechanism a, mechanisms b and c should be associated with lower efficiencies of chemiluminescence due to the transmission coefficients for the crossing process. Distinction between mechanisms b and c can be difficult; evidence that mechanism c could occur in a particular reaction is provided if radiationless transitions are detected in the study of the fluorescence and phosphorescence of the appropriate product. Such studies are important in the investigation of chemiluminescent reactions, since they provide the needed relation between the rates of radiation and of populating the emitting state.

Reaction between Sulfur Monoxide (SO) and Ozone. This process was studied by Halstead and Thrush,[9] who showed that it is bimolecular yielding SO_2 in its ground ($^1A_1$) and first two excited states ($^3B_1$ and $^1B_1$ (?))

(3) (a) M. C. Moulton and D. R. Herschbach, *J. Chem. Phys.*, **44**, 3010 (1966); (b) J. R. Airey, P. D. Pacey, and J. C. Polanyi, "XIth Symposium on Combustion," Combustion Institute, Pittsburgh, Pa., 1967, p 85.

(4) K. E. Shuler, *J. Chem. Phys.*, **21**, 624 (1953).

(5) M. G. Evans and M. Polanyi, *Trans. Faraday Soc.*, **35**, 178 (1939).

(6) (a) M. A. A. Clyne, B. A. Thrush, and R. P. Wayne, *ibid.*, **60**, 359 (1964); (b) P. N. Clough and B. A. Thrush, *ibid.*, **63**, 915 (1967).

(7) (a) H. E. Radford and H. P. Broida, *J. Chem. Phys.*, **38**, 644 (1963); (b) T. Iwai, M. I. Savadatti, and H. P. Broida, *ibid.*, **47**, 3861 (1967).

(8) D. W. Setser and B. A. Thrush, *Proc. Roy. Soc.*, **A288**, 256 (1965).

(9) C. J. Halstead and B. A. Thrush, *ibid.*, **A295**, 380 (1966).

$$SO + O_3 = SO_2X(^1A_1) + O_2 \quad (4)$$

$$= SO_2(^1B_1) + O_2 \quad (4a)$$

$$= SO_2(^3B_1) + O_2 \quad (4b)$$

Experiments were conducted in an argon carrier at pressures between 0.3 and 3.0 mm. The long-lived $^3B_1$ state showed a vibrational distribution corresponding to a temperature a little above ambient, but emission from the $^1B_1$ state showed considerable vibrational excitation extending from its origin which is probably at 91 kcal/mol up to an energy of 101 kcal/mol. With the aid of studies of SO_2 fluorescence, it was shown that the Arrhenius expression for population of the $^1B_1$ state was $k_{4a} = 10^{11} \exp(-4200/RT)$ cm^3 mol^{-1} sec^{-1} and that two-thirds of the triplet emission (which has an activation energy of 3.9 kcal/mol) was caused by collisional quenching from the $^1B_1$ to the $^3B_1$ state. The rate constant for population of the ground state was found to be $k_4 = 1.5 \times 10^{12} \exp(-2100/RT)$ cm^3 mol^{-1} sec^{-1}.

Since $SO(^3\Sigma^-)$ and $O_3(^1A_1)$ yield only one triplet surface which must correlate with ground-state products, the chemiluminescence arises through mechanism b or c. The higher activation energies of reactions 4a and 4b relative to reaction 4 suggest that mechanism b operates and that crossing to the appropriate potential surface occurs at or near the transition state with a transmission coefficient of about 0.1 for reaction 4a.

Several features of this reaction require further investigation, particularly (a) the nature of the extensive vibrational distribution in the $^1B_1$ state, and (b) the rate of population of the $^3B_1$ state for which no quenching data exist.

The Singlet Emission of SO_2. Providing the electronic transition moment of the $^1B_1$–$^1A_1$ system of SO_2 does not change sharply with configuration, the vibrational energy distribution in the $^1B_1$ state can be found from the vibrational sum rule. This rule establishes that a particular vibronic band occurs in the same fraction of transitions from its initial level both in emission or absorption, providing allowance has been made for the different dependence of emission and absorption intensities on frequency. The weakness of the SO + O_3 chemiluminescence makes it impossible to obtain well-resolved spectra, and only bands on the high-frequency side of the origin are resolved. These bands are the strongest ones in the absorption spectrum where they form quite a long progression with spacings of the order of 200 cm^{-1}. It is generally agreed[10,11] that these arise from the (0,0,0) level of the ground state. Clements[10] has interpreted them as a progression purely in ν_2', whereas Metropolis[11] invokes both symmetrical stretching ($\nu_1' = 770$ cm^{-1}) and bending vibrations ($\nu_2' = 320$ cm^{-1}) with a very large interaction term $x_{12}' = -20$ cm^{-1}. The latter interpretation gives more than one assignment to each of the strongest bands,

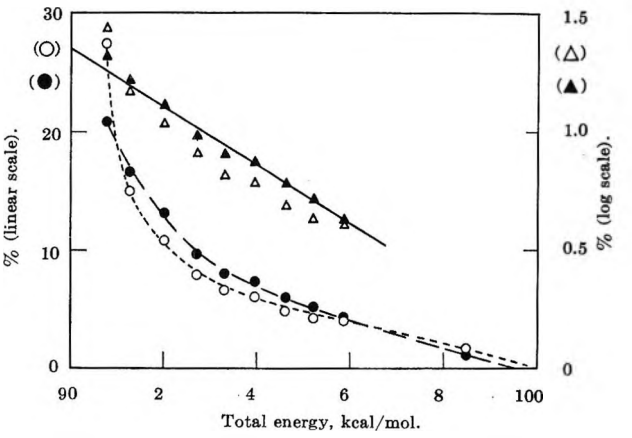

Figure 1. Vibrational energy distribution of $^1B_1$ SO_2 emission from SO + O_3 reaction. Two separate determinations are shown. The highest energy points on the linear scale refer to unresolved emission at energies between 96 and 101 kcal/mol; such points cannot be shown properly on the logarithmic scale.

whereas their envelopes at moderate resolution indicate that one vibronic transition predominates in each band.

The excited state of SO_2 involved is probably the $^1B_1$ state derived from the same $^1\Delta_g$ state of linear SO_2 as is the $^1A_1$ ground state.[9,12] In this situation excitation of ν_2' should predominate, and the isoelectronic species CF_2 has a transition in this region of the spectrum the vibrational structure of which is now interpreted almost exclusively in terms of bending vibrations.[13]

Figure 1 shows linear and logarithmic plots of the vibrational energy distribution in the $^1B_1$ state determined from the vibrational sum rule assuming: (a) that each band is a single, vibronic band or that the same vibronic band predominates in emission and absorption as expected from the Franck–Condon principle; and (b) that each emitting band, being a transition to the (0,0,0) level of the ground state, also contributes background emission to bands at longer wavelengths, the form of this contribution being determined from the overall distribution of the $^1B_1$ chemiluminescence and its intensity from the Franck–Condon factor of the band concerned.

The solid line in Figure 1 corresponds to a vibrational temperature of 1750°K for the bending levels (ν_2'). At the pressures used, $SO_2(^1B_1)$ is removed predominantly by quenching, about one collision in ten with argon being effective. This number of collisions is probably sufficient to redistribute vibrational energy within the excited $^1B_1$ state, and similar excitations of ν_1' and ν_3' must also be present in the emission observed.

The vibrational sum rule yields percentage popula-

(10) J. H. Clements, *Phys. Rev.*, **47**, 224 (1935).
(11) N. Metropolis, *ibid.*, **60**, 295 (1941).
(12) A. D. Walsh, *J. Chem. Soc.*, 2283 (1953).
(13) D. E. Mann and B. A. Thrush, *J. Chem. Phys.*, **33**, 1732 (1960).

tions of emitting levels directly, and the two determinations in Figure 1 account for 70–80% of the total emission, providing Clements' origin at 31,945 cm^{-1} is accepted. This is very good overall agreement, since excitation of ν_1' and ν_3' must produce some small deficit despite the selection rule that $\Delta\nu_3 = 0$ predominates and the probability that transitions involving $\Delta\nu_1 = 0$ are strongest. The relative dispositions of the emission and absorption show that Metropolis' origin for the $^1B_1$ system (29,622 cm^{-1}) is incorrect; it would also give a sum of individual percentage populations totaling several hundred per cent. The vibrational distributions in Figure 1 have therefore been normalized to 100% Clements' origin. On this basis, the mean bending vibrational energy in the $^1B_1$ state is 2.5–3.0 kcal/mol corresponding to about 15% of the (heat of reaction + activation energy) if electronic excitation is subtracted. Because of their larger quanta, ν_1 and ν_3 should each contain about 2 kcal/mol.

Triplet Emission. In recent studies of the sulfur dioxide afterglow (due to O + SO) using a 6-in. diameter linear flow system,[14] we have observed emission by the $^1B_1$ and $^3B_1$ states of SO_2 from the gases close to the Pyrex surface at total pressures between 10 and 50 μ. The spectrum of this emission closely resembles the SO + O_3 chemiluminescence except that: (a) the $^1B_1$ bands between 2950 and 3250 Å are more clearly defined, apparently because the underlying unresolved emission is weaker; (b) the maximum intensity (I_λ) of the singlet emission is shifted from 3400 Å to about 3600 Å; and (c) the triplet emission is relatively somewhat weaker; all the previously reported transitions[9] from levels (0,0,0) and (0,1,0) were detected, but the 3748-Å band from level (1,0,0) was not discernible, even with long exposures, indicating that the vibrational temperature was lower. These observations are consistent with the formation of electronically excited SO_2 in the reaction of gaseous SO with chemisorbed oxygen atoms

$$\text{wall} - \text{O} + \text{SO} \longrightarrow \text{wall} - + \text{SO}_2^* \qquad (5)$$

and the intensity distribution of the emission indicates that the heat of chemisorption of the oxygen atoms responsible is 25–30 kcal/mol, that is, slightly greater than $D(O\text{–}O_2)$. There is evidence for an analogous red glow above the surface when the reaction between O and NO is studied at low pressures.[15] This is almost certainly NO_2 emission due to a process analogous to (5) and resembling the NO + O_3 chemiluminescence (reaction 1) in its spectral distribution.

An analysis of the radial distribution of the $^3B_1$ emission in the flow tube supported the view that $^3B_1$ SO_2 molecules were formed on the flow tube walls and diffused to the center, being removed by a first-order process. Numerical analysis of the spatial distribution at total pressures between 12 and 52 μ for an argon carrier yielded a life of (7.6 ± 1.6) × 10^{-4} sec for the $^3B_1$ state, assuming its diffusion coefficient in argon to be 100 cm^2 sec^{-1} at 1 mm pressure.[16] This value did not decrease with increasing pressure and can therefore be identified with the radiative life of the $^3B_1$ state. It is ten times longer than the radiative life of the $^1B_1$ state.[17] Collisional quenching from the $^1B_1$ to the $^3B_1$ state could not therefore affect its apparent life. Our value may be compared with a lower limit of 5 × 10^{-4} sec in the solid state[17] and a value of 2 × 10^{-4} sec for shock-heated SO_2.[18]

The lack of pressure dependence shows that the half-quenching pressure of the $^3B_1$ state for argon is not less than 50 μ, whereas the pressure dependence of the SO + O_3 emission shows it cannot be greater than 300 μ. If these limits are applied to the $^3B_1$ emission in the SO + O_3 reaction (allowing for population of the $^3B_1$ state by collisional transfer from the $^1B_1$ state), it can be shown that k_{4b} = (1 to 6) × 10^9 $\exp(-3900/RT)$ cm^3 mol^{-1} sec^{-1} and is probably close to the center of the range quoted.

Discussion

The higher activation energies (4.2 and 3.9 as against 2.1 kcal/mol) and lower frequency factors (10^{11}, *ca.* 3 × 10^9 as against 1.5 × 10^{12} cm^3 mol^{-1} sec^{-1}) for the formation of $^1B_1$ and $^3B_1$ electronically excited SO_2 in reaction 4 as compared with ground-state products are consistent with a crossing to the appropriate potential surface at or near the transition state. The low-frequency factor for populating the $^3B_1$ state suggests a weaker crossing process perhaps to a singlet or quintet surface arising from $SO_2(^3B_1)$ + $O_2(^3\Sigma_g^-)$ rather than a triplet, since triplets must be involved in the formation of both ground state and $^1B_1$ SO_2.

Very little is known about vibrational excitation in polyatomic reaction products, but it is highly unlikely that the observed distributions in and between the $^3B_1$ and $^1B_1$ states of SO_2 could arise from the formation of highly vibrationally excited ground state SO_2 molecules which then cross into the emitting states. The higher activation energies for their formation argue against such a process, since there is no evidence that the formation of highly vibrationally excited reaction products is greatly favored by a small increase in reactant energy.

(14) A. McKenzie and B. A. Thrush, to be published.

(15) T. R. Rolfes, R. R. Reeves, and P. Harteck, *J. Phys. Chem.*, **69**, 849 (1965).

(16) Based on unpublished measurements of T. Jones (Leeds University).

(17) K. F. Greenough and A. B. F. Duncan, *J. Amer. Chem. Soc.*, **83**, 555 (1961).

(18) B. P. Levitt and B. D. Sheen, *Trans. Faraday Soc.*, **63**, 540 (1967).

Production of Electronically Excited Atoms. II. $H + HI \rightarrow H_2 + I^*(^2P_{1/2})$

by P. Cadman and J. C. Polanyi

Department of Chemistry, University of Toronto, Toronto 5, Canada *(Received May 7, 1968)*

Measurements of infrared chemiluminescent emission intensity have been used to study the yield of electronically excited $I^*(^2P_{1/2})$ for the reaction $H + HI \rightarrow H_2 + I^*$. The emission was due to the (forbidden) transition, $I^*(^2P_{1/2}) \rightarrow I(^2P_{3/2})$ at 1.315 μ. Atomic hydrogen was formed by discharge techniques and was mixed with HI in a fast-flow system, in the presence of a large excess of argon at 4–6 torr pressure. The absolute concentration of [I*] was measured; from this its rate of formation could be calculated. This rate was then compared with the total rate of formation of atomic iodine, I + I*, measured titrimetrically in the same experiment. There was evidence at higher reagent pressures that atomic iodine was being excited by a secondary process. Extrapolation to low reagent pressure led to a value for the relative yield of I* to I + I* of $k_2^*/k_2 \leq 0.02 \pm 0.015$; *i.e.*, $>98 \pm 1.5\%$ of the reaction goes to form ground-state atomic iodine. Similar results were obtained for D + HI. When combined with earlier chemiluminescent data obtained in this laboratory from the continuous photolysis of HI, the further result was obtained that in the 2537-Å photolysis of HI the relative yield of I* to I + I*, from the primary photolytic act, is $k_1^*/k_1 = 0.55 \pm 0.25$. Further experiments, using continuous photolysis of HI as a source of I*, gave a value for the rate constant of the quenching process, $I^* + H_2 \rightarrow I + H_2$, of $k_6 = 21.5 \pm 2.5 \times 10^{-14}$ cc/mol sec. The yield of I* from $Cl + HI \rightarrow HCl + I^{(*)}$ was shown to be small.

Introduction

Various techniques, among them the study of infrared chemiluminescence employed in this work, have been used in order to study the energy distribution in the products of exothermic reactions. The most common forms of product excitation are vibration, rotation, and translation. *Electronic* excitation is less commonly encountered. Since the mechanism of electronic excitation involves particularly difficult theoretical problems, we have reason to be grateful that relatively few chemical reactions liberate sufficient energy to elevate the products to electronically excited states. This paper describes an attempt to determine the yield of electronically excited halogen atoms from some simple exchange reactions of the type $A + BC \rightarrow AB + C^*$.

In a previous publication,[1] the yield of $I^*(^2P_{1/2})$ electronically excited atoms was determined in the 2537-Å gas-phase photolysis of hydrogen iodide, by emission spectroscopy in the infrared. The processes which produced the electronically excited atoms were (a) direct photolysis of $HI \rightarrow H + I^*$ and (b) the exchange reaction $H + HI \rightarrow H_2 + I^*$. The relevant rate constants are

$$HI \xrightarrow[k_1]{2537\ \text{Å}} \begin{cases} H + I^* & k_1^* \\ H + I & k_1 - k_1^* \end{cases}$$

$$H + HI \xrightarrow[k_2]{} \begin{cases} H_2 + I^* & k_2^* \\ H_2 + I & k_2 - k_2^* \end{cases}$$

The sum of the fractional yields of I* in these two processes was symbolized

$$C = \frac{k_1^*}{k_1} + \frac{k_2^*}{k_2}$$

and was evaluated as being $C = 1.5 \pm 0.4$.

In this earlier work concentrations of $I^*(^2P_{1/2})$ atoms were obtained from the observed emission intensity by using the radiative lifetime for $I^* \rightarrow I + h\nu$ (where $\nu = 7605\ cm^{-1}$, $= 1.315\ \mu$) calculated by Garstang.[2] Recently, this quantity has been measured experimentally;[3,4] the experimentally determined Einstein transition probability for spontaneous emission is $A_{mn} = 22\ sec^{-1}$, as compared with the calculated value of 7.8 sec^{-1}. When C is recalculated using this new radiative transition probability, the value obtained is $C = 0.55 \pm 0.25$. In other recent work,[5] a value of $k_1^*/k_1 \approx 0.55$–0.65 has been obtained for the 2537-Å photolysis of HI. When combined with our revised value of C this leads to $k_2^*/k_2 < 0.25$. (According to the evidence of the present work concerning secondary excitation of I* at higher concentrations of [H], this is best regarded as an *upper limit* on k_2^*/k_2.) This finding is in accord with qualitative evidence arising from the experiments of Donovan and Husain, who concluded that k_2^*/k_2 should be small.

In the present work we have examined process 2 (the exchange reaction H + HI) in the absence of process 1 (the photolysis of HI), by injecting H atoms

(1) P. Cadman, J. C. Polanyi, and I. W. M. Smith, *J. Chim. Phys.*, **64**, 111 (1967); this was part I.

(2) R. H. Garstang, *J. Res. Nat. Bur. Stand.*, **68A**, 61 (1964).

(3) D. Husain and J. R. Wiesenfeld, *Nature*, **213**, 1227 (1967).

(4) D. Husain and J. R. Wiesenfeld, *Trans. Faraday Soc.*, **63**, 1349 (1967).

(5) D. R. Davis, J. M. White, J. Asay, and A. Kuppermann, to be published; A. Kuppermann, private communication.

from a discharge directly into a stream of HI. The investigation has been complicated by the discovery of a secondary process which is also capable of exciting atomic iodine by energy transfer. We have not attemped to characterize this secondary process, but have attempted to reduce it to a minimum with a view to obtaining a dependable upper limit for the fractional yield of I* from the reaction $H + HI \rightarrow H_2 + I^*$.

Experimental Section

The apparatus was very similar to that described in part I.[1] The quartz tube was replaced by a Pyrex tube of the same internal diameter. This tube had two side arms for the introduction of reagents. One of these, located at the spectrometer end of the vessel, was fitted either with a Wood's discharge tube or with a quartz tube which passed through a microwave cavity (see below).[6] The second side arm was located 25 cm downstream (the gas flowed, as before, away from the "front," spectrometer, end of the tube). This second inlet led to a ring of fine Teflon tubing suspended inside the reaction vessel. The Teflon ring constituted the injector for the molecule reagent; it was perforated by 16 small holes which directed jets of reagent in the upstream direction, inward at 45° to the axis of flow. This type of injector has been used previously to ensure rapid mixing of reagents in a flow system at approximately these pressures.[7] As a check on the mixing efficiency, some experiments were repeated with a somewhat poorer mixing system consisting of fewer and wider inlet jets; the results were not altered.

The absolute concentration of atomic hydrogen at the point of entry of the hydrogen iodide into the vessel was obtained by gas-phase "titration" against HI. At high HI flow (as will be shown below) all the H was consumed in reaction with HI; $H + HI \rightarrow H_2 + I$. In this system the fate of I is to recombine giving molecular iodine; consequently, $H = {}^1/_2I_2$. The molecular iodine was collected in two liquid nitrogen-cooled traps in series and was titrated with thiosulfate. The contents of the two traps were titrated separately, so that a correction could be made for the untrapped iodine (<10%).

Figure 1 shows a typical graph of the apparent H-atom concentration, measured by reaction with HI, *vs.* the pressure of HI. For ([HI]/[H]) > 4 the measured [H] reached an approximately constant value, indicating that all the H was reacting with HI. Values of H used in this work were, therefore, obtained in titration experiments with ([HI]/[H]) > 4.

The discharge tube and reaction vessel were coated with phosphoric acid. A measurement was made, *in situ*, of the rate of recombination of H atoms at the walls by means of the H-atom titration technique. The time for H to flow from the discharge tube to the titration point (the HI inlet) was varied systematically (a) by throttling-down the flow through the reaction vessel with the aid of a valve directly in front of the mechanical pump or (b) by moving the microwave discharge away from the vessel, along the side arm. Both techniques gave a collision efficiency of $\gamma \sim 10^{-5}$ for the phosphoric-coated walls. This is similar to published values.[8]

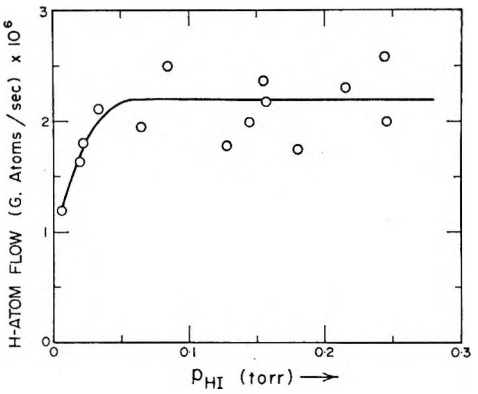

Figure 1. The apparent hydrogen atom flow as a function of the pressure of hydrogen iodide used in the gas-phase "titration." All experiments were conducted in the presence of an excess of argon at a total pressure of 4.8 torr.

The discharge employed in the formation of H atoms was either a Wood's discharge tube with aluminum electrodes (15,000 V, 800 W) or a Raytheon Microtherm 2450-MHz, 120-W, microwave discharge coupled to a barrel-shaped cavity.[6]

The $I^*(^2P_{1/2})$ emission was recorded using a Perkin-Elmer 12G single-pass grating spectrometer, as described previously.[1] The instrument had been calibrated to yield absolute intensity in photons/sec. The recorded intensity could therefore be converted to the absolute concentration of emitters by means of the relationship

$$\text{intensity} = \text{constant} \times k_r[I^*]$$

where constant is the calibration constant[1] and k_r is the rate constant for spontaneous emission, $I^*(^2P_{1/2}) \rightarrow I(^2P_{3/2}) + h\nu$.

$$k_r = A_{mn} = 22 \text{ sec}^{-1}$$

from ref 3 and 4.

Reaction Scheme

Consider the following reaction scheme

$$\begin{aligned} H + HI \xrightarrow{k_2} & \begin{cases} \rightarrow H_2 + I^* & k_2^* \quad \{2U\} \\ \rightarrow H_2 + I & k_2 - k_2^* \quad \{2L\} \end{cases} \quad \{2\} \\ H + \text{wall} \rightarrow {}^1/_2H_2 + \text{wall} & \quad f_2 \quad \{2W\} \\ I^* + \text{wall} \rightarrow I \text{ (or } {}^1/_2I_2) + \text{wall} & \quad f_3 \quad \{3W\} \end{aligned}$$

(6) F. C. Fehsenfeld, K. M. Evenson, and H. P. Broida, *Rev. Sci. Instrum.*, **36**, 294 (1965).

(7) F. A. Morse and F. Kaufman, *J. Chem. Phys.*, **42**, 1785 (1965).

(8) B. A. Thrush, *Progr. Reaction Kinetics*, **3**, 63 (1966).

$$I^* \longrightarrow I + h\nu \qquad k_r \quad \{3R\}$$
$$I^* + HI \longrightarrow I + HI \qquad k_3 \quad \{3\}$$
$$I^* + Ar \longrightarrow I + Ar \qquad k_4 \quad \{4\}$$
$$I^* + H_2 \longrightarrow I + H_2 \qquad k_6 \quad \{6\}$$

Reactions $\{2U\}$ to give the upper state of atomic iodine, $\{2L\}$ to give lower state, and $\{2W\}$ all remove atomic hydrogen. The rate of removal of H by recombination in the gas was calculated and was found to be at least an order of magnitude slower than the rate of removal at the wall; consequently, this process has not been included in the reaction scheme. Another process that might remove H is the rapid reaction of H with molecular iodine. However, the rate of formation of I_2 is low, being governed by the rate of ternary collisions I + I + M or the rate of diffusion of I to the wall followed by diffusion of I_2 into the body of the vessel. As noted below, the reagents H + HI consumed H in $\sim 10^{-3}$ sec, corresponding to a linear displacement of a few millimeters along the reaction tube. Calculations showed that the concentration of I_2 in this short reaction zone must be very small compared with that of HI; consequently, we did not include H + I_2 as a path for the removal of atomic hydrogen.

The remaining five processes listed in the reaction scheme removed I*, either in gas-phase collisions, $\{3\}$, $\{4\}$, and $\{6\}$, by radiation, $\{3R\}$, or by wall deactivation, $\{3W\}$.

Reaction $\{2\}$ (*i.e.* $\{2U\}$ plus $\{2L\}$) has a rate constant at 300°K of 3.3×10^{-11} cc/molecule sec obtained from extrapolation of data given by Sullivan.[9] The rate of removal of H at the vessel wall was probably diffusion controlled at these pressures and hence could be calculated[1] from the first-approximation Chapman–Enskog equation;[10] the value at 4 torr is $f_2 \approx 192$ sec^{-1}. This figure can be compared with the experimental value obtained by Weissman and Mason[11] for H-atom diffusion in H_2 at 300°K, *viz.*, $f_2 = 318$ sec^{-1}, and the value obtained by Wise[12] for an H–H_2–Ar mixture, $f_2 = 216$ sec^{-1}. The method of calculation is described more fully in ref 1. For pressures of HI in excess of 0.001 torr, $k_2[HI] > 10^3$ sec^{-1}; consequently, we can conclude that, in this HI pressure range, $f_2 \ll k_2[HI]$.

The deactivation of $I^*(^2P^1{}_2)$ atoms at the walls of the vessel has been shown to be diffusion controlled.[1] For a 5-cm i.d. tube, it was found that $f_3 = 67$ sec^{-1} at a pressure of 6.4 torr of argon.

The differential rate equations are

$$-\frac{d[H]_t}{dt} = k_2[H]_t[HI] + f_2[H]_t \qquad (1)$$

$$\frac{d[I^*]_t}{dt} = k_2^*[H]_t[HI] - \{k_3[HI] + k_r + f_3 + k_6[H_2]\}[I^*] \qquad (2)$$

$$= k_2^*[H]_t[HI] - k_q[I^*] \qquad (2')$$

Quenching of I* by argon has a negligible probability compared to the other removal processes;[1] consequently, k_4 has not been included in k_q.

These equations can easily be integrated for constant [HI]; *i.e.*, assuming [HI] ≫ [H]

$$[H]_t = [H]_0 \times e^{-\{k_2[HI]t + f_2t\}} \qquad (3)$$

$$[I^*]_t = \frac{k_2^*[H]_0[HI]}{k_q - \{k_2[HI] + f_2\}}\left[e^{-\{k_2[HI] + f_2\}t} - e^{-k_qt}\right] \qquad (4)$$

A second integration is required in order to simulate what the spectrometer records, since it views the reaction tube longitudinally. The decay of I* takes place in a short length of the tube; this is evident from the fact that $k_q \geqslant 10^3$ sec^{-1} making the mean lifetime of I* $\leqslant 10^{-3}$ sec, during which time the gases, which have a linear speed of 300 cm/sec, have flowed 0.3 cm. The fact that I* is removed within a short length of the reaction vessel was confirmed by means of the movable blackened vanes described in ref 1; 95% of the emission was found to originate from within the first 10 cm of the tube, past the HI entry point. Consequently, the spectrometer can be regarded as viewing $[I^*]$ from $t = 0$ to $t = \infty$, and the observed intensity gives a measure of

$$[I^*]_{obsd} = \int_0^\infty [I^*]_t\,dt = \frac{k_2^*[HI]}{k_2[HI] + f_2} \times \frac{[H]_0}{k_q} \qquad (5)$$

At the normal pressures of HI, and the normal total pressure of several torr, $f_2 \ll k_2[HI]$, as noted above. Hence eq 5 reduces to

$$[I^*]_{obsd} = \frac{k_2^*}{k_2} \times \frac{[H]_0}{k_q} \qquad (6)$$

It should be noted that k_q is not a true rate constant, but increases linearly with [HI] and [H_2]. According to (6) the effect of increasing [HI], at constant [H_2] and $[H]_0$, is to decrease $[I^*]_{obsd}$. This assumes, however, that [HI] is increasing in the range where $k_2[HI] \gg f_2$. If [HI] is increased from a low value, then $[I^*]_{obsd}$ will show an initial increase. This is due to the increasing importance of the reaction H + HI relative to removal of H at the wall, corresponding to the ascending portion of the curve in Figure 1. The initial rise and subsequent fall in $[I^*]_{obsd} = fn$. [HI] was obtained when the proper values of the rate constants were inserted into eq 5 or into the numerical calculation referred to below. Both calculations showed that the maximum in [I*] should fall close to the HI pressure for which [HI] = [H].

(9) J. H. Sullivan, *J. Chem. Phys.*, **30**, 1292, 1577 (1959); **36**, 1925 (1962).

(10) J. O. Hirschfelder, C. F. Curtiss, and R. B. Bird, "Molecular Theory of Gases and Liquids," John Wiley and Sons, Inc., New York, N. Y., 1954.

(11) S. Weissman and E. A. Mason, *J. Chem. Phys.*, **36**, 794 (1962).

(12) H. Wise, *ibid.*, **31**, 1414 (1959).

Table I: Slopes of Stern–Volmer Plots and Quenching Constants k_6 for I* + H_2, Determined by the Photolysis of HI in an Excess of Argon with Varying Admixtures of H_2 (See Figure 2)

P_{HI}, torr	0.019	0.09	0.086	0.163	0.247	0.4
Slope, $torr^{-1}$	29.6	15	14.2	8	4.8	4
k_6, cc/molecule sec $\times 10^{14}$	16.6	24.4	22.3	21.7	18.3	25

Mean $k_6 = 21.5 \pm 2.5 \times 10^{-14}$ cc/molecule sec.

Equations 3–6 were based on the assumption that [HI] can be regarded as constant. Numerical integration of eq 1 and 2 on an IBM 7094 computer showed that the analytical expression for $[I^*]_t$ (eq 4) gave values within 25% of the numerically integrated equation when $[HI]_0$ at the point of entry into the vessel was only 20% greater than $[H]_0$. Under our normal operating conditions $[HI]_0 > [H]_0$, and eq 3–6 will not be significantly in error due to depletion of [HI].

Results

In order to obtain k_2^*/k_2 from eq 6, we shall need, in addition to the constants already discussed, a value for k_6, the rate constant for quenching of $I^*(^2P_{1/2}) \rightarrow I(^2P_{3/2})$ in collisions with molecular hydrogen. Figure 2 shows a Stern–Volmer plot for I* + H_2. The excited atoms were produced by the photolysis technique of part I. This has the advantage, for the present purpose, that a major portion of the I* is formed directly in the primary dissociation of HI; consequently, the rate of formation of I* is unlikely to be affected by variation in the pressure of H_2. The second-order rate constant, k_6, can be calculated from the slopes of these plots; the results are presented in Table I. The average value is $k_6 = 21.5 \pm 2.5 \times 10^{-14}$ cc/molecule sec. This is 2.5 times greater than that obtained by Donovan and Husain[13] (8.8×10^{-14} cc/molecule sec) but only one-half as great as the value obtained more recently by Husain and Wiesenfeld.[4] It is unlikely that the difference between the quenching efficiency we obtain for I* + H_2 and that obtained by Donovan and Husain can be explained solely by impurities in our H_2. Oxygen is an efficient deactivator[14] and the most probable impurity. However, it would need 1% oxygen in our H_2 to account for the discrepancy between our quenching constant and that of Donovan and Husain.[13] This level of impurity is highly improbable since our H_2 was Matheson Ultrapure, total impurities less than 10 ppm; it was passed through a Deoxo catalytic purifier which was stated to reduce oxygen impurity to 1 ppm, and subsequently through a liquid nitrogen trap.

Since we must correct for the effect of H_2 as a quencher in our system, we have used the figure for k_6 determined with our reagents.

The first experiments employing a discharge as a source of H_2 made use of a Wood's discharge. The dependence of [I*] on [HI] was examined over a wide range of [HI] pressure in an excess of Ar at a total pressure of 4.3 torr. As noted in the previous section, [I*] should at first increase with HI, in the region of HI pressures where Figure 1 shows that the consumption of H by HI is increasing. According to calculation (previous section), the increasing importance of reaction 2 ends when [HI] ≈ [H]; at higher [HI] quenching of I* by HI should cause the curve at first to level off and then to descend. Experimentally, the levelling-off in Figure 3 comes at [HI] ≈ 3 × [H_2]. If this corresponds to [HI] ≈ [H] we would need to suppose that each H_2 is producing 3 H atoms, corresponding to more than 100% dissociation. These high values for [I*] indicate that some secondary process is exciting atomic iodine.

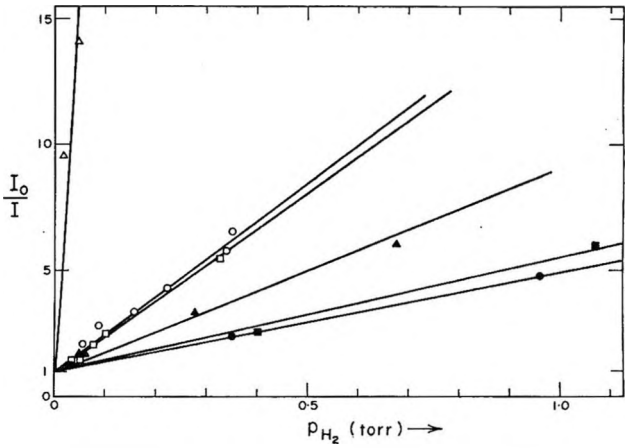

Figure 2. Stern–Volmer plot of the quenching of I* ($^2P_{1/2}$) → I($^2P_{3/2}$) in collisions with hydrogen. An excess of argon brought the total pressure to 6.4 torr in all these experiments. The various plots correspond to various partial pressures of HI, as follows: △, 0.019 torr; □, 0.086 torr; ○, 0.090 torr; ▲, 0.163 torr; ■, 0.247 torr; ●, 0.40 torr.

Figure 4 shows the variation in k_2^*/k_2 calculated from eq 6, with changing pressure of HI. All the experiments recorded in this figure were performed in the region of HI partial pressures where [HI]/[H] > 4; this is the region for which $f_2 \ll k_2$ [HI] (as evidenced by the data of Figure 1) and hence eq 6 should apply. Consequently $(k_2^*/k_2)_{calcd}$ calculated from (6) should be

(13) R. J. Donovan and D. Husain, *Trans. Faraday Soc.*, 62, 1050 (1966).

(14) R. J. Donovan and D. Husain, *ibid.*, 62, 2023 (1966).

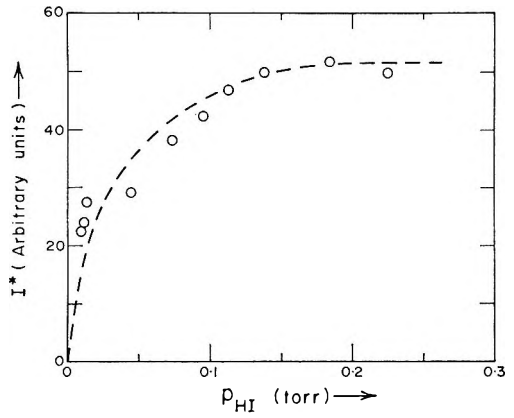

Figure 3. Variation of the emission intensity from the atomic iodine line with hydrogen iodide pressure. Total pressure was maintained constant at 2.2 torr by addition of argon.

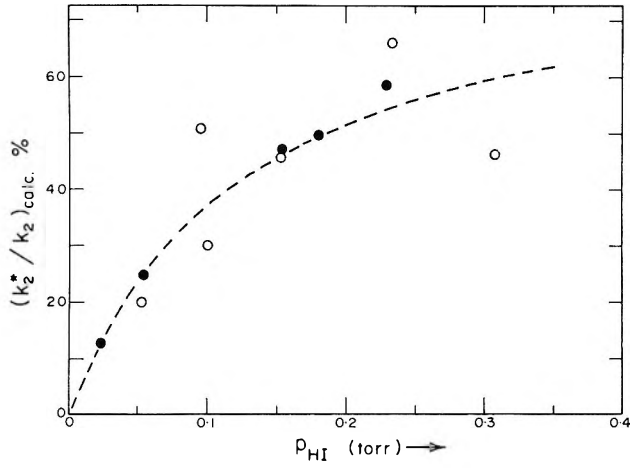

Figure 4. The apparent percentage of reaction 2 yielding I*, calculated from data collected at high H-atom concentration over a range of hydrogen iodide pressures (k_2^*/k_2 should be invariant with p_{HI}). Experiments symbolized by open circles used a Wood's discharge as the source of H: those indicated by the closed circles used a microwave discharge. The partial pressure of atomic hydrogen at the point of entry into the vessel was $p_H \approx 1.5 \times 10^{-2}$ torr; an excess of argon brought the pressure up to a total $p_{tot} \approx 4$–4.5 torr.

a constant. From Figure 4 it is evident that $(k_2^*/k_2)_{calcd}$ increases with HI. Presumably the secondary process is more serious at higher HI pressures. A very similar rise in $(k_2^*/k_2)_{calcd}$ increases with HI. Presumably the secondary process is more serious at higher HI pressures. A very similar rise in $(k_2^*/k_2)_{calcd}$ with increasing [HI] was obtained whether the discharge was a Wood's tube (open circles) or microwave discharge (closed circles). Since the conditions within the discharge are different in these two cases it would seem probable that the excited species responsible for what was termed the secondary excitation of atomic I is formed outside the discharge.

Figure 5 collects a number of experiments performed at various H-atom concentrations over a considerable

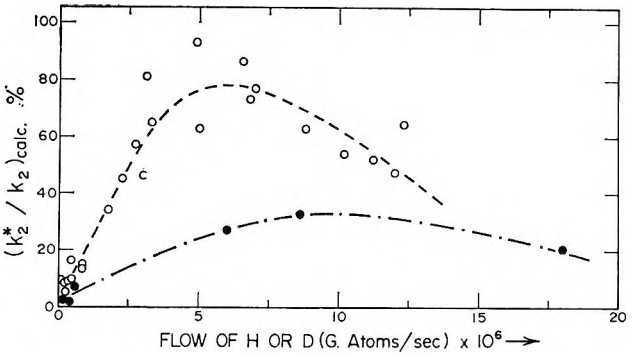

Figure 5. The apparent percentage of reaction 2 yielding I*, calculated from data collected over a range of atomic-H or atomic-D inflows (k_2^*/k_2 should be invariant with p_H or p_D). Open circles refer to the system H + HI; closed circles refer to D + HI. The partial pressure of HI was $p_{HI} \approx 0.34$ torr. The pressure p_H ranged from 5×10^{-4} to 4×10^{-2}, p_D from 5×10^{-4} to 5×10^{-2}. An excess of argon brought the total pressure to *ca.* 5 torr.

span of time. It is evident that the $(k_2^*/k_2)_{calcd}$, taken from eq 6, increases with [H]. It appears that increase in [H], like increase in [HI], has the effect of increasing [I*] more rapidly than the simple reaction scheme, with k_2^* as the only source of I*, would permit. There is an indication of a fall in k_2^*/k_2 at the highest [H]. (This could be due to deactivation of $H_2^\dagger$ by H; see below.)

The secondary process must have a rate which is dependent on [H] and on [HI]. A possible process of this type would involve as a first stage the reaction of atomic hydrogen and HI to give ground state iodine atoms and vibrationally excited H_2

$$H + HI \longrightarrow (H_2^\dagger)_{v \leq 3} + I \qquad \{2L\}$$

Subsequent vibrational-to-electronic exchange would then be held responsible for excitation of the atomic iodine

$$(H_2^\dagger)_{v \geq 2} + I \longrightarrow H_2 + I^* \qquad (7)$$

Since the quenching of I* by H_2 is efficient (collision efficiency approximately 4.4×10^{-3}), this reverse process may also be efficient. The likelihood that $\{2L\}$ is followed by (7) would be increased at high [HI] since the rate of $\{2L\}$ would be enhanced leading to a high local concentration of $[H_2^\dagger]$ and [I] with a consequent increase in the rate of (7) as compared with the rate of collisional deactivation of $H_2^\dagger$. (The deactivation would occur in collisions $H_2^\dagger + H$, $H_2^\dagger + H_2$, and $H_2^\dagger + HI$; $H_2^\dagger + Ar$ would be a less efficient energy transfer.)

Extrapolation of the points in Figure 5 toward low [H] suggests that the true k_2^*/k_2 in the absence of the I* from the secondary process will be a small fraction, $\lesssim 0.03$.

We have made a study of the behavior of $(k_2^*/k_2)_{calcd}$ at the lowest [H] which yielded measurable intensity of I* emission. In this work we used an

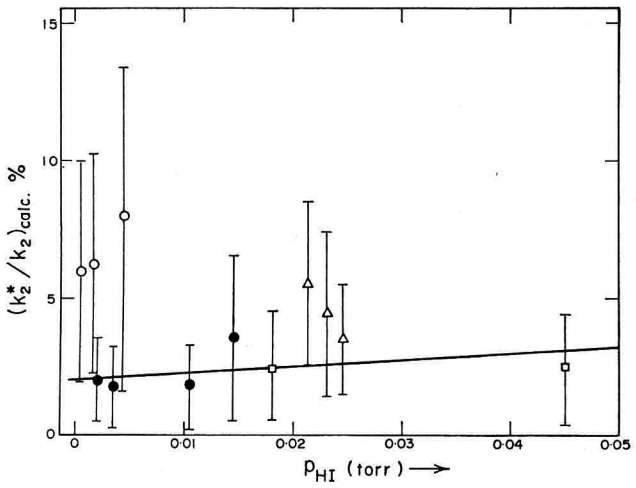

Figure 6. Plot of $(k_2^*/k_2)_{calc}$ at low hydrogen-atom concentrations as a function of p_{HI}. Emission intensity was measured by series of electronic integrations; the error limits were estimated from the scatter in the results from electronic integration under given experimental conditions. The results constitute four sets of data, obtained on different occasions. The pressure of HI was varied in each set, but the rate of inflow of H was constant; the values of p_H at the inlet were for points symbolized: ○, 6×10^{-4} torr; ●, $\leq 4 \times 10^{-4}$; □, 9×10^{-4} torr; △, 9×10^{-4} torr. The last three sets were the most accurate since a large number of integrations were performed at each HI pressure (between 6 and 9 integrations of 5-min duration on the signal, and an equal number on the background). An excess of argon was present in all experiments, bringing the total pressure to *ca.* 4.4 torr.

Elcor Co. electronic integrator to integrate signal and background alternately, each for periods of 5 min. An excess of H_2 was added below the discharge so as to promote collisional deactivation of the agent (perhaps $H_2^\dagger$) responsible for the secondary excitation. The values of $(k_2^*/k_2)_{calcd}$ obtained at low [H] ($p_H \sim 7 \times 10^{-4}$ torr) are plotted against the pressure of HI in Figure 6. Owing to the very low intensity, the error limits on the points are broad, but it appears that $(k_2^*/k_2)_{calcd}$ is roughly invariant with the pressure of HI over a 40-fold variation in HI pressure. If $(k_2^*/k_2)_{calcd}$ is genuinely invariant with HI, then we can write $k_2^*/k_2 \approx 0.02 \pm 0.015$. However, on the basis of Figure 6 we cannot exclude a slight downward trend in $(k_2^*/k_2)_{calcd}$ with decreasing HI. If this slope is genuine, then $k_2^*/k_2 < 0.02 \pm 0.015$. We conclude that $k_2^*/k_2 \leqslant 0.02 \pm 0.015$; only a very small fraction of the reaction H + HI → H_2 + I proceeds along the upper potential energy surface to give I* as product.

We have performed a few experiments on the system D + HI; $(k_2^*/k_2)_{calcd}$ from these experiments are recorded as a function of [D] in Figure 5. The points fall consistently below their counterparts for H + HI; however, in the limit of low [D] the difference is too small to be regarded as trustworthy. We conclude that the yield of I* from D + HI → DH + I is as small as from H + HI, and possibly smaller.

Preliminary experiments were performed on the systems

$$Cl + HI \longrightarrow HCl + I^* \qquad -\Delta H = 34 \text{ kcal/mol} \quad (8)$$

and

$$Br + HI \longrightarrow HBr + I^* \qquad -\Delta H = 16 \text{ kcal/mol} \quad (9)$$

Since the excitation energy for I* is 21.7 kcal/mol, reaction 9 must surmount an activation barrier of *ca.* 6 kcal to produce I*; a very low yield of I* from this reaction was therefore to be expected. The experimental technique was precisely that used in the work on H + HI described above. (Only the microwave discharge was used as a source of halogen atoms.) From experiments in which the infrared chemiluminescence arising from the *molecular* product of these reactions was recorded, we know these to be fast reactions at room temperature.[15] Nonetheless, we were only able to record very weak emission from excited iodine atoms even with the aid of the electronic integrator. It appears that the yield of $I^*(^2P_{1/2})$ is low in both of these reactions. This is in accord with the evidence from the molecular chemiluminescence experiments, performed under different experimental conditions.[15]

If we assume that at the entry to the vessel the percentage dissociation of Cl_2 and Br_2 in these experiments was *ca.* 5%, and if we further assume (arbitrarily) that the quenching efficiency in I* + Cl_2 and I* + Br_2 collisions is the same as that in I* + I_2 collisions, we obtain the result that $k_2^*/k_2 < 0.01$ for reactions 8 and 9. This yield is shown as an upper limit, for the stated assumptions, since the very weak emission could easily be explained by secondary (energy-transfer) processes.

A single experiment was performed on the system

$$O + HI \longrightarrow OH + I^* \qquad -\Delta H = 31 \text{ kcal/mol} \quad (10)$$

using a microwave discharge in O_2 as a source of oxygen atoms. Strong atomic iodine emission was observed. The apparent fractional yield of $I^*(^2P_{1/2})$ from reaction 10 was measured and was found to be 0.8. This figure means little since other species coming from the discharge could be responsible for the excitation of atomic iodine. We merely wish to observe that for reaction 10, in contrast to the three other reactions cited, the possibility that the reaction proceeds preferentially to form electronically excited atomic product is not excluded.

Acknowledgments. The authors are most grateful to Dr. J. Hassler and Dr. I. W. M. Smith for their help with this work. P. C. thanks the University of Toronto

(15) K. G. Anlauf, P. J. Kuntz, D. H. Maylotte, P. D. Pacey, and J. C. Polanyi, *Discussions Faraday Soc.*, **44**, 183 (1967); D. H. Maylotte and J. C. Polanyi, to be published.

for the award of a postdoctoral fellowship. This work was supported by grants from the National Research Council of Canada, the United States Air Force Cambridge Research Laboratories, and the Petroleum Research Fund (administered by the American Chemical Society).

Chemiluminescent Emission in Gaseous Reactions at Low Concentrations

by John Emerson, Robert Reeves, and Paul Harteck

Chemistry Department, Mason Laboratory, Rensselaer Polytechnic Institute, Troy, New York 12181
(Received May 7, 1968)

The advances of electronic technology applied to photochemical systems make it possible to follow radical and atom reactions emitting only a few hundred quanta per second. This technique will make it possible to investigate many reactions by this experimental approach. Exceptionally long-lived low-level luminescence is observed from gases after being irradiated for a few seconds to 1 min with the mercury 2537-Å line or discharged by a Tesla coil. These emissions in the visible and ultraviolet regions with a half-life in the order of hours were investigated for gases such as CO_2 or SO_2 in the pressure region of a few hundred microns. The decay appears to be close to second order. Evacuated or argon filled cells observed as blanks after similar excitation gave no significant luminescence after a few minutes. Initial emission was presumably due to phosphorescence of the glass. The emissions are apparently due to very long-lived radicals or atoms which are consumed partially over chemiluminescent reactions. Concentrations of these radicals and atoms may be less than 10^{10} per cubic centimeter (or square centimeter of surface area). In addition, reactions may be followed where even only a minute fraction results in chemiluminescence or reactions with small light emissions which go so slowly that over only geological ages would they be completed.

Introduction

Chemiluminescence and afterglows from atom and radical reactions have been observed for many years. Readily visible afterglows are observed in the 1-torr range in fast-flow systems.[1] Rayleigh observed the decay of the nitrogen visible afterglow in a closed system over the period of about 1 hr.[2] By quantitatively measuring such afterglows many reactions have been studied, rate coefficients determined, and mechanisms evaluated. In recent years, there has been a general improvement in the quality of electronics and fast rise time photomultipliers to allow essentially low-level photon measurements to be made. Scintillation spectrophotometers are used to measure photons generated simultaneously by β-particle decay of radioactive substance. Although such equipment must include coincidence to measure the β activity, the noncoincidence mode of operation is generally readily used. Using sealed vessels of the necessary size (about 20 cc), low-level luminosity could be observed from various gases after appropriate excitation or from direct chemical reaction. In this work we have made, for example, preliminary observation on emissions which extend in some cases over many hours after excitation for only 10 sec using a Tesla coil discharge. Using a mixture of carbon monoxide and ozone, strong emission can be observed due to the carbon monoxide–ozone reaction where the oxygen atoms are generated in thermal equilibrium with the ozone[3] over many days.

Experimental Section

Cylindrical quartz or Pyrex vessels of about 25 mm diameter and 20 cm^3 volume were evacuated to less than 10^{-3} torr, then heated and exposed to a discharge generated by a Tesla coil in order to degas the cell walls. The cells then were filled with the desired gas or gases and sealed. Two methods of inducing chemiluminescence were used: plasma inside the cell generated a Tesla discharge or exposure to a low-pressure (Hanovia) mercury quartz lamp.[4] The cells were placed in either a Beckman LS-200B, Nuclear Chicago, or Packard Tri-Carb liquid scintillation spectrometer, and the relative luminosity or afterglow emission was observed as a function of time, using the noncoincidence singles mode of operation. In this way, a limit of detection was determined by a background counting

(1) See, for example, *Discussions Faraday Soc.*, **37**, 26 (1964).

(2) Lord Rayleigh, *Proc. Roy. Soc.*, **A151**, 567 (1935); **A176**, 1 (1940).

(3) P. Harteck and S. Dondes, *J. Chem. Phys.*, **26**, 1734 (1957).

(4) Hanovia Chemical and Mfg. Co., Newark, N. J., Model 30600.

rate equivalent to about a total of 300 photons per second.

The discussion of the operation of a liquid scintillator can be found in the manuals of each manufacturer or elsewhere.[5,6] Essentially a high-efficiency, fast-response photomultiplier such as the RCA 8575 is used with high-speed amplification resulting in pulse signals, and the output is equivalent to photons per second when efficiencies are included. By designing the experiment around this standard type equipment which is frequently available in nuclear laboratories, low-level emissions studies can be readily made.

The gases used here were Matheson Research Grade except for the ozone which was made in a Welsbach ozonizer and purified by desorption from silica gel. The ozone–carbon monoxide experiments were made in 2-cm³ Pyrex vials. The purified ozone was added to the evacuated vial and then frozen with liquid nitrogen. Sufficient CO was then added and the vial was sealed. This small vial was inserted inside a standard 20-cm³ counting vessel to which water could be added to control the temperature of the vial itself.

In each run observation of luminescence was over a period of generally 1 to several hr with the counting time for each point being 0.1 to 1 min. Since the counting rate was high in the noncoincidence mode, statistical errors were less than 1%.

Results

Emissions were observed as a function of time for Pyrex and quartz vessels exposed to the mercury 2537-Å line for a period 1 to 10 min or by discharging the gas inside for about 10 sec using a Tesla coil. The emission intensity observed was considerably higher than background or blank sample vials after equivalent treatment except, for example, Pyrex cells exposed to the mercury lamp phosphoresced for 2–3 hr.

Luminescence was observed from oxygen after excitation with the Tesla coil as shown in Figure 1. The counting rate per second (cps) is given as a function of time.[7] The level of intensity was similar for many gases, although argon gave no observable emission as might be expected. At lower pressures, much less than 100 μ, the luminosity was more intense and persistent. The luminosity from nitrogen at a pressure of 300 μ was observed at a higher counting rate than that from oxygen even at 100 μ. SO_2 was also considerably higher at 900 μ as can be seen by comparison with the results given in Figure 2. Typical counting rates observed from cells filled with CO_2 and exposed to the mercury 2537-Å line (uv) are also given in Figure 2.

Excitation of the sample by a low current beam of 1-MeV electrons was considered, but initial experiments showed that the Pyrex glass not only darkened slightly after a total exposure of several 0.5-J pulses of 0.5-μsec duration, but the glass itself was phosphorescing so strongly that the counting scalers were essentially flooded for several days.

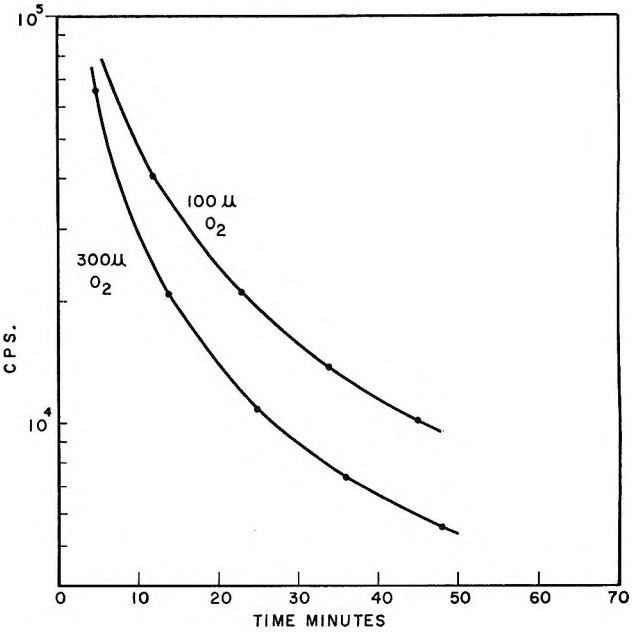

Figure 1. Emmission from oxygen vessel—after Tesla coil, 10 sec.

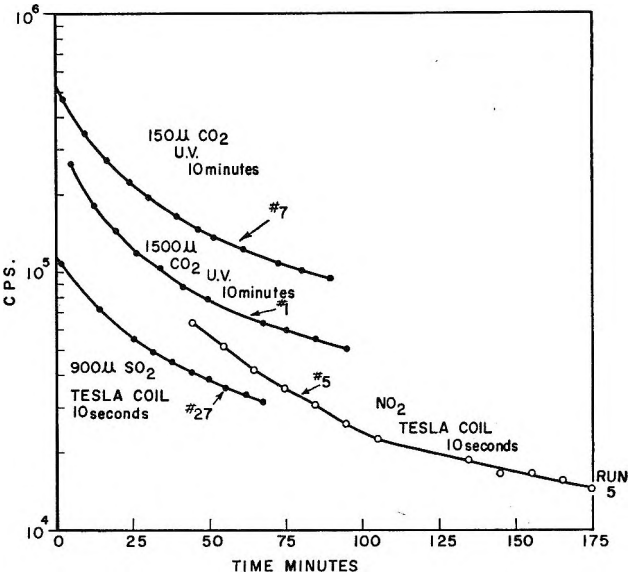

Figure 2. Emission from quartz vessels.

Emission was also observed from a mixture of carbon monoxide with ozone in a 2-cm³ Pyrex vessel filled with 13 torr of ozone and 23 torr of carbon monoxide. The rate of photon emission was relatively constant over

(5) W. J. Price, "Nuclear Radiation Detection," McGraw-Hill Book Co., Inc., New York, N. Y., 1964, Chapter 7.

(6) J. B. Birks, "The Theory and Practice of Scintillation Counting," The Macmillan Co., New York, N. Y., 1964.

(7) Background for irradiation of blank vessels was two orders of magnitude less than irradiated samples. Thus we discarded the background due to phosphorescence of the glass.

long periods of time—the decrease probably corresponding to a decrease in the concentration of ozone due to decomposition on the walls of the vessel. In this case no excitation by a Tesla coil or mercury lamp was used. The emission apparently resulted mainly from the reaction of carbon monoxide with the O atoms. The atoms could be expected to be in thermal equilibrium with the ozone present. This equilibrium is known to be very temperature dependent and the counting rate was observed to increase rapidly with temperature. This dependence was equivalent to slightly more than 20 kcal of activation. The energy of dissociation of ozone into O atoms is about 24 kcal, in good agreement with this observation. However, with samples filled with pure ozone, no appreciable counts above background were observed.

Some typical experimental data are presented in Table I. The results were highly reproducible, showing that reactions have a real meaning.

Table I: Experimental Data

Gas mixture	Pressure, mm	Type of excitation	Counting rate at start, cps
$CO + O_3 + O_2$	25	...	142,436
$H_2 + O_3$	20	...	4,943
O_3[a]	5	...	350
O_2	0.1	Tesla	62,820
SO_2	0.5	Tesla	122,800
CO_2	0.5	Tesla	498,700
Blank (Pyrex)[a]	...	Tesla	170
Blank (quartz)	...	Tesla	Background
Blank (quartz)	...	Uv	Background
Background	...	...	300–330

[a] Background subtracted.

Discussion

The purpose of this work is to bring attention to the possibility of measuring low-level light emissions from gas samples using equipment now generally available with the intent to provide further information to the general field of reaction kinetics involving gases, luminous reactions, and possibly shed additional light on the role that wall reactions may play.

Except for the possibly unique case of the nitrogen atom afterglow, most emissions from reactions terminate in a closed system after a second or so, and it was anticipated that only a flow cell would in general yield any observable emission. First-order decay schemes are usually anticipated, but here emissions were observed in almost all cases with the half-life increasing inversely with time equivalent to a second-order decay scheme. In the same gas the decay rate of the emission was found to increase approximately with the square root of the pressure, although this has been studied only over a limited range.

The kinetic scheme equivalent to $-dA/dt = kA^2$, where I (cps) is proportional to A, would fit virtually all the results obtained for the samples exposed to the mercury line or the Tesla coil. It is not, however, within the scope of this paper to evaluate in detail the mechanism operating in each case. Considerably more work needs to be done on the specific gas studied and especially any effect of the wall. In the case of SO_2, for example, it is well known that the kinetics are very complicated and many reactions occur simultaneously.

In each case the spectral region of emission can be characterized by use of light filters. Addition of glass or quartz wool was made in a few cases, but no major effect was observed. Some metal surfaces are known, however, to have a major effect on emission from gases containing oxygen atoms.[8,9]

Although this type of study will need extensive characterization to produce useful applicable results, it appears to give information in a time region not readily obtainable with atom and radical reactions. Possibilities of a much more direct application are the studies of mixtures of ozone with other gaseous reactants where the ozone acts as a source of O atoms *via* thermal decomposition

$$O_3 + M \rightleftarrows O_2 + M + O \qquad (1)$$

The reaction of CO with O atoms yields emission *via*

$$CO + O \longrightarrow CO_2 + h\nu \qquad (2)$$

Here the role of the third body is not apparent. Assuming a rate for this reaction equal to 3×10^{-18} $(\text{particles/cc})^{-1}$ sec^{-1},[10] and calculating the steady-state oxygen atom concentration assuming the ozone and oxygen molecules to be equivalent,[11] the photons produced *via* reaction 2 are in the right order of magnitude compared to the counting rate (assuming a photomultiplier efficiency overall of about 5% (20 $h\nu$/sec = 1 cps)). The temperature dependence of this emission lends support to this kind of mechanism because the heat of dissociation for ozone is 23.5 kcal/mol.

The capability of measuring coincidence leads to the speculation if any of the observed luminescence could be in coincidence; it might be either by two-photon decay[12,13] or rapid successively emitted photons in a

(8) G. Mannella and P. Harteck, *J. Chem. Phys.*, **34**, 2177 (1961).

(9) P. Harteck and R. R. Reeves, Jr., *Discussions Faraday Soc.*, **37**, 82 (1964).

(10) B. H. Mahan and R. B. Solo, *J. Chem. Phys.*, **37**, 2669 (1962).

(11) The oxygen atom concentration is about 10^6 particles/cc as calculated from the values in the tables in B. Lewis and G. von Elbe, "Combustion, Flames, and Explosions of Gases," Academic Press, New York, N. Y., 1961, p 682. This is in good agreement with the light emission data when efficiencies are included.

(12) M. Lipeles, R. Novick, and N. Tolk, *Phys. Rev. Letters*, **15**, 690 (1965).

(13) R. C. Elton, L. J. Palumbo, and H. R. Grien, *ibid.*, **20**, 783 (1968).

cascade.[14,15] At present the limitations of the efficiency of the photomultipliers and the geometry preclude a high percentage of coincidence counts being observed even if all photon emission would be a true two-photon process. In the case of SO_2 emission it is known that the characteristic SO + O reaction produces a continuum which goes through a maximum, and the characteristic intensity curve *vs.* energy or wavelength is not unlike the curve[16] for β emission where an antineutrino[17] is simultaneously emitted. Counting rates can be made in a noncoincidence mode or in a coincidence mode where the two photons observed must be within a gate time of the circuit of less than 100 nsec for commercial scintillation spectrophotometers. Random emission results in accidental coincidences being observed proportional to the square of the number of random observed pulses.

In high count rates the accidental coincidences can be very large; however, the ratio of accidental coincidence to any real coincidence will decrease with decreasing intensity and obviously the coincidence signals become proportional to the intensity of the measured noncoincidence at low intensity levels. No such coincidence emission was observed here, although the gating times were rather long and the total intensity was rather high to have a sensitive test of such coincidence. From the relative number of accidental coincidences observed compared to the noncoincidence counts, one can readily obtain a measure of the gate time effective within the electronic circuit.

Acknowledgment. The authors wish to thank Mr. R. Waldron and Mr. M. Riozzi for their technical assistance in performing some of the experiments. We also thank Mr. N. I. Sax, New York State Health Radiological Laboratories, for his cooperation in the use of counting equipment. This work was carried out under a research grant from the National Aeronautics and Space Administration.

(14) G. H. Nussbaum and F. M. Pipkin, *Phys. Rev. Letters*, **19**, 1089 (1967).

(15) R. C. Kaul, *J. Opt. Soc. Am.*, **56**, 1262 (1966).

(16) C. S. Wu, "Beta and Gamma-ray Spectroscopy," K. Siegbahn, Ed., North-Holland Publishing Co., Amsterdam, 1965, p 1365.

(17) E. J. Konopinski and M. E. Rose, ref 16, p 1237.

Liquid Benzene Luminescence Quenching by Carbon Tetrachloride. Consideration of the Presence of Solvent Excimers in the Interpretation of the Observed Rates of Quenching

by P. K. Ludwig and C. D. Amata

Department of Chemistry and the Radiation Laboratory,[1] University of Notre Dame, Notre Dame, Indiana 46556
(Received May 7, 1968)

The luminescence behavior of liquid benzene seems in general to follow a simple reaction scheme in which excited benzene monomers only are considered. However, it is found that the experimentally observed benzene luminescence decay time as a function of the aromatic concentration in *n*-nonane deviates from the expected linear relation. This finding together with the spectral evidence for the presence of excited species other than excited benzene monomers in the pure liquid suggests the necessity of using a more complex reaction scheme in describing the benzene fluorescence. The experimental data are discussed in the light of such an extended scheme. The hypothesis of excitation energy migration in liquid benzene is reconsidered. An alternative model is discussed to explain certain "anomalies" of the specific rate of benzene luminescence quenching.

The specific rates of excitation energy transfer from liquid benzene to suitable additives has been found by several workers to be larger than expected on theoretical grounds and furthermore to depend on the benzene concentration.[2-7] The theoretically expected values of these specific rates have been derived from two considerations. If the acceptor has optical properties such that resonance transfer from benzene to it is possible, Förster's theory of resonance transfer[8] has been applied and a critical transfer distance R_0 derived. In the case that no long-range interaction between benzene and the acceptor exists, upper limits of the specific rates of energy transfer (quenching) have been estimated from the theory of diffusion-controlled bimolecular processes.

The observation that specific rates of energy transfer from benzene to a variety of acceptors exceed the values calculated on this basis has been taken as evidence for the occurrence of energy migration through the solvent.[4-7,9] Because of the great theoretical interest in such phenomena in a liquid, it is worthwhile to consider critically the assumptions which are made in interpreting the experimental data and deriving the conclusions regarding energy migration. For example, in the case that resonance energy transfer from benzene to the acceptor is possible, Povinelli[10] has recently shown that some of the reported high specific rates of energy transfer can be the result of an incorrect application of Förster's theory to a liquid of low viscosity because the theory is derived, strictly speaking, for solid systems only. If however, diffusive motion of acceptor and donor is properly taken into account, calculated values of specific rates of energy transfer agree fairly well with those observed. On the other hand, the mathematical difficulties in extending Förster's theory to liquids of low viscosity do not make systems where resonance transfer is possible particularly suitable for studies of energy migration effects. Attention in this paper is focused therefore on processes which presumably involve collisional interactions between donor and acceptor only, that is, short-range interactions only. Specifically, the benzene luminescence behavior in the presence and absence of CCl_4 is studied under conditions of steady-state and nonsteady-state uv excitation and, significantly, as a function of benzene concentration in an optically inert solvent. In this case, the theory of diffusion-controlled processes should be applicable. The main objective of this study is to determine whether in benzene systems solvent excimers may play a role in the energy transfer process and whether they may perhaps account for experimental observations that have been ascribed to energy migration. Almost all

(1) The Radiation Laboratory of the University of Notre Dame is operated under contract with the U. S. Atomic Energy Commission. This is AEC Document No. COO-38-586.

(2) S. Lipsky, W. P. Helman, and J. F. Merklin, "Luminescence of Organic and Inorganic Materials," H. P. Kallmann and G. M. Spruch, Ed., John Wiley & Sons, Inc., New York, N. Y., 1962, p 83.

(3) C. R. Mullin, M. A. Dillon, and M. Burton, *J. Chem. Phys.*, **40**, 3053 (1964).

(4) M. A. Dillon and M. Burton, "Pulse Radiolysis," M. Ebert, J. P. Keene, A. J. Swallow, and J. H. Baxendale, Ed., Academic Press, London, 1965, p 259.

(5) S. Lipsky and M. Burton, *J. Chem. Phys.*, **31**, 221 (1959).

(6) R. Voltz, G. Laustriat, and A. Coche, *Compt. Rend.*, **257**, 1473 (1963).

(7) J. B. Birks and J. C. Conte, *Proc. Roy. Soc.*, **A303**, 85 (1968).

(8) T. Förster, "Fluoreszenz Organischer Verbindungen," Vandenhoeck und Ruprecht, Göttingen, 1951.

(9) C. Tanielian, Thesis, University of Strasbourg, 1965.

(10) R. Povinelli, Thesis, University of Notre Dame, 1967, to be published.

studies of benzene luminescence quenching consider the reactions of excited solvent monomer only despite the fact that the emission spectra of benzene as a function of concentration reveal the presence of excited states other than that of the monomer.

Experimental Section

Materials. Benzene (Eastman) was distilled through a 45-theoretical plate spinning-band column and the middle fraction was retained. Prior to distillation, benzene was repeatedly recrystallized. As an optically inert diluent *n*-nonane (Aldrich) was chosen because of the minimal viscosity change when mixed with benzene. After the hydrocarbon was passed twice through a 4-ft silica gel column, it was distilled in the same manner as benzene.

Techniques. Samples. For both steady-state and nonsteady-state measurements, samples were contained in Suprasil quartz cells. All samples were degassed by the freeze–thaw–pumping technique.

Steady-State Fluorescence Measurements. All fluorescence spectra and intensity measurements were carried out with a Cary 14 spectrophotometer with front-face illumination attachment. The 253.7-nm line from a low-pressure mercury lamp (Hanovia Lo 735A7) used for excitation of the sample was isolated with a Bausch and Lomb monochrometer. To permit determination of relative intensities, the stability of the lamp emission was monitored with a fluorescent standard (*p*-terphenyl in plastic).

Because of the low absorption coefficients of benzene, penetration of the exciting light into the sample cannot be neglected at low concentrations ([B] < 5 vol %). To correct for the concentration-dependent penetration, solutions of *p*-terphenyl with the same optical density as that of the dilute benzene solutions were used to obtain a correction factor for this effect. Because *p*-terphenyl does not exhibit self-quenching, all variation of luminescence intensity for different optical densities can be attributed to penetration effects.

Ultraviolet-Induced Luminescence Intensity–Time (LT) Curves. LT curves at 20° were obtained by using a monophoton technique.[11] A high-pressure hydrogen–mercury lamp described by D'Alessio, Ludwig, and Burton served as a pulsed-excitation source.[12] The emission decay time for the lamp was 2.7 nsec with an associated electric pulse of about 0.3-nsec decay. The emission around 253.0 nm, isolated by a Zeiss interference reflection filter, UV-R-250, served as excitation of the sample perpendicular to the direction of observation of luminescence.

Results

Steady-State Excitation. The reciprocal of the benzene monomer luminescence intensity as a function of benzene concentration is given in Figure 1. Figure 2 represents Stern–Volmer plots for the quenching of

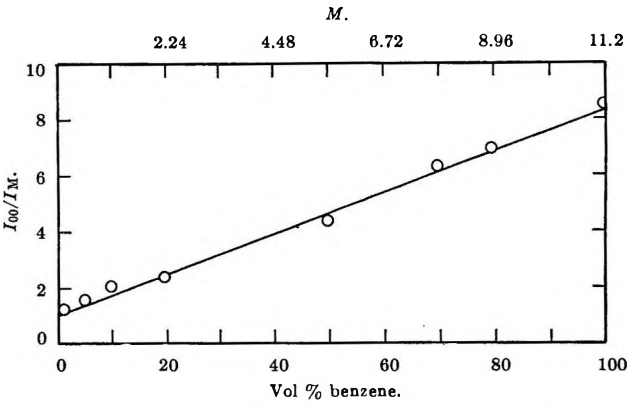

Figure 1. Reciprocal of benzene monomer luminescence intensity as a function of benzene concentration. (Diluent is *n*-nonane; *T*, 20°; $\lambda_{emission}$ 270 nm.)

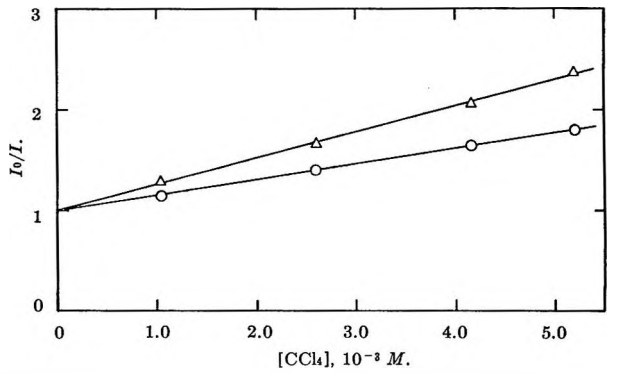

Figure 2. Stern–Volmer plots for benzene luminescence quenching by CCl_4. (Diluent is *n*-nonane; *T*, 20°; $\lambda_{emission}$ 270 nm.) Δ, 100% vol benzene; ○, 0.1 vol % benzene.

monomer luminescence by carbon tetrachloride for various benzene concentrations. Monomer emission is observed at 270 nm; that of the excimer at 330 nm.

Nonsteady-State Excitation. The reciprocal of the benzene luminescence decay time as a function of benzene concentration is given in Figure 3. In all cases, a single exponential decay of luminescence is observed, which is the same for the monomer and excimer emission. Addition of CCl_4 shortens the luminescence decay times.

Discussion

The potential effect of solvent excimers on the experimental observations is inspected by considering two reaction schemes. In the first one, the commonly made assumption is adopted that excited monomers only are of importance for the discussion of the observations, while in the second one, reactions of excimers in addition to that of excited monomers are included.

Simple Reaction Scheme. The luminescence behavior of benzene has frequently been described by the following sequence of processes.

(11) C. D. Amata and P. K. Ludwig, *J. Chem. Phys.*, **47**, 3540 (1967).
(12) J. T. D'Alessio, P. K. Ludwig, and M. Burton, *Rev. Sci. Instr.*, **35**, 1015 (1964).

$$B \xrightarrow{\sim} B^* \quad k_0$$

$$B^* \longrightarrow B \quad k_i$$

$$B^* \longrightarrow B + h\nu \quad k_e$$

$$B^* + B \longrightarrow 2B \quad k_{sq}[B]$$

$$B^* + Q \longrightarrow B + Q \quad k_q[Q]$$

where B, B*, and Q refer to the ground-state benzene molecule, to its excited state, and to the quencher, respectively. The indices of the rate parameters characterize the corresponding process and are self-explanatory. The expression for the luminescence intensity in the steady and nonsteady state as a function of benzene and quencher concentration obtained for this scheme are

$$I_{00}/I = 1 + \gamma_{sq}[B] \quad (1a)$$

$$\tau_0^{-1} = k_e + k_i + k_{sq}[B] \quad (1b)$$

for self-quenching and

$$I_0/I = 1 + \gamma_q[Q] \quad (2a)$$

$$\tau^{-1} = \tau_0^{-1} + k_q[Q] \quad (2b)$$

for foreign quenching.

Here I_{00} refers to the benzene luminescence intensity for low enough concentration so that self-quenching can be ignored. The subscript zero refers to benzene at some concentration in the absence of foreign quencher. τ is the mean lifetime of luminescence, and γ_{sq} and γ_q are defined by

$$\gamma_{sq} = k_{sq}/(k_e + k_i) = k_{sq} \cdot \tau_{00}$$

$$\gamma_q = k_q/(k_e + k_i + k_{sq}[B]) = k_q \cdot \tau_0$$

From eq 2a and 2b and the experimental curves given in Figures 2 and 3, the values of γ_q and k_q given in Table I were obtained.

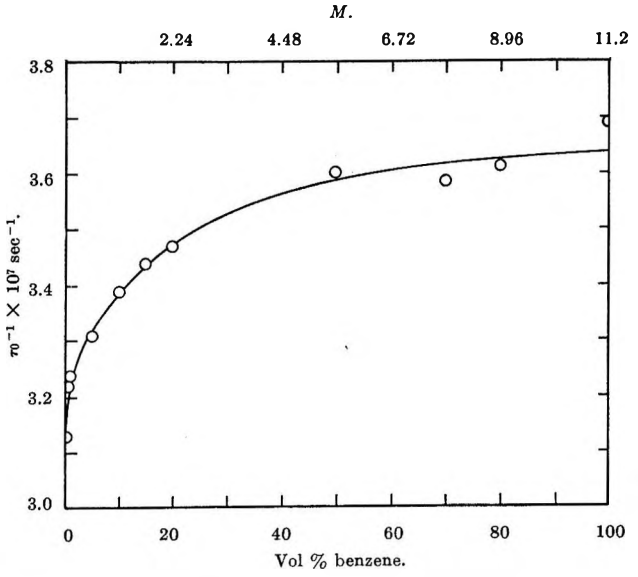

Figure 3. Reciprocal benzene fluorescence decay time as a function of benzene concentration. (Diluent is *n*-nonane; *T*, 20°; $\lambda_{emission}$ 270 nm.)

Table I: Experimental γ_q and k_q Values Obtained with Use of Eq 2a and 2b for Benzene Luminescene Quenching by CCl_4 (Diluent is *n*-Nonane; *T*, 20°)

	Concn, vol %				
	0.1	20	50	80	100
γ_q, M^{-1}	155	165	200	232	260
k_q, $10^{10} \times M^{-1}$ sec^{-1}	0.5	0.5	0.6	0.7	1.0

Comparison of expressions 1 and 2 with the experimental results (Figures 1–3) reveals that the linear variation of the reciprocal luminescence decay time of benzene as a function of its concentration in the absence of quenching (eq 1b) is not observed while the other derived expressions seem to agree with the corresponding observations.

Reaction Scheme Including Excimer. The presence of solvent excimers in benzene systems may be taken into account by the following scheme.[13,14]

$$B \longrightarrow B^* \quad k_0 \quad (0)$$

$$B^* \longrightarrow B \quad k_{im} \quad (I)$$

$$B^* \longrightarrow B + h\nu_1 \quad k_{em} \quad (II)$$

$$B + B^* \longrightarrow B_2^* \quad k_f[B] \quad (III)$$

$$B_2^* \longrightarrow 2B \quad k_{id} \quad (IV)$$

$$B_2^* \longrightarrow 2B + h\nu_2 \quad k_{ed} \quad (V)$$

$$B_2^* \longrightarrow B^* + B \quad k_r \quad (VI)$$

$$B^* + Q \longrightarrow B + Q \quad k_{qm}[Q] \quad (VII)$$

$$B_2^* + Q \longrightarrow 2B + Q \quad k_{qd}[Q] \quad (VIII)$$

The subscripts m and d serve to distinguish between reactions of excited monomers and excimers. Mathematical analysis of this scheme leads to expressions for the steady- and nonsteady-state luminescence intensities as a function of various parameters which are fairly complex and not very conveniently applied to the experimental observations.

However, as discussed elsewhere,[13] from the observed time dependence of benzene luminescence upon excitation by uv pulses of about 1–2 $\times$ 10^{-9} sec duration, it is possible to obtain information on the relative importance of some of the rates of the processes considered in the extended reaction scheme. This information leads to the following two possible inequalities

$$k_f[B] \gg k_m^0;\ k_r \gg k_d^0 \quad (3)$$

or

$$k_d^0 \gg k_m^0,\ k_f[B],\ k_r \quad (4)$$

(13) P. K. Ludwig and C. D. Amata, *J. Chem. Phys.*, in press.

(14) J. B. Birks and I. H. Munro, *Progr. Reaction Kinetics*, **4**, 256 (1967).

Inequality 3 corresponds to a rapid establishment of quasiequilibrium between excited monomer and excimer which may be represented by

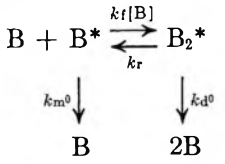

The second condition implies that any excimer that is formed is rapidly deactivated by processes other than dissociation into the excited monomer.

A clear decision which of the two conditions (3) and (4) applies is presently not possible. By analogy to other excimer systems,[14] we assume validity of (3), that is, the establishment of rapid equilibrium between excited monomers and excimers. With this assumption, the relevant theoretical expressions take the simpler form

$$I_m^{00}/I_m = 1 + (k_d^0 k_f[B]/k_m^0 k_r) \quad (5a)$$

$$I_d^{\infty}/I_D = 1 + (k_m^0 k_r/k_d^0 k_f[B]) \quad (5b)$$

$$\tau_0^{-1} = [k_m^0 + k_d^0(k_f/k_r)[B]/[1 + (k_f/k_r)[B]] \quad (5c)$$

for the self-quenching of benzene. Here $k_m^0 = k_{em} + k_{im}$; $k_d^0 = k_{ed} + k_{id}$; I_M^{00} refers to the monomer luminescence intensity in the absence of self-quenching and I_D^{∞} to that of the excimer extrapolated to infinite benzene concentration.

The expressions for foreign quenching are

$$I_m^0/I_m = 1 + \Gamma_m[Q] \quad (6a)$$

$$I_d^0/I_d = 1 + \Gamma_d[Q] \quad (6b)$$

where I_m^0 and I_d^0 represent the monomer and excimer luminescence intensity, respectively, for a particular benzene concentration.

$$\Gamma_m = \Gamma_d = (k_{qm} + k_{qd}(k_f/k_r)[B])/(k_m^0 + k_d^0(k_f/k_r)[B])$$

and

$$k_m = k_m^0 + k_{qm}[Q]$$

$$k_d = k_d^0 + k_{qd}[Q]$$

with $k_m^0 = k_{em} + k_{im}$, $k_d^0 = k_{ed} + k_{id}$. For the reciprocal luminescence decay time as a function of quencher concentration, one obtains

$$\tau^{-1} = \tau_0^{-1} + K[Q]$$

with

$$K = (k_{qm} + k_{qd}(k_f/k_r)[B])/1 + (k_f/k_r)[B]) \quad (6c)$$

Comparison of eq 5 and 6 with the corresponding expressions derived from the simple reaction scheme (eq 1 to 2) shows agreement to the extent that linear relations between the observables and the various parameters are found except for the reciprocal lifetime–benzene concentration dependence (eq 5c).

Despite the similarity of the linear relations 5a, 5b, and 6a–c with those obtained from the simple reaction scheme, the slopes of the corresponding experimental curves have, however, quite different meanings. For example, the slope of a Stern–Volmer plot of fluorescence quenching is according to eq 6a no longer related in a simple manner to the specific rate of quenching as given by (2a). If, therefore, the extended reaction scheme applies, specific rates of quenching cannot be extracted from Stern–Volmer plots in the usual fashion. In other words, such values do not represent meaningful quantities because they are complex functions of other specific rates and the benzene concentration.

The potential role of excimers in energy transfer processes in benzene systems seems to have been largely ignored because the steady-state luminescence behavior appears to be completely describable by the simple reaction scheme. The fact that the emission spectra of liquid benzene solutions suggest the presence of excited species other than monomers does not necessarily invalidate such simplified treatment of the benzene system because excimer formation may be considered as a form of self-quenching assuming that the excimers, once formed, possess a mode of deactivation independent of that of the excited monomers.

From the data presented here on the time dependence of benzene luminescence, however, it appears that excited monomer and excimer are closely connected with one another. As shown in Figure 3, the variation of benzene luminescence decay time with benzene concentration does not conform with the linear relationship 1b derived from the simple reaction scheme. On the other hand, eq 5c reflects the character of the curve of Figure 3. It is, therefore, thought that the more comprehensive reaction scheme must be considered in discussing the luminescence behavior of benzene. In other words, in evaluating self-quenching and foreign quenching experiments, relations 5–6 must be applied rather than eq 1–2.

With regard to the question of energy migration in liquid benzene solutions, it is of particular interest to determine the values of k_{qm} and k_{qd}, the specific rates of quenching of the luminescence of excited monomer and excimer in view of this conclusion. This can be done in the following manner.

Determination of k_{qm} and k_{qd}. Let $I_m^{0\prime}$ denote the monomer luminescence intensity at a given quencher concentration [Q] for so low a benzene concentration that self-quenching is negligible ([B] < 0.1 vol %). One then obtains[13]

$$I_m^{0\prime}/I_m - 1 = k_d k_f/k_m k_r[B]$$

I_m denotes the monomer luminescence intensity at concentration [B] and [Q]. Combination of this

expression with that for the reciprocal decay time, eq 5c, leads to

$$k_m = \tau^{-1}(1 + k_f/k_r[A])I_m^{0\prime}/I_m \quad (7a)$$

$$k_d = \tau^{-1}(1 + k_f/k_r[A])(I_m^{0\prime}/I_m - 1) \times I_m/I_m^{0\prime}k_r/k_f[A] \quad (7b)$$

The ratio k_f/k_r has been given in ref 13, while the other terms on the right-hand side of eq 7a and 7b are obtainable from the experimental data.

The values of k_m and k_d thus calculated for various benzene concentrations vary linearly with quencher concentration, as expected from the relations

$$k_m = k_m^0 + k_{qm}[Q]$$

$$k_d = k_d^0 + k_{qd}[Q]$$

given earlier. The slopes of these curves, therefore, represent the specific rates of quenching. They are listed in Table II.

Table II: Specific Rates of Monomer and Excimer Quenching by CCl_4 for Benzene

Vol %	k_{qm}, 10^{10} M^{-1} sec^{-1}	k_{qd}, 10^{10} M^{-1} sec^{-1}
0.1	0.5	
20	0.4	0.5
50	0.4	0.7
80	0.4	0.8
100	0.5	1.1

Consideration of Values of Specific Rates of Quenching. The most striking result of the previous section is the invariance of the specific rate of benzene monomer luminescence quenching. This is quite different from the results given in Table I where the specific rates of quenching are listed as obtained from the simple reaction scheme and which show an increase with increasing benzene concentration. It is also observed that the value of k_{qm} is well within the limit of what can be expected from the theory of diffusion-controlled processes. One must, therefore, conclude that these data on monomer luminescence quenching by carbon tetrachloride do not support any hypothesis of energy migration in benzene.

While the results for the monomer seem to be quite straightforward, those for the quenching of excimer luminescence require further discussion. Whether the systematic variation of k_{qd} with benzene concentration can be related to a model of energy migration as suggested by Voltz[6] cannot be easily decided. The fact that the specific rate of monomer quenching does not seem to vary with benzene concentration does not seem to make it plausible that energy migration accounts for the observations on the excimer quenching. In addition, the fact that the values of k_{qd} are larger than those of k_{qm} suggests a rather simple explanation.

Model of Diffusion-Controlled Quenching Process. So far it has been assumed that excimers of benzene, particularly, in the pure solvent are dimers. This picture is a simple adaptation of the model of excimers first proposed by Kasper and Förster to interpret the concentration dependence of the emission spectra of certain dyes.[15] Whether this model can be applied to such concentrated solutions as pure benzene cannot really be decided on the basis of the luminescence spectra of benzene solutions. It seems quite possible that more complex excimer may exist.

It is, therefore, suggested that in addition to excited monomers and dimers more complex excited benzene aggregates might have to be considered to form a quasi-equilibrium. If such is the case, the experimentally observed quenching of benzene luminescence by CCl_4 seems to be describable by rather conventional theory of diffusion-controlled processes. For example, the specific rate of quenching as introduced in the simplest reaction scheme would actually represent a value averaged over different excited molecular aggregates. The concentration dependence of such a specific rate simply reflects the weights of each particular aggregate to the observed average and these weights depend on the benzene concentration.

In the next approximation, as given in this paper, if an "equilibrium constant" between excited monomer and the aggregates, summarily denoted as excimers, is established, the specific rate of monomer quenching can be extracted from the experimental data. In principle, one might continue this process if equilibrium constants for the assumed higher complexes could be established. Unfortunately, this is not the case because of the lack of sufficient resolution of the emission spectra of benzene solutions.

The model of benzene luminescence quenching here suggested implies that the specific rate increases with increasing size of the excited molecular aggregate. This is not immediately clear because the effect of an increased interaction radius of the aggregates may be compensated by a decreased diffusion coefficient. However, applying in an admittedly simplified manner Smoluchowski's expression for bimolecular rate constants to the quenching process in question

$$k_q = 4\pi N'(r_q + r_e)(D_q + D_e)$$

(r_q and r_e are the radius of quencher and excimer, respectively; D_q and D_e are their diffusion coefficients), it can easily be shown[16] that k_q has a minimum value for r_e =

(15) K. Kasper and T. Forster, *Z. Phys. Chem.* (Frankfurt am Main), 12, 15 (1951).

(16) This result is obtained when the diffusion coefficients in Smoluchowski's equation are expressed as functions of the radii of the reactants using the Stokes–Einstein formula, $D = kT/6\pi\eta r$, and differentiating k_q with respect to one of the radii.

r_q. Taking the molecular dimensions of CCl_4 and benzene monomer as about equal,[17] a larger aggregate of excited benzene molecules is expected to be quenched more efficiently.

A simple test of this model could be made by a study of benzene luminescence quenching by collisional quenchers with possibly much larger molecular dimensions than the benzene molecule. In this case, a decrease or more likely a reduction of the benzene concentration dependence of k_q is expected.

Conclusions

The experimental results obtained for the steady-state and nonsteady-state luminescence behavior of benzene in the absence and presence of CCl_4 as quencher and as a function of benzene concentration suggest very strongly that in considerations of benzene luminescence the formation and fate of excimers cannot be ignored.

It seems that published data on energy transfer studies in benzene can be understood, at least qualitatively, by inclusion of excimers in the reaction scheme. The data presented here give little support to the existence of energy migration in liquid benzene in the sense of the Voltz model.

(17) R. Daudel, R. Lefebvre, and C. Moser, "Quantum Chemistry," Interscience Publishers, Inc., New York, N. Y., 1959, p125.

Yield of Free Ions in Irradiated Liquids; Determination by a Clearing Field[1]

by Werner F. Schmidt and A. O. Allen

Chemistry Department, Brookhaven National Laboratory, Upton, New York 11973 *(Received May 7, 1968)*

A new method is described for determining the yield of free ions formed by irradiation of a liquid. Yield values are reported for 19 pure liquids at room temperature, for three liquids over a range of temperatures, and for two mixtures over the complete range of compositions. The results are discussed in terms of the mean distances that electrons, formed by ionization, can penetrate into the liquid before becoming thermalized. The free-ion yields in the various liquids show much more variation than anticipated; thus the yield in neopentane is six times as great, and the penetration distance two and one-half times as great, as in normal pentane. The reason for these variations is far from obvious.

The number of free ions formed by irradiation in liquids is of interest in the study of the behavior of free electrons in condensed systems and the basic mechanisms of radiation effects in liquids generally. It has been apparent since 1908[2] that most ions formed in the irradiation of a liquid never become free, but rapidly disappear by "initial" recombination. Applied fields of a few thousand volts per centimeter are sufficient to pull all the free ions to the electrodes without appreciable bulk recombination, but fields of this magnitude already interfere considerably in the process of initial recombination. Determination of the number of ions escaping initial recombination with no applied field can be attempted by extrapolating the high-field results to zero field,[3] but with many liquids this extrapolation is quite uncertain. More accurate in theory but more difficult experimentally is the method of determining the steady-state conductivity under irradiation at essentially zero applied field, together with an estimation of the mobilities of the positive and negative ions, either by an approximate theoretical formula[4] or by direct experimental determination.[5,6] This paper describes a new and less cumbersome method of determining the number of ions escaping recombination in the absence of an applied field and presents values obtained for a number of liquids and liquid mixtures. The method consists of ionizing the liquid by a short pulse of radiation, then immediately applying a clearing field of such magnitude that all the free ions are drawn to the electrodes before any appreciable amount of

(1) Research performed under the auspices of the U. S. Atomic Energy Commission.

(2) G. Jaffe, *Ann. Phys.*, **25**, 257 (1908).

(3) G. Jaffe, *Le radium*, **10**, 126 (1913).

(4) G. R. Freeman and J. M. Fayadh, *J. Chem. Phys.*, **43**, 86 (1965).

(5) A. Hummel, A. O. Allen, and F. H. Watson, Jr., *ibid.*, **44**, 3431 (1966).

(6) W. F. Schmidt, *Z. Naturforsch.*, **23b**, 126 (1968).

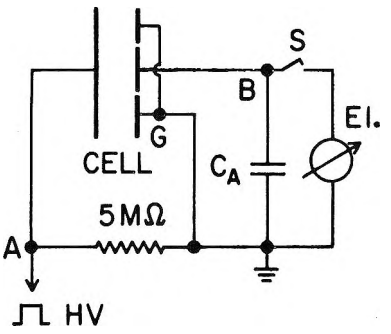

Figure 1. Circuit diagram for measurement of ion yields by a clearing field.

homogeneous recombination has had time to occur. A preliminary account of this work has been published.[7]

Experimental Section

X-Rays were obtained from a Van de Graaff generator, with a beam of 1.6-MeV electrons impinging on a gold target. The circuit used is sketched in Figure 1. An auxiliary capacitor C_A is placed between the collecting electrode of the measuring cell and ground; its capacitance (200 pF) is 300 to 1000 times greater than that of the measuring cell. When the X-ray pulse terminates, high voltage (3–5 kV) is applied at point A by means of an HV-triode (Eimac 25 T) which is triggered by the OFF-pulse of the Van De Graaff pulsing circuit. Essentially all the voltage drop occurs across the cell. The high voltage was applied for a sufficiently long time (1–2 sec) so that the drift of the ions to the cell electrodes was complete. After the high voltage was turned off, point A returned to ground potential through the 5-megohm resistor. Had there been no ions in the cell, point B would return to ground potential also. Any charge collected from the cell during the period of high voltage will, however, result in an equal charge remaining on the condenser C_A, and a corresponding potential will remain on point B. The switch S is then closed and the charge collected is read on the electrometer, Keithley Model 610 B. The rise time of the cell circuit was $<5 \times 10^{-6}$ sec; it depends mainly on the 5000-ohm effective internal resistance of the triode. A platinum point-to-plate contact was constructed for the switch S, in order to avoid difficulties due to contact potentials.

The measurement cells used were of the type shown in Figure 2. They were of tin oxide-coated glass with parallel aluminum electrodes. A number of these cells were used, with interelectrode spacings ranging from 0.42 to 1.02 cm, and measuring electrode areas 1.77 or 3.14 cm^2. The auxiliary cell with platinum electrodes was to provide a final purification of the liquids from conducting impurities by electrolysis. During measurements the upper part of the cell was shielded with lead.

All liquids were thoroughly purified by treatment

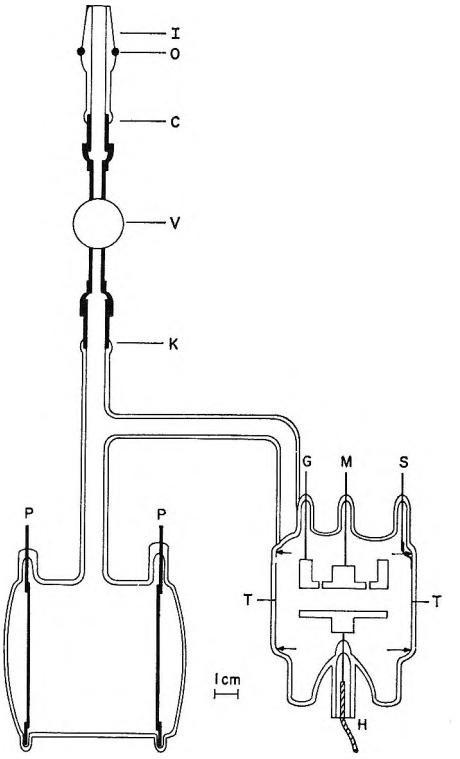

Figure 2. Measurement cell: I, 14/20 standard taper joint; O, Viton O-ring; C,K, Covar-to-Pyrex seals; V, Hoke Series 480 Bellows Seal valve; P, leads to platinum electrodes; G, lead from aluminum guard ring to ground; S, lead from tin oxide coating T (between arrows) to ground; M, measuring electrode; H, lead to high-voltage source.

with appropriate reagents and were then fractionated from drying agents. The hydrocarbons and ethers were finally distilled under vacuum over sodium potassium alloy, while the carbon tetrachloride and germanium tetrachloride were finally distilled under vacuum over calcium hydride. Because these last two liquids are corrosive to aluminum, the carbon tetrachloride was irradiated in a cell provided with electrodes of stainless steel, while the germanium tetrachloride was irradiated in a cell with platinum electrodes.

At first, we irradiated the cell until the concentration of ions had reached a steady state, then applied the high voltage at a varying interval after the radiation was turned off. More consistent results were obtained, however, when the radiation was applied in a short pulse (5×10^{-4} sec) and the high voltage was then applied automatically within a few microseconds after the radiation was shut off.

The buildup of the ion concentration n is given by

$$dn/dt = IG/100 - \alpha n^2 \qquad (1)$$

where I is the dose rate (ev/cm^3 sec), G the free-ion yield, and α the recombination coefficient (cm^3/sec). To prevent loss of ions by recombination during the

(7) W. F. Schmidt and A. O. Allen, *Science*, **160**, 301 (1968).

irradiation, the total dose must be kept small enough and the dose rate large enough so that the last term in the equation is negligibly small ($\alpha DGt_p \ll 100$, where D is the total dose (eV/cm³ delivered in time t_p)). The fraction f of the ions actually reaching the electrodes when a voltage V is applied to a homogeneously ionized medium containing n_0 ion pairs per cm³ in an ion chamber of plate separation d is given[8] by

$$f = u^{-1} \ln (1 + u) \qquad (2)$$

where $u = n_0\alpha d^2/\mu V$. With nonpolar liquids the ratio of the recombination coefficient to the mobility $\alpha/\mu = 4\pi e/\epsilon$, where ϵ is the dielectric constant and e the electronic charge. Doses used here were of such magnitude (a few millirads) that well over 99% of all the free ions formed were collected.

Dosimetry was accomplished by means of an air ionization chamber (Electronic Instruments Ltd., Richmond, Surrey; Model 37A). The instrument was calibrated with standard ^{60}Co sources and compared in the high dose rate ranges with ferrous sulfate solutions. During the measurements the measuring cell and the air ionization chamber were mounted at fixed positions in the radiation field. The ratio of the dose rate between the two positions was determined with the ionization chamber. The absorbed doses in the liquids were calculated from the air dose by using electron densities.

The whole experimental arrangement was tested in air by using as measuring cell an air ionization chamber of air equivalent walls with known volume. A value of $W = 33 \pm 1$ eV was obtained for the energy required to generate one ion pair in air, which is in good agreement with standard determinations.

Results

Figure 3 shows typical data of charge collected *vs.* dose for three liquids. The linearity of the charge–dose curve shows that essentially all the ions formed were collected. The intercept, which depends on the background conductivity of the liquid, is negligible for most of the hydrocarbons used, which have specific conductivities of the order of 10^{-17} ohm^{-1} cm^{-1}, but was appreciable for the ethers, which showed conductivities about 10^{-14} ohm^{-1} cm^{-1}. In these cases the background charge collected usually was found to depend somewhat upon the polarity of the applied voltage, but with either polarity a good straight line was obtained when the charge was plotted against the radiation dose. The value of G (ions of either sign formed per 100 eV) is given by $(10^{10}/dv) \times$ the slope (coulomb/mrad) of the charge–dose line (d = density, v = effective volume). Because of the limitations on the ion concentration, the method should not be used with liquids having specific conductivities of the order of 10^{-13} ohm^{-1} cm^{-1} or greater.

Table I gives the values of G found for a number of

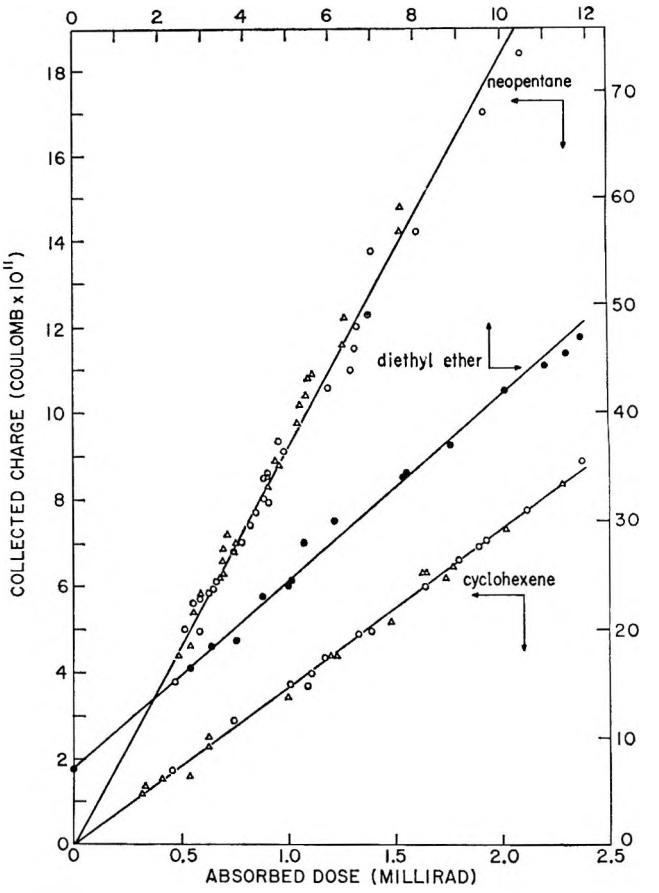

Figure 3. Observed charge–dose curves. Circles, high-voltage electrode negative; triangles, positive. Cyclohexene, d 0.80469 g/cm³, cell volume 3.01 cm³; diethyl ether, d 0.7101, cell volume 1.40; neopentane, d 0.5875, cell volume 1.80.

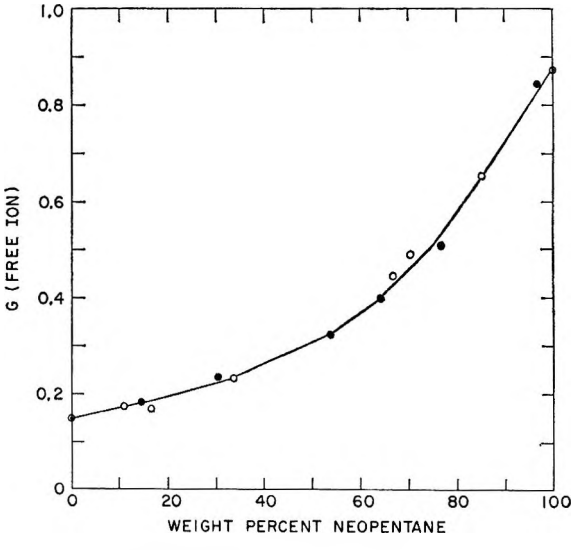

Figure 4. G(ion) in mixtures of neopentane with 3-methylpentane (filled circles) or with cyclohexane (open circles).

(8) J. W. Boag, "Ionization Chambers," in "Radiation Dosimetry," G. J. Hine and G. L. Brownell, Ed., Academic Press, New York, N. Y., 1956, Chapter 4.

Table I: Free Ion Yields in Pure Liquids at 23°

Compound	No. of detns[a]	G, ion pair/ 100 eV	Av devn, %	ϵ[b]	r_c, Å	b/r_c	b, Å	d,[b] g/cm³	bd, g/cm² × 10⁸
n-Pentane	3	0.145	3.4	1.842	306	0.234	71.5	0.623	44.6
Isopentane	4	0.170	0.9	1.838	307	0.248	76.0	0.617	46.9
Neopentane	5	0.857	3.4	1.777[c]	318	0.561	178.4	0.588	104.9
Cyclopentane	1	0.155	...	1.960	288	0.239	68.9	0.742	51.1
n-Hexane	6	0.131	3.8	1.885	299	0.226	67.4	0.656	44.2
3-Methylpentane	2	0.146	4.1	1.901	297	0.235	69.6	0.662	46.0
2,3-Dimethylbutane	2	0.192	1.3	1.953	289	0.259	74.9	0.659	49.4
2,2-Dimethylbutane	2	0.304	3.0	1.926	293	0.314	92.0	0.646	59.5
Hexene-1	2	0.062	3.2	2.046	276	0.178	49.1	0.670	32.9
Cyclohexane	9	0.148	5.5	2.022	279	0.237	66.1	0.776	51.3
Cyclohexene	2	0.150	2.0	2.222	254	0.237	60.1	0.806	48.5
Benzene	3	0.053	1.9	2.278	248	0.170	42.1	0.876	36.9
n-Octane	2	0.124	0.8	1.944	290	0.221	64.2	0.700	44.9
2,2,4-Trimethylpentane	4	0.332	1.1	1.936	291	0.326	95.0	0.689	65.4
1,4-Dioxane	3	0.046	5.0	2.212	255	0.164	41.7	1.030	42.9
Diethyl ether	2	0.350	1.1	4.280	132	0.335	44.2	0.710	31.4
Carbon tetrachloride	2	0.096	1.3	2.232	253	0.203	51.4	1.590	81.7
Germanium tetrachloride	1	0.127	...	2.435	232	0.223	51.7	1.870	96.7
Carbon disulfide	2	0.314	1.3	2.633	214	0.336	71.8	1.259	90.4

[a] Separate fillings of the measurement cell; often different cells with different electrode spacings were used. [b] Data from "Landolt-Börnstein Zahlenwerte und Funktionen," Springer, Berlin; "Handbook of Chemistry and Physics," Chemical Rubber Co., Cleveland, Ohio; "Organic Solvents," Interscience Publishers, New York, N. Y. [c] Calculated from the molar refraction; no data available.

liquids at room temperature (23 ± 1°). When more than one determination is indicated, the separate runs were made with different preparations, usually in different cells. The reproducibility is seen to be better than ±10%. Table II shows the effect of temperature on the G values found for three different liquids.

The saturated hydrocarbons are seen to exhibit a surprising variety of G values. Figure 4 shows how G varies in mixtures of neopentane with either 3-methylpentane or cyclohexane. These mixtures were made up by adding portions of the separate components to the cell by vacuum distillation, then detaching the cell from the vacuum line and weighing it after each addition.

Values of G found here are usually significantly higher than those determined by combining determinations of ion mobility and zero-field conductivity.[4-6] The value for *n*-hexane is, however, in good agreement with the yield obtained by extrapolation of the high-field current–voltage curve to zero field.[9,10]

Discussion

The yield of free ions in a liquid depends upon the average distance that an electron produced by ionization travels before reaching thermal equilibrium. The probability that a pair of separated charges will escape initial recombination is[11] e^{-r/r_c}, where r is the distance between the charges and r_c is the critical distance at which the potential energy of the pair is equal to the thermal energy kT; $r_c = e^2/\epsilon kT$. This expression should hold for X-ray produced ionization, with r the distance at which the pair attains thermal energy or, for ions formed in a group of several pairs, the distance between the last two ions remaining after all others in the group have recombined. It has been assumed that r should depend mainly on the electron density of the medium.[4,5] If this were the case, the ratio of observed G values for different liquids should be readily predictable, since r_c is easily found. Then all the hydrocarbons studied here should have the same G values at room temperature within about ±20%. The variety of values actually observed is therefore quite unexpected.

In the course of thermalization, electrons formed by ionization with a certain given energy will undergo numerous changes in direction and should, when eventually thermalized, find themselves in a random Gaussian distribution of distances from their parent ions. Since the electrons actually start out with a wide variety of energies, the total distribution of distances should be a superposition of Gaussians which one might suspect could be quite far from Gaussian itself. However, Mozumder and Magee[12] have pointed out that the greater part of the initial energy of the electron is lost in

(9) A. Hummel and A. O. Allen, *J. Chem. Phys.*, **46**, 1602 (1967).
(10) A. Jahns and W. Jacobi, *Z. Naturforsch*, **21a**, 1400 (1966).
(11) L. Onsager, *Phys. Rev.*, **54**, 554 (1938).
(12) A. Mozumder and J. L. Magee, *J. Chem. Phys.*, **47**, 939 (1967).

Table II: Free Ion Yields at Various Temperatures

Compound	Temp, °C	G, i.p./100 eV	ϵ[a]	r_c, Å	b/r_c	b, Å	d,[b] g/cm³	bd, g/cm² × 10⁸
n-Pentane	−2	0.121	1.881	328	0.219	71.9	0.647	46.5
	23	0.153	1.842	306	0.238	72.9	0.622	45.3
	26	0.158	1.838	304	0.241	73.3	0.619	45.4
	33	0.163	1.826	299	0.244	73.0	0.612	44.7
	43	0.182	1.811	292	0.254	74.2	0.602	44.7
	56	0.202	1.791	283	0.265	74.9	0.590	44.2
n-Hexane	23	0.131	1.885	300	0.226	67.7	0.656	44.4
	24	0.138	1.884	299	0.229	68.4	0.656	44.8
	41	0.162	1.858	287	0.244	69.9	0.640	44.7
	46	0.168	1.850	283	0.247	69.8	0.636	44.4
	55	0.183	1.835	278	0.255	70.8	0.627	44.4
	60	0.195	1.827	275	0.261	71.8	0.621	44.6
	74.5	0.217	1.802	267	0.272	72.6	0.609	44.2
	79	0.226	1.794	265	0.277	73.3	0.604	44.3
	84	0.239	1.785	262	0.283	74.3	0.600	44.5
	90	0.248	1.774	260	0.287	74.6	0.594	44.3
	98	0.256	1.758	257	0.291	74.7	0.586	43.8
Cyclohexane	22.5	0.148	2.023	279	0.236	65.8	0.776	51.1
	23	0.149	2.022	279	0.236	65.8	0.776	51.1
	32	0.169	2.009	273	0.247	67.3	0.767	51.6
	34	0.166	2.005	271	0.246	66.6	0.766	51.0
	42	0.184	1.992	266	0.255	67.9	0.758	51.5
	49	0.195	1.981	262	0.261	68.3	0.751	51.3
	60	0.213	1.962	256	0.270	69.1	0.741	51.2
	66	0.233	1.950	253	0.280	70.8	0.735	52.0
	75	0.245	1.933	248	0.286	71.1	0.726	51.6
	81	0.153	1.922	246	0.290	71.2	0.721	51.3
	84	0.263	1.917	244	0.295	72.0	0.718	51.6
	95	0.279	1.896	239	0.302	72.4	0.707	51.2

[a] Data from Landolt–Börnstein. [b] Data from American Petroleum Institute, "Selected Values of Physical and Thermodynamic Properties of Hydrocarbons," Carnegie Press, Pittsburgh, Pa.

a distance which is much less than the mean distance which is actually traversed by the electrons, as judged by the observed G values for free ions in hydrocarbons. The electrons rapidly lose energy to electronic and vibrational excitations of the molecules of the medium until they reach subvibrational energies of the order of 0.4 eV. The loss of energy from 0.4 down to the thermal energy of about 0.025 eV is a much more inefficient process, and most of the total thermalization distance is traversed during this final step of energy loss. We therefore make the assumption here that the distribution of thermalization distances r does not depend strongly on the initial energy and is approximately given by the three-dimensional Gaussian distribution function $(4\pi r^2/\pi^{3/2}b^3)e^{-r^2/b^2}$. Since this function gives the probability of a pair existing at a distance between r and $r + dr$, then to get the total probability of escape P we must multiply the Gaussian by the escape probability $e^{-r_c/r}$ and integrate over all r. Substituting x for r/b we find for P

$$P = (4/\pi^{1/2})\int_0^\infty x^2 \exp(-x^2 - (r_c/bx))dx \qquad (3)$$

We see that P is a function of b/r_c only.

To relate P to the experimental G values, we have to make an assumption as to the total number of ions produced. Determination of ion yields in the gas phase has shown that hydrocarbons heavier than propane generally form one ion pair for an amount of energy very close to 23 eV, or G close to 4.3.[13] We shall assume that for all liquids studied here except CS_2 the escape probability P equals $G_{obsd}/4.3$; for CS_2, P was taken as $G_{obsd} \times 0.26$.

The function $P(b/r_c)$ has been calculated. A graph of this function is shown in Figure 5. Knowing P for each liquid we can thus obtain b/r_c, and since r_c is readily found we obtain the values of b which are shown in Tables I and II. Since for any given material we would expect the penetration to vary inversely with the amount of material traversed and hence with the density, we also give the product bd, where d is the density. This product might be expected to be the most meaningful parameter with which to characterize the interaction of an electron with a liquid medium to which it is losing energy. From Table II, we see that indeed

(13) G. G. Meisels, *J. Chem. Phys.*, **41**, 51 (1964).

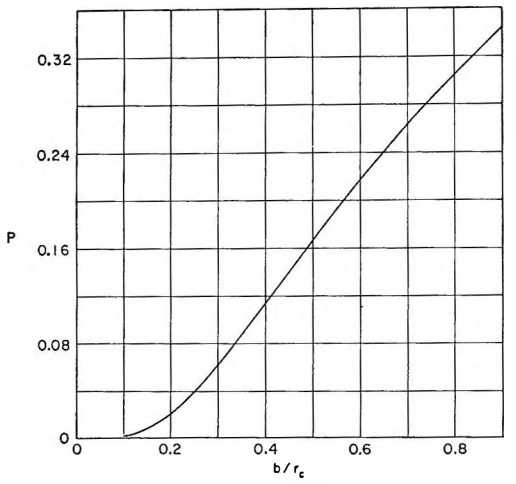

Figure 5. Plot of the function $P(b/r_c)$.

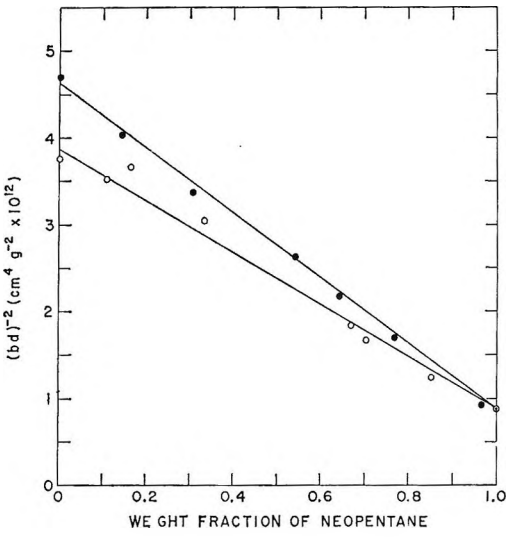

Figure 6. The data of Figure 4 replotted, using the function $1/(bd)^2$ instead of G(ion).

this parameter seems to be independent of temperature for a given liquid, although both the values of G and of b do vary with temperature. We believe that the striking independence of bd on temperature indicates that our assumption of a Gaussian distribution of separation distances is not too bad.

Turning to the results on mixtures, we find that these can be rationalized if we assume that the distribution of the electron about its parent ion is governed by processes similar to those of the random walk. In the course of its thermalization, the electron will certainly undergo numerous interactions which result in its changing direction. Although the mean free path traversed between these events must in general vary with the energy of the electron, it is still possible to say as an approximation that $b = L \times \sqrt{n}$, where b, the Gaussian distribution parameter, is proportional to the average total distance that the electron has separated from its parent ion after undergoing n changes in direction, and L is proportional to an "average mean free path" during the slowing down process. If E_0 is the average energy of the electron at the start of this process, and ΔE is the mean energy lost at each event which causes a change of direction, we may write

$$\begin{aligned} b_m^2 &= L_m^2 E_0/\Delta E_m \\ b_1^2 &= L_1^2 E_0/\Delta E_1 \\ b_2^2 &= L_2^2 E_0/\Delta E_1 \end{aligned} \tag{4}$$

where the subscripts 1 and 2 refer to properties of the two components of the mixture and the subscript m refers to properties of the mixture. We may assume that the mean energy loss per event occurring in the mixture is a simple function of the mixture composition

$$\Delta E_m = X_1 \Delta E_1 + X_2 \Delta E_2 \tag{5}$$

Here we take X_1 and X_2 to be the weight fractions of the two components of the mixture. They might just as well be taken as volume fractions or electron fractions, but fortunately in hydrocarbon mixtures this makes little difference. If we now further assume that the specific slowing down properties which differ so markedly between the different hydrocarbons are expressed in the energy loss term ΔE, and that the actual value of the distance L traversed between these events depends only on the density of the hydrocarbon and not on any other of its properties, we have

$$L_m d_m = L_1 d_1 = L_2 d_2 \tag{6}$$

Combining all the above equations we obtain

$$1/(b_m d_m)^2 = X_1/(b_1 d_1)^2 + X_2/(b_2 d_2)^2 \tag{7}$$

Remembering that $X_2 = 1 - X_1$, we see that in a hydrocarbon mixture we would on the above assumptions expect the parameter $(bd)^{-2}$ to be a linear function of X_1. Figure 6 shows a plot of this quantity for the two mixtures for which the G values were graphed in Figure 4. It is seen that a straight line actually is obtained within the experimental error. Graphs of various other functions of G, b, and bd were tried but did not give straight lines.

We therefore believe that our parameter bd offers a reasonable approximate measure of the ability of a liquid to interact with slow electrons. It is too soon to say much about the meaning of the differences between the different liquids. Looking at the results given in Table I for hydrocarbons, it appears that the value of bd is somewhat higher for ring compounds than for straight chain compounds, but that the really spectacular exaltation occurs in compounds containing a quaternary carbon atom. The parameter is decreased by the introduction of double bonds and by the substitution of oxygen atoms for CH_2 groups in a molecule; both changes tend to increase the local polarizability. It is difficult to compare the nonhydrogenous com-

pounds studied (CCl_4, $GeCl_4$, CS_2) with the others. Their values of b are comparable to those of hydrocarbons, but because of their high densities their values of bd are considerably higher.

The feature of the results most difficult to understand is the very high G value for neopentane. We have been unable to correlate this with any other property of the substance. Generally the properties of the pentane isomers are very similar. Even the electron scattering cross section in the gaseous state is reported by Devins and Crowe[14] to be very similar for the three isomers of pentane. It is still possible that the mean energy loss on scattering in the vapors might be different for the pentane isomers, and this possibility should be investigated in view of the great difference we find in the behavior of the liquids.

We are continuing work in this field in the hope of obtaining deeper insight into these processes.

Acknowledgment. We wish to thank Dr. Harold A. Schwarz for numerous valuable discussions and f programming the calculation of the function $P(b/r_c)$.

(14) J. C. Devins and R. W. Crowe, *J. Chem. Phys.*, **25**, 1053 (1956)

Primary Processes in the Photolysis of SO_2 at 1849 Å[1]

by J. N. Driscoll and Peter Warneck

GCA Corporation, GCA Technology Division, Bedford, Massachusetts *(Received May 7, 1968)*

The production of SO_3 in the 1849-Å photolysis of pure SO_2 and in mixtures containing 5–75% SO_2 in O_2 was studied at atmospheric pressure. An interference filter isolated the 1849–1924-Å lines from a mercury arc and eliminated the emission at longer wavelengths. The quantum yield found for SO_3 formation in pure SO_2 was 0.50 ± 0.07. The addition of oxygen increased the SO_3 quantum yield to a plateau value of 1.04 ± 0.13, but for mixtures containing less than 30% SO_2 the quantum yield declined again. The photodecomposition of SO_2 at 1849 Å is complicated by the occurrence of several primary processes including direct dissociation due to an absorption continuum, excited SO_2 molecule formation, and predissociation. The observed SO_3 quantum yield was utilized to evaluate the relative importance of the various primary processes.

Introduction

The present study was undertaken to obtain information on the production of SO_3 from the photodecomposition of SO_2. Despite a number of investigations[2] concerning the photolysis and photooxidation of SO_2, it appears that the aspect of SO_3 formation has previously not received the attention it deserves. This is particularly true for the 1850-Å wavelength region where several primary processes are involved. The only quantitative data previously reported for SO_3 formation in this spectral region were given by Chen.[3] Unfortunately, his results cover only mixtures of up to 8% SO_2 in oxygen or oxygen plus nitrogen. Moreover, these results are handicapped by incomplete light absorption (for which apparently no corrections were applied) as well as the difficult subtraction of the effect of 1849-Å radiation from that produced by light of longer wavelengths, particularly the powerful 2537-Å radiation. The present study, by contrast, makes use of an interference filter which eliminates the contribution of the 2537-Å line. The evolution of SO_3 during the photolysis of pure SO_2 and mixtures of 5–75% SO_2 with oxygen was investigated. This paper describes the results and their implications concerning the various primary processes for the 1849-Å photochemistry of sulfur dioxide.

Experimental Section

Kornfeld and Weegman[4] had demonstrated previously that at wavelengths near 2000 Å the photodecomposition of SO_2 in a closed vessel quickly approaches a steady state. To make quantum yield determinations more convenient and to avoid photodecomposition of SO_3, the present arrangement, like Chen's, employed a mercury-free flow system whereby product SO_3 was continuously removed from the absorption region. The flow reactor consisted of two

(1) Supported in part by the National Aeronautics and Space Administration.

(2) R. G. W. Norrish and G. A. Oldershaw, *Proc. Roy. Soc.*, **A249**, 498 (1959). For a review of the air pollution aspects, see P. A. Leighton, "Photochemistry on Air Pollution," Academic Press, New York, N. Y., 1961.

(3) S. W. Chen, *Acta Chem. Sinica*, **24**, 187 (1958); *Chem. Abstr.*, **53**, 5884 (1959).

(4) G. Kornfeld and E. Weegman, *Z. Elektrochem.*, **36**, 789 (1930).

concentric Pyrex tubings of which the outer one (2 cm i.d.) served as the gas inlet. Irradiation was performed end-on, through a 2.5-cm diameter Suprasil quartz window, which was fastened to the flow tube by a flange in combination with an O ring. A set of springs provided a tight seal and allowed the removal of deposits from the window after each run. The light source was a U-shaped Hanovia medium-pressure mercury lamp. Air cooling with a blower enhanced the line spectrum by comparison to the continuous background and increased the uv output. A Baird Atomic interference filter was employed to isolate the 1850-Å wavelength region. The filter passed 15% of the 1849-Å Hg line and 10% of the line at 1942 Å, but none of the mercury lines at longer wavelengths, specifically not the strong 2537-Å Hg line.

Actinometry of the radiation passed by the filter presented a problem, because a survey of actinometer systems useful at 1849 Å showed a lack of reliable quantum yield data. Hence, it was preferred to determine the flux of the 1849–1942-Å lines indirectly by actinometry at 2537 Å supplemented by relative intensity measurements of these lines with the aid of a vacuum uv monochromator. The 2537-Å line was isolated with a second interference filter and actinometry was performed with the ferrioxalate system described by Hatchard and Parker.[5] For the relative intensity measurements the monochromator was equipped with a sodium salicylate-coated photomultiplier view plate. The fluorescent yield of sodium salicylate is independent of wavelengths[6] below 3000 Å. In deriving the absolute intensity of the 1849–1942-Å line pair, corrections were applied for the moderate variations of the grating efficiency[7] between 2537 and 1849 Å.

In this manner, the light flux passing the 1849-Å filter and entering the reaction vessel was established to be $7.2 \pm 0.3\ 10^{13}$ photons/sec, of which 84% resided in the 1849-Å mercury line.

Sulfur dioxide was photolyzed for 2–4 hr at atmospheric pressures and a flow rate of 150 cc/min. Matheson anhydrous grade SO_2 was passed through a concentrated sulfuric acid trap (to remove traces of SO_3 and water) before entering the reactor. The effluent SO_3 was collected in an impinger which contained either distilled water or an 80% isopropyl alcohol–water mixture, and was subsequently determined as SO_4^{2-} using the barium chloranilate method.[8] Separate tests using several collecting vessels in series demonstrated that at least 95% of the evolving SO_3 was trapped in the first vessel. Some interference was observed due to dissolved SO_2. Accordingly, blank runs were performed before and after each photolysis, and the SO_3 yield was determined by difference.

Results

At the wavelengths 1849 and 1942 Å, the absorption strength of SO_2 is sufficient[9] to provide essentially complete absorption of the incident radiation within 0.3 cm of the window, even for the lowest SO_2 concentrations employed. In addition, the absorption of oxygen[10] under these conditions can be considered negligible compared with that of SO_2. Thus, if the SO_3 generated is assumed to convert entirely to SO_4^{2-}, the SO_3 quantum yield is given by the SO_4^{2-} yield divided by the radiation dosage. However, during the irradiation of both pure SO_2 and SO_2–O_2 mixtures a fogging of the window occurred which led to noticeable radiation losses. Accordingly, the observed SO_3 quantum yields required a correction. The reduction of intensity caused by the deposits was measured at 1849 Å with the mercury lamp and the monochromator. It was found to be approximately linear with time and amounted to 25–30% after a 2-hr exposure. Examination of the deposit showed that it consisted of two components. One was white and dissolved readily in distilled water. The resulting solution showed a positive test for sulfate but the amount was less than 3% of that collected in the vessel. The other component of the deposit was yellow. It was insoluble in water and could not be removed after repeated rinsings, but it dissolved readily in carbon disulfide, indicating that it probably consisted of sulfur. However, since the total deposit on the window was too small to be weighable, no quantitative information could be obtained. It is not even possible to determine whether deposition of the solids is a major or minor aspect of SO_2 photodecomposition.

The formation of SO_3 was linear with time. Quantum yield data for SO_3 evolution are shown in Figure 1. Each point in Figure 1 represents a minimum of four independent measurements. The SO_3 quantum yield in pure SO_2 is $\varphi(SO_3) = 0.50 \pm 0.07$. The admixture of oxygen increases it to a plateau value of $\varphi(SO_3) = 1.04 \pm 0.13$, but for mixtures containing less than 30% SO_2 the SO_3 quantum yield declines again. The trend is indicative of a finite value for vanishing SO_2 concentration. This behavior of the SO_3 quantum yield is in serious disagreement with the results obtained earlier by Chen,[3] who found increasing SO_3 quantum yields with decreasing SO_2 concentration. From the information given by Chen, it is difficult to evaluate the origin of the discrepancy, but most probably it lies in the method used by him to differentiate between the effects of the 1849- and 2537-Å mercury lines. Additional uncertainties in his work are due to incomplete light

(5) C. A. Hatchard and C. A. Parker, *Proc. Roy. Soc.*, **A236**, 356 (1956).

(6) K. Watanabe and C. Y. Inn, *J. Opt. Soc. Am.*, **43**, 32 (1953).

(7) D. C. Hammer, E. T. Arakawa, and R. D. Birkhoff, *Appl. Opt.*, **3**, 79 (1964).

(8) R. Bertolacini and J. Barney, *Anal. Chem.*, **29**, 281 (1957).

(9) D. Golomb, K. Watanabe, and F. F. Marmo, *J. Chem. Phys.*, **36**, 958 (1962).

(10) K. Watanabe, C. Y. Inn, and M. Zelikoff, *ibid.*, **21**, 1026 (1953).

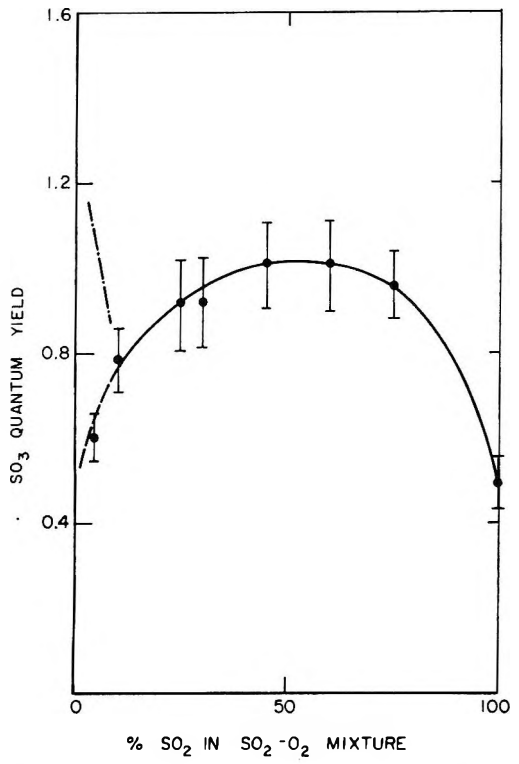

Figure 1. SO_3 quantum yield as a function of % SO_2 in sulfur dioxide–oxygen mixture. Dashed line indicates extrapolation to limiting value as explained in text. Data due to Chen[3] are shown as —·—·.

absorption, and to the use of the uranyl oxalate actinometer at 1849 Å where its quantum yield is uncertain.

Discussion

In the 1849-Å wavelength region, the photolysis of SO_2 is complex due to the occurrence of several primary processes. Their identification and relative role has not been clarified in previous investigations.[3,4] Although the results reported here are limited to the aspect of SO_3 formation in the SO_2 photodecomposition, they can reveal important information on the primary processes in conjunction with the available spectroscopic data. The following discussion, therefore, will place the emphasis on the SO_2 primary processes. Before discussing the results, a brief review of the pertinent spectroscopic information will be given.

The SO_2 absorption spectrum in the wavelength region of interest is characterized by intense bands overlying a dissociation continuum. The onset of the continuum near 2280 Å corresponds energetically to the formation of SO and O in their ground states. At 1849 Å, the contribution of the continuum to the total absorption was estimated previously[11] to be 27%. The overlying bands at the same wavelength belong to the system designated α_4 [12] which has its origin near 1950 Å. This system has been analyzed only recently,[13] but the electronic transition involved is still uncertain. According to Dubois,[13] the system is predissociated with the limit lying at 53,500 cm^{-1} (corresponding to 1870 Å). Although this value coincides only approximately with the onset of predissociation reported by Henri[14] at 1940 Å, both values indicate that at 1849 Å predissociation would be an important process. In addition, Douglas[15] has interpreted the abrupt decrease of fluorescence intensity at exciting wavelengths less than 2000 Å as an indication of predissociation. The resulting species have not yet been identified, but three possibilities must be considered: (a) formation of SO and O in their electronic ground states; (b) excitation of the SO radical to its first singlet state ($^1\Delta$); and (c) the formation of S and O_2. The first and last processes occur with the conservation of spin. The formation of singlet SO is spin-forbidden but a noticeable contribution to the total photolytic effect cannot be ruled out on this basis. However, at the high pressures applied in the present experiments, SO ($^1\Delta$) presumably will undergo rapid quenching so that it could not be distinguished from ground state SO. Thus, processes a and b may be lumped together.

The contribution of predissociation to the total number of primary processes depends on the strength of the predissociation. If it is weak, as it would be if it were forbidden, the initially formed excited SO_2* molecule would loose its energy mainly by fluorescence or, under our conditions, by collisional quenching. If, on the other hand, the predissociation is strong as the results of Dougles suggest, quenching would be negligible compared with the predissociation of the SO_2* molecule. An intermediate case involving both quenching and predissociation is also conceivable.

We now examine the photolysis of pure SO_2 within the framework of the preceding remarks. This requires a consideration of the following primary and subsequent reactions.

$$SO_2 + h\nu \longrightarrow SO + O \qquad \text{cont. } \varphi_1 = 0.27 \qquad (P_1)$$

$$SO_2 + h\nu \longrightarrow SO_2^* \qquad \text{excit. } 1 - \varphi_1 = 0.73 \qquad (P_2)$$

$$SO_2^* + SO_2 \longrightarrow SO_2 + SO_2 \qquad k_1 \qquad (1)$$

$$SO_2^* + SO_2 \longrightarrow SO_3 + SO \qquad k_2 \qquad (2)$$

(k_1, k_2 together: φ_2)

$$SO_2^* \longrightarrow SO + O \qquad \text{prediss. } \varphi_3 \qquad (P3)$$

$$SO_2^* \longrightarrow S + O_2 \qquad \text{prediss. } \varphi_4 \qquad (P4)$$

$$O + SO_2 + M \longrightarrow SO_3 + M \qquad k_3 \qquad (3)$$

Of the primary processes, only the quantum yield for direct dissociation due to the absorption continuum is known.[11] The production of SO_3 is due to two reac-

(11) P. Warneck, F. F. Marmo, and J. O. Sullivan, *J. Chem. Phys.*, **40**, 1132 (1964).

(12) I. Dubois and B. Rosen, *Discussions Faraday Soc.*, **35**, 124 (1963).

(13) I. Dubois, *Bull. Soc. Belge. Phys.*, No. 2, 70 (1964).

(14) V. Henri, "The Structure of Molecules," P. Debye, Ed., Blackie & Son, Ltd., London, 1932.

(15) A. E. Douglas, National Research Council, Canada, Ottawa, private communication.

tions: third-body attachment to SO_2 of oxygen atoms generated by the processes P_1 and P_3, and the reaction of excited SO_2^* with sulfur dioxide. At the high temperatures employed, a recombination of O atoms with SO radicals can be neglected in favor of reaction 3 according to the pertinent rate data of Halstead and Thrush.[16] For sulfur atoms and SO radicals no exothermic reactions with SO_2 are available so that these products will be deposited mainly on the walls. However, the indications of sulfur as a deposit should not be taken as evidence for primary sulfur product ion, since the sulfur may have resulted from a mutual reaction of SO radicals at the walls.

On the basis of the measured quantum yield $\varphi(SO_3) = 0.5$ and the previously determined quantum yield of direct dissociation of SO_2 due to the continuum absorption, $\varphi_1 = 0.27$, one can derive upper limits for the remaining primary processes. Of the total excited SO_2^* production $1 - \varphi_1 = \varphi_2 + \varphi_3 + \varphi_4 = 0.73$, simple quenching assumes $k_1\varphi_2/(k_1 + k_2) \leq 0.5$, and quenching with SO_3 formation $k_2\varphi_2/(k_1 + k_2) \leq 0.23$; the quantum yield for predissociation into SO + O is $\varphi_3 \leq 0.23$, and that for predissociation into S + O_2 is $\varphi_4 \leq 0.5$. Supplementary information concerning the relative contributions of these primary processes can be obtained from the results for SO_2–O_2 mixtures which will be discussed next.

To explain the increase in the SO_3 quantum yield upon the admixture of oxygen to SO_2 requires that one or more of the species SO_2^*, SO, and S undergo reactions with oxygen. Such reactions are

$$SO_2^* + O_2 \longrightarrow SO_2 + O_2 \quad (4)$$

$$SO_2^* + O_2 \longrightarrow SO_3 + O \quad (5)$$

$$SO + O_2 \longrightarrow SO_2 + O \quad (6)$$

$$SO + O_2 (+ M) \longrightarrow SO_3 (+ M) \quad (7)$$

$$S + O_2 \longrightarrow SO + O \quad (8)$$

The plateau observed for the SO_3 quantum yields in mixtures containing about equal quantities of SO_2 and oxygen shows that the reactions responsible for the additional SO_3 formation go essentially to completion. It is interesting to note that reaction 8, involving sulfur atoms from the primary process P_4, leads to equal amounts of SO radicals and oxygen atoms, thereby making it impossible to distinguish between primary processes P_3 and P_4 on the basis of SO_3 evolution.

The reactions given above must be supplemented by at least one further reaction to account for the observed decline of the SO_3 quantum yield when the SO_2 concentration in the SO_2–O_2 mixture is decreased below 30%. The most probable cause of this behavior is that molecular oxygen competes with sulfur dioxide for oxygen atoms

$$O + O_2 + M \longrightarrow O_3 + M \quad (9)$$

The participation of reaction 9 decreases the contribution of reaction 3 to the total production of SO_3 until at vanishing SO_2 concentration only the other sources of SO_3 remain. Accordingly, the SO_3 quantum yield in the domain of low SO_2 concentrations can be expressed as a sum of two contributions

$$\varphi(SO_3) = \varphi_0(SO_3) + \frac{k_3(SO)_2}{k_3(SO_2) + k_9(O_2)}\varphi(O) = \varphi_0(SO_3) + \frac{1}{1 + \dfrac{k_9(O_2)}{k_3(SO_2)}}\varphi(O)$$

where $\varphi(O)$ represents the overall yield of oxygen atoms and $\varphi_0(SO_3)$ represents the limiting SO_3 quantum yield for vanishing SO_2 concentrations. Since these factors are constants, they can be determined from a plot of $\varphi(SO_3)$ *vs.* $1/1 + [k_9(O_2)/k_3(SO_2)]$, which provides a procedure to extrapolate the observed SO_3 quantum yields to the limiting value. The required rate coefficient for reactions 3 and 9 are known.[16–18] Their ratio is $k_9/k_3 = 0.1$ with oxygen as the third body. Making use of this value, the data points are found to fall on a straight line as shown in Figure 2. A least-squares analysis gives a slope of $\varphi(O) = 0.74 \pm 0.11$ and an intercept with the ordinate of $\varphi_0(SO_3) = 0.36 \pm 0.08$. The result that the production of atomic oxygen is

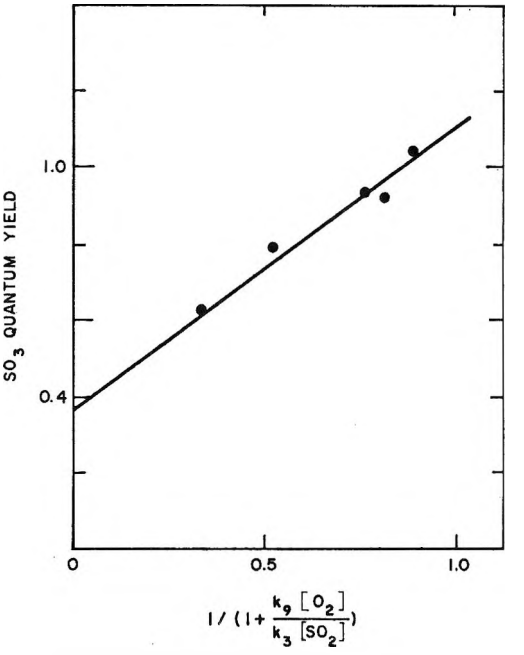

Figure 2. The determination of $\varphi(O)$ and $\varphi_0(SO_3)$ as described in text.

(16) C. J. Halstead and B. A. Thrush, *Proc. Roy. Soc.*, **A295**, 363 (1966).

(17) M. F. R. Mulcahy, J. R. Steven, and J. C. Ward, *J. Phys. Chem.*, 71, 2124 (2967).

(18) F. Kaufman and J. R. Kelso, *Discussions Faraday Soc.*, **37**, 26 (1964).

greater than that of SO_3 from all other sources indicates a noticeable participation of reaction 6. If this reaction were negligible, equal values for $\varphi(0)$ and $\varphi_0(SO_3)$ should have been observed. Thus, not all of the SO radicals generated in the primary processes and *via* reaction 8 are oxidized to SO_3 directly (reaction 7), but a portion of them are converted to oxygen atoms. The occurrence of reaction 6 must be due to the relatively high oxygen pressures used in the present system. This reaction was not observed by Halstead and Thrush at pressures in the vicinity of 1 torr. To estimate the effectiveness of reaction 6 relative to that of reaction 7, consider the extent of oxygen atom generation associated with this path

$$\varphi(O) - {}^1/_2(\varphi(O) + \varphi_0(SO)_3) = \frac{k_6}{k_6 + k_7}\varphi(SO) = 0.19$$

The evaluation of the branching ratio k_6/k_7 requires the insertion of the SO radical quantum yield which is only approximately known. Its lower limit is given by $\varphi(SO) \geq \varphi_1 = 0.27$, while its upper limit is found on the premise that reaction 5 is negligible, $\varphi(SO) \leq {}^1/_2\ (\varphi(O) + \varphi_0SO_3) = 0.55$. With these values one obtains $k_6/k_7 = 0.53$–2.1, which indicates that in the present experiment reactions 6 and 7 proceed with comparable rates.

From the quantum yield values $\varphi(O)$ and $\varphi_0(SO_3)$ one can again derive limits for the various primary SO_2 photodecomposition processes. These limits supplement the limits deduced above from the SO_2 quantum yield in pure SO_2. For this purpose use is made of the relation

$${}^1/_2(\varphi(O) + \varphi_0(SO_3)) = \varphi_1 + \frac{k_5}{k_4 + k_5}\varphi_2 + \varphi_3 + \varphi_4 = 0.55$$

implied by the reaction mechanism. The corresponding upper limit quantum yield for predissociation is $\varphi_3 + \varphi_4 \leq 0.28$. Comparison with the total excited SO_2* yield $1 - \varphi_1 = \varphi_2 + \varphi_3 + \varphi_4 = 0.73$ shows that quenching of SO_2* is an important process. The amount of quenching can be bracketed: $0.47 \leq \varphi_2 \leq 0.73$, with φ_2 in this case referring to quenching by oxygen rather than SO_2 as previously. The major conclusion from these results is that predissociation is not the predominant fate of SO_2*.

On the other hand, the spectroscopic evidence given by Dubois indicates that the predissociation is fairly strong. The apparent discrepancy may be due to the relatively high pressures employed in this work. If the predissociation is of intermediate strength, the excited SO_2 may be quenched before it can predissociate. In this respect it is of interest that the SO_3 quantum yield in pure SO_2 almost equals ${}^1/_2\ (\varphi(O) + \varphi_0(SO_3))$. Thus if quenching of SO_2* predominates, equal efficiencies of SO_3 formation are implied and $k_2/(k_1 + k_2) \approx k_5/(k_4 + k_5)$. However, the uncertainties concerning predissociation are such that it cannot be entirely eliminated. This complicating feature of SO_2 photodecomposition thus precludes a more precise determination of the primary quantum yields than the limiting values determined here.

Production of $N_2(A^3\sum_u^+)$ and $CO(a^3\pi)$ by $Hg(^1P_1)$ Photosensitization: Evidence from 2537-Å Mercury Scintillation[1,2]

by Albrecht Granzow, Morton Z. Hoffman, Norman N. Lichtin, and Satish K. Wason

Department of Chemistry, Boston University, Boston, Massachusetts 02215 (*Received May 7, 1968*)

The dependence of λ 2537-Å scintillation, measured perpendicular to the direction of incident λ 1849-Å radiation, upon pressure of N_2 or CO at constant pressure of mercury is quantitatively consistent with a two-step energy transfer mechanism involving $N_2(A^3\Sigma_u^+)$ or $CO(a^3\pi)$ as intermediates. Examination of the dependence of scintillation intensity upon mercury pressure did not provide information relevant to the question of mechanism. Two alternative mechanisms are not excluded by the pressure dependence data. One involves the single-step quenching of $Hg(^1S_1)$ to $Hg(^3P_1)$, a process which is rigorously forbidden in absorption or emission. The other is a two-step process in which high vibrational states of N_2 play the role of intermediate. Both direct and indirect measurements indicate that the quenching cross sections of N_2 and CO for $Hg(^1P_1)$ are the same, or nearly so.

Introduction

The presence of $N_2(A^3\Sigma_u^+)$ in "active" nitrogen has been established[3] for some time and its formation both in the afterglow by recombination of $N(^4S)$,[3] and in the nitrogen discharge[4,5] recognized. The possibility that $N_2(A^3\Sigma_u^+)$ is responsible for some of the chemical reactivity of "active" nitrogen has also been recognized[6-9] for a number of years. Recently, evidence has been presented[10] that this species is responsible for the decomposition of CO_2, N_2O, and H_2O by "active" nitrogen. Investigation of the chemical and physical properties of $N_2(A^3\Sigma)$ present in "active" nitrogen is, however, complicated by the presence of $N(^4S)$, $N(^2D)$,[5] and $N(^2P)$,[5] as well as other excited states of molecular nitrogen.[3,11] Production of $N_2(A^3\Sigma)$ by reaction of oxygen atoms with N_2H_4 has been reported[12] recently. The possibility, based on energy relationships, that $Hg(^1P_1)$ photosensitization might provide a promising alternative pathway to $N_2(A^3\Sigma)$ stimulated the initiation of the work reported here. These expectations were encouraged soon after work began by the observation by Gover and Bryant[13] of 2537-Å scintillation upon irradiation at λ 1849-Å of mercury vapor in the presence of N_2 or CO. As these workers pointed out, the 6.68 eV energy of $Hg(^1P_1)$ is sufficient to excite $N_2(A^3\Sigma_u^+)$, 0,0 transition energy 6.16 eV, or $CO(a^3\pi)$, 0,0 transition energy 6.01 eV. The proposed processes, however, involve spin inversions which are spectroscopically highly forbidden, and collisional relaxation of the spin selection rules must be assumed.

The efficient excitation of $Hg(^3P_1)$ by collision with $N_2(A^3\Sigma_u^+)$ in "active" nitrogen has also been observed[14] and the rate of this process has been measured.[15] This observation tends to support the suggestion of Gover and Bryant[13] that $Hg(^3P_1)$ may be produced in a two-step mechanism with $N_2(A^3\Sigma)$ as an intermediate but, as Gover and Bryant acknowledge, their data are not capable of distinguishing such a process from a one-step mechanism.

This paper confirms the observations of Gover and Bryant and presents evidence consistent with the mechanism of generation of $N_2(A^3\Sigma)$ encompassed by eq 1–7 as well as the analogous mechanism involving $CO(a^3\pi)$.

$$Hg(^1S_0) + h\nu(1849\ \text{Å}) \xrightarrow{I_{abs}^{1849}} Hg(^1P_1) \quad (1)$$

$$Hg(^1P_1) \xrightarrow{k_f^{1849}} Hg(^1S_0) + h\nu(1849\ \text{Å}) \quad (2)$$

$$Hg(^1P_1) + N_2(X^1\Sigma) \xrightarrow{k_3} Hg(^1S_0) + N_2(A^3\Sigma)_{v\leq 3} \quad (3)$$

$$N_2(A^3\Sigma) \xrightarrow{k_p^{VK}} N_2(X^1\Sigma) + h\nu_{VK} \quad (4)$$

(1) Work supported by the Air Force Office of Scientific Research under Contracts AF-AFOSR-765-65 and 765-67.

(2) See A. Granzow, M. Z. Hoffman, N. N. Lichtin, and S. K. Wason, *J. Phys. Chem.*, **72**, 1402 (1968), for a preliminary communication.

(3) See K. R. Jennings and J. W. Linnett, *Quart. Rev.* (London), **12**, 116 (1958), for a review of early work.

(4) J. F. Noxon, *J. Chem. Phys.*, **36**, 926 (1962).

(5) S. N. Foner and R. L. Hudson, *ibid.*, **37**, 1662 (1962).

(6) K. D. Bayes, *Can. J. Chem.*, **39**, 1074 (1961).

(7) A. N. Wright, R. L. Nelson, and C. A. Winkler, *ibid.*, **40**, 1082 (1962).

(8) A. N. Wright and C. A. Winkler, *ibid.*, **40**, 1291 (1962).

(9) H. B. Dunford, *J. Phys. Chem.*, **67**, 258 (1963).

(10) I. M. Campbell and B. A. Thrush, *Chem. Commun.*, 932 (1967).

(11) B. Brocklehurst and K. R. Jennings, *Progr. Reaction Kinetics*, **4**, 1 (1967).

(12) K. Becker and K. Bayes, *Bull. Am. Phys. Soc.*, **12**, 224 (1967).

(13) T. A. Gover and H. G. Bryant, Jr., *J. Phys. Chem.*, **70**, 2070 (1966).

(14) W. R. Brennen and G. B. Kistiakowsky, *J. Chem. Phys.*, **44**, 2695 (1966).

(15) R. A. Young and G. A. St. John, *ibid.*, **48**, 2572 (1968).

$$N_2(A^3\Sigma) + Hg(^1S_0) \xrightarrow{k_5} N_2(X^1\Sigma) + Hg(^3P_1) \quad (5)$$

$$Hg(^3P_1) \xrightarrow{k_r^{2537}} Hg(^1S_0) + h\nu(2537\ \text{Å}) \quad (6)$$

$$N_2(X^1\Sigma) + Hg(^3P_1) \xrightarrow{k_Q^{N_2}} Hg(^3P_0) + N_2(X^1\Sigma) \quad (7)$$

Experimental Section

Equipment. The emission lines of Hg at 1849 and 2537 Å were produced by a 2-in. diameter flat spiral Hg resonance lamp made of Suprasil quartz (Hanovia Corp.). The lamp jacket was evacuated to 10^{-4} torr in order to prevent the formation of ozone and to avoid transmission of heat from the lamp.

The irradiation cell was constructed of Pyrex tubing; the connections were made by means of O-rings. A side tube attached to the irradiation cell containing high-purity mercury could be immersed in a dewar flask in order to maintain a definite Hg vapor pressure in the irradiation cell.

The 1849-Å Hg line was isolated by means of an LiF window (Harshaw Chemical Co.) that had been irradiated previously with a ^{60}Co γ-ray dose of 2 Mrads.[16] After irradiation, more than 99.5% of the original 2537-Å emission of the lamp is absorbed by the LiF filter. When desired, the 1849-Å radiation was cut off with a No. 7910 Corning filter.

Emission was measured at right angles to the incident light beam with a Jarrel-Ash 0.5-m Ebert monochromator, EMI 6255B photomultiplier, and Tektronix Type 564 storage oscilloscope with Type 2A63 differential amplifier and Type 2B67 time base. The images displayed on the oscilloscope screen were recorded photographically.

In order to monitor the emission at 1849 Å, the whole monochromator had to be flushed with pure nitrogen since oxygen starts to absorb at wavelengths below 1900 Å.

Preliminary spectrographic experiments employed a Bausch and Lomb $f/24$, 1.5-m grating spectrograph in conjunction with Kodak Type 103-0 spectroscopic film.

Materials. Dry Linde high purity nitrogen was further purified by passing the gas through two cooling traps at 77°K and a heated column containing reduced BTS catalyst (Badische Anilin und Soda Fabrik, Germany). This catalyst is reported to reduce oxygen content to less than 0.1 ppm. Carbon monoxide (Matheson, research grade) and helium (Airco) were dried by passage through two liquid N_2 traps. Neon (Matheson, research grade) was used without any further purification.

Measurements. Before any experiment was started, the vacuum line and irradiation cell were evacuated to $<10^{-4}$ torr. For experiments at constant Hg vapor pressure, the mercury trap of the irradiation vessel was surrounded by water at 22°. This temperature corresponds to an Hg vapor pressure of 1.4×10^{-3} torr. The vapor pressure of mercury could be varied over the range $<10^{-8}$ to 2.5×10^{-3} torr by the use of various thermostat liquids in the dewar flask.

The pressure of the investigated gases was varied over the range 760 to 10^{-2} torr and was measured by various pressure gauges (Hg manometer, thermocouple, cold cathode ionization). No measurements were carried out until the intensity of the monitored emission, as represented by the oscilloscope trace, became constant, indicating that equilibrium had been obtained in the irradiation cell.

Data

Preliminary spectrographic experiments revealed that λ 2537-Å emission (scintillation) was unequivocally produced when Hg–N_2 mixtures were irradiated at λ 1849 Å. However, no quantitative evaluation of the dependence of scintillation intensity on N_2 pressure was made by this technique. Instead, the spectrograph was replaced by a monochromator with photoelectric–oscillographic readout and the intensity of λ 2537-Å scintillation was determined as a function of gas pressure for N_2, CO, He, and Ne at constant P_{Hg} (1.4×10^{-3} torr) and incident light intensity. The results, shown in Figure 1, demonstrate that maxima in the λ 2537-Å emission are exhibited by N_2 and CO at 100 and 4 torr, respectively. The intensity at λ 2537 Å also appears to be enhanced above background when He or Ne is irradiated at λ 1849 Å in the presence of Hg vapor, but these apparent scintillations do not exhibit intensity maxima.

Emission at λ 2537 Å can come only from the $Hg(^3P_1)$ state and if this species is indeed present in the system, it is to be expected that it would be readily quenched by N_2 or CO. Quenching data for these gases, which were determined using incident λ 2537 Å and measuring the 2537-Å emission at right angles, yielded the Stern–Volmer plots of Figure 2. From the ratio of the slopes of these plots, the ratio of the quenching rate constants, $k_Q^{CO}/k_Q^{N_2} = 23$ was calculated, in excellent agreement with the ratio of the accepted values[17] of these constants, 21.5. For He and Ne, true quenching curves were not obtained but rather identical enhancement of the 2537-Å phosphorescence with increasing pressure was found.

Scintillation data were corrected for quenching on a point-by-point basis by multiplying the former by corresponding experimental values of I_0/I, where I_0 is the intensity of λ 2537-Å phosphorescence at $P_{gas} = 0$ and I is the intensity at a given pressure. The result is seen in Figure 3; it is apparent that λ 2537-Å scintillation is negligible with He and Ne. In contrast, strong (and similar) scintillation occurs with N_2 and CO.

(16) J. L. Weeks, S. Gordon, and G. Meaborn, *Nature*, **191**, 1186 (1961).

(17) J. G. Calvert and J. N. Pitts, Jr., "Photochemistry," John Wiley and Sons, Inc., New York, N. Y., 1966, p 74.

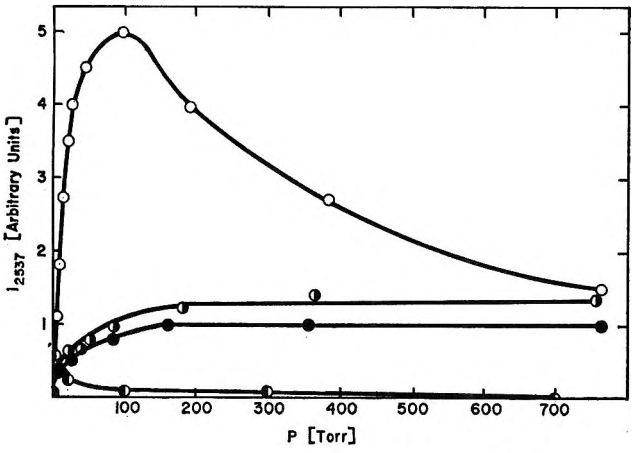

Figure 1. Scintillation at λ 2537 Å under λ 1849-Å irradiation at $P_{Hg} = 1.4 \times 10^{-3}$ torr: ○, N_2; ◐, CO; ◑, Ne; ●, He.

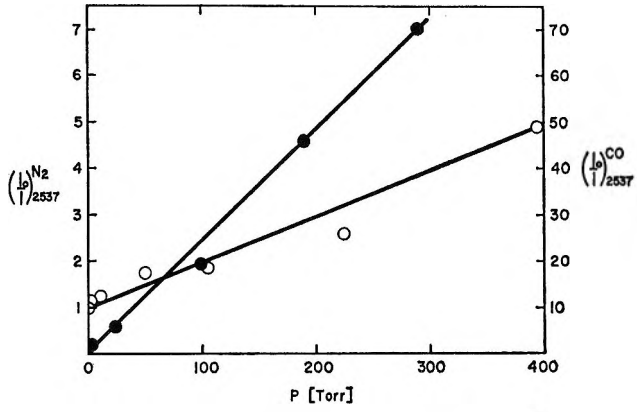

Figure 2. Stern–Volmer plot of quenching of λ 2537-Å radiation by N_2, ○, and CO, ●.

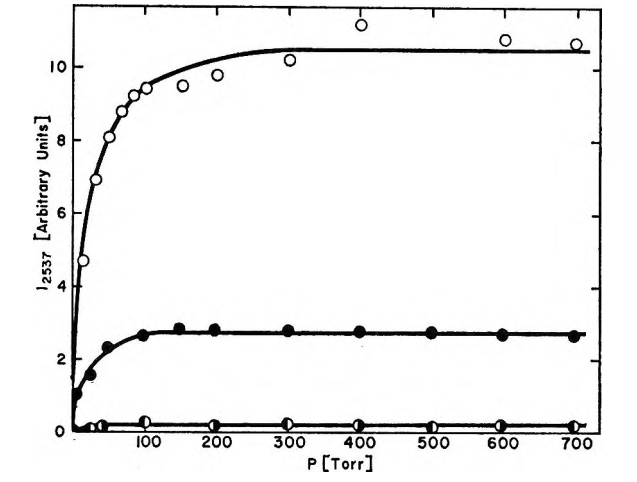

Figure 3. Scintillation at λ 2537 Å, corrected for quenching: ○, N_2; ●, CO; ◑, Ne; ◐, He. ($P_{Hg} = 1.4 \times 10^{-3}$ torr.)

Examination of scintillation intensity as a function of P_{Hg} revealed that the behavior of N_2 is qualitatively unchanged as P_{Hg} is changed although the absolute intensity of the emission is descreased as P_{Hg} is reduced.

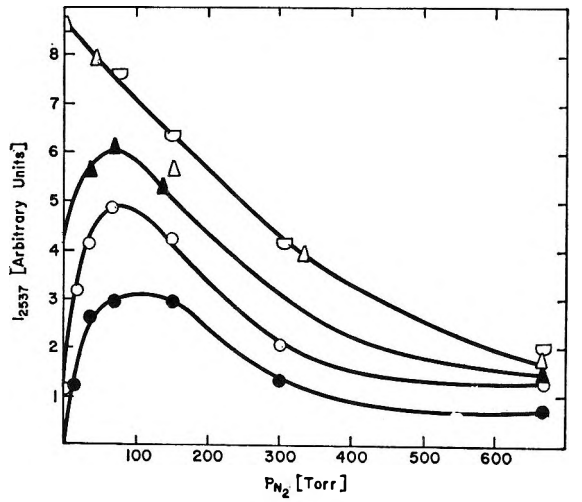

Figure 4. Quenching of λ 2537-Å radiation by N_2 with P_{Hg} equal to 1.2×10^{-3} torr, △; 4.9×10^{-4} torr, ▽; 1.9×10^{-4} torr, ▲; 1.5×10^{-5} torr, ○; $<10^{-8}$ torr, ●.

Quenching data at λ 2537 Å as a function of both P_{Hg} and P_{N_2} are shown in Figure 4. At the higher pressures of Hg, quenching behavior is independent of P_{Hg}; as P_{Hg} is lowered further, the intensity of the λ 2537-Å phosphorescence diminishes in general, and is highly attenuated in the region of low P_{N_2}. It is not clear to what this latter effect is due but it may be associated with less efficient absorption of the incident radiation at low pressures due to the narrow width of the absorption line. At all pressures of Hg, Stern–Volmer behavior is observed for P_{N_2} greater than about 100 torr. Since, fortuitously or not, the maxima in the scintillation and quenching curves both occur at $P_{N_2} \sim 100$ torr, the combined data at that pressure are plotted in Figure 5. The relatively simple dependence of the λ 2537-Å phosphorescence upon P_{Hg} can possibly be explained in terms of the dependence on P_{Hg} of the absorption of incident λ 2537-Å radiation. The intensity of scintillation at λ 2537 Å exhibits a maximum at $P_{Hg} \sim 2 \times 10^{-4}$ torr followed by a sharp decrease. This more complex behavior may possibly be related to the dependence upon P_{Hg} of intensity of absorption of λ 1849-Å radiation. Quantitative interpretation of the dependence upon P_{Hg} of the λ 2537-Å scintillation data does not appear to be possible, however.

By monitoring the λ 1849-Å fluorescence from 1849-Å irradiation it was possible to determine the relative cross sections for the quenching of $Hg(^1P_1)$ by N_2 and by CO. Quenching data at λ 1849-Å for these gases and for He are plotted in Figure 6 in the Stern–Volmer form. Within experimental error, the relative quenching rate constants, and hence the relative quenching cross sections, of N_2 and CO for $Hg(^1P_1)$ are identical. This behavior can be compared with the factor of about 20 by which they differ with respect to quenching of $Hg(^3P_1)$. Quenching by He is negligible within the precision of the data.

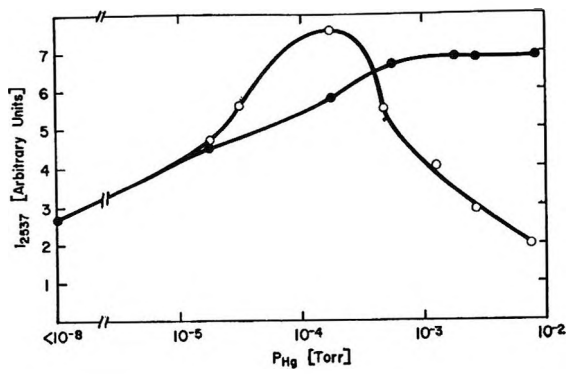

Figure 5. The dependence of λ 2537-Å emission upon P_{Hg} with P_{N_2} = 100 torr under λ 2537-Å, ●, and λ 1849-Å, ○, irradiation.

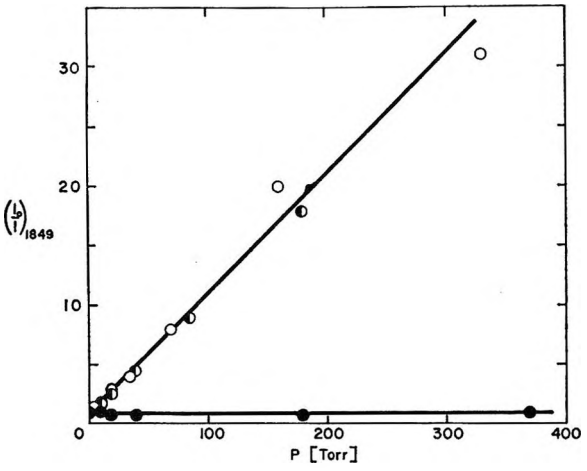

Figure 6. Stern–Volmer plot of λ 1849-Å quenching data for N_2, ○, CO, ◐, and He, ●.

Analysis of the Data

Straightforward application of steady-state kinetics leads to eq 8 (and the analogous expression for CO) where Hg and N_2 refer to species in their ground states, I_{abs}^{1849} is the absorbed flux of λ 1849-Å radiation opposite the monitoring port, I_p^{2537} is the intensity of λ 2537-Å scintillation, and all other symbols are as defined in eq 1–7. Equation 8 predicts that at con-

$$I_p^{2537} = \frac{k_3 k_5 k_p^{2537} I_{abs}^{1849}(\mathrm{Hg})(\mathrm{N_2})}{[k_f^{1849} + k_3(\mathrm{N_2})][k_p^{VK} + k_5(\mathrm{Hg})][k_p^{2537} + k_Q^{N_2}(\mathrm{N_2})]} \quad (8)$$

stant I_{abs}^{1849} and mercury pressure, I_p^{2537} will increase linearly with nitrogen pressure so long as $k_f^{1849} \gg k_3(N_2)$ and $k_p^{2537} \gg k_Q^{N_2}(N_2)$. In the limit of (N_2) sufficiently high to reverse both inequalities, I_p^{2537} will decrease linearly with nitrogen pressure. The data of Figure 2 for CO and N_2, with P_{Hg} equal to 1.4×10^{-3} torr, are consistent with this expectation. Empirical correction for quenching of $Hg(^3P_1)$ by N_2 or by CO is equivalent to multiplying eq 8 by $[k_p^{2537} + k_Q^{N_2}(N_2)]/k_p^{2537}$ to give eq 9. This relationship predicts that, at

$$(I_p^{2537})_{cor} = \frac{k_3 k_5 I_{abs}^{1849}(\mathrm{Hg})(\mathrm{N_2})}{[k_f^{1849} + k_3(\mathrm{N_2})][k_p^{VK} + k_5(\mathrm{Hg})]} \quad (9)$$

constant I_{abs}^{1849} and (Hg), $(I_p^{2537})_{cor}$ should, with increasing pressure of N_2, first increase and then approach constancy when $k_3(N_2) \gg k_f^{1849}$. The data of Figure 3 for both CO and N_2 are consistent with this expectation. It is also apparent that $(I_p^{2537})_{cor}$ is negligible for He and Ar, a result which tends to eliminate a variety of experimental errors as possible explanations of the data for N_2 and CO. Plotting $1/(I_p^{2537})_{cor}$ *vs.* $1/P_{N_2}$ or, respectively, $1/P_{CO}$, corresponds to analyzing the data in the form of eq 10, the reciprocal of eq 9, and provides a more sensitive test of the consistency of the data with the model,

$$\frac{1}{(I_p^{2537})_{cor}} = \frac{k_p^{VK} + k_5(\mathrm{Hg})}{k_3 k_5 I_{abs}^{1849}(\mathrm{Hg})}\left[\frac{k_f^{1849}}{(\mathrm{N_2})} + k_3\right] \quad (10)$$

particularly at lower pressures, as seen in Figure 7.[2] It also makes possible evaluation of k_3 from the ratio of slope to intercept and the known[18] values of k_f^{1849}, 7.7×10^8 sec^{-1}. The significance of the resulting values, 5×10^{11} M^{-1} sec^{-1} for N_2 and 11×10^{11} M^{-1} sec^{-1} for CO, is obscured by our inability to correct for imprisonment of λ 1849-Å resonance radiation; *i.e.*, these values represent only upper limits to $k_3^{N_2}$ and k_3^{CO}. The similarity of the two values is, however, in essential agreement with the finding by direct measurement, as shown in Figure 6, that N_2 and CO are equally efficient quenchers of λ 1849-Å fluorescence. This agreement appears to provide additional support for the proposed two-step mechanism.

According to eq 8, the maximum magnitude of I_p^{2537} should vary directly with I_{abs}^{1849} and should therefore

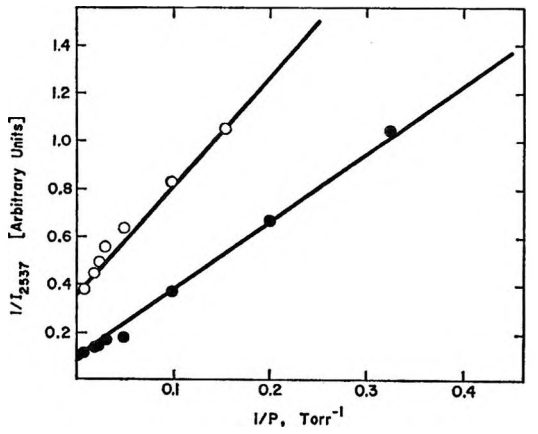

Figure 7. Double reciprocal plot (eq 10) of corrected λ 2537-Å scintillation data at $P_{Hg} = 1.4 \times 10^{-3}$ torr for N_2, ●, and CO, ○.

(18) Reference 17, p 54.

depend on the pressure of mercury. The pressure of N_2 at which it occurs should, however, be independent of P_{Hg}. This expectation is borne out by the data. More discriminating analysis in terms of the model encompassed by eq 1–7 of the dependence of I_p^{2537} upon the concentration of mercury vapor is prevented by the intervention of factors which are not directly relevant to the mechanism. Evidence of this is provided in the "quenching" curves of Figure 4. Clearly, at lower pressures of mercury vapor, N_2 affects I_p^{2537} in one or more ways in addition to quenching $Hg(^3P_1)$, so that empirical corrections for quenching of λ 2537-Å emission by N_2 are not possible. More generally, information as to the nature of the dependence of I_{abs}^{1849} on mercury pressure is lacking. Quantitative *a priori* estimation is prevented by the combination of the extremely high absorptivity of mercury vapor and imprisonment effects. Variation of I_{abs}^{1849} (and I_{abs}^{2537}) with P_{Hg} is probably responsible for most of the variation of scintillation and "quenching" intensities with P_{Hg} at 100 torr of N_2 which is summarized in Figure 5.

A possible alternative explanation for λ 2537-Å scintillation in the presence of N_2 or CO is represented by eq 1, 2, 7, and 11. Presumably both $Hg(^3P_1)$ and

$$Hg(^1P_1) + N_2(X^1\Sigma)_{v=0} \xrightarrow{k_{11}} Hg(^3P_1) + N_2(X^1\Sigma)_{v^*} \quad (11)$$

$N_2(X^1\Sigma)_{v^*}$, where v^* represents a set of high vibrational levels, would possess excess translational energy.[19] Steady-state treatment of this mechanism gives eq 12–14 (and the analogous equations for CO). These

$$I_p^{2537} = \frac{k_p^{2537}k_{11}I_{abs}^{1849}(N_2)}{[k_{11}(N_2) + k_f^{1849}][k_p^{2537} + k_Q(N_2)]} \quad (12)$$

$$(I_p^{2537})_{cor} = \frac{I_{abs}^{1849}(N_2)}{(N_2) + (k_f^{1849}/k_{11})} \quad (13)$$

$$\frac{1}{(I_p^{2537})_{cor}} = \frac{1}{I_{abs}^{1849}}\left[1 + \frac{k_f^{1849}/k_{11}}{(N_2)}\right] \quad (14)$$

equations are as consistent with λ 2537-Å scintillation data at constant P_{Hg} and varying P_{N_2}, P_{CO}, P_{He}, or P_{Ne} as are eq 8–10. They predict no dependence of scintillation intensity on P_{Hg} at constant P_{N_2} other than that due to variation in I_{abs}^{1849}. Unfortunately, the significance of the observed dependence of scintillation intensity on P_{Hg} is too complicated to provide a basis for choice between the two mechanisms. It must be recognized that the transition postulated for mercury, *i.e.*, with $\Delta L = 0$, is strictly forbidden in emission and absorption.[19] There seems to be no precedent for this type of a transition in a collision of the second kind involving a large energy difference although the transition $Hg(^3P_1) \rightarrow Hg(^3P_0)$, for which ΔE is only 0.22 eV is induced efficiently by collision with nitrogen. The possibility of the postulated energy transfer, in which $\Delta S = 2$ and the difference in electronic energy is 1.86 eV, cannot, however, be excluded *a priori*.

A third mechanism substitutes reactions 15, 16 and 17 (and analogous equations for CO) for 3, 4 and 5, respectively, where $N_2(X^1\Sigma)_{v^*}$ designates vibrationally

$$Hg(^1P_1) + N_2(X^1\Sigma)_{v=0} \xrightarrow{k_{15}} Hg(^1S_0) + N_2(X^1\Sigma)_{v^{**}} \quad (15)$$

$$N_2(X^1\Sigma)_{v^{**}} + N_2(X^1\Sigma)_{v=0} \xrightarrow{k_{16}} N_2(X^1\Sigma)_{v^*} \quad (16)$$

$$N_2(X^1\Sigma)_{v^{**}} + Hg(^1S_0) \xrightarrow{k_{17}} N_2(X^1\Sigma)_{v^*} + Hg(^3P_1) \quad (17)$$

excited ground state N_2 with insufficient energy to excite $Hg(^3P_1)$. If excess translational energy is not involved, v^{**} must be at least 19(5.03 eV). This mechanism leads to eq 18 and 19.

$$I_p^{2537} = \frac{k_{15}k_{17}k_p^{2537}I_{abs}^{1849}(Hg)(N_2)}{[k_f^{1849} + k_{15}(N_2)][k_{16}(N_2) + k_{17}(Hg)][k_p^{2537} + k_Q^{N_2}(N_2)]} \quad (18)$$

$$(I_p^{2537})_{cor} = \frac{k_{15}k_{17}I_{abs}^{1849}(Hg)(N_2)}{[k_f^{1849} + k_{15}(N_2)][k_{16}(N_2) + k_{17}(Hg)]} \quad (19)$$

In order for eq 19 to be consistent with the data at constant mercury pressure and varying pressure of N_2, either one of two conditions must maintain. *Either* $k_{17}(Hg) \gg k_{16}(N_2)$ throughout the pressure range observed while $k_f^{1849} = k_{15}(N_2)$ at about 20 torr of N_2 *or* $k_f^{1849} \gg k_{15}(N_2)$ throughout the observed pressure range while $k_{16}(N_2) = k_{17}(Hg)$ at about 20 torr of N_2. The first alternative corresponds to $k_{15} \leqslant 9 \times 10^{11}\ M^{-1}$ sec^{-1} and requires that $k_{17} \gg 4 \times 10^5\ k_{16}$ while the second corresponds to $k_{15} \ll 2.5 \times 10^{10}\ M^{-1}\ sec^{-1}$ and requires that $k_{17} \cong 10^4 k_{16}$. Whether vibrational–vibrational relaxation could be slow enough to meet even the second requirement seems questionable[20] but, again, the present data do not exclude reactions 15–17.

There thus remains the possibility that any or all of the three postulated mechanisms actually occur.[21] A potentially diagnostic experiment involves measurement of the rate of decay of λ 2537-Å scintillation when irradiation at λ 1849 Å in the presence of N_2 is inter-

(19) *Cf.* A. B. Callear in "Photochemistry and Reaction Kinetics," P. G. Ashmore, F. S. Dainton, and T. M. Sugden, Ed., Cambridge University Press, Cambridge, U. K., 1967, pp 175–180.

(20) Reference 19, pp 157–164.

(21) G. Liuti, S. Dondes, and P. Harteck [*J. Chem. Phys.*, **44**, 4051 (1966)] have ascribed the formation of CO_2 and C_3O_2 in the $Hg(^1P_1)$-sensitized photolysis of CO to reaction of $CO(a^3\pi)$ with ground state CO. If such a reaction were sufficiently rapid, it would compete with energy transfer from $CO(a^3\pi)$ to $Hg(^1S_0)$ and prevent scintillation at λ 2537 Å from occurring by the route of eq 3–7. In the absence of quantum yield data for the formation of CO_2 by the above route it is not possible to evaluate the significance of this reaction as a basis for discriminating among the various mechanisms of scintillation.

rupted. Because of the very long radiative lifetime of $N_2(A^3\Sigma)$,[22] reaction 5 would be the rate-determining step of the decay if excitation of $Hg(^3P_1)$ occurred solely *via* $N_2(A^3\Sigma)$. Under favorable circumstances the simultaneous operation of the latter mechanism along with one or both of the other two could also be identified. Such experiments are in progress.

(22) W. Brennen, *J. Chem. Phys.*, **44**, 1793 (1966), reports a lifetime of 12 ± 2.4 sec.

Higher Order Ion–Molecule Reactions. I. Theoretical Basis[1]

by G. G. Meisels and H. F. Tibbals

Department of Chemistry, University of Houston, Houston, Texas 77004 *(Received May 7, 1968)*

Relative ion abundances are calculated on the basis of a collision model for multiple order ion–molecule reactions. Allowance is made for the energy dependency of reaction cross sections and the existence of long-lived intermediates whose dissociation is assumed to follow unimolecular decay kinetics. Cross section and rate constant values severely affect calculated abundance curves and permit the assignment of reaction mechanisms.

I. Introduction

A number of investigations of ion–molecule reactions at pressures up to a few torr[2-8] and even several hundred torr[9] in the ion source of a mass spectrometer have been reported in the last few years. Interest in the results of such investigations stems largely from their obvious relevance to an understanding of gas phase radiation chemical systems where more than one half of the product formation is usually ascribed to reactions of intermediate ions.[10,11] Moreover, product formation in the far vacuum ultraviolet may also involve ions as intermediates.[12]

At least two difficulties arise in the application of information obtained by mass spectrometry directly to radiation and photochemical systems. Mass spectrometric investigations can only report on the nature and abundance of ionic species, and it is often difficult to assign reaction sequences in complex systems where several primary ions undergo ion–molecule reactions.[2b,3] The nature of the neutral entity concomitant with an ionic product can only be inferred if the precursor ion is known, and mechanistic uncertainties can sometimes be resolved only with considerable difficulties. In radiation and photochemical experiments, however, the precise reverse is the case: the nature of the ionic species responsible for and products of a neutral forming step can only be assessed indirectly. The two techniques, although complementary, provide no direct overlap for mutual calibration.

A second difficulty, perhaps somewhat more subtle, is the difference in the kinetic character of the systems. In radiation and photochemistry one provides a continuous, steady source of reactive intermediates, most of which are translationally in thermal equilibrium with their surroundings. Rates of disappearance and metathesis are determined by the usual competition kinetics, and the steady-state assumption can be applied to a good approximation, provided that allowance for possible spatial inhomogeneity of the primary species formation is made. An entirely different situation may exist in the ion source of the mass spectrometer. When ions are sampled from high-pressure α radiolysis,[9] they will typically have survived as long or longer than they would under normal radiolysis and photolysis conditions. Therefore, such experiments yield information princi-

(1) Presented at the Symposium on Photochemistry and Radiation Chemistry sponsored by the National Academy of Sciences at Natick, Mass., April 1968.

(2) (a) C. E. Melton and P. S. Rudolph, *J. Chem. Phys.*, **32**, 1128 (1960); (b) F. H. Field, *J. Amer. Chem. Soc.*, **83**, 1523 (1961).

(3) S. Wexler and N. Jesse, *ibid.*, **84**, 3425 (1962).

(4) M. S. B. Munson, J. L. Franklin, and F. H. Field, *ibid.*, **85**, 3575 (1963).

(5) G. A. W. Derwish, A. Galli, A. Giardini-Guidoni, and G. G. Volpi, *J. Chem. Phys.*, **39**, 1599 (1963).

(6) M. S. B. Munson, *J. Amer. Chem. Soc.*, **87**, 5313(1965).

(7) M. Henchman and C. H. Ogle, *Discussions Faraday Soc.*, **39**, 63 (1965).

(8) J. H. Futrell and T. O. Tiernan, *J. Phys. Chem.*, **72**, 158 (1968).

(9) P. Kebarle and E. W. Godbole, *J. Chem. Phys.*, **39**, 1131 (1963).

(10) P. Ausloos and S. G. Lias, "Gas Phase Radiolysis of Hydrocarbons," in "Actions Chimiques et Biologiques des Radiations," M. Haissinsky, Ed., Masson et Cie, Paris, 1967, Chapter 5.

(11) G. G. Meisels, "Organic Gases" in "Fundamental Processes in Radiation Chemistry," P. Ausloos, Ed., John Wiley and Sons, Inc., New York, N. Y., 1968, Chapter 6.

(12) R. D. Doepker and P. Ausloos, *J. Chem. Phys.*, **43**, 3814 (1965).

pally on the nature of the ion which may be expected to undergo eventual neutralization in the normal radiolytic system. Such experiments can also assist in the assignment of ions resulting from fewer collisions but then pressure must be reduced significantly, or "inert" rare gases are added whose efficiency for deactivation of excited intermediates differs from that of the parent molecule. Most information on the lower order ion–molecule reactions, which presumably give rise to some of the more important relatively simple neutral products, is therefore derived from studies where ion sources are operated in a more or less conventional manner, but at pressures up to *ca.* 1 torr. Thus, the primary ions are formed in an electron beam ribbon and are continually accelerated by an electrostatic field on their way toward expulsion at the exit slit. Their translational energy therefore is continually increased, and the usual steady-state approximation of thermal homogeneous kinetics is *a priori* inapplicable because rate constants and residence times are energy dependent.

Problems of particular interest in an assignment of mechanisms are the collision cross sections or rate constants for the ion–molecule reactions, the verification of the existence of an intermediate complex, and the assessment of its unimolecular dissociation rate constant. An analysis of this sort was first attempted by Field for the ethylene system,[2b] and included an estimate of rate constants based on the premise that the reaction sequence in the ion source could be analyzed using the conventional steady-state assumption.[13] He postulated that all third- and higher order ions were formed by reactions of long-lived intermediate addition complexes such as $C_4H_8^+$. The rate constant for dissociation of intermediate butene ion derived on this basis was also observed in radiation chemical experiments,[14,15] vacuum ultraviolet photochemistry,[16] and in ion-sampling mass spectrometry,[17] lending credulence to this approach. However, Wexler[18] has pointed out that Field's data are also consistent with a mechanism where all tertiary ion formation proceeds only *via* the reactions of the dissociation products of intermediate $C_4H_8^+$ such as $C_3H_5^+$. Wexler was able to account for ion abundance variation using an attenuated beam approach inserting energy independent reaction cross sections. Theoretical considerations,[19] isotopic labeling,[20,21] the ability to affect branching ratios in the sequence ascribed to reactions of a long-lived intermediate butene ion,[21] and ion cyclotron double resonance experiments[22] have recently provided definitive evidence that at low pressures the mechanism leading to third- and fourth-order ions included reactions of $C_3H_5^+$ only.

It is clear that the agreement of the rate constant calculated by the steady-state assumption with that obtained by other essentially non-mass spectrometric methods is specious, and other theoretical methods must be developed. Wexler's ion beam approach has been modified by Derwish, *et al.*,[23] to allow for relatively long-lived intermediate complexes in acetylene ion–molecule reactions. However, these authors assumed energy-independent reaction cross sections and again found it necessary to take recourse to a steady-state assumption. Moreover, they treated the disappearance of complex ions by dissociation in terms of cross sections whose relationship with unimolecular dissociation rate constants depends on ion currents. A model based on energy averaging was developed by Lorquet and Hamill[24] but does not allow for unimolecular dissociation. Hyatt, Dodman, and Henchman developed a model based on residence times in the ion source,[25] but these authors did not make allowance for finite complex lifetimes, and their kinematic treatment does not readily lend itself to such an extension.

In this paper we report the development of a collision theory of higher order ion–molecule reactions based on an examination of simplified classical trajectories. It makes explicit allowance for energy dependency of cross sections and for finite complex lifetimes using first-order decay kinetics. The sensitivity of calculated ion abundances to unknown reaction parameters is examined.

II. Development of Model

A. Physical Model. Our approach is simply one of following the classical, one-dimensional trajectories of individual positive charges and their identity changes in the mass spectrometer ion source. Parent and fragment primary ions are assumed to be formed in an infinitely thin electron beam at L_0 (Figure 1). These and product ions are accelerated by a repeller or draw-out field toward the exit slit at L_x at which there is a sharp boundary beyond which no further reactions occur. The distance L_x is subdivided at points where collisions and unimolecular dissociations take place. Reactions are assumed to involve the formation of an intermediate complex and therefore to occur as a result

(13) F. W. Lampe, J. L. Franklin, and F. H. Field, "Kinetics of Reactions of Ions with Neutral Molecules" in "Progress in Reaction Kinetics," Vol. 1, G. Porter, Ed., Pergamon Press, London, 1961, p. 67.

(14) G. G. Meisels, *J. Chem. Phys.*, **42**, 3237 (1965)

(15) G. G. Meisels, Advances in Chemistry Series, No. 58, American Chemical Society, Washington D. C., 1966, p 243.

(16) R. Gorden, Jr., and P. Ausloos, *J. Chem. Phys.*, **47**, 1799 (1967).

(17) P. Kebarle, R. M. Haynes, and S. Searles, ref 15, p 210.

(18) S. Wexler and R. Marshall, *J. Amer. Chem. Soc.*, **86**, 781 (1964).

(19) G. G. Meisels and F. H. Tibbals, paper presented at the 15th Annual Meeting on Mass Spectrometry at Denver Colo., May 1967.

(20) J. O. Tiernan and J. H. Futrell, *J. Phys. Chem.*, in press.

(21) J. J. Myher and A. G. Harrison, *Can. J. Chem.*, **46**, 101 (1968).

(22) M. T. Bowers, D. D. Elleman, and J. L. Beauchamp, *J. Chem. Phys.*, **72**, 3599 (1968).

(23) G. A. W. Derwish, A. Galli, A. Giardini-Guidoni, and G. G. Volpi, *J. Amer. Chem. Soc.*, **87**, 1159 (1965).

(24) A. J. Lorquet and W. H. Hamill, *J. Phys. Chem.*, **67**, 1709 (1963).

(25) D. H. Hyatt, E. A. Dodman, and M. J. Henchman, ref 15, p 131.

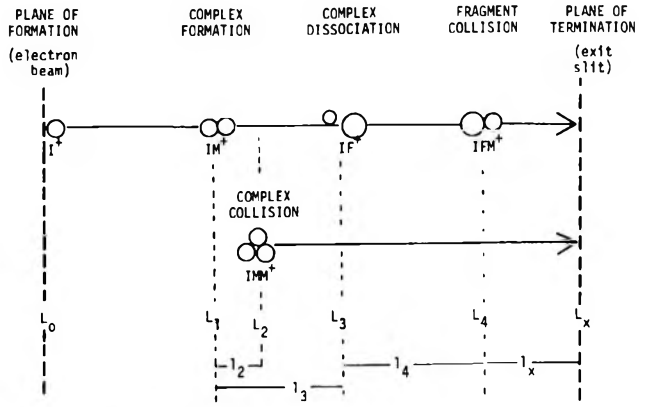

Figure 1. Schematic of collision model and identification of reaction positions.

of capturing collisions. While a stripping[26] or pickup[27] mechanism can easily be accommodated in this treatment, it need not be considered here since the treatment of Hyatt, *et al.*,[25] is satisfactory for such cases. We will be dealing with condensation type reactions which must involve an addition complex persisting more than one or two vibrational periods. The effect of the lifetime of such addition complexes on the calculated higher order ion abundances is our primary concern.

Consider a primary ion (I^+) formed at L_0 and accelerated a distance L_1 where it forms a complex $[IM]^+$ with a neutral species. The sequence may now be distinguished with respect to formation of tertiary ions. In the first, the complex reacts at L_{2c} before it has an opportunity to dissociate, and forms a tertiary "complex" ion $[IMM]^+$. In the second, the complex dissociates at L_{2F} to yield a secondary fragment ion $[IF^+]$ which reacts at L_3 to form a tertiary ion $[IFM^+]$. Dissociation of IM^+ to yield I^+ will change the energy of I^+ and secondary I^+ is therefore treated as and named IF^+. Possible sequences for ions up to fourth order in pressure dependence and the nomenclature for their identification are illustrated in Figure 2.

B. Mathematical Formulation. We consider first the fate of the primary ion which can react by collision only. We define an unnormalized probability function $P_1(L_1, \epsilon_1)$ as the probability density that a primary ion I^+ passing through L_1 will form a collision complex. ϵ_1 is the energy of the ion relative to a neutral reactant in the center of mass system. If one neglects thermal contributions, one can express the relative energy of the reactant pair in terms of the energy E_1 of the ion I^+ in the laboratory coordinate system. Thus, since $E_1 = FeL_1$, where F is the field strength and e is the electronic charge, $P_1(L_1, \epsilon_1)$ can be expressed as a function of L_1 only

$$P_1(L_1, \epsilon_1) = P_1(L_1) \quad (1)$$

The number of primary ions reacting between L_1 and $L_1 + dL_1$ is

$$-di_0(L_1) = i_0(L_1)P_1(L_1)dL_1 \quad (2)$$

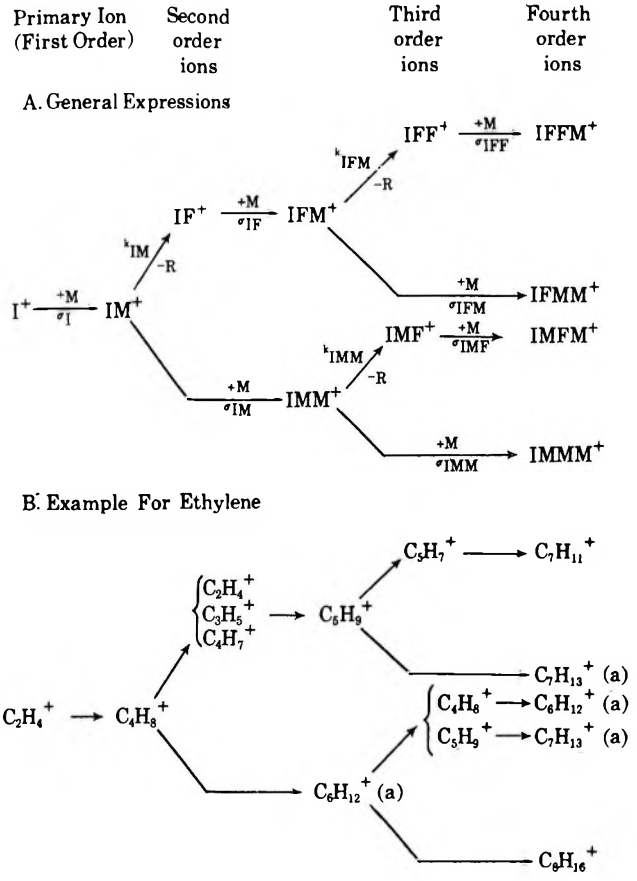

Figure 2. Nomenclature for identification of ions, rate constants, and reaction cross sections. (a) These species apparently predominantly redissociate to starting components as shown explicitly for $C_6H_{12}^+$.

The dependence of the primary ion current i_0 on L_1 arises from the attenuation of the initial ion current $I_0 = i_0(L_0)$ formed in the plane of the electron beam. The intensity of i_0 at L_1 can be expressed as the product of I_0 and an attenuation factor $A_1(L_1)$ by integrating eq 2 between the limits L_0 and L_1 to give

$$i_0(L_1) = I_0\exp\left[-\int_{L'=L_0}^{L_1} P_1(L_1')dL_1'\right] \text{ or}$$

$$i_0(L_1) = I_0A_1(L_1) \quad (3)$$

The translational energies of all ions other than the primary are not only affected by acceleration but are also essentially instantaneously altered at every reaction point. Moreover, the identity of the ion may change by j channels of collision and unimolecular dissociation. For any subsequent process, the energy of the ion is therefore known only when the nature and location of each previous step is specified. In general, if all ions formed at L_n in a sequence of n precisely defined steps are considered, the number which pass some subsequent point L_{n+1} will be given by an equation analogous to (3), or

(26) A. Henglein, ref 15, p 63.

(27) Z. Herman, J. D. Kerstetter, T. L. Rose, and R. Wolfgang, *J. Chem. Phys.*, **46**, 2844 (1967).

$$d^n i_{n,j}(L_1, L_2, \ldots, L_{n+1}) = I_0 \prod_{i=1}^{n+1} A_i(L_1, L_2, \ldots, L_i) \times \prod_{i=1}^{n} P_{i,k}(L_1, L_2, \ldots, L_i) \prod_{i=1}^{n} dL_i \quad (4)$$

where the $P_{i,k}$ terms represent the specific processes leading to the ion of interest, while the A_i factors apply to all j possible exit channels for the ion. The ith attenuation factor, A_i, is obtained by integrating an equation analogous to eq 2 with respect to the variable dL_{i+1}' over the limits L_i to L_{i+1}, or

$$A_i(L_1, L_2, \ldots, L_i) = \exp\left\{-\int_{L_{i-1}}^{L_i}\left(\sum_j P_{i,j}(L_1, L_2, \ldots, L_i')\right)dL_i'\right\} \quad (5)$$

where the summation is again taken over all possible exit channels for the ith ion. This expression for ion attenuation differs slightly from that of Wexler and Jesse[3] by making explicit allowance for the energy dependence of the exponent and by allowing detailed consideration of unimolecular dissociation.

When attenuation is by collision, the probability density $P_{n,j}$ is given by the product of the concentration of neutral reactant species and the cross section for reaction

$$P_{n,\mathrm{coll}}(L_1, L_2, \ldots, L_n) = [\mathrm{M}]\sigma_n(L_1, L_2, \ldots, L_n, E_t) \quad (6)$$

where E_t is an energy not arising from acceleration and can be used to describe possible thermal contributions to the ion energy or excess kinetic energy in the dissociation process. We shall assume at this time that E_t is negligible. The acceleration term is dependent on the reaction path and is shown for the first three processes in Table I. For convenience of expression, we have substituted the identity

$$l_n = L_n - L_{n-1} \quad (7)$$

A critical distinction between stripping[26,27] and complex formation is obvious here. For primary ions where dissociation is not in competition with reaction with neutrals, the integral in expression 5 is essentially an energy averaged or macroscopic cross section[28] which will change with increasing pressure because the region over which it is averaged will put increased emphasis on lower energies.[25]

Table I: Ion Kinetic Energies

Primary ion	$E_1 = F \cdot l_1$
Secondary complex ion	$E_{2c} = (m_1/m_c)F \cdot l_1 + F \cdot l_2$
Secondary fragment ion	$E_3 = [m_3/m_c][(m_1/m_c)F \cdot l_1 + F \cdot l_1] + F \cdot l_3$

When attenuation is by unimolecular dissociation, the probability function $P_{n,j}$ is given by

$$P_{n,\mathrm{dissoc}}(L_1, L_2, \ldots, L_n) = k_n(E_n') \frac{dt_n(L_1, L_2, \ldots, L_n)}{dL_n} \quad (8)$$

where t_n is the time required for the ion formed at L_n to be accelerated to L_{n+1} and k_n is the unimolecular dissociation rate constant for the process of interest. t_n is determined by the equations of motion of the complex ion formed at L_{n-1} and hence can be readily expressed in terms of distance. For example, the time a secondary complex IM^+ of mass m_c has existed is given by

$$t_2(L_2 - L_1) = \sqrt{\frac{2m_c}{Fe}} - \left[\sqrt{\frac{m_1}{m_c}L_1 + L_2 - L_1} - \sqrt{\frac{m_1}{m_c}L_1}\right] \quad (9)$$

The total ion current I_n of species n passing through the exit slit at L_x can now be obtained by successively substituting attenuation factors and expressions for the precursor ion currents into expression 4 and integrating

$$I_n(L_x) = I_0 \int_{L_1'=L_0}^{L_x}\int_{L_2'=L_1'}^{L_x}\cdots\int_{L_n'=L_{n-1}'}^{L_x} \times \prod_{i=1}^{n+1} A_i(L_1', \ldots, L_i') \prod_{i=1}^{n} P_{i,k}(L_1', \ldots, L_i') \prod_{n=1}^{n} dL_i' \quad (10)$$

where $L_{n+1} = L_x$. The identity $\sum_{n,j} I_{nj} = I_0$ can be used to check calculations for self-consistency.

Relationships obtained by the substitution into the precursor functions are given below for the formation of the ions IMM^+ and IFM^+ when only one ion of each type is produced in each reaction step and when each ion is formed *via* a unique sequence of steps.

$$I_{IMM^+}(l_x) = I_0 \int_{l_1=l_0}^{l_x} [\mathrm{M}]\sigma_1(l_1) \exp\left\{-\int_{l=l_0}^{l_x} \times [\mathrm{M}]\sigma_1(l)dl\right\} \int_{l_{2c}=0}^{l_x-l_1} [\mathrm{M}]\sigma_{2c}(l_1, l_{2c}) \times \exp\left\{-k_2t_2 - \int_{l=0}^{l_{2c}} [\mathrm{M}]\sigma_{2c}(l_1, l)dl\right\} dl_1 dl_{2c} \quad (11)$$

$$I_{IFM^+}(l_x) = I_0 \int_{l_1=l_0}^{l_x} [\mathrm{M}]\sigma_1(l_1) \exp\left\{-\int_{l=l_0}^{l_x} \times [\mathrm{M}]\sigma_1(l)dl\right\} \int_{l_{2c}=0}^{l_x-l_1} k_2\frac{dt_2}{dl_{2c}} \exp\left\{-k_2t_2 - \int_{l=0}^{l_{2c}} [\mathrm{M}]\sigma_2(l_1,l)dl\right\} \int_{l_{2f}=0}^{l_x-l_1-l_{2c}} [\mathrm{M}]\sigma_{2f}(l_1,l_{2c},l_{2f}) \times \exp\left\{-\int_{l=0}^{l_{2f}} [\mathrm{M}]\sigma_{2f}(l_1,l_{2c},l)dl\right\} dl_1 dl_{2c} dl_{2f} \quad (12)$$

(28) D. A. Kubose and W. H. Hamill, *J. Amer. Chem. Soc.*, **85**, 125 (1963).

When a species is the product of more than one reaction sequence, the ion current is calculated by summing all I_{nj} which lead to that species.

III. Assumptions and Approximations

Some assumptions and approximations are inherent even in this generalized form. First is the postulate of a collision complex, whose lifetime is of course of primary concern. Second is the neglect of excess kinetic energy in the dissociation coordinate after the fragmentation process. While allowance for this effect is possible in principle, the resultant complex relationship would require an excessive amount of computer time for evaluation since the one-dimensionality of the trajectory would have to be abandoned as an approximation. This should, however, introduce only a minor error since unimolecular reaction rate theory predicts only small if not negligible excess kinetic energy.[29] The randomness of orientation of the dissociation would also tend to decrease a possible effect on further reactions. Third, we have neglected the thermal energies of all species, a common assumption in such treatments. However, the integration procedure requires that the lower limit not be $L_0 = 0$ but have a finite value, and L_0 was therefore chosen to correspond to an initial energy of $0.015kT/F$. Fourth, we have taken the reaction boundary at the planes of formation and exit to be sharp, while in reality the electron beam has finite width and reactions are not quenched precisely at the exit slit. The effects of the last two approximations are now under investigation, and preliminary results for small variations of L_0 have shown little effect on ion abundance. It should perhaps be mentioned that field penetration and inhomogeneity have also been neglected.

Returning to the specific reactionships 11 and 12 and their higher order analogs, it is clear that they contain two unknown components: microscopic cross sections and unimolecular dissociation rate constants. In this communication we use only cross sections of the simple ion-induced dipole sort[30]

$$\sigma(E) = S \cdot \pi e(2\alpha m_1/\mu E)^{1/2} \qquad (13)$$

where S is an efficiency factor, e is the electronic charge, α is the polarizability of the neutral molecule, and μ is the reduced mass of the collision partners. The use of the efficiency factor is dictated by the known deviation of cross sections from those calculated theoretically. The value of S used in the calculation is the first adjustable parameter. Other forms of the cross section dependency on energy, even including discontinuities, can be substituted readily, but are of lesser interest at this time since we are primarily concerned with the low ion energy range of a few tenths of an electron volt where the approximations inherent in eq 13 should be best applicable.

The other adjustable parameters are the rate constants for dissociation of intermediate complexes. It is, of course, possible to estimate these using unimolecular dissociation rate theory,[31] but such an *a priori* approach does not yield values with sufficient reliability to satisfy our requirements since the final ion distribution curves are highly sensitive to the values of rate constants. There is a further difficulty. The assumption of a long-lived collision complex requires that the translational energy of the collision be transformed into internal energy modes, which should affect the value of the rate constant. Therefore, k should really be expressed as a function of energy or $L_1, L_2, \ldots, L_n$ just like the cross section. At this point, however, it is adequate for a test of the general model to assume a fixed rate constant for the dissociation of a given complex, and thus the applicability of simple unimolecular dissociation kinetics.

IV. Numerical Evaluation Procedure

The multiple integrations of equations such as (11) and (12) properly substituted with cross sections from eq 13 cannot be carried out in closed form and were therefore solved on an IBM 7094 computer using FORTRAN IV language. Several numerical integration procedures,[32] including those according to the trapezoidal, Simpson's and Wedell's rule, and the Runge–Kutta method, were attempted. Difficulties were encountered with all these when parameters of interest were varied. Gaussian quadrature was finally adopted as the most appropriate technique for these calculations. In this procedure, the integral of a polynomial of the nth degree or lower can be evaluated exactly by calculation of the integrand at only n values of the variable of integration. The appropriate values of the variables to give such a fit are chosen by this method. An available routine was modified to suit our system.[33]

Sixteen-point gaussian quadrature was found to give satisfactory results for pressures from 0 to 0.2 torr and $k_d \sim 10^{-7}$ sec^{-1}, but rapid decrease of the exponential functions at higher pressures and larger rate constants required a larger number of points, and up to 32-point gaussian quadrature was used for the range from 0.2 to 1.0 torr and $k_d = 10^8$ sec^{-1}.

The accuracy of the integration was confirmed by several means. Different gaussian quadrature procedures were employed, the number of points was varied, and the integration was broken up into subintervals with individual evaluation of the regions and subsequent summation. This assured that the integra-

(29) C. E. Klots, *J. Chem. Phys.*, **41**, 117 (1964).

(30) G. Gioumousis and D. P. Stevenson, *ibid.*, **29**, 294 (1958).

(31) M. Vestal, A. L. Wahrhaftig, and W. H. Johnston, *ibid.*, **37**, 1276 (1962).

(32) J. Todd, Ed., "Survey of Numerical Analysis," McGraw-Hill Book Co., Inc., New York, N. Y., 1962, p 66.

(33) IBM System/360 Scientific Subroutine Package 360A-CM-03X, Verson II, 3rd ed, No. H20-0205-2, IBM Technical Publications Department, White Plains, N. Y., 1966, p 96.

tions converged. Computations were then repeated using the double precision mode, which gave nearly identical results, indicating that the dynamic range of the normal precision mode was sufficient but that errors due to round-off or truncation were limitations. As a further check on such errors, several equivalent programs were written differing in the order of calculating factors in the integrand. The maximum differences found by any of the above comparison methods were less than 2% of calculated individual ion currents or 1% of the total ion current, whichever is larger.

As a last check, the total ion current obtained by summing all individual ion current fractions was compared to the required sum of 1. The deviation of the calculated sum from unity increased from less than 1% at pressures up to 0.2 torr to a maximum of 5% at 1 torr when 24-point gaussian quadrature was employed ($k_d = 10^7$ sec^{-1}). The error obviously increased when a smaller number of points was employed for the evaluation, but also increased with increasing fragmentation rate constant and decreasing field strengths. As indicated above, this can be ascribed to the more rapid decrease of the exponential expressions under these conditions. The total current was always calculated, and the curves were recomputed with a higher order quadrature until the maximum error in I(total) did not exceed 3%

V. Results and Discussion

The most important aspect of these calculations is the evaluation of the effect of the adjustable parameters on the calculated curves. Our theoretical approach would be without value if the results are not sensitive to the assumed mechanism, to the values of the undefined parameters, if there are too many of them, or if their variation has identical effects on the calculated curves. Not more than four of these parameters enter directly into the evaluation of the variation of ion abundance for any given species. These are the collision cross section for and rate constant of dissociation of the precursor ion, and the rate constant for dissociation and the collision cross section for further reactions of the ion itself. The effect of these parameters is demonstrated best by assuming that a particular ion is not produced simultaneously by reactions of both fragment and precursor ions; that is, we assume that IMF^+ and IFM^+ are not of identical m/e. This is not restrictive since abundances of ions arising by both processes can be obtained by summing the probabilities of alternate reaction paths.

Calculated curves can be correlated with experimental results by successive assignment of cross sections and rate constants for first-, second-, third-, etc., order ions, but we shall not attempt such a curve-fitting procedure at this time. Instead we will systematically examine ion abundance curves by varying one factor at a time and keeping all other parameters constant.

The experimental conditions for these calculations were chosen arbitrarily but correspond fairly well to those reported by Wexler,[3] a reaction path length $L_x = 0.29$ cm, a field strength of 6 V cm^{-1} (smaller than that of Wexler), and a gas temperature of 200°. The last factor of course enters only negligibly through the initial ion energy used in the integration. The characteristics of the reaction system closely parallel those of the ethylene system, with $\sigma_{IM} = 7.6 \times 10^{23} E^{-1/2}$ cm^2 where E is the energy of the reactant ion in ergs, $\sigma_{IF} = 6.9 \times 10^{23} E^{-1/2}$ cm^2 and $\sigma_{IFM} = \sigma_{IMM} = 8.2 \times 10^{23} E^{-1/2}$ cm^2 corresponding to the theoretical cross sections of the ions $C_4H_8^+$, $C_3H_5^+$, and $C_5H_9^+$. Only $\sigma_I = 7.7 \times 10^{23} E^{-1/2}$ cm^2 was taken as *ca.* 25% larger than theoretical for ethylene ion as suggested by Wexler.[3] No attempt was made to study variations in σ_I since the magnitude of this cross section is always easily accessible from experiment, and its influence on higher order ion distributions can be predicted qualitatively if the effect of the other factors is understood.

One of the most interesting aspects of these calculations is the assessment of the extent to which second-order intermediate complexes contribute to higher order reactions before they dissociate. The effect of changes in the adjustable parameters on the calculated ion distribution curves is therefore presented at first for the total of all third- and higher order ions arising by reactions of the complex and those formed by collisions of fragment secondary ions. Such ion currents are called unattenuated tertiary ion currents.

Variation of the unimolecular dissociation rate constant between 10^5 and 10^8 sec^{-1} demonstrates that an almost complete change in mechanism occurs over this range (Figure 3). At the highest value of the rate constant reactions occur virtually exclusively *via* a fragment ion mechanism, although a small but real contribution of a few per cent by intermediate complex ions is still observable, and increases with increasing pressure, until at 1 torr 11% of the unattenuated tertiary ion current arises from reactions of the complex (Figure 4). At the other extreme, reactions of the fragment ion are still barely noticeable for a rate constant of 10^5 sec^{-1} but the mechanism is dominated by IM^+ ion reactions. The decrease of IFM^+ with increasing pressure above *ca.* 0.08 torr can be attributed to the removal of precursor complexes by reaction. It is noteworthy that the value of the rate constant reflects itself not only in the relative contributions of the two mechanisms, but also in the character of the curves for the unattenuated tertiary ion abundances. The current fraction of IMM^+ arising from reactions of an undissociated complex shows no maximum but a steady increase with pressure, approaching unity asymptotically at a pressure depending on the rate constant. The current IFM^+, however, has a pronounced maximum whose value depends on the rate constant, but whose position is apparently always at very nearly the same pressure.

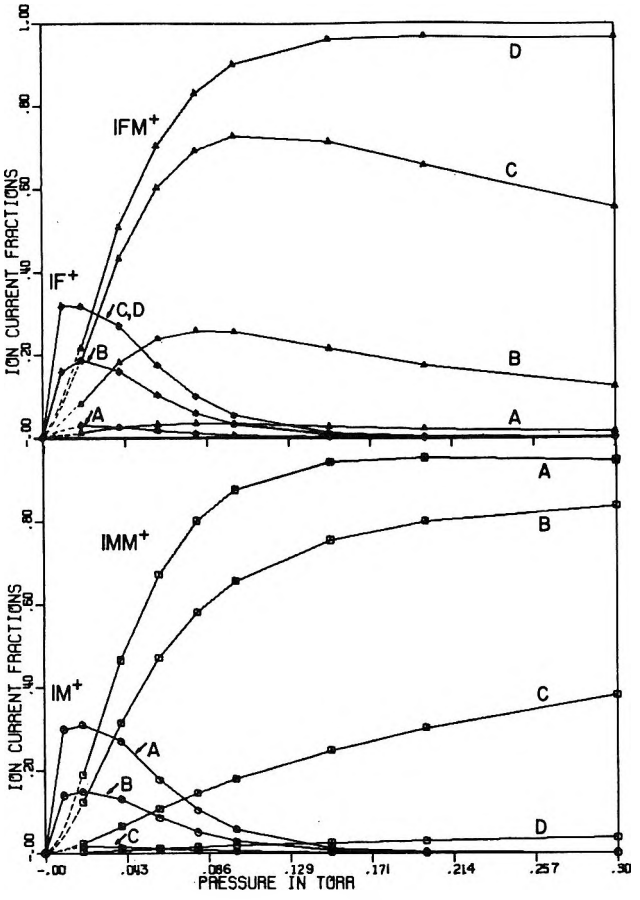

Figure 3. Dependence of secondary and unattenuated tertiary ion currents on the value of k_{IM}: A, $k_{IM} = 10^6$ sec^{-1}; B, $k_{IM} = 10^7$ sec^{-1}; C, $k_{IM} = 10^8$ sec^{-1}; D, $k_{IM} = 10^9$ sec^{-1}. All cross sections and conditions are listed in the text.

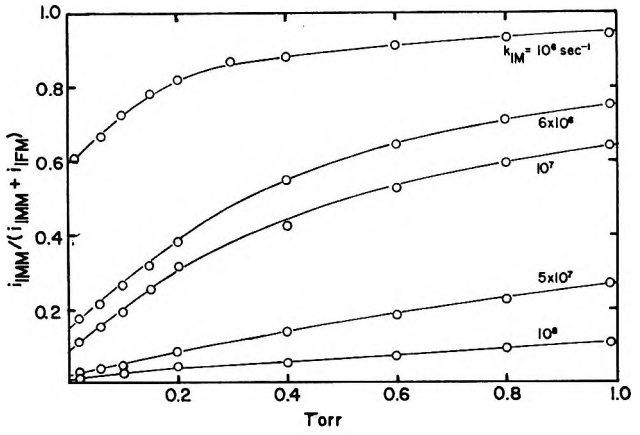

Figure 4. Variation with pressure of the fractional contribution of reactions of IF^+ and IM^+ to the higher order ion currents.

The maximum disappears when virtually all reactions occur *via* fragments ($k_{IM} = 10^8$ sec^{-1}).

The rate constant for dissociation of the secondary complex also has a considerable effect on the relative abundances of the secondary ion currents. However, it is important to recall here that the ion abundances

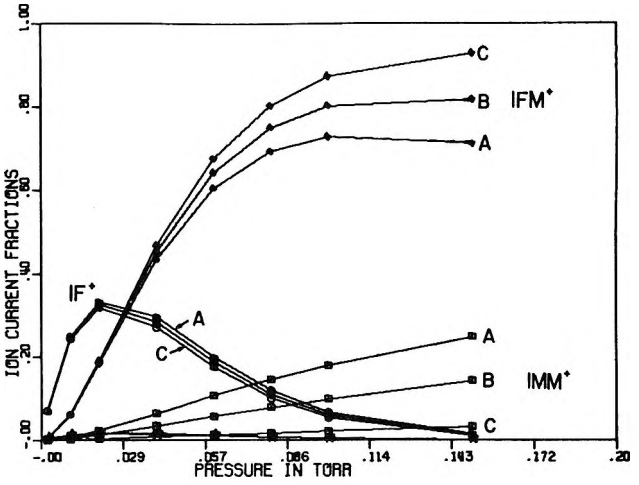

Figure 5. Dependence of secondary and unattenuated tertiary ion currents on the efficiency factor for reactions of IM^+ ($k_{IM} = 10^7$ sec^{-1}): A, $S = 1$; B, $S = 0.5$; C, $S = 0.1$.

calculated are those emerging from the exit slit, and ions of the type IM^+ can undergo fragmentation also before entering the analyzing magnetic field, and thus give rise to metastable peaks. The calculated secondary complex ion current IM^+ therefore includes the metastable ion abundances corresponding to its dissociation. Both will be negligible for rate constants in excess of *ca.* 10^7 sec^{-1}.

Variation of the efficiency of further reaction of the intermediate complex IM^+ by an order of magnitude does not show a considerable effect on the abundance of the secondary ion current for a rate constant of 10^7 sec^{-1} (Figure 5). This is to be expected since at low pressures where the observable current IF^+ is most abundant, IM^+ disappears chiefly by dissociation, and only at higher pressures does collisional removal from the system become significant. Lowering of the cross section σ_{IM} reflects itself much like an increase in the rate constant for these ions. It is important to note that translation into physical observabilities may be quite complicated in this example. Since we are only dealing with capturing collisions, complex formation must occur with collision efficiency and values of S less than unity correspond to return of the collision partners to their original states, almost certainly accompanied by some exchange of energy between internal and translational modes. It is therefore highly probable that collisions will at least reduce the rate constant for dissociation, or even lead to stabilization of the secondary complex. They would thus not change the probability of fragmentation from that calculated using the theoretical σ_{IM} since the intermediate IM^+ would be deactivated even when IMM^+ is produced with less than collision efficiency.

Variation of σ_{IF}, the efficiency of reaction of the secondary fragment ion, has a pronounced effect on the abundance of both the secondary and tertiary fragment

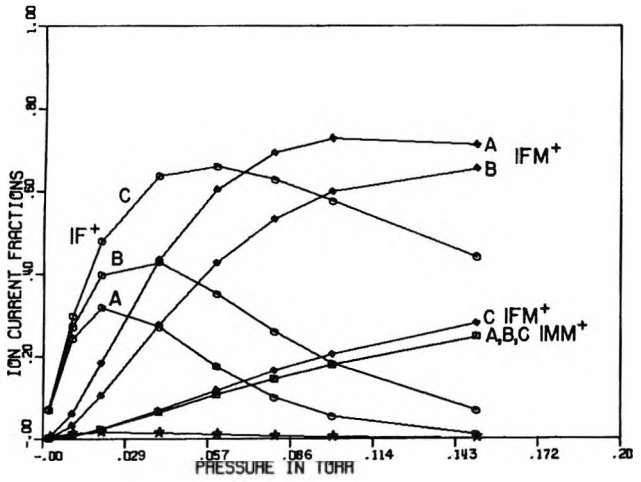

Figure 6. Dependence of secondary and unattenuated tertiary ion currents on the efficiency factor for reactions of IF^+ ($k_{IM} = 10^7$ sec^{-1}): A, $S = 1$; B, $S = 0.5$; C, $S = 0.1$.

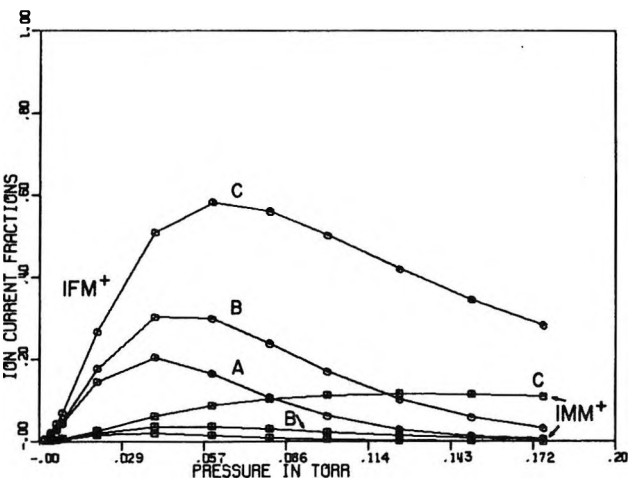

Figure 7. Variation of attenuated tertiary ion currents with pressure for several efficiencies of their future reactions: A, $S = 1.0$; B, $S = 0.5$; C, $S = 0.1$.

ions IF^+ and IFM^+ as expected. A decrease in rate constant for this reaction increases the highest value the secondary current I_{IF} can obtain and shifts the position of the maximum to higher pressures. At the same time the contribution of the fragment ion to tertiary ion formation is reduced, the maximum abundance of IFM^+ is lowered and shifted to higher values of pressure. Thus a decrease in σ_{IF} increases the proportion of I_{IMF^+} at all pressures as the behavior of the latter process remains constant and the removal of precursor complex ions increases (Figure 6).

The tertiary ions can also undergo further reactions. Calculated tertiary ion currents allowing for fourth-order processes are shown in Figure 7. When such reactions occur with collision efficiency, the tertiary ion current vanishes at about 0.15 torr. The value of the maximum in the observed abundance of IFM^+ will thus be indicative of both k_{IM} and σ_{IF}. We have not at this time allowed for disappearance of IFM^+ by unimolecular dissociation.

It is interesting to analyze now what one can deduce from the behavior of the primary and secondary ion currents alone. Observation of an ion current IF^+ in the absence of IM^+ and any metastable corresponding to its formation indicates a rate constant for dissociation of IM^+ greater than 10^7 sec^{-1}. From a semilogarithmic plot of the primary ion abundance *vs.* pressure one can assess σ_I, and from the initial portion of the secondary ion current one can obtain the fractional probability of formation of a given secondary. Assuming that the rate constant is 10^7 sec^{-1} or greater, the efficiency of reactions of IF^+ can be estimated by the value of the maximum in I_{IF} and the pressure at which it occurs. The actual cross section can be deduced with any degree of precision only when k_{diss} is so great (*ca.* 10^8 sec^{-1} or more) that attenuation of IF^+ by reaction of its precursor IM^+ is not in competition with fragmentation. A detailed comparison of calculated values with those reported for the ethylene,[4,18,20,21] acetylene,[23] and methanol[6,25] systems will be given elsewhere.

VI. Significance to Radiation Chemistry

The occasional practice of extrapolating mass spectrometric evidence over orders of magnitude in pressure to radiation chemical systems ignores the possible considerable lifetime of intermediate collision complexes. While direct evaluation of reactions of ion–molecule complexes by conventional mass spectrometry is limited to values of up to *ca.* 10^7 sec^{-1}, only *ca.* 1% of the intermediates will dissociate before collision at a pressure of *ca.* 400 torr, typical of many radiation chemical investigations. Care must therefore be exercised in the correlation of mass spectrometric and radiation chemical results, and overlap of pressures between studies using charged particle and neutral analysis is highly desirable.

Acknowledgment. This investigation was supported in its initial phases by the United States Atomic Energy Commission under Contract AT(40-1)-3606, and subsequently by the National Science Foundation. The IBM 7094 computer employed in these calculations was the facility of the Texas Medical Center, which is supported by U.S.P.H.S. Grant No. FR 00254. It was made available to us as a grantee of the Robert A. Welch Foundation of Texas. We are deeply grateful to these agencies for support of this investigation. We are also indebted to Mr. Michael Raines, undergraduate research participant from Midwestern University, Wichita Falls, Texas, for programming some of the quadrature procedures, and to the referee for his exceptionally careful and constructive comments.

The Gas-Phase Oxidation of Photochemically Generated Isopropyl Radicals[1]

by Graeme S. Milne and Colin Steel

Department of Chemistry, Brandeis University, Waltham, Massachusetts 02154 *(Received May 7, 1968)*

This study is concerned with the gas-phase reactions initiated by the reaction of O_2 with i-$C_3H_7\cdot$ radicals. The latter were generated by the photolysis of azoisopropane. The major reaction products are acetone, 2-propanol, propylene, and acetaldehyde. The effects of surface, light intensity, temperature, pressure of reactants and inert gases, and wavelength of irradiation have been investigated. After seasoning of the reaction vessel, the reactions appear to be homogeneous. The acetone–2-propanol yield depends upon (1) the extent of photolysis and (2) hydrogen donor concentration (*e.g.*, H_2O_2). The acetaldehyde yield depends upon the O_2 and H_2O_2 concentrations, while the propylene yield is very sensitive to inert gas pressure. Changing the temperature from 25 to $-27°$ and the light intensity by 1000-fold has only a minor effect on the products. Existing schemes do not explain the acetone to 2-propanol yields. Instead a new scheme is put forward to account for these products

$$C_3H_7O\cdot + O_2 \longrightarrow (CH_3)_2CO + HO_2\cdot \quad (8)$$

$$C_3H_7O\cdot + HO_2\cdot \longrightarrow (CH_3)_2CH(OH) + O_2 \quad (9)$$

$$C_3H_7O_2 + HO_2\cdot \longrightarrow (CH_3)_2CHOOH + O_2 \quad (10)$$

$$C_3H_7O\cdot + RH \longrightarrow (CH_3)_2CH(OH) + R\cdot \quad (13)$$

where RH is $(CH_3)_2CHOOH$ or any other hydrogen donor. Possible mechanisms are discussed for the formation of propylene and acetaldehyde, although no definitive reaction routes can be given at present for these compounds.

Introduction

There have been many studies of the reactions of photochemically generated alkyl radicals with oxygen. These include the photolyses of azo compounds,[2-4] ketones,[5,6] and alkyl iodides[7,8] in the presence of oxygen, and the mercury photosensitized oxidation of hydrocarbons.[9,10] Much of this work has been comprehensively reviewed by Hoare and Pearson,[11] while the complexities inherent in these studies have been outlined by Johnston and Cramarossa.[12] The products formed in these systems are similar but vary widely in importance from one system to another. As a result, many reaction mechanisms have been suggested, but as yet no one model provides any unity among the studies.

As part of our research in radical scavenging we became interested in this work. We therefore undertook a detailed study of one such system, the photooxidation of azoisopropane. The reasons for choosing azoisopropane were as follows. (1) The primary split into isopropyl radicals and nitrogen is clean and has no side effects. (2) The expected principal products, *viz.*, propylene, 2-propanol, and acetone are stable, both thermally and photochemically under our conditions, allowing the system to be studied as a function of time. In methyl radical systems, for example, HCHO is a product which undergoes subsequent reaction. (3) Although the photooxidation of azomethane,[13] azoethane,[4] and azoisobutane[3] had been reported, there had been no similar work on azoisopropane, and we hoped that our work would fill this gap.

We intended by studying this system over widely varying conditions of reactant pressures, added gases, light intensities, and percentage conversion, to test the current theories to see which of them was most applicable, and to see if they could be extended to explain related systems. In order to avoid thermal reactions with activation energies >4 kcal mol^{-1}, the experiments were carried out at room temperature and below.

Experimental Section

Materials. Azoisopropane was prepared[14] by the standard method and purified by preparative gas chromatography to remove the small amounts of re-

(1) Research sponsored by Directorate of Chemical Sciences, Air Force Office of Scientific Research, Grant 583-66, and by National Science Foundation, Grant GP-8463.

(2) P. L. Hanst and J. G. Calvert, *J. Phys. Chem.*, **63**, 71 (1959).

(3) S. S. Thomas and J. G. Calvert, *J. Amer. Chem. Soc.*, **84**, 4207 (1962).

(4) H. Cerfontain and K. O. Kutschke, *ibid.*, **84**, 4017 (1962).

(5) G. S. Pearson, *J. Phys. Chem.*, **67**, 1686 (1963).

(6) J. E. Jolley, *J. Amer. Chem. Soc.*, **79**, 1537 (1957).

(7) J. Heicklen and H. S. Johnston, *ibid.*, **84**, 4394 (1962).

(8) M. Barber, J. Farren, and J. W. Linnett, *Proc. Roy. Soc.*, **A274**, 306 (1963).

(9) J. A. Gray, *J. Chem. Soc.*, 3150 (1952).

(10) J. S. Watson and B. deB. Darwent, *J. Phys. Chem.*, **61**, 577 (1957).

(11) D. E. Hoare and G. S. Pearson, *Advan. Photochem.*, **3**, 83 (1964).

(12) H. S. Johnston and F. Cramarossa, *ibid.*, **4**, 1 (1965).

(13) M. Shahin and K. O. Kutschke, *J. Phys. Chem.*, **65**, 189 (1961).

(14) R. Renaud and L. C. Leitch, *Can. J. Chem.*, **32**, 545 (1954).

Table I: Effect of Conditioning Reaction Vessel[a]

	P_{azo}, μ	P_{O_2}, μ	$P_{C_3H_6}/P_{tot}$[b]	P_{CH_3CHO}/P_{tot}	$P_{C_2H_6CO}/P_{tot}$	$P_{C_3H_7OH}/P_{tot}$
Unseasoned	249	652	0.155	0.021	0.760	0.064
Seasoned	252	642	0.105	0.023	0.630	0.250

[a] The azoisopropane and oxygen pressures in this and subsequent tables are initial pressures. P_{total} does not include peroxide. [b] $P_{tot} = P_{C_3H_6} + P_{CH_3CHO} + P_{C_2H_6CO} + P_{C_3H_7OH}$.

Table II: Carbon Balance During Photolysis of Azoisopropane–Oxygen Mixtures[a]

Photolysis time, min	γ_{azo}[b]	$\gamma_{C_3H_6}$	γ_{CH_3CHO}[c]	$\gamma_{C_2H_6CO}$	$\gamma_{C_3H_6OH}$	$\gamma_{peroxide}$[d]	$\Sigma\gamma_M$
0	1506.0	0	0	0	0	0	1506
0.5	1418.4	3.6	3.4	28.1	8.9	(6.0)	1468
1.0	1457.4	6.3	6.0	49.3	18.3	(12.6)	1550
2.0	1339.8	13.9	14.1	104.9	43.0	(24.6)	1540
4.0	1219.2	25.4	23.9	204.9	92.1	(45.9)	1611
6.0	901.8	37.8	38.4	280.2	142.8	64.5	1466
9.0	816.6	48.9	47.1	383.1	192.0	85.5	1573
12.0	589.8	58.3	61.8	440.1	261.3	88.8	1500
21.0	359.4	78.0	75.3	637.5	402.0	(68.1)	1620
31.0	172.8	87.0	87.2	689.4	455.7	39.0	1531
44.0	66.6	90.6	90.6	717.0	480.0	...	
61.0	20.4	89.1	86.1	777.0	519.0	...	
74.0	9.6	90.0	91.5	734.4	522.9	...	
						$(\Sigma\gamma_M)_{av}$ =	1539

[a] The initial oxygen pressure was 1200 μ. [b] γ_M = pressure of material M (microns) × number of carbon atoms in M; for example, the initial pressure of azoisopropane, a C_6 hydrocarbon, was 251 μ. [c] Acetaldehyde is treated as if it were a C_3 hydrocarbon; see text. [d] Peroxide analysis was carried out only at times 0, 6.0, 9.0, and 31.0 min. The other values are estimates from the graph of peroxide pressure *vs.* time.

maining impurities. The H_2O_2 was 90% (F.M.C. Corp.). The other chemicals employed were standard laboratory grade reagents and gases.

Reaction Vessels. The smallest surface-to-volume reaction vessel consisted of a 2-l. Pyrex bulb, surface-to-volume = 0.38 cm^{-1}, and the largest surface-to-volume vessel was a coil of 4-mm i.d. Pyrex tubing, surface-to-volume = 10.5 cm^{-1}. This latter vessel had to be conditioned by carrying out several photolyses (Table I), but after conditioning all vessels yielded the same results. We therefore concluded that surface effects were of minor importance. Most of the runs discussed in this paper were carried out in the 2-l. reaction vessel.

Procedure. Reaction mixtures and calibration mixtures for gas chromatography were made up on a conventional greaseless high-vacuum line employing a quartz spiral manometer (Texas Instruments) as the pressure gauge. The initial photochemical runs were carried out using a high-pressure mercury arc and a monochromator. After establishing that there was no wavelength effect using 334- and 365-mμ irradiation (Figures 6 and 7), we employed a photochemical reactor equipped with Sylvania F8T5/BLB Blacklight lamps. These have a continuous emission in the region 305–425 mμ with $\lambda_{em,max}$ 352 mμ. This closely coincides with the n,π^* absorption band of gaseous azoisopropane, λ_{max} 355 mμ, ϵ_{max} 9.0 ± 1.0 M^{-1} cm^{-1}. Unless specifically mentioned, it may be assumed that the light source was Blacklight lamps. Most analyses were carried out using a gas sampling system and a flame ionization gas chromatograph equipped with a 25-ft Ucon 50HB-280X Polar column. This eluted the reactant and products in the order propylene, acetaldehyde, acetone, azoisopropane, 2-propanol. The identity of these compounds was also checked by their retention times on other columns (Poropak Q, Silicone Oil SF-96, 1% SF-96 on alumina) and by mass spectrometry and infrared spectroscopy.

Somewhere along the reaction pathway from isopropyl radicals to acetaldehyde, a carbon–carbon bond must be broken. We have as yet been unable to determine the identity of the product formed from this C_1 fragment. A small peak appears on the gas chromatograph at the correct retention time for methanol, but not in large enough quantities to account for all of the acetaldehyde formed. It is of course possible that most of the C_1 product is formaldehyde which is being retained on the gas chromatograph column. For this reason in the carbon balance (see Table II) acetaldehyde is treated as a C_3 compound.

The concentration of H_2O_2 was determined by reduction of iodide to iodine, while general peroxide analyses

were carried out spectrophotometrically with ferrous thiocyanate using the method of Egerton, *et al.*[15] In one case we checked their data for H_2O_2 and got agreement within 3%.

The H_2O_2 added to the reaction mixtures was not pure, but condensation and analysis of a sample which had been vaporized into a 2-l. bulb and allowed to stand for 4 hr showed that 80 to 90% of the sample consisted of peroxide. The H_2O_2 pressures reported in the Results and Discussion section are therefore approximately 0.9 H_2O_2 and 0.1 H_2O.

Light Intensity. In these experiments the purpose of varying the light intensity was to vary the rate of photolysis, thus varying the rate of isopropyl formation and consequently the steady-state concentrations of the intermediates. Because a broad emission source was used and because ϵ for azoisopropane varies considerably over this region, direct estimates of the number of incident quanta per cm^2 per second are not too meaningful. Instead azoisopropane photolysis at low pressures was used as a relative actinometer[16] and intensities in Figures 6 and 7 are given in arbitrary units; 50 units on this scale corresponds to a photolysis rate of azoisopropane of 1.3×10^{13} molecules/cc sec when the azoisopropane concentration is 1.0×10^{16} molecules/cc. The rate data shown in Figure 1 may also be converted into quantum yields as follows. From Figure 5 it will be noticed that the rates of azo consumption both in the presence and in the absence of oxygen are identical. Quantum yields for the latter process have been determined;[16] hence quantum yields for the products can immediately be determined from Table II.

Results and Discussion

The Formation of Acetone and 2-Propanol. The major products in the photochemical decomposition of azoisopropane–oxygen mixtures are acetone and 2-propanol (Table II). By analogy with previous work, two schemes for their formation might be suggested.

Scheme 1[7,17]

$$C_3H_7N_2C_3H_7 \xrightarrow{h\nu} 2C_3H_7\cdot + N_2 \quad (1)$$

$$C_3H_7\cdot + O_2 \longrightarrow C_3H_7O_2\cdot \quad (2)$$

$$2C_3H_7O_2\cdot \longrightarrow 2C_3H_7O\cdot + O_2 \quad (3)$$

$$2C_3H_7O\cdot \longrightarrow (CH_3)_2CO + (CH_3)_2CH(OH) \quad (4)$$

An alternative to reaction 3, namely, $C_3H_7O_2\cdot + O_2 \rightarrow C_3H_7O\cdot + O_3\cdot$, has been proposed[2] but can be ruled out in this case, since it is 30 kcal endothermic.[18]

Scheme 2[8]

Steps (1) and (2) followed by

$$C_3H_7O_2\cdot \longrightarrow (CH_3)_2CO + \cdot OH \quad (5)$$

$$C_3H_7O_2\cdot + \cdot OH \longrightarrow (CH_3)_2CH(OH) + O_2 \quad (6)$$

Scheme 1 is attractive in that it accounts most simply for acetone and 2-propanol; however, there are other potential routes to these compounds. One of the main sources of evidence that there are both RO· and ROO· radicals in such systems is the work of Bartlett and Guaraldi.[19] Scheme 2 was suggested mainly because on the addition of HI to the system $CH_3\cdot + O_2$, Linnett, *et al.*,[8] did not obtain the expected increase in methanol formation arguing against, they said, a significant concentration of methoxy radicals. Our experimental results, however, are not completely consistent with either of these schemes and although they may be involved they are probably not the major routes to acetone and 2-propanol.

In Figure 1 we show the instantaneous rates of formation of acetone and of 2-propanol. It will be noticed that it is only in the later stages of the reaction that the ratio of the rates of formation of acetone to 2-propanol approaches unity. Initially, the ratio is greater than 1. Indeed in a fresh and unseasoned vessel, the ratio can be as high as 12 [Table I]. Scheme 1 requires the acetone to 2-propanol ratio to remain at unity throughout the course of the reaction.

Scheme 2 requires the ratio to be ≥ 1, depending on the fraction of ·OH radicals which is consumed by step 6, as is indeed found. However, the scheme does not explain why the ratio varies during the course of reaction. Moreover, in the presence of hydrogen donors such as HI or H_2O_2 the ·OH radical would be scavenged preventing 2-propanol formation by step 6.

The data embodied in Figure 1 and Tables II and III are consistent with the scheme

$$\longrightarrow C_3H_7O\cdot \quad (7)$$

$$C_3H_7O\cdot + O_2 \longrightarrow (CH_3)_2CO + HO_2 \quad (8)$$

$$C_3H_7O\cdot + HO_2 \longrightarrow (CH_3)_2CH(OH) + O_2 \quad (9)$$

$$C_3H_7O_2\cdot + HO_2 \longrightarrow (CH_3)_2CHOOH + O_2 \quad (10)$$

$$C_3H_7O\cdot + (CH_3)_2CHOOH \longrightarrow (CH_3)_2CH(OH) + C_3H_7O_2\cdot \quad (11)$$

Reaction 7 is some general sequence leading to alkoxy radicals; we shall discuss it in greater detail below.

A steady-state treatment of (1), (2), (7)–(11) yields

$$\frac{d[C_2H_6CO]}{dt} = \frac{d[C_3H_7OH]}{dt} + \frac{d[C_3H_7OOH]}{dt} = k_1[C_3H_7N_2C_3H_7] \quad (12)$$

(15) A. C. Egerton, A. J. Everett, G. J. Minkoff, S. Rudrukanchana, and K. C. Salooja, *Anal. Chim. Acta*, **10**, 422 (1954).

(16) R. H. Riem and K. O. Kutschke, *Can. J. Chem.*, **38**, 2332 (1960).

(17) J. H. Raley, L. M. Porter, F. F. Rust, and W. E. Vaughan, *J. Amer. Chem. Soc.*, **73**, 15 (1951).

(18) Heats of formation used in this paper are taken from "Photochemistry," by J. G. Calvert and J. N. Pitts, Jr., John Wiley and Sons, Inc., New York, N. Y., 1966, pp 815–823, and from G. E. Coates and L. E. Sutton, *J. Chem. Soc.*, 1187 (1948).

(19) P. D. Bartlett and G. Guaraldi, *J. Amer. Chem. Soc.*, **89**, 4799 (1967).

Table III: Effect of Oxygen Concentration on Product Ratios in Photolysis of Azoisopropane–Oxygen Mixtures

P_{azo}, μ	P_{O_2}, μ	$P_{C_3H_6}/P_{tot}$	P_{CH_3CHO}/P_{tot}	$P_{C_2H_5CO}/P_{tot}$	$P_{C_3H_7OH}/P_{tot}$	P_{tot}, μ[a]
264	48	0.113	0.268	0.451	0.167	28.6
251	82	0.012	0.169	0.527	0.216	24.7
254	209	0.120	0.092	0.528	0.260	14.8
255	783	0.091	0.046	0.640	0.230	29.1
253	4,800	0.058	0.013	0.710	0.220	28.8
253	40,100	0.033	0.004	0.760	0.210	21.4
251	137,000	0.031	0	0.810	0.150	14.5
246	382,000	0.028	0	0.810	0.170	9.7

[a] $P_{tot} = P_{C_3H_6} + P_{CH_3CHO} + P_{C_2H_5CO} + P_{C_3H_7OH}$; this does not include peroxide.

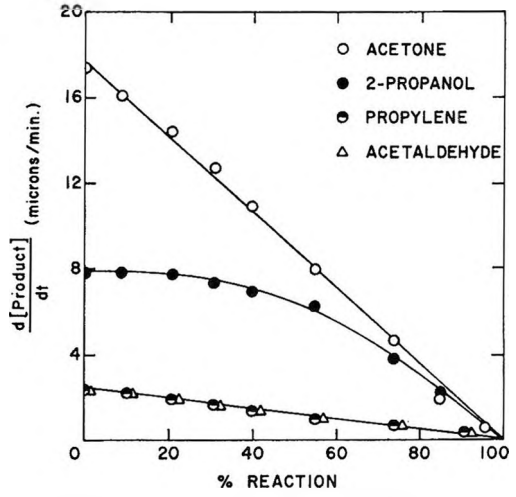

Figure 1. Rates of formation of products in the photolysis of azoisopropane–oxygen mixtures. The initial azoisopropane and oxygen pressures were 250 and 1200 μ, respectively. The rate of disappearance of azoisopropane was strictly first order (see Figure 5).

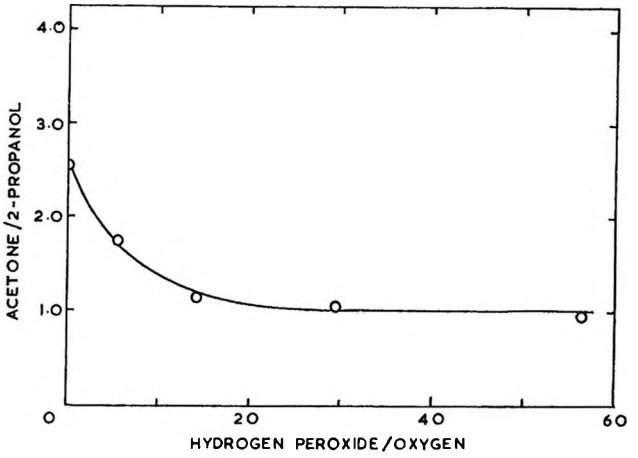

Figure 2. Effect of hydrogen peroxide on the relative yields of acetone and 2-propanol. In all cases $P_{azo} = 250\ \mu$, $P_{O_2} = 45\ \mu$, and $p_{H_2O_2} + p_{N_2} = 2700\ \mu$.

Therefore, contrary to what one might expect from reaction 8, the acetone yield should be insensitive to oxygen concentration (Table III). For every molecule of peroxide consumed in reaction 11, one molecule of 2-propanol is formed. Therefore although the acetone to 2-propanol ratio varies during the course of reaction (Figure 1), the ratio acetone/(2-propanol + peroxide) should remain constant. From the data given in Table II it will be seen that this ratio has a value of about 1:35 throughout the reaction. The fact that this ratio is not unity may mean that there is some other acetone-forming reaction or that some of the $\cdot HO_2$ radicals are removed by reactions other than (9) and (10).

Reactions 9 and 10 together account for the initial formation of 2-propanol and peroxide. However, as peroxide builds up, it acts as a hydrogen donor for alkoxy radicals,[20] reaction 11, and so goes through a maximum, (Table II). Recent work has shown that methyl radicals abstract a hydrogen atom from tertiary butyl hydroperoxide with an activation energy of only 2 to 3 kcal mol.[21] In general, alkoxy radicals undergo metathetical reactions more readily than do the corresponding alkyl radicals;[22] reaction 11 may therefore be expected to be a facile process.

If we add some hydrogen donor to the system, then we might expect the reaction

$$C_3H_7O\cdot + HR \longrightarrow (CH_3)_2CH(OH) + R\cdot \quad (13)$$

Hydrogen peroxide was chosen, because in this case $R\cdot = HO_2\cdot$; this species, itself a good hydrogen donor, should not complicate the analysis. Of course, H_2O_2 would be expected to be a less facile donor than either $(CH_3)_2CHOOH$ or $HO_2\cdot$. In the first place, we see from Table IV and Figure 2 that the addition of H_2O_2 does indeed increase the rate of 2-propanol formation relative to acetone formation. However, in these systems, because of the H_2O_2, we were unable to analyze for $(CH_3)_2CHOOH$ directly. However, we may equate the carbon defect shown in Table IV with $(CH_3)_2CHOOH$. Because (13) can now compete effectively with (11),

(20) E. R. Bell, J. H. Raley, F. F. Rust, F. H. Seubold, and W. E. Vaughn, *Discussions Faraday Soc.*, 10, 242 (1951).

(21) Private communication from K. O. Kutschke.

(22) A. F. Trotman-Dickenson and G. S. Milne, "Tables of Bimolecular Gas Reactions," N.S.R.D.S.-N.B.S. Vol. 9, National Bureau of Standards, 1967.

Table IV: Effect of Hydrogen Peroxide in Photolysis of Azoisopropane–Oxygen Mixtures

Photolysis time, min	γ_{azo}[a]	$\gamma_{C_3H_6}$	γ_{CH_3CHO}	$\gamma_{C_2H_6CO}$	$\gamma_{C_3H_6OH}$	$\Sigma\gamma_M$
0	1212.0	0	0	0	0	1212
3	1008.0	4.4	Trace	66.9	63.0	1142
6	847.2	7.9	Trace	126.0	118.8	1100
12	579.6	13.4	Trace	211.5	214.8	1019
20	369.6	18.9	Trace	305.7	321.9	1016
30	191.4	21.3	Trace	350.4	358.8	923

[a] For definition of γ, see Table II. The initial pressures of azoisopropane, oxygen, and hydrogen peroxide were, respectively, 202, 545, and 2290 μ.

the carbon defect, *i.e.*, $(CH_3)_2CHOOH$, continues to build up throughout the reaction.

A second important piece of information can be obtained from the H_2O_2 addition. If the alkoxy radical formed in reaction 7 arose simply from a reaction such as (3), then the ratio of acetone formation to 2-propanol formation should decrease continuously as we add hydrogen donor. This is not so. Figure 2 shows that a limit of 1.0 is approached in the presence of hydrogen donor. It would therefore appear as if alkoxy radicals and acetone molecules are formed in the ratio 1:1. In a formal sense therefore, we write

$$2C_3H_7O_2\cdot \longrightarrow (CH_3)_2CO + C_3H_7O\cdot + HO_2\cdot \quad (7)$$

Although this reaction is 39.8 kcal mol^{-1} exothermic, more so than the commonly accepted step 3, in fact, it appears too complex for comfort. At present by writing it we simply imply routes, possibly involving reactions such as (3) and (5), leading to acetone and alkoxy in the ratio 1:1. It might be mentioned at this point that if $C_3H_7O\cdot$ radicals were formed by a reaction such as (7), they still could not react mainly by (4) since this would again require a constant ratio of acetone to 2-propanol.

Formation of Acetaldehyde. Although under "normal" conditions acetaldehyde is a minor product, at low oxygen concentrations its yield increases rapidly (Figure 3). These oxygen pressures are still sufficiently large, however, that there is no indication of any direct isopropyl radical reactions; there is, for example, no formation of diisopropyl. Addition of hydrogen peroxide also decreases the acetaldehyde yield (Table IV). The precursor of acetaldehyde must have a relatively long lifetime since it can be intercepted by relatively small concentrations of peroxide and oxygen. If the acetaldehyde were formed by the decomposition of a vibrationally excited molecule, its yield should therefore be very subject to inert gas pressure, while as can be seen from Figure 4, the yield is within experimental error pressure independent.

At first sight, the most attractive route for the formation of acetaldehyde would appear to be

$$C_3H_7O\cdot \longrightarrow CH_3CHO + CH_3\cdot \quad (14)$$

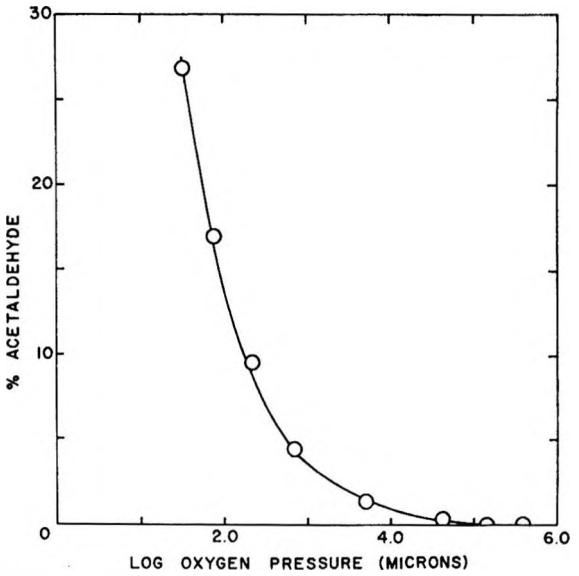

Figure 3. Acetaldehyde yield, *viz.*, $P_{CH_3CHO}/(P_{C_3H_6} + P_{CH_3CHO} + P_{C_2H_6CO} + P_{C_3H_7OH})$, as a function of the oxygen pressure. $P_{azo} = (255 \pm 10)\ \mu$ in all cases.

This unimolecular reaction would then be in competition with reactions 8, 9, and 13, with (8) becoming dominant at high oxygen pressures, and (13) dominant at high peroxide concentration.

However, lifetime calculations for thermally equilibrated $C_3H_7O\cdot$ radicals based on the data of Phillips, *et al.*,[23] yield quite unreasonable results (5.5 sec). A second stumbling block to this scheme is the lack of temperature dependence of the CH_3CHO yield. A 52° change in temperature should reduce the CH_3CHO yield by about 100-fold while in fact the yield was almost temperature independent over the range −27 to +25°. At present we cannot visualize any reasonable scheme consistent with all the experimental factors. It might be mentioned here that over this temperature range there was practically no difference in any of the product ratios.

The Formation of Propylene. Most investigators studying the reactions of alkyl radicals with oxygen

(23) D. L. Cox, R. A. Livermore, and L. Phillips, *J. Chem. Soc., B*, 245 (1966).

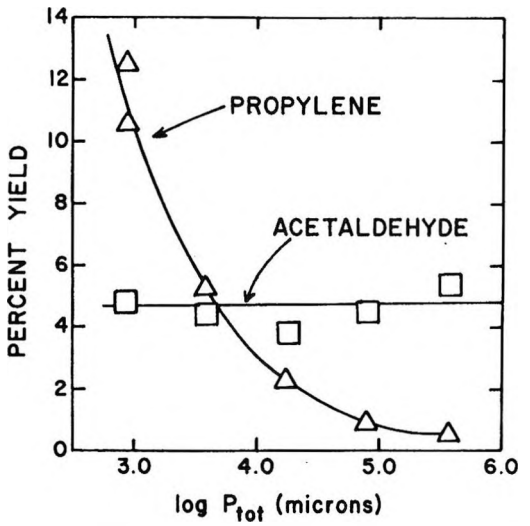

Figure 4. Effect of pressure on the yields of propylene and acetaldehyde. P_{tot} is made up of 250 μ of azoisopropane, 650 μ of oxygen, and varying amounts of nitrogen.

have obtained as a product the corresponding olefins, *viz.* ethylene from ethyl radical, etc. The azoisopropane–oxygen system is no exception in that propylene is a significant product. Under the conditions in which the latter is formed there is no trace of propane or diisopropyl; that is, second-order alkyl radical reactions can be ruled out as the source of propylene. In studying the flash photolysis of azoethane–oxygen mixtures, Dingledy and Calvert[24] proposed the reaction

$$C_2H_5\cdot^* + O_2 \longrightarrow C_2H_4 + HO_2\cdot \quad (15)$$

The equivalent reaction

$$C_3H_7\cdot^* + O_2 \longrightarrow C_3H_6 + HO_2\cdot \quad (16)$$

cannot be invoked under our conditions to account for the propylene formation, since the propylene yield decreases markedly as the oxygen pressure increases (Table III). There is also no evidence for the process

$$C_3H_7\cdot^* \longrightarrow C_3H_6 + H\cdot \quad (17)$$

under our conditions since the ratio C_3H_6/C_3H_8 for the photolysis of azoisopropene in the absence of oxygen remained at 1.0 over the temperature range -25 to $+25°$. In their study of the azoethane–oxygen system, Cerfontain and Kutschke[4] suggested that C_2H_4 arose from the sequence

$$C_2H_5O\cdot + C_2H_5N_2C_2H_5 \longrightarrow C_2H_5OH + \cdot C_2H_4N_2C_2H_5 \quad (18)$$

$$O_2 + \cdot C_2H_4N_2C_2H_5 \longrightarrow C_2H_4 + N_2 + C_2H_5O_2\cdot \quad (19)$$

where reaction 19 accounted for less than 5% of the $C_2H_4N_2C_2H_5$ radicals generated in (18) when the reaction was carried out at room temperature. In our system the equivalent reaction would be

$$C_2H_7O\cdot + C_3H_6N_2C_3H_7 \longrightarrow C_3H_7OH + \cdot C_3H_6N_2C_3H_7 \quad (20)$$

$$O_2 + \cdot C_3H_6N_2C_3H_6 \longrightarrow C_3H_6 + N_2 + C_3H_7O_2 \quad (21)$$

From the rather limited amount of information currently available for the metathetical reactions of alkoxy radicals, we might expect the activation energy for the attack of isopropoxy radical on azoisopropane to be about 4 kcal mol^{-1}. The activation energies for other alkoxy radicals reactions such as (4), (8), and (9) are probably lower and so we might expect a temperature dependence in the yield of C_3H_6. The experimental facts, however, are that this yield is almost invariant over the range -27 to 25°.

Reactions 20 and 21 also require that the rate of azo consumption in the presence of oxygen should be significantly greater than in its absence. Within experimental error, however, we could detect no change (Figure 5). Moreover, the propylene yields are quite sensitive to inert gas pressure (Figure 4 and Table V) and this fact is not explained by reactions 20 and 21. Finally, we must notice that the propylene yields are remarkably insensitive to intensity effects over a wide range (Figures 6 and 7) whereas there are small but significant variations in the yields of acetaldehyde, 2-propanol, and acetone. This would suggest that propylene is formed early in the reaction sequence before the precursor of the oxygen-containing compounds. The process

$$C_3H_7\cdot + O_2 \rightarrow C_3H_7O_2\cdot^* \xrightarrow{+X} \begin{cases} C_3H_7O_2\cdot & (22) \\ C_3H_6 + HO_2\cdot & (23) \end{cases}$$

immediately comes to mind since it would have the correct characteristics, *viz.*, decrease in propylene yield with total pressure, including oxygen, and lack of temperature and intensity dependence. Reaction 23 is 20.8 kcal mol^{-1} endothermic while the process forming $C_3H_7O_2$ is only 28.3 kcal mol^{-1} exothermic. A simple calculation using the formula[25]

$$k(E) = A\left(\frac{E - E_0 + a^+E_z^+}{E + aE_z}\right)^{n-1}$$

with the values $A = 10^{14}$ sec^{-1}, $E = 28.3$ kcal mol^{-1}, $E_0 = 21.0$ kcal mol^{-1}, $a^+ = 0.85$, $a = 0.93$, $E_z^+ = 99$ kcal mol^{-1}, and $E_z = 102$ kcal mol^{-1} shows that the lifetime of $C_3H_7O_2\cdot^*$ could be as low as 10^{-10} sec, although it would be expected to be greater because E_0 would be expected to be larger than the chosen value. Process 23 cannot therefore at present be ruled out.

(24) D. P. Dingledy and J. G. Calvert, *J. Amer. Chem. Soc.*, **85**, 856 (1963).

(25) D. W. Setser and B. S. Rabinovitch, *Can. J. Chem.*, **40**, 1425 (1962).

Table V: Effect of Inert Gas Pressures in the Photolysis of Azoisopropane–Oxygen Mixtures

P_{azo}, μ	P_{O_2}, μ	P_{N_2}, μ	$P_{C_3H_6}$, μ	P_{CH_3CHO}, μ	$P_{C_2H_5CO}$, μ	$P_{C_2H_5OH}$, μ
254	656	0	2.40	1.09	14.38	4.80
249	632	2,900	1.15	0.98	14.46	5.49
257	658	16,900	0.40	0.70	13.10	4.61
252	649	70,000	0.14	0.67	10.19	3.97
251	650	367,000	0.04	0.52	5.69	2.37

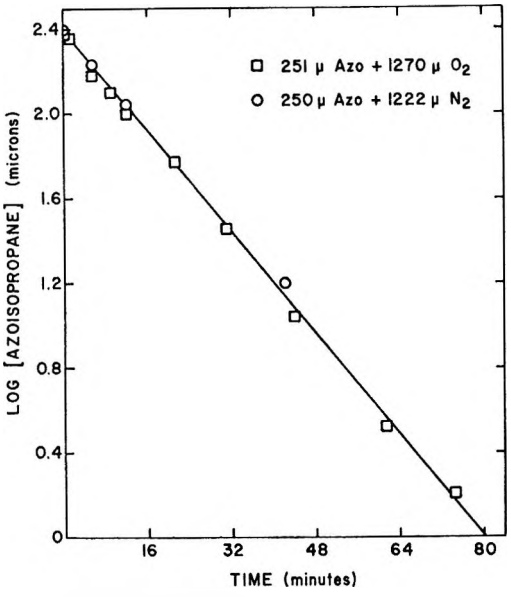

Figure 5. Rate of azoisopropane consumption in the presence and absence of O_2. The light intensities were the same in both cases. The addition of N_2 is necessary because the quantum yield of azoisopropane decomposition is pressure dependent.

Conclusions and Summary

Any explanation of the experimental results must explain the following: (a) the change in the ratio acetone/2-propanol with per cent photolysis; (b) the effect of addition of H_2O_2 which results in an acetone/2-propanol ratio of unity; (c) the negligible effect of temperature on the products; (d) the strong inert gas effect on the propylene yield; (e) the strong oxygen dependence of the yields of acetaldehyde and propylene.

The lack of constancy of the acetone to 2-propanol ratio argues against Schemes 1 and 2. Furthermore, reaction 5 of Scheme 2 would be expected to show some temperature dependence while we should expect that the ·OH radicals which are generated in this reaction would be scavenged by H_2O_2 thus decreasing the 2-propanol yield. Therefore under our conditions it seems unlikely that either Scheme 1 or 2 is of major importance.

Result (a) is interpreted as a competition between reactions 8 and 11. As the hydroperoxide concentration builds up in (10), it is removed by (11); (b) can be seen as the result of reaction 13. At sufficiently high H_2O_2 concentrations all the $C_3H_7O\cdot$ radicals are scavenged to produce 2-propanol. The fact that the acetone/2-propanol ratio does not fall below unity is "explained" by (7). The small effect of temperature can result from the fact that all the reactions have nearly zero activation energy. The pressure dependence in the propylene yield would result if a vibrationally excited species such as $C_3H_7O_2\cdot$ * were involved as the precursor of C_3H_6.

It will be noticed from eq 12 that the ratio acetone/(2-propanol + peroxide) should be independent of intensity. Furthermore, the ratio of the initial rates of formation of peroxide to 2-propanol should depend upon the ratio $C_7H_7O_2\cdot/C_3H_7O$. The steady-state expression for this ratio is complex but to a first approximation it is intensity independent. Thus the ratio acetone/2-propanol might also be expected to be insensitive to intensity as it is (see Figures 6 and 7). We may also note that the data in Figure 5 show that the quantum yields of azo consumption both in the presence and absence of oxygen are identical and remain constant throughout the course of the reaction.

This reaction scheme also explains some of the results found in other systems. Consider first the Hg-photosensitized oxidations of alkanes. The evidence from several studies[9,10] is quite conclusive that the principal product is the hydroperoxide. There is agreement that

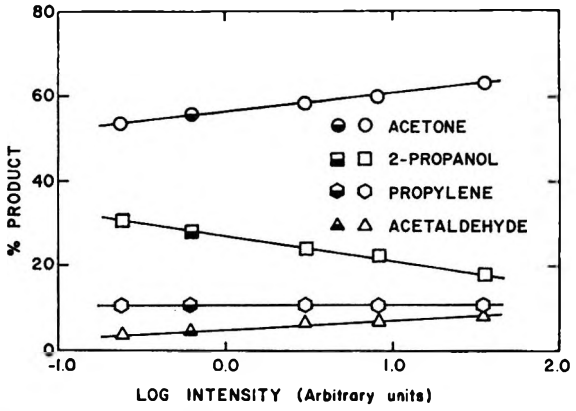

Figure 6. Product yields as a function of intensity at high oxygen pressures. See Experimental Section for the value of intensity units. Acetone yield = $P_{C_2H_6CO}/(P_{C_3H_6} + P_{CH_3CHO} + P_{C_2H_7OH} + P_{C_2H_4CO})$, etc. The open points are "Black light" runs, and the points shaded in the lower half are 365-mμ runs. In all cases $P_{azo} \sim 250$ μ and $P_{O_2} \sim 650$ μ. All runs were carried out to 4% photolysis.

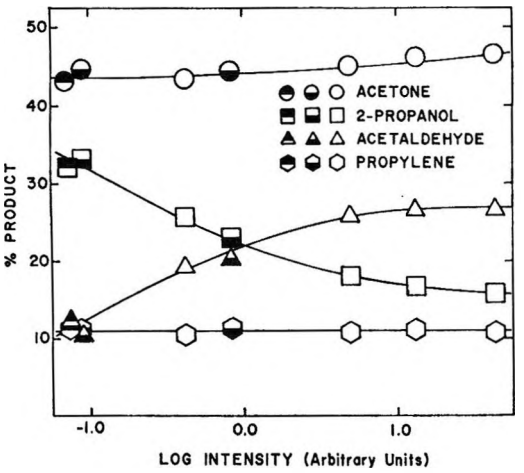

Figure 7. Product yields as a function of intensity at low oxygen pressures. See Experimental Section for the units of intensity. The open points are "Black light" runs, points shaded in the lower half 365-mμ runs, points shaded in the upper half 334-mμ runs. In all cases $P_{azo} \sim 265$ μ and $P_{O_2} \sim 45$ μ. Runs were carried out to 5% completion.

the primary step results in formation of alkyl radicals and hydroperoxy radicals. For example

$$C_2H_6 + \begin{cases} Hg^* \\ O_2^* \end{cases} \longrightarrow C_2H_5\cdot + HO_2\cdot$$

$$C_2H_5\cdot + O_2 \longrightarrow C_2H_5O_2\cdot$$

The peroxy radicals are thus produced in the presence of a high concentration of $HO_2\cdot$ radicals which react as

$$C_2H_5O_2\cdot + HO_2\cdot \longrightarrow C_2H_5O_2H + O_2$$

Thus any oxidation system which contains a high concentration of readily available hydrogen (in the form of $HO_2\cdot$ radicals—or perhaps HI) will be intercepted at the peroxy radical stage resulting in a high yield of hydroperoxide. That this is so can be seen from Table IV where the mass defect ($\equiv (CH_3)_2CHOOH$) accounts for between 30 and 40% of the total products.

In other photochemically initiated systems such as the photolyses of ketones, alkyl iodides, and azo compounds, the $HO_2\cdot$ radicals are produced simultaneously with and as a result of the formation of alkoxy radicals, *e.g.*, reactions such as (7) and (8). The alkoxy radicals compete efficiently with peroxy radicals for the labile hydrogen and result in considerably reduced yields of hydroperoxide. Indeed the evidence from the present system shows that the hydroperoxide itself is attacked by alkoxy radicals even at room temperature; its concentration as a result never rises above 5% of the products in agreement with the work of Calvert, *et al.*,[26] on the photooxidations of $CH_3N_2CH_3$ and $C_2H_5N_2C_2H_5$.

(26) N. R. Subbaratnam and J. G. Calvert, "Chemical Reactions in the Lower and Upper Atmosphere," Interscience Publishers, Inc., New York, N. Y., 1961, p 109.

A Pulse-Radiolysis System for the Observation of Short-Lived Transients

by M. J. Bronskill[1] and J. W. Hunt

Ontario Cancer Institute and Department of Medical Biophysics, University of Toronto, Toronto, Ontario, Canada
(Received May 7, 1968)

Several interesting problems in the field of radiation chemistry occur in the time interval from 0.01 to 1 nsec following the passage of an ionizing particle. Existing pulse-radiolysis systems are unable to investigate these problems because their time resolution is limited to about 1 nsec. In this paper a new technique is described which is theoretically capable of observing transient absorption signals as short-lived as 0.02 nsec. This technique will use the Čerenkov light produced by the 30-MeV electron beam from the Toronto linear accelerator to detect the absorption of transient species produced by the fine-structure pulses (0.01 nsec wide) of the electron beam. A stroboscopic effect is created by varying the phase difference between the Čerenkov light flashes and the fine-structure electron pulses. With this technique a conventional slow detection system can be used to achieve a time resolution of 0.02 nsec. Experimental observations indicate that such a detection system is completely practical, although no short-lived transients have yet been observed.

Introduction

The absence of a suitable short-radiation pulse and a high-speed optical detector limits present pulse-radiolysis systems to a time resolution of about 1 nsec. Nevertheless, the direct observation of events taking place in the "physiochemical" stage of radiolysis (from 10^{-5} to 10^{-1} nsec) may be attainable with a slow system using presently available radiation sources and optical detectors. Such controversial problems as solvated electron formation,[2-4] ion recombination,[5,6] "spur" reactions,[2,7,8] and triplet excited state formation,[9] can be readily studied with such a system.

The study of the radiolysis of dilute aqueous solutions does not provide a completely satisfactory model for the interaction of ionizing radiation with living cells. In living cells a high solute concentration is present (a cell is about 75% water) and hence direct radiation effects become important.[10] Under cellular conditions the solute–radical reactions start to occur at 0.01 nsec. Such reactions can only be studied by pulse-radiolysis techniques if a system having a greatly improved time resolution is devised. In order to attack these problems, a system having a theoretical time resolution of 0.02 nsec has been conceived and constructed.

Stroboscopic Pulse Radiolysis System

A. Radiation Source. The "new breed" of linear accelerators (linacs) available for pulse-radiolysis studies are capable of producing short, intense bursts of high-energy electrons. The important parameters of the linac recently installed in the Physics Department at the University of Toronto are given in Table I. From this machine, a beam current of over 0.5 A has been obtained in a 30-nsec pulse which is focused by quadrupole lenses into a spot less than 4 mm in diameter.

Such a 30-nsec pulse is not actually a continuous stream of electrons but consists of a train of 100 fine-structure pulses spaced 0.35 nsec apart, the period of the accelerating microwave power (Figure 1). The width of these fine-structure pulses is determined by the phase spread of the electron beam on the accelerating wave; this spread is less than 20° for the Toronto linac, giving a pulse width of less than 0.02 nsec. To maintain an average current of 1 A in the 30-nsec pulse, an instantaneous current of over 15 A must be present in the fine-structure pulse.

Table I: University of Toronto Linac Parameters (as Used for Stroboscopic Pulse Radiolysis)

Manufacturer	Vickers-Armstrong Ltd., Swindson, England
Beam energy	>30 MeV
Beam current	1 A (30-nsec pulse) ~30 A (fine-structure pulse)
Accelerating microwave frequency	2.86×10^9 Hz
Time interval between fine-structure pulses	0.35 nsec
Beam diameter (minimum)	<4 mm

(1) Research Student, National Cancer Institute of Canada.

(2) J. W. Hunt and J. K. Thomas, *Radiation Res.*, **32**, 149 (1967).

(3) D. Schulte-Frohlinde, Proceedings of the Third International Congress of Radiation Research, G. Silini, Ed., North-Holland Publishing Co., Amsterdam, 1967, p 251.

(4) V. N. Shubin, V. A. Zhigunov, V. I. Zolotarevsky, and P. I. Dolin, *Nature*, **212**, 1002 (1966).

(5) J. W. Buchanan and F. Williams, *J. Chem. Phys.*, **44**, 4377 (1966).

(6) G. R. Freeman, *ibid.*, **46**, 2822 (1967).

(7) J. K. Thomas and R. V. Benasson, *ibid.*, **46**, 4147 (1967).

(8) A. Kuppermann, Proceedings of the Third International Congress of Radiation Research, G. Silini, Ed., North-Holland Publishing Co., Amsterdam, 1967, p 212.

(9) J. W. Hunt and J. K. Thomas, *J. Chem. Phys.*, **46**, 2954 (1967).

(10) J. Bednar, Proceedings of the 1962 Tihany Symposium on Radiation Chemistry, J. Dobo, Ed., Akademiai Kiado, Budapest, 1964, p 325.

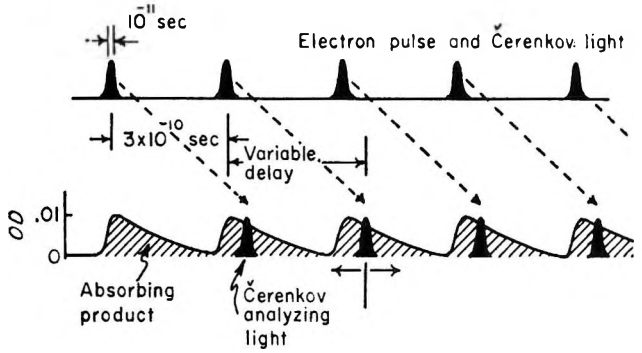

Figure 1. Basic stroboscopic pulse-radiolysis technique using linac beam fine-structure and Čerenkov light to detect short-lived absorption signals. The top line shows the electron fine structure and simultaneous Čerenkov light pulses, separated by 0.3 nsec, the period of the microwave power. The bottom line shows the production and decay of an absorbing product. The Čerenkov light (short, dark pulse) is suitably delayed and used to measure the concentration of the absorbing product.

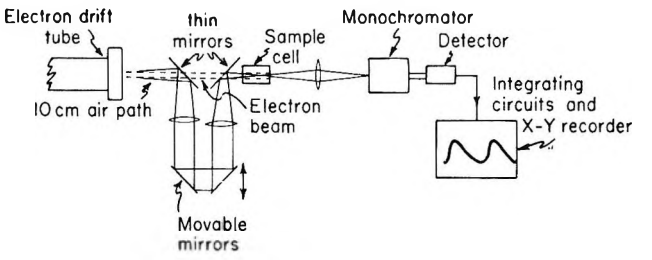

Figure 2. Components of a stroboscopic pulse-radiolysis system. The electron beam (broken line) emerges from the electron drift tube, passes through 10 cm of air and two thin mirrors, and finally irradiates the sample. The analyzing Čerenkov light (solid lines) is produced in the air path of the electron beam. It is transmitted over a variable length optical path and focused to pass through the irradiated sample. This Čerenkov light then is focused through a monochromator and detected by a photomultiplier. Special integrating circuits give a dc signal which may be displayed on a recorder.

B. Principle of Stroboscopic Detection System. No satisfactory optical detection systems are presently available which are capable of making direct observations with the time resolution of the fine-structure pulses (0.02 nsec). It is possible, however, to utilize Čerenkov light produced by these pulses to approach this time resolution, even with comparatively slow optical detectors.

Čerenkov light is produced simultaneously with the passage of a charged particle through a medium at a speed greater than the speed of light in the medium. This occurs when $\beta n > 1$, where β is the ratio of the speed of the charged particle to the speed of light *in vacuo*, and n is the index of refraction of the medium. Čerenkov light has a continuous spectrum and is radiated outward from the path of the charged particle along the surface of a cone of half-angle θ where $\cos\theta = 1/\beta n$.[11]

The time sequence of events for a detection system utilizing Čerenkov light is presented in Figure 1. The electron fine-structure pulses (previously described) are shown producing a rapidly decaying concentration of absorbing species. Simultaneously, the electron fine-structure pulses produce pulses of Čerenkov light. The Čerenkov light pulses are delayed a variable time with respect to the fine-structure electron pulses and then used as analyzing light flashes. Summation over the train of delayed light flashes produces an absorption signal corresponding to a fixed point in time relative to the electron fine-structure pulse. This stroboscopic method makes it unnecessary for the detection system to be particularly fast. The detection system need only add up the total number of photons received from a train of analyzing light flashes to provide a usable signal. By varying the delay of the light flashes, a sweep over the time interval between fine-structure pulses may be obtained.

C. System Design Parameters. The detailed design of a feasible stroboscopic pulse-radiolysis system must overcome three main problems: (1) the incorporation of a suitably adjustable time delay for the Čerenkov light flashes, (2) the production of a detectable concentration of absorption species by the fine-structure electron pulse, and (3) the reduction of noise to well below the signal intensity.

A system has been designed and constructed which is capable of overcoming these obstacles.

1. Time Delay. For the operation of this system, a variable delay of at least twice the time interval between fine-structure pulses is desired in order to show that the absorption signal builds up and decays with the same period as the fine-structure pulses. This variable delay is 0.6 nsec and corresponds to a distance of 18 cm for a light beam in air. The delay is accomplished by reflecting the Čerenkov light beam through 90° onto a pair of movable mirrors which reflect the light back through 180° (see Figure 2) to a fourth mirror in the electron beam. If the pair of mirrors is moved back by 9 cm, the path length is increased by 18 cm, and the desired delay of 0.6 nsec is achieved.

The optical system must collect the analyzing Čerenkov light and focus it through the irradiated volume in the sample cell. The light intensity in the sample cell should not vary as the optical path length is changed. This condition can only be fulfilled by extremely accurate alignment of the optical system. This system must also have constant magnification.

The ultimate time resolutions of such a system is not limited by the width of the fine-structure electron pulse but rather by the problem of synchronizing the fast-moving electron pulses (velocity βc) with the somewhat slower Čerenkov light flashes (velocity c/n) as they pass

(11) J. V. Jelley, "Cerenkov Radiation and Its Applications," Pergamon Press, London, 1958.

through the sample cell. From the front to the back of the cell these pulses lose synchrony by a time

$$t = \frac{nL}{c} - \frac{L}{\beta c} = 0.01L \text{ nsec}$$

where L is the sample cell length and n is the index of refraction of the sample (1.33 for water). The cell length becomes, therefore, a compromise between short time resolution and high sensitivity (*i.e.*, large absorption due to long cell path length). In the detailed system described later, L was chosen as 2 cm, giving a theoretical time resolution of about 0.02 nsec.

Another possible limit on time resolution is caused by differences in the optical path length for individual Čerenkov light rays. In our focusing system, the time spread is negligible, being in the order of 10^{-3} nsec.[12,13]

2. Detectable Concentration of Transient Species. The average dose calculated for each fine-structure pulse in a 5-mm diameter, 1-A, 30-MeV electron beam is about 250 rads. This corresponds to a concentration of solvated electrons of about 6×10^{-7} mol/l., or an absorption signal of about 4%. Such a signal should be easily detectable.

3. Noise. There are two principal sources of noise in this system: the shot noise caused by the finite number of photoelectrons being detected, and noise caused by variations in electron and Čerenkov pulse intensity.

(*a*) *Shot Noise.* An analyzing light beam for pulse radiolysis studies must be sufficiently intense to overcome the statistical fluctuations in the production of photoelectrons at the photocathode of the detecting device. This "shot" noise level varies as the square root of the number of photoelectrons.[2] In order to detect a 4% absorption signal with a 100:1 signal-to-noise ratio, we require at least 4×10^7 photoelectrons during a 30-nsec pulse. Assuming a 10% cathode efficiency and a 10% light collection efficiency, 4×10^9 photons are required in the Čerenkov light pulse at the wavelength of interest. The calculations summarized in Table II show that the necessary light intensity can easily be obtained with a 10-cm air path.

Table II: Čerenkov Light Production by a 30-nsec, 30-MeV, 0.5-A Electron Pulse ($\beta = 0.999$)[a]

Medium	Electron path length, cm	No. of photons produced in a 10-mμ band width at 700 mμ[11]
Water (liquid)	2	4×10^{11}
Zenon (1 atm)	10	1.5×10^{10}
Air (1 atm)	10	1.0×10^{10}

[a] Čerenkov light intensity per unit wavelength (λ) is proportional to $1/\lambda^2$. Thus the figures given in this table should represent minimum values for a 10-mμ band width throughout the visible and near-ultraviolet regions.

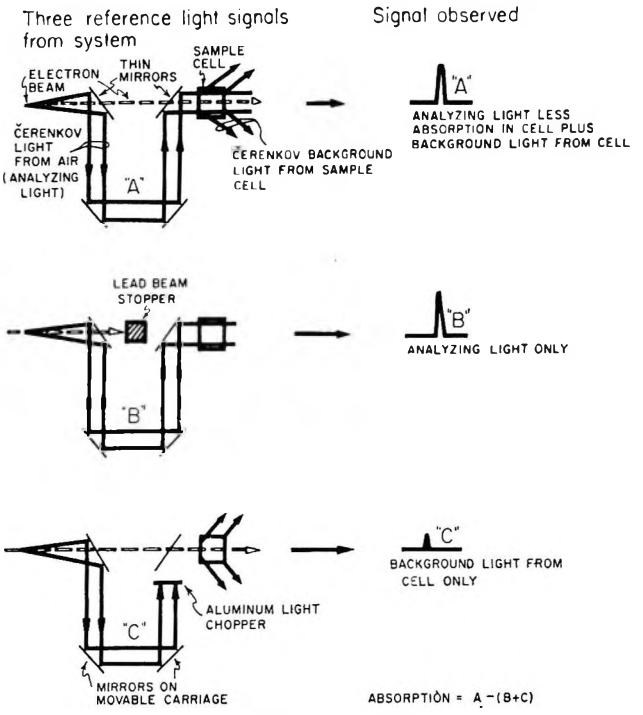

Figure 3. The three types of light pulses used to produce an absorption signal. A rotating "chopper" wheel produces a cycle of three different signals (A,B,C) from consecutive electron pulses. For pulse A, all light and electron paths are open. For pulse B, the electron beam produces the analyzing Čerenkov light, but is blocked from irradiating the sample by a lead block. For pulse C, the electron beam irradiates the sample, but the analyzing Čerenkov light is blocked. Lenses have been omitted from the optical system for simplicity.

(*b*) *Noise from Variation in Pulse Intensity.* Variations in the intensity of the fine-structure electron pulses produce variations in the concentration of absorbing species and variations in the intensity of the Čerenkov analyzing light. The detection system, however, averages the consequent fluctuations in the absorption signal by integrating the light received over 100 pulses. Unfortunately, variations in intensity from one 30-nsec pulse to the next present a more difficult problem. A portion of the light reaching the detection system will be Čerenkov light generated in a cone of about 40° half-angle by the passage of the electron pulse through the sample. This "background" Čerenkov light level must be subtracted before the absorption signal can be obtained.

In order to reduce noise and extract the absorption signal from the background light level, three different types of light pulses can be generated as shown in Figure 3. The "A" light pulse consists of the analyzing Čerenkov light, less the absorption in the sample, plus the background Čerenkov light generated in (and beyond) the sample cell. The "B" light pulse consists

(12) D. A. Hill, D. O. Caldwell, D. H. Frisch, L. S. Osborne, D. M. Ritson, and R. A. Schluter, *Rev. Sci. Instrum.*, **32**, 112 (1961).

(13) E. K. Zavoisky and S. D. Fanchenko, *Appl. Opt.*, **4**, 1155 (1965).

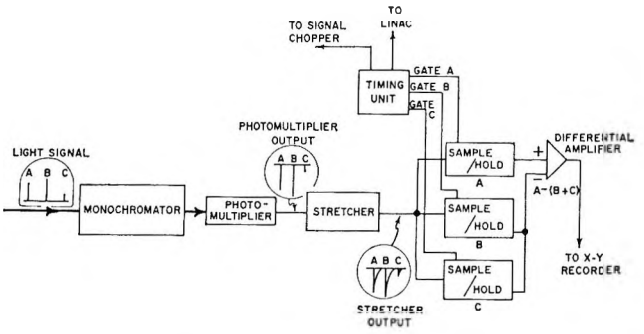

Figure 4. Block diagram of the detection system and signal-processing electronic circuits. The light pulses pass through the monochromator to the photomultiplier where they are converted into electronic pulses. These electronic pulses are "stretched" and fed sequentially to three "holding" circuits. The dc outputs of these holding circuits are proportional to signals A, B, and C. These outputs are fed to a differential amplifier which yields the absorption signal, A − (B + C).

of analyzing Čerenkov light alone with the electron beam blocked in front of the sample cell. The "C" light pulse consists only of background Čerenkov light, since the analyzing light is blocked before the sample cell. The actual absorption signal is A − (B + C) and can be obtained by electronically comparing the three separate light pulses. A chopper wheel, driven by a synchronous motor at constant speed, is phased to provide the three types of light pulses, in sequence, at the rate of 60 Hz. The sequence of signals is ABC-ABCA...etc. The detection system converts these light pulses into electronic pulses which are then processed to yield the absorption signal, A − (B + C), averaged over a period of several seconds, *i.e.*, over several hundred individual pulses. A block diagram of the electronic circuits is shown in Figure 4. By averaging over several hundred pulses, the noise caused by variations in the electron pulse intensity is greatly reduced.

D. Suitable Chemical Systems. The choice of a suitable chemical system for this stroboscopic pulse radiolysis technique must be made with great care. The lifetime of the absorbing species under observation must fall within the time range from 0.02 to 0.3 nsec. Absorbing species with lifetimes longer than 0.3 nsec will be observed, but the kinetics of their decay will be obscured by the buildup of the absorption signal from one fine-structure pulse to the next.

Observation of the decay of the solvated electron in acidic solution is an ideal test system for the stroboscopic pulse radiolysis technique. High concentrations of H^+ can be used to reduce the lifetime of the solvated electron to less than 0.3 nsec. Since the solvation time for electrons in water is thought to be 0.01 nsec[14] or less,[3,4] their buildup and decay should provide an accurate measurement of the time resolution of our apparatus.

Further Details

The analyzing Čerenkov light flashes are generated in 10 cm of air immediately beyond the exit window of the linac. The electron beam, focused to a 5-mm diameter spot by quadrupole magnets, traverses this air path, then passes through two thin (0.01 cm) mirrors to the sample cell. The Čerenkov light rays enter the sample cell at the same point as the electron beam (Figure 2). Once through the sample cell, the light rays are reflected out of the beam line and through a hole in a shielding wall to a separate room containing the monochromator and detection system.

The optical system is designed to keep the position and size of the Čerenkov light image constant as the light path length is varied. The movement of the pair of mirrors is accomplished without vibration by an air cylinder mounted coaxially with a hydraulic checking cylinder (Modernair Corporation, Model 1320). A multi-turn potentiometer is coupled to this linear motion and provides a voltage signal proportional to the mirror position. This signal is fed to the X input of an X–Y recorder while the absorption signal, A − (B + C), is fed to the Y input. Thus the X–Y recorder displays the absorption signal as a function of time within the interval between fine structure pulses, *i.e.*, from 0.02 to 0.3 nsec.

The critical alignment of the optical system is performed by a combination of two methods. A laser shining along the line of the electron beam is used to align all mirrors and lenses up to the sample cell. Once the apparatus is positioned in front of the linac, a light

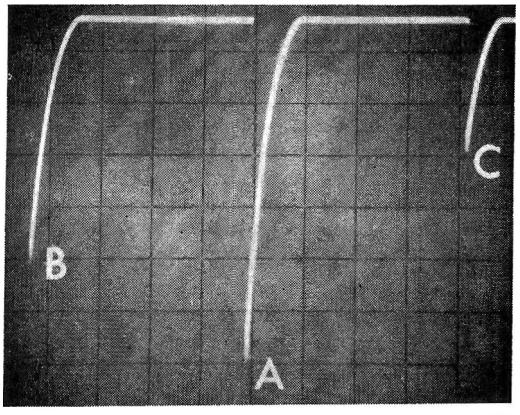

Figure 5. Photograph of an oscilloscope trace showing the three types of analyzing light pulse. This signal was observed at the output of the stretcher circuit (see Figure 4). The vertical scale is 1 V per division and the interval between pulses corresponds to a frequency of 60 Hz. Electron beam current was >0.5 A in a 30-nsec pulse; beam energy was about 30 MeV. The unusual pulse sequence B, A, C was caused by rotating the chopper wheel in the reverse direction to the normal sequence A, B, C.

(14) R. L. Platzman, "Physical and Chemical Aspects of Basic Mechanisms in Radiobiology," U. S. National Research Council Publication 305, 1953, p 22.

beam, imaged on the exit slit of the monochromator, is directed back through the monochromator and optical system to align the components beyond the sample cell.

Because of the high doses absorbed in the sample, a cooling water jacket surrounds the sample cell. In addition, buildup of interfering radiation products is reduced by a flow system which rapidly changes the solution in the sample cell during the run.

Results

Tests of this stroboscopic pulse-radiolysis system are currently in progress. Beam diameters less than 5 mm have been measured with polyvinyl chloride and perspex HX sheets. A dose of over 10 krads/30-nsec pulse has been obtained from a 0.5-A electron beam. This corresponds to a dose of 100 rads per fine-structure pulse.

The Čerenkov analyzing light flashes are very intense and Figure 5 shows a photograph of the three types of light pulses (A, B, and C). The identity of these pulses was confirmed by manually positioning the chopper wheel. The analyzing light level remained constant within 10% as the position of the movable pair of mirrors was changed. This small variation in light level also verified the identity of the three pulses. Only A and B were subject to this variation: C, being independent of the variable optical path, remained constant.

No absorption signals have been observed up to the present time, although all tests prove that the system is feasible. Minor improvements to the linac, optical system, and electronics are underway to alleviate difficulties which have been encountered. These improvements should soon make it possible to observe signals having lifetimes as short as 0.02 nsec.

Acknowledgment. The authors wish to acknowledge the financial support of the National Research Council of Canada. The use of the facilities of the Toronto linac and the cooperation of the linac operating staff, Mr. E. W. Horrigan and Dr. K. G. McNeil, are greatly appreciated. The apparatus was constructed in the machine shop of the Ontario Cancer Institute, in particular by Mr. B. Weckerle. The electronic circuitry was designed by Mr. William B. Taylor and constructed by Mr. K. Grant.

A New Flash-Photolysis System for the Investigation of Fast Reactions

by E.-G. Niemann and M. Klenert

Institut für Strahlenbiologie der Technischen Universität Hannover und Arbeitsgruppe für Strahlenbotanik der Gesellschaft für Strahlenforschung München-Neuherberg, Germany *(Received May 7, 1968)*

For the investigation of fast reactions, especially in photobiology, a new flash-photolysis system has been developed and tested. The photolysis source is a z-pinch arrangement which produces 0.2-μsec light pulses corresponding to a quantum flux of 3×10^{18} quanta/pulse incident on the cuvette. A "kinetic absorption spectroscopy" method is used as the analysis system which gives simultaneous information on the time and wavelength axis in one exposure. The time resolution obtainable with this equipment is in the order of 0.1 μsec, if a wire explosion serves as analysis light source. This source produces nearly rectangular light pulses of about 10-μsec duration. As an example for the use of this photolysis system, some preliminary investigations on hydroquinone solutions are reported. The extension of the arrangement by a new X-ray flash is discussed.

A new flash-photolysis system has been developed in order to increase the time resolution of flash photolysis and to adapt it to the time scales used in pulse radiolysis. On the other hand, the information content of a single analysis had to be improved, as the complexity of the biological systems to be investigated requires the improvement of these properties.

The flash-photolysis light source is a z-pinch arrangement with the irradiation cuvette mounted inside the discharge vessel parallel to the vessel axis.[1] It is operated with a 33-kV, 8.88-μF condenser bank and can be triggered manually or by an optical signal (Figure 1). This setup produces 0.2-μsec flashes (Figure 2) with a maximum radiation density of more than 100 W $Å^{-1}$ cm^{-2} sr^{-1}. The number of quanta entering the cuvette was determined by ferrioxalate actinometry[2] to be 3×10^{18} per pulse.

The analysis system is based on a "kinetic absorption

(1) E.-G. Niemann and M. Klenert, *Appl. Opt.*, **7**, 295 (1968).

(2) C. G. Hatchard and C. A. Parker, *Proc. Roy. Soc.*, **A235**, 518 (1956).

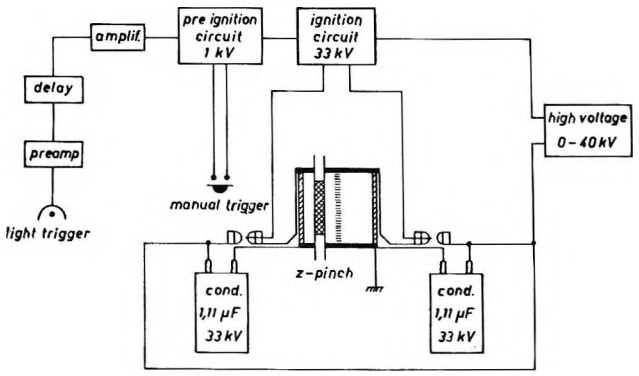

Figure 1. Diagram of the z-pinch arrangement.

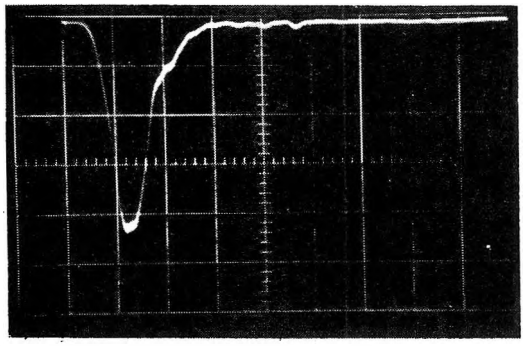

Figure 2. z-Pinch light source. Oscillogram of radiation density over time at 400 nm, 0.2 μsec per large division.

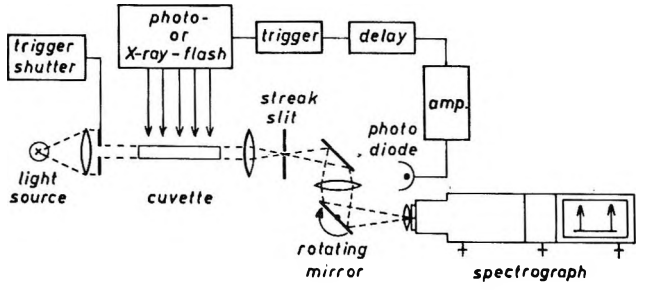

Figure 3. Kinetic absorption spectroscopy, principle of function.

spectroscopy" method which provides a simultaneous resolution of the photolysis process over time and wavelength in one exposure. The principle of this method is illustrated in Figure 3. A continuous light source is focused through the substance under investigation to a horizontal "streak slit" which selects a narrow horizontal section of the image of the light source. An image of this slit is swept over the vertical entrance slit of a spectrograph by means of a fast rotating mirror with horizontal axis. The mirror we used was a 1-in. first surface mirror driven directly by a grinder motor at a maximum of 27,000 rpm which allows a sweep velocity up to 3 mm/μsec on the photographic plate. A fast photodiode is situated in the plane of the entrance slit in a position where it is illuminated by the image of the streak slit before it travels over the spectrograph slit. The signal of this photodiode is amplified and delayed and triggers the irradiation source (photo or X-ray flash) at a time when the streak slit image is at the beginning of its way along the entrance slit. In order to avoid double exposure of the photographic plate and unnecessary illumination of the substance under investigation, the electromechanical shutter near the light source is opened for the period of one rotation of the rotating mirror only. Using a xenon high-pressure lamp[3] as analysis light source, a wide-aperture spectrograph,[4] and a very sensitive emulsion,[5] a time resolution of 1 μsec in the visible region is obtainable.

A further improvement of resolution, particularly in the uv region, is reached by replacing the stationary light source by a quasistationary one, which gives a constant light flux for the period of investigation only. A wire explosion in Freon (CF_2Cl_2) proved to be suitable for this purpose.[6] This source emits a constant luminous flux for about 10 μsec and permits a time resolution of 0.1 μsec in kinetic absorption spectroscopy.

The streak absorption spectrum of a 0.3 mM aqueous hydroquinone solution irradiated at $t = 0$ by the z-pinch is given in Figure 4. Following the flash irradiation,

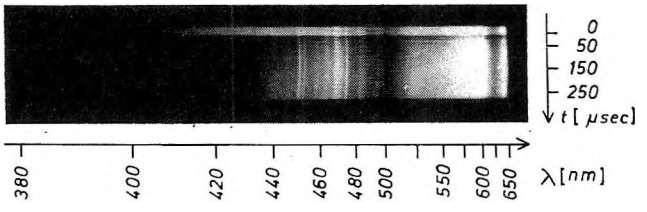

Figure 4. Streak absorption spectrum of a 0.3 mM hydroquinone solution; z-pinch irradiation at $t = 0$.

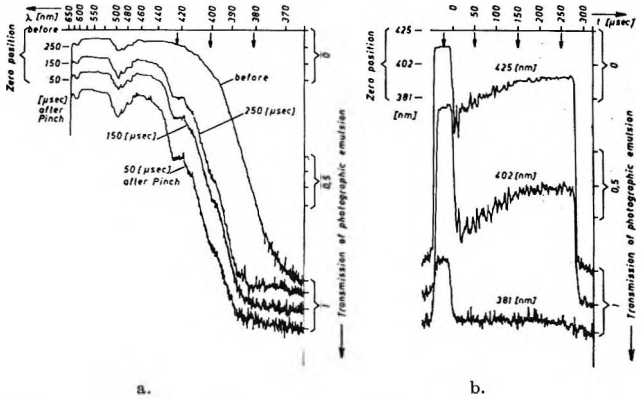

a. b.

Figure 5. Densitometer tracks of the streak spectrum in Figure 4: a, traces at constant time as a function of wavelength; b, traces at constant wavelength as a function of time after irradiation (zero position shifted).

(3) Osram XBO 250 W.
(4) Steinheil Universal Spectrograph, $f/3.5$.
(5) Ilford HPS.
(6) H. W. Seibold and E.-G. Niemann, to be published.

strong transient absorptions are observed in the range from 390 to 440 nm. The evaluation of this type of spectra is done by densitometer measurements along the λ and the t axis as well. Some registration tracks of the hydroquinone photolysis spectrum are assembled in Figure 5. In part a, absorption maxima at 428 and 404 nm are clearly recognizable which are due to the p-hydroxyphenoxyl radical.[7]

The absorption curve $E_i(\lambda)$ of the transient products can be calculated easily by forming the difference between the film density readings before and at time intervals i after irradiation ($S_0(\lambda) - S_i(\lambda)$) and dividing this by the gradation curve $\gamma(\lambda)$ of the emulsion

$$E_i(\lambda) = \frac{S_0(\lambda) - S_i(\lambda)}{\gamma(\lambda)}$$

Registrations over time at constant wavelengths are presented in Figure 5b. As is to be expected, the tracks for 402 and 425 nm yield identical radical half-life values of about 75 μsec. The absorptions of the p-hydroxyphenoxyl radical are superimposed, however, by a long-lived absorption which is seen most clearly in the 381-nm curve. The origin of this absorption could not yet be clarified.

For parallel investigations by flash photolytic and pulse radiolytic methods, the system described will be complemented by the addition of a flash X-ray tube. This device, which is still in the test stage, is operated with a 150-kV condenser bank and produces X-ray pulses of 0.1-μsec duration. The equipment is constructed to give 1 krad per pulse inside the irradiation cuvette. Together with the z-pinch light source and the method of kinetic absorption spectroscopy, it will form a simple and compact arrangement for the flash photolytic and pulse radiolytic investigation of biophysical problems.

(7) H. I. Joschok and L. I. Grossweiner, *J. Amer. Chem. Soc.*, **88**, 3261 (1966).

I^- Photosensitized Reactions in Metaphosphate Glass

by T. Feldmann and A. Treinin[1]

Department of Physical Chemistry, Hebrew University, Jerusalem, Israel *(Received May 7, 1968)*

The photooxidation of Cl^- and Br^- in metaphosphate (MP) glass could be sensitized by I^-. The reaction was investigated by optical and esr methods. The mechanism proposed involves energy transfer from excited I^- to a phosphate polymer, which subsequently dissociates to form the MP color centers. The oxidation of X^- is a dark reaction whereby MP holes are scavenged by halide ions, and X atoms are converted to X_2^- radicals. The esr of Cl_2^- in glass is analyzed. The primary processes involving excited I^- are discussed and an exciton-type mechanism is proposed for the energy transfer.

The halide ions X^- have no excited states in the gas phase,[2] but as shown by spectroscopic and photochemical experiments, such states (so called CTTS states) do exist in solution.[3] Their natural lifetimes, estimated from their integrated absorption bands,[4a] are about 10^{-8} sec, but the actual lifetimes are much shorter.[4b] Dissociation to $X + e_{sol}^-$ and deactivation to ground state are the competing radiationless processes in liquid solutions. The activation energy of dissociation is higher (by *ca.* 5 kcal for I^- and Br^- in aqueous solution) and this by itself can explain their low dissociation yield in ices at 77°K.[5] (In alkaline ices, trapped electrons could not be detected.[6]) The mechanisms of these processes are not clear. Dissociation of X^{-*} may involve diffusion of X from excitation site.[4b] In this case dissociation should be hampered in rigid matrices even at room temperature. Still, efficient photolysis of I^- and Br^- does occur in boric acid[7] and metaphosphate[8] glasses. In the first case this may

(1) On leave of absence at the Department of Chemistry, Brandeis University, Waltham, Mass. 02154.

(2) R. S. Berry, C. W. Reimann, and G. N. Spokes, *J. Chem. Phys.*, **37**, 2278 (1962).

(3) For a recent review, see C. K. Jørgensen, "Halogen Chemistry," Vol. 1, Academic Press, New York, N. Y., 1967, p 280.

(4) (a) J. Jortner and A. Treinin, *Trans. Faraday Soc.*, **58**, 1503 (1962); (b) J. Jortner, M. Ottolenghi, and G. Stein, *J. Phys. Chem.*, **68**, 247 (1964).

(5) P. N. Moorthy and J. J. Weiss, *J. Chem. Phys.*, **42**, 3121 (1965).

(6) P. B. Ayscough, R. G. Collins, and F. S. Dainton, *Nature*, **205**, 965 (1965).

(7) A. Zaliouk-Gitter and A. Treinin, *J. Chem. Phys.*, **42**, 2019 (1965).

(8) T. Feldmann and A. Treinin, *ibid.*, **47**, 2754 (1967).

result from direct oxidation of the excited ion by the highly acidic medium.[9] In the second case, some preliminary results suggest that the excited ion might transfer its energy to phosphate polymers.[8] In the present work, we wish to verify this view.

Experimental Section

Preparation of Glasses. Pure metaphosphate (MP) glasses were prepared as described elsewhere.[10] Halide-containing glasses were produced by melting thoroughly ground mixtures of MP and halide salts at 750° under an atmosphere of N_2. KI, KBr, and KCl of Analar grade were used.

Irradiation and Actinometry. Glass disks were irradiated with an Osram Cd/1 cadmium arc lamp (operated at 12 V and 1.5 A) using a 1-cm layer of water as a filter. The only light absorbed by our glasses was the 2144 (weak), 2265 (weak), and 2288-Å lines. (The last two will be considered together.) To cut off the 2144-Å line, a solution of KBr was used, which transmitted 80% of the 2288-Å line. The intensity ratio $I_{2144}/I_{2288} = 3.3 \times 10^{-2}$ was determined from emission spectrum of the lamp. Intensity of light incident at the front of the glass was measured by differential actinometry with uranyl oxalate,[11] and from known intensity ratio the small contribution from 2144 Å could be found ($\sim 2 \times 10^{-8}$ einstein/min). From this and the absorption spectrum of the glass the amount of light absorbed by X^- at each wavelength was determined. Yields of X_2^- were determined from their absorption peaks, assuming ϵ_{max} to be the same as in aqueous solutions; $\epsilon_{max} \times 10^{-4}\ M^{-1}\ cm^{-1} = 1.2$, 0.8, and 1.4 for Cl_2^-, Br_2^-, and I_2^-, respectively.[12] From the yield with a KBr filter and without, the yield at 2144 Å was obtained. Altogether, the quantum yield of X_2^- was calculated by means of the formula

$$\varphi_{X_2^-} = (1/Ia)(\Delta D_{X_2^-}/\Delta t)(\pi r^2/1000\epsilon_{X_2^-})$$

where Ia is the number of einsteins absorbed by X^- per unit time, $D_{X_2^-}$ and $\epsilon_{X_2^-}$ are the absorbance and molar extinction coefficient of X_2^-, respectively, and r is the radius of the disk in centimeters.

Optical absorption spectra were measured with a Cary 14 recording spectrophotometer. Electron spin resonance spectra were obtained at 9.4 kMc/sec with a Varian 4500 spectrometer.

Results

Under conditions employed, the pure base glass displayed very weak esr signals after only a few hours of irradiation. However, a marked photoactivity was exhibited by I^--doped glass (Figure 1). The two characteristic esr doublets of MP[8] were produced, but the hole doublet (h_1,h_2) was relatively reduced in intensity. A dark reaction involving I^- appeared to be responsible for annihilation of the hole center; it continued to decay after irradiation and rate of decay increased with I^- concentration (Figure 1). The

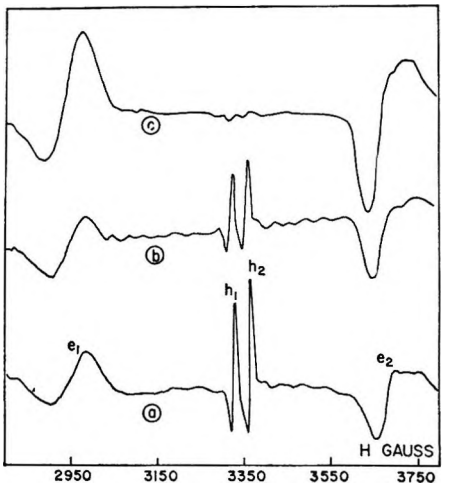

Figure 1. Esr of I^--doped glasses irradiated with Cd lamp for 20 min. Curves a and b: $2.8 \times 10^{-3}\ M$ KI, 8 and 50 min after irradiation, respectively. Curve c: 0.4 M KI, 10 min after irradiation. (All concentrations refer to mixture from which the glasses were prepared.)

"electron" signal (e_1,e_2) was rather stable. Increase in its rate of production with (I^-) was due, at least partly, to increase in light absorption. Thus for the same time of treatment the ratio between intensities of "electron" and hole centers increased with (I^-). In parallel, the spectrum of I_2^- grew up, peaking at 375 mμ.

Higher concentrations of Br^- were required to obtain appreciable light absorption at 2144 Å. Br_2^- (λ_{max} 350 mμ) and the "electron" center were produced, but no hole center. The holes were probably scavenged by Br^-. Cl^- hardly absorbed at 2144 Å. However, when Cl^- or Br^- was added to I^- a striking nonadditive effect was observed. Figures 2 and 3 show the behavior of a glass doped with I^- and large excess of Cl^-. Irradiation led to fast production of Cl_2^-. It was identified by comparing its optical spectrum with that induced by X-rays in Cl^- doped glass (Figure 2). λ_{max} 330 mμ is close to that of Cl_2^- in aqueous solution.[12] (The peak at 230 mμ is probably due to Cl_3^-.[13]) The same glass with no I^- present was not affected by identical treatment (Figure 2); after 2 hr of irradiation Cl_2^- could just be detected. The esr spectrum of the irradiated glass (Figure 3) revealed that the hole doublet was suppressed by Cl^- and a new esr pattern was produced. It showed two strong signals with 50-G separa-

(9) H. M. Buck, W. Th. A. M. Van der Lugt, and L. J. Oosterhoff, *Tetrahedron*, 19, (Suppl. 2), 173 (1963).

(10) T. Feldmann, A. Treinin, and V. Volterra, *J. Chem. Phys.*, 42, 3366 (1965).

(11) J. Jortner, M. Ottolenghi, and G. Stein, *J. Amer. Chem. Soc.*, 85, 2712 (1963). Reflections at the front of the actinometer cell and the glass disk were assumed to be the same.

(12) M. E. Langmuir and E. Hayon, *J. Phys. Chem.*, 71, 3808 (1967).

(13) G. Zimmerman and F. C. Strong, *J. Amer. Chem. Soc.*, 79, 2063 (1957).

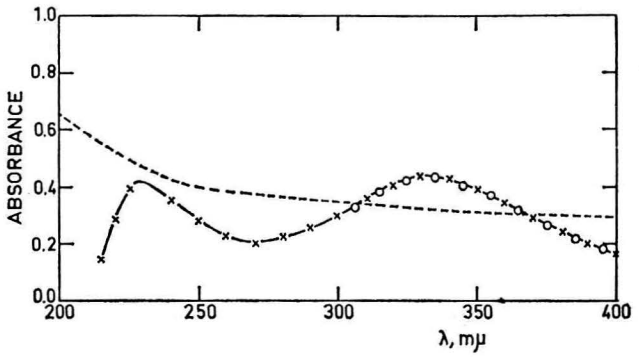

Figure 2. Change in absorption spectra of glasses doped with KCl + KI (10:1) after 10 min exposure to Cd light (×), and with KCl alone after 7 min X irradiation (○). Dashed curve: absorption spectrum of the KCl glass before and after 50 min exposure to Cd light.

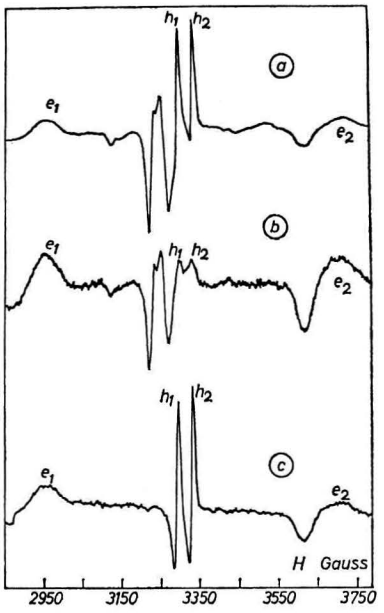

Figure 3. Esr of Cl^- doped glasses. Curve a: 2.1 *M* KCl after 10 min X irradiation. Curves b and c: 2.8 and 0.28 *M* KCl, respectively, with 4.6×10^{-3} *M* KI after 20 min exposure to Cd light. (See remark to Figure 1.)

tion and few weak components. The same pattern was produced by X-rays in MP containing Cl^- alone (Figure 3). Evidently it belongs to a Cl species, most likely Cl_2^-. The esr of Cl_2^- in crystals is well known.[14] It consists of a septet with intensities in the ratio of 1:2:3:4:3:2:1. It displays large hyperfine anisotropy; the first-order splitting A ranges from 101 G at $\theta = 0°$ to 9 G at $\theta = 90°$ (θ is the angle between molecular axis and magnetic field). The line $m_I = +1$ is least sensitive to angular spreading, with $H = 3190 \pm 10$ *G* at 9.3 kMc/sec. Starting with this line, the anisotropy steeply increases as m_I either increases or decreases. For random orientation of Cl_2^- in glass this should lead to gradual smearing of the components on both sides of $m_I = +1$. Those with $m_I = -3, -2, -1$, and $+3$ are expected to be broadened beyond detection. The other two should suffer the same broadening, but taking into account the intensity ratio, the $m_I = +2$ component may not be readily detected. The average separation between the $m_I = 0$ and $+1$ signals is $\sim\int_0^{\pi/2} A(\theta) \sin\theta \, d\theta$. Using available data[14] and carrying out numerical integration, we obtained $A_v = 52$ G. Altogether this description is in complete agreement with the new esr pattern in Figure 3. The $m_I = +2$ component can still be discerned on the low-field side of the sharp signal; the latter at 3200 G evidently corresponds to $m_I = +1$.

Similar experiments with I^-–Br^- mixtures were more difficult to interpret since Br^- also absorbed at 2144 Å when in large excess. Still, under proper conditions, irradiation led to the fast production of Br_2^- (Figure 4; compare curves 1 and 4. The very large hyperfine anisotropy of Br_2^- [14] smeared its esr spectrum beyond detection.) Finally, a glass containing a mixture of Br^- and Cl^- with little I^- was irradiated with Cd light and then with X-rays. By adjusting times of irradiation, the effects produced by the two kinds of radiation were nearly the same (Figure 4).

The quantum yields of X_2^-, produced in the I^-–X^- glasses, were measured under conditions where no holes could be detected. They were nearly the same for Br^- and Cl^-: $\varphi_{2144} \sim 0.2$, $\varphi_{2288} \sim 5 \times 10^{-3}$. Similar increase of φ with $h\nu$ was displayed by I^- alone, but the quantum yield of I_2^- was smaller owing to trapping of I atoms in MP.[8] Their release by heating resulted in growth of both I_2^- and I_3^- spectra and by other annihilation processes.

Discussion

From the effect of X-rays on halide doped glasses[8] it is known that MP holes are efficiently scavenged by Cl^-, Br^-, and I^-.

$$X^- + \text{hole-MP} \longrightarrow X + \text{MP} \qquad (1)$$

This explains annihilation of the hole center and formation of X_2^-. However, the question arises as to the mechanism by which holes are produced by Cd light. In our experiments only little light was absorbed by the base glass and this led to little chemical effect even in the presence of high concentrations of Cl^-, which might compete with geminate recombination. Therefore, the primary excitation of I^- is responsible for this effect. However, it does not seem to involve direct photoionization of I^-. Hole transfer from I to MP is unlikely, since the reverse reaction (eq 1) is efficient even for Cl^-.

The most effective Cd line at 2144 Å falls within the onset of the CTTS band of MP.[10] It is overlapped from its long wavelength side by a weak band, which is probably due to some $n \rightarrow \pi^*$ transition in the phosphate polymers (similar spectra are exhibited by simple

(14) T. G. Castner and W. Känzig, *Phys. Chem. Solids*, **3**, 178 (1957).

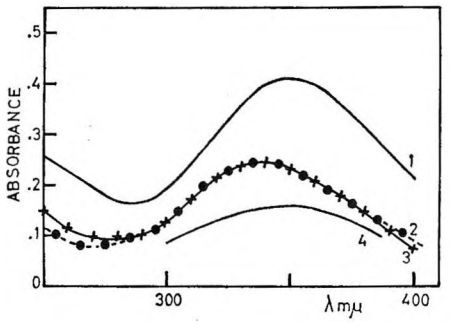

Figure 4. Radiation-induced changes in absorption spectra of glasses doped with halides. Curve 1: 1 *M* KBr + 3 × 10^{-2} *M* KI after 30 min exposure to Cd light. Curves 2 and 3: 4 *M* KCl + 0.15 *M* KBr + 5 × 10^{-3} *M* KI, after exposure for 10 min to X-rays and 15 min to Cd light, respectively. Curve 4: 1 *M* KBr after 45 min exposure to Cd light. (See remark to Figure 1.)

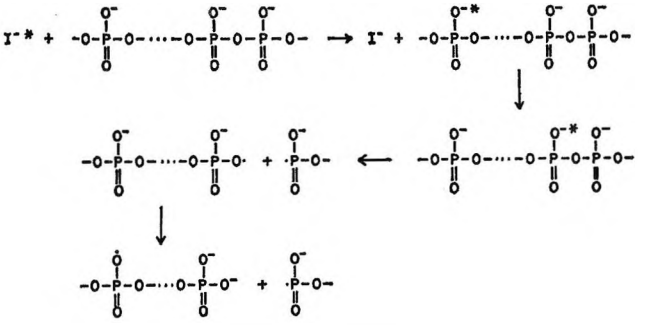

Figure 5. Exciton-type mechanism for I⁻ photosensitized degradation of metaphosphate glass.

phosphate ions[15]). Thus direct excitation of MP to its CTTS state at 2144 Å should be of little probability. Efficient CTTS–CTTS energy transfer from X^- to MP may still occur if other competing reactions are relatively slow. Now, from experiments at 1849 Å[8] it is known that CTTS excitation of MP leads to formation of the "electron" and hole center.

The nature of the CTTS state is not yet clear even in the case of X^-. Its assignment rests on some environmental effects, which do not provide a sensitive tool for studying the detailed charge distribution. There is little reason to believe that the same model will apply to the CTTS state of I^- and a polyphosphate ion. Moreover, the question arises as to the nature of this state in glassy matrices, which possess neither the ordered structure of crystals nor the dipolar polarization properties of liquids. Still, the spectrum of I^- in boric acid glass[7] is rather similar to that in aqueous solution or KI crystal. For this discussion, which is concerned with primary processes involving CTTS states, a crude picture of a hole–electron pair will be used. This pair is mobile in crystals (exciton), confined to the excitation site in the case of randomly dispersed simple ions, and probably shows some freedom of migration along polymer units. Thus in MP it is likely to move freely along the polyphosphate chain, thus more closely resembling an exciton. When such "exciton" reaches a relatively weak chemical bond, some kind of internal conversion to dissociative state can occur. Such conversion was shown to be very efficient in NCS^-.[16]

Figure 5 describes a possible mechanism for formation and destruction of "excitons" in I⁻–MP glass. A highly stretched P–O bond, momentarily formed, should be favored as a site of degradation. Subsequent hole migration away from the ruptured bond should stabilize the hole and "electron" centers, trapped separately on two radicals. Altogether, the net reaction is I^- photosensitized production of MP color centers.

According to the proposed picture, the I^- photosensitized oxidation of Cl^- and Br^- is a dark reaction represented by eq 1.[17] Halide ions compete with matrix on the holes, which are produced with a quantum yield ~0.2. This view is further verified by the experiment with halide mixtures (Figure 4). Owing to its low concentration, I^- could not play any significant role in the X-ray-induced changes and still they were the same as induced by Cd light. Evidently, Cl^- and Br^- compete on the same precursor, which can only be the MP hole center.

The mechanism of energy transfer from I^- to phosphate polymer is not clear. Preliminary study of emission revealed that excitation of I⁻–MP glass led to some broad emission above 250 mμ, which was not displayed by the base glass. Its nature is under investigation, but it seems to originate from MP. The emission spectrum of I^- in glass is expected to be resonance fluorescence. The breadth of its absorption band presumably reflects distribution of environments and since the rigid matrix is not likely to relax fast, emission is expected to be at the same wavelength as absorption. Thus overlap between an emission spectrum of I^- and CTTS absorption of MP should increase with $h\nu$. This explains the effect of wavelength on quantum yield.

The light-absorbing halide may also undergo direct photoionization, in parallel to energy transfer. However, the absence of any esr signals that could be assigned to physically trapped electrons suggests that this is a minor process. Thus energy transfer should be much faster than the dissociation process. Owing to low absorption of MP in the region involved, the former is unlikely to be very fast; its pseudo-first-order rate constant is probably not much larger than the radiative rate constant, ~10^8 sec^{-1}. This suggests that dissociation is hampered in glass. However, the quantum yield of I^- emission should be determined in order to verify this view.

(15) M. Halmann and I. Platzner, *J. Chem. Soc.*, 1440 (1965).

(16) M. Luria and A. Treinin, *J. Phys. Chem.*, 72, 305 (1968).

(17) The possibility that some oxidation product of I^- (or reduction product of MP) is the photosensitizer should also be considered. However, photosensitization was found to occur under conditions where light was in effect totally absorbed by I^-.

In conclusion, our results provide further evidence to the existence of excited halide ions, which in addition to deactivation and dissociation can undergo chemical quenching. They also indicate that apparently inert matrix material may act as a chemical quencher, when its absorption spectrum tails into the region of excitation. A low intrinsic probability for energy transfer can be compensated by a large concentration of quencher and a decrease in rates of other competing processes.

An Efficient and Highly Selective Radiation-Induced Isomerization in the Crystalline State

by David C. Walker

Chemistry Department, University of British Columbia, Vancouver 8, British Columbia, Canada
(Received May 7, 1968)

This paper presents an evaluation and discussion of the G value for a remarkable radiation-induced isomeric transformation of a crystalline organic ester during X-ray crystallographic analysis. The high yield [G(isom) > 57] cannot result from a chain reaction but appears to be a real case of extremely efficient energy transfer or collective excitation peculiar to the pure crystalline state.

Introduction

In a determination of the structure and absolute configuration of hirsutic acid by X-ray crystallographic analysis of its *p*-bromophenacyl ester, Comer and Trotter[1] observed an unusual molecular rearrangement induced by the analyzing X-ray beam. They found an approximately equimolar mixture of the original (I) and rearranged (II) compounds (see Figure 1) after about 10 hr exposure to the soft X-rays and that further exposure to the X-rays caused no further chemical or crystallographic change. Comer and Trotter confirmed their crystallographic results by separating an irradiated crystal, by preparative thin-layer chromatography, into two chemically distinct compounds, shown by chemical analysis and ir, uv, and nmr spectroscopy to be consistent with structures I and II.[1,2] These authors noted the following additional features: (i) the crystal structure was not disrupted as a result of the rearrangement and there were only very minor changes in lattice parameters and intensities of reflections; (ii) the two different molecules were apparently randomly distributed at lattice sites; (iii) the irradiated (but not the unirradiated) crystal contained O--H···O hydrogen bonds; (iv) irradiation of hirsutic acid itself did not lead to any rearrangement, whereas the methyl ester showed a rearrangement similar to the *p*-bromophenacyl ester; and (v) the rearrangement could not be induced thermally or by prolonged exposure to sunlight.[1,2]

From a radiation chemistry standpoint it is clear that, for every other molecule to be altered in exactly the same manner, the rearrangement cannot be a primary radiation effect but must result from a highly selective, rather efficient, secondary utilization of the energy. The purpose of this short paper is to report some radiation dosimetry for the conditions used by Comer and Trotter and to evaluate a radiation yield for this rearrangement.

Experimental Section and Results

(*a*) *Dosimetry.* The X-rays from a 40-kV X-ray tube having a Cu target and Ni filter will correspond predominantly to the Cu Kα line at 8.0 kV. X-Rays of this energy will interact mainly by photoelectric processes, and the absorption coefficient will have a strong dependence on X-ray energy and atomic number of absorber. Consequently, it was decided to measure the total energy incident upon a chemical dosimeter rather than rely on the calibration of a photographic film or ionization chamber.

A hole 0.8 cm in diameter was cut through the lower part of one of the ground-glass walls of a 1-cm square cross section silica spectrophotometric cell and this hole was covered and sealed with polyethylene sheet $<2 \times 10^{-4}$ cm thick; then 2.5 ml of $FeSO_4$ Fricke dosimeter solution (made from Analar grade $Fe(NH_4)_2$-

(1) F. W. Comer and J. Trotter, *J. Chem. Soc. B*, 11 (1966).

(2) F. W. Comer, Ph.D. Thesis, University of British Columbia, 1966.

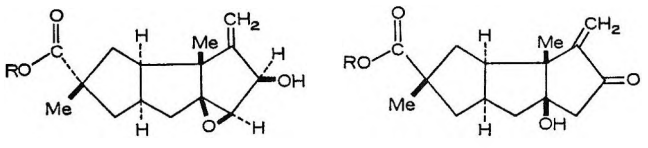

(I) (II)

Figure 1. I, original molecule. II, rearranged isomer; R either *p*-bromophenacyl or methyl group.

$(SO_4)_2$, KCl, and H_2SO_4 and triply distilled water) was placed in the cell. After being filtered by a Ni foil and collimated to a 0.30-cm diameter beam, the X-rays were directed at the solution through the polyethylene window. The geometric arrangement was such that the radiation intensity at the surface of the solution would be almost the same as that received by the crystals in Comer and Trotter's X-ray analysis. After various exposure times, the over-all change in optical density of the solution, due to formation of Fe^{3+} ions, was measured at 304 mμ. A linear plot of optical density *vs.* irradiation time was obtained. The slope of this plot gave $d[D]/dt = (1.17 \pm 0.05) \times 10^{-3}$ min^{-1}. This slope was shown to be unaffected by stirring the solution intermittently during the irradiations so that diffusion of Fe^{2+} into the region very close to the thin window was apparently sufficiently rapid to avoid depletion of Fe^{2+} there. Furthermore, no perceptible change in slope was noted when two thicknesses of polyethylene were used as a window, indicating that the energy absorbed by the window can be neglected.

(*b*) *Calculation of G Value.* The collimated X-ray beam is almost completely absorbed by the 1-cm depth of $FeSO_4$ dosimeter solution. From the observed change in concentration of Fe^{3+} and the known $G(Fe^{3+})$ for the Fricke dosimeter for 8-kV X-rays one can calculate the total energy incident per square centimeter per second on the solution. Combining this with the known linear absorption coefficient and density of the crystals studied, one can evaluate the maximum possible absorbed dose per gram per second by the crystals. Since Comer and Trotter noted that one-half of the molecules were rearranged within a certain time, a minimum value for the radiation yield can be obtained. The net relationship used in this calculation is hence given by the equation

$$G(\text{isomerization}) = \frac{\epsilon l \rho a G'(Fe^{3+}) \times 10^3}{2t_{1/2}MV\mu d[D]/dt} \text{ molecules/100 eV}$$

where $\epsilon = 2200 \pm 10$ M^{-1} cm^{-1}, the extinction coefficient of Fe^{3+} at 304 mμ;[3] $l = 1$ cm, the optical path length used; $\rho = 1.45$ g cm^{-3}, the density of the crystals;[1] $a = 0.0705$ cm^2, the cross-sectional area of the X-ray beam striking the dosimeter solution and the crystals; $G'(Fe^{3+}) = 12.5 \pm 1$, the radiation yield of the Fricke dosimeter for 8-kV X-rays;[4] $t_{1/2} = 10$ hr, the time period within which half the molecules had been rearranged; $M = 461.3$, the molecular weight of the *p*-bromophenacyl ester; $V = 2.5$ ml, the volume of dosimeter solution used; and $\mu = 31$ cm^{-1}, the linear absorption coefficient of the crystals for Cu Kα radiation.[1] Using these data one obtains G(isomerization) $> 57 \pm 5$.

The value for G(isom) is an absolute minimum for four reasons. (i) The rearrangement was observed to be complete within 10 hr of irradiation. In the early stages, at very small percentage conversions, the utilization of energy may have been much more efficient and G(isom) much larger, perhaps even several orders of magnitude larger.[5] (ii) The absorbed dose rate within the crystal will be somewhat less than the maximum value at the surface used in the above calculation. (iii) Even with the Ni filter present there will be some Cu Kβ and "white" X-radiation up to 40 kV. Thus the "weighted" absorption coefficient needed should be less than 31 cm^{-1}. (iv) Back-scatter of X-rays will be greater from the crystals than from the dosimeter.

Discussion

Comer and Trotter have observed a remarkable and interesting radiation chemical process. Perhaps the intramolecular rearrangement was induced by nonlocalized energy deposition (or collective excitation) and perpetuated by an energy transfer process peculiar to the crystalline state—through a sequence of transformations, which derive exothermicity from the relocation of H atoms, leading to intermolecular hydrogen bonding between pairs of dissimilar molecules.

The alternative explanation for G(isom) > 57, namely a chain reaction propogated by a chemically active species such as a free radical or ion, seems very unlikely for this system. First, the isomerization is fairly complex, involving both a hydride ion shift from the secondary OH and a proton transfer from the β-carbon to the epoxy group within the same molecule. Since the isomer so formed then hydrogen bonds with an unaltered molecule without disruption of the crystal lattice, the alteration of the structure proceeds between pairs of molecules, which suggests that an active species is not passed on to adjacent sites. Secondly, the process is complete when every molecule of the crystal is paired in hydrogen bonding. Thirdly, hirsutic acid itself (which Comer and Trotter propose may be already hydrogen bonded through the carboxylic group[1,2]) undergoes no radiation-induced rearrangement, only

(3) A. O. Allen, "The Radiation Chemistry of Water and Aqueous Solutions," D. Van Nostrand Co., New York, N. Y., 1961, p 21.

(4) H. A. J. B. Battaerd and G. W. Tregear, *Rev. Pure Appl. Chem.*, 16, 83 (1966).

(5) Hirsutic acid is a metabolite isolated from a rare strain of stereum hirsutum which is no longer available (T. Money, private communication), so that it is impossible at present to determine the initial G(isom).

its esters. Molecules with a similar skeleton, such as 4β, 5-epoxy-5β-cholestan-3-ol, also show no rearrangement.[2]

Apparently it is a feature of the molecular packing in the crystals of these particular molecules but cannot readily be induced by heat or light. There is no evident resemblance between the system discussed here and either (i) chain reactions such as the radiation-induced polymerization of crystalline monomers (where a chain-propagating species was involved, the reaction was not homogeneous but confined to tracks and gross disruption of the crystal structure resulted[6]), or (ii) efficient scavenging by solutes in crystalline aromatic matrices due to exciton transfer.[7]

Dose rates used in X-ray crystallographic studies are surprisingly high. For instance, with crystals containing a heavy atom as in this work, the dose rate absorbed was about 30,000 rads min^{-1}.

Since crystallographers rarely find molecules which decompose or transform under the X-radiation doses normally used, the type of process reported here is very unusual. However, for those molecules which are affected, the crystallographer's technique affords the radiation chemist a valuable means of following chemical and structural changes, and this example highlights the unique features of the crystalline state under X-ray bombardment.

Acknowledgments. The author is most grateful to Dr. J. Trotter for many helpful discussions and for making available the X-ray equipment. Financial support by the National Research Council of Canada is also gratefully acknowledged.

(6) A. J. Restiano, R. B. Mesrobian, H. Morawetz, D. S. Ballantine, G. J. Dienes, and D. J. Metz, *J. Amer. Chem. Soc.*, **78**, 2939 (1956).

(7) E. Collinson, J. J. Conlay, and F. S. Dainton, *Discussions Faraday Soc.*, **36**, 153 (1963).

A Mixed Triplet-Excimer Intermediate in the Photooxidation of N,N′-Diphenyl-*p*-phenylenediamine by the Diimine

by Michael Ottolenghi

Department of Physical Chemistry, The Hebrew University, Jerusalem, Israel

and René Bensasson

Laboratoire de Chimie Physique de la Faculte des Sciences de Paris, Paris, France *(Received May 7, 1968)*

The flash photolysis of N,N′-diphenyl-*p*-phenylenediamine (RH_2), in the presence of the corresponding diimine (R), has been studied in ethylamine and tetrahydrofuran solutions with varying amounts of acetic acid. At low acid concentrations, when $[CH_3COOH] < 10^{-3}$ *M*, the amine triplet ($^3RH_2$) reacts with a ground-state imine molecule yielding the two radical ions RH_2^+ and R^-, as well as an additional transient, presumably the uncharged RH radical. When the acid concentration exceeds $\sim 10^{-1}$ *M*, R^- and RH are not observed, and around $-100°$, the yield of RH_2^+ is doubled relative to its value in acid-free systems. The detailed effects of imine and acid concentrations indicate that the reaction between $^3RH_2$ and R proceeds *via* a mixed amine–imine triplet excimer ($^3RH_2 \cdot R$). Such an excited complex may undergo dissociation to RH_2^+ and R^- or to two RH radicals. Alternatively, the complex may react with proton donors to give its equilibrated acid form which yields two RH_2^+ ions. The nature of the excimer states responsible for the photochemical events is discussed.

Introduction

N,N′-diphenyl-*p*-phenylenediamine (RH_2) in solution is known to undergo a reversible one-electron photochemical conversion to its semiquinone positive ion, RH_2^+. Such a process, initially investigated in rigid glasses at low temperatures,[1] was recently studied by flash photolysis in a fluid medium.[2] The detailed mechanism of the photooxidation, accounting for the various steps between light absorption by RH_2 and the formation of RH_2^+, is still obscure in the rigid systems. It was shown, however,[2] that in acidified, fluid EPA solutions between -100 and $-160°$, the main

(1) H. Linschitz, J. Rennert, and T. M. Korn, *J. Amer. Chem. Soc.*, **76**, 5839 (1954).

(2) H. Linschitz, M. Ottolenghi, and R. Bensasson, *ibid.*, **89**, 4592 (1967).

path leading to the formation of RH_2^+ involves a reaction between the amine triplet state ($^3RH_2$) and a corresponding, ground-state, imine (R), according to

$$^3RH_2 + R(+2H^+) \longrightarrow 2RH_2^+;\ k_1 = 4.5 \times 10^{17} \times \exp(-6200/RT)\ M^{-1}\ \text{sec}^{-1} \quad (1)$$

No evidence was found for direct photoejection of electrons from RH_2, a process which is well established in the case of numerous aromatic molecules.[3]

The experimental value of the preexponential term in the expression of k_1 yielded evidence against a simple sequence in which a rate-determining bimolecular step ($^3RH_2 + R \rightarrow$ products) is followed by fast protonation of the products, yielding two RH_2^+ ions. Thus, a mechanism was suggested involving a complex between $^3RH_2$ and R.[2]

In the present work we extended the flash experiments to mixed RH_2–R solutions of varying acidity with the purpose of learning more about the protonation step and of gaining new evidence for the role of an amine–imine triplet excimer in the above photooxidation. The results will also bear on the more general problem of photochemical events initiated by excimer formation.

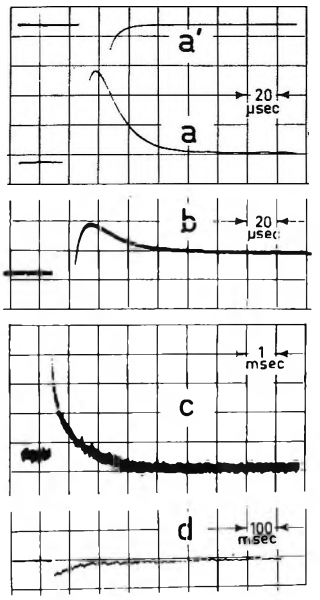

Figure 1. Oscillograms showing decay of transients in the flash photolysis of 3.7×10^{-5} *M* RH_2 and 3.0×10^{-6} *M* R, in a neutral THF solution at −98°: a, λ 600 mμ; $I_0 = 8$; a′, flash-scattered light under same conditions as a; b, λ 540 mμ; $I_0 = 8$; c, d, λ 475 mμ; $I_0 = 40$. I_0 is the dark to light deflection of the trace before flashing.

Experimental Section

1. Materials. Eastman DPPD was treated as previously described.[2] The diimine was prepared by oxidation of DPPD[4] and purified chromatographically after preliminary recrystallizations. Ethylamine (Matheson) was distilled on the vacuum line into a container with lithium wires. After solution of the metal, the solvent was redistilled to a storage container equipped with a side arm coated with a potassium mirror. When brought in contact with the mirror a blue solution was instantaneously formed, from which ethylamine was distilled out to prepare amine–imine or metal–imine solutions. Matheson tetrahydrofuran (THF) was refluxed for 24 hr over sodium and then distilled on the vacuum line to a storage container where it was kept over a liquid K–Na alloy. Acetic acid was Baker analytical grade reagent.

2. Preparation of Samples and Flash Apparatus. Experimental procedures were those previously described for both sample preparation[2] and flash-photolysis setup.[5] All experiments were carried out using an aqueous $CuSO_4$ solution filled into a special quartz jacket surrounding the low-temperature dewar, at the center of which a 50 mm long irradiation cell was axially mounted. The filter solution, adjusted to cut off exciting light below 270 mμ, prevented possible complications due to direct light absorption by the solvent. Glass apparatus was rinsed with alcohol and triply distilled water, and then baked for 2 hr at 500°. Amine–imine solutions in ethylamine were prepared by first dissolving the solutes in analytical grade ethanol or THF. After the original solvent was evaporated on the vacuum line, ethylamine was distilled in from its "blue" stock solution.

Results

1. Acid-Free Solutions. Flash-photolysis experiments on deaerated amine–imine solutions were carried out using pure THF or ethylamine as solvents. In both cases three principal stages were observed for the relaxation kinetics (Figure 1). A fast, exponential, decay of a transient peaking around 610 mμ (see spectra in Figures 2e and 3c) is followed by a slower ($\tau_{1/2} \cong 800$ μsec in THF at −98°) second-order process, due to a species absorbing around 475 mμ (Figure 2f). After the disappearance of both 610- and 475-mμ intermediates, a long-lived absorbance is left whose wavelength dependence is shown in Figures 2a and 3a. Such ("residual") absorbance undergoes a slow decay, leading to recovery of the original spectrum in a second-order process which exhibits the same half-lives at all three maxima (710, 535, and 390 mμ), as well as in the 450–490-mμ region where, due to bleaching of the 450-mμ imine band, ΔD is negative (Figure 1d). An Arrhenius plot for the decay rate constant of this process is presented in Figure 4B. In analogy to our previous observations,[2] we identify the 610-mμ transient as the amine triplet ($^3RH_2$). How-

(3) (a) G. E. Johnson and A. C. Albrecht, *J. Chem. Phys.*, **44**, 3179 (1966), and references therein; (b) L. I. Grossweiner and H. I. Joschek in "Solvated Electron," Advances in Chemistry series, American Chemical Society, Washington, D. C., 1968, p 279.

(4) J. Picard, *Ber.*, **46**, 1853 (1913).

(5) M. Ottolenghi and J. Rabani, *J. Phys. Chem.*, **72**, 593 (1968).

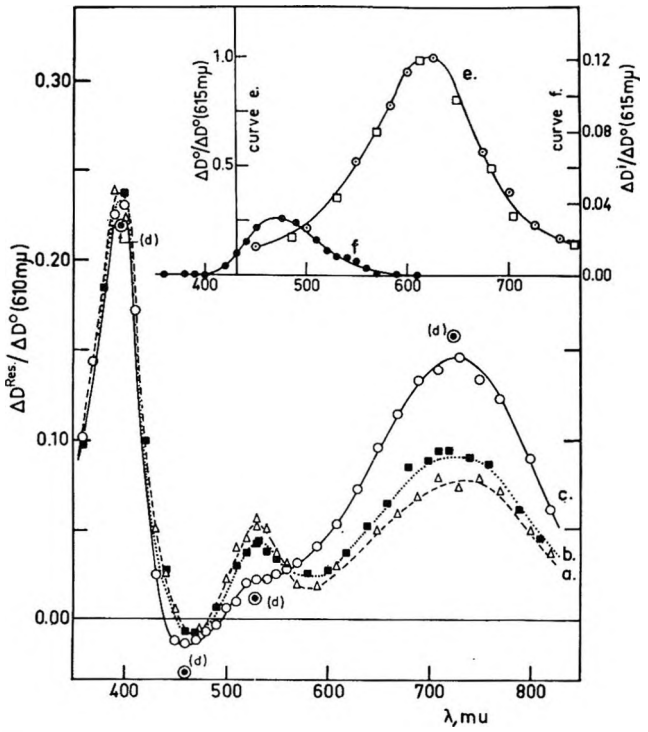

Figure 2. Spectral changes following flash excitation of RH_2 in THF in the presence of the corresponding diimine and varying [CH_3COOH]. ΔD^{RES} is residual absorption left after triplet and 475-mμ transient decays (see Figure 1). ΔD^0 (610 mμ) is "initial" absorption of $^3RH_2$ obtained from extrapolation of log ($\Delta D - \Delta D^{RES}$) *vs.* t plots to 10 μsec after flash triggering: a, [RH_2] = 5.4×10^{-5} M; [R] = 1.15×10^{-5} M in the absence of acid; $t = -98°$; b, [RH_2] = 3.0×10^{-5} M; [R] = 1.3×10^{-5} M; [CH_3COOH] = 6.1×10^{-3} M; $t = -107°$; c, [RH_2] = 2.95×10^{-5} M; [R] = 1.49×10^{-5} M; [CH_3COOH] = 6.0×10^{-2} M; $t = -100°$; d, [RH_2] = 6.0×10^{-5} M; [R] = 2.1×10^{-5} M; [CH_3COOH] = 6.0×10^{-1} M; $t = -99°$; e, spectra of $^3RH_2$ (615-mμ transient); (I) ○, neutral solutions; conditions of curve a; (II) □, acid solutions; conditions of curve c; f, spectrum of intermediate absorption, ΔD^i, (475-mμ transient), conditions as in curve a. ΔD^i is the difference between the absorbance measured immediately after the disappearance of the triplet (~100 μsec) and that measured after the decay of the 475-mμ transient (a few msec).

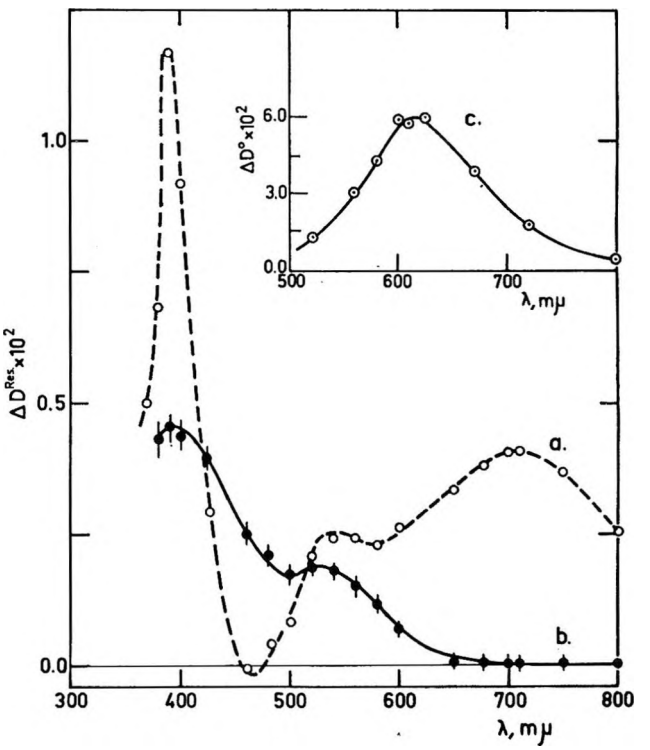

Figure 3. Transient spectra in the flash photolysis of 4.3×10^{-5} M RH_2 and 1.35×10^{-6} M R in ethylamine at −65°: a, residual absorbance change (ΔD^{RES}) measured 10 msec after flashing; half-life of decay of ΔD^{RES} is ~3 sec; b, contribution of transient X to curve a estimated as described in the text; c, spectrum of $^3RH_2$ (from extrapolation to t = 10 μsec after triggering).

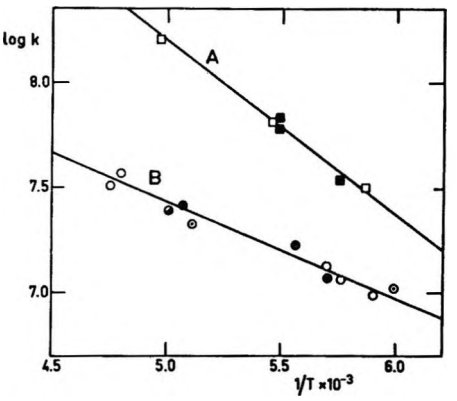

Figure 4. Temperature dependence of radical ions dismutation processes. A, Acid solutions: □, [CH_3COOH] = 6.0×10^{-1} M; [R] = 2.1×10^{-5} M; [RH_2] = 6.0×10^{-5} M; ■, [CH_3COOH] = 6.0×10^{-2} M; [R] = 1.5×10^{-5} M; [$RH]_2$ = 2.95×10^{-5} M. B, Neutral solutions. Imine concentrations are: ⊙, 5×10^{-5} M; ○, 3×10^{-5} M; ◑, 6.1×10^{-6} M; ●, 1.0×10^{-6} M. Values of k were obtained from plots of $1/\Delta D$ at 710 mμ *vs.* t, using [2] 1.1×10^4 M^{-1} cm^{-1} for the molar extinction coefficient of single RH_2^+ (see text) at this wavelength.

ever, in contrast to the photolysis in acid EPA, the RH_2^+ positive ion cannot by itself account for the complete spectrum of the long-lived residual absorption. Thus, the known spectrum of RH_2^+, chemically or photochemically generated in acid media, is characterized by maxima at 710 and 390 mμ but lacks the 535-mμ band and exhibits a considerably lower ΔD(390 mμ)/ΔD(710 mμ) ratio.[1,2] These results suggest that, in acid-free systems, the residual absorption left after the decay of both triplet and 475-mμ transients is a superposition of the spectra of RH_2^+ and of an additional intermediate, X, absorbing around 535 and 390 mμ. The relative contribution of RH_2^+ and X to the spectrum is not only time independent but was also found to be independent of imine concentration, even in the region where their sum strongly depends on [R]. Such information is included in Figure 5a, in which the ratios ΔD(710 mμ)/ΔD^0(610 mμ) and ΔD(535 mμ)/ΔD^0(610 mμ) are plotted *vs.* [R] in THF solutions

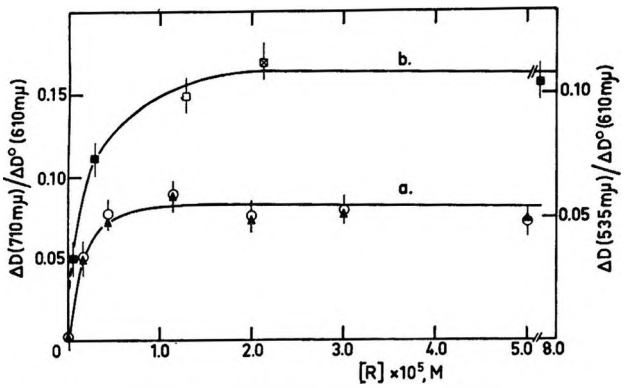

Figure 5. Dependence of radical ions yields on imine concentration in neutral and acid THF solutions; temperature ~−100°: a, no added acid; ϕ, RH_2^+ yields, left-hand scale; ▲, R^- yields, right-hand scale; b, acid solutions (RH_2^+ yields, left hand scale). CH_3COOH concentrations: ϕ, 6.0×10^{-2} *M*; ⧫, 9.5×10^{-2} *M*; ⊗, 6×10^{-1} *M*.

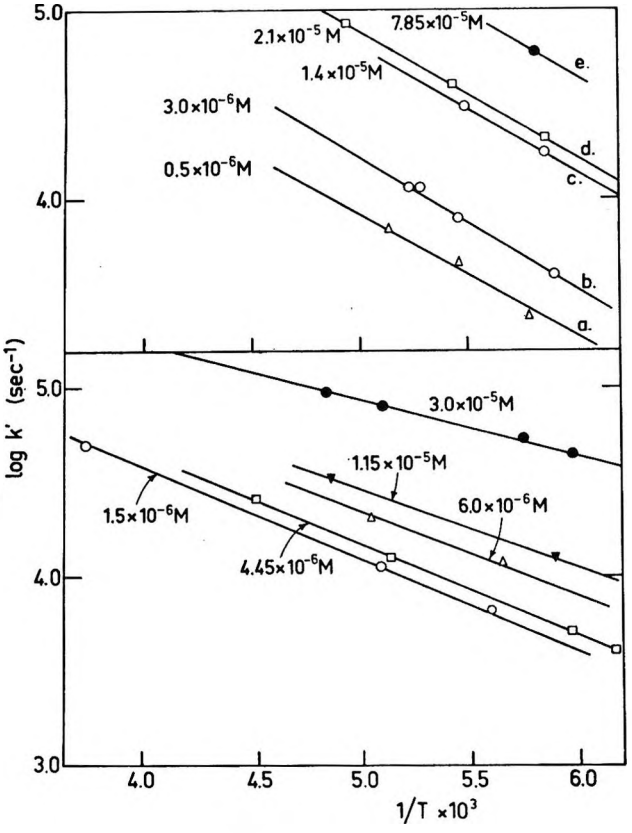

Figure 6. Amine triplet decay rate constants (k') as a function of temperature, imine, and acid concentrations: lower figure, neutral THF solutions; upper figure, acid THF solutions. Values of [CH_3COOH] are: a, b, e, 9.5×10^{-2} *M*; c, 6.0×10^{-2} *M*; d, 6.0×10^{-1} *M*. Numbers in the figure refer to [R] values.

around −100°. (ΔD^0(610 mμ) is the absorbance at 610 mμ, 10 μsec after triggering the flash, and it measures the initial triplet concentration.) At all values of [R], ΔD(710 mμ)/ΔD(535 mμ) ≅ 1.5. This ratio

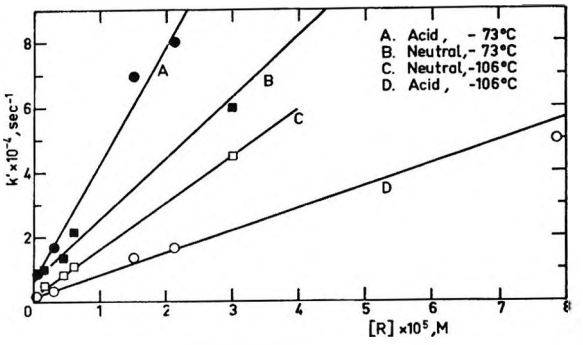

Figure 7. Plots showing the linear relation: $k' = k_0 + k_1$[R] (data taken from Figure 6).

was found to be independent of temperature in the range −24 to −104° as also was the ratio ΔD(710 mμ)/ΔD^0(610 mμ). Finally, we note that the first-order rate constant, k', observed for the triplet decay is directly proportional to the imine concentration (Figures 6 and 7). We therefore conclude (see also ref 2) that both X and RH_2^+ are formed *via* a reaction of the RH_2 triplet with the corresponding ground-state imine.

As to the 475-mμ intermediate, we always observe, independently of imine concentration, a constant ratio of 0.15 ± 0.01 between its own absorbance at 475 mμ and that measured for X and RH_2^+ at 390 mμ.

2. Effects of Added Acid. When CH_3COOH is gradually added to an RH_2 solution in THF at *ca.* −100°, no effects on the general photochemical spectral patterns are noticed as long as the acid concentration is kept below ~10^{-3} *M*. Above this concentration a further increase in [CH_3COOH] is accompanied by a drop in the intensity of the 535-mμ peak and by an increase of the absorbance at 710 mμ (Figure 2). At high acid concentrations ([CH_3COOH] > 2×10^{-1} *M*) a new, acid-independent spectrum is ultimately obtained in which the 535-mμ band is missing and the 710-mμ peak (but not the 390-mμ one) is doubled compared to its value in acid-free THF. The 475-mμ transient exhibits the same sensitivity to acid as the 535-mμ species and is not observed in acid solutions. Figure 5b indicates that the effect of acid on the 535-mμ band is independent of imine concentration in the whole region of the plateau (10^{-5} *M* < [R] < 8×10^{-5} *M*). We note that the new spectrum of the long-lived absorption in acid THF is identical with the one observed by us (and attributed to RH_2^+) in acid EPA systems.[2] This applies also to the spectrum of $^3RH_2$ which was found to be independent of acid concentration (Figure 2e).

The addition of acid affects also the relaxation kinetics in the amine–imine photochemistry. The data concerning the triplet decay rates are presented in Figures 6 and 7. Those related to the slow recovery of the initial absorption are shown in Figure 4A. Here a new bimolecular decay constant is observed ($k = 9.8 \times$

10^{11} exp(−3600/RT) M^{-1} sec^{-1}) which differs from the expression (k = 4.8 × 10^9 exp(−2100/RT) M^{-1} sec^{-1}) measured in acid-free solutions.

By contrast to our observation in neutral solutions, the yields of RH_2^+ in acid were found to be temperature dependent. Thus, in the range between 170 and 210°K we observe $d\Delta D(710\ m\mu)/dT \cong 1.5 \times 10^{-3}$/deg for ΔD values measured under conditions of independency on both acid and imine concentrations.

3. Spectrum and Identification of X. The disappearance of X and of the 475-mμ intermediate upon addition of acid, accompanied by doubling of the absorbance around the characteristic 710-mμ peak of RH_2^+, suggests that the acid effect is one of replacing both transients by RH_2^+. Thus, a reasonable assumption would be that of identifying X and the 475-mμ species with unprotonated forms of RH_2^+ such as R^- or RH.

To obtain independent information concerning the identity of the new species, we carried out experiments in which pure imine was dissolved in a blue solution of potassium in ethylamine. In the imine–metal solution the characteristic 675-mμ metal and 450-mμ imine bands are replaced by a new spectrum exhibiting peaks or shoulders around 675, 580, 450, and 390 mμ (Figure 8, curve a). (After exposure to atmospheric oxygen, the solution is partially bleached, the absorption consisting now of the single 450-mμ imine band.) Obviously, the spectrum in the imine metal system indicates the appearance of a new species, in equilibrium with metal and imine which we identify as the R^- negative ion. A superficial examination of curves a in Figures 3 and 8 suggests the identification of X as the imine negative ion. However, a quantitative comparison between the two species requires evaluation of their exact spectra, free from contributions of overlapping absorptions. The derivation of the spectrum of R^- from the flash experiments in neutral solutions was carried out by assuming the stoichiometry: $RH_2 + R \xrightarrow{h\nu} RH_2^+ + R^-$ which implies: $\Delta D^{RES} = (-\epsilon_{RH_2} - \epsilon_R + \epsilon_{R^-} + \epsilon_{RH_2^+}) \times 5c$, where c is the concentration change in the 5-cm flash cell. The spectrum of R^- (*i.e.*, $\epsilon_{R^-}(\lambda)5c$) was calculated from the last expression and the experimental $\Delta D^{RES}(\lambda)$ values (trace a in Figure 3) by: (a) setting $\epsilon_{RH_2}(\lambda) = 0$ whenever $\lambda > 350$ mμ;[2] (b) assuming $\epsilon_{R^-}(\lambda) = 0$ at $\lambda > 660$ mμ. This seems justified by the similarity of the spectrum in this region and that of single RH_2^+ (acid solutions). Therefore, in the case of Figure 3, $\Delta D(710\ m\mu) = \epsilon_{RH_2^+}(710\ m\mu) \times 5c = 0.042$. This value, together with the known ratio $\epsilon_{RH_2^+}(710\ m\mu)/\epsilon_{RH_2^+}(\lambda)$ (see Figure 1 in ref 2), was used to calculate the contribution of RH_2^+ to trace a in Figure 3; (c) using the known ratio $\epsilon_R(\lambda)/\epsilon_{RH_2^+}(710\ m\mu)$ (Figure 1, ref 2) to calculate $\epsilon_R(\lambda) \times 5c$. A curve obtained for $5c\epsilon_{R^-}(\lambda)$ using such procedure in an ethylamine solution is presented in Figure 3b.

In deriving the contribution of R^- to the spectrum of the metal–imine solutions, a correction had to be carried out for the overlapping absorptions of the free imine (D_R) and metal (D_K) components, since now: $D = D_{R^-} + D_R + D_K$. The assumption was again made that R^- does not contribute at $\lambda > 660$ mμ. This is independently justified in the present case since the shape of the absorption curve above 660 mμ is the same in pure metal and metal–imine solutions (compare a and b in Figure 8). Thus, the wavelength dependence of the absorption due to the free metal, $D_K(\lambda)$, was calculated from the known shape of the metal 675-mμ band (Figure 8b) using $D(700\ m\mu) = D_K(700\ m\mu) = 0.40$ as a normalization factor. Unfortunately, no independent estimate of the imine contribution was available in the metal imine solutions. However, we proceeded with the spectral analysis by using the isosbestic wavelength of the absorption of R^- and R previously established in the treatment of the flash data. We thus take $\epsilon_{R^-} = \epsilon_R$ at λ 450 mμ (see Figure 3 noticing[2] the small, ~10%, contribution of RH_2^+ at this wavelength) and make use of the known spectrum of R,[2] in order to evaluate D_R at all wavelengths. Such a procedure is presented in Figure 8. The resulting spectrum of R^- (trace e) fairly coincides with that calculated from the flash experiments establishing the identity of X and the imine negative ion. The identity of the two spectra may also serve as indirect support for our previous (arbitrary) assumption that in neutral solutions R^- and RH_2^+ are formed in equimolecular amounts, since it was on such a basis that curve b, Figure 3, was calculated. From the above arguments a semiquantitative estimate of the extinction coefficients of R^- in ethylamine is obtained.

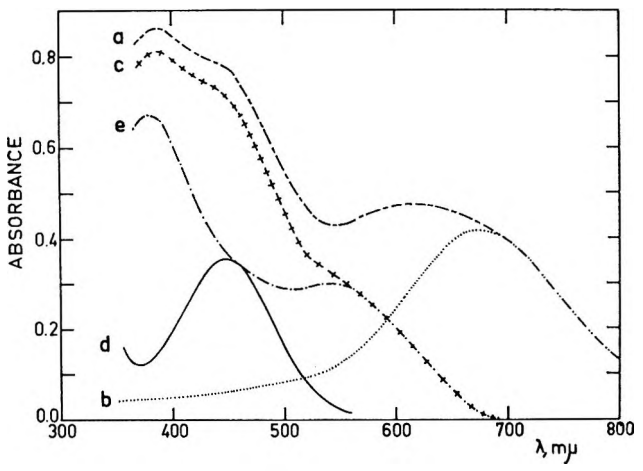

Figure 8. Absorption spectra in a solution of R (7.5×10^{-5} M) and potassium metal in ethylamine at room temperature (1-cm cell): a, spectrum recorded after bringing in contact the imine with a solution of K in ethylamine. b, spectrum of a potassium–ethylamine solution, normalized to D = 0.4 at 700 mμ; c, difference spectrum: D(a) − D(b); d, imine contribution to trace c evaluated as described in the text. e, difference spectrum D(c) − D(d), attributed to R^-.

$\epsilon_{R^-}(535\ m\mu) \cong 6 \times 10^3 M^{-1}\ cm^{-1}$;

$\epsilon_{R^-}(390\ m\mu) \cong 1.5 \times 10^4 M^{-1}\ cm^{-1}$

4. The 475-mμ Intermediate. As previously reported, the yields of the 475-mμ transient around $-100°$ are always proportional to those of R^-, exhibiting a similar dependence on both imine and acid concentrations. Since no growing in of R^- (or RH_2^+) is observed which matches the intermediate decay at 475 mμ, we conclude that the 475-mμ transient is not a precursor of R^-. This indicates that the 475-mμ species and R^- are formed in parallel, *via* similar competing steps, in the reaction between $^3RH_2$ and R. We wish to suggest the RH radical, formed according to $^3RH_2 + R \rightarrow 2RH$, in order to explain the intermediate second-order decay (*via* $2RH \rightarrow RH_2 + R$) of the single band around 475 mμ). Such identification is favored by the large blue shifts, following subsequent protonation, observed for the lowest absorption bands of semiquinone radicals.[6]

Discussion

1. Mechanism of the Reaction between $^3RH_2$ and R. When attempting to explain the experimental observations presented above, three mechanisms can be proposed (I, II, and III)

$$^3RH_2 + R \longrightarrow RH_2^+ + R^- \qquad (\text{and } ^3RH_2 + R \longrightarrow 2RH) \quad \text{(Ia)}$$

$$R^- + 2HA \rightleftharpoons RH_2^+ + A^- \qquad (\text{and } RH + HA \rightleftharpoons RH_2^+ + A^-) \quad \text{(Ib)}$$

$$^3RH_2 + 2HA \longrightarrow {}^3RH_2 \cdot 2H^+ + 2A^- \quad \text{(IIa)}$$

$$^3RH_2 + R \longrightarrow RH_2^+ + R^- \text{ (or } 2RH) \quad \text{(IIb)}$$

$$^3RH_2 \cdot 2H^+ + R \longrightarrow 2RH_2^+ \quad \text{(IIc)}$$

$$^3RH_2 \xrightarrow{k_0} RH_2 \quad \text{(IIIa)}$$

$$^3RH_2 + R \underset{k_b}{\overset{k_a}{\rightleftharpoons}} (^3RH_2 \cdot R) \quad \text{(IIIb)}$$

$$(^3RH_2 \cdot R) \xrightarrow{k_c} RH_2^+ + R^- \quad \text{(IIIc)}$$

$$(^3RH_2 \cdot R) \xrightarrow[2H^+]{k_d} 2RH_2^+ \quad \text{(IIId)}$$

$$(^3RH_2 \cdot R) \xrightarrow{k_e} RH_2 + R \quad \text{(IIIe)}$$

These mechanisms are consistent with (a) the formation of RH_2^+, R^-, and RH from $^3RH_2$ *via* a reaction with R, and (b) the acid effect which, at sufficiently high concentrations of CH_3COOH, replaces R^- and RH by RH_2^+. Mechanism I, in which step b represents a fast equilibrium attained practically simultaneously with step a (we do not observe any $R^- \rightarrow RH_2^+$ conversion after the end of the triplet decay), is inconsistent with the fact that the ratio between RH_2^+ and R^- is unaffected by acid as far as up to $[CH_3COOH] \cong 10^{-3}\ M$. Such behavior could actually be expected only if, in neutral solutions, the equilibrium Ib lay far on the R^- side, which implies (Figures 2 and 3) $\epsilon_{R^-}(530\ m\mu) \ll \epsilon_{RH_2^+}(710\ m\mu)$. This is, however, in variance with (a) the spectra in metal–imine solutions which qualitatively require $\epsilon_{R^-}(535\ m\mu) \cong \epsilon_R(450\ m\mu) \cong \epsilon_{RH_2^+}(710\ m\mu)$, and (b) the agreement (see above) between the spectrum of R^- and that of X calculated assuming $[R^-] = [RH_2^+]$ in neutral solutions.

Mechanism II, in which acetic acid competes with R for the amine triplet (possibly *via* its protonated form $^3RH_2 \cdot 2H^+$), will imply an effect of imine concentration, at constant acid, on the ratio between the yields of R^- and RH_2^+. This, however, is not the case, since as shown in Figure 5, a constant value $\Delta D(710\ m\mu)/\Delta D^0(610\ m\mu) \cong 0.16$, independent of the imine concentration, is reached even when $[CH_3COOH] = 9.5 \times 10^{-2}\ M$, *i.e.*, when still a few per cent of R^- escapes conversion to RH_2^+. Such an argument will not hold if step a in mechanism II is a fast equilibrium between acid and neutral triplet states. However, one will expect in such a case that both the spectrum of $^3RH_2$ and k_0 in the empirical expression $k' = k_0 + k_1[R]$, observed for the triplet decay rate constant, will depend on acid. As shown in Figures 2e and 7 this is not the case. We are therefore led to the conclusion that the above two mechanisms cannot account for the experimental phenomena, implying that the protonation step does not involve directly either R^-, (RH), or $^3RH_2$. The possibility that protonated forms of ground state RH_2 or R account for the observations in acid media could be ruled out by the complete lack of acid effects on the absorption spectra of the amine, the imine, or their mixtures. Thus, in order to explain the detailed effects of imine and acid concentrations, an additional intermediate has to be postulated which: (a) is a precursor of R^-, RH, and RH_2^+ in the acid-free systems; (b) reacts with acid to yield two RH_2^+ ions; (c) is formed from the amine triplet *via* a reaction with R. Accordingly, we suggest mechanism III, involving the mixed amine–imine triplet state excimer $(^3RH_2 \cdot R)$. The assignment of the 475-mμ absorption to the RH radical will imply the additional path

$$(^3RH_2 \cdot R) \xrightarrow{k_f} 2RH \quad \text{(IIIf)}$$

Scheme III will fulfill the experimental relationship $k' = k_0 + k_1[R]$, in three distinct cases: (A) in a mechanism which does not require equilibration of excimer and triplet but assumes a competition between products formation in steps c, f, d, and deactivation of the excimer in process e. This implies $k_a[R] \gg k_c$ and $k_e \gg k_b$; (B) in a simple sequence, with the formation of the complex in IIIb as the rate-determining step ($k_a[R] \ll k_c$, $k_b \ll k_c$); (C) assuming complete

(6) N. K. Bridge and G. Porter, *Proc. Roy. Soc.*, **A244**, 259 (1958).

equilibration of the complex in reaction b, with $k_a[R] \ll k_b$, $k_b \gg k_d$.

The first mechanism seems unprobable, mainly because of the lack of any temperature effect on the yields of the products in neutral solutions. It is unlikely that a competition between deactivation (step e) and products formation (step c and f) will be temperature independent over a range of 80°K. Mechanism B requires k' to be acid independent, which contradicts the observations presented in Figures 6 and 7. We are thus left with the last alternative which requires equilibration of the complex. Examining the details of such a mechanism, we see that step d cannot involve a simple irreversible reaction with acid leading to RH_2^+ formation. This follows from the fact that if this were the case, then $k_1 = k_a(k_c + k_d + k_f)/k_b$.

Since total conversion of R^- (and RH) to RH_2^+ requires $k_d \gg k_c$, one would expect an increase by at least an order of magnitude in the value of k_1 when going from neutral ($k_d = 0$) to acid solutions, where conversion of R^- to RH_2^+ is complete. As shown in Figure 7, this is not observed. We conclude that reaction d should actually involve the steps

$$({}^3RH_2 \cdot R) \underset{}{\overset{2H^+}{\rightleftharpoons}} ({}^3RH_2 \cdot R \cdot 2H^+) \qquad (d_I)$$

$$({}^3RH_2 \cdot R \cdot 2H^+) \xrightarrow{k'_d} 2RH_2^+ \qquad (d_{II})$$

and possibly

$$({}^3RH_2 \cdot R \cdot 2H^+) \xrightarrow{k'_b} {}^3RH_2 + R + 2H^+ \qquad (d_{III})$$

$$({}^3RH_2 \cdot R \cdot 2H^+) \longrightarrow RH_2 + R + 2H^+ \qquad (d_{IV})$$

If the equilibrium in (d_I) is fast, the condition $[RH_2^+] \gg [R^-]$, prevailing in acid solutions, will not imply a drastic change in k_1 as long as k'_d does not differ too much from k_c, and k_b from k'_b.

Attention has to be paid to the temperature dependence of the yields of RH_2^+ observed in acid THF solutions under conditions of total scavenging of $^3RH_2$ by R. Also, the maximum value $\Delta D(390\ m\mu)/\Delta D^0(610\ m\mu) = 0.22$, now observed in THF at −100°, should be compared with the value 0.6 previously measured[2] in acid EPA around −160°. This implies a temperature- and, possibly, solvent-dependent competition between deactivation and one of the steps in scheme III. Since no dependency of the yields on temperature is observed in neutral solutions, it appears that deactivation is associated with the protonation equilibrium (d). In other words, only reaction III (d_{IV}) but not IIIe efficiently competes with the formation of the products. Such a conclusion is not inconsistent with the observed doubling of the yields of RH_2^+ in acid systems. In the absence of deactivation, since not only R^- but also RH is replaced by RH_2^+ in acid solutions, one would expect more than a factor of 2 in the above yield ratio, as long as the extinction coefficient of RH at 475 mμ does not exceed $\sim 2 \times 10^4\ M^{-1}\ sec^{-1}$. Since, within experimental accuracy, the yields are not more than doubled, deactivation in step IIId is probably implied. However, other paths of deactivation, *e.g.*, competing with complex formation in step b, cannot be ruled out definitely. An independent determination of the extinction coefficient of RH may help to clear this point as well as the question of the relative yields of steps IIIc (ionic dissociation) and IIIf (radical formation) in the decay of ($^3RH_2\cdot$).

We cannot at present quantitatively account for the difference between the expression $k_1 = 4.5 \times 10^{17} \exp(-6200/RT)\ M^{-1}\ sec^{-1}$ observed in acid EPA below −100° and the value $k_1 = 8.0 \times 10^{12} \exp(-3700/RT)\ M^{-1}\ sec^{-1}$ measured in acid THF between −50 and −100°. (In neutral THF $k_1 = 4.0 \times 10^{11} \exp(-2140/RT)\ M^{-1}\ sec^{-1}$). We wish to point out, however, that the plot of log k *vs.* $1/T$ in EPA exhibits a break around −100° so that, above such temperature, an activation energy of ~3 kcal is observed, which is less than half the value in the −100 to −160° range. In view of the complexity of mechanism III such behavior is not unexpected.

2. Dissociation Pathways of the Excited Complex. The results and conclusions presented above should be discussed in view of our present knowledge on molecular complexes, in both ground and excited states. Excimer formation for excited aromatic molecules has been extensively investigated for singlet states.[7-10] The corresponding phenomenon for triplets is less known and only a few cases have been reported where excimer characteristics are observed in phosphorescence.[11]

A similar situation prevails in the case of mixed excimers. Such excited complexes are readily accessible, for singlet states, through light absorption by their ground-state form[12] or *via* direct interaction between excited- and ground-state components.[13] Lately, the charge-transfer character of the fluorescing state of some complexes has been clearly demonstrated.[14-17] Al-

(7) Th. Förster and K. Kasper, *Z. Elektrochem.*, **59**, 976 (1955).

(8) J. N. Murrell and J. Tanaka, *Mol. Phys.*, **7**, 363 (1964).

(9) T. Azumi, A. T. Armstrong, and S. P. McGlynn, *J. Chem. Phys.*, **41**, 3839 (1964); **42**, 1675 (1965).

(10) M. T. Vala, I. H. Hillier, S. A. Rice, and J. Jortner, *ibid.*, **44**, 23 (1966).

(11) G. Castro and R. M. Hochstrasser, *ibid.*, **45**, 4352 (1966); C. Lim and S. K. Chakrabarti, *Mol. Phys.*, **13**, 293 (1967).

(12) For reviews, see (a) S. P. McGlynn, *Chem. Rev.*, **58**, 1113 (1958); (b) G. Briegleb, "Elektronen-Donator-Acceptor-Komplexe," Springer Verlag, Berlin-Göttingen-Heidelberg, 1961; (c) R. S. Mulliken and W. B. Person, *Ann. Rev. Phys. Chem.*, **13**, 107 (1962).

(13) (a) H. Leonhardt and A. Weller, *Ber. Bunsenges. Physik. Chem.*, **63**, 791 (1963); (b) A. Weller in Photochemistry Symposium, University of Rochester, 1963.

(14) E. A. Chandross and J. Ferguson, *J. Chem. Phys.*, **47**, 2557 (1967).

(15) H. Beens, H. Knibbe, and A. Weller, *ibid.*, **47**, 1183 (1967).

(16) H. Knibbe, K. Röllig, F. P. Schäfer, and A. Weller, *ibid.*, **47**, 1184 (1967).

(17) M. S. Walker, T. W. Bednar, and R. Lumry, *ibid.*, **47**, 1020 (1967).

though predicted long ago,[12] it is only recently[18] that triplet (CT) states of molecular complexes have been directly observed through their phosphorescence spectra. In the present and previous[2] works we presented evidence for what we believe to be the first detection of a mixed triplet excimer formed by direct interaction of an excited donor with a ground-state acceptor. Since always present at very low concentrations relative to those of its equilibrium components, the excited complex cannot be followed directly by means of absorption or emission spectroscopy. Qualitative information concerning the electronic states of the amine–imine complex can be drawn, however, from the kinetics of the reactions associated with its formation and dissociation.

The data in the preceding sections indicate that ($^3RH_2 \cdot R$) is totally equilibrated with its $^3RH_2$ and R components. This implies that its dissociation to RH_2^+ and R^- (or to 2RH) is slow relative to the dissociation which leads to triplet amine and ground-state imine ($k_c \ll k_b$ in mechanism III). The dissociation mechanism can therefore be visualized in terms of two distinct states, one leading to $^3RH_2$ and R, and the second yielding RH_2^+ and R^-. Both states can be described by assigning appropriate values to the coefficients a, b, c, and d in the generalized wave function Ψ of a bimolecular excited complex[8,9] which in the present case (RH_2 donor and R acceptor) assumes the form

$$\Psi = a\Psi(R^-RH_2^+) + b\Psi(R^+RH_2^-) + c\psi(^3RH_2 \cdot R) + d\psi(RH_2 \cdot {}^3R)$$

In view of the large energy gap between $^3RH_2$ and ^3R, and of the clear donor and acceptor characters of RH_2 and R, respectively, we may assume $a \gg b$ and $c \gg b$. Therefore

$$\Psi = a\psi(R^-RH_2^+) + c\psi(^3RH_2 \cdot R)$$

The two states, for which we shall adopt the notation,[12a] ^3E and $^3N^*$, can now be described in terms of such expression by setting $a > c$ for the primarily ionic ^3E state, and $a < c$ for the locally excited $^3N^*$. A possible potential energy diagram for the system is given in Figure 9. Collision between $^3RH_2$ and R will lead to the $^3N^*$ state. After thermalization, the complex may undergo dissociation to its original components (step IIIb) with activation energy E_b. Alternatively, it may cross to the ^3E state from which, with appropriate activation (E_c), it will yield the radical products RH_2^+ and R^-. Total equilibration of the complex means $k_b \gg k_c$, *i.e.*, $E_c > E_b$. A similar picture, though complicated by proton transfer along additional coordinates, will also apply to the dissociation of ($^3RH_2 \cdot R$) to 2RH and of ($^3RH_2 \cdot R \cdot 2H^+$) to $2RH_2^+$.

3. Kinetics of R^- and RH_2^+ Decay. In neutral THF solutions, second-order kinetics are observed for the slow decays of the 710-, 535-, and 390-mμ bands as well as for the recovery around 470 mμ. Since half-lives of the process were found, within experimental degree of accuracy, to be independent of wavelength, the reaction

$$R^- + RH_2^+ \xrightarrow{k_2} RH_2 + R \qquad (2)$$

is suggested to account for the main path of the semiquinones dismutation. This implies that such a process is much faster than the alternative reactions between two RH_2^+ or two R^- ions. An Arrhenius plot for the second-order rate constant measured in neutral THF solutions at 710 mμ in the range 170–210°K is presented in Figure 4B. The graph shows independency of k_2 on imine concentration yielding the expression $k_2 = 4.8 \times 10^9 \exp(-2100/RT)\ M^{-1}\ \text{sec}^{-1}$. The value of 2.1 ± 0.2 kcal observed for the activation energy is probably too low to account for simple single-staged kinetics. It is possible that the dismutation proceeds *via* an ion-pair intermediate according to $R^- + RH^+ \leftrightarrows (RH_2^+ \cdot R^-) \rightarrow R + RH_2$. The temperature dependence of the rates of the process

$$RH_2^+ + RH_2^+ \xrightarrow{k_3} R + RH_2 + 2H^+ \qquad (3)$$

which takes place in acid solutions when RH_2^+ is the only product, was shown in Figure 4A. For k_3, in the above temperature range, we obtain the expression $k_3 = 9.8 \times 10^{11} \exp(-3600/RT)$, independently of [R] and [CH_3COOH]. Figure 4 shows that second-order rate constants in acid solutions are always higher than those observed for reaction 2 in the absence of acid. Since we have previously required that in a neutral solution $k_3 < k_2$, this implies that k_3 (which is practically

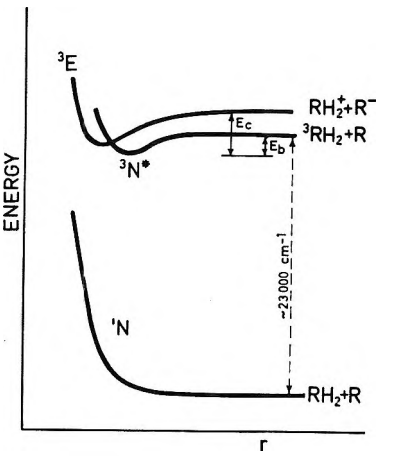

Figure 9. Assumed potential energy curves for the ($RH_2 \cdot R$) complex. ^1N is the repulsive ground state of the system. $^3N^*$ is the lowest locally excited triplet state, and ^3E the predominantly ionic (CT) triplet. r is the coordinate representing the distance between the two components, when their relative orientations are as those at the equilibrium separation.

(18) S. Iwata, J. Tanaka, and S. Nagakura, *J. Chem. Phys.*, **47**, 2203 (1967).

acid independent above [CH_3COOH] $\cong 6 \times 10^{-2}$ M) has a much lower value in an acid-free system. Such behavior may be due to salt effects on k_3 upon increasing acid concentration. Further work, studying salts, solvent, and light intensity effects, may help to clear the dismutation mechanism in both acid and neutral solutions.

Acknowledgment. The authors wish to thank Dr. J. Rabani and Professor H. Linschitz for valuable discussions.

Photoreduction of Aminobenzophenones in Nonpolar Media. Effects of Tertiary Amines[1]

by Saul G. Cohen and Jacob I. Cohen

Department of Chemistry, Brandeis University, Waltham, Massachusetts 02154 *(Received May 7, 1968)*

p-Aminobenzophenone (PAB) is photoreduced very inefficiently if at all by 2-propanol and by 2-butylamine, $\varphi < 0.001$, due to a low-lying chemically unreactive charge-transfer (CT) triplet. PAB is photoreduced by triethylamine with quantum yields at 313–360 mμ varying from 0.22 to 0.57. Quantum yields are higher (i) at higher light intensity, (ii) at lower initial concentrations of PAB, and (iii) in dilute solution of amine in hydrocarbon. Reactivity of the tertiary amine arises from low polarity which leads to a chemically reactive n,π^* triplet, and from heteroatom activation by N. Lower φ at higher concentration of PAB arises from deactivation of PAB triplet by PAB ground state with efficiency half that of diffusion-controlled quenchers, in a process which may convert n,π^* to CT triplet. Self-quenching is also observed in photoreduction of PAB by diisopropylamine, and in photoreduction of dimethylaminobenzophenone by triethylamine, which in general resembles that of PAB. Increase of φ by dilution with cyclohexane may arise from more efficient conversion to n,π^* triplet. Dilution of triethylamine with acetonitrile prevents photoreduction; the dipolar aprotic solvent, like protic solvents, stabilizes and leads to the unreactive CT triplet. Photoreduction of PAB by cyclohexane has $\varphi \cong 0.05$ and leads to ~90% pinacol. Photoreduction of PAB by diisopropylamine, $\varphi \cong 0.04$–0.09, leads to ~100% pinacol; photoreduction in triethylamine leads to 55% pinacol. Decrease of φ with decreasing concentration of triethylamine in cyclohexane is small and leads to $k_d/k_r = 0.011$ M. The effect of naphthalene in quenching photoreduction of PAB by triethylamine, when correction is made for self-quenching, leads to $k_q/k_r = 500$, $k_r \cong 1 \times 10^7$ M^{-1} sec^{-1}. Similar study in 1 M triethylamine in cyclohexane leads to $k_q/k_r = 90$, $k_r \cong 4 \times 10^7$ M^{-1} sec^{-1}, $k_d = 4.6 \times 10^5$ sec^{-1}. The characteristics of photoreduction by amines, reactivity of bridgehead N, low k_d/k_r, low effectiveness of quenchers, moderate quantum yields, no N-deuterium, and small α-deuterium isotope effects, are consistent with rapid interaction of triplet with the nonbonding electrons of N, followed partly by transfer of hydrogen and partly by regeneration of ketone and amine. Photoreduction of *m*-aminobenzophenone by triethylamine is about one-tenth as efficient as that of PAB; *o*-aminobenzophenone is not photoreduced significantly.

The photoreduction of aromatic ketones by primary and secondary alcohols,[2] leading to pinacols and carbinols,[3] is a long known and useful reaction. Hydrocarbons[4,5] and ethers[6–8] were also found to be hydrogen donors, but they were generally less effective than alcohols. The n,π^* excited triplet is thought to be the chemically reactive state of the ketone.[9,10] There are, however, groups of ketones which are either not photoreduced by alcohols or are photoreduced with low efficiency. (i) Ketones which have an appropriate *ortho* substituent may show hydrogen transfer from the substituent to the excited carbonyl, followed by reverse transfer, which leads finally to regeneration of the original ketone.[11–13] (ii) Ketones which have a lowest triplet state of the π,π^* rather than the n,π^* type show low reactivity to alcohols.[12] These may include fluore-

(1) For a preliminary report on part of this work, see S. G. Cohen and J. I. Cohen, *J. Amer. Chem. Soc.*, **89**, 164 (1967).

(2) (a) G. Ciamician and P. Silber, *Ber.*, **33**, 2911 (1900); **34**, 1541 (1901); (b) W. D. Cohen, *Rec. Trav. Chim.*, **39**, 243 (1920); (c) J. N. Pitts, Jr., R. L. Letsinger, R. P. Taylor, J. M. Patterson, G. Recktenwald, and R. B. Martin, *J. Amer. Chem. Soc.*, **81**, 1068 (1959).

(3) W. E. Bachmann, *ibid.*, **55**, 355, 391 (1933).

(4) E. Paterno and G. Chieffi, *Gazz. Chim. Ital.*, (II) **39**, 415 (1909).

(5) G. S. Hammond, W. P. Baker, and W. M. Moore, *J. Amer. Chem. Soc.*, **83**, 2795 (1961).

(6) G. Ciamician and P. Silber, *Ber.*, **44**, 1554 (1911).

(7) E. Bergmann and S. Fujise, *Ann.*, **483**, 65 (1930).

none,[3] xanthone,[14] naphthyl carbonyl compounds,[15,16] polyalkyl-substituted acetophenones,[17] and probably phenyl-substituted benzophenones.[12] (iii) Ketones, including *p*-aminobenzophenone, which have a lowest triplet state in alcohols of the charge-transfer (CT) type will not show efficient photoreduction in such solvents.[18] In a less polar medium, cyclohexane, the levels may be inverted and the chemically reactive n,π^* triplet state may be formed, and photoreduction was observed. Doubt has been expressed as to the formation of a pinacol from the photoreduction of *p*-aminobenzophenone (PAB) by cyclohexane.[19]

We observed[20] that *p*-dimethylaminobenzophenone and *o*- and *p*-aminobenzophenones are readily photoreduced by alcohol in the presence of mineral acid, which protonates the amino group, localizes the electron pair, and leads to the n,π^* triplet. Quaternization of the *p*-amino group also leads to "normal" photoreduction in aqueous alcoholic media.[20b,21] We also observed that aliphatic amines are particularly effective photoreducing agents for aromatic ketones which are photoreduced by alcohols.[22,23] Amines are less polar than alcohols and it appeared reasonable to examine them as photoreducing agents for ketones which lead to π,π^* and CT triplets in alcohols. We now give a more detailed report[1] on the photoreduction of *p*-aminobenzophenone, PAB, and other aminobenzophenones by aliphatic amines. A study of the ketones which lead to π,π^* triplets will be reported later.

Experimental Section

Materials. *o*- and *p*-Aminobenzophenone, obtained from Aldrich, were treated with charcoal, recrystallized twice from 2-propanol, and dried under vacuum, mp 107–108° and 123–124°, respectively. *m*-Aminobenzophenone was prepared by a reported[24] procedure and recrystallized from benzene–cyclohexane, mp 85–86°. *p*-Dimethylaminobenzophenone, available from a previous study,[20] was recrystallized from ethanol, mp 89–90°. Benzophenone, Fisher reagent grade, was recrystallized from ethanol–water, mp 47–48°. Benzhydrol, Eastman White Label, was recrystallized from petroleum ether (bp 60–110°), mp 67–68°.

Amines were distilled immediately before use: *n*-butylamine, Eastman, bp 78°; 2-butylamine, Eastman, bp 63°; and diisopropylamine, Eastman, bp 83–84°. N-Ethyl diisopropylamine, Aldrich, was distilled from sodium hydride and redistilled before use, bp 127–128°. Triethylamine, Eastman, was distilled from sodium hydride and redistilled under argon before use, bp 89–90°. Triethylenediamine, Aldrich, was sublimed twice under vacuum before use.

Acetonitrile was from Matheson Coleman and Bell, Spectrograde. Acetone, benzene, cyclohexane, isooctane were Eastman Spectrograde. Diisopropyl ether, Fisher, was distilled from lithium aluminum hydride before use, bp 68–69°. Methanol was Fisher reagent grade. 2-Propanol, used in kinetics, was Eastman Spectrograde; that used for dilutions was Fisher reagent grade. Argon, Airco welding grade, was passed over Drierite and used. N,N-Dimethylformamide, Fisher reagent grade, formamide, Fisher reagent grade, and N-methylformamide, Eastman White Label, were used directly.

2,2′-Dinaphthyl, Gallard-Schlessinger, was recrystallized from cyclohexane, mp 187.5–188.5°. Naphthalene, Fisher, was recrystallized twice from methanol, mp 80°. *trans*-Stilbene, Pilot Chemical, was recrystallized twice from 2-propanol, mp 125–126°. Benzyl disulfide, Eastman White Label, was recrystallized twice from methanol, mp 69–70°. α-Toluenethiol, Eastman, was distilled, bp 71° (8 mm). Mesityl mercaptan was prepared as described previously.[25] Analysis by glpc, carbowax column, column 185°, detector 280°, injector 250° showed one peak, retention time 6 min. 1,10-Phenanthroline, Eastman, was used directly. Potassium ferrioxalate was prepared according to a reported[26] procedure. Diphenylamine barium sulfonate, Eastman White Label, was used directly.

Irradiation Procedure. Aliquots, 4 or 5 ml, of the ketones in the solutions of varied composition, with and without the several additives, were photolyzed in Pyrex, either in 10-mm i.d. circular tubes or in 1 × 1 × 10 cm square tubes. The circular tubes, used in experiments with unfiltered light, were closed with ground-

(8) (a) S. G. Cohen and S. Aktipis, *Tetrahedron Letters*, **No. 10**, 579 (1965); (b) *J. Amer. Chem. Soc.*, **88**, 3587 (1966).

(9) (a) G. S. Hammond and W. M. Moore, *ibid.*, **81**, 6334 (1959); (b) W. M. Moore, G. S. Hammond, and R. P. Foss, *ibid.*, **83**, 2789 (1961).

(10) H. L. J. Bäckstrom and K. Sandros, *Acta Chem. Scand.*, **14**, 48 (1960).

(11) (a) N. C. Yang and C. Rivas, *J. Amer. Chem. Soc.*, **83**, 2213 (1961); (b) E. F. Zwicker, L. I. Grossweiner, and N. C. Yang, *ibid.*, **85**, 2671 (1963).

(12) J. N. Pitts, Jr., H. W. Johnson, Jr., and T. Kutawa, *J. Phys. Chem.*, **66**, 2456 (1962).

(13) A. Beckett and G. Porter, *Trans. Faraday Soc.*, **59**, 2051 (1963).

(14) A. Schönberg and A. Mustafa, *J. Chem. Soc.*, **67** (1949).

(15) F. Bergmann and Y. Hirschberg, *J. Amer. Chem. Soc.*, **65**, 1429 (1943).

(16) G. S. Hammond and P. A. Leermakers, *ibid.*, **84**, 207 (1962).

(17) N. C. Yang, D. S. McClure, S. L. Murov, J. J. Houser, and R. Dusenbery, *ibid.*, **89**, 5466 (1967).

(18) G. Porter and P. Suppan, *Trans. Faraday Soc.*, **61**, 1664 (1965).

(19) E. J. Baum, J. K. S. Wan, and J. N. Pitts, Jr., *J. Amer. Chem. Soc.*, **88**, 2652 (1966).

(20) (a) S. G. Cohen and M. N. Siddiqui, *ibid.*, **86**, 5047 (1964); **89**, 5409 (1967).

(21) S. G. Cohen, R. Thomas, and M. N. Siddiqui, *ibid.*, **89**, 5845 (1967).

(22) (a) S. G. Cohen and R. J. Baumgarten, *ibid.*, **87**, 2996 (1965); (b) **89**, 3471 (1967).

(23) S. G. Cohen and H. M. Chao, *ibid.*, **90**, 165 (1968).

(24) R. Geigy and W. Konigs, *Ber.*, **18**, 2401 (1885).

(25) C. H. Wang and S. G. Cohen, *J. Amer. Chem. Soc.*, **79**, 1924 (1957).

(26) C. G. Hatchard and C. A. Parker, *Proc. Roy. Soc.*, **A235**, 518 (1956).

glass stopcocks lubricated with silicone grease; the square tubes, used on the monochromator, were closed with Fisher-Porter Teflon valves. The tubes were cooled in Dry Ice–acetone, degassed in three freeze–pump–thaw cycles, and left under argon. In experiments with unfiltered light the tubes were mounted on a turntable 4 or 8 cm from a G.E. H85|A3|UV mercury lamp. In experiments with monochromatic light the tube was placed in a Cary-14 cell holder affixed to the exit slit of a Bausch and Lomb 38-86-01 monochromator, 3.2 mμ/mm dispersion, slit width 3 mm in most experiments. The light source was an Osram SP-200 mercury point source lamp. A Corning 7-54 filter was placed between the exit slit and the cell holder. Tube contents were stirred magnetically and cooled by an air blower. The light intensity was monitored by ferrioxalate actinometry[26] or with benzophenone–benzhydrol[9b] as a secondary actinometer. In experiments on the turntable with unfiltered light, the light intensity was monitored by concomitant photolysis of 0.1 *M* benzophenone in 2-propanol. The rate of benzophenone disappearance, 4 cm from the G.E. lamp, was 0.15–0.20 *M* hr^{-1}, $\varphi \cong 1.1$. In all experiments irradiation tubes were selected in which rates of photoreduction of benzophenone in 2-propanol were the same.

Progress of photoreduction was followed by determination of absorbance at and near λ_{max} of the long wavelength band of the ketone. In some experiments aliquots of photolyzed and unphotolyzed solutions were diluted with 2-propanol in volumetric flasks and absorbances were measured in calibrated 1-cm or 1-mm quartz cells on a Beckman DU-2 or Cary 14 spectrophotometer. In other experiments a Pyrex irradiation tube was used to which a 1-mm quartz absorbance cell was sealed. The solutions were irradiated for a measured period, removed from the irradiator, and examined in the spectrophotometer *via* the absorbance cell at and near the appropriate λ_{max} and returned for further irradiation. Actinometry was carried out between the periods of irradiation. In this way multiple values of rates and quantum yields were determined without use of separate samples. Values obtained by the two procedures were identical.

4,4′-Diaminobenzpinacol. A solution of 0.35 g (1.78 mmol, 0.025 *M*) of *p*-aminobenzophenone, PAB, in diisopropylamine in a 100-ml Pyrex flask was degassed and irradiated under argon for 77.5 hr with the G.E. lamp. The solution was cooled to −20°, and the precipitate was collected and washed with cold diisopropylamine, 0.225 g, 64% yield, mp 170–172° dec. The infrared spectrum in methylene chloride showed a weak multiplet centered at *ca.* 3500 cm^{-1} and strong bands at 1625 and 1510 cm^{-1}. The carbonyl band of PAB at 1650 cm^{-1} was absent. The product was dissolved in methylene chloride, decolorized with carbon, and precipitated with petroleum ether, mp 180–181° dec.

Anal. Calcd for $C_{26}H_{24}N_2O_2$: C, 78.75; H, 6.10; N, 7.07. Found: C, 78.57; H, 6.10; N, 7.28 (Schwarzkopf Laboratories).

The ultraviolet spectrum of a 4×10^{-4} *M* solution in methanol showed absorption: 230 mμ, ε 16,400; 244 mμ(max), ε 23,650; 260 mμ, ε 11,000; 286 mμ(max), ε 2940; 300 mμ, ε 1880; 334 mμ, ε 56. Addition of 1 drop 1 *N* hydrochloric acid discharged the maxima at 286 and 244 mμ and led to a new maximum at 260 mμ, ε 1470. Addition of 1 drop of 1 *M* sodium hydroxide regenerated the original spectrum.

A solution of 0.01053 g (0.0266 mmol, 5.32×10^{-4} *M*) of the initially precipitated pinacol in 50 ml of 2-propanol containing ~0.3 ml of 5 *M* sodium hydroxide was allowed to stand overnight in the dark under argon. The absorbance was measured in a 1-mm cell at 320, 334 (max), and 350 mμ, and compared with that of a similar solution which contained no added alkali. Absorbances of 0.813, 0.995, and 0.832 at the three wavelengths indicated ~99% yield of PAB from the decomposition of the pinacol. The absorbance of the blank, 0.066, indicated the presence of not more than 3.5% PAB in the precipitated pinacol.

4-Aminobenzhydrol. A solution of 1.0 g (5.1 mmol) of PAB in 50 ml of 2-propanol was reduced with 0.15 g (4.0 mmol) of sodium borohydride, leading to 0.70 g, 69% yield, of 4-aminobenzhydrol, mp 116–117° from petroleum ether, lit.[27] mp 121°. The ultraviolet spectrum of a 4×10^{-4} *M* of the hydrol in methanol showed absorption: 230 mμ, ε 8260; 244 mμ(max), ε 12,800; 260 mμ, ε 5750; 286 mμ (max), ε 1630; 300 mμ, ε 1120; 334 mμ, ε 25. Addition of 1 drop of 1 *N* hydrochloric acid discharged the maxima at 244 and 286 mμ and led to a new maximum at 260 mμ, ε 600. Sodium hydroxide restored the original spectrum. A 10-ml solution of 4×10^{-5} *M* 4-aminobenzhydrol in 1:1 2-propanol–water containing 0.3 ml of 5 *N* NaOH, allowed to stand for a month, developed absorbance at 334 mμ, equivalent to less than 1% conversion to PAB.

Effect of Alkali on Irradiated Solutions. (i) Aliquots of a solution of 0.01 *M* PAB in diisopropylamine were irradiated on the turntable for 30–60 min, the absorbances of appropriately diluted aliquots falling from an initial value of 0.738 at 334 mμ to 0.368 and 0.117, respectively, corresponding to rates of photoreduction of 0.010 *M* hr^{-1} and 0.0084 *M* hr^{-1} for the two periods. Aliquots (15 ml) of the diluted unirradiated and irradiated solutions were treated with 0.5 ml of saturated sodium 2-propoxide in 2-propanol and allowed to stand in the dark for 10 days, at which time the absorbances at 334 mμ were 0.733, 0.547, and 0.410, respectively. The increase in absorbance following alkali treatment, due

(27) H. Kippenberg, *Ber.*, **30**, 1136 (1897).

to PAB, corresponded to 99 and 95% formation of the pinacol in the photoreduction.

(ii) Aliquots of a solution of 0.001 *M* PAB in cyclohexane were irradiated for 24 and 60 min on the turntable, and absorbances of aliquots, diluted with 2-propanol, were determined: (a) 0 min, 334 mμ, 0.733, 350 mμ, 0.597; (b) 24 min, 334 mμ, 0.456, 350 mμ, 0.386; (c) 60 min, 334 mμ, 0.268; 350 mμ 0.232. These values correspond to rates of photoreduction of 9.3×10^{-4} and 6.4×10^{-4} *M* hr^{-1} for the two periods. Aliquots (15 ml) of the diluted solutions were treated with 0.2 ml of 5 *M* sodium hydroxide and absorbances were measured after 4 days: (a) 334 mμ, 0.751, 350 mμ, 0.602; (b) 334 mμ, 0.588, 350 mμ, 0.489; (c) 334 mμ, 0.477, 350 mμ, 0.402. The increase in absorbance following alkali treatment indicated 85% pinacol from the data at 334 mμ, 92% pinacol from the data at 350 mμ.

(iii) A solution of $\sim 1 \times 10^{-3}$ *M* PAB in triethylamine was irradiated at 366 mμ on the monochromator in a 1 cm square Pyrex tube, to which was sealed a 1-mm quartz cell in which the absorbance at 317.5 mμ was measured after each period of irradiation with the aid of a neutral density filter: 0 min, 2.16; 15 min, 1.97; 27 min, 1.84. This indicated a rate of 4.3×10^{-4} *M* hr^{-1}, compared with a ferrioxalate rate of 2.48×10^{-3} *M* hr^{-1}, quantum yield $\cong 0.21$. After 343 min of irradiation, the absorbance was 0.33, 88% reaction. An aliquot (1 ml) was treated with 0.2 ml of 5 *m* NaOH, allowed to stand for 3 days, diluted to 25 ml with 1:1 2-propanol–water and examined in the ultraviolet. Absorbances of an unirradiated aliquot so treated were: 334 mμ, 0.750; 350 mμ, 0.610; of an irradiated aliquot diluted but not treated with alkali: 334 mμ, 0.090; 350 mμ, 0.073; and of the aliquot treated with alkali and diluted: 334 mμ, 0.255; 350 mμ, 0.207. Decomposition indicated at each wavelength 50% conversion of reduced PAB to pinacol.

Results

Preliminary experiments were carried out on photoreduction of *o*, *m*, and *p*-aminobenzophenones in a range of solvents. Solutions in Pyrex tubes on a turntable were irradiated with a G.E. H-85 lamp. Irradiation of 0.1 *M* solutions of the three aminobenzophenones in 2-propanol for 71 hr led to very little change in the ultraviolet spectra. Irradiation of a 1×10^{-3} *M* solution of PAB in 2-propanol led to 38% decrease in absorbance after 12 hr, corresponding to a rate of photoreduction of $\sim 3 \times 10^{-5}$ *M* hr^{-1}; benzophenone in 2-propanol was photoreduced at the same time at a rate of 0.16 M^{-1} hr^{-1}. Approximate rates of photoreduction by a variety of compounds are summarized in Table I.

These numbers reflect a reduction of 0.01 *M* PAB in the primary amines to an extent of only 1–2% in 10–20 hr. Disappearance of PAB was slightly more rapid in 2-propanol, and apparently even more rapid in acetone and benzene, though still quite slow. Photoreduction in isooctane and cyclohexane was more efficient, about 1% as fast as that of the standard, benzophenone in 2-propanol. Photoreduction by diisopropylamine was one-tenth as rapid as that of the standard, while the rate by triethylamine was about one-third that of the standard. Photoreduction of *o*-aminobenzophenone was very slow, showing no enhancement in cyclohexane and triethylamine. *m*-Aminobenzophenone was also quite unreactive, triethylamine showing some effectiveness, about 1% of that in the photoreduction of PAB.

Table I: Approximate Rates of Photoreduction in Pyrex, G.E. H85|A3 Lamp: *p*-Aminobenzophenone, PAB; *o*-Aminobenzophenone, OAB; *m*-Aminobenzophenone, MAB

Ketone			Rate, $10^3 \times M$
Compd	*M*	Solvent	hr^{-1}
PAB	0.001	2-Propanol	~0.03
PAB	0.00005	1:1 2-Propanol–H_2O	~0.02
PAB	0.01	*n*-Butylamine	~0.007
PAB	0.01	2-Butylamine	~0.005
PAB	0.01	N-2-Propylacetamide	~0.008
PAB	0.01	Acetone	0.2
PAB	0.01	Benzene	0.2
PAB	0.001	Isooctane	1
PAB	0.001	Cyclohexane	2
PAB	0.02	Diisopropylamine	10
PAB	0.02	Triethylamine	50
PAB	0.02	N-Ethyldiisopropylamine	30
OAB	0.10	2-Propanol	~0.05
OAB	0.0002	1:1 2-Propanol–H_2O	~0.003
OAB	0.01	Cyclohexane	~0.001
OAB	0.01	Triethylamine	~0.06
MAB	0.10	2-Propanol	~0.02
MAB	0.001	Cyclohexane	~0.05
MAB	0.01	Triethylamine	~0.50

Product analysis indicated that photoreduction of PAB in diisopropylamine led to the pinacol, 4,4′-diaminobenzpinacol, which was isolated in 64% yield, mp 180–181° dec. It was readily distinguished from the possible monomolecular product, 4-aminobenzhydrol, mp 116–117°, which was prepared by reduction of PAB by sodium borohydride. The ultraviolet spectra of the pinacol and hydrol are very similar, with molecular extinction coefficients for the pinacol approximately twice those of the hydrol. The spectra are those of an aniline,[28] with maxima at 244 and 286 mμ which are discharged on protonation with HCl and regenerated with neutralization.

The high extinction CT band of PAB at 334 mμ,

(28) J. G. Calvert and J. N. Pitts, Jr., "Photochemistry," John Wiley and Sons, Inc., New York, N. Y., 1966, (a) p 253; (b) p 298; (c) p 267.

$\epsilon \sim 19{,}000$, is absent in the pinacol and in the hydrol. Treatment of the pinacol in alcohol with alkali leads to quantitative generation of the ultraviolet spectrum of one mole of PAB per mole of pinacol. Decomposition to PAB and the hydrol occurs (eq 1), as has been described for the base-catalyzed decomposition of benzpinacol[3] and the pinacols from *p*-dimethylaminobenzophenone[20b] and from *p*-benzoylphenyl-trimethylammonium chloride.[21] Prolonged treatment of the hydrol

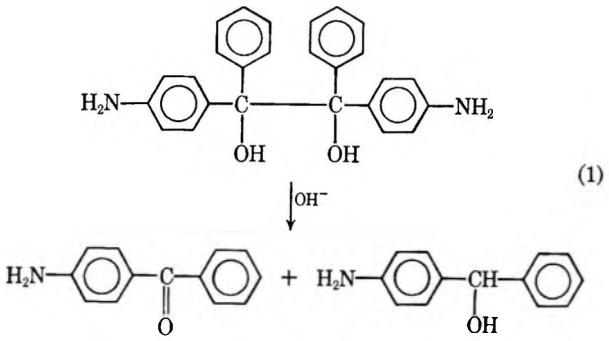

(1)

with alkali led to essentially no PAB. This procedure for pinacol analysis was applied to irradiated solutions. Absorbance measurements at and near λ_{max} for PAB before and after irradiation indicated the total quantity of PAB photoreduced. Base decomposition and increase of absorbance of PAB indicated the quantity which had been photoreduced to pinacol. When conversion of the ketone to pinacol is quantitative, decomposition by base regenerates one-half of the amount of ketone reduced. Other values are proportionate. Small corrections are made for the effects of alkali on the absorbances. This analysis may be general for derivatives of benzpinacol. It is not effective for pinacols from acetophenones which may be quite stable to alkali.[29] Crossed coupling products which may be formed in photoreduction of benzophenones in some solvents are stable and do not appear to interfere. Some results of such analyses applied to photoreduction of PAB in a variety of solvents are given in Table II.

Photoreduction of PAB in diisopropylamine led to essentially quantitative formation of the pinacol, while the more rapid photoreductions in triethylamine and in 1 *M* triethylamine in cyclohexane led to little more than 50% yield of the pinacol. This may be due to formation of the cross-coupling product from combination of the ketyl radical with the tertiary amine derived radical, as has been observed in the photoreduction of benzophenone by dimethylaniline.[30] In one experiment prolonged irradiation of 0.02 *M* PAB in triethylamine, followed by dilution with an equal volume of methylene chloride, led to a material, mp 173–176° dec. It did not regenerate PAB on standing or refluxing with alkali; its infrared spectrum was similar to those of the pinacol and the hydrol, with additional C–H absorption. It decomposed on standing in air and may have been the mixed coupling product. Another material was obtained by glpc, the nmr and mass spectra of which were consistent with the dimer of the tertiary amine derived radical, N,N,N′,N′-tetraethyl-2,3-diaminobutane.[31]

Quantum yield measurements were carried out for the photoreduction of the aminobenzophenones, as affected by reaction conditions: light intensity, concentration of ketone, and reducing medium. The most detailed study was that of the PAB–triethylamine system. The quantum yields for photoreduction of 0.001 *M* PAB in neat triethylamine at 334 mμ were determined by ferrioxalate actinometry as a function of light intensity. Light intensity was decreased by wire screens at the exit slit. Unexpectedly, the quantum yield fell from 0.42 at high light intensity *ca.* 1×10^{16} quanta/sec cm² to 0.25 at *ca.* 6×10^{13} quanta/sec cm². The actinometer and PAB solutions were opaque under all the reaction conditions. Results for *ca.* 15% photoreduction of PAB are given in Table III.

Table II: Yield of Pinacol in Photoreduction of PAB

Reducing agent	PAB, *M*	% Convn	% Pinacol
Diisopropylamine	0.01	50	102
Diisopropylamine	0.01	84	95
Triethylamine	0.02	79	53
Triethylamine	0.001	88	55
1 *M* Triethylamine in cyclohexane	0.001	41	56
1 *M* Triethylamine in cyclohexane	0.001	84	56
Diisopropyl ether	0.001	21	98
Cyclohexane	0.001	38	90
Cyclohexane	0.001	63	88

Table III: Photoreduction of 0.001 *M* PAB in Triethylamine, 334 mμ. Effect of Light Intensity on Quantum Yield φ

PAB irradiation		Actinometer[a]			
Time	*M* hr⁻¹	Time	*M* hr⁻¹	Rel.	φ
25 sec	1.49×10^{-2}	93 sec	4.40×10^{-2}	169	0.42
16 min	8.1×10^{-4}	17 min	3.27×10^{-3}	12.7	0.31
82 min	5.4×10^{-5}	121 min	2.61×10^{-4}	1.0	0.25

[a] Actinometer quantum yield, 1.23; highest light intensity, *ca.* 1×10^{16} quanta/sec cm².

The efficiency of photoreduction of PAB and of *p*-dimethylaminobenzophenone, DMAB, by triethylamine was then examined as a function of the initial concentrations of the ketones at constant light intensities. For PAB, irradiation was at 313 and 334 mμ

(29) D. Laufer, Ph.D. Thesis, Brandeis University, 1963.
(30) R. S. Davidson, *Chem. Commun.*, **16**, 575 (1966).
(31) L. T. Allan and G. A. Swan, *J. Chem. Soc.*, 4822 (1965).

with benzophenone–benzhydrol as a secondary actinometer.[9b] Quantum yields for PAB–triethylamine are independent of wavelength over this range. Three concentrations of ketone were studied at each of the two wavelengths. For DMAB, irradiation was at 334 mμ and three concentrations of ketone were studied. Some results are given in Table IV.

Table IV: Photoreduction of PAB and DMAB in Triethylamine. Effect of Initial Concentration of Ketone on Quantum Yield

		Irradiation				
Ketone	M	mμ	Time, min	Convn, %	Rate, M hr^{-1}	φ
PAB	0.020	313	20	20	0.0121	0.24
PAB	0.010	313	10	27	0.0162	0.31
PAB	0.001	313	1	36	0.0207	0.40
PAB	0.020	334	120	20	0.00204	0.22
PAB	0.010	334	60	27	0.00263	0.28
PAB	0.001	334	5	29	0.00345	0.37
DMAB	0.020	334	20	27	0.0158	
DMAB	0.010	334	8	23	0.0167	
DMAB	0.001	334	0.6	20	0.0197	

In the photoreduction of PAB a 20-fold decrease in initial concentration leads to a 67% increase in quantum yield. While actinometry was not carried out concurrently with the photoreduction of DMAB, the rates indicate a similar but somewhat smaller effect, a 20-fold decrease in concentration leading to a 25% increase in rate. The rate for the 0.001 M solution of DMAB corresponds to a quantum yield of *ca.* 0.4.

The data for PAB in Table IV may be fitted to linear plots of $1/\varphi$ *vs.* concentration of PAB with limiting quantum yields of 0.42 and 0.38 at the high and low light intensity, respectively, and with ratios of slope to intercept of 36 M^{-1} in both cases. This behavior is consistent with quenching by ground-state PAB or by an impurity in it. A sample of the PAB was treated further—recrystallized from 2-propanol, sublimed, and recrystallized twice again. The quantum yield for photoreduction of a 0.02 M solutions of this sample in triethylamine was only 8% greater than that observed in the normally used material, perhaps within experimental error, indicating that the concentration effect may not be due to impurity.

The action of naphthalene as a quencher for photoreduction of PAB by triethylamine at 334 mμ was examined at the same three concentrations of PAB as in Table IV. The energy of the lowest triplet state of PAB is ~67 kcal mol in cyclohexane and 63 kcal/mol in 2-propanol, somewhat lower than the corresponding values for benzophenone.[18] The triplet energy of naphthalene[28b] is about 61 kcal, fairly similar to that of PAB, and it seemed desirable to include comparison with another quencher, *trans*-stilbene, of lower triplet energy, *ca.* 51 kcal/mol. This compound has substantial absorption at 334 mμ, and the comparison was made with irradiation at 366 mμ, and analysis at 350 mμ. Some results with the two quenchers are given in Table V.

Table V: Photoreduction of PAB by Triethylamine. Effects of Naphthalene, N, and *trans*-Stilbene, S

PAB,	Quencher		
M	Compd	M	φ
0.020	...	...	0.20
0.020	N	0.021	0.12
0.020	N	0.050	0.064
0.010	...	...	0.30
0.010	N	0.005	0.23
0.010	N	0.010	0.21
0.010	N	0.015	0.18
0.010	N	0.020	0.17
0.0010	...	...	0.38
0.0010	N	0.010	0.23
0.0010	N	0.021	0.16
0.0020	...	...	0.31
0.0020	S	0.0046	0.22
0.0020	S	0.0094	0.19
0.0020	N	0.0051	0.23
0.0020	N	0.0091	0.18

The last set of data, Table V, indicates that *trans*-stilbene and naphthalene have equal quenching effectiveness. A single linear plot of $1/\varphi$ *vs.* concentration of the two quenchers may be constructed, leading to a value of k_q/k_r (Et_3N), the ratio of slope to intercept, of 69 M^{-1} at 0.002 M PAB in triethylamine. The first three sets of data, Table V, may be plotted similarly, leading to parallel lines, with ratios of slope to intercept of 40 M^{-1} at 0.02 M PAB, 45 M^{-1} at 0.01 M PAB, and 67 M^{-1} at 0.001 M PAB. These values, corresponding to $k_q/k_r(Et_3N)$, or more properly $k_q/(k_d + k_r(Et_3N))$, should, however, be constant. The data of Table IV, for variations in quantum yield with concentration of PAB itself, also fitted a Stern–Volmer plot, with ratio of slope to intercept of 36 M^{-1}, about half the value observed in these quencher studies at low (~0.001 M) concentration of PAB, where the effect of the quencher is dominant and that of the PAB may be neglected. This indicated that the PAB may be treated as a quencher with half the efficiency of naphthalene and *trans*-stilbene. The varying concentration of PAB in the sets of data of Table V should be taken into account in the plots of $1/\varphi$ *vs.* concentration of quencher.

Since PAB undergoes photoreduction better in nonpolar than in polar media,[18] we examined the effect of dilution on the photoreduction by triethylamine. A few experiments were carried out in dilution with benzene and acetonitrile. A more detailed study was made

Table VI: Photoreduction of 0.001 *M* PAB by Triethylamine in Cyclohexane, 313 mμ

Et_3N, *M*	Quantum yield	
7.14 (neat)	0.39[a]	0.32[b]
1.00	0.57[a]	0.55[b]
0.100	0.53[a]	0.51[b]
0.051	0.46[a]	0.45[b]
0.014	0.32[a]	0.32[b]
0[c]	0.052[a]	0.055[b]

[a] Higher light intensity, ferrioxalate rate, 0.030 *M* hr^{-1}. [b] Lower light intensity, ferrioxalate rate, 0.0054 *M* hr^{-1}. [c] Cyclohexane.

on the effect of dilution with cyclohexane, and some of these results are given in Table VI.

At 1 *M* triethylamine in cyclohexane the quantum yields are 46 and 72% greater than in neat triethylamine at the higher and lower light intensity, respectively. This difference arises largely from the difference in quantum yields in neat triethylamine. The quantum yields in the solutions in cyclohexane are essentially independent of light intensity, and a plot of $1/\varphi$ *vs.* $1/(Et_3N)$ leads to a single line for the solution data with ratio of slope to intercept = 0.011 *M*, and with the points for neat amine lying on the ordinate far above the intercept. The quantum yields in all the solutions are much greater than in neat cyclohexane, and triethylamine may be assumed to be the active reducing agent. Supporting evidence is found in analysis of the photolysates for pinacol by base decomposition, Table II. Photoreduction of PAB in 1 *M* triethylamine in cyclohexane and in neat triethylamine leads to essentially the same extent of conversion to pinacol, 54 and 56%, respectively, values very different from that in cyclohexane, 89%, indicating that the cyclohexyl radical is not formed in the solution of the amine in cyclohexane. On this basis the ratio of slope to intercept, 0.011 *M*, is k_d/k_r, the ratio of rate constants for deactivation of the excited ketone to that for abstraction by it of hydrogen from triethylamine.

Experiments were carried out on the quenching by naphthalene of the photoreduction of PAB by 1 *M* triethylamine in cyclohexane. Irradiation was at 334 mμ at low light intensity, ferrioxalate rate 0.00312 *M* hr^{-1}. Some results are given in Table VII. A plot of reciprocal quantum yield against the sum of the concentration of naphthalene and one-half the concentration of PAB is linear, and the ratio of slope to intercept leads to $k_q/k_r = 90$.

Dilution of triethylamine with benzene also leads to increased quantum yield for photoreduction of PAB. Irradiation at 313 mμ of 0.001 *M* PAB in 1 *M* triethylamine in benzene led to photoreduction with zero-order kinetics over the first 50% of reaction with quantum yield 0.56, the same as that in 1 *M* triethylamine in

Table VII: Photoreduction of PAB by 1 *M* Triethylamine in Cyclohexane. Effect of Naphthalene

PAB, $10^3 M$	Naphthalene, *M*	Irradn, min	Convn, %	φ
1.43	...	15	21.5	0.481
1.37	0.0105	25	19.7	0.256
1.40	0.0203	40	21.3	0.176
1.44	0.1006	120	18.0	0.0518

cyclohexane and 40% greater than that in neat triethylamine at the same light intensity. On the other hand, dilution with a dipolar solvent, acetonitrile, leads to greatly decreased efficiency of photoreduction. Irradiation at 313 mμ of 0.001 *M* PAB in 1 *M* triethylamine in acetonitrile led to very slow if any photoreduction, with rate perhaps about 1/300 as great as that in neat triethylamine. Irradiation of 5×10^{-5} *M* PAB in acetonitrile alone led to even slower photoreduction, $\sim 8 \times 10^{-6}$ *M* hr^{-1}, about one-fifth that in 1 *M* triethylamine in acetonitrile.

Quantum yields were also determined for photoreduction of PAB by N-ethyldiisopropylamine and triethylenediamine, by diisopropylamine and 1 *M* diisopropylamine in cyclohexane, by diisopropyl ether and by 1 *M* 2-propanol in cyclohexane, and for photoreduction of *m*-aminobenzophenone, MAB, in triethylamine. Some results are summarized in Table VIII.

Photoreduction by ethyldiisopropylamine was somewhat less efficient than by triethylamine, $\varphi = 0.22$ as compared with 0.39 under similar conditions, Table VI. The solid bicyclic tertiary amine, triethylenediamine, with N atoms in bridgehead positions, used as an 0.05 *M* solution in cyclohexane, showed moderately high efficiency in photoreduction of PAB, $\varphi = 0.21$, somewhat less than half that of triethylamine under similar conditions.

The secondary amine diisopropylamine was about an order of magnitude less efficient than the tertiary amines $\varphi \sim 0.02$–0.04. Again photoreduction was more efficient at low concentration of ketone than at high, and in solution in cyclohexane than in the neat amine. Part of the increase may be due to photoreduction by the hydrocarbon, which is itself more effective ($\varphi \sim 0.05$) than the secondary amine. The effectiveness of cyclohexane was markedly reduced by addition of 1 *M* 2-propanol. Diisopropyl ether had efficiency similar to that of the hydrocarbon. *m*-Aminobenzophenone was photoreduced by 1 *M* triethylamine with low quantum yield, 0.07, about one-seventh that of PAB under similar conditions.

Finally, it was of interest to inquire whether any correlation might be observed between the reactivity of the media in photoreduction of PAB and their effect on the charge-transfer absorption band. Absorption data were obtained on a Cary 14 or Beckman DU-2 spectro-

Table VIII: Quantum Yields for Photoreduction of *p*- and *m*-Aminobenzophenone

Ketone			Irradiation		
Compd	*M*	Medium	Intens[a]	mμ	φ
PAB	0.002	Ethyldiisopropylamine	0.035	313	0.22
PAB	0.001	0.05 *M* Triethylene-diamine in cyclo-hexane	0.030	313	0.21
PAB	0.050	Diisopropylamine	0.056	313	0.024
PAB	0.001	Diisopropylamine	0.054	334	0.038
PAB	0.001	1 *M* Diisopropylamine in cyclohexane	0.030	313	0.087
PAB	0.001	Diisopropyl ether	0.055	313	0.06
PAB	0.001	Cyclohexane	0.030	313	0.053
PAB	0.001	1 *M* 2-Propanol in cyclohexane	0.030	313	<0.01
MAB	0.006	1 *M* Triethylamine in cyclohexane	0.003	334	0.07

[a] Ferrioxalate actinometer rate, M hr^{-1}.

Table IX: Effects of Solvent on the Charge-Transfer Band of *p*-Aminobenzophenone, PAB, and *p*-Dimethylaminobenzophenone, DMAB

Ketone	Solvent	λ_{max}, mμ	Hhw,[a] mμ
PAB	Isooctane	299	40
PAB	Cyclohexane	303	40.5
PAB	Carbon tetrachloride	307	41
PAB	1 *M* Triethylamine in cyclohexane	309	42
PAB	N-Ethyldiisopropylamine	310	36
PAB	Benzene	313	43
PAB	Diisopropyl ether	316	42
PAB	1 *M* 2-Propanol in cyclo-hexane	316.5	55
PAB	Triethylamine	317.5	43
PAB	Diisopropylamine	320	46
PAB	Acetonitrile	320	44
PAB	2-Butylamine	328	48
PAB	Pyridine	330	46
PAB	*n*-Butylamine	331	50
PAB	N,N-Dimethylformamide	333	47
PAB	N-Methylformamide	333	52
PAB	Formamide	333	57
PAB	*t*-Butyl alcohol	333	55
PAB	2-Propanol	334	55
PAB	1:1 2-Propanol–water	334	61
PAB	Water	333	70
DMAB	Cyclohexane	331	35
DMAB	Triethylamine	333	39
DMAB	1:1 2-Propanol–water	360	51

[a] Half-height width.

photometer at 5×10^{-4} to 5×10^{-5} M PAB. Some results are summarized in Table IX in the order of the red shift.

The spectra of PAB show no fine structure at room temperature. The CT band has very high intensity, ε 19,000 M^{-1} cm^{-1}. The λ_{max} of this band is shifted from ~300 mμ in aliphatic hydrocarbons to 328–333 mμ in primary amines, pyridine, amides, alcohols, and water. The shift is accompanied by band-broadening, which is the greatest with alcohols, water, and formamide and may be due in part to hydrogen bonding. This effect is also seen in 1 M 2-propanol in cyclohexane. The tertiary and secondary amines, the ether, benzene, and acetonitrile shift λ_{max} to 310–320 mμ, and the tertiary amine, ether, benzene, and acetonitrile cause little broadening. The limited data for DMAB, ε 24,000, indicate similar behavior. The long wavelength band of the parent compound, benzophenone, is of different type, n,π*, and of low intensity, ε 150, and is quite differently affected by solvent.[32] In aliphatic hydrocarbon, λ_{max} is at 345 mμ, half-height width *ca.* 52 mμ, and the band shows vibrational fine structure. In alcohol the band is shifted to shorter wavelength, 330 mμ, half-height width unchanged, and the fine structure is lost. The short wavelength band of PAB, λ_{max} 236 mμ in cyclohexane, 243 mμ in 2-propanol, ε 13,000, is similar to that of benzophenone, λ_{max} 248 and 252 mμ in cyclohexane and 2-propanol, respectively.

The long wavelength band of *o*-aminobenzophenone shows less clear change with solvent: in triethylamine λ_{max} 375 mμ, half-height width 57 mμ; in 1:1 2-propanol–water λ_{max} 380 mμ, half-height width 64 mμ, ε 5000–6000. The long wavelength band of *m*-aminobenzophenone is of lower intensity, ε 1700–2000, and is displaced but little by solvent change, λ_{max} 341 mμ in triethylamine, 343 in 2-propanol, half-height widths 63 and 78 mμ, respectively.

Discussion

The preliminary irradiations of *o*-, *m*-, and *p*-aminobenzophenones, Table I, confirmed[12] that these compounds underwent photoreduction in 2-propanol very

(32) J. W. Sidman, *Chem. Rev.*, 58, 689 (1958).

slowly if at all. *o*-Aminobenzophenone remained unreactive in cyclohexane and triethylamine, and this may arise from reversible intramolecular abstraction of H from the *ortho* amino group.[11-13] *m*-Aminobenzophenone showed only a slight increase in reactivity in triethylamine, which was unexpected in view of the substantial reactivity of PAB in the tertiary amine.[1] The *meta* amino compound is being studied further along with other carbonyl compounds which may have low-lying π,π^* triplets.

p-Aminobenzophenone, PAB, appeared to show even lower reactivity in primary amines than in 2-propanol. It may be that the chemically unreactive CT triplet is formed to an even greater extent, or that the triplet has more nearly the CT character, in an amine which may solvate or hydrogen bond effectively both ends of the dipolar species, I. The slight reactivity in acetone

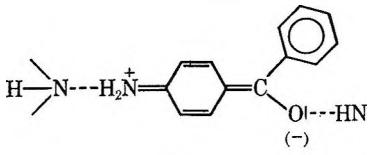

I

and benzene appears to be real and probably greater than that of benzophenone in these solvents. The reactivity in the aliphatic hydrocarbons, isooctane, and cyclohexane (φ = 0.05 in cyclohexane, Table VIII), while generally confirming the work of Porter and Suppan, appeared to be lower than that reported.[18] The secondary amine showed substantial reactivity, that of the tertiary amines was even greater, and these compounds became the basis of the remainder of the study.

The rate of photoreduction of PAB by triethylamine was one-third that of benzophenone by 2-propanol, and if the tertiary amine transfers one reducing moiety while the alcohol transfers two, the initial abstraction by PAB triplet from tertiary amine may be about two-thirds as efficient as the abstraction by benzophenone triplet from 2-propanol. The rate of photoreduction of PAB by triethylamine appeared almost twice as great as that which we reported initially[22a] for photoreduction of benzophenone itself by this amine under similar conditions. However, that rate was low largely because of buildup of a light-absorbing transient,[23] and it was later found to be threefold larger in a dilute solution of triethylamine in benzene[22b] than in the neat amine. Thus the preliminary experiments indicated PAB might be photoreduced by triethylamine almost as effectively as was benzophenone. Presumably, in this medium of low polarity PAB would have a chemically reactive low-lying n,π^* triplet,[18] and heteroatom activation of the amine would lead to higher reactivity than that observed in the hydrocarbons.

Photoreduction of benzophenone by primary and secondary amines containing the >CHNH- group leads to benzpinacol and imines,[22] in essentially quantitative yields, in reactions analogous to photoreduction by alcohols. Similarly, photoreduction of PAB by diisopropylamine led to 4,4′-diaminobenzpinacol, mp 180–181° dec, formed quantitatively, as indicated by base decomposition of the photolysate. The 4,4′-diaminobenzpinacol was characterized by elementary analysis, by its ultraviolet spectrum, which was that of an aniline with molecular extinction coefficients twice those of the corresponding monomolecular reduction product, 4-aminobenzhydrol, and by decomposition with alkali, which generated quantitatively the spectrum of one mole of PAB per mole of pinacol, eq 1. The high yield of pinacol, shown by the base decomposition analytical procedure, may indicate that the initially formed secondary amine derived radical, >ĊNH–, does not survive to enter into a cross-coupling reaction with the ketyl radical but may transfer hydrogen from N to PAB and be converted to the imine. The relatively low rate of photoreduction in the secondary amine may be due to inefficient conversion to a reactive triplet, as described above for primary amines. The analytical procedure indicated (Table II) that the more rapid photoreduction of PAB in triethylamine led to only ~55% pinacol, a result consistent with our failure to obtain high yields of benzpinacol in photoreduction of benzophenone by tertiary amines.[33] The tertiary amine-derived radical, >Ċ–N<, lacking the NH, may have a greater tendency to survive and combine with the ketyl radical, and evidence was found for both this cross-coupling product and the dimer of the amine-derived radical. However, in work now in progress,[34] we have found that diethylvinylamine is formed in photoreduction of benzophenone by triethylamine, indicating that under some circumstances two hydrogen atoms may be transferred even from tertiary amines.

In any event, formation of dimers or crossed products from mixtures of radicals varies with the nature of the radicals and reflects the rates of the several possible processes. The high yield of the pinacol from photoreduction of PAB in cyclohexane, ~90%, is consistent with the results of photoreduction of benzophenone in that solvent,[35] and may indicate rapid dimerization and disappearance of cyclohexyl radicals. Analysis of the photolysate in diisopropyl ether, a single experiment, indicated essentially complete formation of the pinacol, while earlier study of photoreduction of benzophenone in an ether had indicated crossed products.[8b]

Study of the effect of reaction conditions on the quantum yield for photoreduction of PAB by triethylamine led to values ranging from 0.22 to 0.57, depending upon light intensity (Table III), initial concentration of

(33) S. G. Cohen, R. J. Baumgarten, and H. M. Chao, unpublished results.

(34) S. G. Cohen and N. Stein, unpublished results.

(35) C. Walling and M. J. Gibian, *J. Amer. Chem. Soc.*, **87**, 3361 (1965).

PAB (Table IV), and dilution of triethylamine by a nonpolar solvent, cyclohexane (Table VI), or benzene. A stated quantum yield for photoreduction of PAB requires uncommonly clear definition of reaction conditions to have meaning.

Dilution of triethylamine with cyclohexane (Table VI) led to a substantial increase in quantum yield for photoreduction of 0.001 *M* PAB, from 0.39 in neat triethylamine to 0.57 in 1 *M* triethylamine in the hydrocarbon. We have previously observed that dilution of 2-propanol and of tertiary amines with hydrocarbons also leads to more effective photoreduction of benzophenone than that by undiluted alcohol or amine.[22] In each of those cases light-absorbing internally masking transients were formed to substantial extents in the undiluted reducing agents and to a much diminished extent when the systems were diluted with hydrocarbons.[23,36] The increase in efficiency of photoreduction in the hydrocarbon solutions was attributed largely to decreased interference by light absorbing transients.[23,36] In the present photoreductions of PAB evidence for formation of a light-absorbing transient was not found. The optical density due to PAB falls continuously with irradiation and the same results are obtained whether the decreases are measured directly on the irradiated solution, or after dilution and standing, which would decompose intermediates. Also, the absorption band of PAB at which the system is irradiated is very intense, ϵ 19,000, as compared with low intensity of the n,π^* band of benzophenone, ϵ 150, and a light absorbing transient, if formed, would interfere far less with PAB. A satisfactory explanation for the dilution effect is available in the original explanation for the photoreactivity of PAB in cyclohexane,[18] the effect of the nonpolar medium in raising the energy of the chemically unreactive CT triplet relative to that of the reactive n,π^* triplet. It appears that, in the solution of triethylamine in hydrocarbon, a higher yield of the n,π^* triplet is formed, or a triplet containing more n,π^* character and hence more reactive, is formed as compared with what obtains in the more polar solution in triethylamine itself.

At concentrations below 1 *M* triethylamine in cyclohexane the quantum yields decrease remarkably slightly, from 0.57 at 1 *M* amine to 0.32 at 0.014 *M* amine. The data, Table VI, lead to a linear plot of $1/\varphi$ *vs.* $1/(Et_3N)$, and the ratio of slope to intercept leads to $k_d/k_r = 0.011$ *M*, the ratio of rate constants for self- or solvent-deactivation of the excited ketone to that for abstraction by it of hydrogen from the triethylamine. This value, 0.011 *M*, is very low and thus favorable, about one-fifth that for benzophenone–benzhydrol[9b] in benzene and one-tenth that for benzophenone–2-propanol in benzene,[37] and yet both of those reactions have higher quantum yields than the present photoreduction of PAB by triethylamine.

Information as to the values of k_d and k_r may be obtained indirectly by study of the quenching of photoreduction.[9] Quantum yields are determined as a function of concentration of quencher; a plot of $1/\varphi$ against this concentration leads to a linear plot, for which the ratio of slope to intercept leads to the value of $k_q/(k_d + k_r(RH))$. When this experiment was carried out in the system PAB–triethylamine–naphthalene, Table V, a single value for this ratio was not obtained; the results led to values which depended on the initial concentration of PAB, rising from 40 M^{-1} at 0.02 *M* PAB to 67 M^{-1} at 0.001 *M* PAB.

The quantum yields in the absence of quencher were also found to vary with initial concentration of PAB, rising from 0.24 at high concentration of PAB, 0.020 *M*, to 0.40 at low concentration of PAB, 0.001 *M*, Table IV. The photoreduction of *p*-dimethylaminobenzophenone by triethylamine showed a similar inverse relationship between efficiency and concentration of the ketone, Table IV, and a similar effect was observed in the photoreduction of PAB by diisopropylamine, Table VIII. This concentration effect is a very large one. The plot of $1/\varphi$ *vs.* initial concentration of PAB leads to a value of ratio of slope to intercept of 36 M^{-1}, indicating a rate-decreasing effect half as great as that caused by the quenchers, naphthalene and *trans*-stilbene, *i.e.*, with a rate constant half that of diffusion-controlled reactants. The effect is quite capable of perturbing the study of the quenchers carried out over a similar concentration range. Contaminant in the PAB may not cause such an effect, since it would have to have inordinately high quenching activity. Exhaustive purification led to little effect. Wasteful light absorption by dimers or higher complexes of PAB also seem not to be responsible. Absorbancy measurement with thin cells and neutral density filters, difficult to carry out at these high optical densities, gave no positive evidence for complexes. Molecular weight determinations on a 0.05 *M* solution in benzene at room temperature, and in acetonitrile, were also normal. Physical quenching of excited PAB by ground-state PAB seems to be the most reasonable explanation for the concentration effect. No other species appears to be present in sufficient concentration.

Quenching by the ground-state molecule in this case appears to be much more efficient than in the chlorophyl[38] and stilbene systems[39] where the ground-state species appeared to be 1 or 2% as effective as diffusion-controlled quenchers. For PAB to be photoreduced, conditions must be established in which a triplet with

(36) J. I. Cohen, Ph.D Thesis, Brandeis University, 1967; University Microfilms, Inc., Ann Arbor, Mich., 67-16,541.

(37) W. M. Moore and M. D. Ketchum, *J. Phys. Chem.*, **68**, 214 (1964).

(38) H. Linschitz and K. Sarkanen, *J. Amer. Chem. Soc.*, **80**, 4826 (1958).

(39) G. S. Hammond, J. Saltiel, A. A. Lamola, N. J. Turro, J. S. Bradshaw, D. O. Cowan, R. C. Counsell, V. Vogt, and C. Dalton, *ibid.*, **86**, 3197 (1964).

high n,π^* character persists, while the possibility of transition to an unreactive state of CT character of comparable energy is present. The ground state of PAB has dipolar character similar to that of the CT triplet, and interaction of the dipolar ground-state molecule with the excited triplet may in effect solvate and stabilize the CT state relative to the n,π^* state and lead to efficient conversion to the unreactive form. For such a process to account for the similar effect observed with *p*-dimethylaminobenzophenone, stabilization of the CT triplet by interaction with an aprotic dipolar material would be expected. That this may occur is seen in the effect of acetonitrile on the photoreduction of PAB by triethylamine. While dilution of the amine with benzene and cyclohexane increased the efficiency of photoreduction, irradiation of PAB in 1 *M* triethylamine in acetonitrile led to essentially no photoreduction at all. Acetonitrile is a dipolar aprotic solvent, unlike the other deactivating materials, the protic alcohols and amines. Acetonitrile is known for its capacity to solvate dipolar transition states and increase the rates of nucleophilic substitution reactions proceeding *via* such states.[40] In the present instance it may solvate the dipolar CT triplet and deactivate the system. The same kind of interaction may well be involved in the quenching by dipolar ground state PAB and DMAB. Alternatively, it may be stated that energy transfer in the excimer, PAB*(n,π^*)–PAB, leads to PAB–PAB*(CT).

If one accepts that PAB may be treated as a quencher with half the efficiency of naphthalene or *trans*-stilbene, the data of Table V may be modified by adding one-half the concentration of PAB to each concentration of quencher. Each plot of $1/\varphi$ *vs.* this combined concentration of quenching species then leads to essentially the same ratio of slope to intercept, $k_q/(k_d + k_r(\mathrm{RH})) \cong 70\ M^{-1}$. If, as the results in cyclohexane–triethylamine indicate, $k_d \ll k_r$, then $k_q/k_r - \cong 500$. The viscosity of triethylamine was measured, 5.35×10^{-3} poise, 20°, and the diffusion rate constant was calculated,[28c] $1.2 \times 10^{-10}\ M^{-1}\ \mathrm{sec}^{-1}$. If we accept a value of half of this for the quenching constant,[41] $k_q = 6 \times 10^9\ M^{-1}\ \mathrm{sec}^{-1}$, $k_r = 1.2 \times 10^7\ M^{-1}\ \mathrm{sec}^{-1}$, the rate constant for abstraction by triplet PAB from triethylamine. The reported value for k_r in the benzophenone–benzhydrol–benzene system is $5 \times 10^6\ M^{-1}\ \mathrm{sec}^{-1}$, based on $k_q = 2 \times 10^9\ M^{-1}\ \mathrm{sec}^{-1}$, one-fifth the calculated diffusion constant.[42] If a similar lower value of k_q is used for the present data, k_r is also $5 \times 10^6\ M^{-1}\ \mathrm{sec}^{-1}$, for abstraction by triplet PAB from triethylamine.

The data for the quenching by naphthalene of the photoreduction of PAB by 1 *M* triethylamine in cyclohexane, Table VII, lead to $k_q/(k_d + k_r) \cong k_q/k_r \cong 90$. The viscosity of 1 *M* triethylamine in cyclohexane, 8.6×10^{-3} poise, 20°, leads to the diffusion rate constant, $7.7 \times 10^9\ M^{-1}\ \mathrm{sec}^{-1}$. If k_q is set equal to one-half this value, $k_r = 4.2 \times 10^7\ M^{-1}\ \mathrm{sec}^{-1}$, approximately 3.5 times greater than the value in neat triethylamine. From the ratio $k_d/k_r = 0.011$, $k_d = 4.6 \times 10^5\ \mathrm{sec}^{-1}$, a value which may be compared with that for benzophenone triplet[9b] in benzene, $2.6 \times 10^5\ \mathrm{sec}^{-1}$. Thus the low value of k_d/k_r does not appear to arise from a low value of k_d despite the relatively long phosphorescence lifetime of excited PAB in rigid cyclohexane,[18] and it reflects a high value of k_r. Similarly, study of the effects of concentration of amine and of the quenching by naphthalene on the photoreduction of benzophenone by a primary amine, 2-butylamine, in benzene, had indicated[23] a fairly low value of k_d/k_r, 0.03 *M*, and a fairly high value of k_r, 5×10^7 to $1 \times 10^8\ M^{-1}\ \mathrm{sec}^{-1}$ depending upon the value of k_q which is used.

The moderately high reactivity of the bicyclic amine, triethylenediamine, $\varphi = 0.21$, Table VIII, has led us to suggest[1] an electron abstraction mechanism for photoreduction by amines. The heteroatoms of alcohols and amines activate the adjacent C–H for abstraction of the hydrogen by triplet ketones, which have reactivity similar to that of an electrophilic radical.[35] The energy of the transition state may be decreased by a polar contribution to its structure. While stabilization in

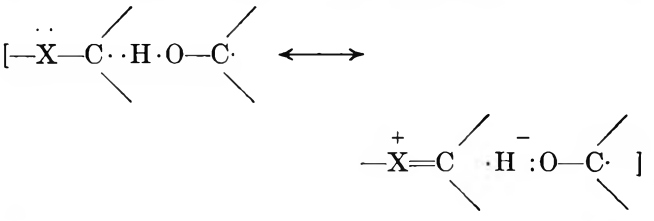

this way may not require full planarity of the –X–C< grouping, the favorable effect of the bridgehead N atoms of the bicyclic amine may indicate that activation by adjacent N may be of a different character. These reactions may proceed by interaction of the triplet ketone with the electron pair of N, forming an ion pair or charge-transfer complex II, followed by proton transfer and electron redistribution.

$$\mathrm{Ar, Ar'C{=}O^* + CH_3CH_2NR_2} \longrightarrow \underset{\mathrm{II}}{[\mathrm{Ar, Ar'C{-}O^-\ CH_3CH_2NR_2^+}]} \quad (2)$$

$$[\mathrm{Ar, Ar'C{-}O^-\ CH_3CH_2NR_2^+}] \longrightarrow \mathrm{Ar, Ar'C{-}OH + CH_3CHNR_2} \quad (3)$$

An initial electron transfer is consistent with absence

(40) A. J. Parker, *Advan. Phys. Org. Chem.*, **5**, 173 (1967).

(41) P. J. Wagner and G. S. Hammond, *J. Amer. Chem. Soc.*, **88**, 1245 (1966).

(42) W. M. Moore and M. D. Ketchum, *ibid.*, **84**, 1368 (1962).

of N-deuterium isotope effect in the antioxidant action of aromatic amines,[43] with the inverse N-deuterium and low α-deuterium isotope effects in photoreduction of benzophenone by primary amines,[23] and with kinetic studies of chemical oxidation of amines.[44] This process may be particularly favored in the bicyclic compound in which *trans*-annular stabilization is possible.[45] Such initial electron or charge transfer has been proposed for the quenching action of amines.[46]

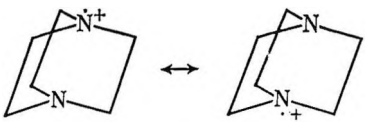

This mechanism is consistent with and may account for the kinetic characteristics of photoreduction by amines—both that of benzophenone[23] and that of the present study of PAB. The reactions show low sensitivity to the concentration of amines, low k_d/k_r, and high k_r. The reactions are not quenched as readily by naphthalene, ferrocene, and oxygen[23] as is photoreduction of benzophenone by alcohol, while the quantum yields are significantly lower. Reversible hydrogen abstraction from amine, where it has been sought,[23] has not been found. These characteristics are consistent with very rapid initial interaction of the triplet with the p-electrons of N and efficient formation of the ion-pair or charge-transfer complex, eq 2, rendering the system relatively insensitive to concentration of amine and to quenchers. This may be followed partly by hydrogen transfer, leading to reaction and the radicals, eq 3, and partly by electron back-transfer, leading to ketone and amine, eq 4, and to lower quantum yield.

$$[\mathrm{Ar,\ Ar'\dot{C}{-}O^-\ \dot{C}H_3CH_2\overset{+}{N}R_2}] \longrightarrow \underset{\mathrm{II}}{}$$

$$\mathrm{Ar,\ Ar'C{=}O\ -\ CH_3CH_2NR_2} \quad (4)$$

This process, eq 2, 3, and 4, allows the amine to act both as an efficient hydrogen donor and as a quencher, and accounts for low quantum yield, high k_r, normal k_d, and low efficiency of quenchers. It accounts particularly well for the kinetic characteristics of photoreduction by amines of benzophenone, a ketone which is known to lead very efficiently to chemically reactive triplets. With PAB the low quantum yield may be due in significant part to inefficient formation of a triplet of high chemical reactivity.

The light-intensity effect, an increase in quantum yield from 0.25 to 0.42 (Table III) with increasing light intensity, is unusual. In the photoreduction of benzophenone by alcohol the reverse has been observed, a decrease in quantum yield with increasing light intensity, due to increased triplet–triplet or radical–triplet quenching[47] and to increased formation of light absorbing transient.[36] The increase in quantum yield for photoreduction of PAB with increasing light intensity may indicate reaction of excited PAB with an intermediate, in a process which has overall greater light efficiency than the more direct single photon process. Such an intermediate may be the complex II, or conceivably an otherwise unreactive product formed from II, such as triethylamine in an excited state.

Finally, the characteristics of the absorption spectra of PAB, Table IX, may be discussed briefly. The effectiveness of the medium as a photoreducing system depends upon (i) its inherent reactivity as a reducing agent for ketone triplet and (ii) its effect on the relative stability of the several triplets of differing chemical reactivity.[18] There may be only an incidental correlation, if any, between these properties and the nature of the singlet–singlet transitions as indicated by the absorption spectra. The hydrocarbon media show λ_{max} at lowest wavelength, ~300 mμ, and sharpest band, and they are the most suitable media for photoreduction by tertiary amines, although they are not very reactive themselves. The hydrogen-bonding compounds, alcohols, water, amides, and primary amines, shift λ_{max} to ~330 mμ and broaden the band. They stabilize the unreactive CT triplet, so that presence of 1 *M* 2-propanol in cyclohexane leads to very low reactivity, Table VIII. Of the aprotic dipolar solvents, dimethylformamide and pyridine affect the spectrum much like the hydrogen-bonding solvents. Acetonitrile, however, leads to a spectrum of intermediate character, much like those in the reactive triethylamine and in diisopropylamine. Nevertheless, acetonitrile prevents reactivity of triethylamine, apparently as its dipolar character leads to a lower lying CT triplet.

Acknowledgment. This work was supported by predoctoral fellowships under Title IV, NDEA, and from the National Institutes of Health, GM-33475, and by the U. S. Atomic Energy Commission, AT(30-1) 2499, and the National Science Foundation, GP-1833, 6366.

(43) G. S. Hammond, C. E. Boozer, C. Hamilton, and J. N. Sen, *J. Amer. Chem. Soc.*, **77**, 3238 (1955).

(44) L. A. Hull, G. T. Davis, D. H. Rosenblatt, H. K. R. Williams, and R. C. Weglein, *ibid.*, **89**, 1163 (1967).

(45) T. M. McKinney and D. H. Geske, *ibid.*, **87**, 3013 (1965).

(46) A. H. Weller and H. Leonhard, *Ber. Bunsenges. Physik. Chem.*, **67**, 791 (1963).

(47) N. C. Yang and S. Murov, *J. Amer. Chem. Soc.*, **88**, 2852 (1966).

The Photoperoxidation of Unsaturated Organic Molecules. III. Autoperoxidation in Polymer Films

by B. Stevens[1] and B. E. Algar

Department of Chemistry, Sheffield University, Sheffield, England *(Received May 7, 1968)*

The autoperoxidation yield of 9,10-dimethyl-1,2-benzanthracene (DMBA) in nylon 6.6 and in polyethylene films has been measured as a function of the partial pressure of environmental oxygen. The observed behavior is similar to that exhibited by the same hydrocarbon in benzene solution under conditions where oxygen quenching of the singlet state of DMBA is restricted by the much lower diffusion coefficient of molecular oxygen in the polymers.

Introduction

Although the presence of $O_2{}^1\Delta_g$ ($^1O_2{}^*$) has yet to be established directly in systems undergoing photosensitized peroxidation, the available evidence[2] strongly supports the intermediary role of this species in the sequential processes

$$S^* + {}^3O_2 \longrightarrow S + {}^1O_2{}^*$$
$$^1O_2{}^* + M \longrightarrow MO_2$$

where the asterisk denotes electronic excitation of the sensitizer S and M is the unsaturated molecule (substrate) from which the peroxide MO_2 is produced.

An analysis of the dependence of the quantum yield of the over-all reaction γ_{MO_2} on concentration of dissolved oxygen, in terms of $^1O_2{}^*$ participation, has shown that at least for (a) the autoperoxidation (S≡M) of 9,10-dimethyl-1,2-benzanthracene[3a] (DMBA) and (b) the anthanthrene-sensitized photoperoxidation of DMBA and 9,10-dimethylanthracene[3b] (DMA), the singlet oxygen molecule is produced entirely by oxygen quenching of the sensitizer triplet state $^3S^*$ and not in the spin-allowed oxygen quenching of the sensitizer singlet state, *i.e.*

$$^1S^* + {}^3O_2 \not\longrightarrow {}^3S^* + {}^1O_2{}^*$$

even when this is exothermic. Oxygen quenching of the sensitizer singlet state does, however, appear necessary to promote the formation of sensitizer triplet state by collision-induced intersystem crossing represented by

$$^1S^* + {}^3O_2 \longrightarrow {}^3S^* + {}^3O_2$$

for those sensitizers with very high (100%) fluorescence quantum yield.[3a]

Processes 1–7 therefore constitute the simplest kinetic scheme consistent with the observed dependence of γ_{MO_2} on such experimental parameters as incident light intensity, substrate concentration, and concentration of dissolved oxygen.[3a]

$$S + h\nu \longrightarrow {}^1S^*$$
$$^1S^* \longrightarrow S + h\nu \quad (1)$$
$$^1S^* \longrightarrow {}^3S^* \quad (2)$$
$$^1S^* + {}^3O_2 \longrightarrow {}^3S^* + {}^3O_2 \quad (3)$$
$$^3S^* \longrightarrow S(+ h\nu) \quad (4)$$
$$^3S^* + {}^3O_2 \longrightarrow S + {}^1O_2{}^* \quad (5)$$
$$^1O_2{}^* \longrightarrow {}^3O_2 \quad (6)$$
$$^1O_2{}^* + M \longrightarrow MO_2 \quad (7)$$

The asterisk denotes electronic excitation, internal conversion of $^1S^*$ does not contribute significantly to the over-all relaxation rate of those aromatic hydrocarbons which undergo autoperoxidation[3a] (with the possible exception of naphthalene[4]), and process 4 includes both radiative and nonradiative relaxation of the triplet state $^3S^*$. Under photostationary conditions, processes 1–7 lead to the following expression for γ_{MO_2}

$$\frac{1}{\gamma_{MO_2}} = \left\{1 + \frac{k_6}{k_7[M]}\right\} \times \left\{1 + \frac{k_1}{k_2 + k_3[O_2]}\right\}\left\{1 + \frac{k_4}{k_5[O_2]}\right\} \quad (I)$$

where k_i is the rate constants of the ith process. Equation I provides a quantitative description of the variation in γ_{MO_2} with concentration of dissolved oxygen over the range 10^{-2} to 3×10^{-6} M for the autoperoxidation of DMBA in benzene,[3a] where at low oxygen concentrations such that

$$k_3[O_2] \ll k_2$$

(1) Department of Chemistry, University of South Florida, Tampa, Fla. 33620.

(2) *Cf.* C. S. Foote, S. Wexler, W. Ando, and R. Higgins, *J. Amer. Chem. Soc.*, 90, 975 (1968), and other papers in this series.

(3) (a) B. Stevens and B. E. Algar, *J. Phys. Chem.*, submitted as part II; (b) B. Stevens and B. E. Algar, *Chem. Phys. Letters*, 1, 219 (1967).

(4) B. Stevens and B. E. Algar, *ibid.*, 1, 58 (1967).

$1/\gamma_{MO_2}$ is a linear function of $1/[O_2]$, and at higher concentrations of dissolved oxygen when

$$k_5[O_2] \gg k_4$$

the nonlinear dependence of $1/\gamma_{MO_2}$ on $1/[O_2]$ reflects a competition between the intramolecular and collision-induced intersystem crossing of the sensitizer (processes 2 and 3); under the same conditions oxygen quenching of the sensitizer to the ground state would effectively inhibit the over-all reaction.

On the other hand, $k_3[O_2] \gg k_2 \sim 0$ for sensitizers of very high (~100%) fluorescence quantum yield (rubrene and DMA) and $1/\gamma_{MO_2}$ varies linearly with $1/[O_2]$ in the (high) experimentally accessible concentration range.[3a]

The over-all quantum yield of peroxide formation is essentially determined (eq I) by the magnitudes of bimolecular quenching frequencies ($k_3[O_2]$, $k_5[O_2]$, $k_7[M]$) relative to the unimolecular relaxation constants (k_1, k_4, k_6) of the electronically excited species involved ($^1S^*$, $^3S^*$, $^1O_2^*$); it is therefore of interest to examine the oxygen concentration dependence of γ_{MO_2} under conditions of limited molecular diffusion to establish the generality of the proposed mechanism and to obtain limiting values for the lifetimes of the metastable intermediates. This communication describes an investigation of the autoperoxidation of DMBA in polymer films at various partial pressures of environmental oxygen.

Experimental Section

Nylon 6.6 and polyethylene films of 0.003-in. thickness were refluxed in a concentrated ethanolic solution of DMBA until the concentration of solute in the film, monitored by absorption spectrophotometry, reached the value required (dictated by the optical density of the films at the actinic wavelength of 365 mμ). At concentrations of the order of 10^{-2} M, obtained after a period of some 30 min, no evidence of solute aggregation was discernible in either absorption or emission, and films containing a similar concentration of pyrene exhibit no trace of the excimer fluorescence band characteristic of this aggregated solute.[5]

The washed and dried films were placed between two 0.25 in. thick plywood squares (2 × 2 in.) bolted together so that a 1 cm diameter circle of the film was visible through 1 cm diameter holes aligned in the plywood plates; the edges of these holes were covered with quartz plates and apertures bored through the assembly in the plane of the film permitted the circulation of a gas stream over the film. In effect the films were suspended in a cylindrical plywood cell parallel to its quartz end windows and subjected to the passage of a N_2–O_2 gas mixture of variable composition.

After establishing the absence of photochemical reaction in the absence of environmental oxygen, the latter gas was admitted to the flowstream and the quantum yields of photoperoxidation computed from the time dependence of the solute optical density at the wavelength of incident radiation as described previously. The prevailing temperature was 23 ± 2°.

Absorption spectra recorded as a function of exposure time were found to exhibit an isosbestic point at 252 mμ, the final spectrum being almost identical with that of the corresponding peroxide in cyclohexane and showing no absorption at wavelengths >350 mμ.

Concentrations of dissolved oxygen in polyethylene were estimated from its solubility (3.44×10^{-3} M at 760 mm) in the completely amorphous polymer with a volume fraction of 0.65, and the partial pressure of oxygen P_{O_2} (atm) in the flowstream, *i.e.*, from the relationship[6]

$$[O_2] = 2.23 \times 10^{-3} P_{O_2} M$$

Solubility data for oxygen in nylon 6.6 could not be found. The bimolecular encounter constant of oxygen in polyethylene was estimated from measurements of the relative fluorescence intensities F_O/F of pyrene in this polymer in nitrogen and oxygen environments, and the relationship

$$F_O/F = 1 + k_{O_2}\tau_F[O_2] = 1.7$$

This yields a value for

$$k_{O_2} = 6.5 \times 10^8 \ M^{-1} \ \text{sec}^{-1} \text{ at } 23°$$

with a fluorescence lifetime for molecular pyrene of 480 sec and the value for $[O_2]$ quoted; in view of the absence of evidence for photoassociation (molecular self-quenching) of this solute in the polymer, it is concluded that this high value for k_{O_2} is due entirely to the rapid diffusion of molecular oxygen in polyethylene.

Results and Discussion

The quantum yields of DMBA autoperoxidation ($[M] = 4 \times 10^{-2}$ M) in nylon 6.6 and polyethylene films are plotted against the partial pressure of environmental oxygen on a reciprocal basis in Figure 1. The linear dependence of $1/\gamma_{MO_2}$ on $1/[O_2]$ is provided by eq I which reduces to

$$\frac{1}{\gamma_{MO_2}} = \frac{1}{\phi_M}\left\{1 + \frac{k_1}{k_2}\right\}\left\{1 + \frac{k_4}{k_5[O_2]}\right\} \qquad \text{(II)}$$

under the condition $k_2 \gg k_3[O_2]$ established by the much lower encounter constant k_3 in the polymer and confirmed by the very small oxygen quenching effect (<5%) of the solute fluorescence.

Within the combined limits of error the identical intercepts of the data lines in Figure 1, given by

$$(\gamma_{MO_2})_{[O_2]=\infty} = \phi_M\gamma_{IS} = 0.68 \pm 0.09$$

indicate that both the $^1O_2^*$ addition efficiency ϕ_M =

(5) *Cf.* B. Stevens, *Spectrochim. Acta*, **18**, 439 (1962).

(6) A. S. Michaels and R. B. Parker, *J. Polymer Sci.*, **51**, 53 (1959); A. S. Michaels and H. J. Bixler, *ibid.*, **50**, 393 (1961).

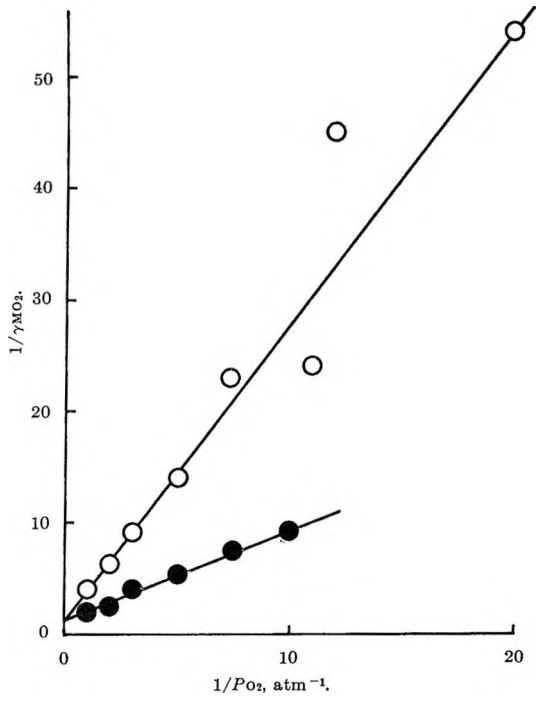

Figure 1. Plot of $1/\gamma_{MO_2}$ for autoperoxidation of DMBA in ○, nylon 6.6, and ●, polyethylene films, against reciprocal partial pressure of environmental oxygen. DMBA concentration, 4×10^{-2} M; λ 365 mμ.

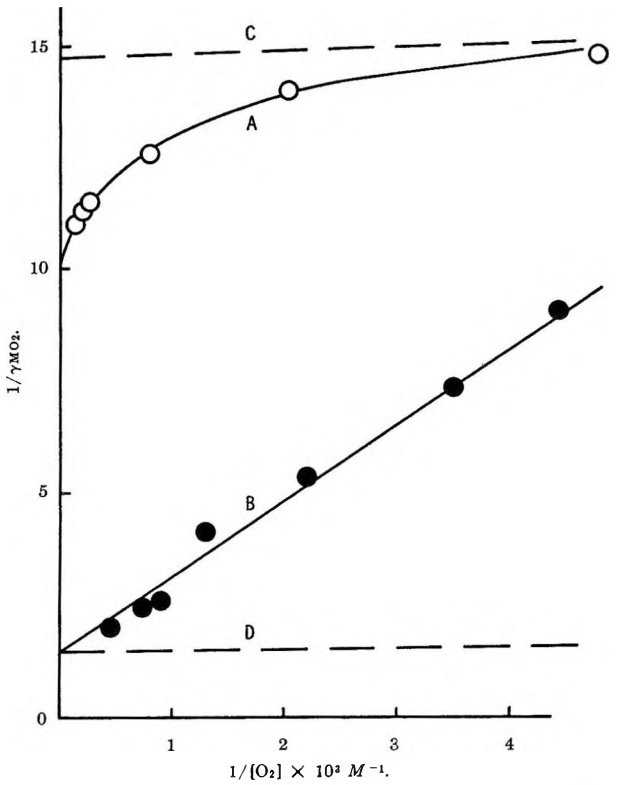

Figure 2. Variation of $1/\gamma_{MO_2}$ with $1/[O_2]$ for autoperoxidation of DMBA in A, benzene solution (10^{-4} M); B, polyethylene film (4×10^{-2} M). Curve C, extrapolation of low $[O_2]$ data for 10^{-4} M benzene solution; D, computed extrapolation of low $[O_2]$ data for 4×10^{-2} M solution in benzene.

$k_7[M]/(k_6 + k_7[M])$ and the intersystem crossing yield $\gamma_{IS} = k_2/(k_1 + k_2)$ of DMBA are independent of the polymer matrix. If γ_{IS} is assigned the value 0.66 ± 0.06 obtained for DMBA in benzene at the same temperature,[3] these data yield the limiting values for

$$\phi_M = 1.0 \pm 0.2$$

$$k_7/k_6 = k_7\tau_{O_2} \gtrsim 130\ M^{-1}$$

i.e., the lifetime τ_{O_2} of $^1O_2$* exceeds 200 nsec if k_7 has an upper limit of 6.5×10^8 M^{-1} sec^{-1} computed from oxygen quenching of pyrene fluorescence in polyethylene (see Experimental Section). This is somewhat lower than the limiting value of $\tau_{O_2} \lesssim 1$ μsec estimated from the photosensitized peroxidation of olefins in various solvents.[2]

The larger slope of the data line for DMBA in nylon film (Figure 1) may be a consequence of either a lower oxygen solubility or a smaller diffusion coefficient for molecular oxygen in this polymer, or both, if the decay constant of solute phosphorescence (which could not be detected at 23°) has the same value in both films.

Figure 2 shows the data for DMBA in polyethylene plotted on the basis of dissolved oxygen concentration in polyethylene film, with data for the same solute in benzene for comparison purposes. The dashed line C represents an extrapolation of the data obtained at very low concentrations of dissolved oxygen in benzene which is described by eq II, and line D denotes a similar extrapolation for the solution data corrected for a change in substrate concentration from the experimental value in solution (10^{-4} M) to that (4×10^{-2} M) used in the polymer film; the extrapolation line D (for benzene solution) is therefore comparable with the data line B obtained for DMBA in polyethylene.

The coincidence of the intercepts $(1/\gamma_{MO_2})_{[O_2]=\infty}$ for the data in solution and in polyethylene confirms the assumption that γ_{IS} is independent of environment, whereas the ratio of the slopes of the comparable data lines for DMBA in benzene and in polyethylene expressed as

$$(k_5\tau_{^3S})_{benzene}/(k_5\tau_{^3S})_{polymer} = 300 \pm 50$$

is a consequence of the difference in both the triplet-state lifetime $\tau_{^3S}$ ($=1/k_4$) of DMBA and the DMBA–oxygen encounter constant k_5 in the different media.

Use of the limiting value $k_5 = k_{O_2} = 6.5 \times 10^8$ M^{-1} sec^{-1} together with the experimental value for the oxygen quenching constant of the triplet state in polyethylene

$$(k_5\tau_{^3S})_{polymer} = 800 \pm 100\ M^{-1}$$

leads to an estimated triplet-state lifetime for the sensitizer (DMBA) given by

$$\tau_{^3S} \lesssim 1.2 \times 10^{-6} \text{ sec}$$

which is two orders of magnitude less than the value

computed for the same parameter in benzene solution; this could be a consequence of a lower encounter probability for oxygen quenching of the triplet than of the singlet state which apparently proceed by different mechanisms.

Conclusions

The oxygen concentration dependence of the quantum yield of DMBA autoperoxidation in nylon and polyethylene films is similar to that observed for the same system in benzene solution and provides additional support for the suggestion that an excited singlet state of oxygen, probably $O_2{}^1\Delta_g$, is the reactive intermediate. Similar conclusions have been reached by Bourdon and Schnuriger,[7] who observe high quantum yields (0.2–0.3) for the erythrosin-sensitized photooxidation of 4-methoxynaphthol in ethyl cellulose under conditions where the average separation of sensitizer and substrate is 80 Å.

(7) J. Bourdon and B. Schnuriger, *Photochem. Photobiol.*, **5**, 507 (1966).

Mechanisms of Photochemical Reactions in Solution. LVI.[1]

A Singlet-Sensitized Reaction

by Steven Murov[2] and George S. Hammond

Contribution No. 3672 from the Gates and Crellin Laboratories of Chemistry, California Institute of Technology, Pasadena, California 91109 (Received May 7, 1968)

Both norbornadiene, **1**, and quadricyclene, **2**, quench the fluorescence of many aromatic hydrocarbons. Surprisingly, **2** is considerably more effective than **1** as a quencher. Quenching by **2** leads to isomerization of the quencher to **1**, but no **2** is produced when **1** acts as a quencher.

We have recently reported that conjugated dienes are remarkably effective in quenching the fluorescence of many aromatic hydrocarbons.[3] The overall process amounts to catalysis of nonradiative decay of fluorescent species. The following formal mechanism provides a basis for discussion.

$$A \xrightarrow{h\nu} A^{*(1)} \tag{1}$$

$$A^{*(1)} \longrightarrow A + h\nu' \tag{2}$$

$$A^{*(1)} + Q \underset{k_{-3}}{\overset{k_3}{\rightleftharpoons}} (A\cdot Q)^{*(1)} \tag{3}$$

$$(A\cdot Q)^{*(1)} \xrightarrow{k_4} \underbrace{A^{*(v)} + Q^{*(v)}}_{\text{vibrationally excited ground-state molecules}} \tag{4}$$

$$R_q = \frac{k_3k_4[A^{*(1)}][Q]}{k_{-3} + k_4} = k_q[A^*][Q] \tag{5}$$

The excited complexes are visualized as being loosely bound and we would expect that they would probably be formed on nearly every encounter in solution. Since quenching rates in many cases are well below diffusion controlled, we infer that reaction 4 is often rate limiting and that $k_{-3} \gg k_4$. Under these circumstances the rate law becomes

$$R_q \cong K_3k_4[A^{*(1)}][Q]$$

Quenching reactivity is controlled by two factors: the stability of the complex, measured by K_3, and the radiationless decay rate, measured by k_4. We are inclined to view the binding energy of the excited complex as arising from exciton and charge-transfer interactions.

$$A^*\cdot Q \longleftrightarrow A\cdot Q^* \longleftrightarrow A^+Q^- \longleftrightarrow A^-Q^+$$

Our principal approach to construction of a more detailed model for quenching has been variation of the structures of both quenchers and quenchees. We hope that consistent patterns of structure–reactivity relationships will emerge. In this spirit we investigated

(1) Part LV: R. S. Cooke and G. S. Hammond, *J. Amer. Chem. Soc.*, **90**, 2958 (1968).

(2) National Institutes of Health Postdoctoral Fellow, 1967–1968.

(3) L. M. Stephenson, D. G. Whitten, and G. S. Hammond, "The Chemistry of Ionization and Excitation," Taylor and Francis Ltd., London, 1967, p 35, and references cited therein.

the behavior of compound **1** (norbornadiene, 2.2.1-bicyclohepta-2,5-diene). Although the diene does not have a classical conjugated structure, interaction between the two double bonds does lower the energies of the lowest, electronically excited states below those of simple olefins. The first absorption maximum is found at 2216 Å.[4] The diene also has low-lying excited triplet states since isomerization to quadricyclene, **2**, can be accomplished using benzophenone as a photosensitizer.[5] Wei and Kuppermann[6] have found a transition at 4.0 eV using electron-scattering spectrometry; the excited state is believed to be the lowest triplet.

Compound **1** quenches naphthalene fluorescence with a rate constant of 1.3×10^7 l. mol^{-1} sec^{-1}. This reactivity is significant, being about the same as that of isoprene (1.4×10^7 l. mol^{-1} sec^{-1}), one of the less reactive conjugated dienes.

As a part of the investigation, we examined solutions after irradiation to determine whether or not any isomerization of **1** to **2** had occurred. No trace of **2** could be found. However, experiments intended to be routine controls showed that **2** *quenches naphthalene fluorescence far more efficiently than* **1**. *Furthermore, extensive isomerization of* **2** *to* **1** *accompanies the quenching action.* Both observations seemed extraordinary to us so the scope of the phenomena has been investigated using a number of aromatic hydrocarbons as sensitizers.

Quenching efficiencies have been measured both by measuring the decrease in fluorescence intensity and by determination of the decrease in fluorescence lifetimes in the presence of quenchers. Results obtained by the two methods are in excellent agreement. Quantum yields for isomerization of **2** to **1** were determined in solutions containing sufficient quadricyclene to quench at least 99% of the fluorescence of the sensitizers.

The mechanism outlined above can be expanded to include chemical reaction of the quencher.

$$Q^{*(u)} \xrightarrow{k_6} Q \qquad (6)$$

$$Q^{*(u)} \xrightarrow{k_7} Q' \qquad (7)$$

The Stern–Volmer relationships used to test the form of the mechanism are

$$\text{Fluorescence intensity} \quad \frac{I_0}{I} = 1 + k_q\tau_0[Q] \qquad (8)$$

$$\text{Fluorescence lifetime} \quad \frac{\tau_0}{\tau} = 1 + k_q\tau_0[Q] \qquad (9)$$

$$\text{Quantum yield} \quad \frac{\phi_0}{\phi} = 1 + \frac{1}{k_q\tau_0[Q]} \qquad (10)$$

I_0 and τ_0 = fluorescence intensities and lifetimes in absence of quencher

ϕ_0 = maximum quantum yield

Figures 1, 2, and 3 show representative plots of data

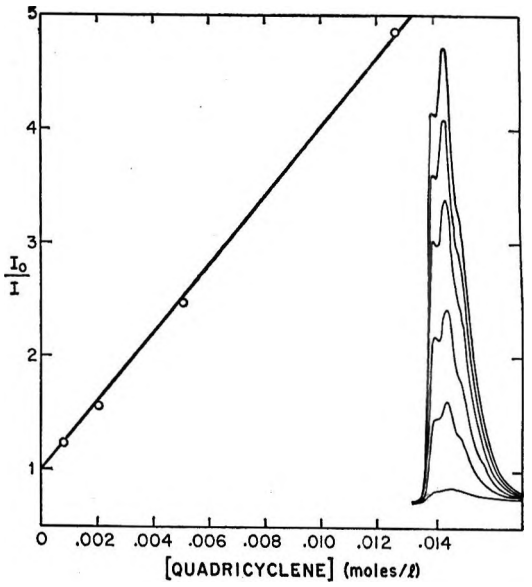

Figure 1. Quenching of naphthalene fluorescence by quadricyclene; relative intensity method; emission spectra shown in the inset.

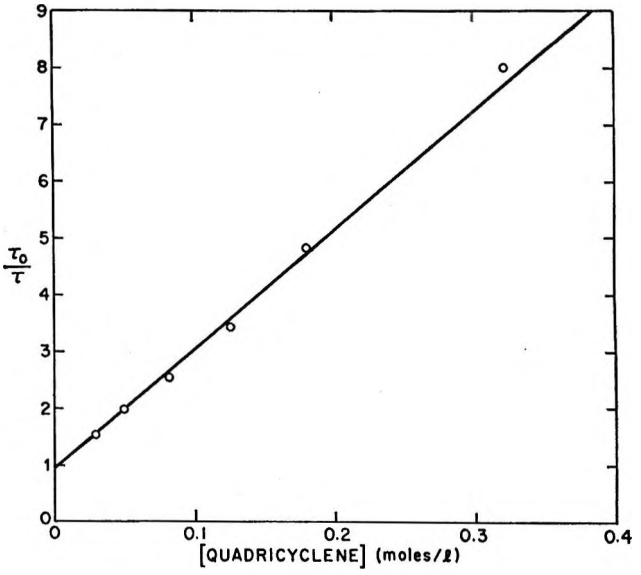

Figure 2. Quenching of 2,6-dimethylnaphthalene fluorescence by quadricyclene; lifetime method.

obtained. Equation 9 may be rearranged to give eq 11 for purposes of direct comparison of quenching and isomerization.

$$\frac{\tau}{\tau_0 - \tau} = \frac{1}{k_q\tau_0[Q]} \qquad (11)$$

Figure 4 shows a comparison of data for quantum

(4) M. B. Robin and N. A. Kuebler, *J. Chem. Phys.*, **44**, 2664 (1966).

(5) G. S. Hammond, N. J. Turro, and A. Fischer, *J. Amer. Chem. Soc.*, **83**, 4674 (1961).

(6) P. S. Wei, Ph.D. Thesis, California Institute of Technology, 1968.

Table I: Rate Constants for Singlet Quenching of Aromatic Hydrocarbons by Quadricyclene

Compound	k_q ($\times 10^{-6}$),[a] l./mol sec	A, eV[b]	I_p[b]	(^1L_b)[c]	(^1L_a)[c]
9,10-Dichloroanthracene	113				3.08
2-Chloronaphthalene	(70)			3.86	
Naphthalene	32	−0.3	8.16	3.88	4.35
Anthracene	31	0.5	7.43		3.31
2,3-Benzfluorene	18			3.65	
1,2,3,4-Dibenzanthracene	10	0.5	7.6	3.32	3.55
Anthanthrene	(7)	1.0	7.11		2.86
2,6-Dimethylnaphthalene	5			3.82	
Pyrene	5	0.5	7.72	3.34	3.72
Octahydro-1,1,4,4,7,7,10,10-octamethylnaphthacene	(3)				
Triphenylene	1.8	−0.05	8.17	3.58	4.36
9,10-Diphenylanthracene	(1.8)				3.11
Perylene	(1.7)	0.8	7.11	3.67	2.86
1,2-Benzanthracene	(1.6)	0.6	7.53	3.22	3.45
3,4-Benzpyrene	(1.6)	0.7	7.37	3.08	3.22
3,4,8,9-Dibenzpyrene	(1.2)	1.1	7.41	3.13	3.88
9,10-Dimethylanthracene	(1.0)				3.11
Chrysene	(0.9)	0.3	7.83	3.44	3.89
1,2,5,6-Dibenzanthracene	(0.3)	0.6	7.58	3.15	3.54
1,2,7,8-Dibenzanthracene	(0.08)	0.6	7.58	3.14	3.33
Tetracene	(<0.08)	1.0	6.95		2.63

[a] Values in parentheses are less accurately known, either because quenching reactivity is low or because relatively few data were taken. [b] Reference 7. [c] Reference 8.

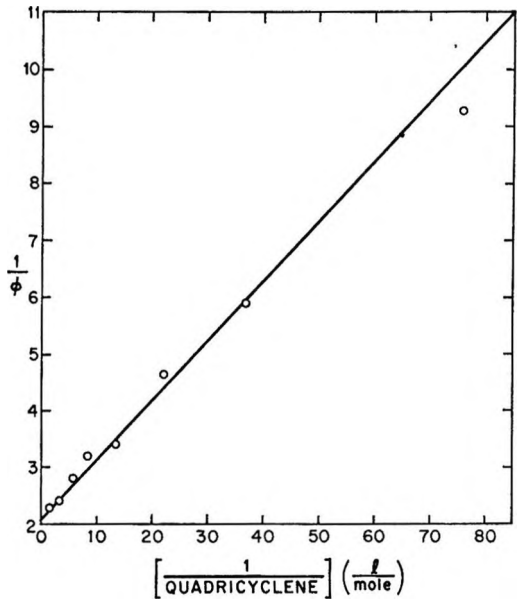

Figure 3. Quantum yield for isomerization of quadricyclene sensitized by 2,6-dimethylnaphthalene.

yields and fluorescence lifetimes in the system 2,6-dimethylnaphthalene–quadricyclene. The slopes of the two lines are identical within experimental error.

Table I shows data for the rates of quenching of various aromatic compounds by **2**.[7,8] Included in the table are available values of the electron affinities (A), ionization potentials (I_p), and energies of transitions to the ^1L_b and ^1L_a states. The data do not reveal any consistent pattern for correlation of quenching reactivity with the various factors that may be expected to contribute to the binding energy of the excited complex, although steric hindrance appears to be a significant inhibitory influence, as is the case with quenching by conjugated dienes.[3] The lack of other clear-cut relationships may reflect both the complexity of the binding interactions and variation in the decay rate, k_4.

Table II shows the data for quantum yields obtained with various sensitizers. There is surprisingly little variation in the values, in view of the considerable variation in k_q and in the excitation energy available in the excited singlet sensitizers. The activation energy for thermal isomerization of **2** to **1** is 38.3 kcal mol^{-1}.[9] This should represent a lower limit to the energy required in the vibrationally excited form of **2** to effect reaction. An easy interpretation of the data involves the assumption that the decay process in most cases leaves energy considerably in excess of the 38 kcal minimum in **2**. The limiting quantum yield of about 0.5 would then measure the partitioning of vibrationally hot molecules between the two decay paths to **1** and **2**. The lower quantum yields obtained with anthanthrene and 9,10-dichloroanthracene could then be taken as an

(7) G. Briegleb, *Angew. Chem.*, **3**, 617 (1964).

(8) E. Clar, "Polycyclic Hydrocarbons," Vol. I and II, Academic Press, New York, N. Y., 1964.

(9) J. R. Erdman, *J. Org. Chem.*, **32**, 2920 (1967).

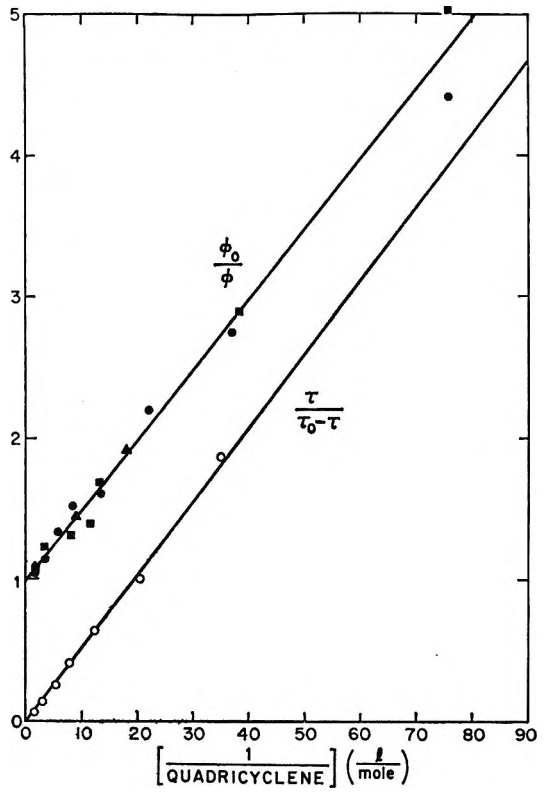

Figure 4. Comparison of quantum yields and fluorescence quenching with quadricyclene and 2,6-dimethylnaphthalene.

Table II: Quantum Yields of Norbornadiene Formation and the Singlet Energies of the Energy Donors

Compound	E_s, kcal	ϕ^a
Naphthalene	89.7	0.53
2,6-Dimethylnaphthalene	88.2	0.58
2,3-Benzfluorene	84.2	0.54
Pyrene	77.2	≥0.47
1,2,3,4-Dibenzanthracene	76.4	0.52
1,2-Benzanthracene	74.3	≥0.57
3,4-Benzpyrene	71.1	≥0.35
9,10-Dichloroanthracene	71.1	0.16
Anthanthrene	66.1	≥0.15

[a] Values indicated as lower limits may be influenced by the slow disappearance of the sensitizer during the experiments.

indication that internal conversion of the less energetic excited complexes from those sensitizers does not always endow the quadricyclene with the minimum energy required for isomerization.

Conclusions drawn from this line of reasoning must be regarded as tentative. One interesting implication comes from consideration of the fact that no detectable chemical action results from quenching of naphthalene by **1**. The diene is more stable than **2** by approximately 20 kcal mol^{-1}.[10] Consequently, 58 kcal/mol must be put in **2** in the quenching act to reach the level of the transition state for the thermal reaction. Although 89 kcal mol^{-1} is potentially available in the excited singlet of naphthalene, the absence of any induced reaction of the quencher suggests that less than 68% of the available energy appears in the quencher.[11]

Triplet-Sensitized Reactions. In our earlier reports[5,12] we assigned triplet mechanisms to all photosensitized interconversions of **1** and **2**. We now know that the singlet mechanism is responsible for the reaction **2** → **1** in the presence of aromatic hydrocarbon sensitizers having low-lying triplet states. We felt that it was worthwhile to reinvestigate some of the results obtained with ketones, which are known to undergo rapid system crossing to triplets. Table III summarizes results of interest. Acetophenone and benzophenone, sensitizers having high energy triplets,[13] effect transformation of the diene to quadricyclene in an entirely unexceptional manner. The triplet mechanism is also undoubtedly responsible for sensitization of the same reaction by 2-acetonaphthone and 2-naphthaldehyde, since quenching of naphthalene fluorescence by the diene is not accompanied by isomerization.

Table III: Quantum Yields for Norbornadiene–Quadricyclene Conversions with Triplet Sensitizers

Starting material	Concn	Sensitizer	ϕ
1	0.528	$C_6H_5COCH_3$	0.91
1	0.579	$(C_6H_5)_2CO$	0.51
1	0.579	2-Acetonaphthone	0.05
1	0.126	2-Acetonaphthone	0.04
1	0.579	2-Naphthaldehyde	0.06
1	0.126	2-Naphthaldehyde	0.02
2	0.632	2-Acetonaphthone	<0.01
2	0.632	2-Naphthaldehyde	Small
2	0.640	$(C_6H_5)_2CO$	0.06
2[a]	0.640	$(C_6H_5)_2CO$	<0.01

[a] Containing 0.413 *M* piperylene.

The small but readily measurable sensitized reversion of **2** to **1** in the presence of benzophenone must also be assigned a triplet mechanism, because the reaction is quenched by piperylene (1,3-pentadiene). It is already known[14,15] that benzophenone singlets are not quenched by piperlyene.

(10) Professor R. B. Turner, unpublished.

(11) Alternatively, we might postulate that the vibrational energy left in the quencher by the decay process is not concentrated in appropriate vibrational modes to lead to reaction. This would also require the hypothesis that internal equilibration of vibrational energy is slower than vibrational relaxation in the liquid phase. Although we cannot argue strongly against this theory, the latter assumption seems unattractive.

(12) G. S. Hammond, P. Wyatt, C. D. DeBoer, and N. J. Turro, *J. Amer. Chem. Soc.*, **86**, 2532 (1964).

(13) W. G. Herkstroeter, A. A. Lamola, and G. S. Hammond, *ibid.*, **86**, 4537 (1964).

Triplet-sensitized reactions involving sensitizers having only low-lying triplet states have been attributed to "nonvertical excitation" of the energy acceptor to form directly a triplet state having a geometrical configuration different from that of the ground state. The energy transfer process must have much in common with the singlet quenching reactions reported in the paper. If spin inversion occurs as a part of the nonradiative change, the direct product from the quenching step may be a vibrationally excited form of the ground electronic state of the quencher in the triplet mechanism, as well as in the singlet reaction.

Experimental Section

Norbornadiene (**1**) was distilled twice. Quadricyclene (**2**) was prepared by photosensitized isomerization of **1**, essentially as described earlier.[12] The product was distilled twice at 50° and 100 torr pressure. Vapor chromatographic analysis showed that the final product contained less than 1% of **1**. Sensitizers were purified by careful, but not exhaustive, recrystallization.

Relative fluorescence intensities were measured with an Aminco spectrofluorometer. The excitation wavelength was adjusted to obtain maximum emission. Samples were made up in ether solution and degassed by three freeze–thaw cycles before the measurements were made. Sample tubes were made from 13-mm Trubore tubing. Measurements were repeated several times and the samples were rotated between measurements in an attempt to detect severe optical imperfections in the tubing.

Fluorescence lifetimes were measured with a TRW Model 75A decay time fluorometer. Quantum yields were measured using a merry-go-round apparatus to assure uniform irradiation of test and actinometric samples. The group of lines near 3130 Å were isolated from the output of a 450-W Hanovia medium-pressure mercury lamp using solution filters. The filters were 1.5 cm of a solution of 26 g of cobalt(II) sulfate in 100 ml of water and 0.6 cm of a solution prepared by dissolving 0.132 g of potassium chromate in 250 ml of 1% aqueous sodium carbonate. A slightly modified version of the ferrioxalate actinometer[16] was used. Analysis for **1** and **2** was done by vapor chromatography using a 5-ft column of 30% Carbowax at 37°.

Acknowledgment. This work was supported by the Directorate of Chemical Sciences, Air Force Office of Scientific Research, Contract No. AF 49(638)-1479.

(14) P. G. Cassman, D. H. Aue, and D. S. Patton, *J. Amer. Chem. Soc.*, **86**, 4211(1964).

(15) A. A. Lamola and G. S. Hammond, *J. Chem. Phys.*, **43**, 2129 (1965).

(16) C. G. Hatchard and C. A. Parker, *Proc. Roy. Soc.*, **A235**, 518 (1956).

Transient Species in the Radiolysis of Solutions of Stilbene

by F. S. Dainton, C. T. Peng,[1] and G. A. Salmon

Cookridge High Energy Radiation Research Centre, University of Leeds, Leeds, United Kingdom *(Received June 3, 1968)*

When solutions of *cis*- and *trans*-stilbene in either benzene or cyclohexane are irradiated with 2-μsec pulses of 3-MeV electrons, absorption bands are observed in the uv (λ_{max} 360 nm) and visible (λ_{max} 480 nm in benzene and 500 nm in cyclohexane) regions. From the effects of additives such as O_2, N_2O, anthracene, and naphthalene, the uv absorption, which decays in a first-order manner, is ascribed to a triplet state while the visible band, which decays according to a second-order law, is attributed to the stilbene anion. Estimates are derived of the rate constants of some energy transfer processes. The results are consistent with radiation-induced geometrical isomerization of stilbene in dilute solutions proceeding to a radiostationary state predominantly *via* triplet states and in concentrated solutions predominantly *via* ions or radicals to exclusively *trans*-stilbene.

Introduction

Irradiation of solutions of stilbene, S, in hydrocarbons with X- or γ rays causes geometrical isomerization. For solutions of stilbene in cyclohexane of less than 10^{-2} *M*, or less than ~0.1 *M* for benzene solutions, the isomerization can occur in both directions, *cis* to *trans* and *trans* to *cis*, so that a radiostationary state is achieved.[2,3] From the similarity of the ratios, $G_{c\rightarrow t}/G_{t\rightarrow c}$ and $\phi_{c\rightarrow t}/\phi_{t\rightarrow c}$, where ϕ is the quantum yield of

(1) Radioactivity Research Center and School of Pharmacy, University of California, San Francisco Medical Center, San Francisco, Calif. 94122.

(2) (a) H. P. Lehmann, G. Stein, and E. Fischer, *Chem. Commun.*, 583 (1965); (b) R. R. Hentz, D. B. Peterson, S. B. Srivastava, H. F. Barzynski, and M. Burton, *J. Phys. Chem.*, **70**, 2362 (1966).

the photoisomerization and from the highly selective effects of additives in either promoting or quenching the isomerization, it has been concluded that triplet states of stilbene, $^3S^*$, are intermediates.[2-4] The internal energy of S_c in the ground, ^1A, state exceeds that of S_t by 6 kcal/mol,[5] and the known vertical excitation energies $S_c \rightarrow {}^3S_c^*$ and $S_t \rightarrow {}^3S_t^*$ are 57 and 49 ± 1, respectively,[6] where $^3S_c^*$ and $^3S_t^*$ represent the first excited triplet states of *cis*- and *trans*-stilbene. Thus $^3S_c^*$ has an internal energy greater than that of $^3S_t^*$ by 14 ± 1 kcal/mol. From the dependence of the energies of the triplet and ground states of stilbene on the angle of twist[7] it would not be surprising if the *cis* and *trans* triplet states did not revert to the same mixture of ground-state isomers. Malkin and Fischer[6] have, in fact, suggested that whereas $^3S_t^*$ gives equal amounts of S_c and S_t, $^3S_c^*$ yields roughly three S_c to one S_t.

These ratios determine the position of the stationary state in irradiated *dilute* solutions of stilbene. At higher stilbene concentrations the stationary state becomes richer in S_t because $G_{c\rightarrow t}$ increases and in 0.6 M solution in benzene may exceed 200.[8] This result has been explained on the basis of an anionic chain reaction in which the propagation step is reaction 1, which in

$$S_t^- + S_c \longrightarrow S_t + S_c^- \qquad (1)$$

ethers has a rate constant of $10^9\ M^{-1}\ \text{sec}^{-1}$.[9] This reaction may proceed *via* the intermediate adduct, $(S\text{-}S\cdot)^-$, which depolymerizes to form predominantly S_t^- and S_t. This prompts the suggestion that *cis* to *trans* isomerization may equally well be induced by radicals, R·, which react with S_c to form a temporary complex RS· in which free rotation can occur and $k_{-2t} > k_{-2c}$.

$$R\cdot + S_c \underset{k_{-2c}}{\overset{}{\rightleftharpoons}} RS\cdot \overset{k_{-2t}}{\rightleftharpoons} R\cdot + S_t \qquad (2)$$

In this paper we report some preliminary results of pulse-radiolysis studies of benzene and cyclohexane solutions of S_c and S_t designed to test whether anions and/or triplet states of stilbene and free radicals can be identified. While the absorption spectra of S^- and S^{2-} are known and extensive studies of the photochemical isomerization have been made, the absorption spectra of $^3S_c^*$ and $^3S_t^*$ are unknown.

Experimental Section

The solutions were irradiated with a 2-μsec pulse of 2.8–2.9-MeV electrons from a Van de Graaff generator. The electron beam was focused by two quadrupole magnets onto the optical cell (10 × 10 × 7 mm) which contained the test solution.

Each pulse was monitored by measuring the charge developed during the passage of the electron beam through a secondary emission chamber. Calibration of the chamber was carried out daily using an oxygenated solution of potassium ferrocyanide (5×10^{-3} M) as the dosimetric fluid and assuming G(ferricyanide) = 3.2,[10] and $\epsilon_{420\ \text{nm}} = 10^3\ M^{-1}\ \text{cm}^{-1}$.[11] Electron density corrections were applied when calculating the dose rates in benzene and cyclohexane.

The optical system and the methods of degassing solutions by argon bubbling and filling and draining the irradiation cell have been described elsewhere.[12]

Unsaturated or aromatic impurities in the cyclohexane were removed by repeated treatment with nitrating mixture, washing with water, drying, and distillation after refluxing over potassium. Benzene was treated with sulfuric acid alone followed by washing, drying, and distillation.

Other chemicals and gases used were of the highest purity available commercially and with the exception of *trans*-stilbene (which was recrystallized three times from ethanol) were not treated further.

All glassware was cleaned with a dilute solution of potassium permanganate in sulfuric acid, rinsed with distilled water, washed with a mixture of nitric acid and 30% hydrogen peroxide, repeatedly rinsed with distilled water, and then dried.

Results and Discussion

1. Transient Spectra in Stilbene Solutions. The spectra measured at the end of the pulse for dilute argon-saturated solutions of stilbene in benzene and cyclohexane are shown in Figures 1, 2, and 3. In each case there is a large peak at ~480 nm and subsidiary peaks in the uv and red regions. The spectra in cyclohexane (Figures 2 and 3) are more intense than those in benzene and part of the absorption between 300 and 500 nm persists for at least 300 μsec in the former solvent. Slight differences exist between the spectra of the pulsed S_c and S_t solutions, *e.g.*, in the position and intensity of the peak at the longest wavelength. However, the presence of a peak at 400 nm for S_c solutions in benzene as compared with its absence for S_t solutions in the same solvent may not be real and is not regarded as significant.

After making allowance for the long-lived absorption which underwent negligible decrease during the experi-

(3) R. A. Caldwell, D. G. Whitten, and G. S. Hammond, *J. Amer. Chem. Soc.*, **88**, 2659 (1966).

(4) E. Fischer, H. P. Lehmann, and G. Stein, *J. Chem. Phys.*, **45**, 3905 (1966).

(5) R. B. Williams, *J. Amer. Chem. Soc.*, **64**, 1395 (1942).

(6) S. Malkin and E. Fischer, *J. Phys. Chem.*, **68**, 1153 (1964); G. S. Hammond, *et al.*, *J. Amer. Chem. Soc.*, **86**, 3197 (1964).

(7) P. Borrell and H. H. Greenwood, *Proc. Roy. Soc.*, **A298**, 453 (1967).

(8) R. R. Hentz, K. Shima, and M. Burton, *J. Phys. Chem.*, **71**, 461 (1967).

(9) R. Chang and C. S. Johnson, *J. Chem. Phys.*, **46**, 2314 (1967).

(10) G. E. Adams, J. W. Boag, and B. D. Michael, *Trans. Faraday Soc.*, **61**, 492 (1965).

(11) G. Hughes and C. Willis, *Discussions Faraday Soc.*, **36**, 243 (1963).

(12) G. A. Salmon, *et al.*, submitted for publication.

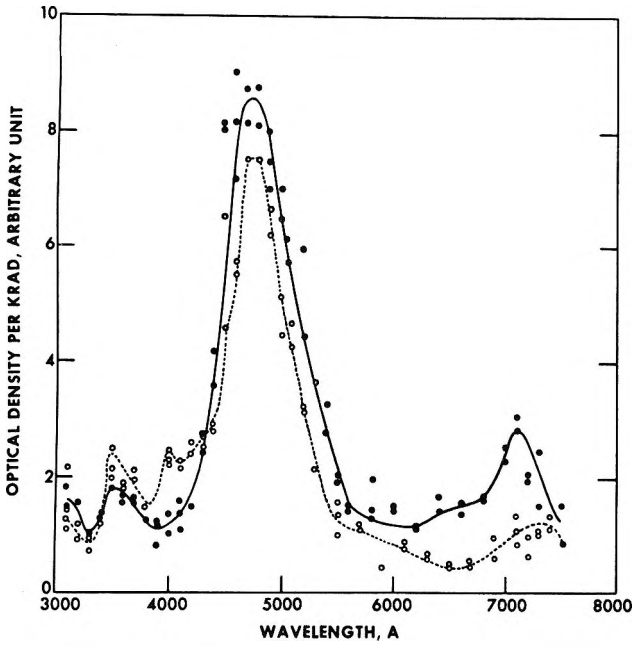

Figure 1. End-of-pulse absorption spectra of benzene solutions of *cis*-stilbene (1.13×10^{-2} *M*) - - -, and *trans*-stilbene (1.062×10^{-2} *M*), ——.

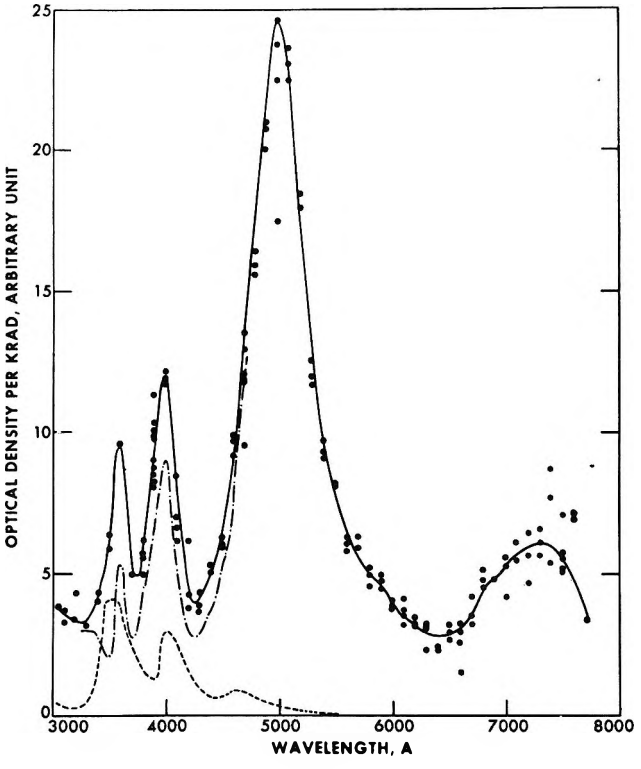

Figure 2. End-of-pulse absorption spectrum of cyclohexane solution of *trans*-stilbene (1.04×10^{-2} *M*), ——. Spectrum corrected for long-lived product is represented by –·–·, and that of long-lived product taken 300 μsec after pulse by - - -.

ment, the residual parts of these ultraviolet absorptions in cyclohexane were found to decay according to a first-order law with $k = 6 \pm 2 \times 10^4$ sec^{-1} for S_c and

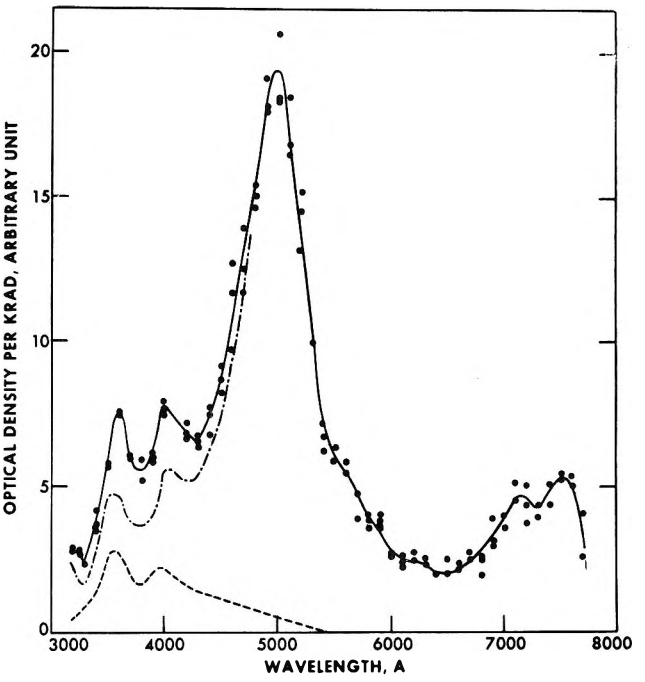

Figure 3. End-of-pulse absorption spectrum of cyclohexane solution of *cis*-stilbene (1.13×10^{-2} *M*), ——. Spectrum corrected for long-lived product is represented by –·–·, and that of long-lived product taken 300 μsec after pulse by - - -.

$7 \pm 3 \times 10^4$ for S_t. This fact combined with the observation that saturation of the solutions with oxygen greatly decreased the apparent $G\epsilon$ of these bands whereas saturation with nitrous oxide did not produce this effect strongly suggests that these bands are due to $^3S_c^*$ and $^3S_t^*$. This assignment is in accord with the findings of Schulte-Frohlinde, *et al.*,[13] that flash photolysis of 10–100 μ*M* solutions of S_t in rigid EPA glass at 77°K produces a spectrum consisting of a strong peak at 379 nm with peaks at 343 and 360 nm, all of which decay in a first-order manner with $k = 34$ sec^{-1}. These authors also found that photoexcitation of S_c does not produce the triplet state but causes it to isomerize instead to 4,4′-dihydrophenanthrene. Loss of $^3S_c^*$ in this way may account for the lower values of $G\epsilon$ found for solutions of S_c in the 300–400-nm region as compared with those for solutions of S_t.

In cyclohexane the dependence of the yield of putative $^3S_t^*$ on the concentration of S_t is very reminiscent of that for naphthalene triplet states on naphthalene concentration in the same solvent, but no experiments were carried out on xenon-saturated solutions to test whether stilbene singlets (*e.g.*, ^1B or $^1G^-$) are precursors of some of the triplets.[14] It is interesting that for S_t in cyclohexane, the 360-nm peak was observable at lower $[S_t]$, $\sim 10^{-5}$ *M*, than the 390-nm peak and was

(13) G. Heinrich, H. Blume, and D. Schulte-Frohlinde, private communication, Aug 1967.

(14) F. S. Dainton, T. Morrow, G. A. Salmon, and G. F. Thompson, *Chem. Commun.*, No. 6, 326 (1968).

also subject to a relatively greater enhancement in the presence of nitrous oxide. Oxygen destroyed only about three quarters of the absorption at 390 nm for S_t in cyclohexane but this residual absorption decayed by a second-order law. This suggests, but does not prove, that absorption in this region in the presence of oxygen may be due to peroxy stilbene diradicals.

Stilbene anions were first reported to be formed in irradiated solutions of stilbene in 2-methyltetrahydrofuran glass[15] and were later identified spectrophotometrically.[16] The spectra of S^- and S^{2-} formed by electron transfer from alkali metals have been extensively investigated and the results are shown in Table I.[17] We conclude that the absorption observed by us for stilbene solutions in benzene at 480 and 500 nm in cyclohexane can be assigned to S^- and/or S^{2-} and that the weak absorption band with a maximum around 710–730 nm is attributable to S^- alone. These assignments are supported by the fact that the presence of oxygen or nitrous oxide causes a very marked decrease

Table I: Peaks in the Absorption Spectra of S^- and S^{2-} [a]

	λ, nm	ε, M^{-1} cm^{-1}
S^-	480	6.2×10^4
S^-	560	8×10^3
S^-	700	1.2×10^4
S^{2-}	480	3.3×10^4
S^{2-}	560	1.5×10^4

[a] See ref 17.

in these absorptions. (See Figures 4 and 5.) The residual $G\epsilon$ at 500 nm in the presence of nitrous oxide and oxygen is less than 10 and 5%, respectively, of its value in their absence. The species S^- is a radical ion and if, as we believe, it is homogeneously distributed, it is expected to disappear in bimolecular reaction such as (3) or (4), where M^+ denotes solvent and solute

$$2S^- \longrightarrow S_2^{2-} \text{ or } S + S^{2-} \quad (3)$$

$$S^- + M^+ \longrightarrow \text{neutralization} \quad (4)$$

cations, the concentration of which must equal that of all the negative ions. The decay of the absorptions in

Table II: Second-Order Rate Constants for Disappearance of S^- Anions

Solute	Solvent	λ_{max}, nm	$G\epsilon$, cm^{-1} M^{-1}	k_2/ϵ, cm sec^{-1}
S_c	Benzene	480	3.15×10^3	3.57×10^7
S_c	Cyclohexane	500	9×10^3	1.8×10^7
S_t	Benzene	480	3.6×10^3	3.6×10^7
S_t	Cyclohexane	500	1.2×10^4	1.1×10^7
S_t	Cyclohexane	710	3.1×10^3	5.6×10^7

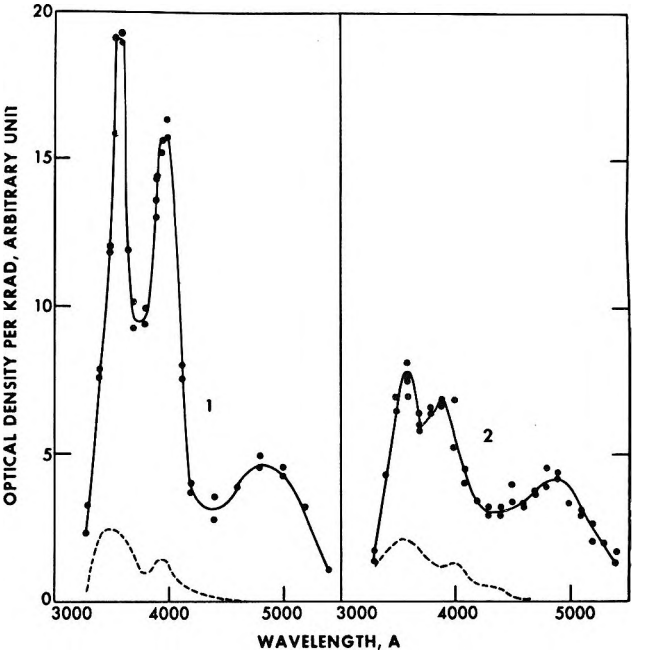

Figure 4. End-of-pulse absorption spectra in cyclohexane with N_2O to saturation: curve 1, *trans*-stilbene (0.893×10^{-2} M); curve 2, *cis*-stilbene (1.13×10^{-2} M). Spectrum of long-lived product taken 300 μsec after pulse is represented by dashed line.

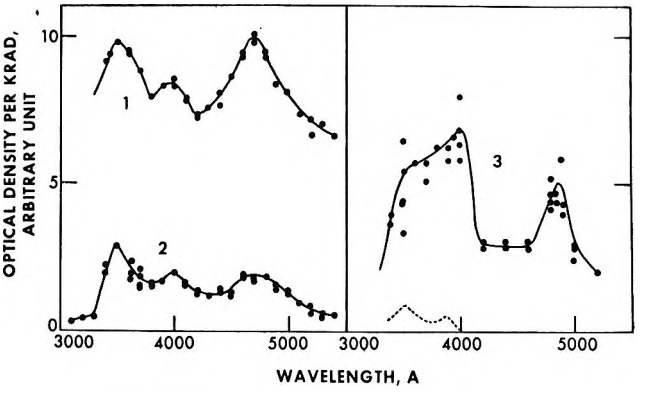

Figure 5. End-of-pulse absorption spectra: curve 1, *trans*-stilbene (0.928×10^{-2} M); curve 2, *cis*-stilbene (1.13×10^{-2} M) in benzene with N_2O to saturation; curve 1 is translated upward in ordinate by 5 arbitrary units for presentation; curve 3, *trans*-stilbene (0.90×10^{-2} M) in cyclohexane with O_2 to saturation. Spectrum of long-lived product taken 300 μsec after pulse is shown by the dotted line.

both wavelength regions was found to be second order with rate constants shown in Table II. Evidently, the extinction coefficients of S_c^- and S_t^- in each solvent are not less than 10^3 and the second-order rate constant are therefore probably in the range 10^{10} to 10^{11} M^{-1} sec^{-1}

(15) F. S. Dainton and G. A. Salmon, *Proc. Roy. Soc.*, **A285**, 319 (1965).

(16) T. Shida and W. H. Hamill, *J. Chem. Phys.*, **44**, 2375 (1966).

(17) E. R. Zabolotny and J. F. Garst, *J. Amer. Chem. Soc.*, **86**, 1645 (1964).

indicating the expected diffusion controlled nature of reactions 3 and 4.

2. Solutions of Stilbene Containing a Second Solute. (a) Directions of Energy and Electron Transfer. Energy- and electron-transfer reactions are generally undetectable when ΔE has positive values even though these are small, but the reverse reaction is usually rapid. It was therefore decided to attempt confirmation of the assignments of the uv and visible absorption bands of the transient species by studying the effects of second solutes having triplet state energies, electron affinities, and ionization potentials different from those of S_c and S_t. The available solutes were naphthalene (N), benzil (Bz), biacetyl (Bi), and anthracene (A), and the major features of the results are indicated in Table III and Figure 6.

Table III: Typical End-of-Pulse $G\epsilon$ Values

Solute	Additive, mM	λ, nm	$G\epsilon \times 10^{-4}$
	A. Benzene Solutions		
cis-Stilbene (0.011 M)	...	350	1.05
	...	480	3.15
	N (0.34)	480	4.0
	A (4.16)	420	37.8
trans-Stilbene (0.010 M)	...	350	0.7
	...	480	3.6
	...	710	1.1
	N (0.2)	480	4.2
	N (0.2)	710	1.1
	B. Cyclohexane Solutions		
cis-Stilbene (0.011 M)	...	360	3.7
	...	400	3.8
	...	500	9.3
	...	710	2.3
	A (4.2)	420	37.8
	Bi (23)	480[a]	3.7
	Bz (9.2)	480[a]	5.0
trans-Stilbene (0.011 M)	...	360	5.4
	...	400	7.1
	...	500	12.1
	N (8.0)	360	4.1
	N (8.0)	400	5.6
	N (8.0)	500	13.0
	A (4.5)	420	24.8
	Bi (23)	480[a]	1.7
	Bz (8.5)	480[a]	4.0

[a] In these solutions the maximum absorption is at 480 nm rather than 500 nm.

When naphthalene, N, is present in comparable concentration to stilbene, there is no detectable formation of naphthalene triplets, $^3N^*$, which have $\epsilon_{max}^{415nm} = 14{,}000\ M^{-1}\ cm^{-1}$, but an increase was observed in the uv absorption which we have ascribed to $^3S_c^*$ or $^3S_t^*$. Mr. Robinson of our laboratory has observed that when the stilbene concentration is reduced to $10^{-4}\ M$ the

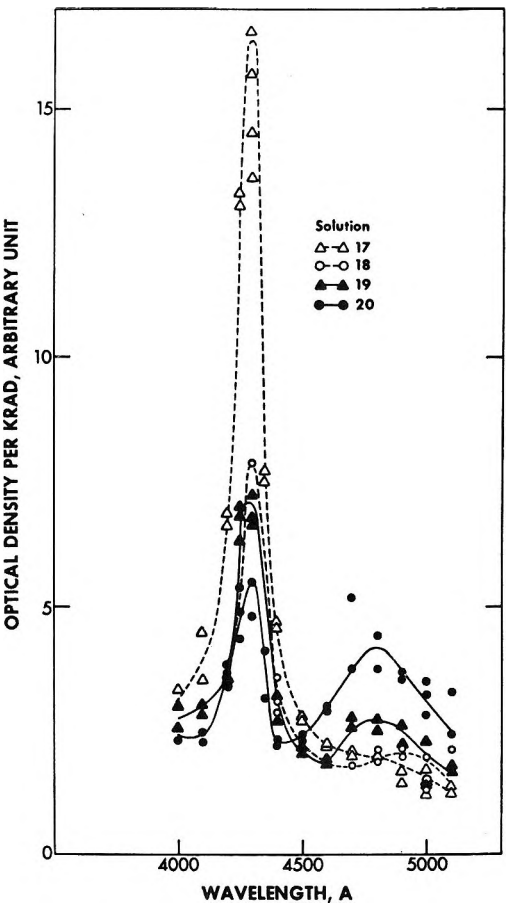

Figure 6. End-of-pulse absorption spectra of binary mixture of *cis*-stilbene ($1.13 \times 10^{-2}\ M$) and anthracene in benzene. Concentrations of anthracene in solutions 17, 18, 19, and 20 were 2.5×10^{-4}, 1.01×10^{-4}, 5.06×10^{-5}, and $2.53 \times 10^{-5}\ M$, respectively.

presence of $10^{-1}\ M$ naphthalene causes a 3–4-fold increase of $G\epsilon^{360\ nm}$. Both these observations suggest that reaction 5 can occur. In the second set of experiments,

$$^3N^* + S_{c\ or\ t} \longrightarrow N + {}^3S_{c\ or\ t}^* \qquad (5)$$

the $^3N^*$ absorption is observed, but its decay rate after the pulse is faster than in the absence of stilbene, and from the fact that the half-life of this decay is about 1 μsec when $[S] = 10^{-4}\ M$ we conclude that $k_5 \simeq 10^{10}\ M^{-1}\ sec^{-1}$.

It is difficult to assess the effect of N on the absorption at 400 nm because of the contribution which $^3N^*$ makes to the absorption at this wavelength. However, measurements taken 20 μsec after the pulse (when the $[^3N^*]$ should be very small indeed) suggest that there has been a slight enhancement of $G\epsilon$ in this region and therefore lends some support to the view that $^3S^*$ has some absorption here. Concentrations of N comparable with those of S have little effect on the 480-nm band in benzene or on the 500-nm band in cyclohexane. This may mean either that N is a much less effective scavenger of electrons (which is unlikely in

view of its positive electron affinity) or that any N^- anions rapidly transfer an electron to stilbene according to eq 6. The fact that a very large excess of N is

$$N^- + S_{c\text{ or }t} \longrightarrow N + S_t^- \quad (6)$$

required ([N] = 10^{-1} M when [S] = 10^{-4} M) before even a slight change of $G\epsilon^{500}$ can be perceived indicates that reaction 6 must be very fast with $k_6 \simeq k_5 \simeq 10^{10}$ M^{-1} sec^{-1}.

The literature values of electron affinities are conflicting, but those[18a,b] in best accord show that the electron affinities of S_c and S_t are 0.40 and 0.38 eV. That for naphthalene is not included, but it would be expected, and there is some indication,[18c] that it would be less than anthracene (0.42 eV) and near that of phenanthrene (0.20 eV) and triphenylene (0.14 eV). It seems a safe assumption that ΔE_6 will be 4 or 5 kcal negative and that eq 6 represents the expected direction of electron transfer. The triplet-state excitation energies are known with greater precision, and certainly $^3N^*$ lies 60.9 kcal above the ground state and hence $\Delta E_5 = -4$ and -11 kcal for *cis*- and *trans*-stilbene, respectively, and we conclude that reaction 5 is probably diffusion controlled.

In cyclohexane solutions containing benzil and biacetyl in concentration comparable to that of the stilbene, the 500-nm absorption is suppressed and an absorption maximum appears at 480 nm. This is consistent with the notion that the electron affinity of these substances exceeds those of S_c and S_t and that stable ketyl anions are derived from the α-diketones. At present, insufficient experiments have been done to assess the relative contribution of these ketyl anions and any remaining stilbene anions to the absorption in the 480–500-nm region.

Anthracene has a triplet excitation energy of only 42.5 kcal so that ΔE_7 would be expected to be -14.5 and -7 kcal for *cis*- and *trans*-stilbene. However, anthra-

$$^3S_{c\text{ or }t}{}^* + A \longrightarrow {}^3S_{c\text{ or }t} + {}^3A^* \quad (7)$$

cene has a slightly larger electron affinity,[18a] so that E_8 would be expected to be negative though small and hence reaction 8 might occur but its reverse should

$$S^- + A \longrightarrow S + A^- \quad (8)$$

not. The observations summarized in Figure 6 are that even very small (20 μM) concentrations of A cause a diminution of absorption at 480 nm and a new band to develop at 425 nm where $^3A^*$ is known to absorb. The fact that when [A] = 2.5×10^{-4} M, *i.e.*, $\sim$2% that of *cis*-stilbene, almost all S^- is removed by the end of the pulse indicates that reaction 8 must indeed be very fast and is probably diffusion controlled. Taking $\epsilon^{425\text{ nm}}$ for $^3A^*$ as 7×10^4 M^{-1} cm^{-1},[19] $G(^3A^*) \simeq 0.5$ for solution 17 in Figure 6. Nevertheless, the data do suggest that 0.25 mM anthracene is sufficient to ensure that reaction 7 is complete within the pulse and hence $k_7 \geq 5 \times 10^9$ M^{-1} sec^{-1}.

(*b*) *Variation in Concentration of Excited States during the Pulse.* It is, of course, unknown whether A^- ions emerging from reaction 8 when neutralized by cations give rise to any $^3A^*$, but it can be said that the dependence of the end-of-pulse-concentration of $^3A^*$ on [A] can be accounted for without recourse to this process. If it is assumed that all excited transients are ultimately derived from excited benzene molecules, B*, the series of equations representing the mechanism can be written as

$$B \longrightarrow B^* \quad (9)$$

$$B^* + S \longrightarrow B + {}^3S^* \quad (10)$$

$$B^* + A \longrightarrow B + {}^3A^* \quad (11)$$

$$B^* \longrightarrow B \quad (12)$$

$$^3S^* + A \longrightarrow S + {}^3A^* \quad (7)$$

$$^3S^* \longrightarrow S \quad (13)$$

$$^3A^* \longrightarrow A \quad (14)$$

where reactions 12, 13, and 14 represent quenching from all causes including impurity but excluding energy transfer involving S or A molecules. During the pulse, [B*] grows at the rate given by

$$[B^*] = G^* I\{1 - \exp[-(k_{10}[S] + k_{11}[A] + k_{12})t]\}/(k_{10}[S] + k_{11}[A] + k_{12}) \quad (15)$$

where I is the dose rate and G^* the yield of B* formed in reaction 9. If, as is likely, $k_{10} \simeq k_{11} \simeq 10^{10}$ M^{-1} sec^{-1}, then under our conditions $k_{10}[S] \gg k_{11}[A]$ and $k_{10}[S] \gg k_{12}$, eq 15 simplifies to

$$[B^*] = G^* I\{1 - \exp(-k_{10}[S]t)\}/k_{10}[S] \quad (16)$$

and since $k_{10}[S]t \simeq 100$ at the end of a microsecond pulse, $[B^*] = G^* I/k_{10}[S]$ and a stationary state in [B*] will be maintained throughout most of the pulse. Hence we obtain

$$[^3S^*] = G^* I\{1 - \exp[-(k_7[A] + k_{13})t]\}/(k_7[A] + k_{13}) \quad (17)$$

but since we have already shown $k_7 \geq 5 \times 10^9$ M^{-1} sec^{-1}, there must also be a steady state in [$^3S^*$] during the pulse and $[^3S^*] = G^* I/(k_7[A] + k_{13})$. Substituting these values for [$^3S^*$] and [B*] in the nonsteady-state equation for [A*] and integrating, we derive

$$[^3A^*] = \alpha\{1 - \exp(-k_{14}t)\}/k_{14} \quad (18)$$

where $\alpha = [A]\, G^*\, I\, [k_{11}/k_{10}[S] + k_7/(k_7[A] + k_{13})]$.

(18) (a) W. V. Sherman, *J. Chem. Soc., A.*, 599 (1966); (b) W. E. Wentworth and R. S. Becker, *J. Amer. Chem. Soc.*, **84**, 4263 (1962); (c) J. B. Binks and M. A. Slifkin, *Nature*, **200**, 766 (1963); **208**, 380 (1965).

(19) G. Porter and M. Windsor, *Proc. Roy. Soc.*, **A245**, 238 (1958).

Now the half-life of $^3A^*$ was measured as being in the range 10–100 μsec depending on the dose given in the pulse and therefore the value of $k_{14}t$ at the end of a 2-μsec pulse is sufficiently small to permit the expansion of eq 18 to only the first term of the series. We thus obtain eq 19. Neglecting, as before, k_{11} [A] in compari-

$$[^3A^*] = G^*It\{k_{11}[A]/k_{10}[S] + k_7[A]/(k_7[A] + k_{13})\} \quad (19)$$

son with k_{10} [S], we arrive at eq 20 expressing the rela-

$$[^3A^*]^{-1} = (G^*It)^{-1}\{1 + k_{13}/k_7[A]\} \quad (20)$$

tionship between the $[^3A^*]$ observed at the end of the pulse and [A]. The data of Figure 6 when suitably plotted to test eq 20 indicate $k_{13}/k_7 = (1.4 \pm 0.6) \times 10^{-5}$ M. Since $k_7 \geq 5 \times 10^9$ M^{-1} sec^{-1} and cannot exceed a diffusion-controlled value, say 2×10^{10}, we conclude that $4 \times 10^5 > k_{13} \geq 1 \times 10^4$ sec^{-1}. This is in accord with the lowest measured values of 6.5×10^4 and 4×10^4 sec^{-1} for $^3S_t^*$ and $^3S_c^*$, respectively, in cyclohexane containing no other solute.

(c) *Regulation of* $[S^-]$ *at the End of the Pulse.* If S and A compete for electrons and the rapid electron-transfer reaction (8) also takes place, then, neglecting charge recombination, the mechanism determining the OD at 480 nm comprises the following reactions and leads to eq 24 for the growth of $[S^-]$ during the pulse

$$B \longrightarrow B^+ + e_s^- \quad (21)$$

$$e_s^- + S \longrightarrow S^- \quad (22)$$

$$e_s^- + A \longrightarrow A^- \quad (23)$$

$$S^- + A \longrightarrow S + A^- \quad (8)$$

$$[S^-] = f_s G_i I\{1 - \exp(-k_8[A]t)\}/k_8[A] \quad (24)$$

where $f_s = k_{22}[S]/(k_{22}[S] + k_{23}[A])$ is the fraction of the available electrons which are captured by stilbene. At the end of the pulse $[A]t = (5\text{–}50) \times 10^{-11}$, so that if reaction 8 is diffusion controlled, $\exp(-k_8[A]t)$ may be neglected at high [A] throughout most of the pulse but cannot be so neglected at low [A]. We therefore deduce that, at low [A], $[S^-]^{-1}$ should be a linear function of [A] but at high [A], $([S^-][A])^{-1}$ should be a linear function of [A]. Though insufficient to permit a definite conclusion, the data suggest that $[S^-]$ is *less* dependent on [A] than this mechanism suggests. We hope that further work will clarify this question.

(d) *Decay of* $^3A^*$. The post-pulse decay of $^3A^*$ is easily measured and we find an empirical relationship that the first-order decay constant increases linearly with the square root of the dose per pulse. The most obvious explanation of this is that $^3A^*$ is subject to collisional quenching by a product formed during the pulse at a rate which is proportional to the square root of the dose rate. At these very high dose rates and consequent high radical concentrations this is entirely expected.

Conclusion

The experiments described have established conclusively that significant yields of anions and triplet states of the solute are formed when benzene or cyclohexane solutions of *cis*- or *trans*-stilbene are irradiated with high energy radiation and justify equally the ionic and triplet state mechanism which have been advanced to account for the radiation-induced geometrical isomerization of concentrated and dilute solutions of these solutes.

Acknowledgment. The authors wish to thank the Science Research Council and the University of California San Francisco Medical Center for financial assistance. We also wish to express our gratitude to Dr. T. Morrow and Mr. G. F. Thompson for their kind cooperation during the course of this investigation and to Mr. E. A. Robinson for making his recent results available.

Energy Transfer in Radiolysis of Rare Gas–Propane Liquid Mixtures[1]

by R. D. Koob[2] and Larry Kevan

Department of Chemistry, University of Kansas, Lawrence, Kansas 66044 *(Received May 7, 1968)*

The γ radiolysis of Xe, Kr, or Ar–C_3H_8 liquid mixtures has been investigated in the presence and absence of O_2 as a radical scavenger. The yields of ionic and excited molecule reactions have been assessed by isotopic analysis of C_3H_8–C_3D_8–O_2–rare gas and $CH_3CD_2CH_3$–O_2–rare gas irradiated mixtures. These yields have been related to the nature and efficiency of the energy transfer process by comparison with detailed radiolysis and photolysis results for pure liquid propane. Phase effects have been analyzed by comparison with gas-phase data. In xenon mixtures the gas–liquid phase change decreases ionic decomposition by 71% and excited molecule decomposition by only 8%, but in krypton mixtures both ionic and excited molecule decomposition yields are similar in gas and liquid phases. In liquid mixtures propane decomposition due to ionic fragmentation is 93, 76, and 39% in Ar, Kr, and Xe mixtures, respectively. The excited molecule fragmentation products show that the average energy of the excited molecule is high and about constant in Ar, Kr, and Xe mixtures. It is concluded that ion neutralization produces most of the excited molecules and that charge transfer from rare gas ions is the predominant energy transfer process. Overall energy transfer efficiencies in nonscavenged systems follow the trend: Xe > Kr > Ar.

Introduction

The radiolysis of propane has been extensively studied in both gas[3–10] and liquid phases.[11–15] The use of isotopically labeled propane has allowed a quantitative assessment of the decomposition reactions of excited ions and excited neutral molecules.[10] In the presence of excess rare gas, the radiation energy is originally absorbed by the rare gas and then transferred to propane. A careful study of excess rare gas–propane systems can thus give information about the nature and efficiency of the energy transfer processes.

Xenon–propane and krypton–propane mixtures have been studied in the gas phase. The results were analyzed in terms of energy transfer from both excited and ionized rare gas species.[9,10] A study of liquid phase rare gas–propane mixtures has indicated that energy is transferred from the rare gas mainly by ionic species.[12] In the present work isotopic data for rare gas (Ar, Kr, Xe)–propane liquid mixtures is presented and used to assess yields of ionic and excited molecule reactions. These yields have been related to the nature of the energy transfer process by comparison with detailed radiolysis and photolysis results for pure liquid propane. Phase effects have been analyzed by comparison with gas phase data. The overall efficiency of energy transfer has been evaluated for nonscavenged systems and found to follow the trend: Xe > Kr > Ar.

Experimental Section

Phillips research grade propane was purified by gas chromatography after which only 2 ppm of propane impurity remained. Deuterated propanes were about 95% isotopically pure. Oxygen (Air Products), 99.6% pure, and rare gases (Air Products), 99.99% pure, were used as received. Samples were condensed in order of increasing vapor pressure into 4 cm long Pyrex ampoules fabricated from 2-mm i.d. heavy-wall capillary tubing, and were irradiated by Co^{60} γ rays at a nominal dose rate of 0.5 Mrad/hr to H_2O. In all samples the liquid phase occupied 60% or more of the ampoule volume. To obtain thorough mixing, C_3H_8–Xe and C_3H_8–Kr mixtures were held at −78° for 24 hr before irradiation. C_3H_8–Ar mixtures were held at −130° for 30 min before irradiation. In addition to irradiation at the γ-source temperature (35°), samples were irradiated in crushed Dry Ice (−78°) and in a liquid nitrogen cooled air stream (−130°).

Ferrous sulfate dosimetry was used to determine the total dose to the sample. The dosimetry solution was O_2 saturated and irradiated in ampoules similar to those used with actual samples. The dosimetry results show that the actual dose to the liquid in the heavy-wall glass

(1) This work was supported by the Petroleum Research Fund and the U. S. Atomic Energy Commission. This is A.E.C. Document No. COO-1528-22.

(2) National Science Foundation Predoctoral Fellow, 1964–1966; National Institutes of Health Predoctoral Fellow, 1966–1967.

(3) P. Ausloos and S. Lias, *J. Chem. Phys.*, **36**, 3163 (1962).

(4) P. Ausloos, S. G. Lias, and I. B. Sandoval, *Discussions Faraday Soc.*, **36**, 66 (1963).

(5) P. Ausloos and R. Gorden, *J. Chem. Phys.*, **41**, 1278 (1964).

(6) P. Ausloos and S. G. Lias, *ibid.*, **44**, 521 (1966).

(7) J. H. Futrell and T. O. Tiernan, *ibid.*, **37**, 1694 (1962).

(8) L. W. Sieck, N. K. Blocker, and J. H. Futrell, *J. Phys. Chem.*, **69**, 888 (1965).

(9) L. I. Bone, L. W. Sieck, and J. H. Futrell, *J. Chem. Phys.*, **44**, 3667 (1966).

(10) (a) L. I. Bone, L. W. Sieck, and J. H. Futrell, "The Chemistry of Ionization and Excitation," G. R. A. Johnson and G. Scholes, Ed., Taylor and Francis, Ltd., London, 1967, pp 223–236; (b) L. I. Bone, Ph.D. Thesis, Ohio State University, 1966.

(11) R. D. Koob and L. Kevan, *J. Phys. Chem.*, **70**, 1336 (1966).

(12) R. D. Koob and L. Kevan, ref 10a, pp 141–150.

(13) R. D. Koob and L. Kevan, *Trans. Faraday Soc.*, **64**, 422 (1968).

(14) R. D. Koob and L. Kevan, *ibid.*, **64**, 706 (1968).

(15) R. D. Koob, Ph.D. Thesis, University of Kansas, 1967.

Table I: Radiolysis Product Yields per 100 eV (G) in Rare Gas–Propane Liquid Mixtures at 0.8-Mrad Dose[a]

Products	Xe–C_3H_8–O_2 (−78°) 25:1:0	Xe–C_3H_8–O_2 (−78°) 25:1:0.1	Kr–C_3H_8–O_2 (−78°) 25:1:0	Kr–C_3H_8–O_2 (−78°) 25:1:0.1	Ar–C_3H_8–O_2 (−130°) 25:1:0	Ar–C_3H_8–O_2 (−130°) 25:1:0.1
CH_4	1.38	0.88	3.3	2.7	2.14	1.32
C_2H_4	0.35	1.21	0.60	0.85	0.12	0.12
C_2H_6	1.20	0.64	3.0	1.9	1.98	1.16
C_2H_2	0.08	0.10	0.30	0.32	0.12	0.12
C_3H_6	0.77	0.60	0.66	0.39	0.13	0.04
i-C_4H_{10}	0.55	0.07	0.66	0.02	0.37	0.03
n-C_4H_{10}	0.43	0.08	0.48	0.05	0.28	0.04
i-C_5H_{12}	0.46	0.01	0.39	0.02	0.26	0.03
n-C_5H_{12}	0.29	0.04	0.36	0.29	0.25	0.14
2,3-Me_2C_4	0.58	0.01	0.30		0.17	
2-MeC_5	0.98	0.03	0.24	0.12	0.14	0.06
n-Hexane	0.40	0.01	0.09		0.03	

[a] Data are averages of three or more samples; precision is better than 15% or 0.01G; values for CH_4 and C_2H_6 in krypton scavenged systems are corrected from those reported previously in ref 12.

ampoules is about 5% higher than if the liquid is irradiated in a vessel whose diameter is large compared to the average range of the secondary electrons produced by γ radiation. The total dose absorbed by the liquid mixtures was calculated by correcting the dose to the dosimetry solution using electron fraction (electron density) and stopping-power per electron[16] correction factors. In the xenon mixtures an 11% correction for the photoelectric effect was included. Yields are reported as G values, the number of product molecules produced per 100 eV absorbed by the entire mixture.

After irradiation the sample ampoules were inserted into a brass cylinder which was then evacuated. The brass cylinder was heated with heating tape until the sample exploded and vaporization was complete. Analysis was performed by gas chromatography. By employing a switching system that allowed two different columns to be placed first in series and then in parallel, all components of the sample, with the exception of isobutane, were determined in a single aliquot.[13,15] In the series arrangement a thermal conductivity detector is used for measurement of the parent hydrocarbon and the rare gas. Flame ionization detection is used in the parallel arrangement to analyze the hydrocarbon products.

Isotopic ratios were measured on a Nuclide Model 12-90G mass spectrometer. Ethane and ethylene were trapped after gas chromatographic separation at 77°K from a helium stream; the helium was pumped away from the sample before it was injected into the mass spectrometer. Methane could not be trapped quantitatively from a helium stream, so CO_2 was used as a carrier gas and methane was trapped at 77°K by total collection of the CO_2 stream. The sample was held at 77°K for mass spectrometric analysis so that only methane was injected.

Fragmentation patterns, for CD_4, CD_3H, CD_2H_2, CDH_3, CH_4, C_2D_6, C_2H_6, C_2D_4, and C_2H_4 were measured for authentic samples on the Nuclide mass spectrometer. Other fragmentation patterns were obtained from the literature[17,18] and normalized to fragmentation patterns of knowns.[15]

Results

Table I shows the product yields of rare gas–propane (25:1) mixtures in G units, where G equals the number of molecules produced per 100 eV of radiation energy absorbed by the mixture. H_2 yields were not measured. Both unscavenged and O_2 scavenged results are shown. In the O_2 scavenged mixtures O_2 was equal to about 10% of the total propane. Higher concentrations of O_2 caused no further significant decrease in the product yields. The dose of 0.8 Mrad corresponds to 0.03% conversion in pure propane. However, in the rare gas mixtures over 95% of the deposited radiation energy is absorbed by the rare gas and the effective dose and % conversion of propane are higher because of rather efficient energy transfer. In the xenon and krypton mixtures the total conversion of propane is about 0.7% and in the argon mixtures the conversion is about 0.3%. Note that the yield of ethylene in Xe–C_3H_8–O_2 and Kr–C_3H_8–O_2 mixtures is greater than the ethylene yield in Xe–C_3H_8 and Kr–C_3H_8 mixtures in the absence of O_2. This is due to the occurrence of secondary reactions produced by the effective high dose to these mixtures. Thus the unscavenged yields in Table I do not represent initial yields. On the other hand, the O_2 scavenged yields are found to be independent of dose and are considered to represent initial yields.

The xenon and krypton mixtures were studied at

(16) N. A. Baily and G. C. Brown, *Radiation Res.*, 11, 745 (1959).
(17) E. I. Quinn and F. L. Mohler, *J. Res. Nat. Bur. Stand.*, 65A, 93 (1961).
(18) V. H. Dibeler, F. L. Mohler, and M. de Hemptinne, *ibid.*, 53, 107 (1954).

Table II: Isotopic Fractions in Irradiated Mixtures of Rare Gas Sensitized C_3H_8–C_3H_8–Scavenger Systems[a]

Fraction	Gas, 1 atm, NO scavenger[b] 25° Xe	25° Kr	Liquid, O_2 scavenger[c] −78° Xe	−78° Kr	−130° Ar
$\frac{CD_4 - CD_3H}{CD_4 + CD_3H + CH_2D_2}$[d]	...	...	0.82	0.80	0.76
$\frac{C_2D_6 - (C_2D_5H + C_2D_4H_2)}{C_2D_6 + (C_2D_5H + C_2D_4H_2)}$	0.03	0.05	0.0	0.0	0.0
$\frac{C_2D_4H_2}{C_2D_4H_2 + C_2D_5H}$	0.17	0.13	0.36	0.34	0.36
$\frac{C_2D_4 - C_2D_3H}{C_2D_4 + C_2D_3H}$	0.74	0.72	0.81	0.81	0.79
$\frac{C_3D_6 - C_3D_5H}{C_3D_6 + C_3D_5H}$	0.85	0.86	...	...	...

[a] All fractions have been corrected to $C_3D_8:C_3D_8 = 1$; dose = 0.8 Mrad. [b] Reference 10; typical ratios for rare gas:C_2D_8:C_3H_8:NO = 90:5:5:1. [c] Typical ratios for rare gas:C_3D_8:C_3H_8:O_2 = 90:2:2:0.2. [d] CH_2D_2 was ~3% of ($CD_4 + CD_3H + CD_2H_2$).

−78° while the argon mixtures were studied at −130°; this temperature difference was required by the freezing points and critical temperature of the rare gases in order to maintain a liquid phase in all mixtures. Separate experiments on pure propane[13] show that the temperature effects between −78° and −130° in O_2-scavenged systems are small.

In order to assess the decomposition yields and mechanisms, the system rare gas ≫ C_3H_8 = C_3D_8 ≫ O_2 was examined. Isotopic analysis of nonscavengeable CH_4, C_2H_6, and C_2H_4 was performed. Isotopic analysis of propylene did not give accurate results due to insufficient separation between propylene and propane on our chromatographic column. Table II gives values for the important isotopic fractions from the analysis. All ratios are normalized to represent a 1:1 ratio of C_3H_8:C_3D_8. Isotopically mixed propanes in C_3D_8 account for less than 5% of the total propane and corrections for these were minor or unnecessary. For a given compound the expression, (sum of isotopically pure components − sum of isotopically mixed components)/sum of all components, is a direct measure of the fraction of that compound formed intramolecularly. The isotopically mixed components arise from bimolecular reactions. If isotope effects are neglected, the yields of intramolecular and bimolecular reactions can be expressed in terms of only the more highly deuterated symmetrical components (*e.g.*, C_2D_6 rather than $C_2D_6 + C_2H_6$, C_2D_5H rather than $C_2D_5H + C_2H_5D$, etc.). This is advantageous because the deuterated components are more accurately measured by mass spectrometry. Within experimental error $C_2D_3H = C_2H_3D$ and $C_2D_5H = C_2H_5D$.

Table III shows the isotopic analysis of methanes produced in the irradiation of the system rare gas–$CH_3CD_2CH_3$–O_2. The CH_3D/CH_4 ratio increases for Ar to Kr to Xe. To provide information about the overall efficiency of energy transfer in rare gas–propane mixtures the yields for loss of C_3H_8 are calculated in Table IV. These yields are based on the total carbon yield found in the products.

Table III: Distribution of Isotopic Methanes from Irradiated Rare Gas–$CH_3CD_2CH_3$–O_2 Mixtures[a]

Product	Rare gas: Xe	Kr	Ar
	Irradiation temp, °C: −78	−78	−130
CH_4	0.63	0.70	0.85
CH_3D	0.31	0.23	0.12
CH_2D_2	0.08	0.07	0.03
CH_3D/CH_4	0.49	0.33	0.14

[a] Dose = 0.8 Mrad.

Figures 1 and 2 show radiolysis yields in Ar–C_3H_8 liquid mixtures as a function of F, the fraction of radiation energy absorbed by argon. The definition of F is given by eq 9 in the Discussion.

Discussion

A. Propane Decomposition Modes in Propane–Rare Gas Mixtures. In propane–rare gas mixtures with a large excess of rare gas almost all of the radiation energy is initially deposited in the rare gas. In order to decompose propane, energy must be transferred to propane molecules from the excited and ionized rare gas species produced by the radiation. The important species in liquid rare gases have been discussed;[12] it was concluded that all R* states above the appearance potential of R_2^+ react to yield R_2^+, that the majority of R^+ reacts to yield R_2^+, and that low-lying R* states mostly react to yield excimers, R_2^*. Thus, R_2^+ and R_2^* are considered to be the principal species by which energy is transferred to propane.

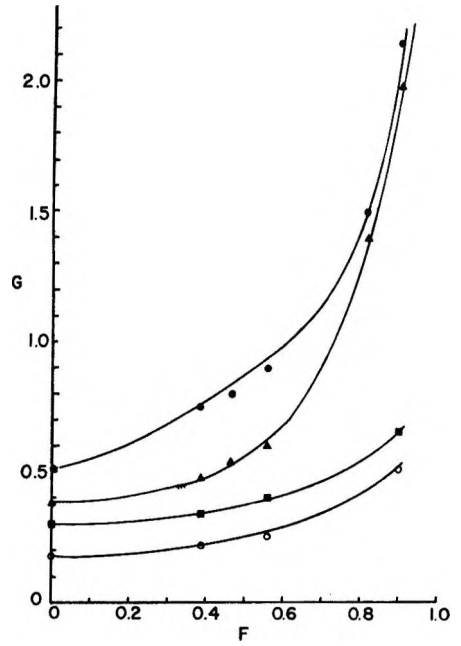

Figure 1. Radiolysis yields (G) in Ar–C_3H_8 liquid mixtures at −130° *vs.* F, the fraction of energy absorbed by Ar: ●, CH_4; ▲, C_2H_6; ■, C_4H_{10}; ○, C_5H_{12}.

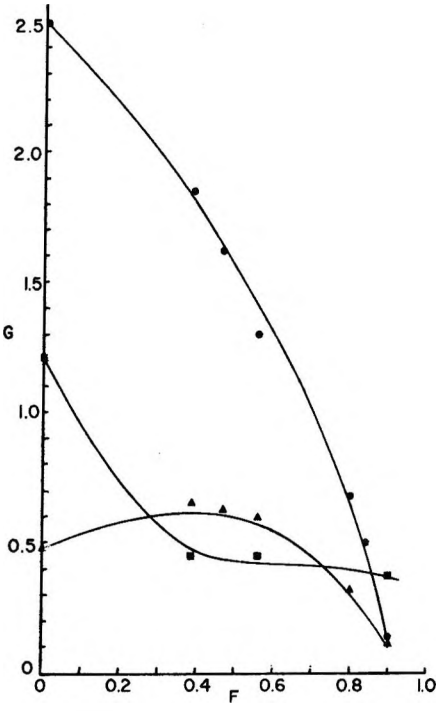

Figure 2. Radiolysis yields (G) in Ar–C_3H_8 liquid mixtures at −130° *vs.* F, the fraction of energy absorbed by Ar: ▲, C_2H_4; ●, C_3H_6; ■, C_6H_{14}.

Changes in nonradical product distributions from the liquid phase rare gas sensitized radiolysis of propane for Ar, Kr, and Xe, have been reported previously.[12] The isotopic information herein allows quantitative assessment of the formation mechanisms for nonradical products and of the ionic and excited molecule decomposition modes of propane in the three rare gas mixtures. Table I shows that O_2 acts as an efficient thermal radical scavenger in the liquid mixtures. The specific scavenging reactions involving O_2 are not well known. Oxygenated products are presumably formed and are not normally observed due to their long gas chromatographic retention times. The residual yield of pentanes in the O_2-scavenged krypton mixtures has been suggested to be due to ionic reactions[12] and will not be considered here. The other residual products in the O_2-scavenged systems are mainly ethane, ethylene, propylene, and methane, and are defined as nonradical products. The nonradical products are considered to arise by intramolecular decomposition of the parent excited ion and excited molecule or by bimolecular ionic reactions. Radical decomposition followed by cage disproportionation is counted as intramolecular decomposition in the framework of the isotopic analysis given here.

Table IV: Radiolysis Yields per 100 eV (G) for Total Propane Decomposition in Propane Systems

System	Phase	Temp, °C	$G(-C_3H_8)$[a] Unscavenged	$G(-C_3H_8)$[a] O_2-scavenged
C_3H_8	Liquid	−78	9.3	1.6
C_3H_8	Liquid	−130	6.4	1.6
Xe–C_3H_8 (25:1)	Liquid	−78	8.8	2.6
Kr–C_3H_8 (25:1)	Liquid	−78	8.4	4.2
Ar–C_3H_8 (25:1)	Liquid	−130	4.4	1.9
C_3H_8	Gas	35	12.1	2.9
Xe–C_3H_8[b] (10:1)	Gas	Room temp	11.7	4.4
Kr–C_3H_8[b] (10:1)	Gas	Room temp	11.0	3.3

[a] Based on total carbon yield in products. [b] Reference 10.

1. Ethane Formation. The entire ethane yield is accounted for by the bimolecular ionic reactions 1 and 2. This is shown by the second line of data in Table II; C_2D_5H is characteristic of reaction 1 and $C_2D_4H_2$ is

$$C_2H_5^+ + C_3H_8 \longrightarrow C_2H_6 + C_3H_7^+ \quad (1)$$

$$C_2H_4^+ + C_3H_8 \longrightarrow C_2H_6 + C_3H_6^+ \quad (2)$$

characteristic of reaction 2. The isotopic data indicate that $C_2H_5^+$ and $C_2H_4^+$ ions are produced in the radiolysis of all the rare gas–propane liquid systems. The yield of $C_2D_3H_3$ is less than 2% of the total ethane.

Reaction 3 which is observed to form about 4% of the

$$C_3H_8^* \longrightarrow C_2H_6 + CH_2 \quad (3)$$

total ethane in the rare gas–propane gaseous systems[5,10] is not observable (<2% of total ethane) from our liquid-phase data.[19]

Table V: Decomposition Yields (G) of Excited Ions and Neutral Molecules in Irradiated Rare Gas-Propane Systems

Reaction	Gas, 25°, 1 atm[a] Xe	Gas, 25°, 1 atm[a] Kr	Liquid −78° Xe	Liquid −78° Kr	Liquid −130° Ar
$C_3H_8^{+*} \rightarrow C_2H_4^+ + CH_4$	0.69	0.53	0.11	1.75	1.00
$\rightarrow C_2H_5^+ + CH_3$	2.03	1.93	0.41	1.25	0.74
$\rightarrow C_3H_5^+ + H_2 + H$	0.16	0.11	0.06	0.04	0.0
$\rightarrow C_2H_3^+ + CH_3 + H_2$	0.27	0.21	0.23	0.16	0.02
$C_3H_8^* \rightarrow C_3H_6 + H_2$	0.88	0.68	0.54	0.35	0.04
$\xrightarrow{b} C_2H_4 + CH_4$	0.46	0.33	0.59	0.41	0.06
$\rightarrow C_2H_4 + CH_3 + H$	0.31	0.22	0.39	0.28	0.04

[a] Calculated from isotopic data in ref 10 (Table II); G values calculated from M/N yields in ref 10. [b] Also includes: $C_3H_8^* \rightarrow [CH_3 + C_2H_5] \rightarrow CH_4 + C_2H_4$.

The relative importance of reaction 2 to ethane production is given by the isotopic ratio in line 3 of Table II. The H_2^- transfer reaction seems to be at least twice as important in the liquid phase as in the gas phase.

Table V summarizes the yields of various decomposition modes of excited ions and molecules in irradiated propane. The yield of $C_3H_8^{+*} \rightarrow C_2H_5^+ + CH_3$ is given by $[C_2D_5H/(C_2D_5H + C_2D_4H_2)] \times G(C_2H_6)$; recall that all yields refer to the scavenged system.

2. Ethylene Formation. The isotopic ratio in line 4 of Table II shows that 20% of the ethylene arises from bimolecular ionic reactions; this is slightly less than the ratio observed in the gas phase. The equality of C_2D_3H and C_2H_3D yields allows us to assign 20% of the ethylene to bimolecular reaction 4. The ionic de-

$$C_2H_3^+ + C_3H_8 \longrightarrow C_2H_4 + C_3H_7^+ \quad (4)$$

composition yield to give $C_2H_3^+$ is given by $[2C_2D_3H/(C_2D_3H + C_2D_4] \times G(C_2H_4)_{bimolec}$ and is tabulated in Table V.

Isotopic data show that the remaining 80% of the ethylene yield is produced by intramolecular decomposition. Since ethylene elimination from the propane ion is not a major decomposition mode for gas-phase propane,[10] the intramolecular ethylene yield is assigned to neutral excited propane decomposition *via* reactions 5 and 6.

$$C_3H_8^* \longrightarrow C_2H_4 + CH_4 \quad (5)$$

$$C_3H_8^* \longrightarrow C_2H_4 + CH_3 + H \quad (6)$$

The relative yields of (5) and (6) can be evaluated from vacuum uv photolysis of scavenged liquid propane. The yield ratio of methane:ethylene gives $k_5/(k_5 + k_6)$. Photolysis of C_3H_8–O_2 liquid mixtures at 25° with a krypton (10.0 eV) resonance lamp gives methane:ethylene equal 0.60.[20] No other liquid-phase photolysis data are available. The unscavenged solid phase-photolysis of propane at 77°K gives methane/ethylene = 1 with xenon (8.4 eV), krypton (10.0 eV), and argon (11.6–11.8 eV) resonance lamps.[21] We have used $k_5/(k_5 + k_6) = 0.60$ to assess the contributions of reactions 5 and 6 in Table V. Since the methane–ethylene ratio probably increases as the temperature decreases in the liquid-phase photolysis, the 0.60 value is regarded as a lower limit. The lower limit yield of reaction 5 = $[k_5/(k_5 + k_6)] \times G(C_2H_4)_{intramolec}$ while the upper limit yield of reaction 6 = $[k_6/(k_5 + k_6)] \times G(C_2H_4)_{intramolec}$.

The products of reaction 5 can also be formed by a second mechanism shown in (7). This reaction has

$$C_3H_8^* \longrightarrow [CH_3 + C_2H_5] \longrightarrow CH_4 + C_2H_4 \quad (7)$$

been postulated to be important along with reaction 5 in the solid-phase vacuum photolysis of propane.[21] An analysis of the isotopic methane produced from $CH_3CD_2CH_3$ suggests that reaction 7 may also occur in liquid-phase radiolysis.

3. Propylene Formation. The isotopic distribution of propylene was not measured in liquid mixtures because of experimental complications. In gas-phase xenon and krypton mixtures, isotopic data[5,7,10] show that 85% of the propylene comes from molecular decomposition and the remaining 15% from hydride transfer involving $C_3H_5^+$. The analogous molecular decomposition and hydride transfer reactions that form ethylene occur in nearly similar proportion in both gas and liquid phases. Based on the liquid-phase isotopic ratios for ethylene and a comparison of the isotopic ratios for ethylene and propylene in the gas phase, it is estimated that in the liquid phase 90% of the propylene arises from molecular decomposition and 10% from hydride transfer. The yield of the molecular decomposition to give C_3H_6 is then calculated in Table V as 0.90 $G(C_3H_6)$, and the yield of the ionic decomposition to give $C_2H_5^+$ is given by 0.10 $G(C_3H_6)$.

$C_3H_7^+$ ions are formed in all hydride transfer reac-

(19) The isotopic data on ethane in ref 12 were incorrect due to incomplete analysis and gave an erroneous conclusion about reaction 3.

(20) R. D. Koob and L. Kevan, to be published.

(21) R. E. Rebbert and P. Ausloos, *J. Chem. Phys.*, **46**, 4333 (1967).

tions. In the liquid phase most of these ions will be neutralized to form C_3H_7 which will be scavenged. Some C_3H_6 may also be formed; this source of C_3H_6 is included in the C_3H_6 attributable to molecular decomposition.

4. Methane Formation. Isotopic analysis of the methane product fraction shows that about 80% of the methane is eliminated intramolecularly. The remaining 20% is due to bimolecular processes which could include abstraction by "hot" methyl radicals which are not scavenged and hydride transfer to CH_3^+. In the following calculations 20% of the methane yield is attributed to bimolecular reactions but no further speculation on these reactions will be made.

Intramolecular elimination of methane may occur from neutral decomposition (5) and (7) or ionic decomposition (8). The yield of reaction 5 + 7 has been

$$C_3H_8^{+*} \longrightarrow C_2H_4^+ + CH_4 \qquad (8)$$

calculated in Table V. The yield of reaction 8 is then calculated by difference from the observed intramolecular CH_4 yield [$0.8\ G(CH_4)_{obs} - G(5) = G(8)$]; these values are tabulated in Table V. The same relationship was used to calculate the values for the gas phase; this assumes that the methane isotopic composition in the gas phase is the same as found in the liquid phase. $G(8)$ must be regarded as an upper limit since $G(5)$ is a lower limit and since a small contribution from $C_3H_8^{+*} \rightarrow C_2H_4^* + CH_3 + H$ may be present.

B. Decomposition of $CH_3CD_2CH_3$. In the gas phase an independent evaluation of the yields of reactions 5 and 8 is possible by measuring the isotopic methane eliminated from $CH_3CD_2CH_3$ or $CD_3CH_2CD_3$.[3-5] Gas-phase photolysis of scavenged $CH_3CD_2CH_3$ produces $CH_3D/CH_4 = 2.96$ and 5.50[4] for excitation by Xe and Kr resonance lines, respectively. In contrast, fragmentation of the parent ion of $CH_3CD_2CH_3$ according to reaction 8 gives $CH_3D/CH_4 = 0.13$ and 0.23 for ionization by 13- and 70-eV electrons, respectively.[4] Radiolysis of scavenged $CH_3CD_2CH_3$ at 500 torr gives $CH_3D/CH_4 = 0.77$,[3] which indicates that the greater part of the intramolecular methane is formed *via* reaction 8. This conclusion is in reasonable quantitative agreement with the decomposition mechanisms deduced independently by balancing yields.[10,14]

In light of the last paragraph, let us see what can be deduced for the liquid phase. Liquid photolysis of $CH_3CD_2CH_3$ at 25° with a krypton resonance lamp gives $CH_3D/CH_4 \simeq 1.9$.[20] Photolysis of solid $CH_3CD_2CH_3$ at 77°K gives $CH_3D/CH_4 = 2.39$, 1.50, and 1.16 for xenon, krypton, and argon resonance lamps, respectively.[21] These ratios are all much lower than in the gas phase. The liquid-phase result is in reasonable agreement with the solid-phase result even disregarding the temperature difference. The energy dependence in the solid is opposite to the energy dependence in the gas. These results have been attributed to contributions from both reactions 5 and 7 in the solid-phase photolysis. Reaction 7 increases with respect to reaction 5 with increasing excitation energy. The liquid-phase ionic decomposition reaction (8) should have CH_3D/CH_4 ratios equal to or less than the gas-phase ratios.

In the liquid-phase radiolysis of scavenged $CH_3CD_2CH_3$, the CH_3D/CH_4 ratio = 0.23 from 35 to −130°.[14] On the basis of the liquid-phase photolysis results this low value indicates that reaction 8 contributes over 90% of the intramolecular methane. This conflicts with a 60–65% contribution calculated by balancing yields (Table III in ref 14). The discrepancy can be resolved if it is postulated that the CH_3D/CH_4 ratio characteristic of excited molecule decomposition under radiolytic conditions is much lower than is indicated by the photolysis results. If a significant fraction of the excited molecules were formed by parent ion neutralization, the associated CH_3D/CH_4 ratio would be much lower according to the observed energy dependence of the ratio in condensed phases. In addition, other processes such as hot methyl radical reactions could complicate the interpretation of the CH_3D/CH_4 ratio. It is concluded that in condensed phases the CH_3D/CH_4 ratio is only a qualitative but nevertheless significant guide to the relative importance of ionic decomposition reaction 8 *vs.* excited molecule decomposition reactions 5 and 7.

In the scavenged rare gas–$CH_3CD_2CH_3$ liquid mixtures, the CH_3D/CH_4 ratios are also low (Table III). On the basis of the solid-phase photolysis data, these indicate that reaction 8 contributes 100, 86, and 84% of the intramolecular methane in Ar, Kr, and Xe mixtures, respectively. From Table V one calculates the contributions to be 95, 81, and 18%, respectively. The only discrepancy is in Xe mixtures which are the only rare gas mixtures in which excited molecule decomposition of propane is more important than ionic decomposition. Under such conditions, as with pure propane, parent ion neutralization can become significant and lower the observed CH_3D/CH_4 ratio.

The trend with rare gas in CH_3D/CH_4 ratios in Table III is identical with the trend found in solid-phase photolysis. This suggests that reaction 7 is probably important in the rare gas mixtures. However, the same trend is also produced by increasing the fraction of reactions 5 and 7 compared to 8 as the rare gas is changed from Ar to Kr to Xe; this increase is observed according to Table V. Thus no quantitative assessment of the relative importance of reactions 5 *vs.* 7 will be made on the basis of the present data alone.

C. Effect of Phase and Rare Gas on Decomposition Modes. An analysis of Table V enables one to discuss the effects of phase change in xenon- and krypton-sensitized systems on the two major precursors in the scavenged system, excited propane ions and excited neutral molecules. The temperatures of the gas- and

liquid-phase systems are different, but in a scavenged system the principal effects are more likely attributed to phase rather than to temperature.

In xenon mixtures the change from gas to liquid decreases total propane decomposition by 50%. The amount of ionic decomposition is decreased by 74% while excited molecule decomposition is decreased by only 8%. These changes are almost identical with those found in direct radiolysis of propane.[14] Ionic decomposition apparently becomes less important in the liquid compared to the gas due to deactivation of excited ions followed by ion neutralization. This is consistent with pressure effects on ionic decomposition that have been reported for the gas phase.[4] Since the rate of fragmentation increases with the amount of vibrational excitation in the parent ion, the ionic fragmentation observed in the liquid must be due to the more highly excited propane ions whose fragmentation rates can compete with collisional deactivation. This conclusion is supported by the krypton data.

In krypton mixtures there is little change in the total amount of propane decomposition. Both the ionic and excited molecule decomposition yields are about the same in gas and liquid. In comparison with the xenon mixtures, we conclude that most of the propane ions produced by krypton sensitization are so highly excited that they can undergo fragmentation in both gas and liquid. As in xenon mixtures, the *net* phase effect on excited molecule decomposition is quite small.

In the argon liquid mixtures the ionic decomposition yield is also high. Consequently, most of the propane ions produced by argon sensitization are so highly excited that they can undergo fragmentation. In a previous paper[12] on rare gas sensitization of liquid propane in which few isotopic data were available, it was concluded that as the rare gas is changed fron Ar to Kr to Xe the ionic fragmentation processes become relatively less important while the molecular decomposition processes become relatively more important. From the results in Table V this conclusion can now be put on a quantitative basis. In scavenged liquid-phase systems the per cent of propane decomposition due to ionic fragmentation is 93% in argon mixtures, 76% in krypton mixtures, and 35% in xenon mixtures. In the gas phase the corresponding percentages are 70% in krypton mixtures and 66% in xenon mixtures; the trend seen in the liquid is not very apparent in the gas.

D. Energy Transfer Efficiency and Mechanism. The overall product yields in unscavenged propane–excess rare gas mixtures arise mainly from energy transfer. The magnitude of the product yields depends on two factors, the efficiency of energy transfer from rare gas to propane and the particular decomposition modes by which propane utilizes this energy. The product distributions in pure propane and in argon–propane (25:1) mixtures are quite different. Figures 1 and 2 show how these yields change as a function of the fraction of radiation energy absorbed by argon, F. F was calculated according to eq 9

$$F = D_m(f_r n_r S_r)/(f_r n_r S_r + f_c n_c S_c) \quad (9)$$

where D_m is the total radiation dose absorbed by the mixture, f is weight fraction, n is electrons per gram, S is stopping power per electron, subscript r refers to Ar and subscript c refers to C_3H_8.

If it is assumed that the total decomposition yield, $G(-C_3H_8)$, is independent of the individual decomposition modes, then an energy transfer efficiency can be defined by eq 10[23]

$$\% \text{ transfer efficiency} = [G_m - G_c(1 - F)] \times 100/G_c \quad (10)$$

where G_m and G_c refer to $G(-C_3H_8)$ for the rare gas mixture and for pure C_3H_8, respectively. Equation 10 has been used to obtain energy transfer efficiencies in rare gas–C_2F_6 mixtures in both gas and liquid phases.[22,23] For 25:1 rare gas–C_3H_8 liquid mixtures using the G values in Table IV, eq 10 gives 90, 84, and 59% for transfer efficiencies in Xe, Kr, and Ar, respectively. For 10:1 gas-phase mixtures, eq 10 gives 87 and 77% for Xe and Kr, respectively.

The dimeric ion has been postulated to be the most abundant species from which energy transfer may occur in liquid rare gases.[12] It is interesting that the transfer efficiency is highest for Xe which is the rare gas having an ionization potential closest to that of propane. It appears that the greater the ionization potential difference between rare gas and propane the lower is the energy transfer efficiency. This behavior qualitatively parallels charge-transfer cross sections between rare gas ions and propane as determined by mass spectrometry.[24] Radiolysis of rare gas–C_2F_6 mixtures also exhibits this pseudo-resonant charge transfer behavior.[22,23] We suggest that charge transfer is the predominant energy transfer process occurring in the rare gas–propane liquid mixtures.

The excited molecule decomposition spectrum of products (Table V) is strikingly similar in Xe, Kr, and Ar mixtures (29% CH_4, 48% C_2H_4, 23% C_3H_6), and quite different from the spectrum in liquid-phase photolysis with a krypton lamp[20] (14% CH_4, 23% C_2H_4, 63% C_3H_6). The higher ethylene/propylene ratio in the rare gas mixtures indicates formation of more highly excited molecules[5] than in direct photolysis. The source of these highly excited molecules could be ion neutralization; this is compatible with our conclusion that charge transfer is the predominant energy transfer process. Energy transfer from excited rare gas atoms, R*, to propane in the liquid phase is probably small because of formation of dimeric rare gas ions by R*.

(22) L. Kevan, *J. Chem. Phys.*, **44**, 683 (1966).
(23) A. Sokolowska and L. Kevan, *J. Phys. Chem.*, **72**, 253 (1968).
(24) D. Smith and L. Kevan, to be published.

Nature of the Transient Species in the Photochemistry of Negative Ions in Aqueous Solution

by R. Devonshire and J. J. Weiss

Laboratory of Radiation Chemistry, University of Newcastle upon Tyne, Newcastle upon Tyne, England *(Received May 7, 1968)*

For further elucidation of the theory of the photochemical primary processes of negative ions in solution, the absorption spectra of the unstable intermediates have been investigated by a novel spectrophotometric technique. It has been found that ultraviolet irradiation of the negative ions such as OH^-, Cl^-, Br^-, and I^- as well as sulfite, phosphate, sulfate, carbonate, and ferrocyanide, leads to an unstable species with an absorption spectrum which is in every case the same and identical with the spectrum of the hydrated electron obtained in the radiation chemistry of aqueous systems. The spectra of the simultaneously produced radical ions such as Br_2^-, I_2^-, SO_4^-, and the phosphate radical have also been determined. It is suggested that the mechanism of the photochemical primary process in aqueous solution is a predissociation of the excited negative ion leading to the trapping of an electron at some distance from its parent center. The trapping of electrons in uv-irradiated alkaline ice matrices at 77°K has also been discussed, and it is concluded that this involves the formation of radiation-produced vacancies in which the electron can be trapped.

Introduction

During the past few years, interest in photochemical processes in aqueous systems has been revived and considerably stimulated by results from radiation chemistry. Photochemical primary processes of negative ions in aqueous solutions were first considered by Franck and Scheibe,[1] who suggested that in the case of simple ions such as I^-, interaction with photons leads to ionization of the electron. Subsequently, Franck and Haber[2] suggested the more "chemical" primary process, $I^- \cdot H_2O + h\nu \rightarrow I + H + OH^-$, to account for the formation of hydrogen and iodine in the uv-irradiation of deaerated solutions of iodides. Such a primary process described reasonably well the experimental observations, particularly in acid solutions, as was shown subsequently by Rigg and Weiss.[3]

Recent work has centered mainly around two problems, namely (i) the photolytic formation of solvated electrons and (ii) the question of geminate recombination of the electron with its parent center.

With regard to the photochemical primary process, it should be pointed out that the absorption spectra of halide ions in aqueous solution show considerable similarity to those in the alkali halide crystals. It is therefore more likely that the electron is, in the first instance, put into an excited orbital of the halogen atom which has its radial wave function changed by the environment.

More recently, some results have been published on the absorption spectra of the unstable intermediates produced in the photolysis of negative ions in solutions. Matheson, Mulac, and Rabani,[4] by means of flash-photolysis technique, established some definite evidence of an unstable intermediate absorbing in the region of the hydrated electron. Their results would suggest that, *e.g.*, in the case of Cl^-, the absorption maximum of this species is at about 670 nm. Some preliminary measurements[5] in our laboratory gave an absorption maximum at 720 nm for I^- and at somewhat longer wavelengths for sulfite and ferrocyanide. We have now carried out more precise measurements of the absorption spectra of this unstable species in the photolysis of a number of different ions such as OH^-, Cl^-, Br^-, I^-, ferrocyanide, sulfite as well as sulfate, phosphate, and carbonate by a somewhat novel spectrophotometric technique. This is based on measuring absorption spectra in the stationary state by photoexcitation with a modulated light source and monitoring the analyzing light by a phase sensitive detector method.[6]

Experimental Section

The uv exciting light which is absorbed by the solute is modulated at 100 cps. If the half-times of the reactions by which the transient species disappear are considerably less than 10^{-2} sec, the concentrations of the unstable intermediates closely follow the variations in the intensity of the photoexciting light source. If, under these conditions, a steady light beam of given

(1) J. Franck and G. Scheibe, *J. Phys. Chem.* (Leipzig), **A139**, 22 (1928).

(2) J. Franck and F. Haber, *Sitzungsber. Preuss. Akad. Wiss.*, 250 (1931).

(3) T. Rigg and J. J. Weiss, *J. Chem. Soc.*, 4198 (1952).

(4) M. S. Matheson, W. A. Mulac, and J. Rabani, *J. Chem. Phys.*, **67**, 2613 (1963).

(5) J. J. Weiss in "The Chemistry of Ionization and Excitation," G. R. A. Johnson and G. Scholes, Ed., Taylor & Francis Ltd., London, 1967, p 17.

(6) D. J. Dyson and M. A. Slifkin, *J. Sci. Instrum.*, **40**, 599 (1963).

intensity is passed through the solution, the transmitted light will contain a 100-cps component at the wavelengths where the intermediate absorbs.

With the present instrument the smallest detectable fraction of modulation defined as $f = (I_0 - I)/I_0$, at a signal to noise ratio of 5:1 is approximately $1:0 \times 10^{-5}$. When f is small it is proportional to the optical density. For measurements of the hydrated electron spectrum at 700 nm, this means that the smallest concentration which is detectable in our device is approximately 5×10^{-12} M. A more detailed discussion of the instruments performance will appear in another paper.

Optical Detection System. The arrangement is shown in Figure 1. The 150-W quartz tungsten–iodine lamp is run from a 24-V battery supply. The heat filter glass C eliminates fluctuations in the light intensity passing through the cell caused by temperature gradients in the solution around the end window. The optical filter D minimizes stray light effects in the monochromator and also reduces a small spurious signal caused by absorption of scattered light by iodine in the lamp. Light filter G reduces the scattered uv light entering the detection system.

For experiments using the 185-nm mercury line for photoexcitation, the arrangement of the absorption cell and the uv source is shown in Figure 2. The low-pressure Spectrosil mercury lamp A is run from a leakage reactance transformer supplying 120 mA and 1650 V at 50 cps. The metal tube C is perforated along its length and enables a continuous stream of pure nitrogen gas to pass over and between the mercury lamp and the absorption cell. This minimizes fluctuations in light intensity due to absorption by oxygen and by radiation-produced ozone. The absorption cell D is a 50-cm Spectrosil tube of 0.5 cm internal diameter. The optical windows were attached to the tube ends with Araldite and are blacked out, apart from the central portion, to prevent light traveling down the tube walls. The cell is in a fixed position and is filled by pushing the solution through the side arm E by a slight pressure of gas.

Electronic Detection System. A block diagram is shown in Figure 3. The high-voltage supply to the photomultiplier is a Dynatron Type N103. The photomultiplier dynode chain current and anode current are chosen to give a linear response between light intensity and the anode current. The amplifier (LA635), phase sensitive detector (PD629), phase shifter (PS946), and the meter (MU947) are commercial units obtained from Brookdeal Electronics Ltd. The reference signal to drive the phase sensitive detector is picked up by a photoresistor from a 6.5-V torch bulb, run from a mains transformer. To improve the signal-to-noise ratio, the band width of the amplifier is limited to about 200 cps. The time constant of the meter unit is typically about 3 sec, and a determination of the

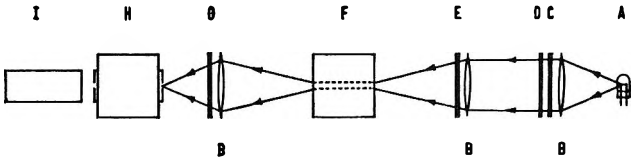

Figure 1. Schematic drawing of optical arrangement: A, quartz tungsten–iodine lamp; B, quartz lenses; C, glass heat filter; D, light filter; E, light shutter; F, absorption cell assembly (shown in Figure 2); G, light filter; H, quartz prism monochromator; I, photomultiplier.

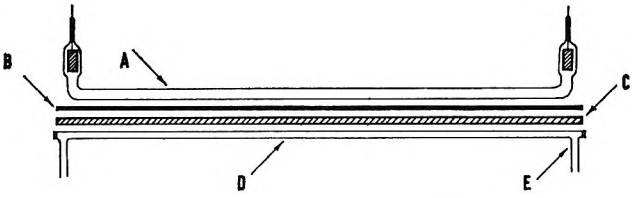

Figure 2. Experimental arrangement of absorption cell and uv exciting lamp (the vertical scale is expanded): A, Spectrosil low-pressure Hg lamp; B, mechanically operated shutter; C, nitrogen gas supply; D, spectrosil absorption cell; E, side arms for filling.

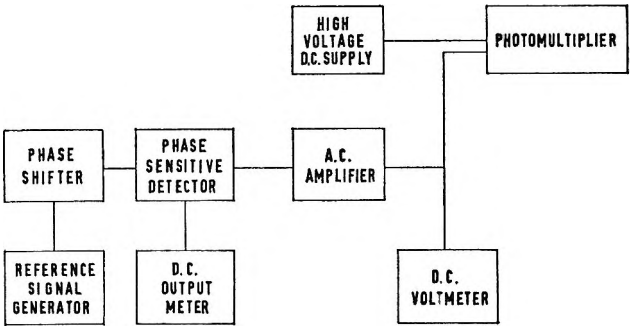

Figure 3. Block diagram of the electronic detection system.

fraction of modulation at a particular wavelength can therefore be made in approximately 20 sec.

Preparation of Solutions. All reagents were B.D.H. Analar grade and were used without further purification. The pH adjustments were made using $HClO_4$ and carbonate-free NaOH and measured on a Pye Model 79 pH meter. All the solutions were prepared with triply distilled water. The oxygen and argon gases were British Oxygen Co. best grade.

Argon-saturated solutions were prepared by bubbling the gas through a sintered glass disk in a flask of 1 l. of triply distilled water for 0.5 hr and then, if required, adding the necessary amount of $HClO_4$ and NaOH to adjust the pH, followed by a further short period of bubbling. Finally, the weighed amount of solute was added and the solution vigorously bubbled for 1 hr. The solution was then pushed into the cell under a slight pressure of argon, the absorption cell having previously been flushed out with the gas. A measurement was made and then by releasing the pressure at the

exit side arm of the absorption cell the irradiated solution was replaced by a fresh aliquot of solution. In this manner up to 50 experimental points could be obtained from each degassing procedure. The absorption cell was not thermostated as this would involve sacrificing a large fraction of the light intensity. However, each solution was irradiated for only 30 sec and any heating effects should be negligible. This was confirmed by measurements with a thermocouple on a solution where there was total absorption of both the 185- and 254-nm lines of the mercury lamp.

Solutions were made up to give an optical density of about 2 at 185 nm as taken from recent measurements.[7] In the 0.5 cm of the absorption cell, the optical density of water at this wavelength is 0.9 at 25°.

Results

Figure 4 shows the spectrum of the transient from argon-saturated, 1.4×10^{-3} *M* NaOH (carbonate free). Each point is the average of at least five determinations. The systematic error is better than 2% at the peak of the absorption spectrum. The spectrum of the hydrated electron obtained by Fielden and Hart[8] from pulse radiolysis experiments is superimposed. The spectra have been normalized to the value at 700 nm. The agreement is excellent but our values tend to be somewhat higher at the shorter wavelengths. The differences are very close to the limits of error but are in the same direction. This must either be attributed to absorption from another transient or to an increasing contribution from stray light at the lower wavelengths.

The ratio of the extinction coefficients $E_{700\text{ nm}}/E_{578\text{ nm}} = 1.7$ is in agreement with Fielden and Hart[8] but different from an earlier value of 1.4 given by Keene.[9]

This system was also used to test the linearity of response of the equipment, as there are no other transient species present which absorb strongly in the region 375–750 nm; by increasing the light level so that the photomultiplier anode current was ten times its normal value, the spectrum was redetermined and the agreement was entirely satisfactory.

Phosphate Ion (HPO_4^{2-}). Figure 5 shows the transient spectrum obtained from oxygen saturated 6.7×10^{-3} *M* Na_2HPO_4 at pH 8.9 (OH^- absorbs less than 1% of the exciting light at this pH). The spectrum, having a peak at 480 nm and a pronounced shoulder around 575 nm, is attributed to the HPO_4^- radical ion.

The top line in Figure 6 is the transient spectrum from an argon-saturated solution at the same pH. The radical (Figure 5) shows no absorption at 700 nm and by subtracting the electron spectrum of Figure 4 from Figure 6 to give a zero value at 700 nm, a spectrum identical, within experimental error, with that of Figure 5 is obtained.

Halide Ions. Figure 7 shows the transient spectrum from neutral oxygen saturated 3.3×10^{-4} *M* KI. A

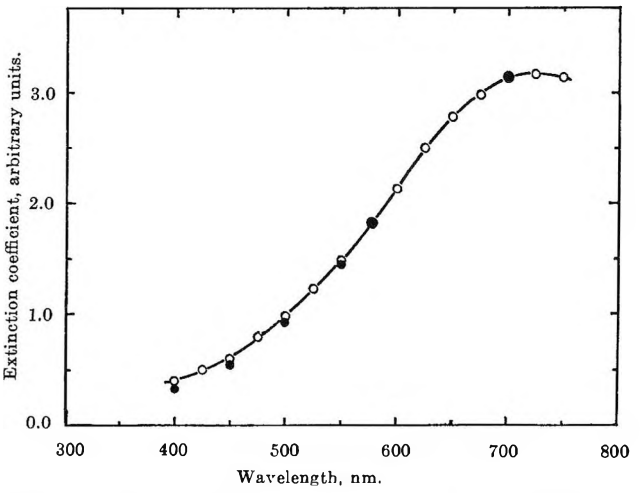

Figure 4. Absorption spectrum of the hydrated electron from argon-saturated aqueous 1.4×10^{-3} *M* NaOH: ○, measured values; ●, measurements ↔ of Fielden and Hart.[8]

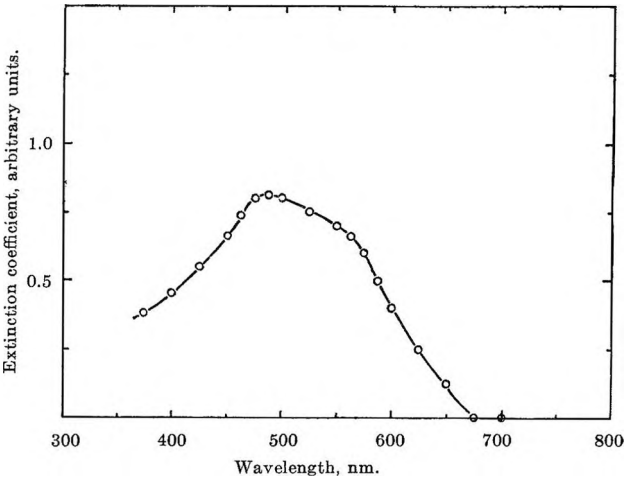

Figure 5. Phosphate radical ion spectrum from oxygen-saturated aqueous 6.7×10^{-3} *M* Na_2HPO_4 (pH 8.9).

correction has been applied to the experimental points on the part of the spectrum marked by a broken line, as during the time the measured signal is approaching its steady value, I_3^- is formed as a product of the photochemical reaction causing a fall in the transmitted light intensity. The correction was made by multiplying the signal by a factor corresponding to the ratio of the initial divided by the final light intensities.

The main absorption band of the I_2^- radical ion has a similar shape and peak position to that reported in the literature,[4,10] but additionally a broad absorption band with a maximum at 750 nm is observed. This is

(7) J. L. Weeks, G. M. A. C. Meaburn, and S. Gordon, *Radiation Res.*, 19, 559 (1963); M. Halman and I. Platzner, *J. Chem. Soc.*, 1440 (1965).

(8) E. M. Fielden and E. J. Hart, *Trans. Faraday Soc.*, 63, 2975 (1967).

(9) J. P. Keene, *Discussions Faraday Soc.*, 36, 307 (1963).

(10) L. I. Grossweiner and M. S. Matheson, *J. Phys. Chem.*, 61, 1089 (1957).

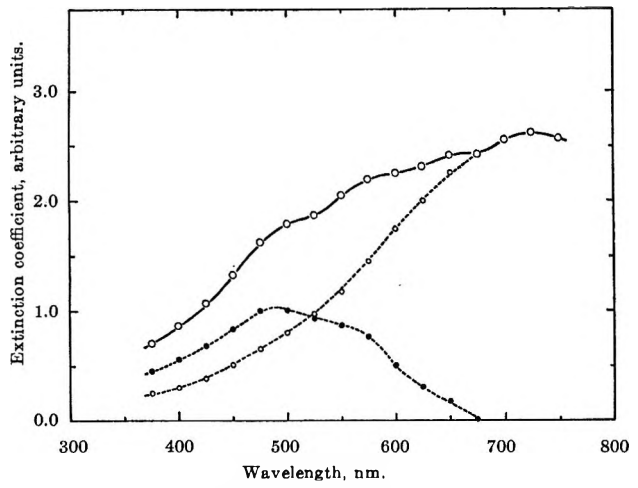

Figure 6. Transient spectrum from argon-saturated aqueous 6.7×10^{-3} M Na_2HPO_4 (pH 8.9), —○—; - - -●- - -, radical spectrum from Figure 5; - - -○- - -, difference spectrum.

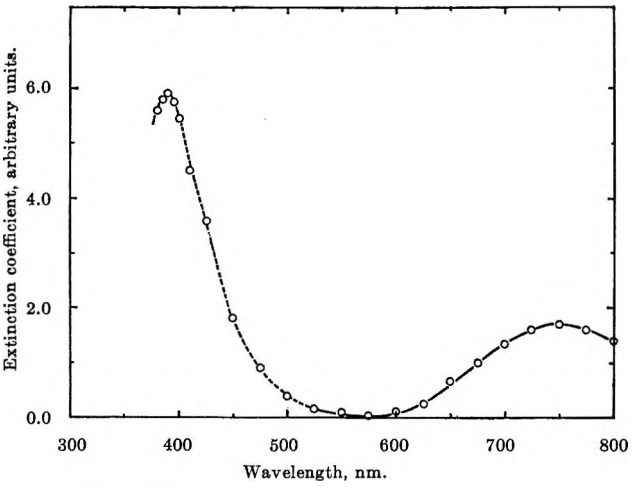

Figure 7. I_2^- spectrum from neutral oxygen-saturated aqueous 3.3×10^{-4} M KI. A correction has been applied to the part of the curve having a dotted line.

part of the I_2^- absorption spectrum and the ratio $E_{390\ nm}/E_{750\ nm} = 3.5$.

Figure 8 shows the spectrum from oxygen-saturated 3.3×10^{-4} M KBr at pH 2.8. The points in the region 575–775 nm were measured at higher amplification. Br_2^- also has an absorption band at longer wavelengths, which is smaller but appears to consist of two bands, one with a maximum at 700 nm and another at 760 nm. The ratio of $E_{365\ nm}/E_{700\ nm}$ is approximately 20.

The edge of the Cl_2^- absorption band could be measured in neutral oxygen-saturated 10^{-3} M NaCl, but the peak position at 350 nm could not be detected as it is beyond the range of the present instrument.

The peak position and the $E_{700\ nm}/E_{578\ nm}$ ratio of the hydrated electron absorption found in an argon-saturated solution of NaCl at pH 8 are identical with that given in Figure 4. The comparison could be made very

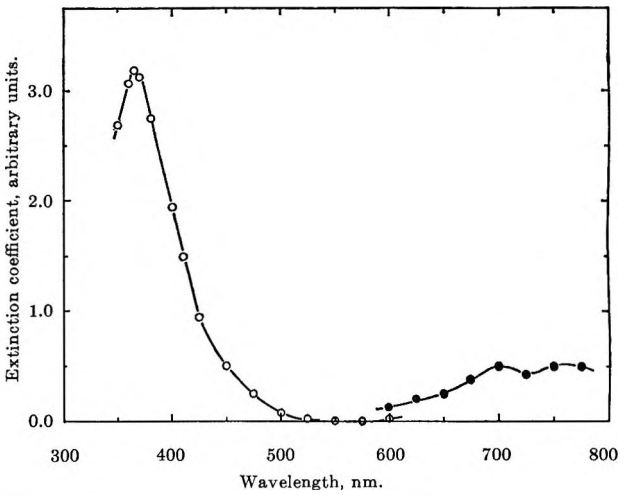

Figure 8. Br^-_2 spectrum for oxygen-saturated aqueous 3.3×10^{-4} M KBr, pH 2.8. (The part of the spectrum with filled circles was measured at a higher amplification.)

accurately in the cases of OH^- and Cl^- as there are no interfering absorptions above 500 nm.

The hydrated electron spectrum from I^- and Br^- found by subtracting the spectra given in Figures 7 and 8, respectively, from those obtained in argon-saturated solutions of KI and KBr are also identical with that of Figure 4, within experimental error.

Sulfate and Sulfite Ions. The sulfate radical spectrum from neutral oxygen saturated $2{:}2 \times 10^{-2}$ M Na_2SO_4 is shown in Figure 9. The peak position at 455 nm is identical with that found in previous studies.[11] Measurements in alkaline argon saturated solutions of Na_2SO_4 above 500 nm gave erratic results, and a reproducible spectrum could not be obtained.

The spectrum from oxygen saturated 1.0×10^{-2} M Na_2SO_3 was identical with that from an argon-saturated solution apart from a small difference around 450 nm. The spectrum in the argon-saturated solution was identical with that of the hydrated electron. This behavior is attributed to the removal of the electron scavenging oxygen by the rapid photoinitiated chain oxidation of some of the sulfite.[12]

Carbonate Ion. The carbonate radical spectrum found in oxygen saturated 4×10^{-3} M Na_2CO_3 at pH 9.0 had a peak value at 600 nm similar to that of Keene, *et al.*[13]

Ferrocyanide Ion. Measurements in this system are difficult because of the rapid production of ferricyanide which absorbs strongly in the visible. This limits the measurements to the range 600–775 nm. The peak of

(11) P. N. Moorthy and J. J. Weiss, *J. Chem. Phys.*, 42, 3127 (1965); V. E. Heckel, A. Henglein, and G. Beck, *Ber. Bunsenges. Physik. Chem.*, 70, 149 (1966); E. Hayon and J. J. McGarvey, *J. Phys. Chem.*, 71, 1472 (1967); L. Dogliotti and E. Hayon, *ibid.*, 71, 2511 (1967).

(12) H. S. Backstrom, *J. Amer. Chem. Soc.*, 49, 146 (1927).

(13) J. P. Keene, Y. Raef, and A. J. Swallow in "Pulse Radiolysis," Academic Press, London, 1965, p 99.

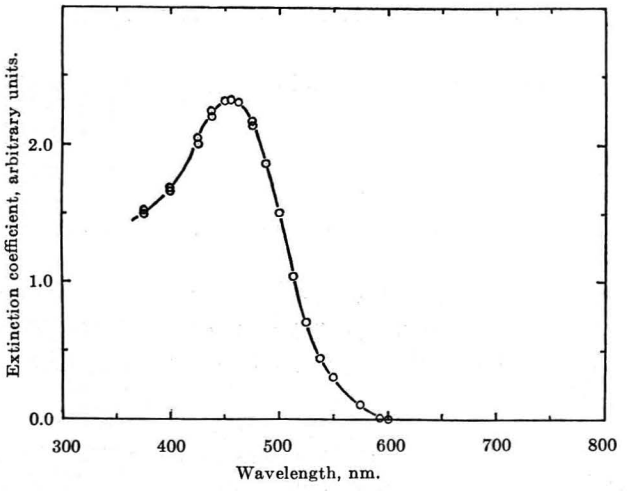

Figure 9. Sulfate radical ion spectrum obtained from neutral oxygen-saturated aqueous 2.0×10^{-2} M Na_2SO_4.

the hydrated electron absorption was 720 nm as in Figure 4, but a value for the ratio $E_{700\ nm}/E_{578\ nm}$ could not be determined here.

Discussion

The nature of the unstable intermediate is closely linked with the mechanism of these photochemical reactions. In recent discussions of the the kinetics, it has been assumed that geminate recombination between the electron and its parent center plays an important role.[14] If this was the case one might perhaps have expected some variation in the absorption spectra of the electron due to the proximity of the parent center. However, at the time scale of events of the experiments it is quite clear that this is not the case. It is therefore of interest to reexamine the importance of geminate recombination. Simple physical considerations of the effect of scavenger concentration on the quantum yields leads one to question the evidence in support of geminate recombination because scavengers do affect the quantum yield at a concentration which is about two orders of magnitude lower than one would expect from theory, and it appears that the assumption of geminate recombination was based almost entirely on the dependence of the quantum yields on the square root of scavenger concentrations, as deduced from the theory of Noyes.[15] In a recent paper, Czapski and Ottolenghi[16] have shown that geminate recombination is unlikely to be important in these photochemical processes and that the yields can be satisfactorily explained on the basis of back reactions of the electron with the final products, *e.g.*, with I_3^- or ferricyanide. This, incidentally, is very similar to the conclusions reached previously by Rigg and Weiss[3] in 1952, who proposed a similar mechanism with hydrogen atoms instead of electrons as intermediates and which would still essentially be valid in acid solutions in the absence of H atom scavengers.

The fact that one finds in every case the same unstable species, *i.e.*, the hydrated electron, and also that geminate recombination does not play an important part under the conditions in question allows one to draw certain conclusions regarding the mechanism of these reactions. Light absorption would lead to an excited state of the hydrated ion which could return to the ground state either with or without emission of radiation according to

$$I^- + h\nu \longrightarrow (I^-)^* \qquad \text{excited ion} \qquad (1)$$

$$(I^-)^* \longrightarrow I^- + \text{energy} \qquad (2)$$

Such a process could be favored at low temperatures. The other possibility would be predissociation of the excited ion whereby the electron is removed some distance from its parent center and then is trapped in a suitable (tetrahedral) cavity in the water. This can be represented by

$$(I^-)^* \longrightarrow I + e \qquad (3)$$

$$e + \text{trap} \longrightarrow e_t \qquad \text{trapped electron} \qquad (4)$$

If any scavenger (*e.g.*, N_2O, H_3O^+) is present in the solution it could react with the electron at any stage of its existence.

Some remarks may be in order about the mechanism of trapping of the electron. In aqueous media this may not present any difficulties and the electron could be trapped in a tetrahedral cavity of the water structure, giving an F center like unit. The situation is, however, different in solid ice matrices, particularly at low temperatures where the effect of the radiation would include the formation of a vacancy. The mechanism of the formation of vacancies in solids has been discussed in some detail.[17] It would involve the primary formation of a "relaxed exciton" which upon predissociation could create a vacancy for the electron. Such a mechanism cannot be completely disregarded even in aqueous systems and further experiments, particularly the effect of the concentration of I^-, might give some information about this in the I^- photolysis.

In uv-irradiated acid ice matrices at 77°K one finds the formation of H atoms[18] which presumably originate from the interaction between electrons and hydrogen ions or with acid anions.

In a sense more interesting are the alkaline ice matrices where uv irradiation of phenolate ion[19] or of ferrocyanide[20] in these matrices at 77°K gives an ab-

(14) F. S. Dainton and S. R. Logan, *Proc. Roy. Soc.*, **A287**, 281 (1965).

(15) R. M. Noyes, *J. Amer. Chem. Soc.*, **77**, 2042 (1955).

(16) G. Czapski and M. Ottolenghi, in press.

(17) H. N. Hersh, *Phys. Rev.*, **148** (2), 928 (1966); D. Pooley, *Proc. Phys. Soc.*, **87**, 245 (1965).

(18) P. N. Moorthy and J. J. Weiss, *J. Chem. Phys.*, **42**, 3121 (1965).

(19) J. Jortner and B. Sharf, *ibid.*, **37**, 2506 (1962).

(20) P. B. Ayscough and R. G. Collins, *J. Phys. Chem.*, **70**, 3128 (1966).

sorption which is similar to that obtained on γ irradiation of alkaline ice and also an esr spectrum characteristic of the electron.[20] The mechanism of this F center formation could be similar to the one which has been proposed in alkali halide crystals where it has now been established that the anion vacancies are produced by the radiation itself. It is suggested that in the case of, *e.g.*, phenolate ion PhO^- in alkaline ice matrices, one has the reactions

$$PhO^- + h\nu \longrightarrow (PhO^-)^* \quad (5)$$

$$(PhO^-)^* + OH^- \longrightarrow (PhO^- \cdot OH^-)^* \quad (6)$$

leading to the formation of an excited adduct with OH^- ions. This can either return to the ground state with emission of luminescence

$$(PhO^- \cdot OH^-)^* \longrightarrow PhO^- + OH^- + h\nu' \quad (7)$$

or dissociate to give a radical, the electron, and a vacancy

$$(PhO^- \cdot OH^-)^* \longrightarrow PhO + OH^- + e + \text{vacancy} \quad (8)$$

This can lead to an F center, when the electron is trapped in the anion vacancy. A corresponding mechanism would hold for, *e.g.*, alkaline ice ferrocyanide matrices.

Acknowledgment. R. D. wishes to thank the Science Research Council for financial support.

Flash Photolysis in the Vacuum Ultraviolet Region of the Phosphate Anions $H_2PO_4^-$, HPO_4^{2-}, and $P_2O_7^{4-}$ in Aqueous Solutions

by J. Robert Huber and E. Hayon

Pioneering Research Laboratory, U. S. Army Natick Laboratories, Natick, Massachusetts 01760
(Received May 7, 1968)

Photoexcitation of the phosphate anions $H_2PO_4^-$, HPO_4^{2-}, and $P_2O_7^{4-}$ has been studied using a vacuum ultraviolet flash apparatus. The main primary photolytic act in aqueous solutions of these three inorganic phosphate ions has been shown to lead to the photodetachment of an electron from the respective anions, $M_{aq}^{-n} + h\nu \rightarrow M_{aq}^{-(n-1)} + e_{aq}^-$. The absorption spectrum of the photo-ejected electron has been determined in aqueous solutions of HPO_4^{2-} and $P_2O_7^{4-}$ ions. Transient optical absorption spectra corresponding to various phosphate radical anions have been observed. The transient species $H_2PO_4\cdot$ and $HPO_4\cdot^-$ produced from the photolysis of $H_2PO_4^-$ and HPO_4^{2-} have λ_{max} 500 nm, ϵ^{500} 650 ± 50 M^{-1} cm^{-1} and λ_{max} 500 nm, ϵ^{500} 600 ± 50 M^{-1} cm^{-1}, respectively, and decay by second-order processes. In solutions containing oxygen, a transient spectrum with λ_{max} ~250 nm is produced in the three phosphate ions and is assigned to the O_2^- radical. This latter radical apparently decays to give rise to a relatively long-lived transient with λ_{max} ~260 nm and a half-life of a few hundred milliseconds. Results obtained in this study are compared with those obtained in the pulse radiolysis of aqueous solutions of the same phosphate ions.

In a previous publication,[1] the primary chemical species produced in the photochemistry of the inorganic ions SO_4^{2-}, CO_3^{2-}, and OH^-, whose absorption maxima lie below 2000 Å, have been observed using a vacuum uv flash photolysis apparatus. This apparatus has been modified and the optical detection system considerably improved (see Experimental Section) for the study of short-lived species produced in the optical excitation of systems in the condensed phase. This paper deals with the examination of the primary processes occurring in the photolysis of aqueous solutions of mono- and dibasic phosphate and pyrophosphate ions.

The absorption spectra of these ions have been recently determined by Halmann and Platzner,[2] their extinction coefficients in the wavelength region below 2000 Å obtained, and the steep absorption bands below 2000 Å tentatively assigned to a charge-transfer-to-

(1) E. Hayon and J. J. McGarvey, *J. Phys. Chem.*, 71, 1472 (1967).
(2) M. Halmann and I. Platzner, *Proc. Chem. Soc.*, 261 (1964); *J. Chem. Soc.*, 1440 (1965).

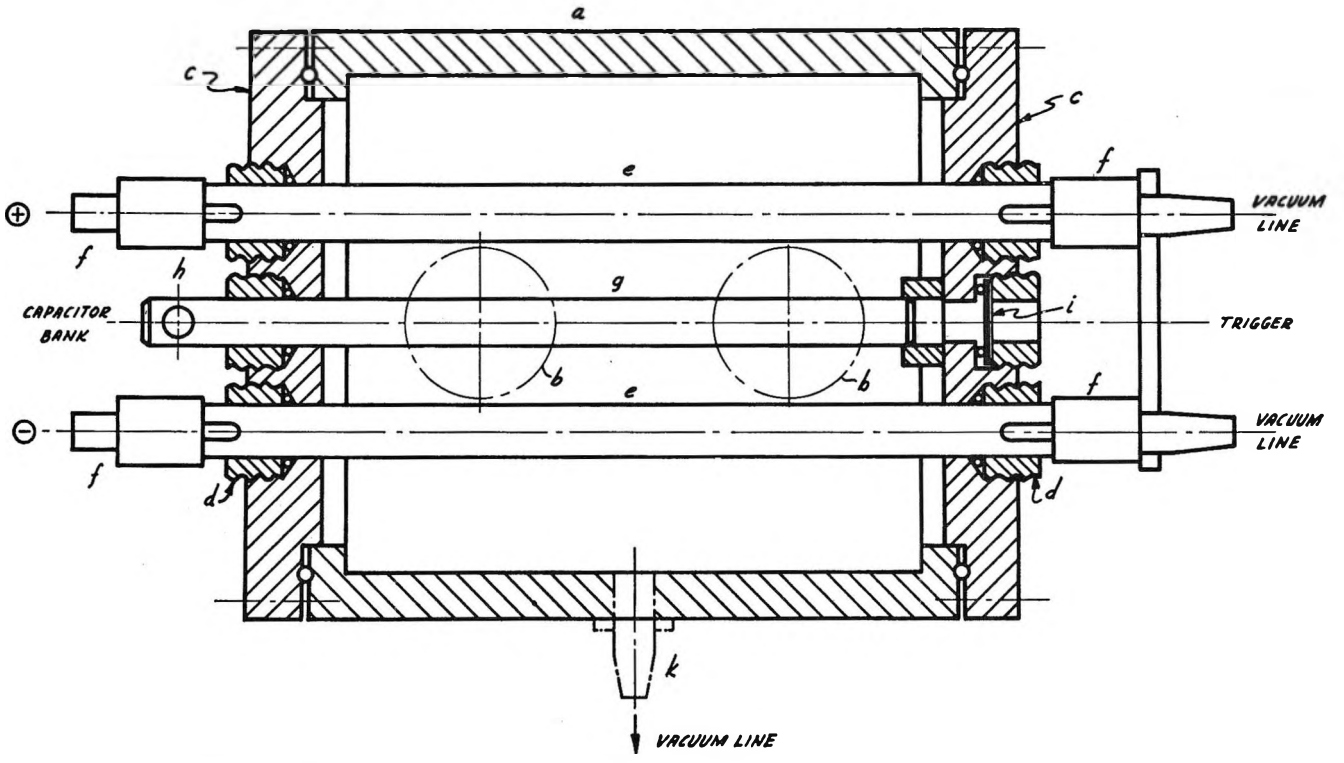

Figure 1. Schematic of vacuum uv flash-photolysis apparatus: a, aluminum cylindrical chamber; b, viewing windows; c, PVC cover; d, PVC nut; e, Spectrosil flash tube; f, stainless steel–tungsten electrode; g, Spectrosil reaction cell; h, inlet joint for reaction cell; i, Spectrosil window; k, connection to vacuum pump.

solvent (CTTS) type of transition. In a later publication, these authors studied[3] the photolysis at 1849 Å of aqueous solutions of dibasic phosphate ions, Na_2HPO_4, in the presence and absence of dissolved nitrous oxide gas. From the well-known electron-scavenging properties of N_2O in solution, Halmann and Platzner[3] concluded that the absorption spectrum of HPO_4^{2-} ions is due to a CTTS transition.

The flash-photolysis study of $H_2PO_4^-$, HPO_4^{2-}, and $P_2O_7^{4-}$ ions reported below shows conclusively that the primary photolytic act resulting from the excitation of these ions leads to the photodetachment of an electron which rapidly becomes solvated in the hydration sphere of these ions.

Experimental Section

Flash-Photolysis Apparatus. The setup used in the present work is shown in Figure 1. The quartz tubes are made of Spectrosil quartz (Thermal Syndicate Co., transmission at 165 nm $\geq 25\%$) with an outer diameter of 21 mm and a wall thickness of about 1.5 mm. These tubes are placed inside an aluminum cylinder chamber with two viewing windows on the top and a connection to the vacuum pump at the bottom. Two PVC covers fitted with O-rings to make it vacuum-tight are placed on each end of the cylinder. Before introduction into the cylindrical chamber, two of the four stainless steel–tungsten electrodes are sealed to the Spectrosil tubes with epoxy resin (Emerson L 28), while the other two electrodes are sealed, after introduction into the chamber, with wax (Apiezon Hard Wax W). The two flash tubes are linked in series and connected to a 100-μF capacitor bank. The flash tubes are triggered by means of a Thyratron circuit and a pulse transformer (pulse height >50 kV, pulse duration <1 μsec).[4]

In this work flash energies between 900 and 2000 J were used, providing a flash duration $1/e$ time of 25–30 μsec. The flash tubes were filled with argon or an argon–nitrogen mixture (80 vol % Ar, 20 vol % N_2) at 25–50 torr pressure. The whole cylindrical chamber was pumped out to a pressure less than 1 torr. An estimate of the lower limit of the number of photons below 200 nm incident on the reaction vessel was obtained by determining the amount of O_2^- radicals produced in the flash photolysis of air-saturated water at pH 5.5. Taking the quantum yield for $H_2O \xrightarrow{h\nu} H + OH$, $\phi = 0.5 \pm 0.1$,[5] $H + O_2 \rightarrow O_2^- + H^+$, $\epsilon_{O_2^-}^{260}$ 900 M^{-1} cm^{-1},[6] it was estimated that with a flash energy of 1600 J more than 1×10^{17} quanta in the wavelength range below 200 nm were incident on the 20 cm long reaction vessel.

Reaction Vessel. The reaction cells were made of

(3) M. Halmann and I. Platzner, *J. Phys. Chem.*, **70**, 2281 (1966).
(4) J. A. Sousa, private communication.
(5) J. Barrett and J. H. Baxendale, *Trans. Faraday Soc.*, **56**, 37 (1960).
(6) G. Czapski and L. M. Dorfman, *J. Phys. Chem.*, **68**, 1169 (1964).

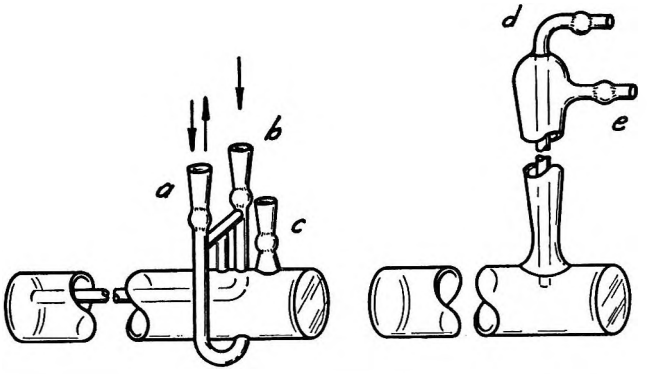

Figure 2. Optical cells used with vacuum uv flash unit. For argon-saturated solutions: a, inlet–outlet filling of reaction cell; b, gas inlet for flushing cell; c, stoppered joint. For air-saturated solutions: d, outlet of reaction cell; e, gas inlet for removing solution.

Spectrosil quartz and are shown in Figure 2. The overall length of these cells is 28 cm with an effective optical path length of 20 cm, measured inside the cylindrical chamber. The inside diameter of the cells was 14 mm.

Optical Detection System. The monitoring light source used was either a high-pressure xenon arc lamp (Osram XBO 450-WE fed from a 20-V battery bank or a water-cooled deuterium lamp (Hanau D 150-W). Collimated light from these lamps passed once through the reaction cell and was split afterward into two beams each falling on the entrance slit of a monochromator (Bausch and Lomb, 500 and 100 mm). One of the beams was at a fixed wavelength and was used as a reference. This was necessary because the light output of the flash tubes, especially below 200 nm, was decreasing with increasing number of flashes, caused by unidentified impurities deposited on the inside surface of the quartz. The emerging light beams were monitored by EMI 9558 QB photomultiplier tubes and the traces were recorded on Polaroid film (300 speed, Type 47) using a Tektronix RM 565 dual-beam oscilloscope. Spectra of the transient species were taken by the point-by-point method at a given time t after the flash and the reaction rate constants were determined using a computer by least-squares approximation of first- or second-order reactions. The rate constants given in this paper have not been corrected for the effect of change in ionic strength on the rates of reactions.

Materials. The $NaH_2PO_4 \cdot H_2O$, $K_2HPO_4 \cdot 3H_2O$, and $Na_4P_2O_7 \cdot 10H_2O$ were all of reagent grade quality obtained from Baker and Adamson. The water used was purified by distillation, radiolysis, and photolysis as described elsewhere.[7] The absorption spectra of the anions $H_2PO_4^-$, HPO_4^{2-}, and $P_2O_7^{4-}$ all have their maxima below 200 nm and their exctinction coefficients have been determined.[2] The linear extinction coefficient of liquid water has also been obtained.[8] The concentrations of anions used were such that essentially all the radiation was absorbed by the anions and none by the water.

Results and Discussion

Photolysis of $H_2PO_4^-$ Anions. The flash photolysis of air-free aqueous solutions of 10^{-1} M $H_2PO_4^-$ ions was found to produce a transient species with a broad optical absorption spectrum, stretching from about 250 to 680 nm, λ_{max} 500 nm and a half-life of about 300 μsec. (See Figure 3.) The decay of this species follows a second-order process, with $2k/\epsilon = 2.2 \times 10^6$ at 500 nm. (See Table I.) In air-saturated solutions, a species identical with that produced in air-free solutions is obtained having a maximum at 500 nm. In addition, however, another transient absorption is produced which absorbs below 300 nm and has $\lambda_{max} \simeq 250$ nm (see Figure 3). The absorption of this transient species appears to be similar to the optical absorption spectrum for the O_2^- radical produced in the pulse radiolysis of neutral aerated aqueous solutions[6] and in the flash photolysis of aerated aqueous solutions of SO_4^{2-}, CO_3^{2-}, and OH^- ions.[1]

From an examination of the absorption spectrum of monobasic phosphate ions and the observed blue shift of the spectrum in D_2O, it has been suggested[2] that it is due to a CTTS type of transition. The optical excitation of $H_2PO_4^-$ ions should therefore lead to ionization, with the ejection of an electron

$$H_2PO_4^- \cdot H_2O \overset{h\nu}{\rightleftharpoons} (H_2PO_4^- \cdot H_2O)^* \rightleftharpoons H_2PO_4\cdot + e_{aq}^- \quad (1)$$

No transient absorption spectrum due to the solvated electron could, however, be detected in the flash photolysis of air-free aqueous solutions of $H_2PO_4^-$ ions at the time resolution of the apparatus, $\geqslant 30$ μsec. In the flash photolysis of HPO_4^{2-} and $P_2O_7^{4-}$ ions (see below), the absorption spectra of e_{aq}^- in these systems could be observed and was determined. The reason for this difference is explained on the basis of the relatively higher reactivity of e_{aq}^- with $H_2PO_4^-$ ions, compared to HPO_4^{2-} and $P_2O_7^{4-}$ ions.

$$e_{aq}^- + H_2PO_4^- \longrightarrow HPO_4^- + H \quad (2)$$

The rate constant $k(e_{aq}^- + H_2PO_4^-) = 7.7 \times 10^6$ M^{-1} sec^{-1} [9] indicates that the lifetime of the hydrated electron in 0.1 M $H_2PO_4^-$ solutions would be about 1 μsec, that is shorter than the time resolution of this apparatus.

On flashing N_2O-saturated solutions of $H_2PO_4^-$ ions, a spectrum identical with that produced in air-free solutions is obtained, with a second-order decay constant $2k/\epsilon = 3.0 \times 10^6$ at 500 nm. Nitrous oxide is known to react effectively with e_{aq}^-

$$e_{aq}^- + N_2O \longrightarrow N_2 + OH + OH^- \quad (3)$$

(7) E. Hayon, *Trans. Faraday Soc.*, **60**, 1059 (1964).

(8) J. L. Weeks, G. M. A. Meaburn, and S. Gordon, *Radiation Res.*, **19**, 559 (1963).

(9) M. Anbar and P. Neta, *Int. J. Appl. Radiat. Isotopes*, **18**, 493 (1967).

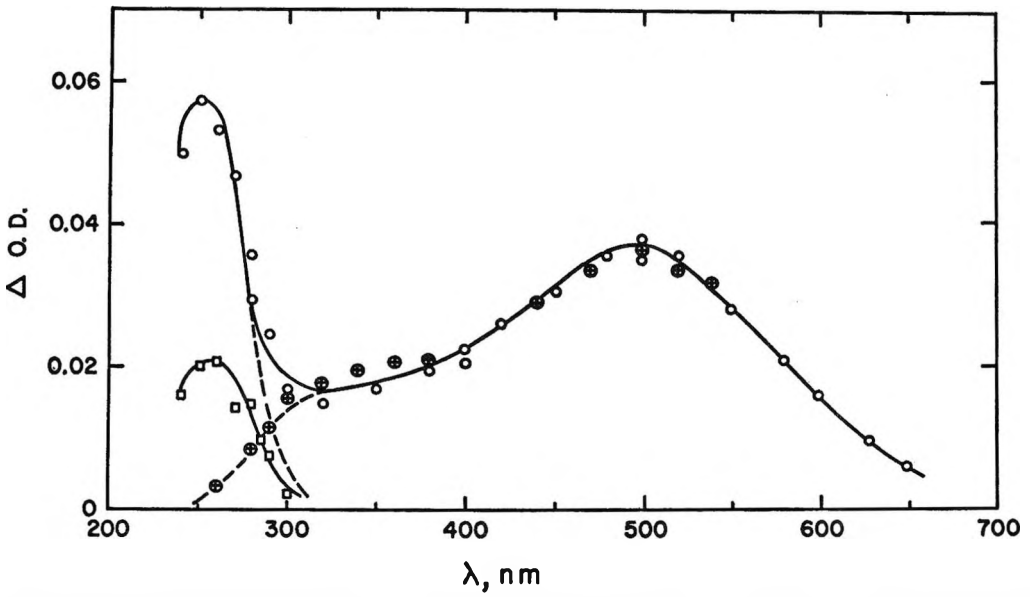

Figure 3. Transient absorption spectra of intermediates produced in the photolysis of 10^{-1} M $H_2PO_4^-$ ions in air-free (⊕) and air-saturated (O) aqueous solutions at pH 4.5. OD's measured 120 μsec after start of flash. Symbol □ is transient spectrum of long-lived species produced in air-saturated solutions with OD measured 16 msec after start of flash.

Table I: Decay Rates of Transient Species Produced in the Flash Photolysis of Aqueous Solutions of 10^{-1} M $H_2PO_4^-$ Ions, pH 4.5

System	λ, nm	Transient species	Decay rate	Absolute rate, M^{-1} sec^{-1}
Argon-saturated	500	$H_2PO_4\cdot$	$2k/\epsilon = 2.2 \times 10^6$	$1.4 \pm 0.3 \times 10^9$ [a]
Argon-saturated	470	$H_2PO_4\cdot$	$2k/\epsilon = 3.5 \times 10^6$	...
Argon-saturated	420	$H_2PO_4\cdot$	$2k/\epsilon = 3.1 \times 10^6$	...
N_2O-saturated	500	$H_2PO_4\cdot$	$2k/\epsilon = 3.0 \times 10^6$	$2.0 \pm 0.5 \times 10^9$ [a]
Air-saturated	500	$(H_2PO_4\cdot O_2)$	$k = 3.5 \pm 0.3 \times 10^3$ sec^{-1}	...
Air-saturated	500[c]	$(H_2PO_4\cdot O_2)$	$k = 3.4 \pm 0.3 \times 10^3$ sec^{-1}	...
Air-saturated	260	O_2^-	$k = 1.7 \pm 0.5 \times 10^2$ sec^{-1}	...
Air-saturated	260	O_2^-	$2k/\epsilon = 5.0 \pm 0.5 \times 10^5$	$4.5 \pm 0.5 \times 10^8$ [b]

[a] Derived using $\epsilon^{500} = 650 \times 50$ M^{-1} cm^{-1}. [b] $\epsilon O_2^{260} = 900$ M^{-1} cm^{-1}. [c] In 3×10^{-2} M $H_2PO_4^-$.

with $k_3 = 5.6 \times 10^9$ M^{-1} sec^{-1}.[9] Since the reaction of OH radicals with $H_2PO_4^-$ ions is known to be slow, $k_4 \ll 10^7$ M^{-1} sec^{-1} [9]

$$OH + H_2PO_4^- \longrightarrow HPO_4\cdot^- + H_2O \quad (4)$$

$$OH + H_2PO_4^- \longrightarrow H_2PO_4\cdot + OH^- \quad (4')$$

no significant increase was expected or found in the amount of the transient phosphate radical species at 500 nm. This contrasts to the observed[10] doubling of the amount of transients produced in the photoionization of SO_3^{2-}, $S_2O_3^{2-}$, and CNS^- ions in N_2O solutions compared to air-free solutions, by a similar reaction mechanism.

The nature of the intermediate with λ_{max} 500 nm (Figure 3) produced in the photolysis of 0.1 M $H_2PO_4^-$ ions at pH 4.5 is considered to be, according to reaction 1, the $H_2PO_4\cdot$ radical. However, since the pK of this radical is not known it could be present in its alkaline form.

$$H_2PO_4\cdot \rightleftharpoons HPO_4\cdot^- + H^+ \quad (5)$$

Indeed the absorption spectrum and decay rate of this radical is closely similar to that produced in the flash photolysis of 3×10^{-2} M HPO_4^{2-} ions at pH 9.3 (see below).

On photolysis in the presence of oxygen, the following reactions can be considered

$$e_{aq}^- + O_2 \longrightarrow O_2^- \quad (6)$$

$$O_2^- + O_2^- \xrightarrow{2H_2O} H_2O_2 + O_2 + 2OH^- \quad (7)$$

$$H_2PO_4\cdot + O_2 \longrightarrow (H_2PO_4\cdot O_2) \quad (8)$$

with $k_6 = 1.9 \times 10^{10}$ M^{-1} sec^{-1}.[9] On the basis of reaction 6, and taking $\epsilon_{C_2}{}^{260} = 900$ M^{-1} cm^{-1},[6] it was possible to determine the extinction coefficient of $H_2PO_4\cdot$ radicals at 500 nm, assuming that on extrapolation to zero time after the start of the flash $[O_2^-]_{t=0}$ =

(10) L. Dogliotti and E. Hayon, *J. Phys. Chem.*, **72**, 1800 (1968).

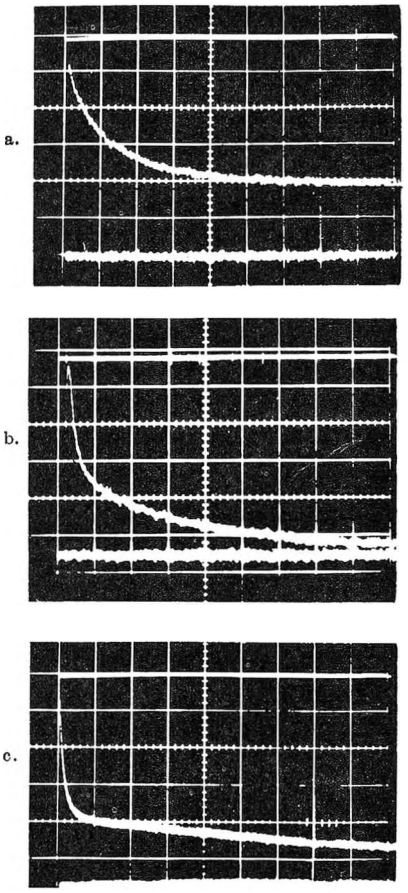

Figure 4. Oscilloscope traces obtained in the flash photolysis of aqueous solutions of 5×10^{-3} M HPO_4^{2-} ions, pH 8.7:
a, air-saturated solution, 250 nm, 2 msec/large division;
b, O_2-free solution, λ 500 nm, 500 μsec/large division;
c, air-saturated solution, 250 nm, 20 msec/large division.

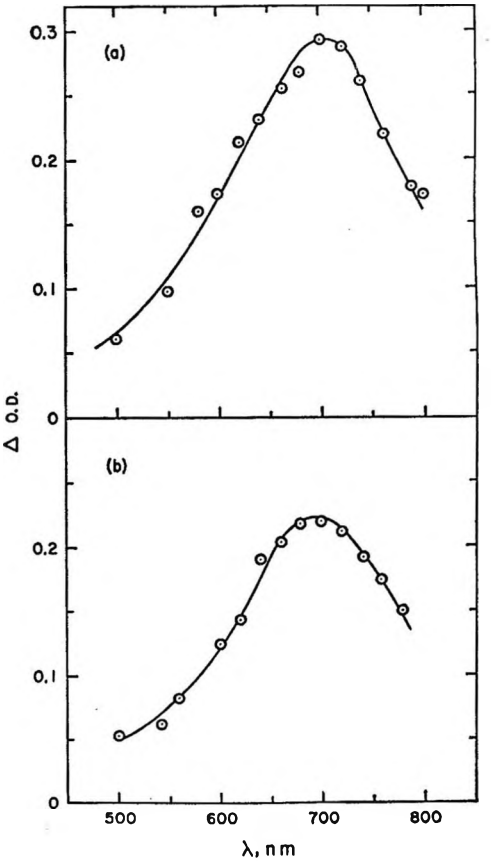

Figure 5. Optical absorption spectrum of the solvated electron produced in the photolysis of air-free solutions of (a) 3×10^{-2} M HPO_4^{2-}, pH 9.3, and (b) 10^{-2} M $P_2O_7^{4-}$, pH 10.5. OD measured 50 μsec after start of flash.

$[H_2PO_4\cdot]_{t=0}$. Using this method, $\epsilon_{H_2PO_4\cdot}^{500} = 650 \pm 50$ M^{-1} cm^{-1} was derived, and $2k(H_2PO_4\cdot + H_2PO_4\cdot) = 1.4 \pm 0.3 \times 10^9$ M^{-1} sec^{-1} was obtained.

In the presence of oxygen, the phosphate radical at 500 nm was found to decay by an apparent first-order process, $k = 3.5 \pm 0.3 \times 10^3$ sec^{-1}. To explain the difference in the decay order in O_2 compared to air-free solutions, it is suggested that the phosphate radical may react very rapidly with O_2, according to reaction 8. The same decay rate was obtained in air- and O_2-saturated solutions.

The decay order of the O_2^- radical at 260 nm could not be definitely established ($k = 1.7 \pm 0.5 \times 10^2$ sec^{-1} or $2k/\epsilon = 4.5 \pm 0.5 \times 10^5$). This is due to the formation of a relatively long-lived species, C, with λ_{max} ~260 mm, Figure 3, which is apparently produced from the decay of O_2^- radicals.

Photolysis of HPO_4^{2-} Ions. On flash photolysis of air-free aqueous solutions of dibasic phosphate ions two transient species are observed: a fast decaying species and a relatively longer-lived species; see Figure 4a. The fast-decaying species was found to have an optical absorption maximum at about 700 nm, Figure 5a, and is attributed to the solvated electron produced on photoexcitation of HPO_4^{2-} ions

$$HPO_4^{2-}\cdot H_2O \xrightleftharpoons{h\nu} (HPO_4^{2-}\cdot H_2O)^* \rightleftharpoons HPO_4^{-}\cdot + e_{aq}^- \quad (9)$$

The second intermediate was found to have a broad absorption spectrum in the wavelength region 280–680 nm, with $\lambda_{max} \simeq 500$ nm, see Figure 6, and is assigned to the $HPO_4\cdot^-$ radical anion.

The short-lived species with $\lambda_{max} \simeq 700$ nm was found to decay by a pseudo-first-order process. Support for the assignment of this radical to the solvated electron was derived from its close resemblance to the absorption spectrum of e_{aq}^- produced in the pulse radiolysis of neutral air-free water[11] and the disappearance of this optical absorption in N_2O- and air-saturated solutions of HPO_4^{2-} ions. Both N_2O and O_2 react with e_{aq}^- at almost diffusion-controlled rates, and therefore account for the disappearance of the spectrum with $\lambda_{max} \simeq 700$ nm.

The absorption spectrum of $HPO_4\cdot^-$ produced from

(11) J. W. Boag and E. J. Hart, *Nature*, 197, 45 (1963); J. P. Keene, *Radiation Res.*, 22, 1 (1964).

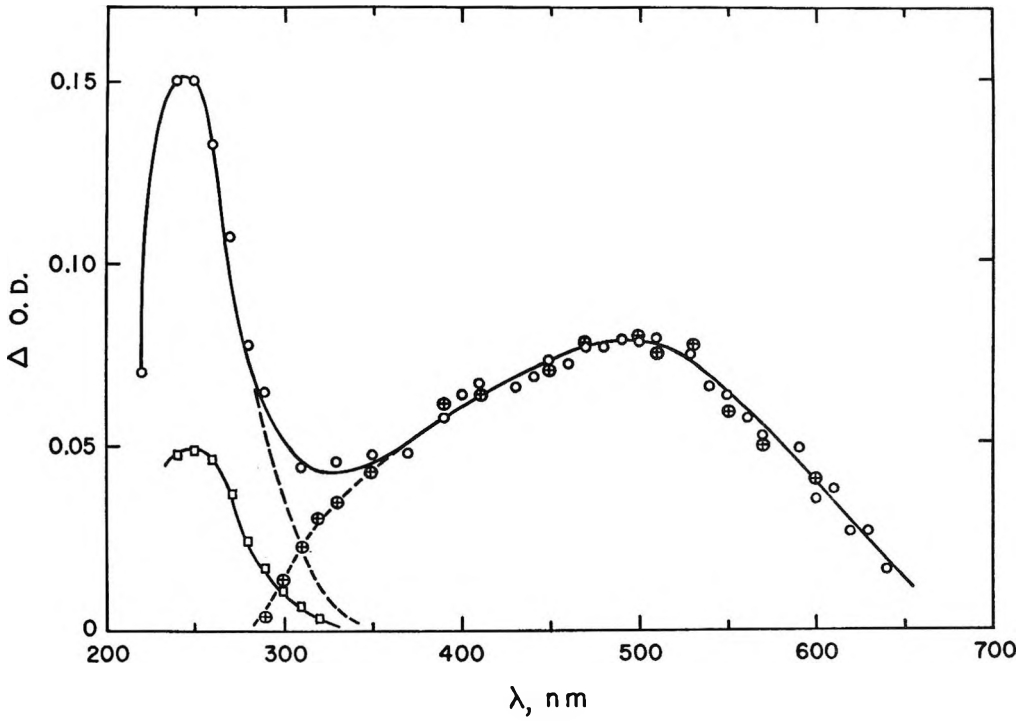

Figure 6. Transient absorption spectrum of intermediates produced in the photolysis of 3×10^{-2} M HPO_4^{2-} ions in air-free (⊕) and air-saturated (O) aqueous solutions at pH 9.3. OD's measured 200 μsec after start of flash. Symbol □ represents transient spectrum of long-lived species produced in air-saturated solutions, measured 16 msec after start of flash.

Table II: Decay Rates of Transient Species Produced in the Flash Photolysis of Aqueous Solutions of 3×10^{-2} M HPO_4^{2-} Ions, pH 9.3

System	λ, nm	Transient species	Decay rate	Absolute rate, M^{-1} sec^{-1}
Argon-saturated	500	$HPO_4\cdot^-$	$2k/\epsilon = 1.9 \times 10^6$	$1.1 \pm 0.3 \times 10^9$ [a]
Argon-saturated	470	$HPO_4\cdot^-$	$2k/\epsilon = 2.0 \times 10^6$	...
Argon-saturated	410	$HPO_4\cdot^-$	$2k/\epsilon = 3.1 \times 10^6$	...
N_2O-saturated	500	$HPO_4\cdot^-$	$2k/\epsilon = 1.2 \times 10^6$	$7.2 \pm 1.8 \times 10^8$ [a]
	470	$HPO_4\cdot^-$	$2k/\epsilon = 1.1 \times 10^6$	...
Air-saturated	500	$(HPO_4^-\cdot O_2)$	$k = 5.3 \pm 0.5 \times 10^2$ sec^{-1}	...
Air-saturated	500[b]	$(HPO_4^-\cdot O_2)$	$k = 4.8 \pm 0.5 \times 10^2$ sec^{-1}	...
Air-saturated	250	O_2^-	$2k/\epsilon = 4.5 \times 10^5$	$4.6 \pm 1.0 \times 10^8$ [c]
Air-saturated	250[b]	O_2^-	$2k/\epsilon = 6.0 \times 10^5$	$6.2 \pm 1.0 \times 10^8$ [c]
Air-saturated	270	C	$k = 1.3 \pm 0.2$ sec^{-1}	...

[a] Based on $\epsilon^{500} = 600 \pm 50$ M^{-1} cm^{-1}. [b] In 5×10^{-3} M HPO_4^{2-}. [c] Based on $\epsilon_{O_2}^{250} = 1030$ M^{-1} cm^{-1}.

the optical excitation of HPO_4^{2-} ions at pH 9.3 is rather similar to the intermediate produced in $H_2PO_4^-$ solutions at pH 4.5. It decays by a second-order process, with $2k/\epsilon = 1.9 \pm 0.4 \times 10^6$ at 500 nm in air-free solutions; see Table II. Based on the amount of e_{aq}^- produced and $\epsilon_{e_{aq}^-}^{720} = 18{,}500$ M^{-1} cm^{-1},[12] an extinction coefficient $\epsilon_{HPO_4^-}^{500} = 690 \pm 100$ M^{-1} cm^{-1} has been derived. However, due to possible errors involved in extrapolating $[e_{aq}^-]$ to zero time, the extinction coefficient used was based on the O_2^- method, as described above. Using $\epsilon_{O_2^-}^{260} = 900$ M^{-1} cm^{-1}, a value of $\epsilon_{HPO_4^-}^{500} = 600 \pm 50$ M^{-1} cm^{-1} was derived and is used in this paper. The second-order recombination rates for HPO_4^- radicals at pH 9.3 was found to be $1.1 \pm 0.3 \times 10^9$ M^{-1} sec^{-1} in N_2O-saturated solutions. Again, as in the photolysis of $H_2PO_4^-$ ions, the amount of transient produced on photolysis of N_2O-saturated solution of HPO_4^{2-} ions is not significantly increased over that in air-free solutions. This is because reaction 10 is relatively very slow

$$OH + HPO_4^{2-} \longrightarrow HPO_4^- + OH^- \qquad (10)$$

On photolysis of air-saturated solutions of HPO_4^{2-}

(12) E. M. Fielden and E. J. Hart, *Trans. Faraday Soc.*, **64**, 2975 (1968).

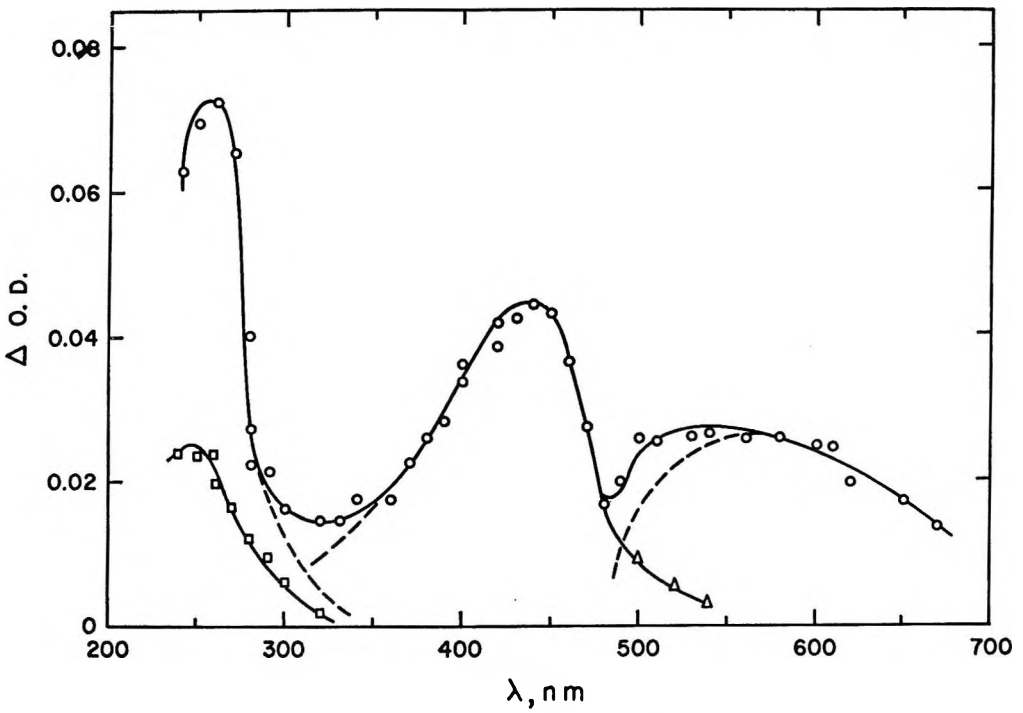

Figure 7. Transient absorption spectrum of intermediates produced in the photolysis of 10^{-2} M $P_2O_7^{4-}$ ions in air-saturated solutions (○) at pH 10.5. OD's measured 120 μsec after start of flash. Symbol △ represents continuation of spectrum of species with λ_{max} 440 nm obtained after correction for absorption of species with $\lambda_{max} \simeq 580$ nm. Symbol □ represents spectrum of long-lived species produced in air-saturated solution, with OD measured at 16 msec after start of flash.

ions, the HPO_4^- radical anion is produced in addition to O_2^- radicals and a long-lived transient species C (see Figure 6) as was observed in the photolysis of $H_2PO_4^-$ ions. The oscilloscope traces for the decay of O_2^- radicals and transient C are shown in Figures 4b and c.

The absorption spectra of the two transient species absorbing below 300 nm are identical with those observed in aerated solutions of H_2PO_4 ions (Figure 3) and $P_2O_7^{4-}$ ions (Figure 7). Their decay rates are also much the same. The decay rate in aerated 3×10^{-2} M HPO_4^{2-} for the species assumed to be O_2^- is $2k/\epsilon = 4.5 \times 10^5$ at 250 nm, or $2k = 4.6 \times 10^8$ M^{-1} sec^{-1} taking $\epsilon_{O_2^-}^{250} = 1030$ M^{-1} cm^{-1}. This second-order decay rate is considerably greater than $2k_7 = 3.4 \times 10^7$ M^{-1} sec^{-1},[6] as derived from pulse-radiolysis studies. Using the same purified water as employed in the flash-photolysis work, we obtain a value of $2k_7 = 3.0 \pm 0.2 \times 10^7$ M^{-1} sec^{-1} on pulse radiolysis of aerated water at pH 5.7. While efforts have been made to resolve this difference, no apparent explanation is available at the present time. Preliminary work on the flash photolysis of aerated water at pH 5.7 would appear to indicate that two similar transient species absorbing below 300 nm are produced.[13]

$$H_2O \xrightarrow{h\nu} H + OH \qquad (11)$$

$$H + O_2 \rightleftharpoons O_2^- + H^+ \qquad (12)$$

The long-lived species with $\lambda_{max} \simeq 260$ nm decays by a first-order process, $k = 1.3 \pm 0.2$ sec^{-1}. It is considered to be formed from the decay of O_2^- radicals, since a constant ratio exists between the OD's of O_2^- and transient C (see Figures 3, 6, and 7) which is independent of the absolute amounts of O_2^- produced in the system.

Photolysis of $P_2O_7^{4-}$ Ions. Two transients were observed in the flash photolysis of air-free aqueous solutions containing 10^{-2} M $P_2O_7^{4-}$ ions at pH 10.5. A short-lived species with $\lambda_{max} \sim 700$ nm, Figure 5b, which decays by a pseudo-first-order process and is assigned to the absorption spectrum of the solvated electron

$$P_2O_7^{4-} \cdot H_2O \overset{h\nu}{\rightleftharpoons} (P_2O_7^{4-} \cdot H_2O)^* \rightleftharpoons e_{aq}^- + (P_2O_7^{3-}) \qquad (13)$$

In addition, a second transient species is produced which absorbs in the range 480–750 nm, with $\lambda_{max} \sim 580$ nm. This species decays by a second-order process with $2k/\epsilon = 4.5 \times 10^5$ at 550 nm. In N_2O-saturated solutions, the e_{aq}^- spectrum disappeared and the species with $\lambda_{max} \simeq 580$ nm was increased by a factor of about 2. On the basis of reactions 13, 3, and 14, the species with λ_{max} 580 nm is

$$OH + P_2O_7^{4-} \longrightarrow P_2O_7^{3-} + OH^- \qquad (14)$$

tentatively attributed to the $P_2O_7^{3-}$ radical anion.

In aerated solutions, the species with $\lambda_{max} \simeq 580$ nm (A) is formed, and in addition three other species with

(13) J. R. Huber and E. Hayon, unpublished results.

Table III: Decay Rates of Transient Species Produced in the Flash Photolysis of Aqueous Solutions of 10^{-2} *M* $P_2O_7^{4-}$ Ions, pH 10.5

System	λ, nm	Transient species	Decay rate[b]
Argon-saturated	550	A	$2k/\epsilon = 4.5 \times 10^5$
N_2O-saturated	580	A	$2k/\epsilon = 2.6 \times 10^5$
N_2O-saturated	610	A	$2k/\epsilon = 3.0 \times 10^5$
Air-saturated	550	A	$2k/\epsilon = 3.0 \times 10^5$
Air-saturated	530	A	$2k/\epsilon = 3.2 \times 10^5$
Air-saturated	440	B	$k = 3.3 \pm 0.3 \times 10^3$ sec^{-1}
Air-saturated	440[a]	B	$k = 3.0 \pm 0.3 \times 10^3$ sec^{-1}
Air-saturated	260	O_2^-	$2k/\epsilon = 5.3 \times 10^5$

[a] In 10^{-3} *M* $P_2O_7^{4-}$. [b] Deviation in decay rate good to ±20%.

λ_{max} ≃440 nm (B), λ_{max} 250 nm (O_2^-), and λ_{max} ~260 nm (C), are produced; see Figure 7 and Table III. Species A decays by second-order process with $2k/\epsilon = 3.0 \times 10^5$ at 500 nm. Species B decays by a first-order process with $k = 3.3 \times 10^3$ sec^{-1}. The O_2^- radical produced appears to decay by a second-order process, with $k_7 = 4.8 \times 10^8$ M^{-1} sec^{-1}.

Comparison with Pulse-Radiolysis Study of Phosphate Ions. The pulse radiolysis of water and aqueous solutions produces the reactive species e_{aq}^-, H, and OH, in addition to H_2 and H_2O_2.

$$H_2O \rightsquigarrow e_{aq}^-, H, OH, H_2, H_2O_2$$

It is these species which react with the solutes present in solution. The pulse radiolysis of aqueous solutions of $H_2PO_4^-$, HPO_4^{2-}, and $P_2O_7^{4-}$ ions produces transient species similar to those observed in flash photolysis, and these have been shown[14] to result mainly from the reaction of OH radicals with the oxyphosphate anions. Thus transient species with λ_{max} ≃500 nm due to $H_2PO_4\cdot$ and/or $HPO_4^-\cdot$ radicals are produced on radiolysis of mono- and dibasic phosphates. On pulse radiolysis of $P_2O_7^{4-}$ ions, species A with λ_{max} ≃580 nm is observed and appears to be produced by reaction of OH radicals with $P_2O_7^{4-}$ ions. Similarly, species B with λ_{max} 440 nm is formed in the pulse radiolysis of $P_2O_7^{4-}$ ions in the presence of oxygen, but not in argon or N_2O-saturated solutions. Further work is in progress to elucidate the nature of the species B and C produced in these systems.

(14) E. D. Black and E. Hayon, to be published.

Photochemistry of Aqueous $Cr(CN)_6^{3-}$

by A. Chiang and A. W. Adamson

Department of Chemistry, University of Southern California, Los Angeles, California 90007 *(Received May 7, 1968)*

Aqueous $Cr(CN)_6^{3-}$ undergoes photoaquation when irradiated at either of the first two ligand field bands, at 377 and 307 mμ, with nearly wavelength- and temperature-independent quantum yields. The yield for cyanide production is 0.17 at 25°, but analysis of the product spectra indicates that the dominant immediate product is $Cr(CN)_4(H_2O)_2^-$, as the result of an efficient secondary photolysis of the primary product, $Cr(CN)_5(H_2O)^{2-}$. The primary quantum yield is then 0.09 at 25°. If added cyanide is present, photostationary states may be reached, with photoaquation balanced by thermal anation. The results are discussed in relation to the photochemistry of Cr(III) ammines. In particular, the relatively small quantum yield found for $Cr(CN)_6^{3-}$ is not expected in terms of the position of cyanide ligand in the spectrochemical series. The discrepancy is very likely related to the bonding character of cyanide as a ligand.

Introduction

Aqueous $Cr(CN)_6^{3-}$ has been known for some time to be photolyzed by visible and near-ultraviolet light to give free cyanide ion;[1] the process is one of photoaquation.[2] Photoexchange with added cyanide ion occurs, presumably through the reverse anation reaction.[3] However, no detailed studies of the photochemistry of this complex have been reported; one difficulty has been that $Cr(CN)_5(H_2O)^{2-}$ and the fur-

(1) R. Schwarz and K. Tede, *Chem. Ber.*, **60B**, 69 (1927).

(2) L. Moggi, F. Bolletta, V. Balzani, and F. Scandola, *J. Inorg. Nucl. Chem.*, **28**, 2589 (1966).

(3) A. G. MacDiarmid and N. F. Hall, *J. Amer. Chem. Soc.*, **75**, 5204 (1953); **76**, 4222 (1954).

ther possible aquation products had not been characterized. Recently, however, some spectra for the series $Cr(CN)_a(H_2O)_b^{3-a}$ have been published[4] so that some guide to the spectrophotometric analysis of irradiated solutions is now available. An interesting additional point is that the acid-catalyzed thermal aquation rate of $Cr(CN)_5(H_2O)^{-2}$ is sufficiently faster than that of $Cr(CN)_6^{3-}$ that the first observed product is $Cr(CN)_4(H_2O)_2^-$ (taken to be the *cis* isomer).[5]

There is a fairly extensive literature on the photochemistry of Cr(III) complexes in general, which has been reviewed.[6-10] So far, however, all reported investigations have been with essentially σ-bonding ligands (ammines, oxalates, etc.), and it was of interest to us to determine whether certain patterns of behavior for such complexes would carry over to a highly π-bonded species such as $Cr(CN)_6^{3-}$. Thus the series $Cr(urea)_6^{3-}$, $Cr(H_2O)_6^{3+}$, $Cr(C_2O_4)_3^{3-}$, $Cr(NCS)_6^{3-}$, $Cr(NH_3)_6^{3+}$, and $Cr(en)_3^{3+}$, which is in the order of increasing ligand field strength, photoaquates with quantum yields which are largely wavelength independent and which increase steadily from 0.1 to 0.5 (see ref 10). The expectation from this observation is then that $Cr(CN)_6^{3-}$ should show a wavelength-independent photoaquation yield greater than 0.5; cyanide lies higher than ethylenediamine in the spectrochemical series. Also, the ligand field strength effect and other observations provided a rationalization for some empirically determined photolysis rules for Cr(III) complexes,[11] on the basis of which some further predictions can be made. Thus the first photolysis product, $Cr(CN)_5(H_2O)^{2-}$, should further photoaquate, in high-quantum yield, to $Cr(CN)_4(H_2O)_2^-$. To the extent that photoaquations are stereospecific, the diaquo species should be the *trans* isomer, which should then be stable toward further photoaquation. However, should *cis* isomer be present, either because it was in fact the photolysis product, or because of a thermal isomerization, then further stages of photoaquation should occur. Since the thermal anation reactions are moderately fast,[5] continued photolysis should lead eventually to a photostationary state. It will be seen that some but not all of the above expectations are obeyed.

Experimental Section

Materials. $K_3Cr(CN)_6$ was prepared according to a literature procedure[12] and recrystallized twice from water; its spectrum agreed well with that previously reported (*e.g.*, ref 13). The actinometer compound, $KCr(NH_3)_2(NCS)_4$, was obtained from the ammonium salt (Reinecke's salt) by recrystallization from aqueous potassium nitrate. Other chemicals used were of reagent grade.

Apparatus and Procedures. The light source of the nominally 370-mμ photolyses was a General Electric AH6 lamp, with that wavelength region isolated by means of a glass filter having a broad window (40-mμ half-width) centered at 360 mμ. The 305-mμ irradiations were carried out by means of a Hanovia medium-pressure mercury lamp, using an interference filter whose window was at 305 mμ (5-mμ half-width). The two wavelength regions correspond to the first two ligand field bands of $Cr(CN)_6^{3-}$ (377 and 307 mμ).

The 370-mμ irradiations were done in a 2-cm path length Pyrex cell, equipped with a water jacket through which thermostated water was circulated. The available intensity of 305-mμ light was much lower, and hence its heating effect, so it was sufficient to irradiate solutions in 1-cm path length quartz spectrophotometer cells of the cylindrical type. In both cases, the light beam was sufficiently collimated and the solution absorption such that all incident light was contained by the irradiated solution. The absorbed light intensity was determined by reineckate actinometry,[14] in the case of the 370-mμ irradiations, and by ferrioxalate actinometry, in the case of those at 305 mμ (*e.g.*, ref 15). Actinometric measurements were usually made before and after a photolysis run, and in general, often enough to verify that no important change in lamp output had occurred during the experiment.

Where only the sequence of spectral changes was wanted, the irradiation was carried out directly on a solution contained in a 5-cm quartz spectrophotometer cell. Such spectra were measured on a Cary 14 spectrophotometer. Where, however, released cyanide analyses were also performed, spectral changes were usually monitored at selected wavelengths by transferring a sample to a spectrophotometer cell and making the measurement with a Beckman Model DU instrument. Solutions buffered to a stated pH contained *ca.* 0.25 *M* mixtures of KH_2PO_4 and K_2HPO_5.

A modified Liebig titration gave good results for free cyanide determination. Solutions were made 0.3 *M* in ammonia and 0.02 *M* in potassium iodide and titrated with aqueous silver nitrate to the first permanent cloudiness. The silver salts of the various Cr(III) cyano complexes are insoluble, but evidently

(4) R. Krishnamurthy, W. B. Schaap, and J. R. Perumareddi, *Inorg. Chem.*, **6**, 1338 (1967).

(5) W. B. Schaap and R. Krishnamurthy, private communication.

(6) F. Basolo and R. G. Pearson, "Mechanisms of Inorganic Reactions," 2nd ed, John Wiley and Sons, Inc., New York, N. Y., 1967.

(7) E. L. Wehry, *Quart. Rev.* (London), **21**, 213 (1967).

(8) J. Szychlinsky, *Wiad. Chem.*, **16**, 607 (1962).

(9) A. W. Adamson, *Coord. Chem. Rev.*, **3**, 169 (1968).

(10) A. W. Adamson, W. L. Waltz, E. Zinato, D. W. Watts, P. D. Fleischauer, and R. D. Lindholm, *Chem. Rev.*, in press.

(11) A. W. Adamson, *J. Phys. Chem.*, **71**, 798 (1967).

(12) J. F. Bigelow, *Inorg. Syn.*, **2**, 203 (1946).

(13) R. Krishnamurthy and W. B. Schaap, *Inorg. Chem.*, **2**, 605 (1963).

(14) E. E. Wegner and A. W. Adamson, *J. Amer. Chem. Soc.*, **88**, 394 (1966).

(15) J. Lee and H. H. Seliger, *J. Chem. Phys.*, **40**, 519 (1964); C. G. Hatchard and C. A. Parker, *Proc. Roy. Soc.*, **A235**, 518 (1956).

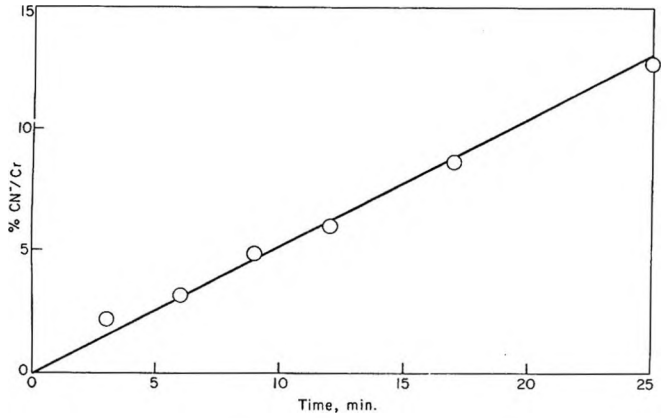

Figure 1. Photolysis of aqueous $Cr(CN)_6^{3-}$ at 370 mμ. Concentration of complex: 0.0204 *M*, pH 6.85 (phosphate buffer), 25°. Absorbed light intensity: 7.2×10^{-4} einstein/l. min.

not as much so as silver iodide; no induced cyanide release was observed. Also, added known amounts of free cyanide were accurately reported by the procedure.

Results

Quantum Yield for Cyanide Release. The results for a typical run at 370 mμ are shown in Figure 1; the cyanide release was linear with time, so that the system appeared to be simple in behavior. The general set of quantum yield data is summarized in Table I. A small temperature dependence is indicated at 370 mμ, and, within experimental error, there was no wavelength dependence.

Table I: Quantum Yields for Cyanide Release

$Cr(CN)_6^{3-}$, *M*	Wavelength, mμ	Temp, °C	pH[a]	Quantum yield
2.04	370	25	6.75	0.15
1.97	370	25	6.85	0.16
2.00	370	25	6.75	0.16
1.94	370	15	6.85	0.11
2.11	370	15	6.85	0.10
5.23	305	25	6.85	0.18[b]

[a] Phosphate buffer present. [b] Two runs combined.

Identification of Photolysis Products. The above results would normally be interpreted as giving quantum yields for the reaction

$$Cr(CN)_6^{3-} + H_2O \xrightarrow{h\nu} Cr(CN)_5(H_2O)^{2-} + CN^- \quad (1)$$

but examination of the spectra of the photolyzed solutions showed that the principal product during the first states of photolysis was probably $Cr(CN)_4(H_2O)_2^-$. The spectra for several aquocyano chromium (III) complexes are displayed in Figure 2 (from ref 4), while the spectral changes that actually occur during photolysis at 370 mμ and pH 6.85 are shown in Figure 3. First, the presence of three well-defined isosbestic points in Figure 3 indicates that essentially only one photolysis product was present. However, not only do these isosbestic points not correspond to those expected were $Cr(CN)_5(H_2O)^{2-}$ the product, but, as a clear discrepancy, the optical density at 377 mμ decreases rather than increases during irradiation.

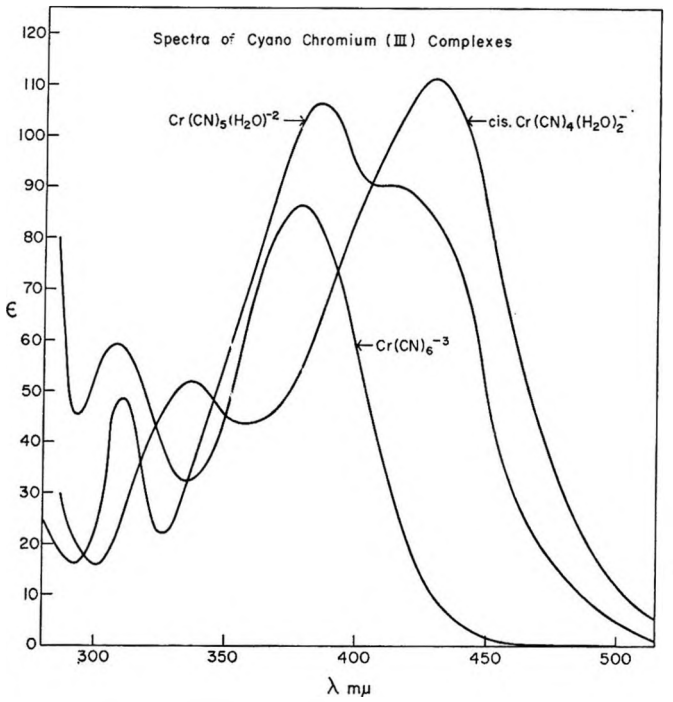

Figure 2. Spectra of $Cr(CN)_a(H_2O)_b^{3-a}$ complexes. From ref 4.

Concurrent cyanide titrations and optical density measurements at 377, 410, and 430 mμ allowed, in combination with the data of Figure 3, a calculation of the complete spectrum of this single photolysis product. This last is included in Figure 3, and it corresponds fairly closely to the reported spectrum for the tetracyano complex. On this basis, the primary quantum yields are given by the values of Table I divided by 2.

The failure of the literature and our derived spectrum for $Cr(CN)_4(H_2O)_2^-$ to agree exactly could be due to experimental error, but additional possibilities exist. First, the isomeric nature of our product is not known and may not be the same as that from the thermal kinetic studies (assumed to be *cis*[4]). Second, the detailed spectra of the various aquocyano species are pH dependent. Thus, irradiation of an unbuffered solution of $Cr(CN)_6^{3-}$ leads to a somewhat different sequence of spectra, showing no isobestic points; a similar observation (of lack of isosbestic points) was made by Moggi, *et al.*[2]

Photostationary States. Prolonged irradiation at 370 mμ of solutions buffered at pH 6.85 led to progressive

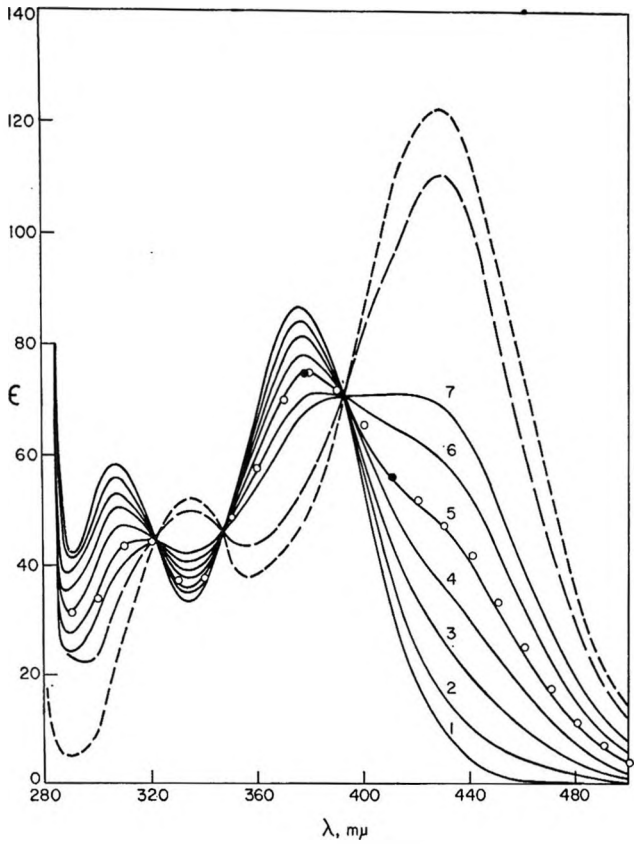

Figure 3. Spectral sequence on photolysis of aqueous $Cr(CN)_6^{3-}$ at 370 mμ. Curves 1–7 for 0-, 10-, 25-, 42-, 60-, 90-, and 120-min irradiations at pH 6.90 (phosphate buffer) at 25°; other conditions roughly comparable to Figure 1. Solid circles: points established by separate run with concurrent cyanide and spectrophotometric determinations; slope of optical density change *vs.* cyanide release when applied to curve 5 identified it as corresponding to 33% conversion to tetracyano complex. Open circles: points for 33% conversion calculated according to the product spectrum given by the dashed line. Dotted line: spectrum for $Cr(CN)_4(H_2O)_2^-$ from ref 4.

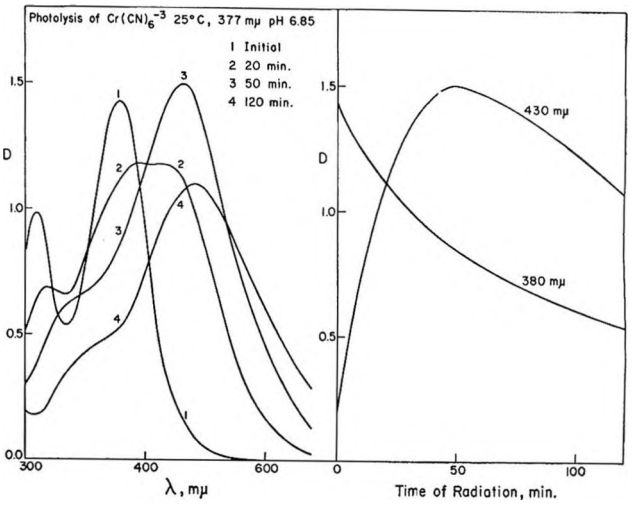

Figure 4. Spectral sequence on long-term photolysis of aqueous $Cr(CN)_6^{3-}$ at 25°, pH 6.85 (phosphate buffer), 370-mμ radiation. Right-hand graph shows the optical density changes at selected wavelengths. From ref 9.

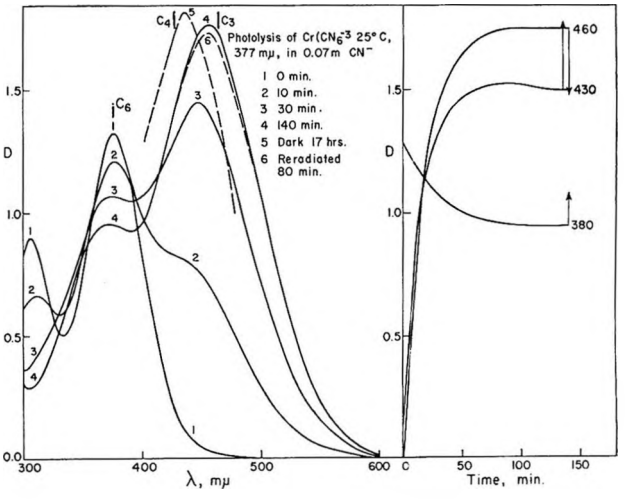

Figure 5. Spectral sequence on long-term photolysis of $Cr(CN)_6^{3-}$ in 0.07 *M* cyanide at 25°, natural pH, 370-mμ radiation. Right-hand graph shows the optical density change at selected wavelengths; the arrows indicate the the direction of change in the dark, after terminating the irradiation.

spectral changes as shown in Figure 4. The spectrum terminal for this experiment corresponds to $Cr(CN)_3(H_2O)_3$ as the principal product present.

If the initial solution was made 0.07 *M* in cyanide ion, the continued irradiation at 370 mμ led eventually to a photostationary state, as shown in Figure 5. This state corresponds to a mixture of the tri- and the tetracyano complexes, and, in the dark, thermal anation returned the system to more nearly pure tetracyano complex. Re-irradiation gave essentially the same photostationary state as before. Another indication that thermal anation reactions occurred was that if added thiocyanate ion was also present, continued irradiation of aqueous $Cr(CN)_6^{3-}$ produced solutions whose spectra indicate the presence of coordinated thiocyanate.

Discussion

The most important discrepancy between our results and the predictions made in the Introduction is that the primary quantum yield is only about 0.09, or much lower than expected in terms of the correlation between quantum yield and position in the spectrochemical series. It seems likely that the special behavior of $Cr(CN)_6^{3-}$ as compared to nitrogen and oxygen complexes is related to the high degree of π bonding probably present in the former. Detailed explanation is less easy to contrive, however. The excited state which is the immediate precursor to chemical reaction has alternatively been supposed to be the first doublet state (^2E_g),[16] or the lowest-lying

(16) See H. L. Schläfer, *J. Phys. Chem.*, 69, 2201 (1965).

quartet state ($^4T_{2g}$).[11] It was in terms of the latter intermediate that the correlation between ligand field strength and quantum yield could be explained—as a consequence of σ antibonding character in the reactive excited state. That is, it appeared that the position of a ligand in the spectrochemical series gave not only the degree of ligand field stabilization in the ground state of Cr(III) complexes but also the degree of bond weakening in the excited state.

Pursuing this last emphasis, the first spin-allowed transition for a cyano complex probably involves the promotion of an electron from a π-bonding orbital to either a metal σ antibonding or a cyanide π antibonding one.[4,10,13,17] The extreme position of cyanide in the spectrochemical series may thus be more a reflection of π-bonding ability than of bond weakening in the excited state.

Since quantum yields reflect the competition between chemical reaction and radiationless deactivation, it might be that it is the latter which is relatively fast for the cyano complex, as compared to the ammine family. Lifetimes for radiationless deactivation should be a function of the degree of excited-state distortion,[11] and an alternative supposition is that such distortion is less in a highly π-bonded system.

If, on the other hand, it is supposed that reaction occurs from the ^2E_g state, produced by intersystem crossing, then it seems less easy to explain why a π-bonded complex should be less photosensitive than a largely σ-bonded one. The ^2E_g state involves only spin pairing within the σ-nonbonding (or, alternatively, the π-bonding) set of d orbitals, so distortion or bond weakening effects should not be present.

The appearance of $Cr(CN)_4(H_2O)_2^-$ as the first observed product seems best explained on the basis that the immediate product, $Cr(CN)_5(H_2O)^{2-}$, shows the expected high photosensitivity for cyano complexes, and is subject to an efficient secondary photolysis. A quantum yield above 0.5 for its photoaquation, coupled with an extinction coefficient reasonably above that for $Cr(CN)_6^{3-}$ in the region of 370 mμ, would account for the situation. An alternative and not disproven possibility is that simultaneous aquation of two cyano groups occurs in the primary step. Such diaquations have not previously been reported, however, and seem improbable, nor is it likely that a fast thermal aquation of $Cr(CN)_5(H_2O)^{2-}$ occurs; the required maximum half-life of about 1 min would be in orders of magnitude disparity with the very slow aquation rates for the other members of the series.[5]

Finally, the prediction that if $Cr(CN)_5(H_2O)^{2-}$ undergoes secondary photolysis the product should be *trans*-$Cr(CN)_4(H_2O)_2^-$ appears not to be borne out. Although no definite isomer assignment is possible, the product spectrum is quite similar to that assigned to the *cis* isomer; again, however, the basis for this last assignment is on indirect kinetic evidence. The predicted relative insensitivity of the photoproduced $Cr(CN)_4(H_2O)_2^-$ to further photolysis is to a degree confirmed by the persistence of isosbestic points up to at least 50% conversion of the hexacyano complex to the tetracyano one (Figure 3).

Acknowledgment. The investigations have been supported in part by Contract AT(11-1)-113 between the University of Southern California and the U. S. Atomic Energy Commission.

(17) Note J. J. Alexander and H. B. Gray, *Coord. Chem. Rev.*, **2**, 29 (1967).

Substituent Effects in Cyclohexadienyl Radicals as Studied by Pulse Radiolysis

by B. Cercek

Paterson Laboratories, Christie Hospital and Holt Radium Institute, Manchester 20, England *(Received May 7, 1968)*

The effect of electron-donating and electron-withdrawing substituents on the second-order decay of hydroxycyclohexadienyl radicals, $\cdot HOC_6H_5X$, and their reactivity toward oxygen has been studied using the technique of pulse radiolysis. The reactions of $\cdot HOC_6H_5X$ radicals are enhanced by electron-donating substituents and retarded by substituents that are electron-withdrawing. The activation energies for the second-order decay of $\cdot HOC_6H_5X$ radicals increase with increasing dipolar character of the species.

Introduction

A multitude of radicals can be produced and their reactivities measured by the technique of pulse radiolysis. Various physicochemical parameters can be studied within a group of related radicals. This paper explores the correlations of tautomeric and inductive effects of substituents with reactivity as well as activation energies in monosubstituted hydroxycyclohexadienyl radicals.

Experimental Section

Materials. All solutions were prepared using distilled water redistilled from alkaline permanganate. The quality of the water was checked by measuring the half-life of the hydrated electron in deaerated water. It was at least 100 μsec after a dose of about 30 rads/2-μsec pulse. The reagents were used without further purification. Benzene sulfonamide, chloro-, bromo-, and iodobenzene were B.D.H. laboratory reagents. Benzene was of Analar grade (B.D.H.). Xylene, toluene, phenol, benzoic acid, nitrobenzene, N,N-dimethylaniline, and aniline were of Analar grade, Hopkin and Williams Ltd. Benzophenone, acetophenone, benzonitrile, and anisole were Hopkin and Williams Ltd. general purpose reagents.

Procedure. Details of the pulse-radiolysis technique have been extensively described elsewhere.[1] Kinetic spectroscopy was used following 2-μsec pulses of 4-MeV electrons giving doses from 500 to 5000 rads per pulse. The optical density changes were recorded at the absorption maxima for OH addition products.[2-4]

In experiments in which the effects of temperature were measured, a large volume of the preheated solution was flowed through the irradiation cell until the desired temperature, measured by a thermistor in the exit of the cell, was reached and remained constant before, during, and after the pulse of radiation. The activation energies were calculated from Arrhenius plots (logarithm of the rate constants *vs.* the inverse of the absolute temperature). The reproducibility of the activation energies was within 10%.

The second-order decay of monosubstituted hydroxycyclohexadienyl radicals, $\cdot HOC_6H_5X$, (X equals H or the substituent) was measured over the range from 19 to 80°. The solutions used were deoxygenated and N_2O-saturated by bubbling for at least 45 min with N_2O. The solute concentration was adjusted so that over 99% of the hydrated electrons reacted with N_2O and were converted to OH radicals. Neglecting the small amount of unconverted H radicals ($G(H) \sim 0.6$) only hydroxycyclohexadienyl radicals were produced *via* reaction 1.

$$HO + C_6H_5X \longrightarrow \cdot HOC_6H_5X \qquad (1)$$

The first-order decay of $\cdot HOC_6H_5X$ radicals with oxygen was measured in oxygen-saturated solutions at 19 ± 1°. The solute concentration was adjusted so that over 99% of the hydrated electrons and H atoms were scavenged by oxygen.

Results and Discussion

To study the tautomeric and inductive effects of different substituents on the reactivty of hydroxycyclohexadienyl radicals, the reactions of $\cdot HOC_6H_5X$ with oxygen, reaction 2, and the reaction of these radicals with each other, reaction 3, were selected.

$$\cdot HOC_6H_5X + O_2 \longrightarrow \cdot O_2(HO)C_6H_5X \qquad (2)$$

$$2 \cdot HOC_6H_5X \longrightarrow \text{products} \qquad (3)$$

The rate constants for reactions 2 and 3 and activation energies for reaction 3 are summarized in Table I. The reproducibility of the rate constants and activation energies was within 10%.

Structure of the Radicals $\cdot HOC_6H_5X$. It follows from current theories[5] that the reactivity of monosubstituted benzene derivatives, C_6H_5X, toward radicals is greater in the *ortho* and *para* positions than in the *meta* position. In fact, it has been shown in radiolytic hydroxylation

(1) J. P. Keene, *J. Sci. Instrum.*, **41**, 493 (1964).

(2) L. M. Dorfman, I. A. Taub, and R. E. Bühler, *J. Chem. Phys.*, **36**, 3051 (1962).

(3) D. F. Sangster, *J. Phys. Chem.*, **70**, 1712 (1966).

(4) B. Cercek, *ibid.*, **71**, 2354 (1967).

(5) G. H. Williams, "Homolytic Aromatic Substitution," Pergamon Press, Oxford, 1960, pp 6–25.

Table I: The Reaction Rate Constants of Substituted Hydroxycyclohexadienyl Radicals with Oxygen and Each Other

Substituent X	$\cdot HOC_6H_5X + O_2$ $k_2(\times 10^{-6}\ M^{-1}\ sec^{-1})$	$\alpha = \log \frac{k(\cdot HOC_6H_5X + O_2)}{k(\cdot HOC_6H_6 + O_2)}$	$\cdot HOC_6H_5X +$ $\cdot HOC_6H_5X$ $k_3(\times 10^{-8}\ M^{-1}\ sec^{-1})$	$\beta = \log \frac{k(2 \cdot HOC_6H_5X)}{k(2 \cdot HOC_6H_6)}$	Activation energy for reaction 3, kcal mol^{-1}
1. NO_2	2.5	−2.20	5.0	0.037	6.0
2. CN	2.9	−2.14	3.92	−0.066	4.7
3. COC_6H_5	3.7	−2.03	3.66	−0.095	4.7
4. $COCH_3$	3.82	−2.02	4.2	−0.033	4.3
5. SO_2NH_2	4.2	−1.98	3.68	−0.092	5.4
6. COOH	5.25	−1.88	3.95	−0.062	4.3
7. I	7.0	−1.76	4.0	−0.055	5.0
8. Cl	7.95	−1.70	4.36	0.03	3.5
9. Br	9.6	−1.62	4.2	−0.03	3.9
10. OH	4.9	−1.91	11.0	0.38	6.7
11. OCH_3	16.4	−1.39	5.73	0.10	5.8
12. NH_2	25.4	−1.197	16.0	0.547	3.9
13. $N(CH_3)_2$	23.2	−1.24	7.3	0.206	4.6
14. H	400	0	4.55	0	3.5
15. CH_3	390	−0.01	3.85	−0.07	3.0
16. C_2H_5	555	0.14	4.2	−0.03	3.6

studies[6-13] that about 75% of the OH radicals appear in the *ortho* and *para* positions. Furthermore, for electron-donating substituents the attack of the OH radicals has been shown to be on the *para* position and that its addition to the *meta* position may be neglected.[14]

A priori, the radicals $\cdot HOC_6H_5X$ could have any of the structures shown in Table II. However, some of these may be neglected for the following reasons. (a) Structures containing formal bonds between nonneighboring carbon atoms should possess a greater amount of energy than any other structure. They represent an energetically unfavored state; hence, the fraction of radicals having this type of structures should be small.[15] (b) The amount of energy required to localize the radical spot in the *para* and *ortho* position to an electron-withdrawing substituent should be greater than in the *ortho* position to an OH group.[16,17] Moreover, a substituent in the *ortho* position to the radical spot should, because of the steric hindrance, strongly decrease, if not completely prevent, the reaction. (c) It has been shown that the optical absorption spectra of all the transients studied can be ascribed to species of the hydroxycyclohexadienyl type;[4] thus, structures with the radical spot on the substituent are not relevant. (d) For electron-donating substituents the attack of the OH radicals has been shown to be on the *para* position; thus, its addition to the *meta* position may be neglected.[14] On the basis of these arguments only the following structures of the radicals $\cdot HOC_6H_5X$ in Table II need to be considered when evaluating the results; in the case of: (1) electron-withdrawing substituents: radicals I, IV, VIII, XIII, and XIV, and (2) electron-donating substituents: radicals I, IV, XIII, and XIV.

Evaluation of the Substituent Effects. In general, radical reactions are facilitated by electron-donating groups and are hindered by groups that are electron-withdrawing.[18,19] A measure for the electron-donating

Table II: Possible Structures of the Radicals $\cdot HOC_6H_5X$

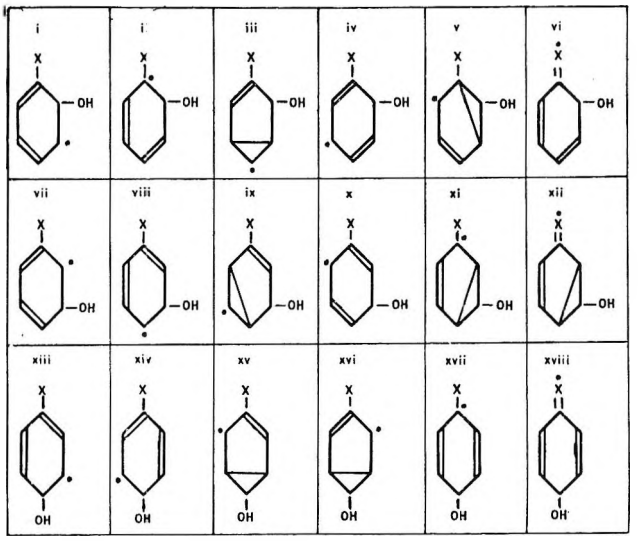

(6) G. Stein and J. Weiss, *J. Chem. Soc.*, 3245 (1949).
(7) H. Loebl, G. Stein, and J. Weiss, *ibid.*, 2704 (1950).
(8) H. Loebl, G. Stein, and J. Weiss, *ibid.*, 405 (1951).
(9) G. Stein and J. Weiss, *ibid.*, 3265 (1951).
(10) G. R. A. Johnson and J. Weiss, *ibid.*, 3275 (1951).
(11) A. M. Downes, *Australian J. Chem.*, 11, 154 (1958).
(12) I. Loeff and A. J. Swallow, *J. Phys. Chem.*, 68, 2470 (1964).
(13) R. W. Matthews and D. F. Sangster, *ibid.*, 71, 4056 (1967).
(14) M. Anbar, D. Meyerstein, and P. Neta, *J. Phys. Chem.*, **70**, 2660 (1966).
(15) G. H. Williams, "Homolytic Aromatic Substitution," Pergamon Press, Oxford, 1960, pp 17, 18.
(16) G. H. Williams, ref 15, pp 18–20.
(17) D. Grässlin, F. Merger, D. Schulte-Frohlinde, and O. Volkert, *Z. Phys. Chem.* (Frankfurt am Main), 51, 84 (1966).

or electron-withdrawing power of a group, X, is its Hammett substituent constant, σ.[20] On this basis the method of "linear free energy reactivity relationships"[20-22] should be a reasonable first-order approximation in evaluating the influence of substituents on the reactivity of hydroxycyclohexadienyl radicals. In order to make use of this method all rate constants of the $\cdot HOC_6H_5X$ radicals were related to that of $\cdot HOC_6H_6$ and expressed in terms of

$$\alpha = \log \frac{k(\cdot HOC_6H_5X + O_2)}{k(\cdot HOC_6H_6 + O_2)};$$

$$\beta = \log \frac{k(2 \cdot HOC_6H_5X)}{k(2 \cdot HOC_6H_6)}$$

for reactions 2 and 3, respectively. The values of α and β are given in Table I.

In the transients $\cdot HOC_6H_5X$, with an electron-withdrawing substituent the radical spot is located in either the *meta* or *para* position, in relation to the substituent X (Table II, structure I, IV, VIII, XIII, and XIV), whereas in the case of electron-donating substitutents the radical spot is located in the *meta* position (Table II, structures I, IV, XIII, and XIV). Therefore, both σ-*para* and σ-*meta* values of the Hammett constants were used for electron-withdrawing substituents and only σ-*meta* values for electron-donating ones in the correlation plots with the α and β values. In these plots the σ values may be regarded as a parameter related to the increase or decrease of electron density at the radical spot.

As shown in Figures 1 and 2, in which the α and β values are plotted *vs.* σ values, a correlation was obtained for 13 out of 16 radicals $\cdot HOC_6H_5X$ studied. The reactivities of $\cdot HOC_6H_6$, $\cdot HOC_6H_5CH_3$, and $\cdot HOC_6H_5C_2H_5$ for reaction 2 were found to be about 40 times greater and for reaction 3 about one-fourth as large as that expected from the general trend of the other 13 radicals. An explanation for these deviations will be discussed later. A calculation of the statistical reliability by the t-test method[23] revealed that the probability of obtaining such a correlation out of a set of uncorrelated data is smaller than 0.1% and 5% for the correlations in Figures 1 and 2, respectively. Radicals $\cdot HOC_6H_6$, $\cdot HOC_6H_5CH_3$, and $\cdot HOC_6H_5C_2H_5$ were not included in the statistical test. In view of the high level of statistical significance, these results can be regarded as collateral evidence that reactions of radicals are facilitated by electron-donating groups and are hindered by groups that are electron withdrawing.

The correlations in Figures 1 and 2 can be described by the following Hammett type equations:[20] $\alpha = \rho_\alpha\sigma + C_\alpha$ and $\beta = \rho_\beta\sigma + C_\beta$, where σ denotes the Hammett substituent constant, σ and ρ_β the reaction constants, C_α and C_β the empirical correlation constants for reactions 2 and 3, respectively. The following values

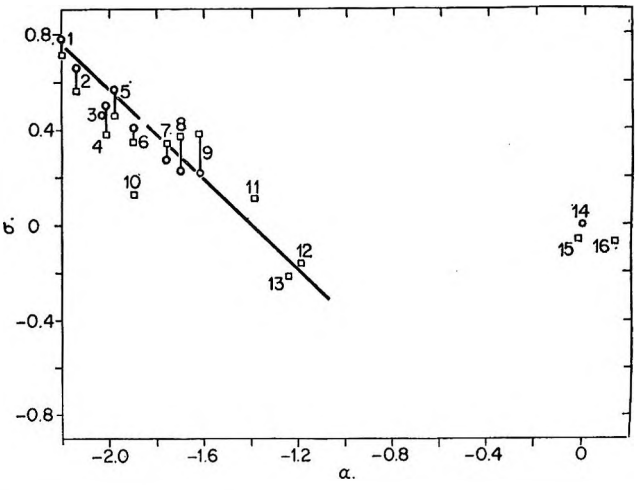

Figure 1. Correlation of the Hammett substituent constants, σ,[5] with the α values: squares, σ_m; circles, σ_p. The numbers given at every point refer to the substituents listed under the same number in Table I. Ordinate, Hammett substituent constants; abscissa, log $[k(\cdot HOC_6H_5X + O_2)/k(\cdot HOC_6H_6 + O_2)] = \alpha$.

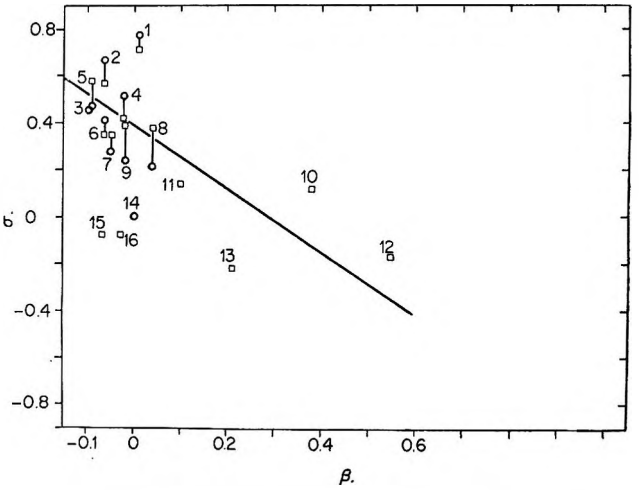

Figure 2. Correlation of the Hammett substituent constants, σ,[5] with β values: squares, σ_m; circles, σ_p. The numbers given at every point refer to the substituents listed under the same number in Table I. Ordinate, Hammett substituent constants; abscissa, log $[k(2 \cdot HOC_6H_5X)/k(2 \cdot HOC_6H_6)] = \beta$.

for the constants $\rho_\alpha = -1.0$, $\rho_\beta = -0.75$, $C_\alpha = -1.4$ and $c_\beta = 0.3$ were found.

Activation Energies for Biradical Reactions. We have shown before[24] that about 75% of the nitrohydrox-

(18) A. Streitwieser, "Molecular Orbital Theory for Organic Chemists," John Wiley & Sons, Inc., New York, N. Y., 1961, p 397.

(19) S. W. Charles, J. T. Pearson, and E. Whittle, *Trans. Faraday Soc.*, 59, 1156 (1963).

(20) J. Hine, "Physical Organic Chemistry," McGraw-Hill Book Co. Inc., New York, N. Y., 1962, pp 85-87.

(21) S. Ehrenson, *Progr. Phys. Org. Chem.*, 2, 195 (1964).

(22) C. D. Ritchie and W. F. Sager, *ibid.*, 2, 323 (1964).

(23) R. A. Fischer, "Statistical Methods for Research Workers," Oliver and Boyd, Edinburgh, 1938, p 177.

(24) K.-D. Asmus, B. Cercek, M. Ebert, A. Henglein, and A. Wigger, *Trans. Faraday Soc.*, 63, 2435 (1967).

ycyclohexadienyl radicals dimerize forming unstable nitrocyclohexadienes and 25% react by disproportionation, a reaction in which an H atom is being abstracted. Since the aromatic C–H bond strength increases with increasing π-electron density,[25] it seems reasonable to expect that the proportion of radicals which dimerize will increase as the π-electron density increases. The nitro group is the strongest electron-withdrawing substituent. It therefore can be expected that the hydroxycyclohexadienyl radicals react mainly by dimerization, interacting at identical ends of the dipoles, *i.e.*, in *meta* and *para* positions to the substituent X. Thus the repulsive forces in the activated complex should increase with increasing dipolar character of the radicals $\cdot HOC_6H_5X$. For several reactions of the aromatic compounds the electrical properties of the substituents were found to be correlated with the activation energies.[26] A similar attempt for the radicals $\cdot HOC_6H_5X$ showed that the activation energies for the biradical reactions could be correlated with the electron-withdrawing ($+\sigma$ values) and electron-donating properties ($-\sigma$ values) of the substituent X. As shown in Figure 3, the activation energies, E, increase with increasing values of the Hammett substituent constants, σ. The statistical reliability of the obtained correlation for electron-withdrawing substituents is greater than 99.5%; as there are only four measurements, a statistical t-test[23] could not be applied to electron-donating substituents. Nevertheless, the general trend shown for electron-withdrawing substituents seems to be holding for electron-donating substituents as well. These results can best be explained by the dipole character of these radicals and repulsion between interacting dipoles in the activated complex. It has been reported that increased electron withdrawal lowers the activation energy for the decomposition of diaroyl peroxides. Since the decomposition of diaroyl peroxides into radicals can be regarded as the analogous reverse process to radical dimerization, the reverse effect of electron-withdrawing substituent has been described before.[27]

Reactivities of $\cdot HOC_6H_6$, $\cdot HOC_6H_5CH_3$, *and* $\cdot HOC_6H_5C_2H_5$. Finally, we have to consider why the reactivities of these radicals depart from the general trends of the "linear free energy reactivity relationships" for reactions 2 and 3. In view of the large deviation, a factor of 40 in Figure 1, from the otherwise statistically highly significant correlation, one might be tempted to suggest that a different type of reaction is being observed. For example: a reaction of the benzyl or phenyl type radicals produced by the abstraction of H atoms from either the $-CH_3$ and $-C_2H_5$ groups or the benzene ring. However, this explanation is not likely for the following reasons. (a) The phenyl radical is not known to have an optical absorption in the 315-nm region.[28] (b) No isotope effect could be found for the OH radical with benzene.[29] (c) The abstraction of H atoms from $-CH_3$ and $-C_2H_5$ would lead to the formation of benzyl type radicals. These have an optical absorption in the same wavelength region[30] as the radicals $\cdot HOC_6H_5CH_3$ and $\cdot HOC_6H_5C_2H_5$. However, the molar extinction coefficient of the benzyl radical at 317 nm is 12,000 M^{-1} cm^{-1}, whereas that of the observed transients at this wavelength is 3400 ± 400 M^{-1} cm^{-1}. This is in agreement with the value of 3500 M^{-1} cm^{-1} for the hydroxycyclohexadienyl radical.[29] Thus not more than an insignificant part of OH radicals could yield the benzyl type transients, a result which cannot account for the observed deviations.

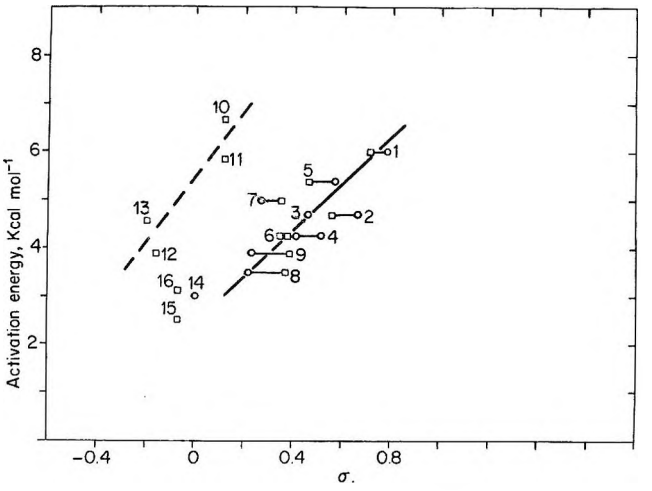

Figure 3. Activation energies for the second-order decay of $\cdot HOC_6H_5X$ radicals as a function of the Hammett substituent constants, σ[5]: squares, σ_m; circles, σ_p. Ordinate, activation energy in kcal mol^{-1}; abscissa, Hammett substituent constants, σ.

Another explanation for the deviations could be found in entropy effects. This is supported by the fact that the activation energies of $\cdot HOC_6H_6$, $\cdot HOC_6H_5CH_3$, and $\cdot HOC_6H_5C_2H_5$ do not significantly depart from the correlation plot in Figure 3. Taking the activation energies as being equal to the enthalpies of activation, $\Delta H^{\ddagger}$, it is obvious from the relationship $\Delta F^{\ddagger} = \Delta H^{\ddagger} - T\Delta S^{\ddagger}$ that the breakdown in the general trend of the free energy–reactivity relationship could be attributed to a change in the entropy of activation, $\Delta S^{\ddagger}$. A likely cause for this effect could be the absence

(25) W. Hückel, "Theoretische Grundlagen der Organischen Chemie," Akademische Verlagsgesellschaft Geest and Partig K-G, Leipzig, 1948, p 528.

(26) S. Glasstone, K. J. Laidler, and H. Eyring, "The Theory of Rate Processes," McGraw-Hill Book Co., New York, N. Y., 1941, p 456.

(27) G. H. Williams, "Homolytic Aromatic Substitution," Pergamon Press, Oxford, 1960, p 40.

(28) G. Porter and B. Ward, *Proc. Roy. Soc.*, **A287**, 457 (1965).

(29) L. M. Dorfman, I. A. Taub, and R. E. Bühler, *J. Chem. Phys.*, **36**, 305 (1962).

(30) R. J. Hagemann and H. A. Schwarz, *J. Phys. Chem.*, **71**, 2694 (1967).

of a lone pair of electrons in the substituents $-CH_3$ and $-C_2H_5$ necessary for the hydrogen bonding with water molecules. Selective forces of this kind can destroy "linear free energy reactivity relationships" as suggested previously.[31]

Acknowledgment. The author wishes to express his thanks to Dr. M. Ebert for his helpful criticisms and discussions during the writing of this paper.

(31) C. D. Ritchie and W. F. Sager, *Progr. Phys. Org. Chem.*, 2, 381 (1964).

The Absorption Spectra and Kinetics of Hydrogen Sesquioxide and the Perhydroxyl Radical[1]

by Benon H. J. Bielski and Harold A. Schwarz

Chemistry Department, Brookhaven National Laboratory, Upton, New York 11973 *(Received May 7, 1968)*

An absorption spectrum below 280 mμ attributable to hydrogen sesquioxide was found in the pulse radiolysis of air-saturated perchloric acid solutions. The decay of the spectrum is in agreement with previous results obtained by reaction of the H_2O_3 with ferrous sulfate in a flow system. The activation energy for the decomposition at pH 2 is 16.5 kcal/mol. The maximum half-life for H_2O_3 in aqueous solution is 17 sec in 0.027 *M* acid and at 0°. Neither the absorption spectrum nor the decay kinetics that we find for the perhydroxyl radical offer any support for the existence of the protonated form, $H_2O_2^+$.

In 1963, Czapski and Bielski reported the production of a new compound, hydrogen sesquioxide, in the radiolysis of air-saturated water.[2] Acidic solutions flowing through a narrow tube were irradiated with an electron beam, and the oxidizing products remaining a few centimeters further on were allowed to react with ferrous sulfate solution in a mixing chamber. An unstable compound was found which was identified as H_2O_3 on the basis of the yield and kinetics and which was believed to be formed by the reaction

$$OH + HO_2 \longrightarrow H_2O_3 \qquad (1)$$

This compound is of considerable interest as it is the third member of the homologous series starting with water and hydrogen peroxide. We have observed hydrogen sesquioxide spectroscopically in pulse-radiolysis experiments and have extended the kinetic studies.

The hydrogen sesquioxide absorption is in the same spectral region as the perhydroxyl radical which made further study of this radical necessary. Previous studies have indicated that the perhydroxyl radical exists in three forms, O_2^-, HO_2, and $H_2O_2^+$, each form exhibiting different kinetics.[2-4] Our results are in agreement with the first two forms but not $H_2O_2^+$.

Experimental Section

A pulsed 2-MeV Van de Graaff generator was used as the electron source. Pulse lengths of a few hundred microseconds to several tenths of a second were used as the species being studied were long-lived (several milliseconds to seconds). The quartz irradiation cell was 2 × 2 × 0.8 cm with one 2 × 2 cm face thinned to 0.5 mm to allow penetration of the electron beam.[5] The analyzing light from a deuterium lamp crossed the cell perpendicular to the electron beam three times for a total optical path length of 6.1 cm and entered a Bausch and Lomb *f*/3.5 monochromator mounted on the same optical bench as the lamp and radiation cell. This arrangement was required for maximum stability as it minimized the effect of room vibrations. Tandem monochromators were used below 240 mμ to eliminate scattered light which was always kept below 2% of the analyzed light beam. The light from the monochromator fell on a photomultiplier, and the signal was fed to a dual beam oscilloscope so that both the rapid (HO_2) and slow (H_2O_3) decay could be followed.

The electron beam current striking the sample and cell holder was monitored and related to ferrous dosimetry at low currents to determine absolute yields.

(1) Research carried out under the auspices of the U. S. Atomic Energy Commission.

(2) G. Czapski and B. H. J. Bielski, *J. Phys. Chem.*, 67, 2180 (1963).

(3) K. Schmidt, *Z. Naturforsch.*, 16B, 206 (1961).

(4) B. H. J. Bielski and A. O. Allen, "Proceedings of the 2nd Tihany Symposium on Radiation Chemistry," Akademiai Biado, Budapest, 1967, p 81.

(5) R. J. Hagemann and H. A. Schwarz, *J. Phys. Chem.*, 71, 2694 (1967).

The acidity was varied with perchloric acid (Czapski and Bielski found the intermediate in both perchloric and sulfuric acid solutions[2]), and Baker and Adamson reagent grade hydrogen peroxide was used.

Results

Hydrogen sesquioxide decays in a first-order reaction, presumably to water and oxygen

$$H_2O_3 \longrightarrow H_2O + O_2 \qquad (2)$$

while the perhydroxyl radical reacts bimolecularly to give oxygen and hydrogen peroxide

$$2HO_2 \longrightarrow O_2 + H_2O_2 \qquad (3)$$

The optical density at any time after the electron pulse is given by

$$OD - OD_\infty = A_{H_2O_3}e^{-k_{H_2O_3}t} + \frac{A_{HO_2}}{1 + \frac{2k_{HO_2}A_{HO_2}}{l\epsilon}t}$$

where $A_{H_2O_3}$ and $k_{H_2O_3}$ are the initial optical density of the H_2O_3 present and rate constant for reaction 2, A_{HO_2} and k_{HO_2} are the initial optical density and rate constant for reaction 3, l is the optical path length, and ϵ is equal to the extinction coefficient of the perhydroxyl radical minus one-half the extinction coefficient of hydrogen peroxide. Note that A_{HO_2} is not the initial optical density of HO_2 but is given by the initial HO_2 concentration multiplied by $l\epsilon$.

The experimental results of optical density *vs.* time were resolved into the four components $A_{H_2O_3}$, $k_{H_2O_3}$, A_{HO_2}, and $k_{HO_2}/l\epsilon$ by a least-squares procedure[6] in which estimates are made for the rate constants, $k^\circ_{H_2O_3}$ and $2k^\circ_{HO_2}/l\epsilon$, and the data fitted to the equation

$$OD = X_1e^{-k^\circ_{H_2O_3}t} + X_2\frac{1}{1 + \frac{2k^\circ_{HO_2}}{l\epsilon}X^\circ_2 t} + \Delta k_{H_2O_3}\frac{\partial OD}{\partial k_{H_2O_3}} + \Delta k_{HO_2}\frac{\partial OD}{\partial k_{HO_2}}$$

The four linear variables, X_1, X_2, $\Delta k_{H_2O_3}$, and Δk_{HO_2}, were determined and the Δk's added to the respective rate constant estimates and the process iterated until the Δk's were less than 1% of the rate constants at which time the X's could be identified with the optical densities, $A_{H_2O_3}$ and A_{HO_2}. Sometimes individual samples were handled this way and sometimes groups of samples were analyzed for the best values of the rate constants.

The resolution of the curves into two components with four constants is meaningful primarily because the time constants are widely separated. The first half-life of the HO_2 decay was generally a factor of 10 to 100 smaller than the half-life of the H_2O_3 decay. The use of the dual-beam oscilloscope allowed us to determine the optical density and rate constant for H_2O_3 decay to about 10% even when it was only 5% of the total absorption. The H_2O_3 was generally the smaller component except in samples irradiated with pulse lengths longer than a few tenths of a second at wavelengths below 210 mμ.

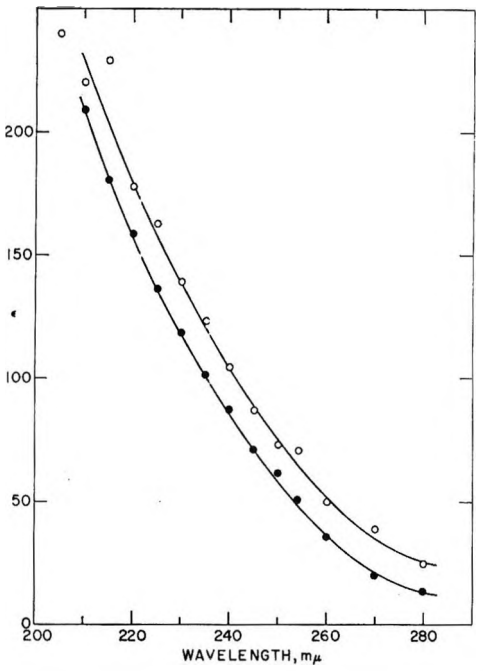

Figure 1. Absorption spectrum of H_2O_3. The molar extinction coefficient (M^{-1} cm^{-1}) as determined in: ○, 0.5 M $HClO_4$, and ●, 10^{-2} M $HClO_4$.

Hydrogen Sesquioxide. The absorption spectrum of hydrogen sesquioxide, determined in air-saturated perchloric acid solutions, is given in Figure 1. The extinction coefficient is given by

$$A_{H_2O_3} = l\epsilon_{H_2O_3}G(H_2O_3) \times \text{dose}$$

where $G(H_2O_3)$ = 1.7 molecules/100 eV absorbed in the solution.[2] The spectrum is very similar to that of hydrogen peroxide but more intense. The difference between the results in 10^{-2} M $HClO_4$ and 0.5 M $HClO_4$ may be either a slight shift in spectrum or a systematic observational error (of the order of 0.001 ODU).

Additional evidence that H_2O_3 is formed by reaction 1 is that (a) it is not formed in solutions containing 10^{-4} M ethanol, which is sufficient to react with all the hydroxyl radicals, and (b) the yield of H_2O_3 as a function of acidity can be predicted by the known pK of the HO_2 radical, 4.5.[7,3] At higher pH, reaction 1 is in competition with

$$OH + O_2^- \longrightarrow OH^- + O_2$$

(6) W. C. Hamilton, "Statistics in Physical Science," The Ronald Press Co., New York, N. Y., 1964, p 124.

(7) G. Czapski and L. M. Dorfman, *J. Phys. Chem.*, **68**, 1169 (1964).

(8) J. Rabani, W. A. Mulac, and M. S. Matheson, *ibid.*, **69**, 53 (1965).

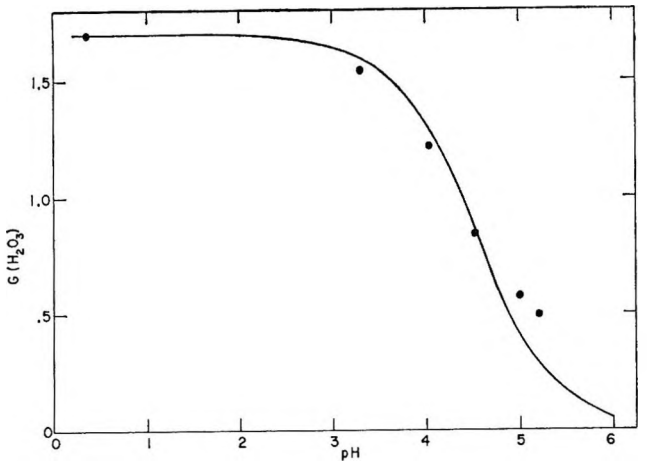

Figure 2. The yield of H_2O_3 as a function of pH. The curve is computed from the assumption that OH reacts equally well with HO_2 and O_2^-.

and the assumption that the rate constant for the above reaction is equal to k_1 (both are probably diffusion controlled) leads to the equation

$$G(H_2O_3) = \frac{1.7}{1 + \frac{k_{HO_2}}{(H^+)}}$$

The yield of H_2O_3 (normalized to 1.7 at high acidity) is given as a function of pH in Figure 2 along with the curve for the above equation.

Czapski and Bielski found that the rate constant for decomposition of H_2O_3 was strongly dependent on acid concentration and was in agreement with the mechanism

$$H_2O_3 + H^+ \longrightarrow H_3O^+ + O_2 \quad (4)$$

$$H_2O_3 \longrightarrow H^+ + HO_3^- \quad (5)$$

$$HO_3^- + H^+ \longrightarrow H_2O_3 \quad (6)$$

$$HO_3^- \longrightarrow OH^- + O_2 \quad (7)$$

They found $k_4 = 6\ M^{-1}\ sec^{-1}$, $k_5 = 9.2\ sec^{-1}$, and $k_6/k_7 = 1700$.[2] Our results in Figure 3 are in good agreement with theirs between 1 M and 10^{-4} M acid, which is the range they studied except that our rate constants are slightly larger near the minimum at 0.035 M H^+. We have extended the acid range to pH 5.2 and find that the rate constant continues to increase, whereas the above mechanism would predict a leveling off at 9.2 sec^{-1}. The increase is likely due to the reaction

$$OH^- + H_2O_3 \longrightarrow H_2O + HO_3^- \quad (8)$$

Reactions 4–8 give the equation

$$k_{H_2O_3} = k_4(H^+) + \frac{k_5 + k_8(OH^-)}{1 + \frac{k_6(H^+)}{k_7}}$$

The solid curve of Figure 3 is computed with the constants of Czapski and Bielski and a value of $1.5 \times 10^{10}\ M^{-1}\ sec^{-1}$ for k_8. Apparently reaction 8 is diffusion controlled, which is in accord with similar reactions.[9] The variation of $k_{H_2O_3}$ with temperature is given in Figure 4. The activation energy at pH 0.5 is 13.3 kcal/mol and at pH 2 is 16.5 kcal/mol.

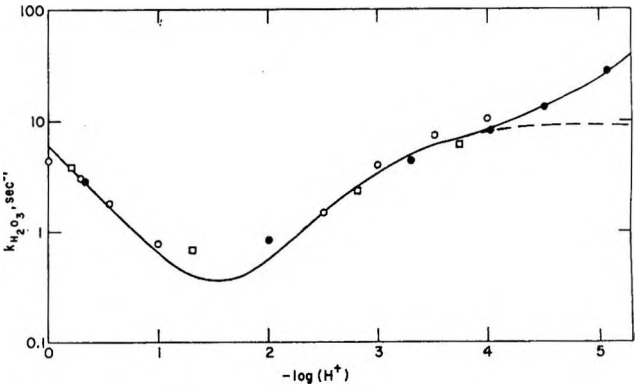

Figure 3. The effect of acidity on the rate constant for H_2O_3 decomposition: ●, 210 mμ; □, 240 mμ; ○, 254 mμ. The results at shorter wavelength are most precise as H_2O_3 is larger portion of optical density.

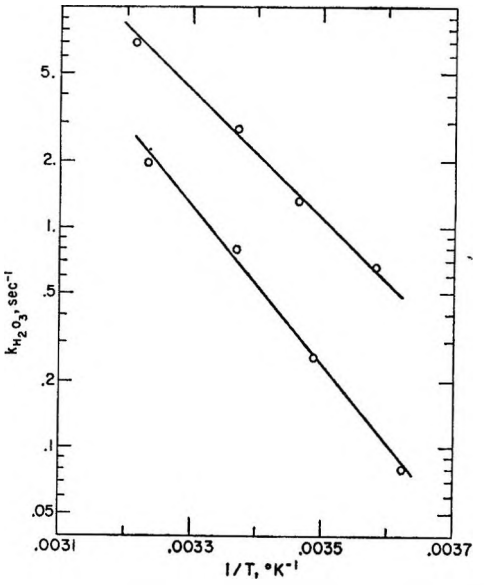

Figure 4. Temperature effect on H_2O_3 decomposition in 0.5 M $HClO_4$ (upper curve) and 10^{-2} M $HClO_4$ (lower curve).

A third absorption appeared in the more concentrated perchloric acid solutions, apparently a product of perchloric acid as it was not observed in sulfuric acid solutions. The optical density of this species was a few per cent of the H_2O_3 optical density and its lifetime varied from about 20 sec at room temperature to about 5 sec at 35°. It presented no particular difficulty to the analysis of the results but complicated the issue

(9) N. Eigen, W. Kruse, G. Maass, and L. DeMaeyer, *Progr. Reaction Kinetics*, 2, 285 (1964).

sufficiently at higher temperatures to limit our temperature range to below 40°.

Perhydroxyl Radical. Czapski and Dorfman found that the absorption spectrum of O_2^- was red-shifted from that of HO_2 by 10 mμ,[7] a fact which allowed them to determine the pK of the radical in a manner uncomplicated by kinetic considerations. They found the two extinction coefficients to be equal at 241 mμ and we have chosen this wavelength for the bulk of our kinetic studies and for our determination of the extinction coefficient of the radical.

In order to estimate the extinction coefficient, a system was needed in which the yield of HO_2 is reasonably well known. Hydrogen peroxide converts all of the radicals in the system to HO_2 through the reactions[10]

$$\begin{aligned} e + H^+ &\longrightarrow H \\ e + H_2O_2 &\longrightarrow OH^- + OH \\ e + O_2 &\longrightarrow O_2^- \\ H + O_2 &\longrightarrow HO_2 \\ H + H_2O_2 &\longrightarrow H_2O + OH \\ OH + H_2O_2 &\longrightarrow H_2O + HO_2 \end{aligned} \qquad (9)$$

It is seen that in the presence of hydrogen peroxide all hydrogen atoms and electrons eventually yield HO_2 (or O_2^-) as long as reaction 9 accounts for all of the hydroxyl radicals. The yield of HO_2 is equal to $G_e + G_H + G_{OH}$ which is 6.6 in 0.5 M $HClO_4$, 6.4 in 10^{-2} M $HClO_4$,[11] and 6.1[12] at pH 5. Optical density–dose curves for 7×10^{-3} M H_2O_2 solutions containing 10^{-2} M $HClO_4$ are given in Figure 5. It is difficult to work in more concentrated solutions of peroxide because of the absorption of the solution. It may be seen that the concentration of HO_2 approaches a plateau at high doses but sufficient data can be obtained to find the initial slope. The dose units of Figure 5 are such that the slope of the curve gives $G\epsilon$ directly for the radical. Similar data (though not to such large doses) were obtained for solutions in 0.5 M $HClO_4$ and 10^{-5} M $HClO_4$. The resulting values of $G\epsilon$, all at 241 mμ, are 6.3×10^3 at pH 2, 6.3×10^3 at pH 5, and 6.2×10^3 at pH 0.3. The corresponding values of ϵ (equal to $\epsilon_{HO_2} - {}^1/_2 \epsilon_{H_2O_2}$) are 984, 1033, and 939 M^{-1} cm^{-1}.

The spectrum of the HO_2 radical in 0.5 M $HClO_4$ and 10^{-2} M $HClO_4$ corrected for the hydrogen peroxide absorption is given in Figure 6. The spectra were obtained from solutions without peroxide present. The shapes of the two spectra are identical and the absolute values of the extinction coefficients are within experimental error. There is no evidence for any shift corresponding to $H_2O_2^+$. The spectrum in 10^{-2} M $HClO_4$ agrees reasonably well with that of Czapski and Dorfman.[7] They found ϵ_{HO_2} at 241 mμ to be 1070 M^{-1} cm^{-1} but this value includes an uncertain contribution from the hydroxyl radical.

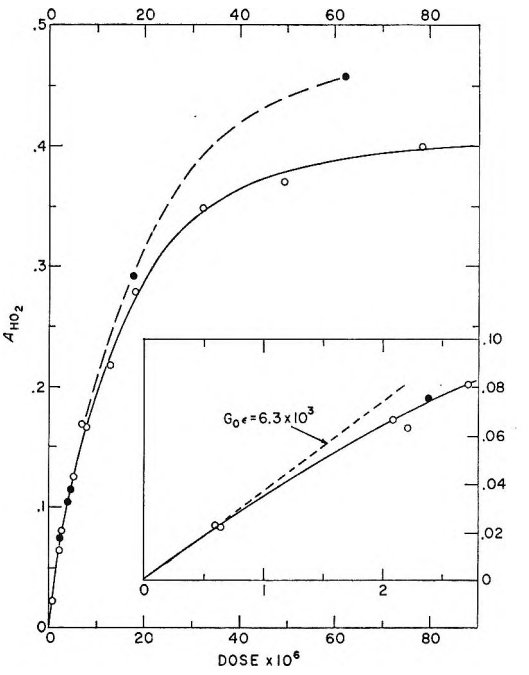

Figure 5. Optical density change, A_{HO_2}, produced in air-saturated (○) and oxygen saturated (●) 10^{-2} M $HClO_4$, 7×10^{-3} M H_2O_2, solutions as a function of dose. The units of dose are electron volts per liter divided by 6.023×10^{25} so that the slope gives $G\epsilon$ directly.

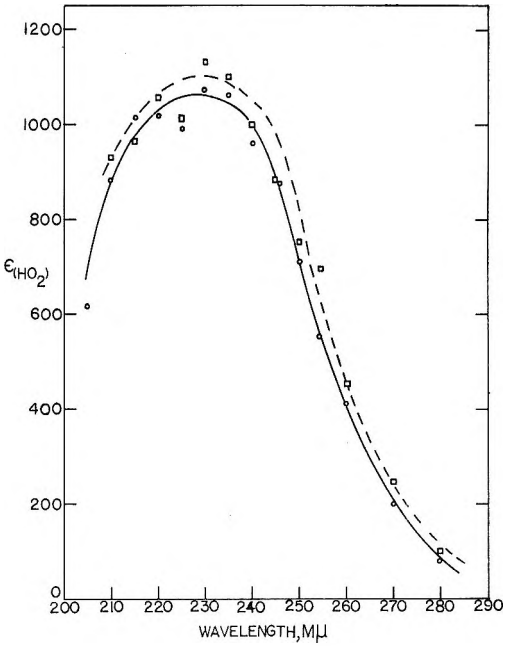

Figure 6. The absorption spectrum of the HO_2 radical determined in 0.5 M $HClO_4$ (○) and 10^{-2} M $HClO_4$ (□).

(10) A. O. Allen, "The Radiation Chemistry of Water and Aqueous Solutions," D. Van Nostrand Co., Princeton, N. J., 1961, p 41.

(11) A. O. Allen, V. D. Hogan, and W. G. Rothschild, *Radiation Res.*, **7**, 603 (1957).

(12) B. H. J. Bielski and A. O. Allen, *J. Phys. Chem.*, **71**, 4544 (1967).

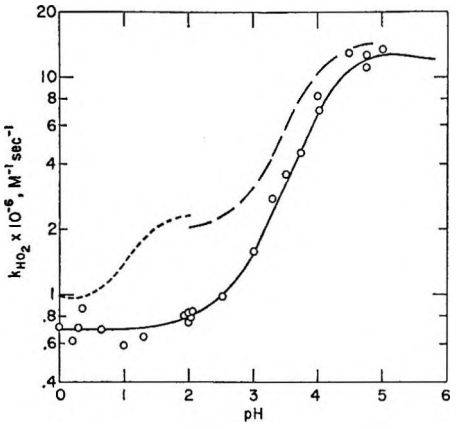

Figure 7. The effect of pH on the rate of disappearance of perhydroxyl radicals. The solid curve is calculated according to reactions 10 to 12 as described in the text. The dashed curves are the results of Czapski and Bielski above pH 2 and Bielski and Allen below pH 2.

We have determined k/ϵ at various acidities in air-saturated solutions without hydrogen peroxide, and with the measured extinction coefficients have computed the rate constants which are given in Figure 7. The agreement with other work is good at pH 5, poor at pH 2, and better again at pH 0. The original evidence for the existence of $H_2O_2^+$ was inferred from the curve of Bielski and Allen below pH 2.[4] We do not confirm this curve and again find no evidence for $H_2O_2^+$. The reaction scheme

$$HO_2 + HO_2 \longrightarrow O_2 + H_2O_2 \qquad (10)$$

$$HO_2 + O_2^- \xrightarrow{H_2O} OH^- + H_2O_2 + O_2 \qquad (11)$$

$$O_2^- + O_2^- \xrightarrow{2H_2O} 2OH^- + H_2O_2 + O_2 \qquad (12)$$

leads to the equation

$$k_{HO_2} = \frac{k_{10} + k_{11}X + k_{12}X^2}{(1 + X)^2}$$

where $X = K_{HO_2}/H^+$. The solid curve in Figure 7 is calculated from this equation using $K_{HO_2} = 3 \times 10^{-5}$,[7,8] $k_{10} = 0.7 \times 10^6$, $k_{11} = 3.0 \times 10^7$, and $k_{12} = 1.2 \times 10^7$ M^{-1} sec^{-1}.

The second-order kinetics for the HO_2 decay held when the initial concentration of the radical was varied from 1×10^{-5} to 5×10^{-5} M both in the presence and absence of added peroxide. However, one bottle of H_2O_2 which had been standing in a refrigerator for a year gave erratic results. The decay rate was high by a factor of 1.5 to 3 and the kinetics were not second order. A fresh bottle gave better results but still tended to give high rates when the HO_2 concentration was below 1×10^{-5} M (an effect not found with solutions containing no added peroxide). This effect might explain part of the irreproducibility of the radiolysis of peroxide solutions and in particular offers an explanation for the peroxide catalysis of the HO_2 decay noted by Hart and Matheson.[13]

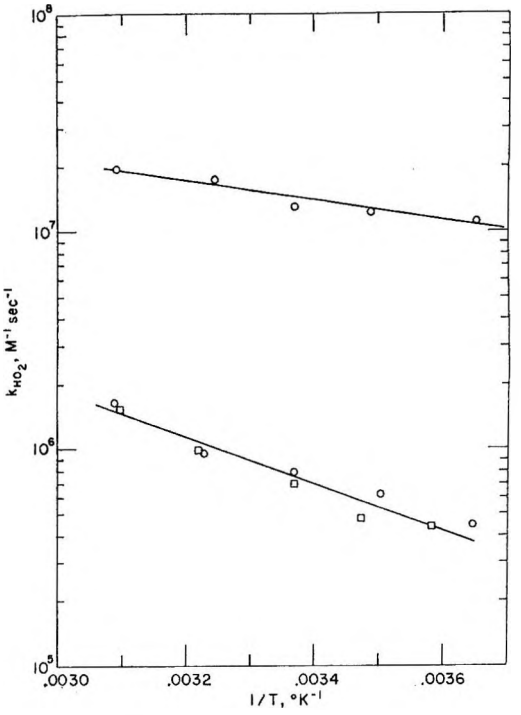

Figure 8. Effect of temperature on rate constant for perhydroxyl radical disappearance at pH 5 (upper curve) and pH 2 (○) and pH 0.3 (□) (lower curve).

The effects of temperature on the rate constant at pH 0.3, pH 2, and pH 5 are given in Figure 8. The rate constants are calculated assuming the extinction coefficients to be independent of temperature. The results at pH 0.3 and pH 2 should correspond to reaction 10 and the activation energy is found to be 4.9 kcal/mol (to be compared with 5.9 kcal/mol found by Bielski and Saito[14]). The activation energy at pH 5 is 2.1 kcal/mol and should correspond to reaction 12.

Discussion

The major feature of the perhydroxyl radical kinetics is our lack of evidence for $H_2O_2^+$ in disagreement with other work. The magnitude of the discrepancy with other spectroscopic studies is best seen by comparing values of k/ϵ which is the slope of the normal second-order plot of the recriprocal of the optical density *vs.* time. Czapski and Dorfman find a value of 1.7×10^4 for k/ϵ at pH 5 and 254 mμ.[7] We find 1.35×10^4 at 241 mμ which would be 1.5×10^4 at 254 mμ according to the spectrum of Czapski and Dorfman. The agreement is satisfactory. At pH 2 we studied the kinetics at 254 mμ and found k/ϵ to be 1.3×10^3, which is a factor of 2.6 smaller than the value of 3.3×10^3 found by Czapski and Dorfman and the value of 3.5×10^3 found by Baxendale.[15] The discrepancy is not likely to

(13) E. J. Hart and M. S. Matheson, *Discussions Faraday Soc.*, 169 (1952).

(14) B. H. J. Bielski and E. Saito, *J. Phys. Chem.*, **66**, 2266 (1962).

(15) J. H. Baxendale, *Radiation Res.*, **17**, 312 (1962).

be instrumental as we agree at pH 5. Impurity effects would give large values of k/ϵ as would most instrumental troubles (stray light, inhomogeneities, etc.). We have searched diligently but have been unable to obtain values other than those reported here and conclude that they are right.

The chemical results given as the dashed curves in Figure 7 were obtained by the reaction of the HO_2 and O_2^- with tetranitromethane (TNM) in a flow system a known distance past the point of irradiation.[2,4]

$$HO_2 + C(NO_2)_4 \longrightarrow H^+ + O_2 + C(NO_2)_3^- + NO_2$$

The basic form of the radical reacts rapidly with TNM ($k = 2 \times 10^9\ M^{-1}\ sec^{-1}$) while HO_2 reacts very slowly (k is less than 2×10^4).[8] Perhaps in acid solution the HO_2 also reacts with the product NO_2 which would change the stoichiometry and hence the rate constant by a factor of 2.

Support for our results comes from an esr study of the HO_2 kinetics in which it was found that the rate constant was independent of sulfuric acid concentration from pH 0.5 to pH 1.55.[14] Though the rate constant found in the esr work was $2.4 \times 10^6\ M^{-1}\ sec^{-1}$, the uncertainty in the absolute value was 50% due to difficulties of calibration.

We conclude that there is no kinetic evidence for $H_2O_2^+$ and that $k_{10} = 2.8 \times 10^9 \exp(-4900/RT)$ and $k_{12} = 4 \times 10^8 \exp(-2100/RT)$.

The observation of the absorption spectrum of H_2O_3 offers a rapid and accurate method of studying the compound. At low acidities eq 1 reduces to

$$k_{H_2O_3} = k_4(H^+) + \frac{k_5 k_7}{k_6(H^+)}$$

In 0.5 M $HClO_4$ solutions the second term is negligible so that the upper curve of Figure 4 corresponds to 0.5 k_4. The curve obtained from 10^{-2} M acid is predominantly due to the second term, and from the two the maximum half-life of H_2O_3 in aqueous solutions is found to be 17 sec in 0.027 M acid at 0°. This time is sufficiently long to encourage future efforts directed toward isolation and conventional chemical studies.

Since the second term of eq 2 predominates in 10^{-2} M $HClO_4$, the lower curve of Figure 4 corresponds to $[(0.01k_4k_7)/k_6]$ or $0.01Kk_7$ as k_4/k_6 is the acid dissociation constant of H_2O_3. The activation energy of 16.5 kcal/mol would be equal to ΔH(ionization) + E_7. Since $k_4 = 9.2\ sec^{-1}$ and k_6 is a simple neutralization reaction, rate constants for which are generally above $10^{10}\ M^{-1}\ sec^{-1}$, $pK_{H_2O_3} \sim 9.5$ at 24°. This value fits well with the systematics of hydrogen oxygen compounds for which

$$pK = 19 - 7\frac{[O]}{[H]}$$

where [O] is the number of oxygen atoms in the molecule and [H] is the number of hydrogen atoms. The heat of ionization of H_2O_3 cannot be measured directly by kinetic methods, but since the entropy of ionization of water and hydrogen peroxide are so similar, one may assume that the entropy for H_2O_3 is the same.[16] In this case ΔH(ionization) = 5.2 kcal/mol and the activation energy for reaction 7 is 11 kcal/mol. The absolute value of k_7 at room temperature can be estimated to be $10^7\ sec^{-1}$ from $k_6/k_7 = 1700\ M^{-1}$ and the assumption that $k_6 = 2 \times 10^{10}\ M^{-1}\ sec^{-1}$. Combining this with the activation energy of 11 kcal/mol leads to $k_7 \approx 10^{16} \exp(-11{,}000/RT)$. The preexponential factor, though not a record, is large for a small molecule and suggests a large increase in entropy on forming the transition state.

The data presented here do not tell much about the energetics of H_2O_3 except that according to reactions 5, 6, and 7 the activation energy of 16.5 kcal/mol corresponds to a net process of

$$H_2O_3 \longrightarrow H^+ + OH^- + O_2$$

Since the heat of neutralization of H^+ and OH^- is 13.4 kcal/mol the decomposition of H_2O_3 according to reaction 2 is most likely exothermic, which is not surprising. Benson has estimated the heat of formation of H_2O_3 to be -13.5 ± 4 kcal/mol so that reaction 2 should be exothermic to 55 kcal/mol.[17]

Acknowledgment. We wish to thank Mr. D. A. Comstock for his excellent technical assistance throughout this work.

(16) K. Yu. Salmis, K. P. Meschenko, and I. E. Flis, *Zh. Neorg. Khim.*, **2**, 1985 (1957).

(17) S. W. Benson, *J. Amer. Chem. Soc.*, **86**, 3922 (1964).

Pulse-Radiolysis and Flash-Photolysis Study of Aqueous Solutions of Simple Pyrimidines. Uracil and Bromouracil

by R. M. Danziger, E. Hayon, and M. E. Langmuir

Pioneering Research Laboratory, U. S. Army Natick Laboratories, Natick, Massachusetts 01760
(Received May 7, 1968)

The pulse radiolysis of uracil and 5-bromouracil has been studied at pH 1.0, 5.5, and 11.0 in argon-, air- and N_2O-saturated aqueous solutions. The main precursor which gives rise to the observed transient optical absorption spectra in these systems was the OH radical. The transient species, which decay according to the second-order rate law, are considered to be formed from the addition of OH radicals to the 5,6 double bond of the pyrimidine molecule. In the flash photolysis of neutral and acidic solutions of 5-bromouracil, two major transients are produced with λ_{max} at 320 nm and 420 nm which decay by second-order processes. One of the main primary photolytic processes is homolytic cleavage of the C–Br bond to produce Br radicals, as evidenced by the formation of Br_2^- radical anions on photolysis in the presence of bromide ions. Photolysis of the bromouracil anion (RO^-) in air-free alkaline solution produces two major species with absorption maxima at 330 and 420 nm. The "330" transient appears to result from the photoionization of RO^- to $RO\cdot + e_{aq}^-$. A similar $RO\cdot$ transient species is formed in the pulse radiolysis of alkaline air-free aqueous solutions of RO^- ions, produced by abstraction of an electron from RO^- by OH radicals.

Introduction

Radiation chemical studies of some simple pyrimidines such as uracil, thymine, and cytosine in dilute aqueous solutions have shown[1-7] that OH radicals formed in the radiolytic decomposition of water add preferentially to the 5,6 carbon–carbon double bond to form the hydroxypyrimidyl radical. In oxygenated solution, this radical is scavenged by oxygen and eventually yields the 5,6 glycol as a major radiolysis product.[1,2] In a recent investigation on the X irradiation of aqueous solutions of uracil-2-^{14}C, Smith and Hays[8] have identified the following compounds: dihydrouracil, 6-hydroxy-5-hydrouracil (under N_2, not O_2 atmosphere), isobarbituric acid, *cis*- and *trans*-glycols of uracil, and alloxan. A qualitative and quantitative lack of agreement exists in the data from the different laboratories, due probably to the dependence of G values on pH, oxygen, solute concentration, and impurities.

The photochemistry of aqueous solutions of uracil and bromouracil has been studied by a number of investigators.[9-14] In some of the studies the excitation wavelength was not clearly defined, and the effect of oxygen on the nature of the products was not established. Addition of water to the 5,6 double bond was found to be induced by uv radiation at 2537 Å, and the hydration product has been reported to be 50% reversible in uracil and irreversible in 5-bromouracil on acidification and heating.[9,13] Dimers have been detected in the photolysis at room temperature of aqueous solutions of uracil[13] and bromouracil.[11] In the case of bromouracil, the dimer has been identified[11] as 5,5′-diuracil. No conclusive evidence has yet been obtained for the participation of triplet states in the photochemistry of uracil or bromouracil in aqueous solutions, and the nature of the primary photolytic processes which give rise to the observed chemical products is still undefined.

In view of the above situation, a preliminary study of the radiation chemistry and photochemistry of aqueous solutions of uracil and bromouracil has been initiated, using the fast-reaction techniques of pulse radiolysis and flash photolysis.

Experimental Section

Pulse-Radiolysis Setup. The Natick 24-MeV Varian linear accelerator has been used in this work, and full

(1) G. Scholes, J. F. Ward, and J. Weiss, *J. Mol. Biol.*, **2**, 379 (1960).

(2) (a) B. Ekert and R. Monier, *Nature*, **188**, 309 (1960); (b) R. Latarjet, B. Ekert, and P. Demerseman, *Radiation Res. Suppl.*, **3**, 247 (1963).

(3) A. Kamal and W. M. Garrison, *Nature*, **206**, 1315 (1965); J. Holian and W. M. Garrison, *Radiation Res.*, **27**, 527 (1966).

(4) G. Scholes, *Progr. Biophys.*, **13**, 59 (1963).

(5) J. Weiss, *Progr. Nucleic Acid Res. Mol. Biol.*, **3**, 103 (1964).

(6) H. Reuschl, *Z. Naturforsch.*, **21b**, 643 (1966).

(7) E. Gilbert, O. Volkert, and D. Schulte-Frohlinde, *ibid.*, **22b**, 477 (1967); O. Volkert, W. Bors, and D. Schulte-Frohlinde, *ibid.*, **22b**, 480 (1967).

(8) K. C. Smith and J. E. Hays, *Radiation Res.*, **33**, 129 (1968).

(9) A. D. McLaren and D. Shugar, "Photochemistry of Proteins and Nucleic Acids," Pergamon Press, Oxford, 1964, p 162.

(10) K. C. Smith, *Radiation Res. Suppl.*, **6**, 54 (1966).

(11) H. Ishihara and S. Y. Wang, *Nature*, **210**, 1222 (1966); *Biochemistry*, **5**, 2307 (1966).

(12) W. Rothman and D. R. Kearns, *Photochem. Photobiol.*, **6**, 775 (1967).

(13) A. A. Lamola and J. P. Mittal, *Science*, **154**, 1560 (1966).

(14) R. B. Setlow, *ibid.*, **153**, 379 (1966).

details of the experimental conditions will be published elsewhere.[15] Briefly, the Linac was operated at about 7 MeV, 200–500 mA current, providing single pulses of electron of 1–2-μsec duration. The total dose, measured using 2×10^{-4} M KBr solutions and $\epsilon_{Br_2^-}{}^{360} = 7.8 \times 10^3$ M^{-1} cm^{-1},[16] was about 8×10^{17} eV/ml per pulse in a rectangular optical cell with dimensions of 30 mm (path length) $\times$ 15 $\times$ 15 mm. Due to small fluctuations in the dose per pulse, the monitoring light beam was split in two and each beam was allowed to enter a monochromator and photomultiplier unit assembly. Two EMI 9558 QB photomultiplier tubes were employed throughout this work. One monochromator was kept at a fixed wavelength, to act as an internal dosimeter, and was used to normalize the fluctuation in output of the accelerator. A high-pressure xenon arc lamp (Osram XBO 450 W) operated from a highly current-regulated power supply was used as the monitoring light source.

Flash-Photolysis Setup. The flash-photolysis lamps and experimental layout used in this work have been described elsewhere.[17]

General Procedures. The optical absorption spectra of the transient species produced were obtained by the point-by-point method. Reaction rate constants were determined using a computer by least-squares approximation of first- and second-order reactions.[15,17] Solutions were prepared using water purified by triple distillation, radiolysis, and photolysis.[18] Reagents were the best available supplied by Calbiochem Co. and Baker and Adamson. The pH's were adjusted using perchloric acid and sodium hydroxide.

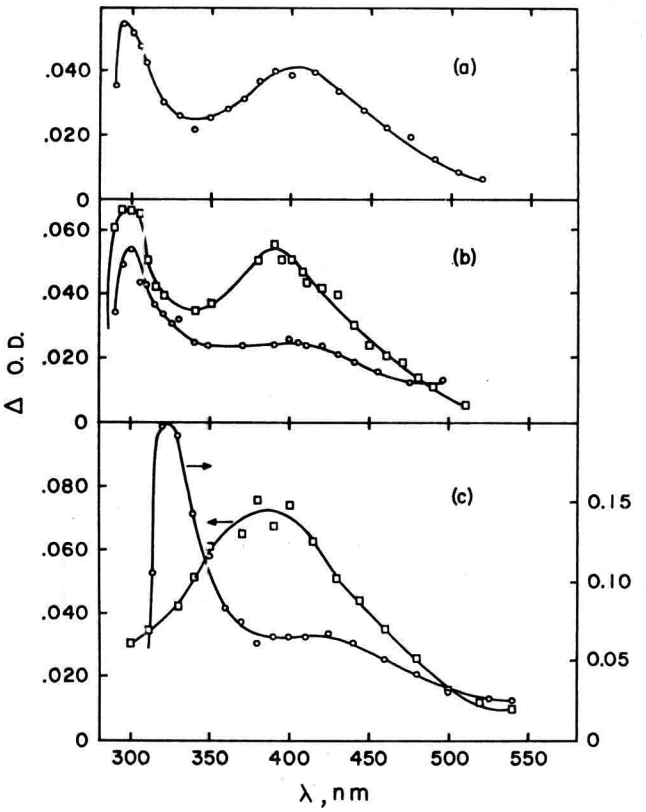

Figure 1. Optical absorption spectra of transient species produced in the pulse radiolysis of aqueous solutions of 2×10^{-4} M uracil in: (a) acid, pH 1.0; (b) neutral, pH 5.5; and (c) alkaline, pH 11.0. Solutions were saturated with argon (○), N_2O (□), and air (●); 1–1.5-μsec pulses of 7-MeV electrons were used, and OD's were measured 4 μsec after pulse.

Results and Discussion

Pulse Radiolysis of Uracil. In the pulse radiolysis of oxygen-free aqueous solutions of 2×10^{-4} M uracil (U) at pH 5.5 a transient optical absorption spectrum is observed which absorbs in the wavelength range 280–500 nm; see Figure 1b. This species has two absorption maxima at ~400 and ~300 nm, and its disappearance follows the second-order rate law, as shown in Table I. A similar absorption spectrum is obtained on pulse radiolysis of deaerated uracil solutions at pH 1.3, Figure 1a.

The radiation chemistry of water and aqueous solutions is known to produce the reactive intermediates e^-, H, and OH radicals, in addition to the "molecular" products H_2 and H_2O_2

$$H_2O \rightsquigarrow e_{aq}^-, \text{ H, OH, } H_2, \text{ and } H_2O_2 \qquad (1)$$

The following reactions can be considered to take place

$$e_{aq}^- + U \rightarrow (U^-) \qquad (2)$$

$$e_{aq}^- + N_2O \rightarrow N_2 + OH + OH^- \qquad (3)$$

$$OH + U \rightarrow (U \cdot OH) \qquad (4)$$

with $k_2 = 7.7 \times 10^9$ M^{-1} sec^{-1}, $k_3 = 5.6 \times 10^9$ M^{-1} sec^{-1}, and $k_4 = 3.5 \times 10^9$ M^{-1} sec^{-1}.[19] On pulse radiolysis of N_2O-saturated uracil solutions, a twofold increase in the 400-nm transient species was observed (Figure 1b) compared to argon-saturated solutions. Since $G(e_{aq}^-) \sim G(OH)$, and under the experimental conditions used (2×10^{-4} M U and 2×10^{-2} M N_2O) all the e_{aq}^- would react with N_2O, the species with λ_{max} ~400 nm can be attributed to the reaction of OH radicals with uracil.

Based on calculations of the electronic structure of the pyrimidine molecule,[20] the 5,6 carbon–carbon double bond has been shown to be the most reactive site of the pyrimidine molecule. Hence, it is suggested that the

(15) E. D. Black and E. Hayon, to be published.

(16) M. S. Matheson, W. A. Mulac, J. L. Weeks, and J. Rabani, *J. Phys. Chem.*, **70**, 2092 (1966).

(17) (a) L. Dogliotti and E. Hayon, *ibid.*, **71**, 2511 (1967); (b) M. E. Langmuir and E. Hayon, *ibid.*, **71**, 3808 (1967).

(18) E. Hayon, *Trans. Faraday Soc.*, **60**, 1059 (1964).

(19) M. Anbar and P. Neta, *Intern. J. Appl. Radiation Isotopes*, **18**, 493 (1967).

(20) B. Pullman and A. Pullman, "Quantum Biochemistry," Interscience Publishers, New York, N. Y., 1963.

Table I: Second-Order Decay Rates of Transient Species Produced in the Pulse Radiolysis of Aqueous Solutions of 2×10^{-4} M Uracil

pH	System	λ, nm	$2k/\epsilon$	Absolute rate, M^{-1} sec^{-1} [c]
1.3	Argon-saturated	305	$5.6 \pm 1.3 \times 10^5$	9.0×10^8 [d]
1.3	Argon-saturated	340	$1.3 \pm 0.3 \times 10^6$	...
1.3	Argon-saturated	390	$1.6 \pm 0.4 \times 10^6$	...
5.5	Argon-saturated	310	$1.3 \pm 0.4 \times 10^6$	2.1×10^9 [d]
5.5	Argon-saturated	410	$1.8 \pm 0.4 \times 10^6$	1.8×10^9 [e]
5.5	N_2O-saturated	310	$2.2 \pm 0.5 \times 10^6$	...
5.5	N_2O-saturated	400	$1.3 \pm 0.3 \times 10^6$	...
11.0	Argon-saturated	320	$1.1 \pm 0.2 \times 10^6$	8.2×10^9 [f]
11.0	Argon-saturated	400	$8.6 \pm 1.8 \times 10^5$ [a]	...
11.0	Argon-saturated	400	$3.0 \pm 1.0 \times 10^5$ [b]	...
11.0	N_2O-saturated	390	$8.6 \pm 2.2 \times 10^5$ [a]	2.2×10^9 [g]
11.0	N_2O-saturated	390	$3.2 \pm 0.8 \times 10^6$ [b]	...

[a] Fast-decaying transient. [b] Slow-decaying transient. [c] Deviation ±15%. [d] Based on $\epsilon^{300} = 1.9 \times 10^3$ M^{-1} cm^{-1}. [e] Based on $\epsilon^{400} = 1.0 \times 10^3$ M^{-1} cm^{-1}. [f] Based on $\epsilon^{300} = 7.5 \times 10^3$ M^{-1} cm^{-1}. [g] Based on $\epsilon^{390} = 2.6 \times 10^3$ M^{-1} cm^{-1}.

"400-nm" transient is the result of OH-radical addition to the 5 or 6 position

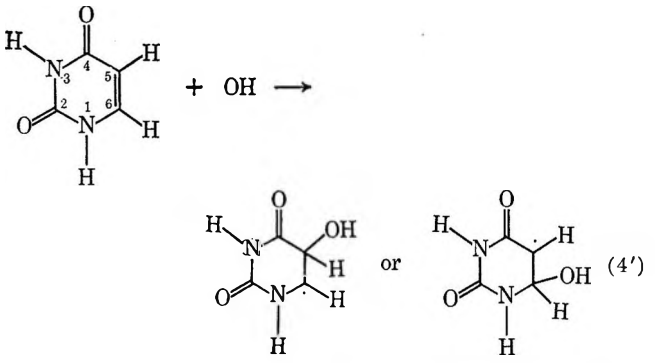

Support for reaction 4′ can be derived from the observed formation of pyrimidine glycols and of hydroxy-hydro compounds.[4,8] Due to the irreproducibility in the formation of the 300-nm species in the pulse radiolysis of neutral air-free solutions, it is not possible to establish its radical precursor.

Uracil is very reactive toward e_{aq}^- with $k_2 = 7.7 \times 10^9$ M^{-1} sec^{-1}, but no intermediate has been observed within the time resolution of this work ($\gtrsim$ 1–2 μsec) in the radiolysis of neutral air-free solutions, which can be definitely attributed to such a reaction. In alkaline solution, however, a strong absorbing species is produced, with $\lambda_{max} \sim 320$ nm, on pulse radiolysis of oxygen-free 2×10^{-4} uracil at pH 11.0, as shown in Figure 1c. In N_2O-saturated solution, at pH 11.0, this transient absorption at 320 nm is not observed. Consequently, it is tentatively suggested that the 320-nm transient is the mononegative uracil radical anion (U^-). This species is not observed at lower pH's, due possibly to the protonation of U^-. Further work is in progress to establish this point.

Two other transient species are produced in the pulse radiolysis of Ar- or N_2O-saturated uracil solutions at pH 11.0. One species has a maximum at $\lambda_{max} \sim 400$ nm and is shown in Figure 1c. The other transient species decays more slowly than the λ_{max} 400-nm species and appears to have a rather broad band in the region 400–580 nm. Both species decay by second-order processes, and their decay rates are given in Table I. A permanent product(s) which absorbs at wavelengths below 360 nm is also produced in N_2O- and Ar-saturated solutions of uracil at pH 11.0.

The first pK of uracil due to dissociation at the C_2 position is at pK = 9.5.[21] At pH 11.0 one could therefore expect different sites of radical attack on the uracil anion, RO^-, compared to its un-ionized form present in neutral solutions. It is suggested that at pH 11.0 the OH radicals can add to the 5,6 double bond or abstract an electron from the C_2-carbonyl to produce an RO radical

$$OH + RO^- \longrightarrow RO\cdot + OH^- \qquad (5)$$

In the pulse radiolysis of neutral and acidic solutions of uracil in the presence of oxygen, a very short-lived intermediate with a lifetime of <3 μsec was observed in the wavelength range 300–500 nm. Due to its fast decay, it was not possible to study its physical properties. This transient species is probably the hydroxyperoxy radical of uracil, produced by successive addition of OH radical and O_2 to the 5,6 double bond, and could be the precursor of uracil hydroperoxide which is known to be formed in oxygenated neutral and acidic solutions of uracil.[1,22]

Pulse Radiolysis of Bromouracil Solutions. The pulse radiolysis of neutral, argon-saturated aqueous solutions of 2×10^{-4} M bromouracil (BrU) produces a

(21) K. Berens and D. Shugar, *Acta Biochim. Polon.*, **10**, 25 (1963).
(22) R. Latarjet, B. Ekert, S. Apelgot, and N. Reybeyrotte, *J. Chim. Phys.*, **58**, 1046 (1961).

Table II: Second-Order Decay Rates of Transient Species Produced in the Pulse Radiolysis of Aqueous Solutions of 2×10^{-4} *M* 5-Bromouracil

pH	System	λ, nm	$2k/\epsilon$	Absolute rate, M^{-1} sec^{-1} [a]
1.0	Argon-saturated	320	$3.6 \pm 0.7 \times 10^5$	2.0×10^9 [b]
1.0	Argon-saturated	440	$1.8 \pm 0.5 \times 10^6$	...
1.0	Air-saturated	320	$1.5 \pm 0.3 \times 10^6$	1.4×10^{10} [f]
1.0	Air-saturated	420	$5.4 \pm 1.1 \times 10^6$	...
5.5	Argon-saturated	330	$2.8 \pm 0.4 \times 10^5$	1.5×10^9 [b]
5.5	Argon-saturated	380	$5.5 \pm 0.9 \times 10^5$	...
5.5	N_2O-saturated	330	$2.3 \pm 0.4 \times 10^5$	...
5.5	N_2O-saturated	380	$5.5 \pm 0.8 \times 10^5$	...
5.5	Air-saturated	330	$2.7 \pm 0.5 \times 10^6$	1.9×10^9 [c]
10.4	Argon-saturated	330	$1.2 \pm 0.3 \times 10^6$	1.2×10^9 [d]
10.4	Argon-saturated	430	$1.4 \pm 0.4 \times 10^5$	...
10.4	N_2O-saturated	330	$5.5 \pm 1.5 \times 10^4$	...
10.4	N_2O-saturated	440	$2.3 \pm 0.5 \times 10^5$	...
10.4	Air-saturated	330	$1.7 \pm 0.4 \times 10^5$	1.3×10^9 [e]
10.4	Air-saturated	430	$4.7 \pm 1.0 \times 10^5$	...

[a] Deviation ±15%. [b] Based on $\epsilon^{330} = 5.4 \times 10^3\ M^{-1}\ cm^{-1}$ at pH 5.5. [c] Based on $\epsilon^{330} = 6.9 \times 10^3\ M^{-1}\ cm^{-1}$ at pH 5.5. [d] Based on $\epsilon^{330} = 9.7 \times 10^3\ M^{-1}\ cm^{-1}$ at pH 10.4. [e] Based on $\epsilon^{330} = 7.5 \times 10^3\ M^{-1}\ cm^{-1}$ at pH 10.4. [f] Based on $\epsilon^{330} = 9.0 \times 10^3\ M^{-1}\ cm^{-1}$ at pH 1.0.

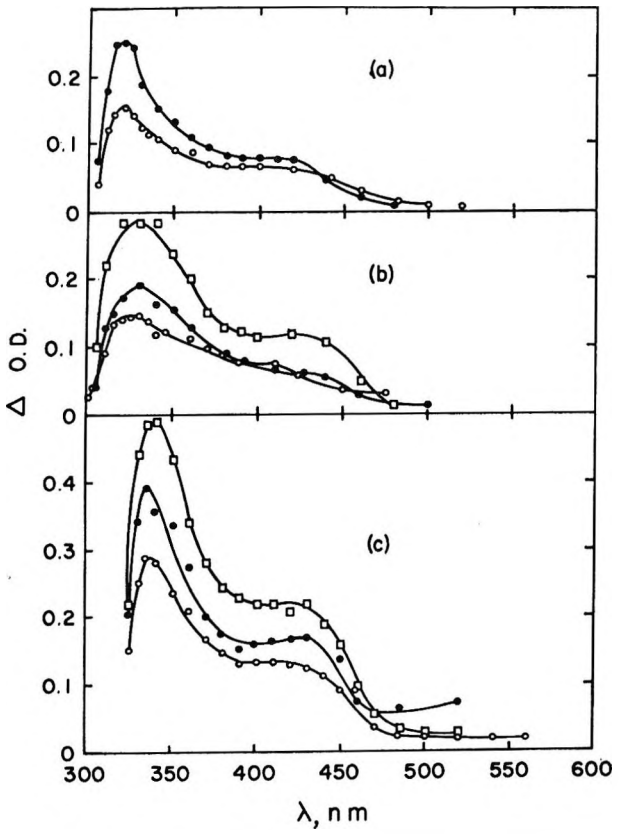

Figure 2. Optical absorption spectra of transient species produced in the pulse radiolysis of aqueous solutions of 2×10^{-4} *M* bromouracil in: (a) acid, pH 1.0; (b) neutral, pH 5.5; and (c) alkaline, pH 11.0. Solutions were saturated with argon (○), N_2O(□), and air (●); 1–1.5-μsec pulses of 7-MeV electrons were used, and OD's were measured 4 μsec after pulse.

transient absorption spectrum with $\lambda_{max} \sim 330$ nm, Figure 2b. From a study of the decay rate, at different wavelengths, it would appear that only one species is formed in this system; see Table II. On irradiation in the presence of N_2O, about a twofold increase in the amount of transient is observed. This would seem to indicate that OH radicals are the precursors of this species. A very similar absorption spectrum is obtained on pulse radiolysis of air-free 2×10^{-4} *M* bromouracil at pH 1.0, Figure 2a.

The intermediate produced is considered to be the OH radical adduct of bromouracil, at the 5,6 double bond of the molecule

$$OH + BrU \longrightarrow (BrU \cdot OH) \qquad (6)$$

with $k_6 = 3.6 \times 10^9\ M^{-1}\ sec^{-1}$.[23] In air-saturated neutral and acidic solutions of bromouracil, a similar optical absorption spectrum is obtained, Figure 2a and b. The species appears to have a higher extinction coefficient but decays at the same rate as the species produced in oxygen-free solutions (see Table II). The species in air is suggested to be the hydroxy-peroxy bromouracil radical, produced by successive addition of an OH radical and O_2 at the 5,6 position.

In alkaline solutions, at pH 10.4, the transient species formed has $\lambda_{max} \sim 335$ nm and shows the similar twofold increase in N_2O compared to argon-saturated solutions. Based on the results and mechanism proposed for the flash photolysis of alkaline bromouracil solutions (see

(23) I. Kraljic, "The Chemistry of Ionization and Excitation," G. R. A. Johnson and G. Scholes, Ed., Taylor and Francis Ltd., London, 1967, p 305.

below), it is suggested that the species observed at pH 10.4 in pulse radiolysis is produced mainly by the reaction of OH radicals with the C_2-carbonyl bromouracil anion RO^- (pK = 8.1[20]) to form the RO· radical, reaction 7.

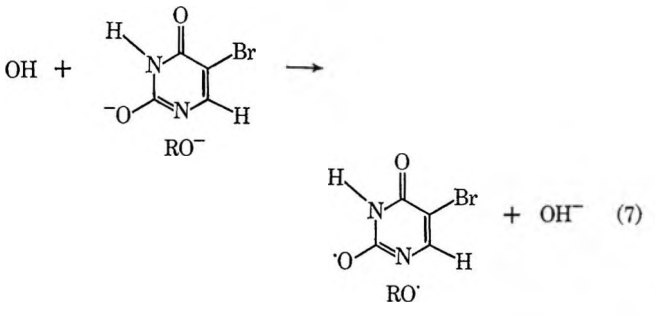

No evidence has so far been obtained in this investigation for the formation of transient species produced by the reaction of H atoms with either uracil or bromouracil. The solvated electron is expected to react with BrU to debrominate it and produce Br^- ions plus uracil radicals. Dehalogenation by e_{aq}^- in aliphatic halogenated compounds is well known, but no conclusive evidence has been obtained for similar dehalogenation of aromatic or heterocyclic compounds.

Figure 3 shows the dependence of the amount of transient produced upon concentration of uracil and bromouracil. The increase in yields in the concentration range of 2×10^{-4} to 2×10^{-3} M is considered to be mainly a result of scavenging by the solutes of the precursors of molecular hydrogen peroxide. The extinction coefficients obtained in 2×10^{-4} M solutions of uracil and bromouracil were calculated on the basis of $G(OH) = 2.3$.

Flash Photolysis of Bromouracil. The main absorption band of 5-bromouracil at pH 5.5 has a maximum at ~280 nm and a minimum at ~240 nm. Below 240 nm, BrU absorbs strongly down to 200 nm and below. On flash photolysis of 10^{-4} M BrU at pH 5.5 using a 20% acetic acid solution filter (cutoff 238 nm) no transient species were observed in the region 280–600 nm. On flash photolysis of BrU solutions at pH 5.5 in the absence of a solution filter, two transient species are produced which absorb in the wavelength region 300–500 nm, with maxima at 320 and 420 nm. The transient optical absorption spectra observed in air-free and air-saturated solutions are shown in Figure 4. The above-mentioned observation indicates that it is the bromouracil absorption band below ~240 nm which gives rise to the transient species detected on photolysis. It further indicates that these transients are not the precursors of the dimers or hydration products reported[9,13] to be formed on photoexcitation at 2537 Å.

In the presence of air at pH 5.6, the 320-nm peak increases and the 420-nm peak decreases in optical density with respect to that observed under deaerated conditions. The 420-nm transient decay rate is also

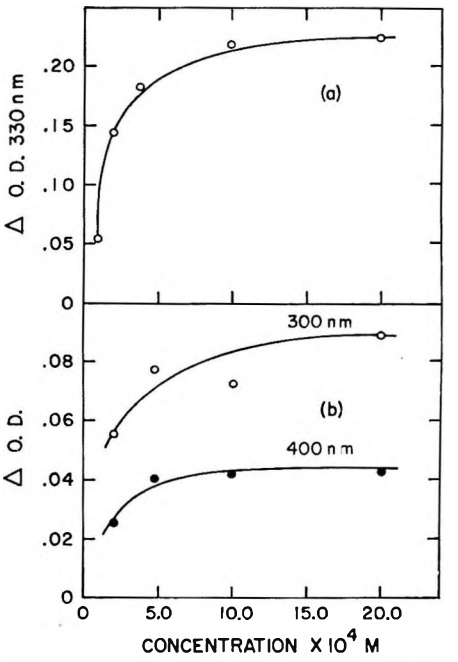

Figure 3. Dependence upon solute concentration of the yield of transient species produced in the pulse radiolysis of argon-saturated aqueous solutions of (a) bromouracil and (b) uracil.

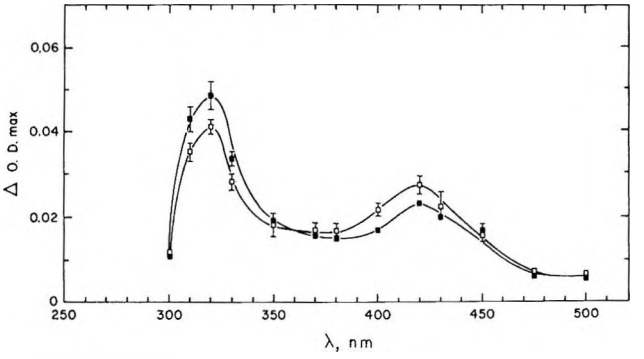

Figure 4. Flash photolysis of 10^{-4} M 5-bromouracil at pH 5.7 in N_2-saturated (□) and air-saturated (■) aqueous solutions; OD measured 200 μsec after start of flash.

increased by a factor of 2 (Table IV) in the presence of air, while air does not affect the decay rate of the 320-nm species. From these facts we conclude that the 320- and 420-nm peaks are due to two transients (see also below). A very similar transient spectrum is obtained on flask photolysis of 1×10^{-4} M BrU in the presence or absence of oxygen at pH 1.5 (see Figure 5). The second-order decay rates of the two species produced in acid solution are also very close to those obtained in neutral solutions (Tables III and IV).

Flash Photolysis of BrU in the Presence of Ethanol. Under deaerated conditions, ethanol in the concentration range 1.7×10^{-3} to 1.7×10^{-1} M was added to 1×10^{-4} M BrU at pH 5.5. The addition of ethanol decreases at the same rate the amount of transient

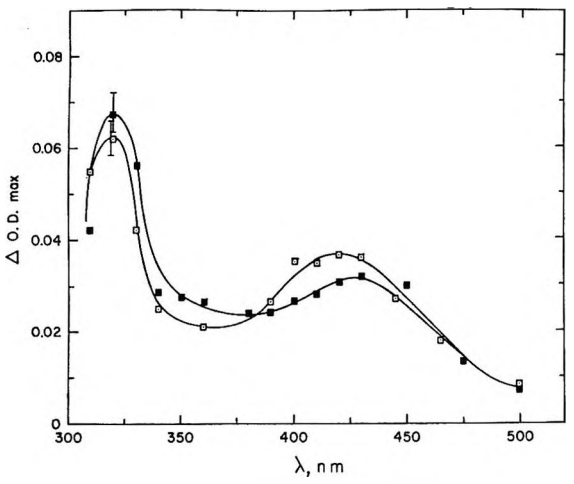

Figure 5. Flash photolysis of 10^{-4} M bromouracil at pH 1.5 in N_2-saturated (⊡) and air-saturated (■) aqueous solutions; OD measured 200 μsec after start of flash.

Table III: Second-Order Decay Rates of Transient Species Produced in the Flash Photolysis of Aqueous Solutions of 10^{-4} M 5-Bromouracil

pH	System	λ, nm	$2k/\epsilon$
1.5	Air-saturated	320	$7.7 \pm 1.0 \times 10^5$
1.5	N_2-saturated	320	$6.1 \pm 1.2 \times 10^5$
1.5	N_2O-saturated	320	$6.4 \pm 1.0 \times 10^5$
5.6	Air-saturated	320	$6.1 \pm 0.9 \times 10^5$
5.6	N_2-saturated	320	$6.9 \pm 1.4 \times 10^5$
10.5	Air-saturated	330	$3.2 \pm 0.9 \times 10^5$
10.5	N_2-saturated	330	$1.3 \pm 0.3 \times 10^5$
10.5	N_2O-saturated	330	$1.6 \pm 0.3 \times 10^5$

Table IV: Second-Order Decay Rates of Transient Species Produced in the Flash Photolysis of Aqueous Solutions of 10^{-4} M 5-Bromouracil

pH	System	λ, nm	$2k/\epsilon$[a]
1.5	Air-saturated	420	$1.4 \pm 0.2 \times 10^6$
1.5	N_2-saturated	420	$1.3 \pm 0.4 \times 10^6$
1.5	N_2O-saturated	420	$1.4 \pm 0.3 \times 10^6$
5.6	Air-saturated	420	$2.1 \pm 0.6 \times 10^6$
5.6	N_2-saturated	420	$1.3 \pm 0.6 \times 10^6$
5.6	N_2O-saturated	420	$1.2 \pm 0.4 \times 10^6$
10.5	Air-saturated	420	$4.9 \pm 1.0 \times 10^5$
10.5	N_2-saturated	420	$3.4 \pm 0.7 \times 10^5$
10.5	N_2O-saturated	420	$7.3 \pm 1.0 \times 10^5$

[a] All values lie within the limits given.

species formed at 320 and 420 nm. In 1.7×10^{-1} M ethanol, no transients were observed. The decay kinetics in the presence of ethanol were complex, *i.e.*, neither first nor second order.

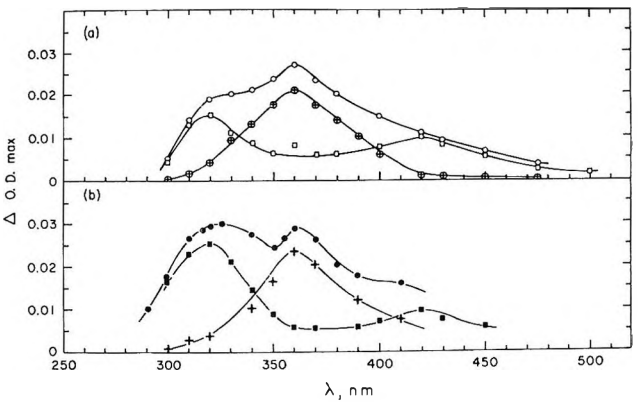

Figure 6. Flash photolysis of 5-bromoacil (BU) solutions, pH 5.7, in 20-cm optical cells, using 10^{-2} M KBr filter (cutoff 218 nm); OD_{max} measured at 200 μsec after start of flash. (a) 10^{-4} M BU, N_2-saturated (□); 10^{-4} M BU plus 10^{-4} M KBr, N_2-saturated (○); (⊕) is difference in OD, *i.e.*, ⊕ = ○ − □; (b) 10^{-4} M BU, air-saturated (■); 10^{-4} M BU plus 10^{-4} M KBr, air-saturated (●); (+) = ● − ■.

Flash Photolysis of BrU in the Presence of Br^- Ions. This experiment was carried out to test whether one of the primary photolytic processes resulting from the optical excitation of BrU involves cleavage of the C_5 carbon–bromine bond. Neutral solutions containing 1×10^{-4} M BrU in the presence of 10^{-4} M KBr were flashed using a 10^{-2} M KBr solution filter (cutoff 218 nm). The transient absorption spectrum obtained is given in Figure 6. On subtraction of the absorption spectrum obtained on flash photolysis of BrU in absence of Br^- ions from this "overall" spectrum, one obtains a "difference" spectrum with $\lambda_{max} \sim 360$ nm which is identical with that due to Br_2^- radical anions.[17b] The second-order decay rate of Br_2^- radicals produced in the photolysis of BrU is $2k = 2 \times 10^9$ M^{-1} sec^{-1}, taking $\epsilon^{360} = 7.8 \times 10^3$ M^{-1} cm^{-1}.[16] This compares with the literature value of $2k(Br_2^- + Br_2^-) = 3 \times 10^9$ M^{-1} sec^{-1}.[17b] These runs were performed using a 10^{-2} M KBr filter solution to prevent formation of Br_2^- radicals from the direct photolysis of Br^- ions. No Br_2^- is produced on flash photolysis of 10^{-4} M KBr in the absence of 10^{-4} M BrU, using a 218-nm cutoff filter. From the OD of Br_2^- radicals produced under the stated conditions, one can calculate that 0.14 μM Br_2^- radicals are produced per flash.

The above results indicate fairly conclusively that (a) one of the primary photolytic processes resulting from the absorption by bromouracil of uv radiation below 240 nm leads to the homolytic cleavage of the C_5 carbon–bromine bond

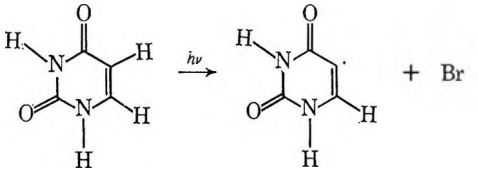

(8)

In the presence of bromide ions, Br atoms form Br_2^- radical anions

$$Br + Br^- \longrightarrow Br_2^- \quad (9)$$

(b) Bromine atoms are not the precursors of either the 320- or 420-nm species produced in the flash photolysis of BrU in the absence of Br^- ions. This is shown by the OD's at 320 and 420 nm which remain the same in the presence or absence of Br^- ions. The Br_2^- radicals also decay by recombination with each other, and not by reaction with either BrU or with the transient species. Further confirmation for reaction 8 is the observation and determination of 5,5′-diuracil by Ishihara and Wang[11] in the photolysis of aqueous solutions of 5-bromouracil.

On flash photolysis of 1,3-dimethyl-5-bromouracil,[24] only one transient species is produced with λ_{max} ~320 nm. Cleavage of the C–Br bond also occurs. From these results it is tempting to suggest that the 320-nm transient produced on flash photolysis of BrU or dimethyl bromouracil is due to the uracil radical

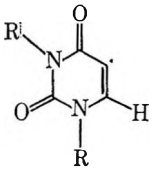

If this assignment is correct, one should observe this species in the pulse radiolysis of air-free neutral BrU solutions where debromination by e_{aq}^- if it occurs would produce the same transient species. However, there is no evidence for the formation of this species in pulse radiolysis.

Flash Photolysis of BrU in Alkaline Solutions. The flash photolysis of air-free 10^{-4} *M* BrU at pH 10.5 has been studied, and the transient optical spectrum obtained with maxima at 330 and 420 nm is shown in Figure 7a. On photolysis of the same system in N_2O-saturated solutions, the 330-nm peak is about doubled while the 420-nm peak remains unchanged, Figure 7a. N_2O-saturation of the solution causes no change in the decay rates of the two transients at 330 and 420 nm; see Tables III and IV. From the known reactivity of N_2O toward solvated electrons, it is suggested that in alkaline solutions the primary photolytic process resulting from photoexcitation of the bromouracil anion RO^- (pK = 8.1) leads to an electron ejection

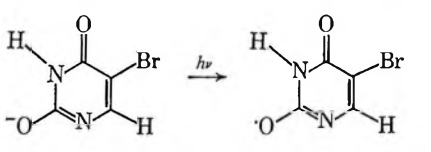

followed by

$$e_{aq}^- + N_2O \longrightarrow OH + N_2 + OH^- \quad (3)$$

$$OH + RO^- \longrightarrow RO\cdot + OH^- \quad (7)$$

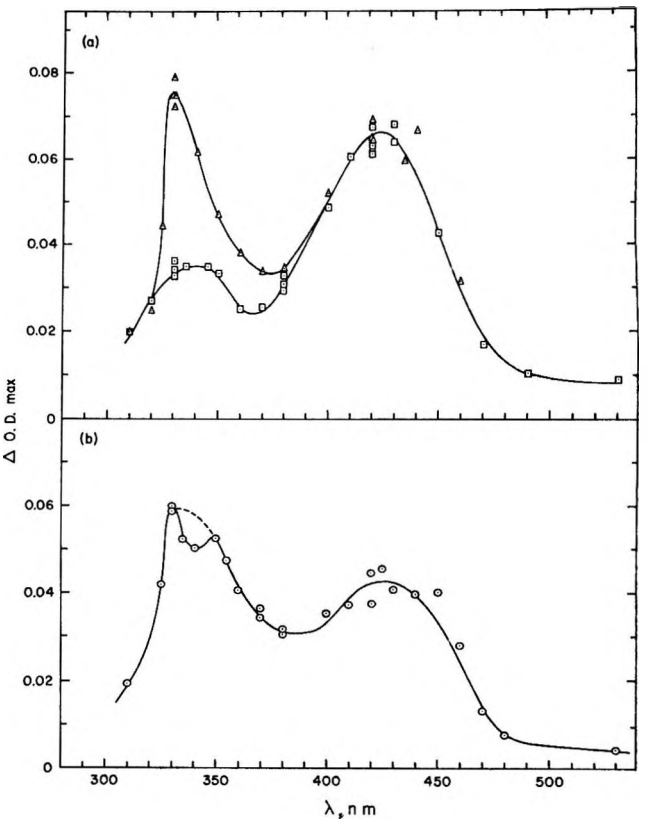

Figure 7. Flash photolysis of 10^{-4} *M* 5-bromouracil at pH 10.5 in (a) N_2-saturated (⊡), N_2O-saturated (△), and (b) air-saturated (⊙) solutions; OD measured 200 μsec after start of flash.

The above sequence of reactions is consistent with the experimental observations. The transient absorption spectra and decay rates of the 330-nm species produced in the pulse radiolysis and flash photolysis of air-free bromouracil at pH 10.4 are in good agreement with each other. On the basis of the above results the 330-nm species produced in alkaline solution is attributed to the RO· radical, with the free electron on the C_2-carbonyl group.

The photolysis of BrU in alkaline solutions is expected to yield the same type of C–Br cleavage which occurs in neutral solutions. No Br_2^- was found in the flash photolysis of BrU in presence of Br^- ions at pH 10.4. In the direct photolysis of Br^- ions at pH 10.4, the yield of Br_2^- is considerably reduced compared to neutral solution. This reduction in the yield of Br_2^- in alkaline solutions does not allow one to establish, within our experimental limits, reaction 8 at pH 10.4.

Figure 7b shows the transient optical absorption spectrum produced on flash photolysis of air-saturated BrU at pH 10.4. It would appear that two species are produced in the wavelength region 300–370 nm, in addition to the 420-nm species. Under the conditions of

(24) M. E. Langmuir and E. Hayon, unpublished results.

this experiment (10^{-4} M BrU, 2.5×10^{-4} M O_2), most of the e_{aq}^- produced in reaction 9 are expected to react with O_2

$$e_{aq}^- + O_2 \longrightarrow O_2^- \qquad (11)$$

with $k_{11} = 2 \times 10^{10}$ M^{-1} sec^{-1}.[19] One of the species absorbing in the 300–370-nm region could therefore be produced by reaction of a primary produced radical with O_2^- radicals.

Flash Photolysis of Uracil. A very weak transient is observed on flash photolysis of 10^{-4} M uracil at pH 5.5 in the presence or absence of air, under the experimental conditions of the flash units used.[17] This transient has a maximum at ~310 nm and is long-lived, $t_{1/2}$ ~0.5 sec. Using different filter solutions, it was established that this species is produced by optical excitation of the uracil band below ~225 nm. Because of the low absorption of the transient species, it was not possible to study it on a quantitative basis.

Flash Photolysis of 5-Iodouracil. A few experiments have been carried out on the flash photolysis of 5-iodouracil in neutral solution. Transient species are produced in the region 300–450 nm. On flash photolysis in the presence of iodide ions, I_2^- radicals are produced indicating that one of the primary photolytic processes occurring is the scission of the carbon–iodine bond to produce iodine atoms. Again, as in the case for bromouracil, the observed transient species are produced by photoexcitation of iodo–uracil in the absorption band <245 nm.

Electrons, Ions, and Excited States in the Pulse Radiolysis of Dioxane

by J. H. Baxendale and M. A. J. Rodgers

Chemistry Department, The University, Manchester, United Kingdom *(Received May 7, 1968)*

Changes in the absorption attributable to the solvated electron in dioxane toward shorter wavelengths are produced by the addition of water and lithium aluminum hydride. With water the change occurs gradually as the water content increases, as might be expected from a change in solvation environment. With lithium aluminum hydride the lifetime of the electron is increased appreciably due to the replacement of reactive cations by the inert Li^+ which probably also accounts for the wavelength shift. Anthracene anions, formed with $G = 0.12$ in pure dioxane are also stabilized and their yield increased by the hydride. The mechanism of anthracene triplet formation has been studied by observing the effect of additives on the triplet yield. Water and lithium aluminum hydride have little effect, and it is concluded from this that ions of solute or solvent are not precursors. Kinetic observations and the effects of benzene and acetone are consistent with the assumption that excited states of the solvent are involved in its formation.

In preliminary pulse radiolysis work on 1,4-dioxane, we observed[1] transient absorptions which were ascribed to solvated electrons, ions of solutes such as benzophenone and anthracene, and the triplet state of anthracene. A recent γ-radiolysis study[2] showed that the reactions of electrons and their concomitant solvent cations may be interfered with by added solutes to produce changes in product yields so that yields of charged species considerably higher than indicated by pulse radiolysis and conductivity measurements[3] could be measured.

Work on fluorescence[4] of aromatics in dioxane had concluded that the excited solvent molecules, which were presumed precursors of the fluorescence, did not contribute significantly to the radiolysis products. Estimates of the kinetic parameters for the energy transfer process were also made. However, some doubt is thrown on the validity of these conclusions by the subsequent discovery that the dioxane used was not pure.[5] The present study extends the pulse radiolysis work with a view to examining the effects of the solutes which were used in the γ radiolysis. Also, measurements on the formation of the anthracene triplet seemed to offer an alternative to fluorescence measurements as a means of studying excited states in this medium.

Experimental Section

Materials. The rigorous procedure used to purify the

(1) J. H. Baxendale, E. M. Fielden, and J. P. Keene, *Science*, **148**, 637 (1965).

(2) J. H. Baxendale and M. A. J. Rodgers, *Trans. Faraday Soc.*, **63**, 2004 (1967).

(3) (a) A. Hummel, A. O. Allen, and F. H. Watson, *J. Chem. Phys.*, **44**, 3431 (1966); (b) G. R. Freeman and J. M. Fayadh, *ibid.*, **43**, 86 (1965).

(4) E. A. Rojo and R. R. Hentz, *J. Phys. Chem.*, **69**, 3024 (1965).

(5) R. R. Hentz, F. W. Mellows, and W. V. Sherman, *ibid.*, **71**, 3365 (1967).

1,4-dioxane has been described elsewhere.[2] Care was taken to prevent the access of air and water at all stages by handling in an excess pressure of pure nitrogen. Blue fluorescent anthracene (B.D.H.) was recrystallised from ethanol, and analytical reagent quality hydrochloric acid and benzene were used without further treatment. Lithium aluminum hydride was used as supplied.

Apparatus and Procedures. The radiation source was a 4-MeV linear accelerator giving 0.5- or 2-μsec electron pulses at doses up to about 6000 rads/pulse. The associated optics, electronics, and glassware for pulse radiolysis studies has been described in detail elsewhere.[6] Reaction cells of 16- and 25-mm optical path were used in the present work.

Spectra of transient species were obtained by the mapping procedure, *i.e.*, reading the absorptions from the C.R.O. traces following an electron pulse at each wavelength. The yields of species were calculated from absorption measurements taken from photographed traces using doses calibrated with the Fricke dosimeter. For the calculation of triplet anthracene yields an absorption coefficient of 76,000 M^{-1} cm^{-1} was used.[7]

Results

Solvated Electrons in Dioxane. The previously observed small transient absorption increasing from 500 to 800 nm has been attributed to the solvated electron.[1] The evidence for this assignment is that the absorption is in the region to be expected for this solvent, it is prevented by a small amount of hydrochloric acid or oxygen, and it is replaced by an absorption due to the anion of anthracene or benzophenone when these solutes are present to capture the electron.

We have confirmed these observations and have extended the wavelength range to 1100 nm without observing a maximum in the absorption (Figure 1). We also find that nitrous oxide, another efficient electron scavenger, prevents its appearance.

In pure dioxane the absorption decays very rapidly and has disappeared within 2 μsec of the end of the pulse. This lifetime is considerably shorter than that of the solvated electron in water in similar concentration conditions, where it is removed by reaction with itself, with water, and with the species H_3O^+, H, and OH produced simultaneously. Dioxane is fairly stable to the alkali metals and it seems unlikely that it will react rapidly with the electrons so that reaction with radiolysis products must occur. The much lower yield of electrons in dioxane as measured either by conductivity[3a,b] (G = 0.04) or by the yield of benzophenone anion[1] (G = 0.1) compared with that in water (G = 2.6) reflects the greater difficulty in escaping the coulombic field of the cation which accompanies the electron,[3] so that most electrons are removed by charge neutralization before they can be detected. On this interpretation it should be possible to increase the observable yield of electrons and probably increase their lifetime, if the original cation could be removed and replaced by one which is less reactive to electrons. Lithium aluminum hydride is a solute which might be expected to give this result since it will react rapidly with the organic cation, and the net effect would be to replace it by the ion Li^+, possibly by a reaction such as

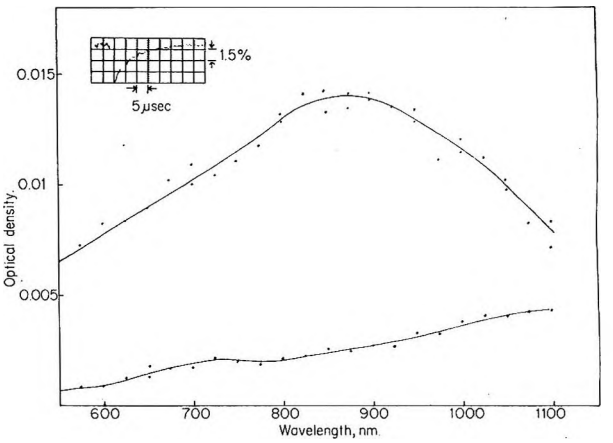

Figure 1. Solvated electron absorption in dioxane. Spectra immediately following a 2-μsec electron pulse of 6 krads, in pure dioxane (lower curve) and a 10^{-3} M $LiAlH_4$ solution (upper curve). Inset: decay of absorption at 950 nm in presence and $LiAlH_4$; 5 μsec per division and *ca.* 1.5% absorption per division.

$$Li^+AlH_4^- + RH^+ \longrightarrow Li^+ + AlH_3 + R + H_2$$

We find, as shown in Figure 1, that both the absorption and its lifetime are markedly changed in the presence of $LiAlH_4$. The absorption is increased and shifted to shorter wavelengths so that a peak is now present at 900 nm. Simultaneously, the half-life of the absorption is increased to about 10 μsec. Furthermore, nitrous oxide again prevents any absorption from appearing in this region of the spectrum; hence it would appear probable that the new absorption is still that of solvated electrons. In these circumstances the lifetime of the electron is presumably determined either by reaction with free radicals produced at the same time or by neutralization by Li^+. The latter is suggested by the fact that solutions of alkali metals are not as stable in dioxane as they are in certain other ethers. The shift of the absorption from the infrared is probably due to the more polar environment provided by the Li^+ ion. Similar shifts have been observed in the absorption of hydrated electrons in the presence of LiCl.[8]

In view of the ability of water to change the γ radiolysis of dioxane,[2] it was of interest to investigate its

(6) J. P. Keene in "Pulse Radiolysis," M. Ebert, J. P. Keene, A. J. Swallow, and J. H. Baxendale, Ed., Academic Press, London, 1965, p 1.

(7) G. Porter and M. W. Windsor, *Proc. Roy. Soc.*, **A245**, 238 (1958).

(8) M. Anbar and E. J. Hart, *J. Phys. Chem.*, **69**, 1244 (1965).

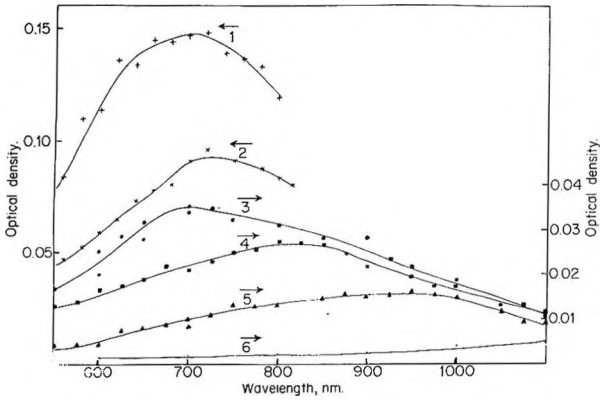

Figure 2. Solvated electron absorptions in dioxane–water mixtures. Spectra taken immediately following a 2-μsec electron pulse of 6 krads: 1, 74 mol % H_2O; 2, 53 mol % H_2O; 3, 34 mol % H_2O; 4, 21 mol % H_2O; 5, 9 mol % H_2O; 6, pure dioxane.

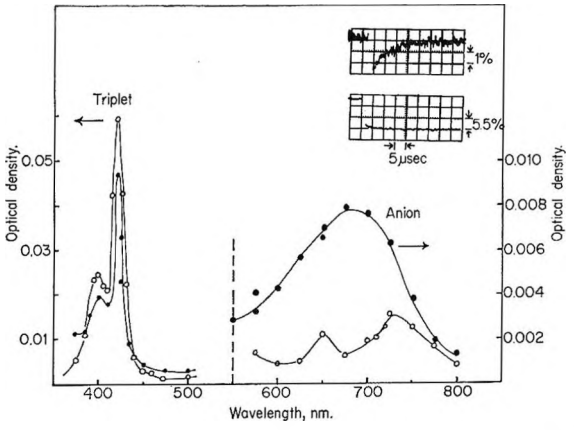

Figure 3. Transient absorptions of solute anion and triplet species produced in dioxane solutions of anthracene. Spectra 10 μsec following a 2-μsec electron pulse of 6 krads: open circles, 10^{-3} M anthracene in dioxane; filled circles, 5×10^{-4} M anthracene and *ca.* 10^{-3} M $LiAlH_4$ in dioxane. Inset: (a) anion decay at 720 nm without $LiAlH_4$; (b) anion decay at 720 nm with 2×10^{-2} M $LiAlH_4$.

effect on the electron absorption. Figure 2 shows that there is a gradual shift from the infrared with increasing water content until at 34 mol % water the peak absorption corresponds to that of the hydrated electron. However, the general absorption is broader at the red end than the latter, which suggests the existence of a variety of environments or traps of differing polarities, constituted presumably by a mixture of dioxane and water molecules.

Anthracene Anion Formation in Dioxane. As mentioned above, anthracene captures the solvated electrons to form the anion which is recognizable by its absorption spectrum (Figure 3). The yields of anions formed in this way in alcohols have been used as a measure of the electron yields,[9] and a preliminary estimate for dioxane using the benzophenone anion gave $G = 0.1$, although a higher yield of 0.6 is possible if the ketyl radical,[1] which is also observed, has the anion as its

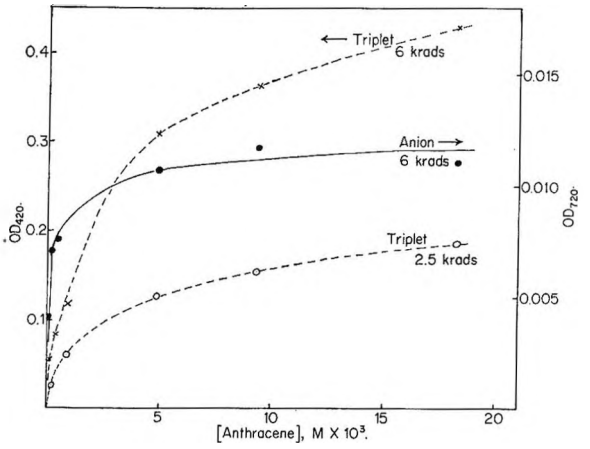

Figure 4. Yields of anthracene anion and triplet in dioxane solutions. Absorptions measured immediately after 2-μsec electron pulses of 6 and 2.5 krads.

precursor. From the γ-radiolysis studies[2] it was concluded that with high solute concentrations a much higher electron yield is required to account for the results. We have now examined the anthracene anion formation and yields in more detail.

A 2-μsec electron pulse on anthracene solutions in dioxane gives, in the present experimental conditions, the anion having a half-life of about 5 μsec (Figure 3). Yields were obtained by measuring peak absorptions at 720 nm from traces as shown in Figure 3 and assuming $\epsilon_{720} = 1.0 \times 10^4\ M^{-1}\ cm^{-1}$ as is found for the anion in tetrahydrofuran.[10] These are minimum yields since some decay must occur during the 2-μsec pulse. As shown in Figure 4, the anion absorption increases with anthracene concentration but appears to reach a constant value beyond about 10 mM. This gives G(anion) = 0.12, in reasonable agreement with the benzophenone experiment.

It should be possible to observe higher anion yields by reducing the effect of the organic cation as above using $LiAlH_4$. We find, as shown in Figure 3, that the long wavelength absorption is substantially increased and, as in pure dioxane, it persists longer. The absorption now exhibits a single maximum at 675 nm and, although not showing the characteristic two peaks of the anthracene anion, the difference may again be due to environmental changes. In support, we find that a degassed solution of anthracene and lithium aluminum hydride (respectively, 5 and 20 mM) in tetrahydrofuran (a better solvent for hydride), when irradiated to about 10^{18} eV g^{-1} formed a persistent yellow-green color which disappeared when air was admitted. An esr examination of the colored solution gave a 75-line spectrum, corresponding in outline and

(9) I. A. Taub, D. A. Harter, M. C. Sauer, and L. M. Dorfman, *J. Chem. Phys.*, **41**, 979 (1964).

(10) D. Gill, J. Jagur-Grodzinski, and M. Szwarc, *Trans. Faraday Soc.*, **60**, 1424 (1964).

spacings to that reported for anthracene anion. This latter species is blue, and it is likely that the yellow component in the liquor is due to another product, possibly involving AlH_3.

These experiments strongly suggest that the hydride is effective in removing the reactive organic cations and replacing them with lithium ions.

Anthracene Triplet Formation in Dioxane. In addition to the anion absorption, anthracene solutions give a prominent transient absorption due to the triplet state (A^T). This is relatively long-lived although its half-life decreases with pulse dose; *e.g.*, with 2 mM anthracene it is about 150 μsec at 150 rads and about 50 μsec at 6000 rads. The decay deviates appreciably from first order and more so at higher doses, and it seems probable that in addition to the quenching processes which have been shown to occur in the photochemical system,[11] such as triplet–triplet annihilation and concentration quenching, there is also quenching by radiation products—possibly free radicals.

The triplet absorption can be observed at anthracene concentrations as low as 10 μM, and even here it has reached a maximum during the time of the pulse; *i.e.*, the formation of A^T is too fast to be observed. The yield of A^T, $G(A^T)$, measured at this maximum increases with anthracene concentration and at concentrations of *ca.* 20 mM approaches a constant value (Figure 4). The form of the curves in Figure 4 is that to be expected if A^T is formed from a precursor P which reacts as

$$P \xrightarrow{k_P} \text{inactive product}$$

$$P + A \xrightarrow{k_{PA}} A^T + \text{inactive product}$$

These reactions lead to the equation

$$[G(A^T)]^{-1} = [G(P)]^{-1}[1 + k_P/k_{PA}(A)]$$

which in terms of observed optical densities, D, can be written

$$D_{max}/D = 1 + k_P/k_{PA}(A)$$

Figure 5 shows that this equation holds reasonably well down to about 300 μM anthracene and covers at least 85% of the A^T formed. From Figure 5 we obtain $G(P) = 1.03$ and $k_P/k_{PA} = 2.5 \times 10^{-3}$ M. Below 300 μM anthracene A^T is bigger than expected from the equation as can be seen from the extended plot in Figure 6.

It should appear that on this interpretation at least two precursors are involved, a short-lived one, P, which contributes the major part of A^T and requires high anthracene concentration to scavenge it appreciably, and another, Q, which gives A^T efficiently even at very low concentrations of anthracene. The results in Figure 6 can be analyzed numerically in these terms by subtracting the calculated contribution of P to $G(A^T)$ at the lower concentrations and thus leaving that from Q. This residue when plotted in the same way, *i.e.*, assuming similar kinetics apply to P and Q, gives a line from which the corresponding values $G(Q) = 0.03$ and $k_Q/k_{QA} = 4.3 \times 10^{-5}$ M are obtained. Thus the species Q only contributes 3% to the total A^T produced.

However, although this treatment provides a useful way of extrapolating to obtain $G(Q)$, the kinetic interpretation is not consistent with the observation that the formation of A^T is too fast to be observed at 10 μM anthracene. Thus even if k_{QA} is *ca.* 10^{11} M^{-1} sec^{-1}, *i.e.*, A^T forms with a half-life of 1 μsec, the buildup of A^T would have been observed at least in part. It seems unlikely that k_{QA} has a higher value than this

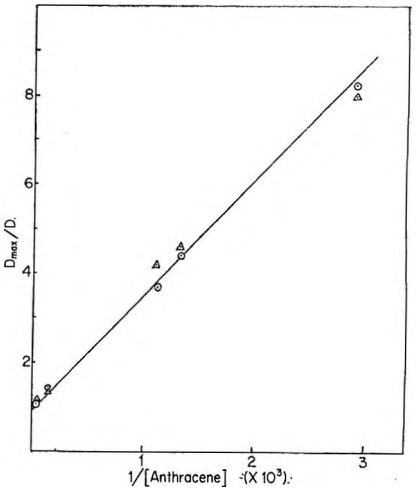

Figure 5. Plot of variation of triplet yield with anthracene concentration according to equation in text. High-concentration range: ⊙, 6-krad pulse; △, 2.7-krad pulse.

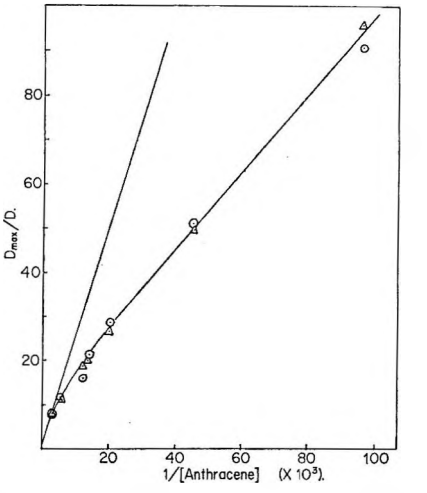

Figure 6. Plot of variation of triplet yield with anthracene concentration over whole range: ⊙, 6-krad pulse; △, 2.7-krad pulse.

(11) G. Jackson, R. Livingston, and A. C. Pugh, *Trans. Faraday Soc.*, **56**, 1635 (1960).

and hence it is improbable that this part of A^T is formed in a bimolecular process.

This argument cannot of course be applied to P, and if the kinetics are as above, and if the diffusion-controlled value for $k_{PA} = 8RT/3000 = 5 \times 10^9\ M^{-1}$ sec^{-1} is assumed, then $k_P = 1.25 \times 10^7\ sec^{-1}$ and P would have a half-life of 55 nsec.

Effect of Electron and Cation Scavengers on Anthracene Triplet Yield. In the preliminary work we reported that 0.1 *M* hydrochloric acid reduces the triplet yield by a factor of 4.[1] It was suggested that the effect arises from the reaction of the acid with the anthracene anion or the solvated electron which would normally give rise to the triplet state on neutralization by the concomitant cation. As shown in Table I, we have confirmed this effect of HCl, but in these and the earlier experiments aqueous acid was used so that water (never more than 0.5 mol %) was also present. Since water has been shown[2] to have a marked effect on the γ radiolysis of dioxane, it may well be significant here and we have therefore measured the triplet yields in aqueous dioxane with the results shown in Table II.

Table I: Effect of HCl on Anthracene Triplet Absorption[a]

[HCl], m*M*	0	11.1	16.7	32.7	57.5	127
OD at 420 nm	0.51	0.32	0.26	0.190	0.134	0.120

[a] Anthracene 17 m*M*; 2-μsec pulse of 6 krads, approximately.

Table II: Effect of Water on Anthracene Triplet Absorption[a]

H_2O, mole %	Dose *ca.* 6000 rads: OD at 420 nm	Dose *ca.* 6000 rads: OD (cor)	Dose *ca.* 1200 rads: OD at 420 nm	Dose *ca.* 1200 rads: OD (cor)
0	0.38	0.38	0.071	0.071
10	0.35	0.36	0.062	0.063
19.5	0.30	0.31	0.055	0.058
31	0.31	0.33	0.052	0.056
41.5	0.29	0.33	0.045	0.052
50	0.29	0.35	0.037	0.045

[a] Anthracene 17 m*M*; OD at 420 nm = OD (cor) $\times$ weight fraction of dioxane.

It will be seen that if the yield of triplet is calculated on the basis of the energy absorbed in dioxane only (this is measured by OD (cor) in Table II), then with the higher dose pulse there is only a small decrease in yield even at 50 mol % water. The extent of this decrease is the same when the dose is reduced by a factor of 5, which suggests that perhaps a small amount of impurity has been introduced. However, it is clear that water at the concentration present with the acid does not play a significant part in decreasing the triplet yield.

The effect of nitrous oxide, a well-known efficient electron scavenger, is shown in Table III. The yield is decreased, and from the smaller effect at higher anthracene concentrations it appears that nitrous oxide and anthracene compete for a precursor to the triplet. Measured by the amount required to reduce the yield to one-half, it will be seen that anthracene and hydrochloric acid are about equally reactive toward the precursor whereas nitrous oxide is lower by about a factor of 5.

Table III: Effect of N_2O on Anthracene Triplet Absorption[a]

[Anthracene], m*M*	OD at 420 nm: Ar-saturated	OD at 420 nm: N_2O-saturated	% decrease
0.05	0.0130	0.00135	90
0.150	0.0234	0.0069	30
0.500	0.0446	0.0150	33.5
34.0	0.237	0.106	45

[a] Pulse dose about 6000 rads. N_2O is 200 m*M* at saturation.

Because of the possible importance of a cation either from dioxane or from anthracene as a precursor to the triplet state, and in view of the work described above with lithium aluminum hydride, it was of interest to investigate the effect of the latter on the formation of the triplet. The result is shown in Figure 3 where it will be seen that although the absorption and lifetime of the anthracene anion are considerably increased, the yield of triplet is scarcely affected. Most of the decrease shown in Figure 3 is due to the lower concentration used. We also find that all the absorption is again present immediately after the pulse.

Excitation Transfer. Earlier work on the fluorescence of terphenyl in γ-irradiated dioxane solution[4] indicated that benzene could act as an intermediary in the transfer of the excitation to terphenyl. We have observed a similar effect with respect to the triplet anthracene excitation. This can be made apparent in two ways. Thus beginning with an anthracene concentration which is insufficient to give the maximum A^T, an addition of benzene increases the A^T yield and with further additions it ultimately reaches the same maximum value as is given by high concentrations of anthracene. About 1.0 *M* benzene is required to produce the optimum yield. Alternatively, we find that a lower concentration of anthracene is required to attain the optimum triplet yield if the dioxane contains benzene. The latter is shown in Figure 7a. An exactly analogous behavior is shown by acetone, the only difference being that acetone is effective at a lower concentration as shown in Figure 7b.

Since these additives do not alter the yield of A^T it would appear that the precursor transfers its excitation facility quantitatively perhaps by producing excited

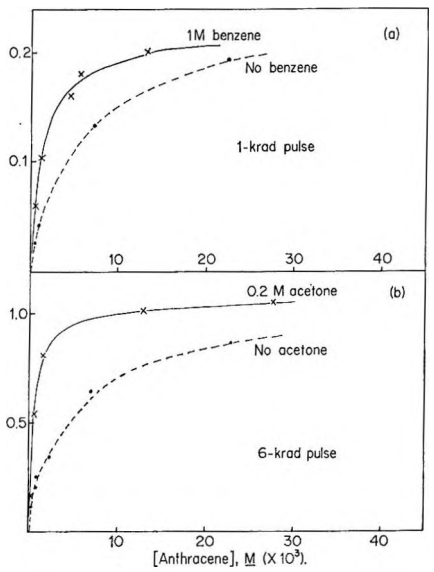

Figure 7. Enhancement of triplet yield of anthracene in dioxane by: (a) 1.0 M benzene (1-krad pulse); (b) 0.2 M acetone (6-krad pulse). Ordinates, OD at 420 nm.

benzene or acetone. If, as seems reasonable, the additives react with the precursor with the same order of efficiency as does anthracene, then at these high concentrations the situation will be

$$P + B \longrightarrow B^*$$

$$B^* \xrightarrow{k_B} B$$

$$B^* + A \xrightarrow{k_{BA}} B + A^T$$

i.e., excited benzene becomes the precursor to A^T. Using the same equation and plot as above for anthracene alone, k_B/k_{BA} and the corresponding term for acetone can be obtained from the data in Figure 7. These are found to be 1.5×10^{-3} M and 6.0×10^{-4} M, respectively.

Discussion

Excited states of solutes produced by ionizing radiation on dilute solutions may arise either by energy transfer from an excited state of a solvent molecule or species derived from it, by the neutralization of a charged solute molecule in various ways, or by direct excitation of the solute molecule, for example by electrons with energies below the excitation energy of the solvent. In the case of triplet states, these may be produced directly or derived from an excited singlet state by intersystem crossing. There are at present few systems for which the experimental evidence can distinguish unequivocally between direct excitation, of either solute or solvent, and charge neutralization involving either solute and/or solvent as the primary source of the excitation energy, although in benzene[12] and in acetone[13] solutions the immediate precursor to the excited solute molecule would seem to be an excited solvent molecule.

The observation that additives such as HCl and N_2O, which are known to react with electrons and should therefore interfere with the charge neutralization process, depress the yield of triplet anthracene in dioxane and cyclohexane, has been adduced[1] as evidence that the neutralization process is the origin of the excitation energy.

It is difficult to reconcile this conclusion with the present observation that quite large amounts of water in dioxane have little effect on $G(A^T)$. From the γ-radiolysis work it would appear that water undoubtedly reacts with a cation derived from the solvent and hence must profoundly change the charge neutralization step. In the same way the lack of effect of lithium aluminum hydride which appears to remove reactive cations argues against a solvent or solute cation being involved.

Our observation that the excitation can be transferred quantitatively to anthracene *via* benzene or acetone also makes it improbable that direct excitation of the solute by sub-excitation electrons is occurring, for it seems unlikely that in this case all three solutes would give the same yield. Moreover, the form of the yield–concentration curve for anthracene alone is not that to be expected from this effect which would lead to a more slowly varying function of anthracene concentration at the high concentration end. It is possible, however, that the few per cent of the triplet which we have seen to be readily produced at low anthracene concentrations derives from this process, since it is difficult to see how it could develop so rapidly from a bimolecular reaction.

We are led to the conclusion that in dioxane the major part of the anthracene triplet is produced by energy transfer from an excited solvent molecule which is itself formed by direct excitation. The effects of HCl and N_2O are, we suggest, due to their reaction with, and hence quenching of, this excited solvent molecule. In support, we note that in the γ radiolysis a higher yield of hydrogen was produced by adding HCl to dioxane than could be obtained with water.[2] The extra hydrogen might arise from the reaction with the excited state, and its magnitude $G(H_2) = 1.05$ is similar to the value of $G(A^T)$ as would be required by this mechanism. Moreover, analysis of the results of Table I in terms of the competition reactions of the precursor P

$$P \xrightarrow{k_P} \text{inactive product}$$

$$P + A \xrightarrow{k_{PA}} A^T + \text{inactive product}$$

(12) R. B. Cundall and P. A. Griffiths, *Discussions Faraday Soc.*, 56, 1635 (1963).

(13) S. Arai and L. M. Dorfman, *J. Phys. Chem.*, 69, 2239 (1965).

$$P + HCl \xrightarrow{k_{PB}} \text{product} + H \text{ (or } H_2)$$

gives $k_P/k_{PA} = 6.8 \times 10^{-3}$ M. Now an exactly analogous analysis in terms of the same equations can be made of the extra $G(H_2)$ produced at various HCl concentrations given earlier.[2] This gives $k_P/k_{PA} = 6.6 \times 10^{-3}$ M in good agreement.

We saw above that on the assumption that the rate constant for the energy transfer step was given by the diffusion equation, the excited dioxane species would have a half-life of 55 nsec. The absorption spectrum of dioxane in the vapor state[14] shows vibrational structure centered around 180 nm which has been assigned to the first singlet–singlet transition. Hence the first excited singlet state is well defined, and using the oscillator strength of the transition, $f = 0.11$, the usual formula gives a radiative lifetime of 3 nsec in the gas phase. This is much shorter than is evidenced by the present work and suggests that some state other than the first excited singlet is involved.

Analysis of the observations on the benzene and acetone solutions given above indicates that the half-lives of the excited benzene and acetone molecules produced by transfer from the primary excited dioxane are 100 and 250 nsec, respectively. This assumes that the bimolecular rate constants for transfer are all 5×10^9 M^{-1} sec^{-1}. In fact, k_{PA} may be somewhat higher than the others in view of the larger molecular size of anthracene, so that 100 and 250 nsec are probably lower estimates.

Considering first benzene, it is fairly certain that at this concentration of benzene any excited state will exist as excimer, and the rate constants for emission and decay[15] to the triplet state suggest that it is the triplet excimer which transfers to anthracene. The lifetimes of the triplet monomer and dimer are known with less certainty and it is not unreasonable that the 100 nsec refers to one of these.

If the excitation transfer was from a singlet state dioxane to give a singlet acetone or benzene which then decayed to the triplet before transferring to anthracene, it seems unlikely that the final yield of A^T would be the same for acetone and benzene as is in fact observed. This suggests that the excited dioxane is in a triplet state. The above value for the lifetime of the acetone triplet state is much smaller than the 1 μsec in hexane[16] and 6 μsec in acetone[13] which have been quoted, but it has recently been pointed out[17] that 80% of the decay in hexane is due to a hydrogen abstraction reaction with the solvent. Dioxane is likely to be more reactive than hexane in this respect and the above value of 0.25 μsec would not seem unreasonable.

(14) G. J. Hernandez and A. B. F. Duncan, *J. Chem. Phys.*, **36**, 1504 (1962).

(15) J. B. Birks, C. L. Braga, and M. D. Lumb, *Proc. Roy. Soc.*, **A283**, 83 (1965).

(16) F. Wilkinson and J. T. Dubois, *J. Chem. Phys.*, **39**, 377 (1963).

(17) P. J. Wagner, *J. Amer. Chem. Soc.*, **88**, 3672 (1966).

Pulsed Radiolysis of Liquid Cyclohexane and *n*-Hexane. I. Yield of Hydrogen Atoms Measured by the Cyclohexadienyl Radical Absorption in Solutions Containing Benzene. II. Absorption Spectra and Reactions of Cyclohexyl and Hexyl Radicals[1]

by Myran C. Sauer, Jr., and Inder Mani

Chemistry Division, Argonne National Laboratory, Argonne, Illinois *(Received May 7, 1968)*

The pulsed radiolysis of solutions of benzene in cyclohexane and *n*-hexane yields the cyclohexadienyl radical, ($C_6H_7\cdot$), absorbing at 315 mμ. Studies of the intensity of this absorption as a function of benzene concentration indicates that thermal hydrogen atoms react by (1) $H\cdot + RH \rightarrow H_2 + R\cdot$ and (2) $H\cdot + C_6H_6 \rightarrow C_6H_7\cdot$, with $k_2/k_1 = 35 \pm 15$ for cyclohexane and 37 ± 10 for *n*-hexane. The *G* values for thermal hydrogen atoms are found to be 1.3 ± 0.4 in cyclohexane and 1.8 ± 0.4 in *n*-hexane. In the pure solvents, absorbing radicals were produced with maxima at 240 mμ in cyclohexane (cyclohexyl, $\epsilon^{240} = 2.1 \pm 0.4 \times 10^3\ M^{-1}\ cm^{-1}$) and at 235 m$\mu$ in *n*-hexane (hexyl, $\epsilon^{235} = 1.4 \pm 0.3 \times 10^3\ M^{-1}\ cm^{-1}$). The maxima were unchanged when the radicals were produced in aqueous solution, but the values of ϵ^{240} were lower ($1.48 \pm 0.15 \times 10^3\ M^{-1}\ cm^{-1}$ and $0.96 \pm 0.10 \times 10^3\ M^{-1}\ cm^{-1}$ for cyclohexyl and hexyl, respectively). The rate constants for radical + radical reaction are, in units of $10^9\ M^{-1}\ sec^{-1}$, for cyclohexyl 2.0 ± 0.6 and 1.4 ± 0.2 in cyclohexane and water, repectively, and for hexyl 3.1 ± 0.9 and 1.2 ± 0.2 in *n*-hexane and water, respectively.

Introduction

That thermal hydrogen atoms are produced during the radiolysis of liquid cyclohexane and *n*-hexane is supported by many data, although there is considerable variation in the *G* values reported.[2-9] The evidence for thermal hydrogen atoms is based on the effects of scavengers which compete with the abstraction reaction with the saturated hydrocarbon. This paper describes a similar scavenger experiment, which differs, however, in that the product of the reaction of hydrogen atoms with the scavenger is observed as a transient optical absorption using the pulsed-radiolysis technique.

The scavenger used is benzene, and the observed transient product is the cyclohexadienyl radical ($C_6H_7\cdot$). The absorption spectrum of this radical has recently been observed by the addition of hydrogen atoms to benzene in the gas phase and in aqueous solution, and the rate constants for the addition reactions have been measured.[10] By measuring the yield of this radical as a function of benzene concentration in cyclohexane or *n*-hexane solutions, we have been able to observe the competitive behavior of the hydrocarbon involved and to make an estimate of the yield of thermal hydrogen atoms.

Experimental Section

Materials. Cyclohexane, Phillips 99.5%, was passed through an activated silica gel column. For some experiments, cyclohexane, Phillips Research grade, was also used after passing through silica gel. However, no difference in results was observed in the present experiments. *n*-Hexane, Phillips Pure grade, was passed through activated silica gel. Benzene, Phillips Research grade, was used without further purification. Nitrous oxide (Matheson Co., about 0.03% O_2 found by gas chromatographic analysis) was used directly from the cylinder.

Preparation of Samples. Solutions of known composition of benzene in cyclohexane or *n*-hexane were prepared volumetrically. The solutions were degassed on a vacuum line by shaking while pumping. When volatile binary solutions were degassed as above, the final composition of the solution was determined, after irradiation, by gas chromatographic measurements. Solutions saturated with nitrous oxide at atmospheric pressure were prepared by first degassing the

(1) Based on work performed under the auspices of the U. S. Atomic Energy Commission.

(2) (a) J. F. Merklin and S. Lipsky, *J. Phys. Chem.*, **68**, 3297 (1964); (b) C. E. Klots, Y. Raef, and R. H. Johnson, *ibid.*, **68**, 2040 (1964).

(3) R. J. Hagemann and H. A. Schwartz, *ibid.*, **71**, 2694 (1967).

(4) R. A. Holroyd, *ibid.*, **70**, 1341 (1966).

(5) J. L. McCrumb and R. H. Schuler, *ibid.*, **71**, 1953 (1967).

(6) T. J. Hardwick, *ibid.*, **66**, 1611 (1962).

(7) G. E. Adams, J. H. Baxendale, and R. D. Sedgewick, *ibid.*, **63**, 854 (1959).

(8) I. Mani and R. J. Hanrahan, *ibid.*, **70**, 2233 (1966).

(9) W. A. Cramer and G. J. Piet, *Trans. Faraday Soc.*, **63**, 1402 (1967).

(10) M. C. Sauer, Jr., and B. Ward, *J. Phys. Chem.*, **71**, 3971 (1967).

hydrocarbon solution and subsequently equilibrating with nitrous oxide.

Pulse-Radiolysis Apparatus. This is described in detail elsewhere.[11,12] The solutions were irradiated in 3 and 4 cm long quartz cells using 0.4- or 1.0-μsec pulses of 12- to 15-MeV electron beam from an Arco linear accelerator. An analyzing light beam passed through the cell twice and then through a monochromator to a 1P28 photomultiplier tube. The output of the tube was amplified and displayed on a Tektronix 555 oscilloscope. In recording point by point spectra, the light beam was split, as has been described earlier,[12] in order that a second monochromator could be used as a monitor of pulse intensity. The apparatus used for low-temperature irradiation has been previously described.[12]

The photographic pictures of the oscilloscope traces were analyzed by an automatic, computerized technique described in detail elsewhere.[12-14]

Dosimetry. Dosimetry was performed by the observation of the transient I_2^- in 10^{-3} *M* aerated aqueous potassium iodide solution. The extinction coefficient of I_2^- at 385 mμ is 14,000,[15] and the radiolytic yield $G_{I_2^-}$ is 2.40. The absorption in hydrocarbons relative to the aqueous dosimetry was corrected on the basis of the electron density ratio. The intensity of the pulse (absorbed in aqueous solution) usually used (80 mA, 0.4 μsec half-width) was 1.2×10^{17} eV/ml.

Results and Discussion

Transient Spectra. When a solution of from 0.1 to 35% benzene in either cyclohexane or *n*-hexane is pulse-irradiated and the absorption in the region of 315 mμ is observed, one finds that the absorption is at a maximum immediately following the 1-μsec pulse, and subsequently decays. That there is no formation curve observable on this time scale is expected because the disappearance of hydrogen atoms due to abstraction from the alkane is rapid, having a half-time of the order of magnitude of 10^{-7} to 10^{-8} sec at room temperature.

For a given solution, the maximum optical density was determined at about ten different wavelengths in the 315-mμ region, using a single electron pulse for each wavelength. The spectrum was the same in the case of benzene dissolved in cyclohexane or *n*-hexane, and was independent of benzene concentration, except at 100% benzene, where the absorption maximum was about 325 mμ. Also, the spectrum did not vary as the absorption decayed, nor did solutions saturated with N_2O (*ca.* 0.12 *M*) at 1 atm show any appreciable difference in spectrum (Figure 1, open circles). The spectrum is shown by the filled circles and the solid curve in Figure 1. The maximum absorption is at 315 mμ, which is slightly different from the wavelength of maximum absorption of the cyclohexadienyl radical in aqueous solution[10] (311 mμ, dashed curve), and differs more from the spectrum in the gas phase[10] (300 mμ, dotted curve). All indications are that the observed spectrum is that

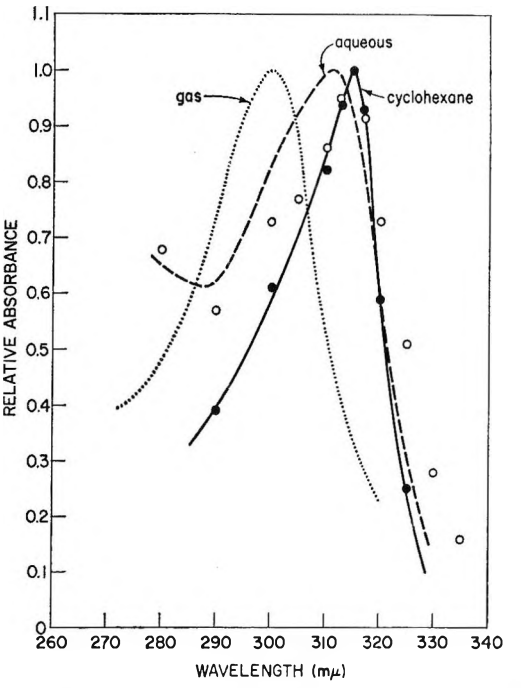

Figure 1. Absorption spectra of the cyclohexadienyl radical in cyclohexane containing 6% benzene, ●, solid curve; in cyclohexane containing 6% benzene, saturated with N_2O, ○; in aqueous solution, dashed curve (ref 10); in gas phase, dotted curve (ref 10).

of the cyclohexadienyl radical. All three spectra have been arbitrarily normalized to unity at the maxima. The actual absorption coefficients will be discussed later.

In order to determine whether any correction is necessary due to absorbing species originating from the solvent itself, samples of pure cyclohexane and *n*-hexane were examined. Figure 2 shows the absorption spectra obtained; the open circles represent points taken in cyclohexane, and the open triangles are for *n*-hexane. The amount of absorption at 315 mμ was found to be negligible in the case of *n*-hexane and small in the case of cyclohexane insofar as the measurement of the cyclohexadienyl yield is concerned. Figure 2 shows λ_{max} of 240 mμ (cyclohexane) and 235 mμ (hexane). Measurements at wavelengths below 250 mμ are difficult because of scattered light problems. The data in the case of *n*-hexane are more strongly conclusive with respect to the existence of an absorption maximum than in the case of cyclohexane; however, we feel that both peaks are real. An absorption with a maximum at 255 mμ has previously been observed[16] in the pulsed radiol-

(11) M. C. Sauer, Jr., S. Arai, and L. M. Dorfman, *J. Chem. Phys.*, **42**, 708 (1965).

(12) S. Arai and M. C. Sauer, Jr., *ibid.*, **44**, 2297 (1966).

(13) M. C. Sauer, Jr., Argonne National Laboratory Report, ANL-7113, Oct 1965.

(14) M. C. Sauer, Jr., Argonne National Laboratory Report, ANL-7146, Jan 1966.

(15) J. K. Thomas, *Trans. Faraday Soc.*, **61**, 702 (1965).

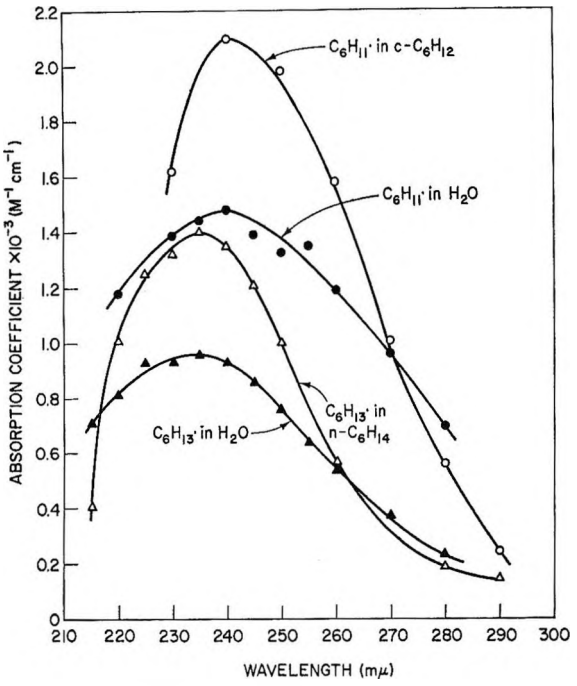

Figure 2. Absorption spectra of cyclohexyl and hexyl radicals: ○, cyclohexyl in cyclohexane; ●, cyclohexyl in water; △, hexyl in *n*-hexane; ▲, hexyl in water.

ysis of cyclohexane. The 15 mμ difference may be due to a scattered light problem, mainly in the latter absorption data.

We agree with the suggestion[16] that the absorption spectrum in pure cyclohexane is due to the cyclohexyl radical; similarly, the absorption spectrum at 235 mμ in pure hexane is most likely due to hexyl radicals. It is difficult to imagine any other species which would be in high enough concentration to explain the observed optical densities. We can estimate the decadic absorption coefficients of the cyclohexyl and hexyl radicals, using our observed optical densities, on the basis of the reported G values for these radicals, and the results of dosimetry on the electron beam (see Experimental Section). Using G(cyclohexyl) = 4.4 ± 0.2,[17,18] $\epsilon_{\text{cyclohexyl}}^{240} = 2.1 \pm 0.4 \times 10^3\ M^{-1}\ \text{cm}^{-1}$, and using G(hexyl) = 5 ± 0.5,[19] $\epsilon_{\text{hexyl}}^{235} = 1.4 \pm 0.3 \times 10^3\ M^{-1}\ \text{cm}^{-1}$. The same results were obtained for research grade and pure grade cyclohexane. The value of ϵ for cyclohexyl is about five times higher than the previously reported[16] value. No reason for the discrepancy is obvious.

In order to gain additional evidence as to whether the absorptions in the region of 240 mμ are due to hexyl and cyclohexyl radicals, we have studied the transient spectra produced in aqueous solutions, saturated with N_2O at 1 atm to convert solvated electrons into OH·, and saturated with either cyclohexane or *n*-hexane. The spectra obtained are shown in Figure 2 (filled circles, cyclohexane; filled triangles, *n*-hexane) and are similar to the spectra obtained in the pure hydrocarbons. The transients appeared simultaneously with the pulse and subsequently decayed. The absorption coefficients of these radicals in aqueous solution can be estimated as follows. Under conditions of N_2O saturation, the N_2O scavenges solvated electrons and a second species[20] yielding a G(OH·) from N_2O of 3.1. The total yield of OH· is 5.5, since G(OH·) is 2.4 in the absence of N_2O. Approximately 99% of the OH· will react with the hydrocarbon under the conditions used, *i.e.*, cyclohexane concentration of 0.0017 M,[21] and OH· concentration produced per pulse of $1.2 \times 10^{-6}\ M$. However, about 12% of the hydrogen atoms, which are produced with a G of 0.6, will react with OH·, H·, or radicals. Therefore, a reasonable estimate of the G value of cyclohexyl radicals produced by OH· and H·, and corrected as indicated above, is 5.9 ± 0.1. (The same value also holds in the case of the aqueous hexane solutions.) Using this value, we obtain for the cyclohexyl radical $\epsilon = 1.48 \pm 0.15 \times 10^3\ M^{-1}\ \text{cm}^{-1}$ at 240 mμ, and for the hexyl radical $\epsilon = 0.96 \pm 0.10 \times 10^3\ M^{-1}\ \text{cm}^{-1}$ at 235 mμ. The fact that the maximum ϵ values are about 30% lower than in the case of the pure hydrocarbons as solvents is probably due to the broadening of the spectra in aqueous solutions. Since the presence of oxygen in the system would lead to absorption[22] in the region of 240 mμ, the O_2 content of the N_2O was checked and found to be small enough (0.03%) that the O_2 concentration in the aqueous solution was negligible (less than $10^{-7}\ M$).

Rate Constant for the Reaction of Hydrogen Atoms with Cyclohexane. At room temperature, the formation of the transients in cyclohexane and *n*-hexane was simultaneous with the 1-μsec pulse. An attempt was made to observe any formation due to the reaction of thermal hydrogen atoms with the hydrocarbon by examining the transient in liquid *n*-hexane at −78°. However, no formation was apparent, indicating that the abstraction reaction is too fast even at −78°. If the abstraction reaction had a half-time of about 1 μsec, the formation should have been observable. (However, the observation of the formation is made difficult by the fact that less than half of the hexyl radicals originate *via* thermal hydrogen atoms.) Therefore, the data suggest that the rate constant of the ab-

(16) M. Ebert, J. P. Keene, E. J. Land, and A. J. Swallow, *Proc. Roy. Soc.*, **A287**, 1 (1965).

(17) From the total radical yield of G = 4.8 based on iodine uptake[18] and the fact that 90 to 95%[4] of the total radicals are cyclohexyl.

(18) P. J. Horner and A. J. Swallow, *J. Phys. Chem.*, **65**, 953 (1961).

(19) From data given in "Radiolysis of Hydrocarbons," by A. V. Topchiev, English edition, R. A. Holroyd, Ed, Elsevier Publishing Co., New York, N. Y., 1964, pp 77, 78.

(20) D. A. Head and D. C. Walker, *Can. J. Chem.*, **45**, 2051 (1967).

(21) "Solubilities of Inorganic and Organic Compounds," Vol. 1, Part 1, H. Stephen and T. Stephen, Ed., Pergamon Press, New York, N. Y., 1963, p 452.

(22) G. Czapski and L. M. Dorfman, *J. Phys. Chem.*, **68**, 1169 (1964).

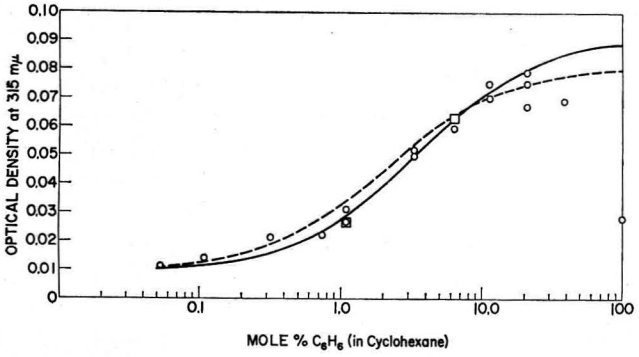

Figure 3. Yield of cyclohexadienyl radical as a function of benzene concentration in cyclohexane. Each point represents a separate experiment. The square points (□) represent solutions saturated with N_2O at 1 atm. The solid and dashed curves are calculated, as described in the text.

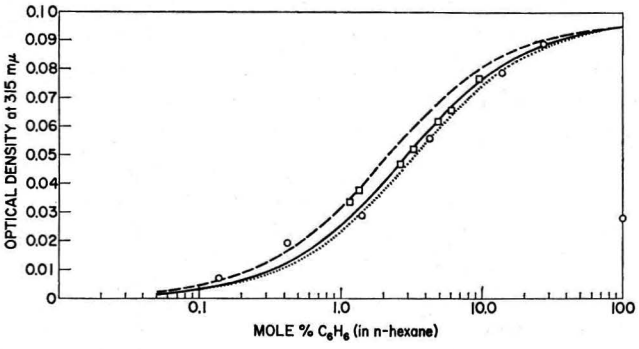

Figure 4. Yield of cyclohexadienyl radical as a function of benzene concentration in *n*-hexane. The circles represent data obtained in this work; the squares represent hydrogen yield data of Rajbenbach and Kaldor,[23] normalized as described in the text.

straction reaction must be greater than about $10^5\ M^{-1}$ sec^{-1} at $-78°$.

The reaction of H· with cyclohexane was further investigated by saturating an aqueous solution at pH 3 (perchloric acid) with cyclohexane (0.0017 M[21]) and observing the formation of the cyclohexyl radical under conditions of low pulse intensity (to prevent reactions of H· with itself and radicals). The lowest intensity which was usable produced $0.36 \times 10^{-6}\ M$ hydrogen atom per pulse, and at this intensity about 90% of the hydrogen atoms react with the cyclohexane. The rate constant obtained after allowing for the latter is $4 \pm 1 \times 10^7\ M^{-1}$ sec^{-1}. (As expected, the hydroxyl radicals react with the cyclohexane much faster, producing an "initial" concentration of cyclohexyl radicals nearly simultaneously with the pulse). It is interesting to note that the rate constant for addition of H· to benzene in aqueous solution[10] is $1.1 \times 10^9\ M^{-1}$ sec^{-1}, which is 28 times the rate constant for abstraction from cyclohexane given above. Therefore, the ratio is in agreement with the analogous ratio in cyclohexane solution of 35 ± 15, which will be derived in the next section.

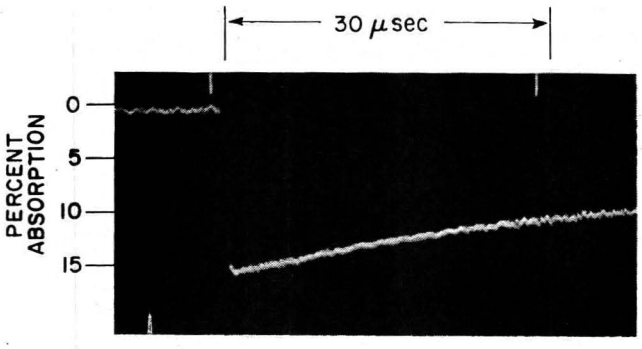

Figure 5. Optical absorption at 315 mμ produced by pulse irradiating a 20% benzene in cyclohexane solution.

Dependence of Cyclohexadienyl Radical Yield on Benzene Concentration. Figures 3 and 4 show the yield of cyclohexadienyl radical for various mole percentages of benzene in cyclohexane and *n*-hexane, respectively. The yield is given arbitrarily in terms of the observed initial optical density, *i.e.*, before appreciable decay of the cyclohexadienyl radical occurred. A typical decay curve is shown in Figure 5. The observed optical densities were corrected to a common basis by irradiating a KI dosimeter solution before and after each hydrocarbon solution, for small changes in the dose per pulse during a given day, and for larger changes (up to 30%) from one day to another.

The data in Figures 3 and 4 were tested to determine how well they correspond to the hypothesis that there exists a competition for thermal hydrogen atoms between the saturated hydrocarbon (RH) and benzene, where the yield of thermal hydrogen atoms is independent of benzene concentration. (We know, of course, that the yield of hydrogen atoms in pure benzene must be considerably less than that in pure cyclohexane, since the optical density observed in pure benzene is considerably less than that observed in a solution containing 20% benzene. Therefore, one would expect that the yield of hydrogen atoms would decrease somewhat at the highest benzene concentrations.) If k_1 and k_2 are the rate constants for the reactions

$$H\cdot + RH \longrightarrow H_2 + R\cdot \qquad (1)$$

$$H\cdot + C_6H_6 \longrightarrow C_6H_7\cdot \qquad (2)$$

and D_{max} is the constant yield of thermal hydrogen atoms in units of optical density, then we can test the hypothesis by assuming various values of D_{max} and k_2/k_1 and calculating, as a function of (C_6H_6), the optical density which should be observed, D_{calcd}, from the relationship

$$D_{calcd} = D_{max}\frac{k_2(C_6H_6)}{k_2(C_6H_6) + k_1(RH)} \qquad (I)$$

Figure 3 shows the observed optical densities due to the cyclohexadienyl radical in benzene–cyclohexane solutions. Note that the two square points are for

solutions saturated with N_2O, and show that N_2O has no effect on the observed optical density. This will be discussed in a later section. An attempt was made to fit the experimental points with curves calculated from eq I modified to take into account an optical density at 315 mμ of 0.004 from pure cyclohexane (which was assumed independent of added benzene). However, a reasonable fit could not be obtained unless an additional "constant correction" of 0.005 was included. With this modification, eq (I) becomes

$$D_{\text{calcd}} = 0.009 + (D_{\max} - 0.009)\left(\frac{k_2(C_6H_6)}{k_2(C_6H_6) + k_1(RH)}\right)$$

and yields, for example, the two curves shown in Figure 3. The solid curve represents the case where $k_2/k_1 = 30$, and the dashed curve the case where $k_2/k_1 = 50$, with values of $D_{\max}$ as shown by the y coordinate of the curves at 100% benzene. The fit seems better for the lower value of k_2/k_1, but in view of the assumptions, and the nature of the experimental data, a value of 35 $\pm$ 15 for k_2/k_1 is not unreasonable. The value of $D_{\max} - 0.009$ is 0.077 $\pm$ 0.007, which will be used later to calculate the G of thermal hydrogen atoms.

The fact that a correction term for some undefined process has to be added above somewhat weakens the contention that eq I correctly describes the variation of cyclohexadienyl with benzene concentration. However, in the case of n-hexane, one can represent the data satisfactorily on the basis of eq I *without* making any such corrections. The experimental data on the optical density due to the cyclohexadienyl radical as a function of benzene concentration are shown by the circles in Figure 4. The squares represent the data of Rajbenbach and Kaldor[23] on the depression of the H_2 yield by benzene added to a 3.7 mol % perfluorocyclobutane in n-hexane solution. The latter authors interpret the depression of the hydrogen yield by benzene when perfluorocyclobutane is present to be due to the reaction of thermal hydrogen atoms with benzene, and obtain $G(H\cdot) = 1.36$ and $k_2/k_1 = 37$. Their data have been normalized by assuming that $D_{\max} = 0.095$ corresponds to $G(H\cdot) = 1.36$. The squares and the circles easily fit on a common curve, which certainly indicates that the depression of the hydrogen yield and the increase in cyclohexadienyl yield with increasing benzene concentration are caused by the same process. The solid curve in Figure 3 is the theoretical curve calculated from eq I using $k_2/k_1 = 37$ and $D_{\max} = 0.095$. For comparison, theoretical curves calculated using k_2/k_1 of 50 (dashed line) and 32 (dotted line) are shown. A reasonable estimate of k_2/k_1 is 37 $\pm$ 10, and $D_{\max}$ may be stated as 0.095 $\pm$ 0.007, for use later in estimating $G(H\cdot)$.

Therefore, the data are in fair agreement with the contention that thermal hydrogen atoms react with benzene to form the cyclohexadienyl radical, in competition with abstraction from RH, with the agreement being better in the case of n-hexane.

Effect of Nitrous Oxide. Two solutions of benzene in cyclohexane were saturated with N_2O at 1 atm, which yields a concentration of 0.12 M N_2O.[24] As can be seen in Figure 3, the presence of N_2O had no effect on the yield of the cyclohexadienyl radical as measured by the optical density at 315 mμ. In addition, the spectrum (Figure 1) was not appreciably different with added N_2O.

Nitrous oxide is known to lower the H_2 yield,[25] supposedly by interfering with recombination processes involving electrons and positively charged species. Therefore, the fact that N_2O has no effect on the cyclohexadienyl radical yield is an indication that this radical originates only from thermal hydrogen atoms and that charged species are not precursors of thermal hydrogen atoms. These conclusions are in agreement with the mechanism recently summarized by Rajbenbach and Kaldor[23] and with their conclusions concerning the effect of scavengers on the hydrogen gas yields in n-hexane radiolysis. Other possible explanations of the lack of effect of N_2O on the yield and spectrum of the $C_6H_7\cdot$ require the occurrence of unlikely coincidences. For example, the results could be explained if the reaction of e^- with N_2O eventually yielded an OH radical, but in the absence of N_2O, the electron yielded a thermal hydrogen atom. The OH radical would have to yield exactly the same spectrum and optical density upon addition to the benzene as would have resulted from the hydrogen atom. That all of these conditions hold seems unlikely.

G Value for Thermal Hydrogen Atoms. The value of $G(H\cdot)$ can be estimated from the values of $D_{\max}$ discussed in a previous section, using the energy absorbed as determined in the dosimetry experiments, and the value of $\epsilon_{C_6H_7\cdot}^{315}$. The latter value has not been determined in hydrocarbon solutions, but has been measured in aqueous solution[10] as 5.4 $\pm$ 0.5 $\times$ 10^3 M^{-1} cm^{-1} at 311 mμ. Since the spectrum is apparently somewhat broader in aqueous solution (Figure 2), we have estimated that in cyclohexane or hexane $\epsilon_{C_6H_7\cdot}^{315} = 6.5 \pm 1.5 \times 10^3$ M^{-1} cm^{-1}.

For cyclohexane, using $(D_{\max} - 0.009) = 0.077 \pm 0.007$, we obtain $G(H\cdot) = 8.2 \times 10^3/\epsilon_{C_6H_7\cdot}^{315}$, and for n-hexane, $G(H\cdot) = 1.18 \times 10^4/\epsilon_{C_6H_7\cdot}^{315}$, using $D_{\max} = 0.095 \pm 0.007$. Using these values, we obtain

$$G(H\cdot) = 1.3 \pm 0.4 \text{ in cyclohexane}$$

$$G(H\cdot) = 1.8 \pm 0.4 \text{ in } n\text{-hexane}$$

These values can be compared with previous determinations of $G(H\cdot)$ in cyclohexane[2-9] and n-hexane.[23]

(23) L. A. Rajbenbach and U. Kaldor, *J. Chem. Phys.*, **47**, 242 (1967).

(24) J. K. Thomas, private communication.

(25) G. Scholes and M. Simic, *Nature*, **202**, 895 (1964).

The majority of the reported values of $G(H\cdot)$ are greater than unity.

Decay of Transients. The decay of transients was found to be second order in all cases, as would be expected for decay by radical–radical reactions. An estimate can be made of the rate constant for the main radical–radical reaction occurring if the G values for all radicals are known, and if ϵ is known for the observed radical. Values of ϵ have been discussed in a previous section.

In the case of pure cyclohexane, the cyclohexyl radical is by far the most important radical, having a G value of 4.4 ± 0.2. The sum of the G values of other radicals is 0.3 ± 0.2.[19] The observed slope of the second-order plot is 2.6 ± 0.2 × 10^5 sec^{-1}. This would be equal to $-2k/\epsilon l$, where l is the optical path length in centimeters, ϵ is the absorption coefficient of the cyclohexyl radical in M^{-1} cm^{-1}, and k is the rate constant of the reaction R· + R. → products, *i.e.*, as in the equation $d(R\cdot)/dt = -2k(R\cdot)^2$, if the cyclohexyl radical were the only radical species reacting. In the case where other radicals are present, one can make a correction if the assumption is made that all radical–radical rate constants are equal (except for the statistical factor of 2 in the case of unlike radicals). We obtain

$$\text{slope} = \frac{2k(1 + C)}{\epsilon l} \qquad \text{(II)}$$

where C is the ratio of the concentration of "other" radicals to the concentration of the observed radical, R, and can be obtained from the G values given above, and is $C = 0.07$. (This ratio remains constant during the reaction under the assumption made.) Since l = 8 cm, and ϵ is estimated as 2.1 ± 0.4 × 10^3 M^{-1} cm^{-1} in a previous section, we obtain $k = 2.0 \times 10^9$ M^{-1} sec^{-1} for the reaction between two cyclohexyl radicals, which is in the range expected for a diffusion-controlled reaction. Ebert, *et al.*,[16] obtained $2k = 2.5 \times 10^9$ M^{-1} sec^{-1}; the approximate agreement is surprising in view of the already noted discrepancy in the value of $\epsilon_{cyclohexyl}$.

In the case of *n*-hexane, the ratio of "other" radicals to hexyl radicals is $C = 0.25$.[19] Even though C is larger than in the case of cyclohexane, the assumption of equal reaction rate constants should still have little effect on the value of k; the value obtained for k is 3.1 × 10^9 M^{-1} sec^{-1}, using $\epsilon = 1.4 \pm 0.3 \times 10^3$ and the experimental second-order slope of 7.0 ± 0.6 × 10^5 sec^{-1}. For both cyclohexane and *n*-hexane, a reasonable estimate of the absolute error in the rate constant is ±30%. This makes the difference between the values of 2.0 × 10^9 for cyclohexyl in cyclohexane and 3.1 × 10^9 for hexyl in *n*-hexane of questionable significance. It is interesting to note, however, that the viscosities of *n*-hexane and cyclohexane are[26] 0.00294 and about 0.0080 P at 25°, respectively. Although the observed difference in the rate constants is in the right direction, it is far from the factor of about 2.7 predicted on the basis of the (approximate) inverse dependence[27] of rate constant on viscosity in the case of diffusion-controlled reactions. The experimental values of the rate constants may be compared with values calculated from the equation[27]

$$k = \frac{4\pi\sigma_{AB}DN}{1000} \qquad \text{(III)}$$

where σ_{AB} is the encounter radius of the reaction pair, N is the number of molecules per mole, and D is the sum of the diffusion coefficients of the two reactants. (In this case, since the two reactants are identical, the value of D for the radical is used, which is equivalent to applying a statistical factor of $^1/_2$ to the above equation.) The value of D is estimated using the approximate relation[27]

$$D = \frac{kT}{6\pi\eta r} \qquad \text{(IV)}$$

where k is the Boltzmann constant, T is the absolute temperature, η is the viscosity of the solvent, and r is the radius of the radical. Using the viscosities stated earlier, 4 Å as the radius of the radicals, and 8 Å as the encounter radius, we obtain for cyclohexyl in cyclohexane $k = 4.0 \times 10^9$ M^{-1} sec^{-1}, and for hexyl in *n*-hexane $k = 1.1 \times 10^{10}$ M^{-1} sec^{-1}. The observed value is one-half of the calculated value in the case of cyclohexyl. The agreement is fair, considering experimental errors and the approximate nature of (IV). However, in the case of hexyl, the observed value is only 0.28 times the calculated value, indicating that the reaction of two hexyl radicals in *n*-hexane may be less efficient than the reaction of two cyclohexyl radicals in cyclohexane.

The decay of the cyclohexyl and hexyl radicals produced in aqueous solution was also investigated (see section on transient spectra) and the rate constants determined as $k_{cyclohexyl + cyclohexyl} = 1.4 \pm 0.2 \times 10^9$ M^{-1} sec^{-1} and $k_{hexyl + hexyl} = 1.2 \pm 0.2 \times 10^9$ M^{-1} sec^{-1}. Using 4 Å for the radical radius, 8 Å for the encounter radius, and 0.01 P for the viscosity of water, we calculate (for either hexyl or cyclohexyl) $k = 3.3 \times 10^9$ M^{-1} sec^{-1}. A summary of the results concerning the cyclohexyl and hexyl radicals is given in Table I.

The rate constant for decay of the transients in *n*-hexane was also observed at −78° and found to be slower by a factor of 3.9 ± 0.5, which indicates an overall activation energy of 1.4 ± 0.1 kcal/mol. However, eq III and IV predict that k is directly proportional

(26) "Handbook of Chemistry and Physics," 46th ed, R. C. Weast, Ed., The Chemical Rubber Co., Cleveland, Ohio. 1965–1966, pp F-34, F-36.

(27) A. A. Frost and R. G. Pearson, "Kinetics and Mechanism," 2nd ed, John Wiley & Sons, Inc., New York, N. Y., 1961, p 271.

Table I: Summary of Results Concerning Cyclohexyl and Hexyl Radicals

R·	Solvent	λ_{max}, mμ	$\epsilon_{R\cdot}$ at λ_{max}, $(M^{-1}\ cm^{-1})$ × 10^{-3}	$k_{R\cdot + R\cdot}$ $(M^{-1}\ sec^{-1})$ × 10^{-9} Obsd	Calcd[a]
Cyclohexyl	Cyclohexane	240	2.1 ± 0.4	2.0 ± 0.6	4.0
Cyclohexyl	Water	240	1.48 ± 0.15	1.4 ± 0.2	3.3
Hexyl	*n*-Hexane	235	1.4 ± 0.3	3.1 ± 0.9	11.0
Hexyl	Water	235	0.96 ± 0.10	1.2 ± 0.2	3.3

[a] See text.

to the absolute temperature, which means that the activation energy due to the changes in other parameters in the equations is 1.1 kcal/mol. Using the relationship[28] between viscosity and temperature

$$\eta = Ae\left(\frac{\Delta E_{vis}}{RT}\right)$$

and available values of η for *n*-hexane[29] between 0 and 60°, we can estimate by extrapolation that ΔE_{vis} will be $\leqslant$1.6 kcal/mol between 25 and −78°. Since the rate constant for diffusion-controlled encounters between two radicals is expected to be approximately directly proportional to temperature and inversely proportional to viscosity as can be seen from eq III and IV, the approximate agreement between the observed activation energy (1.1 kcal) and the activation energy for diffusion ($\leqslant$1.6 kcal) is expected.

The decay of the cyclohexadienyl radical produced in the solutions of benzene in cyclohexane or hexane was found to be second order, as expected, and the slopes of the second-order plots were examined to estimate the sum of the G values of all radicals. As has been mentioned, the slope is related to the rate constant and a ratio of radical concentrations by eq II. In this case, C is the ratio of the G value of other radicals to the G value of cyclohexadienyl radical for a particular solution, and ϵ is the optical absorption coefficient of the cyclohexadienyl radical. The G value of "other" radicals was calculated as follows, using eq II. The values of k determined for hexyl ($3.1 \times 10^9\ M^{-1}\ sec^{-1}$) and cyclohexyl ($2.0 \times 10^9\ M^{-1}\ sec^{-1}$) in pure hexane and cyclohexane, respectively, were used, and the G values of cyclohexadienyl at any benzene concentration were calculated from Figures 3 and 4, using the experimental values of G(H·) and the relationship between H· and cyclohexadienyl which has already been discussed. These calculations yield the following information. In the case of cyclohexane, the G value for total radicals (including cyclohexadienyl) increases from 3 at 21% benzene to about 5 at 0.1% benzene, which gives us a qualitative idea of the interference of benzene in the production of radicals. In the case of *n*-hexane, the G value for total radicals goes from about 4 at 27% benzene to about 5 at the lowest concentrations of benzene. Of course, these calculations are approximate to the extent that the assumption is made of equal rate constants for all radical–radical reactions. However, the calculated G(radicals) are probably not grossly in error.

Acknowledgment. We thank J. K. Thomas for discussing with us his work on the pulsed radiolysis of hydrocarbon liquids and for suggestions concerning the work presented here. We also thank B. E. Clifft, B. J. Naderer, and D. B. Donkersloot for operating the linac, and B. E. Clifft for the development of various aspects of the equipment which facilitated the experimental work.

(28) W. J. Moore, "Physical Chemistry," 2nd ed, Prentice-Hall, Inc., Englewood Cliffs, N. J., 1955, p 431.

(29) "International Critical Tables," Vol. 7, E. W. Washburn, Ed., McGraw-Hill Book Co., Inc., New York, N. Y., 1928, p 218.

The Photochemistry of Charge-Transfer Systems. I.

Complexes of Iodine with Amines[1]

by Arthur M. Halpern and Karl Weiss

Photochemistry and Spectroscopy Laboratory, Department of Chemistry, Northeastern University, Boston, Massachusetts 02115 *(Received May 7, 1968)*

The flash photolysis of the iodine complexes of quinuclidine (ABCO), triethylenediamine (DABCO), and ammonia has been investigated in methylcyclohexane solution. By means of appropriate filters, excitation was achieved in the charge-transfer band (<350 mμ), the complexed iodine band near 400 mμ, and the uncomplexed iodine band at 520 mμ. In contrast with the behavior of the triethylamine–iodine complex, photolysis of the complexes of the cage amines ABCO and DABCO in the visible bands gives rise to reversible photochemical changes. The transients generated are identified as amine–iodine atom complexes by their spectral characteristics and by their decay mode. The magnitudes of the second-order rate constants indicate that the atom recombination rates are diffusion controlled. Photolysis of the ABCO–amine complex in the charge-transfer band results in the irreversible destruction of the complex. With ammonia, excitation in the shifted and "free" iodine bands produces the same transient absorption, which is also ascribed to the donor-atom complex. The decay is first order and is considered to involve an intra- and intermolecular reaction with ammonia. The photolysis of iodine in pure methylcyclohexane generates transient absorption with λ_{max} 330 mμ which is ascribed to the solvent–iodine atom complex, whose association constant is estimated to have a lower limit of 1 l./mol.

Introduction

The interaction between electron donor and acceptor molecules gives rise to new spectral features which are ascribed to charge-transfer complexes. In general, distinct charge-transfer bands appear and the absorption due to the components of the complex is shifted relative to their absorption in the uncomplexed state. The photochemistry of these complexes has received relatively little attention. One can envision several consequences of irradiation in the charge-transfer or shifted component bands: (1) complete electron transfer leading to radical ions of the donor and acceptor, (2) the production of metastable donor and/or acceptor excited states, or (3) fragmentation of the components. These intermediates can react further and photochemical changes different from those resulting from excitation of the separated components can be anticipated. We have initiated a detailed investigation of the photochemistry of charge-transfer complexes, and in this first paper report on the behavior of iodine–amine systems in solutions.

A number of flash photolysis studies of molecular iodine in the gas phase,[2] in "inert" solvents,[3-5] and in solutions of electron donors[6-9] have been reported. In all cases, homolytic dissociation of the iodine molecule occurs, and in solvents such as carbon tetrachloride and *n*-hexane, the rate of iodine atom recombination is close to diffusion-controlled.[3,4] Photolysis in solvents such as aromatic hydrocarbons,[9] alcohols, and alkyl halides[6] gives rise to transient absorption which has been ascribed to iodine atom–donor charge-transfer complexes. Only fleeting reference has been made to the behavior of iodine–amine complexes.[6] It was reported that photolysis of iodine in triethylamine produces no transient absorption below 9000 Å, and that solutions in pyridine give rise to very weak transient absorption at 4400 Å.

Our experiments were conducted in methylcyclohexane solutions using quinuclidine (azabicyclo-(2,2,2)-octane, ABCO, I), triethylenediamine (1,4-diazabicyclo-(2,2,2)octane, DABCO, II), and ammonia as donors.

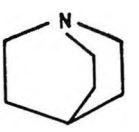

I

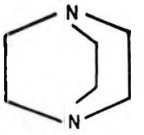

II

Preliminary experiments showed that, in contrast with the behavior of simple alkylamines such as triethylamine, the photolysis of the complexes of ABCO and DABCO produces no permanent changes under appropriate conditions and that transient formation and

(1) Presented at the Symposium on Photochemistry and Radiation Chemistry, U. S. Army Natick Laboratories, Natick, Mass., April 22-24, 1968.

(2) R. Marshall and N. Davidson, *J. Chem. Phys.*, **21**, 658 (1953).

(3) R. L. Strong and J. E. Willard, *J. Amer. Chem. Soc.*, **79**, 2098 (1957).

(4) S. Aditya and J. E. Willard, *ibid.*, **79**, 2680 (1957).

(5) N. K. Bridge, *J. Chem. Phys.*, **32**, 945 (1960).

(6) T. A. Gover and G. Porter, *Proc. Roy. Soc.*, **A262**, 476 (1961).

(7) S. J. Rand and R. L. Strong, *J. Amer. Chem. Soc.*, **82**, 5 (1960).

(8) R. L. Strong, S. J. Rand, and J. A. Britt, *ibid.*, **82**, 5053 (1960).

(9) R. L. Strong, *J. Phys. Chem.*, **66**, 2423 (1962).

decay are entirely reversible. With ammonia there is a slow dark reaction; nonetheless, the photochemical changes are amenable to study with this donor as well.

Experimental Section

Materials. Methylcyclohexane (Matheson Coleman and Bell) Spectroquality solvent was tested for interfering impurities, and was found to be suitable for use without further purification. Ammonia gas (Matheson Coleman and Bell) was dried by passage through a 1 m long tube filled with potassium hydroxide. The preparation of ABCO from its hydrochloride, and the purification of this amine and iodine are described elsewhere.[10,11] An ultrapure sample of DABCO was obtained from the Hondry Process Co.

Apparatus and Procedure. Spectral measurements were made with a Beckman DK-1 recording spectrophotometer. The flash apparatus is described in detail in the second paper of this series. It is based on four xenon-filled (10 mm) flash tubes, with 16 cm between tungsten electrodes, which are energized with two 14-μF capacitors charged to 10 kV. Each capacitor services a set of two lamps connected in series. The flash duration is somewhat wavelength dependent; at 440 mμ, the maximum intensity is reached *ca.* 10 μsec after onset of the flash and it decays with a half-life of 10 μsec. A continuous analyzing beam is provided by a 450-W xenon arc lamp which is stabilized by means of two parallel banks of three 6-V automobile batteries connected in series. Scattered light is minimized by a 6-m separation between the monochromator (Jarrell-Ash f/6.3 grating spectrograph modified by replacing the film holder with a slit assembly) and by appropriately placed baffles. The intensity variations of the monitoring light at a given wavelength are detected with an EMI 9558AQ photomultiplier tube, and the resulting signals are displayed and photographed on a Tektronix Type 535-A oscilloscope. Digitization of the oscilloscope recordsi s accomplished by means of a Gerber digital data reduction system, Model GDDRS-3B. The change in optical density is computed from the equation $\Delta D_\lambda = \log [V_0/(V_0 - V_t)]$, where V_0 and V_t are the voltages which are proportional to the light intensities transmitted by the ground state and transient, respectively.

The solutions were flashed in 14-cm long, 1.2-cm diameter cylindrical Pyrex cells with optically flat windows. To confine light absorption to the free iodine band at 520 mμ, the photolysis cell was covered with a Roscolene No. 807 dark lemon plastic filter (Rosco Laboratories, Inc., Harrison, N. Y.), while for photolysis in the shifted iodine band near 400 mμ a Roscolene No. 863 medium blue filter was employed. It was found that the light stability of these filters is substantially improved by covering them with one layer of "Scotch" brand transparent tape. A 6-cm path length cell, which was attached to the solution reservoir of the photolysis cell, permitted measurement of the ground-state absorption before and after the flash excitation. Excitation in the charge-transfer band was studied only for the ABCO–iodine complex. For this experiment a 12-cm path length jacketed quartz cell was employed. An aqueous filter solution containing cobalt sulfate (0.46 M) and nickel sulfate (0.66 M) confined light absorption to the charge-transfer band at 270 mμ.

The flash experiments were always conducted with solutions freshly prepared from accurately weighed samples of iodine and the amines. Solutions of the ammonia complex were prepared by saturating iodine dissolved in methylcyclohexane with the gas; with this donor, the composition of the solution is not accurately known. It was found that for all three donors the amount and decay behavior of the transients is unaffected by the presence of oxygen. Consequently, undegassed solutions were employed for most of the experiments.

Results

(*a*) *Spectral Features and Photochemical Behavior of the Complexes.* The ground-state absorption spectrum of the ABCO–iodine complex is shown in Figure 1 for a solution containing donor and acceptor in the ratio 7:1. For comparison, the spectrum of iodine in methylcyclohexane is included in this figure. In the complex, the visible iodine band is shifted from 520 to 400 mμ and a strong charge-transfer band appears at 272 mμ (ϵ_{max} 2.8 $\times$ 10^4 l. mol^{-1} cm^{-1}). At lower donor-to-acceptor ratios both uncomplexed and shifted iodine bands are evident, and with appropriate filters selective excitation can be achieved in each of these three spectral regions. These spectral features, with some variation in the positions of the band maxima, are common to all amine–iodine systems.

Our earliest experiments were performed with the triethylamine–iodine complex, which has a charge-transfer band with λ_{max} 278 mμ and a shifted iodine band with λ_{max} 412 mμ. Continuous irradiation of solutions in the latter band with a filtered tungsten source results in the rapid disappearance of the color and the formation of a colorless solid. In dichloromethane, this solid showed no absorption maximum above 200 mμ; the addition of a small amount of free iodine to this solution furnished a spectrum characteristic of the I_3^- ion. Under comparable conditions, the complexes of the cage amines ABCO and DABCO are stable with respect to the formation of permanent photochemical products. Flash photolysis of their solutions in the visible region generates transient species, and after as many as 100

(10) A. M. Halpern, J. L. Roebber, and K. Weiss, *J. Chem. Phys.*, in press.

(11) A. M. Halpern and K. Weiss, *J. Amer. Chem. Soc.*, submitted for publication.

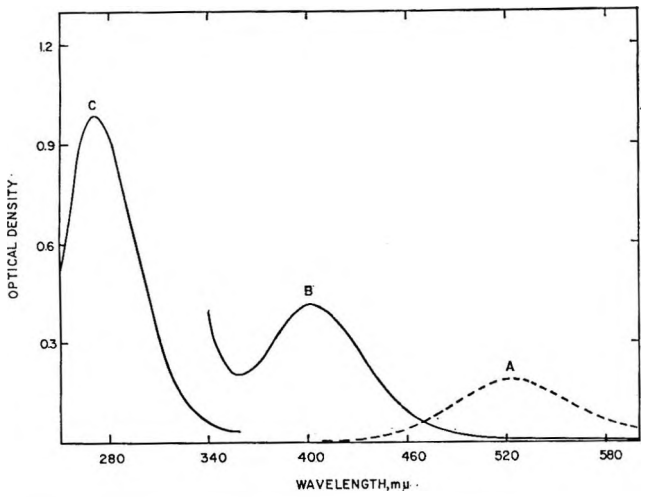

Figure 1. Ground-state absorption spectrum of the ABCO–iodine complex in methylcyclohexane at 23°: curve A, $(I_2) = 3.3 \times 10^{-5}$ *M*, $l = 6$ cm; curve B, $(I_2) = 3.3 \times 10^{-5}$ *M*, (ABCO) $= 2.3 \times 10^{-4}$ *M*, $l = 6$ cm; curve C, as B, $l = 1$ cm.

flashes with an energy input of 1400 J there is no significant change in the ground-state absorption spectrum. ABCO and DABCO are probably the strongest donors known with respect to complex formation with iodine.[11] For ABCO, the association constant is $(3.3 \pm 0.4) \times 10^5$ l./mol at 23°. With DABCO, both 1:1 and 1:2 complexes are formed; the corresponding association constants at 23° are $(6.8 \pm 0.3) \times 10^4$ l./mol (K_1) and $(2 \pm 1) \times 10^3$ l./mol (K_2). These values indicate that at the iodine concentrations employed in this study ($\sim 5 \times 10^{-5}$ *M*) and with donor-to-acceptor ratios greater than 5, the iodine is almost completely complexed. Moreover, under these conditions the 1:2 complex of DABCO is an insignificant component of the solutions.

Flash excitation of the ABCO–iodine complex (Figure 1) in the charge-transfer band at 272 mμ results in its irreversible decomposition. Owing to the high extinction associated with this band, a solution containing only 4×10^{-6} mol/l. of the complex had to be used for this experiment. After 20 1400-J flashes, about half of the complex had disappeared. No transient species with absorption below 700 mμ was observed. The products of this reaction have not, as yet, been further investigated.

(*b*) *Transient Spectra.* The photolysis of iodine in methylcyclohexane in the absence of amines generates a transient with broad absorption between 240 and 420 mμ with λ_{max} 330 mμ (Figure 2a, solid curve). Transient absorption in this spectral region has been observed with solutions of iodine in several normal hydrocarbons, isopentane, and cyclohexane.[5,6] On the basis of kinetic evidence (*vide infra*), we ascribe it to the solvent-complexed iodine atom. The kinetic results also allow the extinction coefficient at 330 mμ in methylcyclohexane to be estimated as 1.6×10^3 l. mol^{-1} cm^{-1}.

The transient spectra for the iodine complexes of ABCO, DABCO, and ammonia are shown in Figures 2b, 2c, and 2d, respectively. In each case the ground-state absorption of the complex is represented by the dashed curve. With ABCO and DABCO, more than 99% of the iodine is complexed and irradiation was confined to the shifted iodine band (blue filter). Ammonia is a relatively weak donor toward iodine (the association constant is 67 l./mol at 20° in *n*-heptane[12]) and the solution saturated with ammonia ($\sim 10^{-2}$ *M*) shows absorption due to both uncomplexed and complexed molecular iodine. Irradiation in either of these bands produces the transient spectrum with λ_{max} 350 mμ shown in Figure 2d. The DABCO–iodine complex transient absorption (λ_{max} 520 mμ) is clearly separated from the ground-state absorption and, furthermore, bleaching is evident near 400 mμ. The ABCO–iodine transient absorption (Figure 2b) completely overlaps the ground-state absorption. For this system the transient spectrum changes with the donor-to-acceptor ratio. This is illustrated in Figure 3. With an (ABCO)/(I_2) ratio of 1.0, the maximum appears at 360 mμ, and it shifts to longer wavelengths as the ratio is increased. Figure 4, in which the ratio $\Delta D_{410}/\Delta D_{360}$ measured 50 μsec after onset of the flash is plotted against the donor-to-acceptor ratio, shows that the transient spectrum remains constant when (ABCO)/(I_2) > 5. The second-order decay kinetics leaves no doubt that in the amine-containing systems the new transient absorption is due to the amine-complexed iodine atom. The spectral shift noted with DABCO suggests that at low donor-to-acceptor ratios there is a competition between solvent and amine for the iodine atom and that complexes with both of these compounds coexist. These results further indicate that the second-order rate constants for transient disappearance should vary with the donor concentration. This is indeed found to be the case.

Gover and Porter[6] have considered competing equilibria involving the iodine atom (presumably *solvated*) and its complexes with the solvent, S, and an electron-donor, D, *i.e.*

$$I\cdot + D \underset{}{\overset{K_D}{\rightleftharpoons}} DI\cdot \qquad (1)$$

$$I\cdot + S \underset{}{\overset{K_S}{\rightleftharpoons}} SI\cdot \qquad (2)$$

and have developed an expression for the estimation of K_D which is based on the assumption that $1 \gg K_S(S)$. We have applied this method to the DABCO–iodine system and find, from a plot of $1/\Delta D_{520}$ *vs.* $1/(D)$ for solutions of varying donor concentrations which is linear as anticipated (Figure 5), that $K_D = 2 \times 10^3$ l./mol. This is more than an order of magnitude smaller than the association constant for the 1:1 complex

(12) H. Yada, J. Tanaka, and S. Nagakura, *Bull. Chem. Soc. Jap.*, **33**, 1660 (1960).

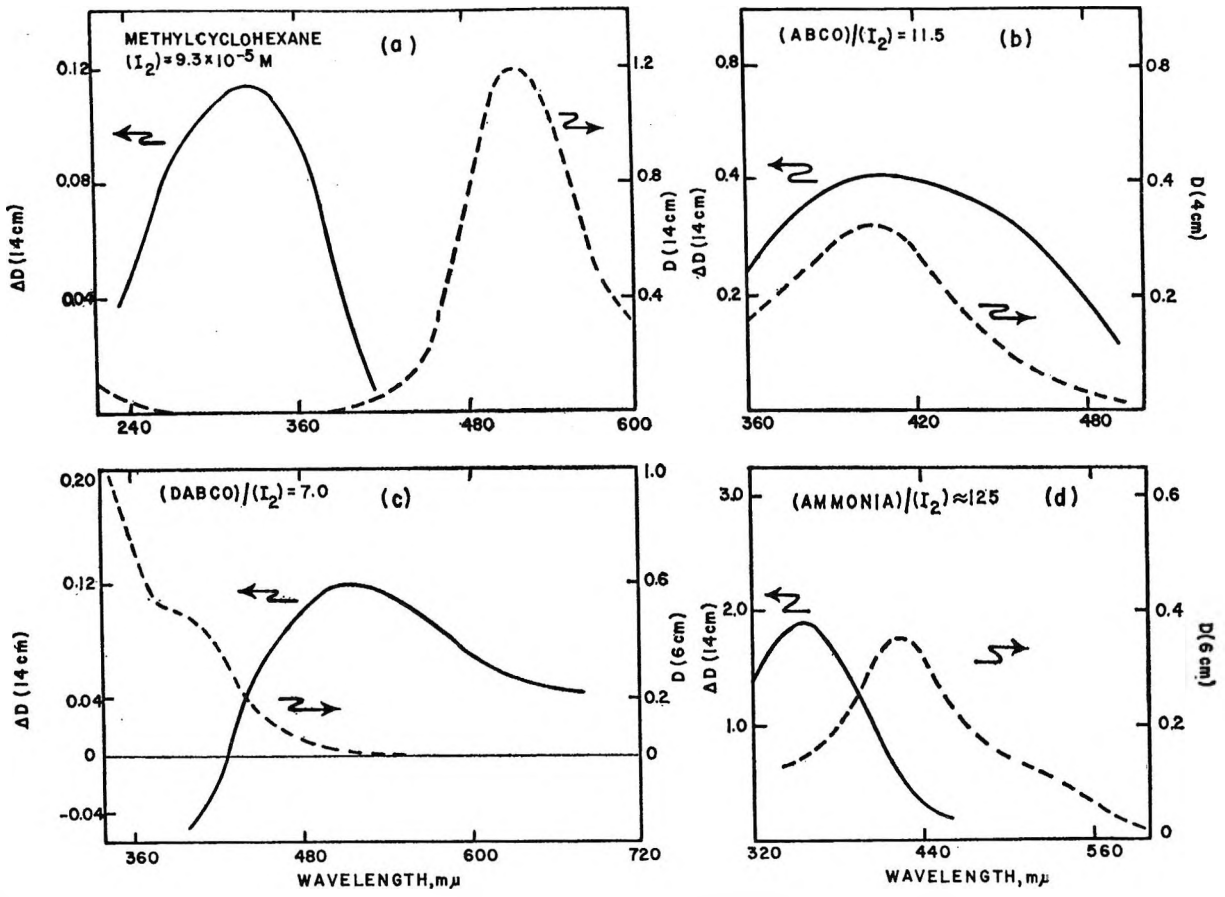

Figure 2. Transient spectra for amine–iodine complexes and solvent: (a) iodine in the pure solvent; (b) $(I_2) = 2.8 \times 10^{-5}\ M$, (ABCO) $= 3.2 \times 10^{-4}\ M$; (c) $(I_2) = 3.4 \times 10^{-5}\ M$, (DABCO) $= 2.4 \times 10^{-4}\ M$; (d) $(I_2) = 8.1 \times 10^{-5}\ M$, $(NH_3) \simeq 10^{-2}\ M$. The dashed curves represent the ground-state absorption of iodine and the complexes. For the complexes, the blue filter was used to confine excitation to the shifted visible iodine bands.

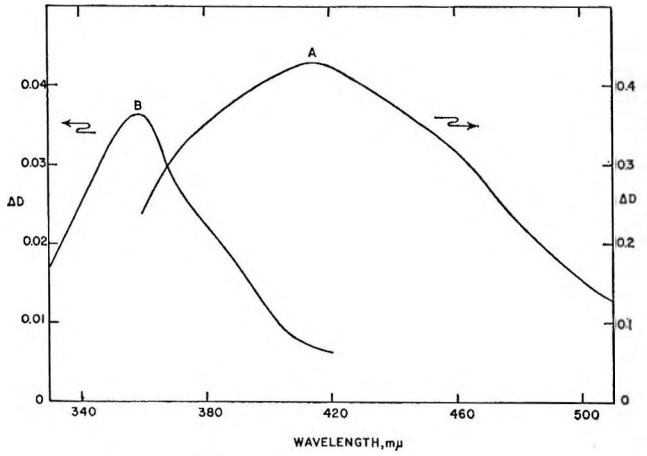

Figure 3. Transient spectra for the ABCO–iodine complexes: curve A, (ABCO)/(I_2) = 100, 44 μsec after flash; curve B, (ABCO)/(I_2) = 1.0, 56 μsec after flash. The iodine concentration is $3.8 \times 10^{-5}\ M$ in both solutions.

of molecular iodine ($K_1 = 6.8 \times 10^4$ l./mol), although a larger value is expected on the basis of the substantially higher electron affinity of the atom than that of the molecule.[13] Owing to the overlapping absorption of several species in the measurement region near 400 mμ, K_D cannot be determined for the ABCO system by this method.

(c) *Kinetics.* Since, with the exception of the ammonia complex, the decay was very fast, the initial decay data had to be corrected not only for signal contributed by the stray light, but also for the continued formation of transient during the decay of the flash pulse. The latter correction, although applicable to all the systems studied, is most easily developed for the photolysis of iodine in the pure solvent where only one transient absorbs. For the solvent–iodine atom complex, the pertinent equation is[9]

$$-\mathrm{d(SI\cdot)}/\mathrm{d}t = 2k(\mathrm{SI\cdot})^2 - 2\Phi I_{abs} \qquad (3)$$

where Φ is the quantum yield of atom complex formation and I_{abs} is the rate of light absorption. If we incorporate the definition $\Delta D_\lambda = \epsilon_\lambda (\mathrm{SI\cdot})l$, where ϵ_λ is the extinction coefficient and l the path length (cm), and recognize that when ΔD_λ has its maximum value $\Delta D_\lambda{}^0$ at a time t_0, $\mathrm{d}\Delta D_\lambda/\mathrm{d}T = 0$, we have

(13) G. Briegleb, "Elektronen Donator-Acceptor Komplexe," Springer-Verlag, Berlin, 1961, p 183.

$$2k(\Delta D_\lambda{}^0)^2 = 2\Phi\epsilon_\lambda{}^2 l^2 I_{abs} \quad (4)$$

Since the fraction of exciting light absorbed by the system is small, I_{abs} at any time t may be taken as proportional to the voltage $V_f(t)$ representing the flash intensity at t (measured in the excitation spectral region); *i.e.*, $I_{abs} = aV_f(t)$, where a is a constant. Equation 4 then becomes $2k/a' = V_f(t_0)/(\Delta D_\lambda{}^0)^2$, where $a' = 2\Phi\epsilon_\lambda{}^2 l^2 a$. In terms of the change in optical density, eq 3 may be rewritten as

$$\frac{-d\Delta D_\lambda}{dt} = \frac{a'}{\epsilon_\lambda l}\left[\frac{2k}{a'}(\Delta D_\lambda)^2 - V_f(t)\right] \quad (5)$$

The bracketed quantity on the right is computed from

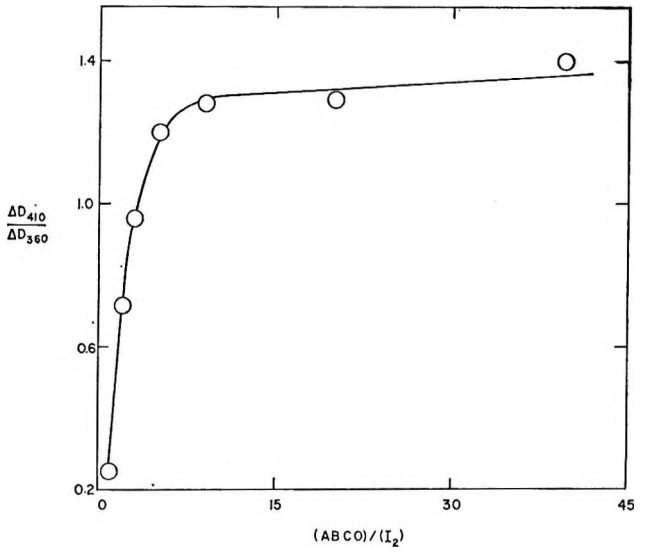

Figure 4. Absorption at 410 and 360 mμ as a function of the (ABCO)/(I_2) ratio. ΔD was measured 50 μsec after the flash. The iodine concentration is 3.8×10^{-5} *M*.

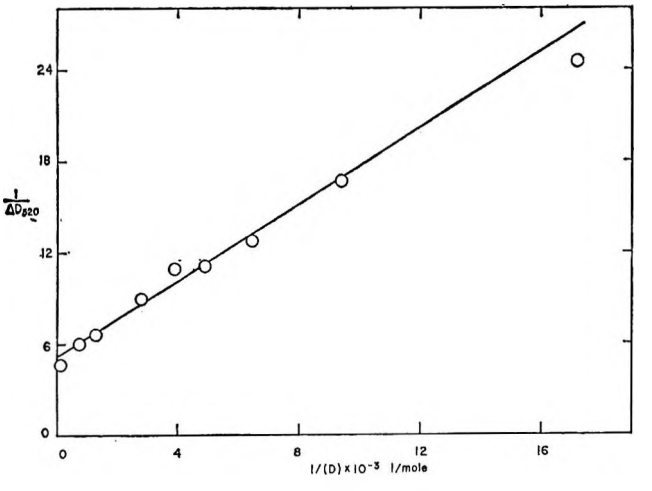

Figure 5. Plot of $1/\Delta D_{520}$ against the reciprocal of the donor concentration for the determination of K_D (or $K_D/(1 + K_S(S))$) for the DABCO–iodine system by Gover and Porter's method.[6] The iodine concentration is 5.1×10^{-5} *M*, and the measurements were taken 50 μsec after the flash.

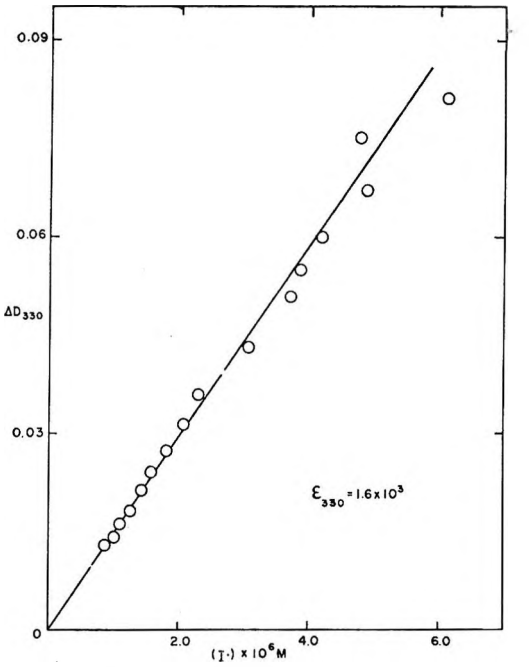

Figure 6. Determination of ϵ_{330} for the methylcyclohexane–iodine atom complex. The path length is 14 cm and $(I_2) = 9.3 \times 10^{-5}$ *M*.

the ratio $2k/a'$ (obtained from the steady-state condition above, in units of volts) and from the values of $(\Delta D_\lambda)^2$ and V_f at given times. At these time values, $-d\Delta D_\lambda/dt$, obtained from differentiation of a ΔD_λ *vs.* time curve, is plotted against the square-bracketed term. For a second-order process, the plot should be linear with an intercept of zero and slope equal to $a'/\epsilon_\lambda l$. Since $2k/a'$ is known, k/ϵ_λ may be obtained.

For iodine in pure methylcyclohexane both the rate of transient decay at 330 mμ and the atom recombination rate at 520 mμ can be measured. For the latter, we may equate the total iodine concentration at any time to twice the difference between the initial and actual molecular iodine concentration; *i.e.*, $(I\cdot)_{Total} = 2[(I_2)^0 - (I_2)]$. Knowledge of the extinction coefficient of iodine at 520 mμ (920 ± 10 l. mol^{-1} cm^{-1})[11] then provides the rate constant $k = (1.3 \pm 0.3) \times 10^{10}$ l./mol sec. If the assumption is now made that all iodine atoms are complexed with the solvent, *i.e.*, $(I\cdot)_{Total} = (SI\cdot)$, the extinction coefficient of SI· at 330 mμ may be estimated by plotting the iodine atom concentration against ΔD_{330} at equivalent time points. This Beer's law plot is shown in Figure 6. The value $\epsilon_{330} = 1.6 \times 10^3$ l. mol^{-1} cm^{-1} gives $k = (1.5 \pm 0.2) \times 10^{10}$ l./mole sec for the decay, which is in good agreement with the rate constant for the recombination process.

Inasmuch as the amine systems involve several complexed atom species, it is appropriate to replace the $2k$ of eq 3 by k_{expt}. As can be seen in Figure 2c, the DABCO–iodine system is also amenable to recombination rate measurements. The shifted iodine band,

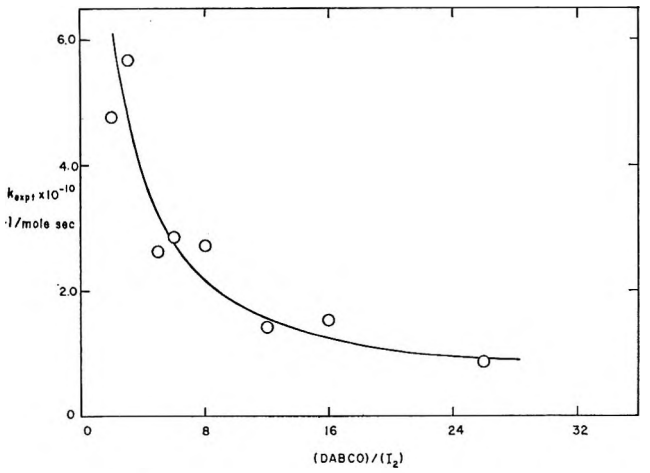

Figure 7. k_{expt} as a function of the (DABCO)/(I_2) ratio. The iodine concentration is 5.1×10^{-5} M.

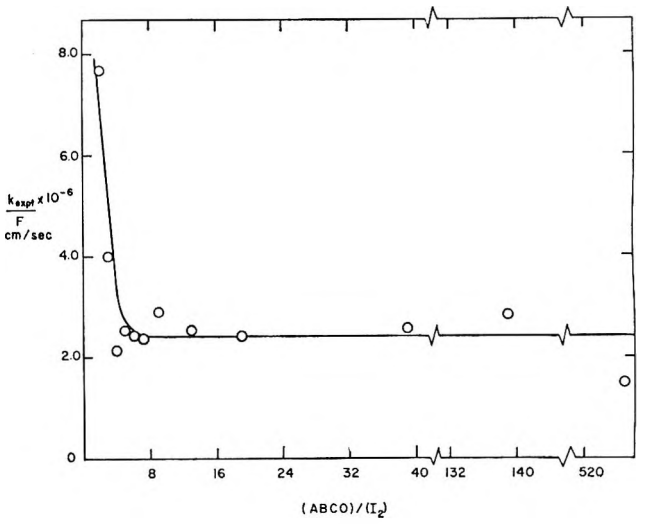

Figure 8. k_{expt}/F as a function of the (ABCO)/(I_2) ratio. The iodine concentration is 3.8×10^{-5} M.

which appears as a shoulder at 395 mμ on the more intense charge-transfer transition, is evidently not significantly overlapped by the transient absorption which maximizes at 520 mμ. Thus, for this system, recombination and decay rate constants can be determined independently from measurements at 495 and 520 mμ, respectively. At high donor concentration the iodine atoms are presumed to be predominantly complexed with the amine, and under these conditions the linear plot of the iodine atom concentration against ΔD_{520} yields $\epsilon_{520} = 3.4$ l. mol^{-1} cm^{-1}. With (DABCO)/(I_2) = 6, the recombination rate constant (k_{expt}) is $(3.4 \pm 0.4) \times 10^{10}$ l./mol sec and the decay rate constant is $(3.6 \pm 0.4) \times 10^{10}$ l./mol sec.

For the DABCO–iodine system, the experimental second-order rate constant decreases with increasing donor-to-acceptor ratio. This behavior, which is predicted by eq 10, is illustrated in Figure 7. This dependence of the experimental rate constant is a result of the partitioning of iodine atoms between free amine and solvent as formulated in the Discussion section. Over the range studied ((DABCO)/(I_2) = 2 to 25), k_{expt} changes by an order of magnitude, and it appears to level off at about 1×10^{10} l./mol sec.

In the case of ABCO, we have already presented evidence that several species absorb in the 400-mμ region. Apart from the ground-state complex (DI_2) there are the transient atom complexes SI· and DI·, so that the change in optical density at 410 mμ is

$$\Delta D_\lambda = \epsilon_{SI,\lambda}(SI\cdot)l + \epsilon_{DI,\lambda}(DI\cdot)l - \epsilon_{DI_2,\lambda}[(DI_2)^0 - (DI_2)]l \quad (6)$$

where $(DI_2)^0$ is the initial equilibrium molecular complex concentration. In view of this complexity, we report only k_{expt}/F cm/sec values here, where F is a function of the extinction coefficients of eq 6 and the donor concentration. The variation of k_{expt}/F with donor concentration is shown in Figure 8. The function rapidly approaches the limiting value of *ca.* 2.5×10^6 cm/sec at a donor-to-acceptor ratio of 5. As will be shown below, this limiting value provides an estimate of the bimolecular rate constant for the combination of DI· complexes.

We have obtained evidence for the presence of yet another transient species in the ABCO–iodine system, which absorbs near 360 mμ. At this wavelength about 90% of the transient absorption decays rapidly. This is followed by a slow decay with a half-life of several milliseconds. This residual absorption is too small to allow evaluation of order and reliable rate constants. This complex behavior is absent at wavelengths greater than 380 mμ. It is in any case clear from the stability of the system to prolonged flash irradiation that the process is reversible. We can make no meaningful speculation regarding its nature on the basis of the limited amount of information at hand. It is, however, recognized that this weak, lingering transient renders material balance equations involving iodine atoms approximate.

The ammonia–iodine complex shows an entirely different behavior from that of the DABCO and ABCO complexes. Since the molecular complex of this donor is weak, the transient absorption with λ_{max} 350 mμ (Figure 2d) may well include a substantial contribution from the solvent–iodine atom complex (Figure 2a). The decay kinetics for a freshly prepared ammonia-saturated solution are strictly first order with $k = (3.5 \pm 0.2) \times 10^3$ sec^{-1}, corresponding to $t_{1/2} = 200$ μsec. The rate constant shows some dependence on the history of the solution. Thus $t_{1/2}$ is larger in aged and repeatedly flashed solutions. This effect is undoubtedly related to the changing nature of the solution, which becomes increasingly turbid in the dark. With prolonged flash excitation, there is a decrease in the amount of ground-state complex. When a solu-

tion containing only sufficient ammonia to complex one-third of the molecular iodine is excited in the uncomplexed iodine band (yellow filter), the decay is more rapid than for the ammonia-saturated case, and the behavior resembles that observed for iodine alone in the solvent. We surmise that, under these conditions, the solvent-complexed iodine atom predominates.

Discussion

The photolysis of iodine in methylcyclohexane follows the pattern observed with other inert solvents.[3,7] The excited iodine dissociates into iodine atoms, which evidently complex rapidly with the solvent. In other words, in the pure solvent (7.8 *M*), the equilibrium of eq 2 is displaced substantially to the right-hand side. The equality of the rate constants for recombination and decay (*vide supra*) suggest that certainly no more than 10% of the iodine atoms are uncomplexed (probably *solvated* as distinguished from *solvent-complexed*). This furnishes a *lower* limit of *ca.* 1 l./mol for K_S. The rate constants in methylcyclohexane compare favorably with those reported for the photolysis in *n*-heptane and in *n*-decane (Table I).[4] The Debye

Table I: Summary of Rate Constants for Iodine Atom Recombination in Solution

System[a]	Reaction (equation)	$k \times 10^{-10}$ (l./mol sec)	Ref
MCH	9	1.3 ± 0.3[b]	*d*
	9	1.5 ± 0.2[c]	*d*
n-Hexane		1.8 ± 0.6[b]	4
n-Decane		1.6 ± 0.4[b]	4
CCl_4		0.72 ± 0.01[b]	2
		0.69 ± 0.06[b]	4
		0.57 ± 0.05[b]	3
ABCO–MCH	7	0.4[c]	*d*
DABCO–MCH	7	0.30 ± 0.15[c]	*d*
	8	1.0 ± 0.5[c]	*d*
Hexamethylbenzene–CCl_4		0.79 ± 0.12[b]	9
		0.75 ± 0.11[c]	9

[a] At room temperature; MCH = methylcyclohexane. [b] From rate of reappearance of I_2. [c] From rate of transient decay. [d] This study.

equation ($k_{diff} = 8RT/3000\eta$, where η is the viscosity in poises) provides the value 1.45×10^{10} l./mol sec at 25° in methylcyclohexane, which agrees well with the observed constants.

For the amine–iodine systems, we have the ground-state equilibrium

$$D + I_2 \underset{}{\overset{K_1}{\rightleftharpoons}} DI_2$$

As pointed out previously, for ABCO and DABCO the molecular iodine is predominantly complexed at high donor concentrations. Consequently, the approximation $(DI_2)^0 - (DI_2) = {}^1/_2(I\cdot)_{Total}$ is valid. The excitation produces iodine atoms

$$DI_2 \xrightarrow{h\nu} DI_2^* \longrightarrow DI\cdot + I\cdot \text{ or } 2I\cdot + D$$

which are rapidly partitioned between the donor and solvent (eq 1 and 2). Since we have reasoned above that, even in the pure solvent, complexation is essentially complete, SI· and DI· are the only atom species which need be considered. The bimolecular decay processes are then

$$2DI\cdot \xrightarrow{2k_7} DI_2 + D \quad (7)$$

$$DI\cdot + SI\cdot \xrightarrow{k_8} DI_2 + S \quad (8)$$

$$2SI\cdot \xrightarrow{2k_9} I_2 + 2S \quad (9)$$

Since only DI· absorbs at 520 mμ for the DABCO system, this scheme yields the rate equation

$$\frac{-d\Delta D_\lambda}{dt} = [2k_7 + k_8/K'(D)]\frac{(\Delta D_\lambda)^2}{\epsilon_{DI,\lambda} l} \quad (10)$$

Here $K' = K_D/K_S(S)$, and the square-bracketed quantity represents k_{expt}. Indeed, a plot of k_{expt} against 1/(D) is reasonably linear (no curvature, but considerable scatter of points), and extrapolation yields $k_7 \simeq 3 \times 10^9$ l./mol sec. With $K' \simeq 2 \times 10^3$ l./mol, the slope gives $k_8 \simeq 1 \times 10^{10}$ l./mol. The error in these constants is large (±50%) so that they may well be equal.

In connection with this calculation it must be pointed out that, with $K_S \simeq 1$ l./mol, $K_S(S) \simeq 8$ and the previously made approximation $1 \gg K_S(S)$ does not hold. Consequently, the constant obtained by Gover and Porter's method[6] is not K_D, but $K_D/(1 + K_S(S))$. The new value of K_D is then *ca.* 2×10^4 l./mol, which is closer to but still less by a factor of about 3 than the K_1 value for DABCO.

For ABCO complex, eq 6 applies and the differential equation

$$\frac{-d\Delta D_\lambda}{dt} = \frac{[2k_7 + k_8/K'(D)](\Delta D_\lambda)^2}{[\epsilon_{DI,\lambda} - \epsilon_{DI_2,\lambda}/2 + (\epsilon_{SI,\lambda} - \epsilon_{DI_2,\lambda}/2)/K'(D)]l} \quad (11)$$

can be derived, for which k_{expt} is defined as for eq 10 and the square-bracketed quantity in the denominator is the function F (*vide supra*). The appearance of Figure 8 relative to Figure 7 can now be qualitatively understood since $\epsilon_{DI_2,\lambda} > 2\ \epsilon_{SI,\lambda}$. As predicted by eq 11, k_{expt}/F is not a linear function of 1/(D). At high donor-to-acceptor ratios $k_{expt}/F \simeq 2k_1/(\epsilon_{DI,\lambda} - \epsilon_{DI_2,\lambda})$, and if we take $\epsilon_{DI,410}$ for the ABCO complex as approximately equal to $\epsilon_{DI,520}$ for the DABCO complex ($\sim 4 \times 10^3$ l. mol^{-1} cm^{-1}), we obtain $k_7 \simeq 4 \times 10^9$ l./mol sec.

In the ammonia system, we believe that the complexed iodine atoms react with the donor. Since the conversion into atoms is small and the solutions are

buffered with respect to the ground-state molecular complex by the presence of donor and uncomplexed iodine, a single flash excitation will always appear to be reversible. The reaction undoubtedly involves hydrogen abstraction and may be intramolecular (*i.e.*, the iodine atom reacts with the donor molecule to which it is attached) or bimolecular. The products of this reaction are worthy of study.

The rate constants obtained in this investigation as well as some pertinent literature values are summarized in Table I.

It is noteworthy that, contrary to the results for the DABCO and ABCO systems, Strong[9] has found that the rate constant of the iodine atom recombination for the hexamethylbenzene–iodine complex in carbon tetrachloride is independent of the donor concentration. The value $K_D = 2.7$ l./mol is reported for this system. If the iodine concentration is $\sim 10^{-4}$ M in these experiments, the smallest donor concentration quoted corresponds to a donor-to-acceptor ratio of 620. Under these conditions the dependence on donor concentration is not likely to be detected.

While the associated constant for the DABCO–iodine atom complex is distinctly smaller than anticipated, the charge-transfer transition energies as reflected in the transient absorption maxima do, in all cases, show the expected red shift relative to the corresponding molecular iodine complexes. The iodine complexes of ammonia,[14] ABCO, and DABCO[11] have maxima at 229, 272, and 310 mμ, respectively; the corresponding atom complexes peak at about 350, 410, and 520 mμ, respectively. For each donor, the energy separation is approximately the same (1.7 ± 0.1 eV). Finally, we note that although the charge-transfer transition energies do increase with increasing ionization potential of the amine (ammonia, 10.15 eV; ABCO, 7.72 eV; DABCO, 7.2 eV[10]) as predicted by theory,[15] they do not follow the approximate correlation noted by Gover and Porter[6] for some other iodine atom complexes.

Acknowledgments. This research was supported by the Air Force Cambridge Research Laboratories, Office of Aerospace Research, under Contract F 19628-67-C-0118. We are grateful to Dr. J. L. Roebber for many helpful discussions and to Mr. E. Reid for his aid with the computation work, which was carried out at the M.I.T. Computation Center.

(14) Reference 13, p 33.

(15) Reference 13, Chapter 6.

The Pulse Radiolysis of Benzene–Biacetyl Solutions

by R. B. Cundall, G. B. Evans, P. A. Griffiths,

Department of Chemistry, The University, Nottingham, England

and J. P. Keene

Paterson Laboratories, Christie Hospital and Holt Radium Institute, Manchester 20, England
(Received May 7, 1968)

Phosphoresence emission from biacetyl has been used to study singlet and triplet excited states produced in the pulse radiolysis of benzene. Cyclohexene acts as a selective scavenger of the triplet state of benzene while the lowest excited singlet state is practically unaffected. The quenching of the benzene excited singlet and triplet states by biacetyl is effectively diffusion controlled and a lifetime of the order of 10^{-8} sec is derived for the excited benzene triplet. A species with an absorption maximum at 317 mμ has identical decay kinetics with the phosphorescence and is assumed to be the biacetyl triplet. Using this absorption and an extinction coefficient of 6400 M^{-1} cm^{-1}, it is concluded that in irradiated benzene the initially formed excited state yields are $G(^1B_{2u}) = 1.43$, $G(^3B_{1u})$ 1.24, and a total measured excited-state yield of 2.67. Some observations are made on the quenching of the biacetyl triplet by cyclohexene ($k = 1.18 \times 10^5$ M^{-1} sec^{-1}). A free-radical quenching species is produced by radiolysis of the benzene and is formed from a species, probably ionic, which achieves a steady state during the pulse. The mechanism assumed involves energy transfer from the $^1B_{2u}$ and $^3B_{1u}$ (or corresponding excimers) states of benzene to the solute. The presence of higher excited states of benzene may explain the difference between the measured yields and values obtained in other experiments.

Introduction

Excited states are primary products of the interaction of ionizing radiation with matter, and excitation transfer has a significant role in the radiation chemistry of solutions. Fluorescence emission shows that excited singlet states are formed and spectroscopic and chemical methods demonstrate that triplet states of solutes are produced in a range of organic solvents.

Singlet, triplet, and possibly higher multiplets may be formed by interactions with charged particles or from the recombination of charged species. These initially formed excited states may undergo any of a number of possible processes, chemical reaction, energy transfer, internal conversion, intersystem crossing, or mutual interaction such as triplet–triplet annihilation to produce excited singlets. Internal conversion of higher states to produce the lowest excited state of the appropriate manifold is usually assumed to be fast, but benzene and its alkyl derivatives appear to be significant exceptions.[1]

Many studies of excitation transfer in radiation chemical systems have failed to distinguish the possibility of singlet–singlet from triplet–triplet transfer. This paper describes experiments carried out to determine the yields of different excited states in irradiated benzene. Pulse radiolysis is well adapted to the study of light emissions, and biacetyl has been selected because of its high phosphorescence yield in fluid media. The high sensitivity of emission detection allows measurements to be made at low doses. Earlier work has shown the efficiency with which olefins undergo triplet–triplet energy transfer with the $^3B_{1u}$ state of benzene.[2] The fluorescent $^1B_{2u}$ state is only slightly affected by olefins. Cyclohexene addition has been used to distinguish the contributions of singlet–singlet and triplet–triplet energy exchange processes in the radiation-induced excitation of biacetyl in benzene.

Experimental Section

The pulse-radiolysis studies were made using the apparatus described by Keene.[3] Optical measurements were made after 2- or 0.2-μsec pulses of 4-MeV electrons at various dose rates. The monochromator was used with entrance and exit slit widths of 1.6 and 2.8 mm, respectively, giving a half band width of 10 mμ.

Benzene was purified by shaking with concentrated sulfuric acid, washing with water, partial crystallization with rejection of the unfrozen liquid, drying with phosphorus pentoxide, and distillation. Biacetyl and cyclohexene were twice vacuum distilled and stored over anhydrous sodium sulfate. Biacetyl was kept in the dark to prevent photolysis. Oxygen, sulfur hexafluoride, and nitrous oxide were used direct from the cylinder. Oxygen was removed from the solutions by flushing with argon.

Results

Emission Spectra. At a dose of 60 rads/2-μsec pulse a long-lived emission from a solution in benzene was observed with a maximum at 520 mμ. The spectrum of the emission is shown in Figure 1, due correction having been made for the wavelength response of the

(1) C. L. Braun, S. Kato, and S. Lipsky, *J. Chem. Phys.*, **44**, 3667 (1966).

(2) R. B. Cundall and P. A. Griffiths, *Trans. Faraday Soc.*, **61**, 1968 (1965).

(3) J. P. Keene, *J. Sci. Instrum.*, **41**, 493 (1964).

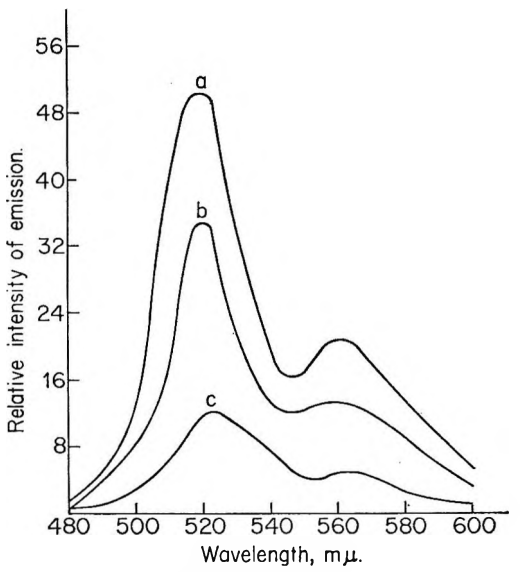

Figure 1. Emission spectrum of biacetyl in benzene taken 20 μsec after 2-μsec pulses at a dose of 60 rads: a, 1.15×10^{-2} *M*; b, 5.72×10^{-3} *M*; c, 1.15×10^{-3} *M*.

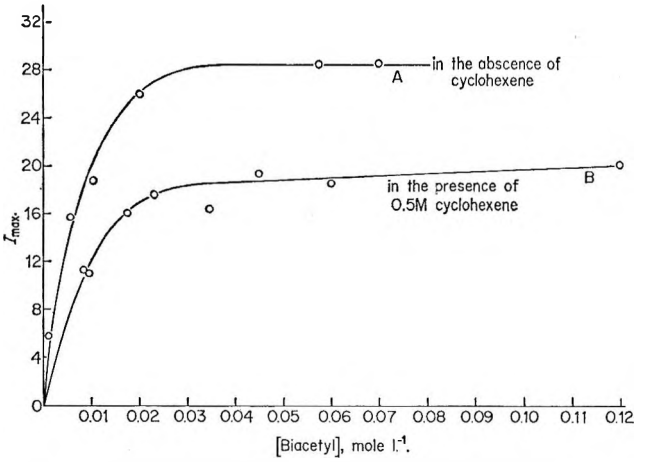

Figure 2. The dependence of the intensity of biacetyl phosphorescence on biacetyl concentration. I_{max} is the intensity immediately after the pulse (2 μsec, 60 rads): A, biacetyl in benzene; B, biacetyl + 0.5 *M* cyclohexene in benzene.

photomultiplier by use of the manufacturer's standard curves. The relative intensity values shown were taken 20 μsec after the pulse but the form of the spectrum was not time dependent. The derived spectrum agrees with the long-lived biacetyl emission spectra published by Backström and Sandros[4] and Dubois and Wilkinson.[5] Changing the concentration of biacetyl changed the intensity of emission but did not affect the shape of the spectrum. No postpulse emission was observed from benzene at any wavelength within the range of the apparatus.

Effect of Concentration and Dose. The dependence of the intensity of phosphorescence at 520 mμ on the concentration of biacetyl at a constant dose of 60 rads/pulse is shown by curve A in Figure 2. The decay of the phosphorescence is exponential, *i.e.*, first order, and I_{max} refers to the relative value of the emission at the end of the pulse obtained by extrapolation of the linear plot of log (intensity of emission, *I*) *vs.* time. The half lifetime of emission in one series of experiments remained constant at 125 μsec down to 5×10^{-3} *M*, but at 10^{-3} *M* biacetyl a half lifetime of 145 μsec was recorded. The actual lifetimes observed were dependent on samples used but in all cases were of the order of those quoted and tended to increase at the lowest biacetyl concentrations.

At a fixed concentration of biacetyl the intensity of the emission is linearly dependent on dose. This is exemplified by data at three concentrations shown in Table I. The half lifetime of the emission decreased with increasing dose during the pulse in most of the experiments. Deviations from this were almost certainly due to adventitious impurities in different samples. No emission was observed with pulses in excess of 1000 rads due to the very short half-life of the phosphorescence under these conditions, the impossibility of distinguishing it from the "tail" of the Cerenkov emission, and the strong fluorescence emitted during the pulse.

Table I

Concn of biacetyl, M^{-1}	Approx. dose, rads/2-μsec pulse	I_{max}, relative units	Half-life of emission, μsec
6.9×10^{-2}	20	9.2	125
6.9×10^{-2}	150	67.5	60
6.9×10^{-2}	500	208	26.5
5.75×10^{-2}	20	9.85	122
5.75×10^{-2}	60	28.5	124
5.75×10^{-2}	100	49.5	100
5.75×10^{-2}	500	270	50
1.15×10^{-2}	60	18.6	126
5.75×10^{-3}	60	15.8	120
1.15×10^{-3}	60	5.2	145
1.0×10^{-3}	20	1.55	235
1.0×10^{-3}	150	19.4	84
1.0×10^{-3}	500	46.8	56

Repeated pulsing of solutions up to the order of 1000 pulses at a dose of 60 rads/pulse gradually reduced the intensity and lifetime of the phosphorescence emission.

Effect of Oxygen, Sulfur Hexafluoride, and Nitrous Oxide. No emission was observed from an air-or oxygen-saturated solution and thorough deaeration was necessary in the experiments. Sometimes the intensity and lifetime of the emission increased up to a constant level after a small number of successive low dose pulses indicating that trace quantities of oxygen were present in

(4) H. L. J. Backström and K. Sandros, *Acta Chem. Scand.*, 12, 823 (1958).

(5) F. Wilkinson and J. T. Dubois, *J. Chem. Phys.*, 38, 2541 (1963); 39, 377 (1963).

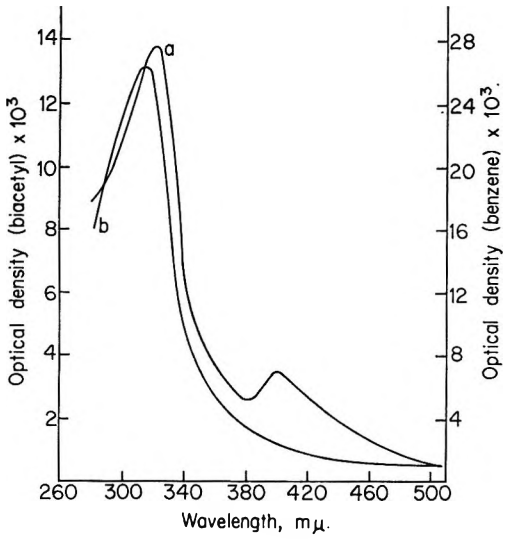

Figure 3. Absorption spectra: a, species produced in pure benzene after pulses (2 μsec) of 7000 rads (right-hand axis); b, species produced in 5.75×10^{-3} M biacetyl in benzene after 500-rad pulses (2 μsec) (left-hand axis).

the solution and were being consumed by reaction with radicals produced by radiolysis. Only very small amounts of oxygen or other impurity could be removed by this process.

In a number of experiments it was shown that the effect of saturating the solution with nitrous oxide was slight; I_{max} was reduced by less than 4%. Sulfur hexafluoride saturation had a similar lack of effect.

Absorption Spectra. In pure deaerated benzene using pulses of approximately 7000 rads, two transients were found, one with a maximum at 320 mμ (half-lifetime of approximately 500 μsec) and another very much weaker with a maximum at 400 mμ (half-lifetime of approximately 5 μsec). The former agrees with an absorption found by Dorfman[6] at 323 mμ attributed to the phenylcyclohexadienyl or cyclohexadienyl radical. McCarthy and MacLachlan[7] also observed this species which disappeared by a bimolecular reaction. Rate constants for this radical–radical interaction of 2.8 and 6.2×10^9 M^{-1} sec^{-1}, respectively, have been assigned by these two groups assuming $G = 0.3$. The species observed at 400 mμ is probably an excited polyphenyl produced by the radiolysis of benzene.

Using a pulse of 500 rads and a 5×10^{-3} M solution of biacetyl, a transient absorption was observed at 315 mμ with a half-lifetime of 120 μsec. This coincided exactly with the half-lifetime of the phosphorescence of the biacetyl triplet. This observation was repeated in a number of experiments. The benzene and biacetyl absorption spectra are shown in Figure 3.

Effect of Cyclohexene. The variation of phosphorescence intensity with biacetyl concentration was studied with a solution of 0.5 M cyclohexene in benzene (curve B, Figure 2). An overall reduction in intensity of phosphorescence occurred although a plateau value was not achieved. The observed half-lifetime of emission was considerably decreased by the presence of cyclohexene, but increasing the concentration of biacetyl from 8.05×10^{-3} to 1.2×10^{-1} M increased the half-lifetime of biacetyl triplet decay from 6.5 to 31 μsec. This observation has also been confirmed in other experiments.

The effect of varying the concentration of cyclohexene on the phosphorescence of a 3.7×10^{-2} M biacetyl solution in benzene was also examined. Increasing the concentration of cyclohexene from 4×10^{-3} to 1.8×10^{-1} M gradually reduced the phosphorescence from $I_{max} = 33$ to $I_{max} = 18.6$. Further addition of cyclohexene up to 7×10^{-1} M did not further significantly affect the intensity of emission, Figure 4. The half-lifetime of emission decreased from 110 μsec for a solution containing no cyclohexene to 15 μsec for a 7×10^{-1} M cyclohexene solution. It was noticeable that in the presence of cyclohexene the strictly linear plots of log I *vs.* t obtained in the absence of cyclohexene changed slightly in the presence of cyclohexene. A trend toward second-order kinetics was apparent at the end of the biacetyl triplet decay.

Measurement of G Values. The molar extinction coefficient of the triplet state of biacetyl at the maximum absorption wavelength of 317 mμ has been determined by Land[8] to be 6200 and 6600 M^{-1} cm^{-1} relative to the 1,2-benzathracene and anthracene triplet extinction coefficients. The mean value of 6400 M^{-1} cm^{-1} was used in this work. Emission at any dose can be related to a G value calculated from the extinction coefficient and observed optical density. For a 0.04 M

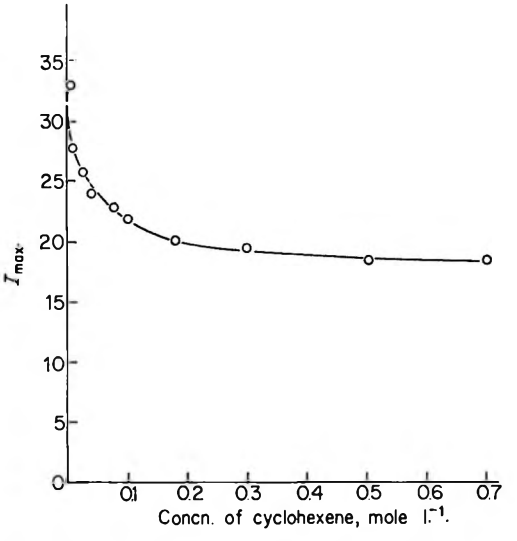

Figure 4. The effect of cyclohexene on the emission from a 3.7×10^{-2} M solution of biacetyl in benzene.

(6) L. M. Dorfman, I. A. Taub, and R. E. Buhler, *J. Chem. Phys.*, **36**, 3051 (1962).

(7) A. MacLachlan and R. L. McCarthy, *J. Amer. Chem. Soc.*, **84**, 2519 (1962).

(8) Dr. E. J. Land, private communication.

biacetyl solution in benzene the measured triplet state yield was 2.67/100 eV. In 0.14 M nitrous oxide the yield was 2.56/100 eV. In the presence of 0.5 M cyclohexene the yield decreased to about 1.4 molecules/100 eV, *i.e.*, a reduction of 45%

Discussion

The results are interpreted by a mechanism in which there is transfer of electronic excitation from solvent molecules excited by radiation to the biacetyl solute. The lack of effect of electron scavengers suggests that charge recombination on the solute is an unimportant process for biacetyl excitation.

The primary excitation processes are

$$C_6H_6 \text{ -ww-> } {}^1C_6H_6 \quad (1)$$

$$\text{-ww-> } {}^3C_6H_6 \quad (2)$$

It will be assumed that only the lower $^1B_{2u}$ and $^3B_{1u}$ (assumed) states are involved in populating the triplet state of biacetyl. Transfer from higher energy states would probably dissociate biacetyl. The limited evidence available indicates that the conventional idea of rapid internal conversion of higher states to the lowest excited states may not be valid in the case of benzene.[1,9]

The single excited benzene molecules may undergo intersystem crossing

$$^1C_6H_6 \longrightarrow {}^3C_6H_6 \quad (3)$$

Experiments using 2537-Å light show that the efficiency of (3) in liquid benzene is 0.6,[10] and the fluorescence yield is 0.06.[11] Since the lifetime of the singlet state determined by fluorescence decay measurements is about 20 nsec,[12] $k_3 = 3.1 \times 10^7$ sec^{-1}.

In the presence of biacetyl (B) singlet–singlet energy transfer may occur

$$^1C_6H_6 + B \longrightarrow C_6H_6 + {}^1B \quad (4)$$

k_4 has been measured by ourselves in a series of fluorescence quenching experiments to be 3.0×10^{10} M^{-1} sec^{-1} in reasonable agreement with the value of 4.0×10^{10} M^{-1} sec^{-1} obtained by Dubois.[13] The singlet excited benzene may revert to the ground state by either

$$^1C_6H_6 \longrightarrow C_6H_6 \quad (5)$$

or

$$^1C_6H_6 \longrightarrow C_6H_6 + h\nu_f \quad (6)$$

Reaction 5 is apparently responsible for deactivation of about 30% of the excited benzene singlet in the absence of quenchers. Excimer formation[14] occurs but for simplicity will be formally ignored. The assumption that processes 3, 4, and 5 are first order is not likely to introduce serious error.

Triplet benzene molecules may undergo either triplet–triplet transfer

$$^3C_6H_6 + B \longrightarrow C_6H_6 + {}^3B \quad (7)$$

or deactivation

$$^3C_6H_6 \longrightarrow C_6H_6 \quad (8)$$

Normally k_8 would be expected to be of the order of 10^3 M^{-1} sec^{-1}, but it appears that 10^8 is typical for benzene and its homologs.[2,13] The reasons for this are not understood.

The excited biacetyl molecules may undergo

$$^1B \longrightarrow {}^3B \quad (9)$$

$$^1B \longrightarrow B + h\nu_f \quad (10)$$

$$^3B \longrightarrow B + h\nu_p \quad (11)$$

$$^3B \longrightarrow B \quad (12)$$

Almgren[15] has determined the fluorescence quantum yield for biacetyl in benzene to be 0.0027; the triplet yield is practically unity.

Mutual annihilation of triplet states

$$^3C_6H_6 + {}^3C_6H_6 \longrightarrow {}^1C_6H_6 + C_6H_6 \quad (13)$$

$$^3B + {}^3B \longrightarrow {}^1B + B \quad (14)$$

is not important at the low doses used. This is indicated by the linear increase in yield with dose and first-order biacetyl triplet decay.

When cyclohexene (C) is present

$$^3C_6H_6 + C \longrightarrow C_6H_6 + {}^3C \quad (15)$$

$$^1C_6H_6 + C \longrightarrow C_6H_6 + C \quad (16)$$

$$^3C \longrightarrow C \quad (17)$$

Reaction 15 will be efficient since olefin triplet states are lower in energy than the benzene triplet.[2] Rate constants for triplet–triplet transfer are around 5×10^9 M^{-1} sec^{-1},[16] and a similar value for k_{15} is expected in this case.

The quenching of benzene singlet states by olefins has been studied spectrofluorimetrically.[11] Pure monoolefins have rate constants for quenching of benzene fluorescence $k_{16} \simeq 2 \times 10^5$ M^{-1} sec^{-1}, but exposure to air produces a marked increase due to the presence of oxidation products, and a value of 4×10^7 M^{-1} sec^{-1} is

(9) J. K. Foote, M. H. Mallon, and J. N. Pitts, Jr., *J. Amer. Chem. Soc.*, **88**, 3698 (1966); F. Mellows and S. Lipsky, *J. Phys. Chem.*, **70**, 4076 (1966).

(10) W. Tippett and R. B. Cundall, to be published.

(11) G. B. Evans, Ph.D. Thesis, University of Nottingham, 1967.

(12) J. B. Birks and I. D. Munro, *Progr. Reaction Kinetics*, **4**, 239 (1967); I. Berlman, "Handbook of Fluorescent Spectra," Academic Press, New York, N. Y., 1965.

(13) J. T. Dubois and J. W. van Loben Sels, *J. Chem. Phys.*, **45**, 1522 (1966); also "Proceedings of the International Symposium on Luminescence," Munich, 1965, p 109.

(14) J. B. Birks, C. L. Braga, and M. D. Lumb, *Proc. Roy. Soc.*, **A283**, 83 (1965).

(15) M. Almgren, *Photochem. Photobiol.*, **6**, 829 (1967).

(16) *E.g.*, W. G. Herkstroeter and G. S. Hammond, *J. Amer. Chem. Soc.*, **88**, 4769 (1966).

a reasonable estimate for k_{16} for the samples used. An amount equal to 0.1% of an efficient quenching impurity, such as a diene, could cause all the observed quenching; cyclohexadiene had a rate constant of $2.1 \times 10^{10}\ M^{-1}\ \text{sec}^{-1}$ for the quenching of benzene fluorescence.[11] Reaction 17 must be very rapid since there is no evidence for triplet excitation transfer from cyclohexene. This is expected from the theoretically predicted overlap of triplet and ground-state potential energy surfaces in the case of olefins.[17] Singlet–singlet energy transfer from benzene to the olefin is inefficient since the lowest olefin excited singlet is higher in energy than the $^1B_{2u}$ state of benzene and chemical interaction has a low yield.

It is necessary to include the very effective quenching of biacetyl triplets by some radiolytic product X (which cannot be ionic)

$$^3B + X \longrightarrow (?) \qquad (18)$$

Radicals are the most likely species since the main quencher disappears within a few milliseconds. It is clear that the radiolytic products quench the triplet biacetyl and not its precursor. Extended irradiation produces a permanent quenching species, probably a polyphenyl. Cyclohexene also quenches the biacetyl triplet

$$^3B + C \longrightarrow \text{product} \qquad (19)$$

probably by chemical interaction.[4]

Kinetic Treatment. For convenience the scheme is simplified as

$F_1 = \dfrac{k_{11}}{k_{11} + k_{12}}$ (the fraction of biacetyl triplet states which phosphoresce)

$F_2 = \dfrac{k_1}{k_1 + k_2}$ (the fraction of excited benzene formed in the singlet state)

$F_3 = \dfrac{k_4(B)}{k_4(B) + k_5 + k_6 + k_3}$ (the probability that excited benzene singlet states will transfer to biacetyl)

In the presence of cyclohexene, F_1 becomes

$$F_1^1 = \frac{k_{11}}{k_{11} + k_{12} + k_{19}(C)}$$

and F_3 becomes

$$F_3^1 = \frac{k_4(B)}{k_4(B) + k_5 + k_6 + k_3 + k_{16}(C)}$$

F_4, the probability that the excited singlet biacetyl crosses to the triplet states, is unity. The probability that singlet excited benzene crosses to the triplet state is

$$F_5 = \frac{k_3}{k_3 + k_5 + k_4(B)}$$

which in the presence of cyclohexene becomes

$$F_5^1 = \frac{k_3}{k_3 + k_5 + k_4(B) + k_{16}(C)}$$

If F_6 is the probability that triplet benzene transfers to biacetyl

$$F_6 = \frac{k_7(B)}{k_7(B) + k_8}$$

in the presence of cyclohexene this becomes

$$F_6^1 = \frac{k_7(B)}{k_7(B) + k_8 + k_{15}(C)}$$

Finally

$$F_7 = \frac{k_2}{k_2 + k_1}$$

the fraction of excited benzene formed in the triplet state.

It follows that

$$G(^3B) \propto I = \alpha[F_2\{F_3F_4) + (F_5F_6)\} + F_6F_7]$$

where α is a proportionality factor including the rate constant for phosphorescence and dose received.

When biacetyl is in excess, $k_4(B) \gg k_3 + k_5$, so $F_5 \to 0$ and $F_3 = F_4 = F_6 = 1$; *i.e.*, all the excitation energy of benzene is transferred to the biacetyl and $I = \alpha$.

In the experiments with the higher concentrations of biacetyl (0.037 M) and 0.5 M cyclohexene, $k_{15}(C) \gg k_7(B)$ so $F_6^1 \to 0$ and the observed emission is due to singlet–singlet energy transfer followed by intersystem crossing.

The difference between the yields under the two specified conditions measures the contribution to the biacetyl triplet emission from triplet transfer ($k_{16}(C)$ is less than 1% of $k_4(B)$ when biacetyl is in excess).

When the phosphorescence yield of a 0.037 M solution of biacetyl in benzene is plotted as a function of (C), it can be seen that cyclohexene scavenges benzene triplet molecules and prevents triplet–triplet transfer to biacetyl.

If we write the difference in intensities in the absence and presence of cyclohexene as $I - I_s$, then $I - I_s = \alpha F_6^1 F_7$, or

$$\frac{1}{I - I_s} = \frac{1}{\alpha F_7 F_6} + \frac{k_{15}(C)}{\alpha F_7 k_7(B)}$$

A plot of $(I - I_s)^{-1}$ *vs.* (C) is shown in Figure 5.

From the slope and intercept it is possible to calculate that $k_{15}/k_7 = 1.09 \pm 0.2$, *i.e.*, biacetyl and cyclohexene are of approximately equal efficiency in deactivating the benzene triplet. This justifies the assumption that the triplet–triplet energy transfer is near the limit of diffusion control. An approximate calculation of k_{15}/k_7 can be made from the data of curve B of Figure 2.

(17) *E.g.*, R. S. Mulliken and C. C. J. Roothaan, *Chem. Rev.*, **41**, 219 (1947).

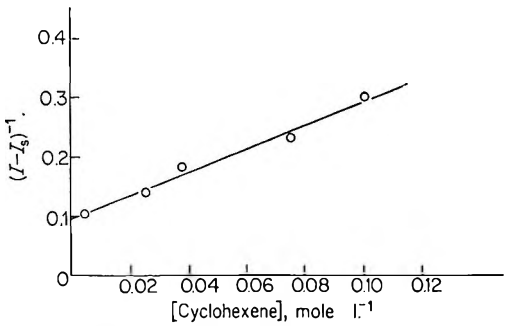

Figure 5. Plot of $(I - I_s)^{-1}$ *vs.* (C).

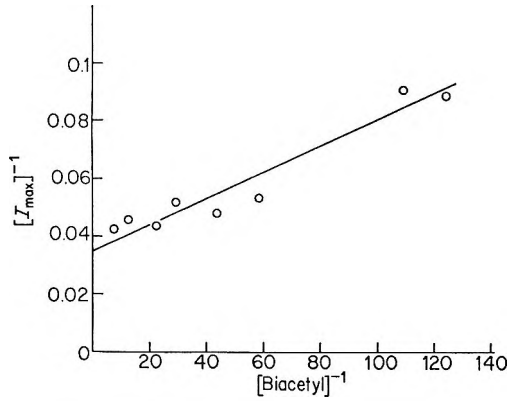

Figure 6. Plot of I^{-1} *vs.* $(B)^{-1}$ in the presence of 0.5 *M* cyclohexene.

The slope at higher biacetyl concentrations is a result of competition between biacetyl and cyclohexene for the benzene triplet. The value obtained for k_{15}/k_7 is about 1.2.

In the presence of excess cyclohexene and when the biacetyl concentration is low, $k_{15}(C) \gg k_7(B)$, $F_6^1 \rightarrow 0$, and the intensity of emission I is given by

$$I = \alpha F_2 F_3^1 F_4$$

or

$$\frac{1}{I} = \frac{1}{\alpha F_2 F_4} + \frac{k_3 + k_5 + k_6 + k_{16}(C)}{\alpha F_2 F_4 k_4(B)}$$

(as shown in Figure 6)

$$\frac{\text{intercept}}{\text{slope}} = \frac{k_4}{k_3 + k_5 + k_6 + k_{16}(C)} = 81$$

From this we obtain $k_4 \approx 10^{10}\ M^{-1}\ \text{sec}^{-1}$, in good agreement with direct observation, taking $k_3 + k_5 + k_6 = 6 \times 10^7\ \text{sec}^{-1}$ and $k_{16} \approx 4 \times 10^7\ M^{-1}\ \text{sec}^{-1}$.

From the intercepts of Figures 5 and 6 and the ratio of k_1/k_2 which can be obtained from Figure 2, we can deduce the lifetime of the benzene triplet. The intercept of Figure 5 is $(\alpha F_6 F_7)^{-1}$ and that for Figure 6 is $(\alpha F_2 F_4)^{-1}$. The ratio is $k_7(B)/[k_7(B) + k_8(k_2/k_1)]$ and from this can be deduced $k_7/k_8 = 40$. Assigning k_7 a value of $0.5\text{–}1.0 \times 10^{10}\ M^{-1}\ \text{sec}^{-1}$,[16] then we deduce that k_8 is $1.2\text{–}2.4 \times 10^8\ \text{sec}^{-1}$. This triplet lifetime of about 10^{-8} sec is in agreement with estimates by other methods.[2,13] The short lifetime is not restricted to radiation chemical systems since practically identical behavior is found in analogous photochemical systems.[2,10] The reason for the rapid deactivation is unknown but it should be pointed out that it has not been proved that it is the $^3B_{1u}$ (the long-lived phosphorescent state observed in solid media[18]) which is involved in energy transfer processes in liquid-phase radiolytic or photochemical systems. If a higher triplet, *e.g.*, the $^3E_{1u}$ which is lower in energy than the $^1B_{2u}$,[19] is the one involved in energy transfer, the short lifetime may be understandable. The participation of a triplet excimer is probable. This would bring about some delocalization of the excitation and increase the rate of quenching either by solute or triplet–triplet annihilation. It is difficult to see why the possible excimer should have such a short lifetime.

Decay of the Biacetyl Triplet. The shorter lifetime of the biacetyl triplet in radiolytic experiments as compared with analogous photochemical systems[4,15] may be due in part to impurities but quenching by radiolytic products clearly occurs. The data in Table I indicate some evidence for apparent self-quenching at higher biacetyl concentrations. Backström and Sandros[4] report such an effect which was slight and variable ($k = 460\ M^{-1}\ \text{sec}^{-1}$). The data in this work give only approximate Stern–Volmer plots from which an approximate rate constant of $5 \times 10^4\ M^{-1}\ \text{sec}^{-1}$ can be deduced. This may be due to products formed by interaction between biacetyl and products of benzene radiolysis.

In the experiments reported there is some variation in lifetime with the different samples of solvent but there is in all cases a clear tendency for the decay time to decrease with dose (2-μsec pulses) and the decay rate is approximately proportional to $(\text{dose})^{1/2}$, Figure 7.

Extrapolation of the data to very low doses at low biacetyl concentrations gives a lifetime in the order of milliseconds in agreement with photochemical results. The decrease in lifetime of the biacetyl triplet is similar to that reported by McCollum and Wilson,[20] who treated the situation by a kinetic scheme in which the quenching radical concentration was assumed to reach the steady state. This is not possible under the conditions reported here and it seems that the triplet-state quencher is a species *derived* from intermediates which exist in a steady state during the pulse. This could be an ion or excited state which undergoes rapid decomposition into free radicals. The effect of repeated pulsing shows that the most effective quencher is not a permanent product. A limited amount of data showed no

(18) M. R. Wright, R. P. Frosch, and G. W. Robinson, *J. Chem. Phys.*, **33**, 934 (1960).

(19) S. D. Colson and E. R. Bernstein, *ibid.*, **43**, 2661 (1965).

(20) J. D. McCollum and W. A. Wilson, A.S.D. Technical Report, 61-1700, 1961.

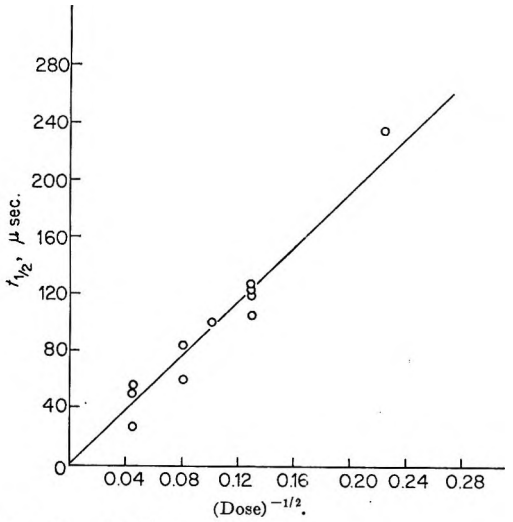

Figure 7. Plot of $t^{-1/2}$ for decay of the biacetyl triplet *vs.* $(\text{dose})^{-1/2}$ (rads).

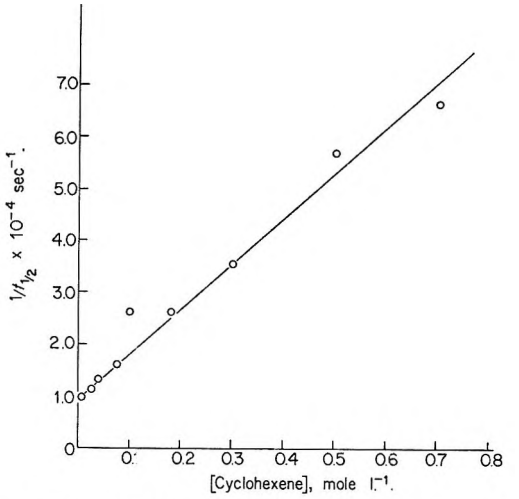

Figure 8. Plot of $(t_{1/2})^{-1}$ for biacetyl triplet decay *vs.* (C).

difference in lifetime was obtained in going from 2- to 0.2-μsec pulses at constant dose.

Backström and Sandros[4] have also shown that cyclohexene quenches biacetyl phosphorescence. In Figure 8, $(t_{1/2})^{-1}$ is plotted against (C). From the intercept it can be calculated that $k_{19} = 1.18 \times 10^5\ M^{-1}\ \text{sec}^{-1}$ in good agreement with Backström and Sandros ($1.0 \times 10^5\ M^{-1}\ \text{sec}^{-1}$). The effects of varying both cyclohexene and biacetyl concentrations indicate that the radiolytic products from the solvent competitively react with both these additives to yield products of different quenching efficiency. There is no evidence at the low doses used that radiolytic products affect the measured yield of excited states of benzene. This is probably not the case at higher dose rates or in experiments with prolonged irradiation at high dose rates.

General Remarks

The combined yield of triplet and singlet states of benzene of 2.67 is lower than that of about 5 per 100 eV deduced from *cis–trans* isomerization studies.[2,21] If higher electronically excited states, *e.g.*, the $^1E_{1u}$, $^1B_{1u}$, or $^3E_{1u}$ are involved, then transfer to the biacetyl may not form the phosphorescent state due to decomposition. Activation and isomerization of an olefin is still feasible. Formation of the $^1E_{1u}$ state from the $^1A_{1g}$ ground state is not symmetry forbidden as is the $^1B_{2u}$ state and might be readily formed by interaction with fast electrons. The experiments do not give any direct information on the origin of excited states but show that the $^1B_{2u}$ and $^3B_{1u}$ states of benzene are formed by irradiation and behave in the same way as in photochemical experiments. In this type of study it is essential to bear in mind that the addition of a solute may markedly change the primary radiation processes. Further experiments with alkyl-substituted benzenes are in agreement with the conclusions presented.

Acknowledgments. We are grateful to Dr. E. J. Land for his cooperation and the Petroleum Research Fund of the American Chemical Society for support. Thanks are also due to Professor G. Stein for many stimulating discussions.

(21) R. B. Cundall and P. A. Griffiths, *Discussions Faraday Soc.*, **36**, 111 (1963); W. G. Burns, R. B. Cundall, P. A. Griffiths, and W. R. Marsh, *ibid.*, **64**, 129 (1968); E. Fischer, H. P. Lehman, and G. Stein, *J. Chem. Phys.*, **45**, 1503 (1966); M. A. Golub and C. L. Stephens, *J. Phys. Chem.*, **70**, 3576 (1966); R. R. Hertz, D. B. Peterson, S. B. Srivastava, H. F. Barzynski, and M. Burton, *ibid.*, **70**, 2362 (1966).

Positive Charge Migration in γ-Irradiated Organic Solids and Trapping by Alkanes at 77°K

by Pieter W. F. Louwrier and William H. Hamill

Department of Chemistry and the Radiation Laboratory,[1] University of Notre Dame, Notre Dame, Indiana 46556
(Received May 7, 1968)

Alkanes (RH) of seven or more carbon atoms in matrices of CCl_4 or 3-methylpentane (3MP) at 77°K are strongly colored by ^{60}Co irradiation. The absorption bands are structureless, the half-width is ~400 nm, and λ_{max} increases from 560 nm for C_7H_{16} to ~910 nm at $C_{15}H_{32}$ and higher. They are attributed to the alkane radical ions, RH^+. One-component alkane systems, with CCl_4 or CO_2 as electron traps, are not colored, and higher alkanes do not trap holes in 3-methylhexane and higher alkane matrices, possibly because the difference of ionization potentials (trap depth) becomes too small above hexane. For 2-methyldecane (2MD) in 3MP, the yield of $2MD^+$ increases to a sharp maximum at 0.5 mol % 2MD and diminishes to half below 2% 2MD when observed shortly after irradiation. Upon standing, $OD(2MD^+)$ decreases, the rate being faster at higher % 2MD. Both effects are attributed to positive charge migration by electron tunneling from RH to RH^+. Optical excitation of RH^+ transfers holes to CCl_4 or tetramethyl-*p*-phenylenediamine, and bleaching is more efficient on the blue side of the RH^+ band, indicating excited hole migration.

The migration of positive charge (holes) in γ-irradiated organic solids and liquids was demonstrated by formation of the well-known radical positive ion of dimethyl-*p*-phenylenediamine (DMPD) at small concentrations of the latter when used as an authentic test substance.[2] The yield of $DMPD^+$ was enhanced by added alkyl chloride which traps electrons, preventing charge recombination. This effect serves as a partial test for identifying unknown color centers as positive ions since yields of negative ions will be suppressed by halides. Several positive ions of olefins and aromatic hydrocarbons were characterized by this method using a matrix of 3-methylpentane (3MP).[3] This test is somewhat complicated by the fact that alkyl halides in 3MP trap holes as well as electrons. The alkyl iodides, for example, give several strong bands from 300 to 900 nm.[4-6] It could also be shown that positive ions generate new color centers by the reaction $RI^+ + I^- \rightarrow RI \cdot I$ which showed the necessity to distinguish between color centers due to positive ions themselves and others which are uncharged but have positive ion precursors and will therefore be enhanced somewhat by electron traps.

Although there is no identifiable color center in the γ-irradiated pure 3MP matrix attributable to the trapped hole, both polycrystalline CCl_4 and glassy *n*- and *sec*-butyl chloride matrices produce such color centers. The butyl chloride matrices were found to be quite suitable for preparing positive ions, among them many aromatic amines, aromatic hydrocarbons, ketones, and olefins.[7] Using tetramethyl-*p*-phenylenediamine (TMPD) as a test additive for trapping holes, the yield of conducting holes was found to be ~3 per 100 eV of absorbed energy.

Preliminary observations[8] with higher alkanes (RH) in a matrix of CCl_4 provided evidence for hole trapping to form the radical ions RH^+. The optical absorption bands ranged from λ_{max} 560 nm for *n*-heptane to $\lambda_{max} \cong 950$ nm for *n*-hexadecane. Such species have not been detected previously in condensed systems, to our knowledge, and therefore provide novel and quite interesting subjects for investigation. This study is concerned with positive charge trapping by alkanes, particularly in matrices of other alkanes.

Experimental Section

Samples in CCl_4 matrices were prepared in air using Suprasil cells 1.8 mm thick, plunged into liquid nitrogen and γ-irradiated. They were transferred quickly in darkness to a windowed silica dewar containing liquid nitrogen, and the spectra were recorded using a Cary Model 14R spectrophotometer equipped with a high-intensity light source and using OD = 2 attenuation in the reference beam. Irradiation with ^{60}Co γ rays ranged from 3×10^{18} to 4×10^{19} eV g^{-1}.

To transfer charge effectively from the matrix-trapped holes absorbing at ~400 nm to the additive, samples were warmed to 143°K (pentane slush). Color centers were optically bleached, as required, using the

(1) The Radiation Laboratory of the University of Notre Dame is operated under contract with the U. S. Atomic Energy Commission. This is AEC Document No. COO-38-603.

(2) M. Kondo, M. R. Ronayne, J. P. Guarino, and W. H. Hamill, *J. Amer. Chem. Soc.*, 86, 1297 (1964).

(3) J. P. Guarino and W. H. Hamill, *ibid.*, 86, 777 (1964).

(4) E. P. Bertin and W. H. Hamill, *ibid.*, 86, 1301 (1964).

(5) R. F. C. Claridge and J. E. Willard, *ibid.*, 89, 510 (1967).

(6) J. P. Mittal and W. H. Hamill, *ibid.*, 89, 5749 (1967).

(7) T. Shida and W. H. Hamill, *ibid.*, 88, 5376 (1966), and earlier articles in this series.

(8) T. Shida, unpublished results.

IR-2 lamp of the spectrophotometer and appropriate Corning filters. The band maxima are reliable within ~10 nm for C_6–C_{11}, ~25 nm for C_{12}–C_{16}, and ~50 nm for C_{17}–C_{19} alkanes. The long wavelength absorption limits cannot be established at all for C_{16} and higher alkanes, and are admittedly inaccurate for lower alkanes.

Samples in 3MP matrices were prepared in air (excepting a few samples for solvent-trapped electrons which were air-free) using Suprasil 1 × 1 cm mandrel-drawn cells and immersed in liquid nitrogen throughout. The added higher alkanes were insoluble above ~4 mole %. When CO_2 was used to trap electrons it was bubbled into the sample through a capillary for 10 min at ambient temperature; glasses were clear and no trapped electron band ($\lambda_{max} \cong 1600$ nm) was detectable.

Higher alkanes were obtained from Aldrich Chemical Co. and CCl_4 was Fisher certified reagent grade, both used as received. Phillips pure grade 3MP was passed through a column of activated silica gel.

Results

The band maxima observed for higher alkanes in a matrix of CCl_4, as well as long wavelength onsets, are summarized in Table I, together with Shida's earlier measurements. The spectra of the ions of the 2-methyl alkanes are the same as those in a 3MP matrix except for blue shifts of ~25 nm. Within the limits of detection the band maxima increase monotonically with carbon number to a limit of ~900 nm and are the same for *n*- and 2-methyl alkanes of the same carbon number. The low energy onset of each band lies ~500 nm beyond the maximum. Holes can be transferred from the CCl_4 matrix to additive RH by warming to 143°K and from RH^+ back to the matrix by optical excitation in the RH^+ absorption band repeatedly. All other spectra of higher alkane positive ions were measured in the 3MP matrix.

The spectra in Figure 1 of the positive ions from several alkanes in 3MP are attributed to the radical ions $C_nH_{2n+2}^+$. In these and many other systems CO_2 was used as the electron trap because it strongly enhances yields of RH^+, does not itself give an absorption band at $\lambda > 300$ nm, and is not expected to form a charge-transfer complex or to trap holes. Although CCl_4 is a very efficient trap for electrons it is responsible for a strong band at $\lambda_{max} \cong 470$ nm in 3MP which is caused by trapped holes and may be due to CCl_4^+. The spectra of the four isomeric $C_{10}H_{22}$ alkanes shown in Figure 2 are seen to be very dependent upon molecular structure. These differences argue against ion rearrangement to most stable structures, which are improbable in rigid matrices in any event.

The yields of RH^+ in 3MP do not increase monotonically with the concentration of RH, as shown in Figure 3, and the spectra are unchanged. The highest OD's occur well below the solubility limits and the glasses were quite clear. The yields of RH^+ can be estimated only for $2MD^+$ (2-methyldecane), but the results suggest that oscillator strengths increase markedly with the carbon number. This is more clearly shown in Figure 1. The decreased yields of RH^+ at higher concentrations of RH suggested increasing hole mobility. To test this assumption, varied amounts of 2MD were added to 3MP containing 0.1 mol % *sec*-C_3H_7Cl and 0.035 mol % TMPD. Because of evidence that *sec*-C_3H_7Cl trapped holes more than CCl_4, a second

Table I: Absorption Maxima and Onsets of Alkane Radical Cations Produced by γ Irradiation of Solutions in CCl_4 at 77°K

	λ_{max}, Shida,[a] nm	λ_{max}, this work, nm	Onset, estd, nm
n-Heptane	560	...	...
n-Octane	650	645	1150
2-Methyloctane	...	685	1200
n-Nonane	700	700	1200
2-Methylnonane	...	740	1270
n-Decane	740	750	1270
2-Methyldecane	...	775	1300
n-Undecane	780	790	1325
2-Methylundecane	...	880	1325
n-Dodecane	830	850	1300
n-Tridecane	800–850	875	1300
n-Pentadecane[a]	915	920	1400
n-Hexadecane[a]	950	910	...
n-Heptadecane[a]	...	875	...
n-Octadecane[a]	...	900	...
n-Nonadecane[a]	...	900	...

[a] These alkanes give such broad absorption spectra that the maxima are only estimates. The onset is hard to define, and for that reason, omitted.

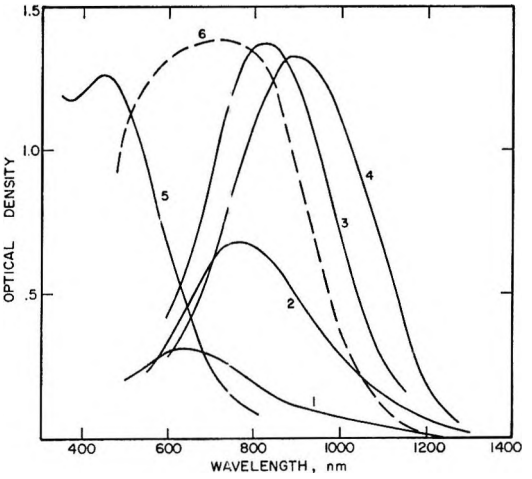

Figure 1. Absorption spectra of irradiated 0.65 mol % solutions of some branched alkanes in CO_2-saturated 3MP at 77°K, dose 1.4×10^{19} eV/g: 1, 2-methyloctane × 2; 2, 2-methylnonane; 3, 2-methyldecane; 4, 2-methylundecane; 5, 2,2-dimethylheptane; *sec*-C_3H_7Cl as electron trap; 6, 2,6-dimethylheptane in CCl_4. Curves 5 and 6 are not on scale.

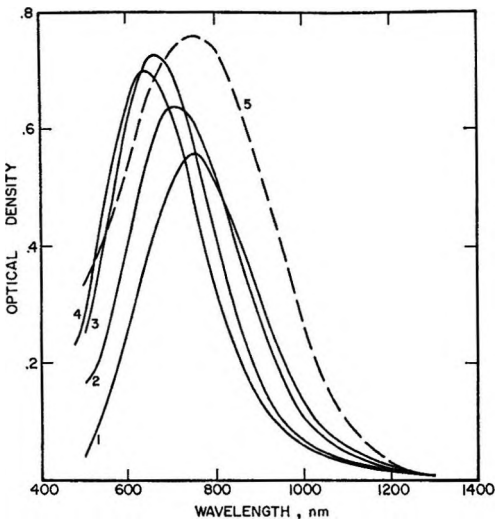

Figure 2. Absorption spectra of irradiated 0.65 mol % solutions of isomeric $C_{10}H_{22}$ alkanes in 3MP, 0.5 mol % CCl_4 as electron trap, at 77°K, dose 8.4×10^{18} eV/g: 1, 2-methylnonane; 2, 3-methylnonane; 3, 4-methylnonane; 4, 5-methylnonane; 5, 0.5 mol % 2-methylnonane in CCl_4; 1.8-mm cell, dose 5.6×10^{18} eV/g.

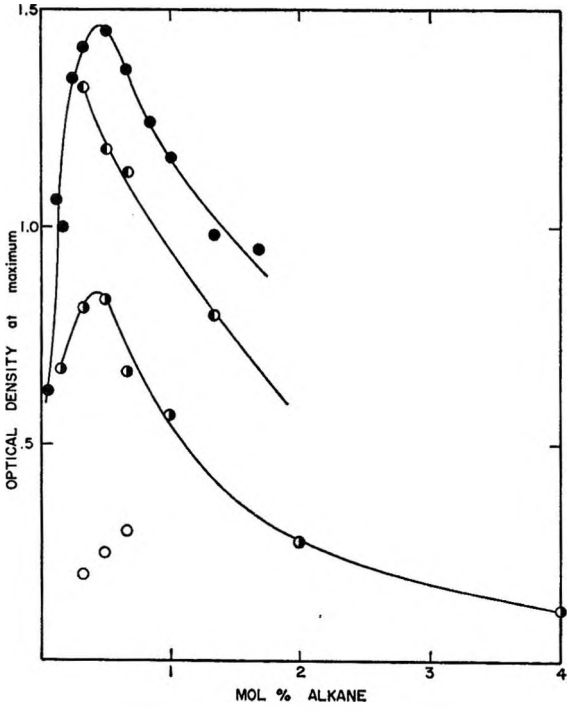

Figure 3. Optical density at absorption maximum of irradiated solutions of some branched alkanes in CO_2-saturated 3MP at 77°K as a function of alkane concentration, dose 1.4×10^{19} eV/g: ○, 2-methyloctane × 2; ◑, 2-methylnonane; ●, 2-methyldecane; ◐, 2-methylundecane − 0.2.

series of measurements was conducted using 0.015 mol % TMPD and 0.48 mol % CCl_4 in 3MP. Both sets of results appear in Figure 4 and show significant increase in OD($TMPD^+$) with increasing concentration of 2MD which correlates with decreasing OD($2MD^+$) of

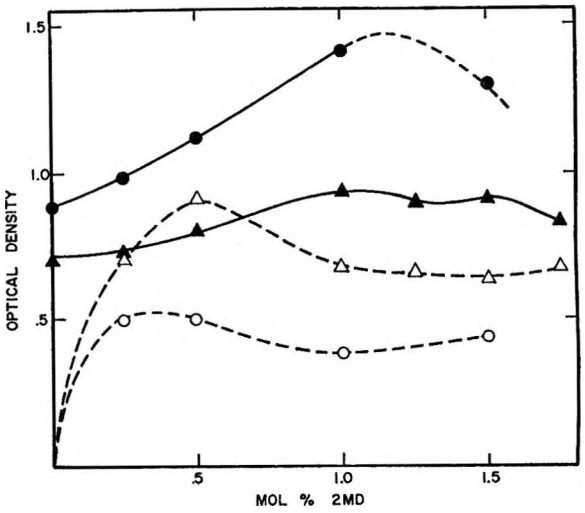

Figure 4. Optical densities at absorption maxima of irradiated solutions of 2MD and TMPD in 3MP at 77°K as a function of 2MD concentration. Experiment 1: 0.035 mol % TMPD; 0.1 mol % *sec*-C_3H_7Cl; dose 1.05×10^{19} eV/g; ●, $TMPD^+$; ○, $2MD^+$. Experiment 2: 0.015 mol % TMPD; 0.48 mol % CCl_4; dose 9.6×10^{18} eV/g; ▲, $TMPD^+$; △, $2MD^+$.

Figure 3. It is qualitatively clear that appropriate concentrations of 2MD provide a hole conduction mechanism, while at lower concentrations 2MD provides hole traps.

There is a remarkably disproportionate competition for holes between TMPD and 2MD. At 2×10^{19} eV g^{-1} with CO_2-saturated 3MP and 0.5 mol % 2MD, OD($2MD^+$) is depressed from 0.73 to 0.56 by only 0.006 mol % TMPD. When the $2MD^+$ was optically bleached, OD($TMPD^+$) at 645 nm increased from 0.38 to 0.58. This provides a minimal value $\epsilon(2MD^+) = 6.8 \times 10^3\ M^{-1}\ cm^{-1}$. Also, when 0.015 mol % TMPD was added to 0.5 mol % 2MD and 0.48 mol % CCl_4 in 3MP at 9.5×10^{14} eV g^{-1}, OD($2MD^+$) decreased to 0.91 from 1.14 without TMPD, while OD($TMPD^+$) was 0.80 with 2MD and 0.70 without. Assuming $\epsilon(TMPD^+)\Delta OD(TMPD^+) = \epsilon(2MD^+)\Delta OD(2MP^+)$ gives $\epsilon(2MD^+) = 8.2 \times 10^3\ M^{-1}\ cm^{-1}$ and 0.89 for the 100-eV yield. The oscillator strength is ~0.24.

The increased yield of $TMPD^+$ from bleaching $2MD^+$ provides the clearest evidence that bands associated with added higher alkanes are due to trapped holes. A qualitatively similar hole transfer by optical excitation of RH^+ was observed for the biphenyl positive ion using 0.02 mol % biphenyl and 1 mol % propyl chloride with 2MD in 3MP.

A series of measurements shown in Figure 5 was performed using 0.5 mol % 2MD in CO_2-saturated 3MP with various concentrations of CCl_4. The OD at 470 nm for the positive ion band arising from CCl_4 exhibits a normal concentration dependence. The OD for $2MD^+$ increased slightly at small concentrations of CCl_4, probably due to more efficient electron trapping. The expected enhancement of the $2MD^+$ band at

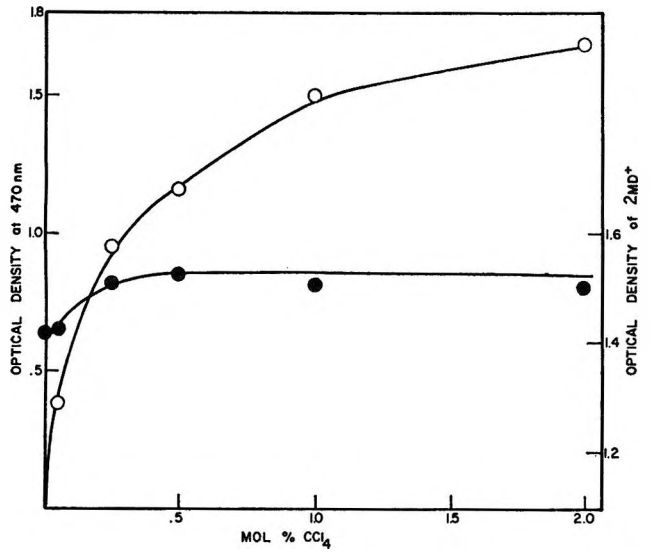

Figure 5. Optical densities of $2MD^+$ and of the band at 470 nm due to CCl_4 in irradiated CO_2-saturated solutions of 0.5 mol % 2MD at 77°K as a function of CCl_4 concentration; dose 1.4×10^{19} eV/g: ●, $2MD^+$; ○, OD at 470 nm, not corrected for increase in background due to irradiation products other than $2MD^+$.

higher concentrations of CCl_4 from more nearly complete electron trapping was not observed and may have been fortuitously canceled by competition for holes.

To test this possibility, a sample containing 2 mol % CCl_4 and 0.75 mol % 2MD was irradiated and then optically bleached with Corning filters 7–69 and 7–56 ($\lambda > 940$ nm) in one experiment, then with a narrow band-pass filter (λ_{max} 687 nm and half-width ~15 nm) in another experiment. The results, which appear in Figure 6, demonstrate unmistakably that both additives trap holes. Since the minimum energy required to produce an ion from CCl_4 is 11.65 eV, while the ionization potential of 3MP is 10.08 eV,[9] the hole is considered to be excited. It follows that 2MD traps excited holes.

To test the possibility that added 2MD was affecting electron trapping or electron mobility, samples containing 0.03 mol % $C_6H_5CCl_3$ in 3MP are examined at 0, 0.35, 0.65, 1.00, 1.35, 1.65, and 2.00 mol % 2MD. The reaction measured was $C_6H_5CCl_3 + e^- \rightarrow C_6H_5CCl_2 + Cl^-$, and any subsequent hole migration would not be expected to affect the yield. In fact, the $OD(C_6H_5CCl_2)$ was 0.64 ± 0.03, with no systematic trend, over the range of measurement.

To determine whether higher alkanes in 3MP facilitate hole conduction over longer times, a series of measurements shown in Figure 7 was conducted using 0.3, 0.5, 0.6, 0.75, and 1.15 mol % 2MD measuring $OD(2MD^+)$ at intervals for nearly 3 hr. The rates of decay of the $2MD^+$ band, normalized to a common intensity at the end of the irradiation, increased with increasing concentration of 2MD. The concentration dependence of the yields of $2MD^+$ at long times is approximately the same as that at short times.

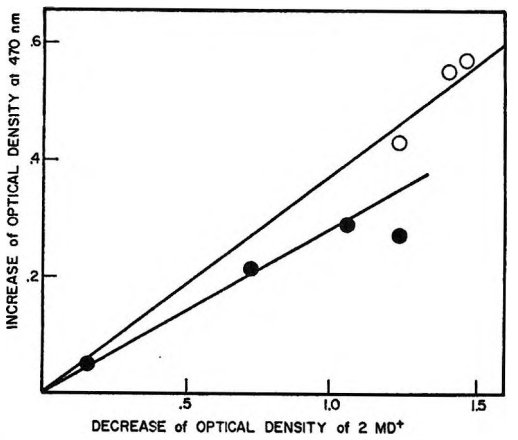

Figure 6. Bleaching of the $2MD^+$ absorption band in an irradiated solution of 0.75 mol % 2MD and 2 mol % CCl_4 in 3MP at 77°K. Dose 1.4×10^{19} eV/g: ○, bleaching with Corning filters 7.69 and 7.56 (λ_{max} 937 nm, half-width ~120 nm); ●, bleaching with narrow band pass filter, (λ_{max} 687 nm, half-width ~15 nm).

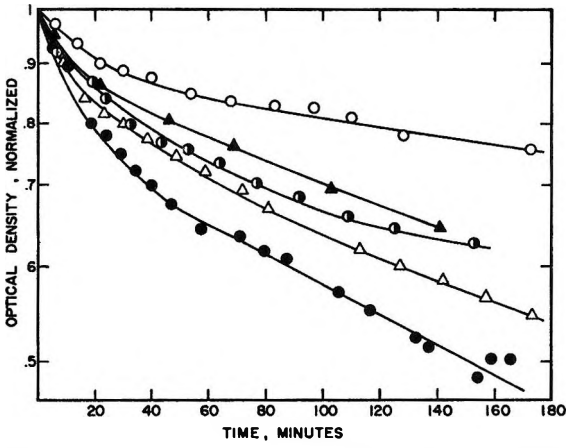

Figure 7. Decay of the $2MD^+$ absorption in irradiated CO_2 saturated solutions of 2MD in 3MP at 77°K as a function of 2MD concentration, normalized to a common intensity at the end of the irradiation: ○, 0.3 mol % 2MD; ▲, 0.5 mol % 2MD; CCl_4 is used as an electron trap; ◑, 0.6 mol % 2MD; △, 0.75 mol % 2MD; ●, 1.20 mol % 2MD.

It was thought that some information concerning hole trapping and migration might be obtained using alkane matrices above 3MP in carbon number. No trapped holes RH^+ are observed in pure 3MP, or with added electron traps, but by extrapolation from higher RH^+ the absorption band would lie at short wavelength and be obscured by unidentifiable absorbing species. This difficulty is avoided by using higher alkanes, with known RH^+ bands, as matrices. The 2-methylalkanes from C_9H_{20} to $C_{12}H_{26}$, as well as 4-methylnonane, using CCl_4 as electron trap, gave no RH^+ bands, nor did 2-methyldecane with CO_2. Therefore

(9) K. Watanabe, T. Nakayama, and J. Mottl, *J. Quant. Spectrosc. Radiat. Transfer*, 2, 369 (1962).

RH^+ cannot be stabilized in the RH matrix for this range of carbon numbers.

In a matrix of 2-methyloctane with CO_2, neither 1% 2-methylundecane nor 1% 2,2-dimethylheptane gave the expected RH^+ bands. In a matrix of 3-methylheptane, added 5-methyltetradecane gave no RH^+ band, nor did 2MD in 3-methylhexane. In the 2-methyloctane matrix, TMPD with CO_2 formed $TMPD^+$. Both pure 2-methyloctane and pure 2-methyldecane do trap electrons.

The effect of trap depth, *i.e.*, the difference of ionization potentials of matrix and additive, was also tested by adding 5% 2-methylpentene-1 to 3MP saturated with CO_2. There was no decay after 80 min, in contrast to the results with 2MD in Figure 7. In two other runs, $TMPD^+$ and $(C_6H_5)_2^+$ in 3MP with CO_2 also did not decay after 80 min. Since there was no loss for deeply trapped charges in 3MP, recombination by viscous drift of ions is negligible.

Discussion

The optical absorption bands produced by addition of higher alkanes RH to CCl_4 and 3MP matrices are clearly due to trapped holes and are quite satisfactorily assignable to the corresponding radical positive ions. This is consistent with the dependence of λ_{max} on carbon number and structure. The enhancement of their yields by addition of electron traps and the transfer of holes from "RH^+" color centers to TMPD under optical excitation establish the positive charge. Since 983 nm (~1.3 eV) suffices for hole transfer, and assuming that $3MP^+$ is an intermediate, the color center could not be a carbonium ion since transfer would require at least 2 eV. A charge-transfer complex, *e.g.*, from $RH^+ + Cl^- \rightarrow RH{\cdot}Cl$, is incompatible with results obtained using CO_2 as electron trap. The assumption of neutral radiolytic products would be quite at variance with the observations. The assignment to radical ions is also qualitatively consistent with the optical excitation of holes into the conducting state since there are many excited states of the higher alkane radical ions[10] and all these should lie above the ground state of $3MP^+$. That is, $RH^{*+} + 3MP \rightarrow RH + 3MP^+$ accounts for photoconductivity, and an analogous process can account for hole transfer to CCl_4. If the ion so produced is CCl_4^+, it must lose energy by relaxation to prevent transfer back to the 3MP matrix.

Hole trapping by higher alkanes in CCl_4 is to be expected since the (vacuum) ionization potentials are *ca.* 10.0 and 11.65 eV.[9] The separation between 3MP ($I \cong 10.08$ eV[9]) and higher alkanes is probably very small, but the trend is correct.

The remarkable decrease in yields of RH^+ with increasing concentrations of RH is almost without precedent for ions in rigid matrices but somewhat resembles the dependence of biphenyl anion (ϕ_2^-) yields in 3MP on the concentration of added 2-methylpentene-1 (2MP-1).[11] That is, yields of ϕ_2^- at constant concentration of ϕ_2 increased with added 2MP-1 to ~2 mol %, then decreased markedly with increasing amounts of 2MP-1. The decrease was attributed to hole conduction by tunneling along interrupted chains of 2MP-1 and loss of ϕ_2^- by recombination. The model proposed for the earlier work can be used here without essential modification. The strongly increasing yields of RH^+ for small concentrations of RH is normal, the hole traps being very shallow but effectively isolated. With increasing concentrations of RH, hole transfer from RH^+ to RH within a few molecular diameters is postulated to occur by electron tunneling. At ~1 mol % RH sequences of such charge transfers may readily provide a conduction path sufficient for recombination of an appreciable fraction of all charge pairs, the probability depending on the charge separation distribution function and the local field. The probability of producing RH^+ by hole trapping at first increases with concentration of RH, then saturates while the probability of losing RH^+ by recombination as a result of tunneling increases steadily. Hole migration in pure 3MP is postulated to occur by resonant charge transfer, and is therefore very fast and between nearest neighbors.

The concentration dependence of the slow decay of RH^+ in 3MP appears not to depend on ion migration and therefore presumably involves an electronic mechanism. The temperature dependence implies a relaxed ion $RH^+(r)$ which is thermally activated to a configuration $RH^+(v)$ corresponding to vertical ionization of RH. Hole migration must involve electron transfer from RH rather than 3MP since the mobility increases with increasing % RH, the interaction being greater the less the width of the barrier. Also, if $RH^+(v)$ accepted an electron from 3MP, the hole would be trapped more efficiently by increasing % RH. The tunneling model will also be applied tentatively to this type of charge transfer. For both fast and slow charge migration, the same $RH^+(v)$ occupying some narrow range of vibrational states is assumed. That is, fast migration of holes between $RH^+(v)$ and RH may occur repeatedly and holes become self-trapped when relaxation to $RH^+(r)$ occurs, while thermal activation can restore the conducting state. It should be noted that electron transfer to $RH^+(v)$ will probably leave RH vibrationally unexcited and the internal energy of $RH^+(v)$ is not necessarily dissipated rapidly.

A very rough estimate of the rate of tunneling can be made using eq 1[12]

$$T \cong \frac{16E(V_0 - E)}{V_0^2} \exp\left(-2a\hbar^{-1}\sqrt{2m(V_0 - E)}\right) \quad (1)$$

(10) K. Fueki, *J. Phys. Chem.*, **68**, 2656 (1964).

(11) J. B. Gallivan and W. H. Hamill, *J. Chem. Phys.*, **44**, 2378 (1966).

(12) W. Kauzmann, "Quantum Mechanics," Academic Press, Inc., New York, N. Y., 1957, p 195.

where T is the transmission coefficient, E is the energy of the electron, and V_0 is the height of the barrier having width a, taken as 2×10^{-7} cm. $V_0 - E$ can be identified with the difference of ionization potentials of additive and matrix, *ca.* 0.05 eV, and the ratio E/V_0 approximated by unity. Then the preexponential factor is of the order 10^{-1}. If the hole approaches the barrier ν sec^{-1}, the rate of penetration would be $R \cong s\nu T$, where s is a statistical factor proportional to the cross product of the number of donor sites and the number of acceptor sites. If $s \cong 10$ and $\nu \cong 10^{14}$, the rate of hole tunneling would be *ca.* 10^{13}, largely unidirectional because of the Coulombic field and able to compete with vibrational relaxation. It should be considered that for an initial charge distribution centered at 10^2 Å and $a = 20$ Å, only three or four charge transfers would remove nearly all trapped charge because stabilization must be impossible in such matrices at very high fields as charge separation diminishes.

No holes are trapped as RH^+ in a matrix of RH, and the evidence for relaxation excludes 0–0 transitions. Resonant nonadiabatic transfer is possible, however, if the hole transfer time between neighboring alkane molecules is *ca.* 10^{-14} sec, which has been estimated.[13] The small average vibrational relaxation per transfer may be compensated by internal energy acquired from the Coulombic field.

The maxima of ion yields for alkane and alkene provide rough measures of tunnneling efficiencies, *viz.* ~3% 2MP-1 and 0.5% RH, and $a \propto (\text{concn})^{1/3}$. The ratio of the a's so determined (~2) approximates the inverse ratio of the $(V_0 - E)^{1/2}$ terms (~3), as required.

Optical bleaching of RH^+ in 3MP is attributed to charge transfer from the excited ion to the matrix. More efficient bleaching at shorter wavelength is plausibly related to formation of a more highly excited ion, RH^{*+}, which can produce a more highly excited $3MP^{*+}$, and the more highly excited hole could survive more charge transfers. If charge transfer in the matrix is quite fast, *i.e.*, resonant, not only electronic but also vibrational energy may survive several jumps. These excited states gradually relax and the ground-state ion is trapped by further internuclear relaxation.

Acknowledgment. Discussions with J. L. Magee, K. P. Funabashi, and A. Mozumder are gratefully acknowledged.

(13) W. L. McCubbin, *Trans. Faraday Soc.*, **59**, 769 (1963)

Comparison of Photo- and γ-Induced Ionization Processes in the Condensed Phase by Means of Electron Spin Resonance Spectroscopy[1]

by Kozo Tsuji and Ffrancon Williams

Department of Chemistry, University of Tennessee, Knoxville, Tennessee 37916 *(Received May 7, 1968)*

The production of electrons by photoionization and γ irradiation has been studied in several rigid organic glasses by the esr technique. A steady-state concentration of electrons is achieved rapidly during photoionization but not by γ irradiation. In the latter case the concentration increases linearly with dose to a maximum value and then declines. After irradiation, the trapped electrons undergo thermal decay at rates which are highly characteristic of the matrix system and the experimental conditions but are almost independent of the method of electron generation. During photoionization, esr evidence for a transient triplet state of N,N,N′,N′-tetramethyl-*p*-phenylenediamine (TMPD) was obtained in several solvents at 77°K. After warming up samples which had been photoionized at 77°K, well-resolved esr spectra of TMPD·$^+$ were obtained in alcohol systems. Two slightly different spectra were observed depending on the experimental conditions, and these have been assigned to TMPD·$^+$ and its dimer although the identification of the latter is inconclusive. When the light beam is cut off in TMPD photoionization, there is a sudden decrease in the electron concentration which is not related to the thermal decay of trapped electrons. A mechanism of photoionization has been proposed which includes the participation of a delocalized state as a precursor to ionization and of excited electrons. Photobleaching of trapped electrons has been studied in several solvent systems and evidence has been obtained for the reactions of excited electrons with alcohol.

Photoionization in rigid glasses has been studied extensively since the original work of Lewis and his coworkers.[2a] The main experimental investigations have been concerned with the optical detection of the photoionized molecules and trapped electrons[2b] and with the phenomena of photoconductivity[3] and recombination luminescence.[4] In a recent communication,[5] we described the use of the electron spin resonance (esr) method to detect the electrons produced by the photoionization of N,N,N′,N′-tetramethyl-*p*-phenylenediamine (TMPD) in a number of rigid solvents. By showing the existence of a simple photodynamic ionization equilibrium, this experiment illustrated the power of the esr technique to probe the dynamics of molecular ionization processes in the condensed phase. One particular advantage of the esr method is that it can be easily used to monitor the electron population during as well as after illumination.

It is of considerable interest to compare the results of photoionization and γ irradiation in model systems because the electrons are initially released with different energy distributions according to the nature of the incident radiation. Gallivan and Hamill[6] have described studies along these lines by means of the optical method. In previous work[7,8] we have shown by esr and optical investigations that thermal decay of trapped electrons in 3-methylpentane (3-MP) glasses is strongly influenced by the presence of polar additives such as tertiary amines and that the character of the effect is similar irrespective of whether γ irradiation or photoionization is used as the method of electron generation. From these experiments, it has been concluded that the mobility of the trapped electron is the decisive factor in controlling the rate of thermal decay.

In the present paper, we report in detail on photoionization experiments using esr detection. Attention is directed to the excited (or "mobile") electrons which are present under continuous photoexcitation and how these differ in properties and reactivity from the electrons which are generated during γ irradiation. The kinetics of thermal decay of trapped electrons has been examined. Finally, the influence of solvents on the nature of the photoionization process has been studied.

Experimental Section and Results

A general account of the preparative methods and measurement techniques has been given elsewhere,[9]

(1) This research was supported by the U. S. Atomic Energy Commission under Contract No. AT-(40-1)-2968 at the University of Tennessee. This is AEC Document No. ORO-2968-36.

(2) (a) G. N. Lewis and D. Lipkin, *J. Amer. Chem. Soc.*, **64**, 2801 (1942); (b) H. Linschitz, M. G. Berry, and D. Schweitzer, *ibid.*, **76**, 5833 (1954).

(3) A. C. Albrecht and M. E. Green, *J. Chem. Phys.*, **31**, 261 (1959).

(4) W. M. McClain and A. C. Albrecht, *ibid.*, **43**, 465 (1965); **44**, 1594 (1966).

(5) J. Lin, K. Tsuji, and F. Williams, *ibid.*, **45**, 4982 (1967).

(6) J. B. Gallivan and W. H. Hamill, *ibid.*, **44**, 1279 (1966).

(7) J. Lin, K. Tsuji, and F. Williams, *Chem. Phys. Lett.*, **1**, 66 (1967).

(8) M. A. Bonin, J. Lin, K. Tsuji, and F. Williams, Advances in Chemistry Series, No. 82, American Chemical Society, Washington, D. C., 1968, p 269.

and only those experimental details which are particularly relevant to the present investigation will be included in this report. All samples for esr studies were prepared from solvents which had been dried and degassed by standard techniques.[8,9] The hydrocarbons were purified by passage over silica gel and distillation and then stored over sodium–potassium mirrors on the vacuum lines. Triethylamine (TEA) was distilled and stored in the same manner. The alcohols were dried by standing over preheated magnesium sulfate, again under vacuum. The TMPD solutions were made up as described before.[9]

Since this paper is concerned only with esr measurements, mention should be made at the outset of the apparent discrepancy which came to light in previous work[9] when the rate of thermal decay of trapped electrons in γ-irradiated 3-MP at 77°K was followed independently by esr and optical methods. Through the use of the large V-4535 cylindrical cavity from Varian Associates, we have recently shown[10] that when the esr measurements are made with samples of 3-MP (in 10-mm square cells) which are identical in size with those previously employed in the optical work,[6,9a] the decay rates measured by the two methods at 77°K almost coincide with each other. This result suggests that the optical and esr absorption spectra refer to the same population of trapped electrons in 3-MP. We have also verified by esr studies that the rate of decay of trapped electrons is a function of sample size, and this finding accounts for the previous anomaly[9] between the esr and optical studies. As to the explanation for this effect, we incline to the view that the constitution of the glass is affected by changes in the rate of cooling when samples of different size are glassified at 77°K by immersion in liquid nitrogen before irradiation. Consequently, the thermal mobility of the trapped electron may be sensitive to the degree of structural organization which pervades the glass. Whatever the exact reason for the observed behavior, it is important from a practical standpoint that sample sizes should be standardized for comparative measurements even when the same detection technique is being used throughout. In the present esr work, we have used sample tubes made from thin-walled Spectrosil cylindrical tubing (i.d. 3.5 ± 0.5 mm). The rectangular Varian V-4531 multipurpose cavity was used and the arrangement for the esr studies at 70 and 77°K has been described.[9] In some experiments, the Varian V-4557 variable-temperature accessory was used to raise the temperature of the sample above 77°K in the esr cavity.

Many details of the irradiation techniques have been described.[5,8,9] Samples in a dewar were shielded from stray light and irradiated with γ rays in a Gammacell-200 cobalt-60 source at a dose rate of 2.6×10^{17} eV g^{-1} min^{-1} at either 70 or 77°K and then transferred in the dark into the esr cavity at the temperature of interest. Irradiations with ultraviolet light were generally carried out with the sample in the esr cavity. The light source was the B-H6 mercury arc, and the filtration system[5] provided a passband centered at 320 nm corresponding to the absorption maximum of TMPD.[11] Photobleaching studies were carried out in the different wavelength regions using ultraviolet, visible, and infrared lamps together with appropriate filters. The details pertaining to the particular experiments are given in the description of the results.

In Figure 1 some typical recorder traces are shown of the esr signals due to the electrons generated during photoionization of TMPD in various rigid glasses at 77°K. We have presented evidence elsewhere[5,7-9] that the esr singlet spectrum observed under our experimental conditions is characteristic of electrons and is easily distinguishable from the CO_2^- singlet spectrum[12] according to the differences in photobleaching behavior and microwave power saturation properties.[9] An earlier report by Dolan[13] referred to the production of a singlet spectrum with a half-width of 9 G by the photoionization of TMPD in 2-MP at 77°K. This spectrum which was attributed to a trapped electron must have been due to some extraneous species because the linewidth ΔH_{ms} of the trapped-electron singlet is only 4.0 ± 0.2 G.[9] Dolan's assignment[13] has also been refuted[14] on the basis of the observed photobleaching characteristics.

For purposes of kinetic differentiation, it is convenient to break down each of the experimental traces in Figure 1 into four portions. First, there is the initial growth of the signal intensity to the steady state. By allowing the lamp to reach full intensity before subjecting the sample to irradiation, it has been established that this growth is not connected with the rise time of the lamp, and so the initial increase in signal intensity is controlled by the kinetics of electron reactions in the glass. It is noteworthy that the increase of the intensity to the steady state is much slower for MTHF than for the other solvents examined in Figures 1 and 2. The second portion denotes the period where the intensity of the electron signal has reached a steady state. Although it is not evident in the comparatively short times over which the traces of Figure 1 were recorded, other experiments showed that there was a definite tendency for the signal intensity to decrease slowly on prolonged irradiation, and this was accompanied by an increase in the intensity of the underlying

(9) (a) J. Lin, K. Tsuji, and F. Williams, *J. Amer. Chem. Soc.*, **90**, 2766 (1968); (b) K. Tsuji and F. Williams, *ibid.*, **89**, 1526 (1967).

(10) K. Tsuji and F. Williams, submitted for publication.

(11) W. C. Meyer and A. C. Albrecht, *J. Phys. Chem.*, **66**, 1168 (1962).

(12) P. M. Johnson and A. C. Albrecht, *J. Chem. Phys.*, **44**, 1845 (1966).

(13) E. Dolan, *ibid.*, **37**, 2508 (1962).

(14) D. W. Skelly, R. G. Hayes, and W. H. Hamill, *ibid.*, **43**, 2795 (1965).

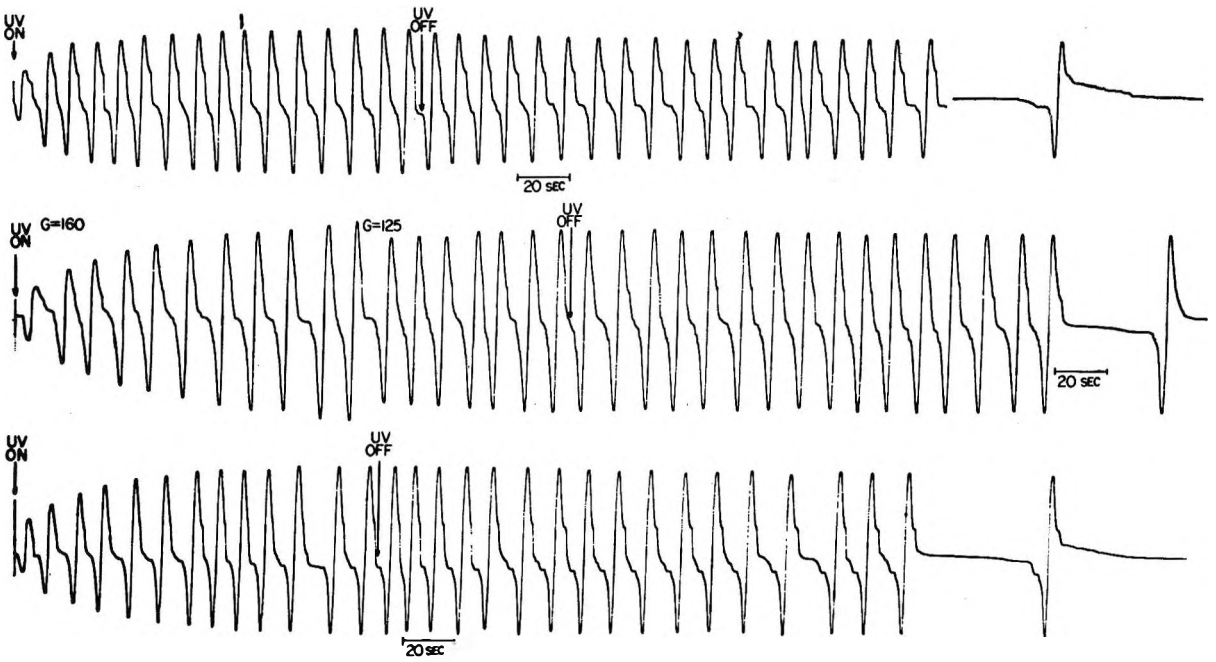

Figure 1. Recorder traces showing repeated scans of esr signal due to electrons during and after the photoionization of TMPD at 77°K: upper, 3-MHX; center, MTHF; lower, methanol-d_4 (CD_3OD); microwave power, 0.01 mW; response time, 0.3 sec.

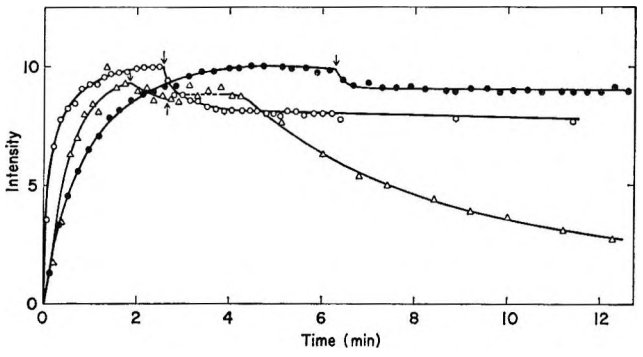

Figure 2. Typical growth and decay curves of esr signal due to electrons by photoionization of TMPD: ●, TEA at 77°K; ○, 3-MHX at 77°K; △, 3-MP irradiated at 70°K, decay at 77°K; ———, period during which temperature, cavity Q, and resonant frequency was changing; ↓ shows the point at which the light was cut off; ↑ shows the point at which helium gas was turned off.

spectrum. The third period begins on turning off the light, when a sharp decrease in the signal intensity was observed in the photoionized 3-MHX glass over a period of about 1 min, after which time the subsequent decay became much slower. As can be seen from Figure 1, the relative magnitude of this initial "fast" decay after irradiation appears to be influenced to some extent by the nature of the solvent. While the effect is clearly in evidence for 3-MHX, the corresponding decrease in MTHF and CD_3OD is much less striking. The fourth and last period refers to the "long-time" decay which will be considered later.

Profiles of the experimental behavior are shown in Figure 2. In the case of 3-MP, the "long-time" thermal decay after irradiation at 77°K is quite rapid so several experiments were carried out at 70°K where this part of the decay is known to be very slow on the indicated time scale.[9] Although the effect was not as pronounced as for 3-MHX, there was still a definite decrease in the signal intensity within a short interval immediately after irradiation and before the helium bubbling was turned off. After discontinuation of helium bubbling, the sample temperature reached 77°K within about 1 min but the measurements made during this intervening period have only a qualitative significance because small changes occurred in the resonant frequency and the Q value of the cavity. In a previous paper,[9a] we omitted consideration of this factor in the graphical presentation of a similar set of data. After the 3-MP sample had attained 77°K and there was no further change in the microwave resonance conditions, thermal decay of the electron signal could be followed in the usual manner. Also shown in Figure 2 are the experimental results for TEA and 3-MHX. These samples were at 77°K during and after irradiation, and since the long-time decay of the signal is very slow in these glasses, the form of the fast decay process immediately after irradiation was more clearly revealed. It might be noted again that the magnitude of this initial decrease for 3-MHX is about a factor of 2 greater than for TEA.

In addition to the singlet spectra due to electrons located at $g \approx 2$ which were observed at low power (0.01 mW), it was also possible to detect a broad singlet ($\Delta H_{ms} \approx 20$ G) at the half-field position (1550 G) *during*

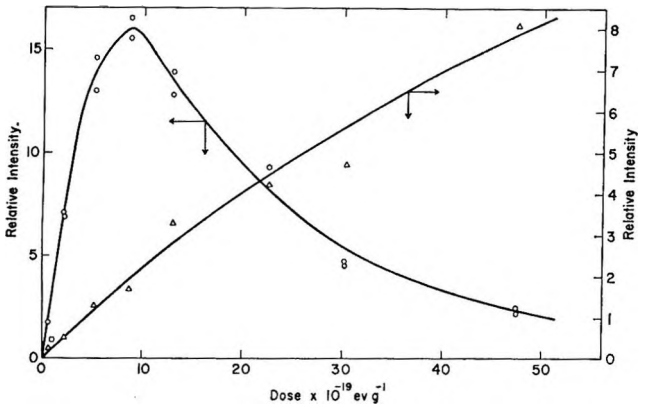

Figure 3. Dose dependence of electron and free-radical concentrations in γ-irradiated 3-methylhexane at 77°K. The ordinate scales are arbitrary and unrelated: electron, ○; free radical, △; electron, □ (sample was preirradiated to a dose of 3×10^{20} eV g^{-1} and bleached before irradiation).

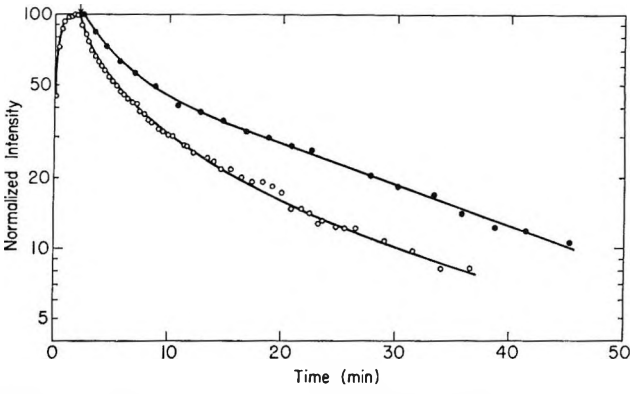

Figure 4. First-order curves for thermal decay of trapped electrons in 3-MP at 77°K: ○, 3-MP–TMPD photoionization; ↓ shows the point where ultraviolet light was cut off; ●, pure 3-MP, γ irradiated at 70°K to a dose of 3.9×10^{18} eV g^{-1}.

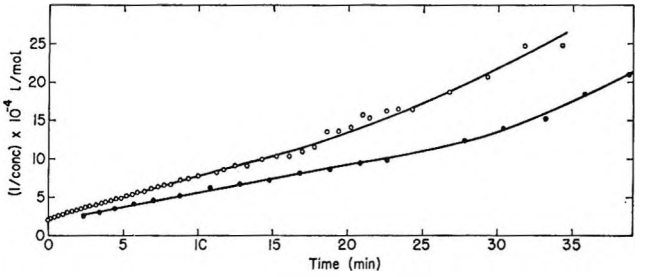

Figure 5. Second-order curves for thermal decay of trapped electrons in 3-MP at 77°K. Other details as in Figure 4.

photoionization of TMPD in several organic glasses, including 3-MHX, 3-MP, MTHF, C_2H_5OH, C_2H_5OD, and CD_3OD. This signal was weak and could be observed clearly only at a power of 1 mW. After the ultraviolet irradiation was stopped, the signal disappeared within 5 sec. When pure organic glasses without TMPD were irradiated under the same conditions, no signal was observed at the half-field position. Therefore, it is reasonable to suppose that the transient signal is due to the $\Delta M_s = 2$ transition of the triplet state of TMPD which has been proposed[4] as an intermediate in the photoionization process.

The manner in which the intensity of the electron signal induced in 3-MHX by γ irradiation depends on the dose is illustrated in Figure 3. For comparison, the corresponding growth curve for the underlying (free-radical) signal due to all of the other radiation-induced paramagnetic centers has been plotted alongside. The trapped electron is relatively stable in 3-MHX at 77°K over the duration of most of these irradiations, so the observed behavior is not a consequence of thermal decay. Over the range in which the free-radical signal grows almost linearly with dose, the intensity of the electron signal first increases, then passes through a maximum value, and finally decreases on prolonged irradiation. When the electron signal was photobleached after a γ-irradiation dose of 3×10^{20} eV g^{-1}, further irradiation of 3-MHX without warming up resulted in a decreased initial yield of trapped electrons compared to the results obtained for previously unirradiated samples. However, if the irradiated sample was warmed up to the liquid state and reirradiated as before, the initial yield remained the same. Similar results have been reported by Willard and coworkers[15] for methylcyclohexane. These findings illustrate some important differences between the behavior on γ irradiation and photoionization. Probably the most marked contrast is in the absence of a steady-state concentration of (e^-) at high γ-irradiation doses.

Thermal decay after either photoionization or γ irradiation is most conveniently compared at 77°K in 3-MP because of the suitable time scale. Representative first- and second-order plots are shown in Figures 4 and 5, respectively. In order to obtain a sufficient concentration of trapped electrons, pure 3-MP was γ irradiated at a temperature of ≈70°K which was obtained by the helium-bubbling technique, and the decay curve was obtained at 77°K according to the general procedure given earlier in this report. In the case of photoionization, the decay studies were made by cutting off the light after the steady-state concentration of (e^-) had been attained at 77°K. In the present work, the decay of the signal was sufficiently slow that it could be followed by repeated scanning at frequent intervals.

The semilogarithmic curves of Figure 4 demonstrate that, in both cases, thermal decay does not proceed by simple first-order kinetics over the entire range of con-

(15) (a) M. Shirom and J. E. Willard, *J. Amer. Chem. Soc.*, 90, 2184 (1968). (b) Recently in this laboratory, Mr. M. A. Bonin has observed a blue emission from the inner wall of a Pyrex dewar containing liquid nitrogen after prolonged irradiation in the γ source. The possibility that this effect may have caused some accidental photobleaching of trapped electrons at the high γ-irradiation doses in our experiments will be investigated.

centration. In the case of electrons produced by γ irradiation, the curve is linear after the concentration has decreased to about 35% of the initial value. As has been pointed out,[6] the shape of the decay curve is largely unaffected by the γ-irradiation dose so in this case the kinetics is independent of the absolute concentration of trapped electrons despite the fact that the simple first-order relation does not apply. From Figure 5 it can be seen that second-order kinetics is formally applicable to the initial portion of the decay in each case. In at least 10 runs following photoionization, the plot was linear up to 20 min after irradiation, and the apparent second-order rate constant is 90 M^{-1} sec^{-1}.

An attempt was made to describe the growth curve during photoionization according to zero-order formation and second-order decay of (e^-). The best fit to the experimental results was obtained with a second-order rate constant of 670 M^{-1} sec^{-1}, but the measure of agreement was far from perfect over the initial portion of the curve. The absolute value of this rate constant was obtained by combining the time characteristic which best fitted the growth curve with the known steady-state concentration of trapped electrons (5×10^{-5} M). Regardless of the uncertainty concerning the precise values and their interpretation, it is clear that the apparent recombination rate constant *during* photoionization is much greater than the value which obtains during thermal decay in the dark, and this can be understood in terms of the important contribution of photobleaching. Independent evidence for this conclusion comes from photobleaching studies at 320 nm of γ-irradiated pure MTHF showing that the decay of trapped electrons occurred rapidly ($t_{1/2} \approx 200$ sec) under the same experimental conditions used for photoionization. The decay was even more rapid ($t_{1/2} \approx 5$ sec) for the electrons in γ-irradiated pure TEA which are known to have photobleaching characteristics similar to those of hydrocarbons.[8] Kinetic analysis of the photobleaching decay curve for trapped electrons in γ-irradiated pure MTHF showed that a simple second-order treatment of the recombination was not applicable, so this might help to explain the failure to fit the data for the growth curve to the calculated expression based on second-order decay.

It has been shown[7,9,12,16] that carbon dioxide is an efficient electron scavenger in γ-irradiated and photoionized organic glasses. Figure 6 shows that the increase in the intensity of the $CO_2\cdot^-$ signal which occurred after γ irradiation is much greater than that after photoionization in 3-MP glasses at 77°K. As indicated in Figure 6, this increase was unaffected by photobleaching with infrared light which is known to remove trapped electrons. It appears then that the growth of $CO_2\cdot^-$ after irradiation is not simply due to electron capture by CO_2.

It is well known[6,9] that trapped electrons in hydrocarbons are efficiently photobleached by infrared light with wavelengths greater than 1000 nm. This effect is illustrated in Figure 7 for a photoionized sample of TMPD in 3-MHX. Subsequent photobleaching with red light ($\lambda > 640$ nm) removed much of the underlying signal which was insensitive to the earlier photobleaching of the electron signal, and this contribution might be due to $TMPD\cdot^+$. There are many reports in the literature[4,6] that the optical absorption spectrum of $TMPD\cdot^+$ in 3-MP persists after the removal of the trapped electrons, although it has been found[17] that when very pure TMPD is used, only a small percentage of the initial absorption remains after complete photobleaching of the electrons. However, it must be said that the present esr results are consistent with the general view that some $TMPD\cdot^+$ species are not removed by photobleaching all the trapped electrons.

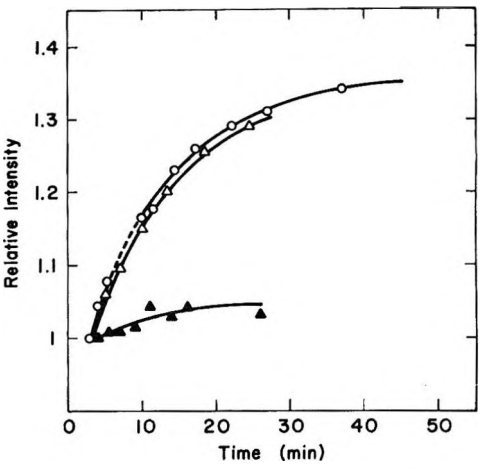

Figure 6. Growth curve of intensity of $CO_2\cdot^-$ after irradiation at 77°K: O, 3-MP–CO_2, γ-irradiation dose 2.9×10^{18} eV g^{-1}; ———, sample was irradiated with infrared light; △, 3-MP–CO_2–TMPD, γ-irradiation dose 2.9×10^{18} eV g^{-1}; ▲, 3-MP–CO_2–TMPD, ultraviolet irradiation.

Whereas the residual free-radical signal in hydrocarbons after TMPD photoionization and photobleaching (Figure 7) was extremely small, this was not the case after the photoionization was carried out in alcohol matrices. In Figure 8 the results of γ irradiation and photoionization are compared for the CD_3OD system. Photobleaching by visible light removed the singlet spectrum of the trapped electron, but a poorly resolved quintet spectrum attributable to $\cdot CD_2OD$ can be seen to remain in each case, although the asymmetry of the spectrum suggests a possible contribution from $CD_3O\cdot$. The presence of these free radicals after γ irradiation is to be expected, but the fact that the same species are also formed in the photoionization experiment suggests that in this case their formation may occur by reaction of the electrons with the alcohol matrix under photo-

(16) M. Shirom, R. F. C. Claridge, and J. E. Willard, *J. Chem. Phys.*, 47, 286 (1967).

(17) J. Lin, Ph.D. Thesis, University of Tennessee, 1968.

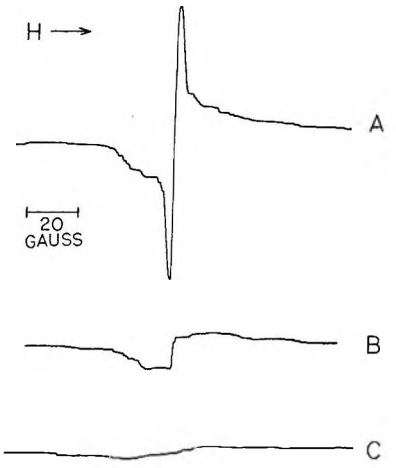

Figure 7. Effect of photobleaching on esr signal from photoionized TMPD in 3-methylhexane at 77°K: A, immediately after irradiation; B, after photobleaching with λ >1000 nm; C, after photobleaching with λ >640 nm; microwave power, 0.01 mW. The same gain settings were used throughout.

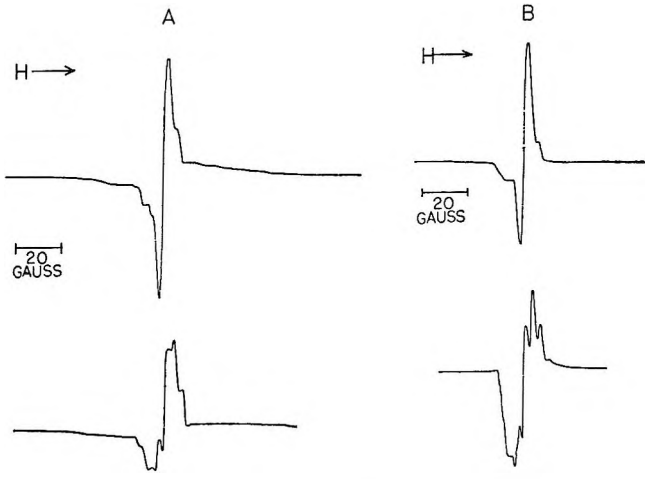

Figure 8. Esr spectra of photoionized TMPD in CD_3OD (A) and γ-irradiated CD_3OD (B) at 77°K. In both cases, the upper and lower spectra refer to sample before and after bleaching with visible light; microwave power, 0.01 mW. The same gain settings were used before and after bleaching.

excitation. This possibility will be discussed more fully below. When TMPD was not present in the 3-MHX or alcohol glasses, no esr signal was observed under the same conditions of ultraviolet irradiation and esr measurement.

Another marked difference between hydrocarbon and nonpolar media (including MTHF) on the one hand and alcohol systems on the other concerned the chemical behavior in the photoionized glasses on warming. In all the nonpolar media we have examined, the esr signal completely disappeared by the time the photoionized sample reached the fluid state, and as indicated in Table I, the trapped electron always disappeared at a

Table I: Decay Temperatures (°K) for Intermediate Species during Warm-up after Photoionization of TMPD in Organic Glasses at 77°K

Solvent	Trapped electron	Free radical	$TMPD^{\cdot+}$
MTHF	93	98	103
3-MP	77–84	≈103	≈103
CD_3OD	103	113	Stable[a]
C_2H_5OD	98	103	Stable[a]

[a] Stable at 300°K for days.

lower temperature than the underlying signal which possibly included a contribution from $TMPD^{\cdot+}$.

The sequence of changes which occurred on warming samples of TMPD in C_2H_5OH and C_2H_5OD after photoionization at 77°K will now be described. The spectrum of the trapped electron shown in Figure 9A disappeared when the sample was warmed to 98°K, and there remained a five-line spectrum together with some additional unresolved hyperfine structure. This five-line spectrum, which is attributed to the free-radical $CH_3\dot{C}HOD$, disappeared on raising the temperature to 103°K, and the spectrum shown in Figure 9B was obtained. No remarkable change occurred on warming until 153°K when the resolution of this spectrum began to improve. A similar pattern of changes was observed for photoionized TMPD in C_2H_5OH and CD_3OD. At higher temperature, a well-resolved spectrum was observed for every photoionized TMPD–alcohol system and a typical spectrum is shown in Figure 10. This spectrum is designated D in the later discussion. In a few experiments, a slightly different spectrum M shown in Figure 11 was obtained, and this spectrum is identical with the published spectrum for Wurster's blue perchlorate in methanol at 223°K (see Figure 6 in ref 18b). The coupling constants in the present work are $A_H^{CH_3}$ = 6.77 G and A_H^{CH} = 1.97 G, which almost exactly agree with the literature values[18,19] for Wurster's blue perchlorate ($TMPD^{\cdot+}ClO_4^-$). The coupling constant for the nitrogen atoms has been reported to be 0.28 G[18] and 6.99 G[19] in two independent investigations, but whichever of these is correct, this coupling constant can only be obtained from very well-resolved spectra.[18,19] Our spectrum M does not show sufficient resolution, and the intensity is too weak to analyze the wings for this purpose. In two experiments, spectrum M changed irreversibly into spectrum D as the sample temperature was raised above ≈205°K, and this latter spectrum persisted even at room temperature although the intensity gradually decreased. The sample was blue and the color persisted for at least 1 day.

(18) (a) K. H. Hausser, *Naturwissenschaften*, **47**, 251 (1960); (b) K. H. Hausser, *Z. Naturforsch.*, **14a**, 425 (1959).

(19) J. R. Bolton, A. Carrington, and J. dos Santos-Veiga, *Mol. Phys.*, **5**, 615 (1962).

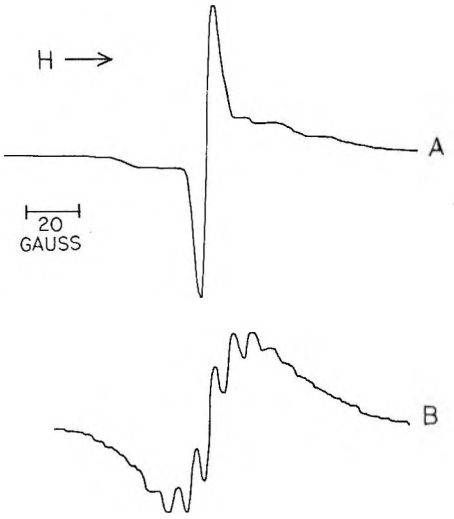

Figure 9. Esr spectra of photoionized TMPD in C_2H_5OD: A, immediately after photoionization at 77°K; microwave power, 0.01 mW; B, after warm-up to 103°K; microwave power, 0.4 mW.

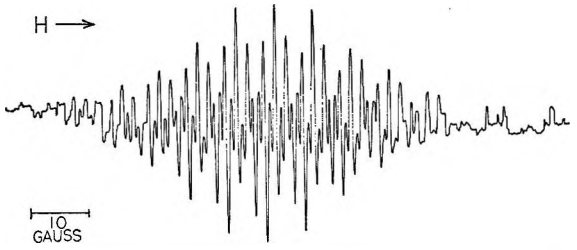

Figure 10. Esr spectrum of photoionized TMPD in C_2H_5OH at 213°K; sample irradiated at 77°K; microwave power, 0.4 mW; modulation amplitude, 0.25 G.

Photoionization of TMPD–alcohol systems could also be carried out at temperatures much higher than 77°K where the system was no longer a rigid glass. The spectra obtained for the TMPD–C_2H_5OD system after photoionization at 183°K are shown in Figure 12. Spectrum A shows 13 lines with additional substructure. Spectra B and C show better resolution due to motional narrowing and spectrum C is identical with the spectrum in Figure 10. When the sample which gave spectrum C was cooled down to 133°K, the spectrum at this temperature resembled that shown in Figure 9B.

A solution of TMPD in CD_3CN formed a polycrystalline matrix at 77°K, and after photoionization at this temperature, the broad singlet spectrum ($\Delta H_{ms} \approx$ 23 G) shown in Figure 13A was obtained. As the sample temperature was raised after irradiation, the singlet spectrum narrowed considerably until at 213°K, the width (ΔH_{ms}) was reduced to about 2 G as a result of exchange narrowing presumably caused by coagulation of $TMPD\cdot^+$.[20] On further warming to 221°K, a resolved spectrum similar to that shown in Figure 10 was observed. At higher temperatures somewhat above the melting point, dielectric loss due to the large sample prevented the observation of the spectrum. The sample was blue at room temperature and the color remained for several days. When the sample was recooled to 77°K, the spectrum did not revert to A in Figure 13 but resembled C instead. Thus, the physical change (coagulation) in the nature of $TMPD\cdot^+$ on warming in CD_3CN is irreversible, and this behavior is in marked contrast to that exhibited by the TMPD–alcohol systems. The intensities of the spectra obtained for the photoionized TMPD–CH_3CN system under the same irradiation conditions were weaker than in the corresponding experiments with CD_3CN, so the results are not so clear in this case.

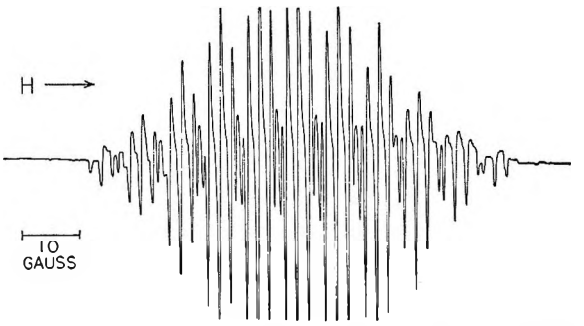

Figure 11. Esr spectrum of photoionized TMPD in C_2H_5OD at 203°K; sample irradiated at 84°K; microwave power, 0.4 mW; modulation amplitude, 0.25 G.

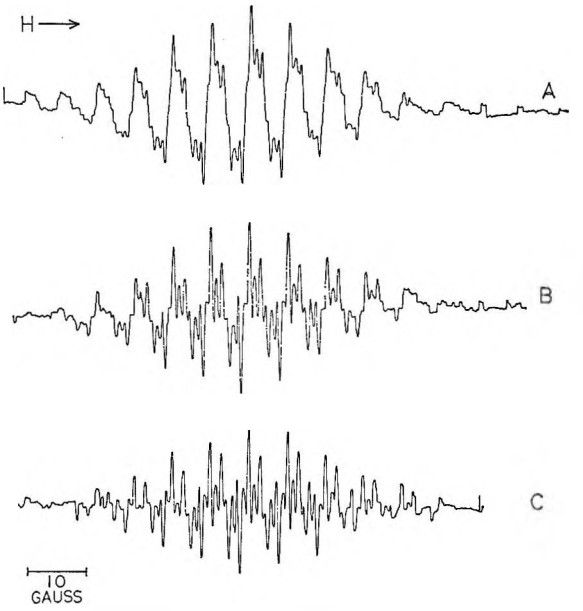

Figure 12. Esr spectra of photoionized TMPD in C_2H_5OD; sample irradiated at 183°K: A, 183°K; B, 203°K; C, 213°K; microwave power, 1 mW.

Discussion

Nature of Electrons Produced by Photoionization and γ Irradiation. There is a striking similarity between the

(20) *Cf.* G. T. Pott and J. Kommandeur, *J. Chem. Phys.*, **47**, 395 (1967).

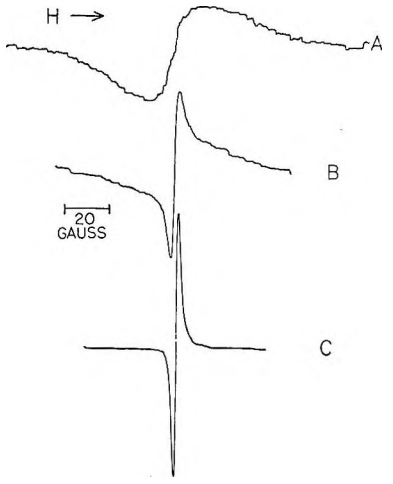

Figure 13. Esr spectra of photoionized TMPD in CD_3CN. Sample irradiated at 77°K: A, 77°K, 0.01 mW; B, 163°K, 0.4 mW; C, 213°K, 0.4 mW.

initial growth curves of electrons shown in Figure 2 and the photoconductivity effects reported by Johnson and Albrecht.[21] In both cases, a steady-state condition is achieved within 3 min in a hydrocarbon matrix containing TMPD under constant illumination at 320 nm. The electron population measured by the esr technique in the steady state is made up largely of electrons which are trapped in the matrix, because only a relatively small decrease in signal intensity is observed immediately after the light is cut off. In contrast, the photoconductivity decreases immediately after irradiation and the remaining dark conductivity is almost negligible in comparison. Therefore, although a steady state of electrons is achieved in the two cases, the nature of the electrons responsible for the photoconductivity and esr signal must be different. This conclusion is in accord with Johnson and Albrecht's proposal that the photoconductivity arises from a short-lived "mobile" state of the electrons which is present only during illumination. We prefer to regard this state as corresponding to optically excited electrons.[8] Further evidence that the excited electron is responsible for the photoconductivity comes from their experiments[21] showing that a transient photoconductivity spike is induced by 546-nm light after previous photoionization at 320 nm. This spike is readily interpreted[21] as coming from the excitation of trapped electrons in the matrix, and this is consistent with our results showing that trapped electrons remain in the matrix after photoionization although they undergo a slow process of thermal decay, especially in 3-MP. In fact, there is semiquantitative agreement between the decay curve (Figure 4) of the esr signal and the decrease in the height of the photoconductivity spike[21] after photoionization in 3-MP at 77°K.

The preceding results suggest that a close relationship prevails between the trapped and excited electrons during illumination, and since both populations reach a steady state during photoionization, it is reasonable to suppose that they are in photodynamic equilibrium. On this basis, the over-all mechanism for TMPD (M) photoionization can be represented as

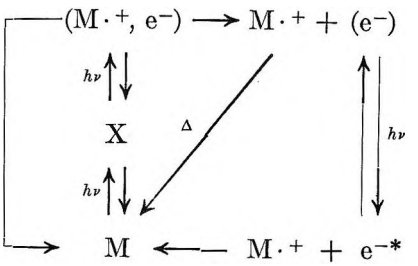

In this scheme, three states of the electron can be distinguished. The delocalized state (M·+, e−) is regarded[8] as the precursor from which the electron may be captured by a solute molecule or be trapped in the matrix (e−). This state is considered to embrace a variety of states proceeding to the complete ionization of the TMPD molecule. Optical excitation of (e−) can result in the formation of an excited state e−* whose reactivity and properties are quite different from those of (e−). The intermediate X is included in the scheme to indicate that the photoionization process is biphotonic, for which there is considerable evidence.[21-23] The diagonal arrow refers to a thermal recombination process of the *trapped* electron.

At first sight, it might be thought that the sharp decrease in the intensity of the esr signal after the light beam is cut off is due to the decay of excited electrons. However, the time scale for this process is much longer than the decay of photoconductivity.[21] Also the magnitude of the decrease in the esr signal, especially in hydrocarbons, is rather large to be attributed solely to excited electrons since the electron concentration responsible for the photoconductivity is considered to be negligibly small.[21] An alternative explanation[24] for the initial decrease in the esr signal is that it involves the recombination of some (M·+, e−) species which are close to the fully ionized condition.

It is immediately apparent from a comparison of

(21) G. E. Johnson and A. C. Albrecht, *J. Chem. Phys.*, **44**, 3162, 3179 (1966).

(22) K. D. Cadogan and A. C. Albrecht, *ibid.*, **43**, 2550 (1965); *J. Phys. Chem.*, **72**, 929 (1968).

(23) Y. Nakato, N. Yamamoto, and H. Tsubomura, *Bull. Chem. Soc. Jap.*, **40**, 2480 (1967); **39**, 2603 (1966).

(24) Another possibility is that the sharp singlet observed at the $g \simeq 2$ position during photoionization includes a *small* contribution resulting from a $\Delta M_s = 1$ transition of the TMPD triplet state. Although it is well known that the anisotropy of the $\Delta M_s = 1$ transition for the randomly oriented triplet state in glasses usually gives rise to a broad signal which is difficult to observe, there may be some narrow lines in the spectrum close to $g \simeq 2$ whose positions depend on the zero-field splitting parameters. The involvement of the triplet state is suggested by the fact that the signal from the $\Delta M_s = 2$ transition at the half-field position and the rapidly decaying portion of the signal at $g \simeq 2$ both disappear with time constants of the order of seconds, but if this is the correct explanation, it is still not clear why the magnitude of the fast decay at $g \simeq 2$ should be affected by the solvent.

Figures 2 and 3 that there is a significant difference in the phenomenology between TMPD photoionization and γ irradiation. A steady-state concentration of electrons was set up rapidly in the former case, while in the latter, the electron concentration first increased linearly with dose and then decreased considerably on prolonged irradiation ($>10^{20}$ eV g^{-1}). It is interesting to note that the maximum concentration of electrons attained by the γ irradiation of 3-MHX at 77°K[9a] is at least one order of magnitude greater than the typical steady-state concentration established in our photoionization experiments.[5] Since no esr measurements could be carried out during γ irradiation, it is impossible to tell whether or not there is a rapidly decaying electron contribution corresponding to that observed in the photoionization experiment. However, we know that the electrons produced by γ irradiation are easily photobleached at 320 nm and that the apparent recombination rate constant during the photoionization is much larger than any thermal contribution. The maximum in the electron concentration produced by γ irradiation does not seem to correlate with any contribution from excited electrons, and the general behavior seems to indicate that the role of excited electrons is much more important in the case of photoionization. On this basis, we would expect the conductivity measured in glasses *during* γ irradiation to be much less than the steady-state photoconductivity even though the trapped-electron concentrations might be similar in the two cases. The essential difference between the two cases lies not only in the character of the ionization process itself but in the capacity of the ultraviolet radiation to excite the trapped electrons which are embedded in the matrix. From these considerations, the processes occurring during γ irradiation may be represented by the modified scheme

$$S \overset{\gamma}{\rightleftharpoons} (S\cdot^+, e^-) \underset{\Delta}{\rightleftharpoons} S\cdot^+ + (e^-)$$

In this case there is no means for the trapped electron (e^-) to recombine except by diffusive recombination, and a stationary concentration of (e^-) is not attained in rigid media. An upper limit to the (e^-) concentration is set by the number density of trapping sites. At high doses, the traps themselves appear to be destroyed[15] by some mechanism peculiar to γ irradiation.

The delocalized state ($S^+\cdot$, e^-) is considered to be the precursor of complete ionization in the general manner already discussed under photoionization. That is, electron separation proceeds through this state and the extent of trapping or capture should then be determined by the way this state interacts with its environment before collapse to the neutral molecule. From previous work,[8] it is known that (e^-) yields in γ-irradiated hydrocarbons are sensitive to the crystallinity and polarity of the matrix, so these effects could arise through this mechanism.

Thermal Decay and Photobleaching Studies. The qualitative similarity in the decay rates of trapped electrons in 3-MP at 77°K after photoionization and γ irradiation (Figures 4 and 5) suggests that the electron distributions in the two cases are not widely different. Although we have not investigated the kinetics of thermal decay as a function of initial steady-state concentration, it would be possible to explain the observation of second-order kinetics following photoionization if a random distribution of positive ions and electrons were to be generated; however, Albrecht and McClain[4] have obtained evidence from recombination luminescence that the individual ion pairs are highly correlated. A precise interpretation of the kinetic results is beset with many uncertainties, and we do not feel that unequivocal conclusions can be drawn from this information alone.

Microwave power saturation studies to be published elsewhere have shown that there is little or no difference in the shape of the esr saturation curves for electrons produced by photoionization and γ irradiation, and again this is consistent with the close resemblance in the kinetic behavior. However, these findings should not be construed to mean that the *original* spatial distributions are necessarily similar, because the excitation of trapped electrons occurs continuously throughout photoionization and this process can modify the distribution.

The intensity of the $CO_2\cdot^-$ signal increases very much after γ irradiation but only very slightly after photoionization in 3-MP at 77°K. This is one of the few significant differences which we have observed between the postirradiation effects of photoionization and γ irradiation, but interpretation is made difficult by the absence of any effect due to infrared photobleaching on the growth curve.

Photobleaching of trapped electrons in 3-MHX by near-infrared radiation ($\lambda > 1000$ nm) occurs with comparable facility after photoionization and γ irradiation. The effects were also similar to those on CD_3OD samples bleached by visible light (Figure 8), but in this matrix an increase in the underlying signal was observed after bleaching which at least in the case of the photoionized sample can be attributed to a reaction of the photoexcited electron e^{-*} with the alcohol. As mentioned earlier, it is likely that the radicals $\cdot CD_2OD$ and $CD_3O\cdot$ are produced by this reaction. The only reasonable mechanism leading to these species in the photoionized sample involves the reactions

$$CD_3OD + e^{-*} \longrightarrow [CD_3OD\cdot^-] \longrightarrow CD_3O^- + D\cdot$$

$$D\cdot + CD_3OD \begin{cases} \longrightarrow \dot{C}D_2OD + D_2 \\ \longrightarrow CD_3O\cdot + D_2 \end{cases}$$

The first reaction has been suggested before[25a] in the photobleaching of γ-irradiated methanol systems, while the second reaction probably requires the participation of a hot D· atom at these low temperatures. It is possible that these reactions also occur during photoionization.[25b] In the case of the γ-irradiated sample, other reactions such as that of e^{-*} with the positive species ($CD_3OD_2^+$) may also contribute in the photobleaching process.

Ionization of TMPD and Solvent Effects. It has been proposed that the photoionization of TMPD occurs by a biphotonic mechanism through the triplet state as the intermediate.[22,23] The present work provides unambiguous esr evidence for the triplet state. Our measurements can only indicate that the lifetime in each solvent system at 77°K was less than 5 sec, but this is consistent with the kinetic results ($\tau \approx 2.3$ sec) obtained from a study of recombination luminescence[4] in 3-MP at 77°K. It follows that the intermediate X included in the previous scheme for photoionization is probably the triplet state of TMPD.

An esr spectrum was observed in the case of alcohol and acetonitrile systems even after the photoionized glasses had been warmed up to the liquid state. These results are in agreement with the findings of Tsubomura and coworkers[23] by optical absorption studies of $TMPD\cdot^+$ produced by photoionization. The esr spectrum in both solvents was the same and this is the spectrum D (Figures 10 and 12) referred to earlier. It is hardly likely that this spectrum would be independent of the solvent if the paramagnetic species responsible were formed by some reaction with the solvent. At 183°K this spectrum (Figure 12A) is partially resolved and shows 13 lines with a hyperfine splitting of about 6.8 G which corresponds to the reported spectrum of Würster's blue perchlorate ($TMPD\cdot^+ClO_4^-$) under conditions of poor resolution.[26] From the better resolved spectrum D shown in Figure 10, the coupling constants for the methyl and ring protons agree with the values quoted earlier for the spectrum M which coincides in every respect with the authentic spectrum of $TMPD\cdot^+ClO_4^-$ in methanol at 223°K. The difference between the spectra D and M resides only in the additional doublet splitting of ≈0.8 G which is observed in D. We interpret the spectrum D as belonging to a different form of $TMPD\cdot^+$. The small splitting of ≈0.8 G cannot be attributed to nuclear hyperfine interaction in the single molecule, and it is postulated that it is due to an interaction between two $TMPD\cdot^+$ cation radicals in close proximity since there is supporting evidence from many sources[27] that $TMPD\cdot^+$ has a tendency to dimerize both in the solid state and in solution. Of particular interest is the recent finding[27a] that the optical absorption spectrum of the $TMPD\cdot^+$ dimer is observed at 143°K after the photoionization of TMPD in ethanol at 77°K. This parallels our esr observations except that the esr spectrum of the dimer is not fully resolved at this particular temperature. Although these authors[27a] suggest that the dimer of the *p*-phenylenediamine cation radical ($PD\cdot^+$) in an ethanol solution of $PD\cdot^+Br^-$ is diamagnetic and that the ground state is consequently a singlet, this may not be true in every instance of dimer formation. In the case of a paramagnetic dimer, a triplet-state esr signal should also be manifested, but in the present work the signal intensity corresponding to the $\Delta M_s = 1$ transition was already very weak, and therefore it is not surprising that no evidence could be obtained for the $\Delta M_s = 2$ transition. Another possible interaction which should be considered is that of $TMPD\cdot^+$ with a neutral molecule of TMPD. The corresponding naphthalene dimer cation $(C_{10}H_8)_2\cdot^+$ is known.[28] In this case, the dimer cation would be in a doublet state. It is impossible to say which, if any, of these interactions is responsible for the spectrum D,[29] and a final interpretation must await further work on this subject. Although it has been established that either of the species responsible for the spectra D and M can predominate in the *same* solution under different conditions, the precise factors governing the relation between these species are not clear.

The stability of $TMPD\cdot^+$ in alcohol and acetonitrile systems after photoionization is explicable in terms of reactions between e^{-*} and the solvent as already discussed earlier in this paper for alcohol and elsewhere for acetonitrile.[8] Such reactions provide a pathway whereby the electron is replaced by stable anions such as $C_2H_5O^-$ and CN^- which can coexist with $TMPD\cdot^+$ in the liquid state.

Acknowledgments. The authors wish to thank Mr. Michael A. Bonin and Mr. Jacob Lin for assistance in the preparation of some samples used in this work.

(25) (a) T. Shida and W. H. Hamill, *J. Amer. Chem. Soc.*, **88**, 3689 (1966). (b) It has been suggested by the reviewer of this paper that the photosensitized production of free radicals may also proceed by a mechanism of energy transfer from an excited state of TMPD.

(26) (a) T. R. Tuttle, Jr., *J. Chem. Phys.*, **30**, 331 (1959); (b) S. I. Weissman, *ibid.*, **22**, 1135 (1954).

(27) (a) K. Kimura, H. Yamada, and H. Tsubomura, *ibid.*, **48**, 440 (1968), and other references quoted in this paper; (b) L. Michaelis and S. Granick, *J. Amer. Chem. Soc.*, **65**, 1747 (1943).

(28) (a) B. Badger, B. Brocklehurst, and R. D. Russell, *Chem. Phys. Lett.*, **1**, 122 (1967); (b) I. C. Lewis and L. S. Singer, *J. Chem. Phys.*, **43**, 2712 (1965); (c) O. W. Haworth and G. K. Fraenkel, *J. Amer. Chem. Soc.*, **38**, 4514 (1966).

(29) The hyperfine splittings in the esr spectrum of the anthracene cation dimer[28c] are approximately one-half of the corresponding values in the monomeric cation radical. According to expectations based on a similar interpretation, spectrum D is *not* attributable to a $(TMPD)_2\cdot^+$ cation dimer.

Low-Energy, High-Angle Electron-Impact Spectrometry

by Aron Kuppermann,[1a] J. K. Rice,[1a,b] and Sandor Trajmar[1c]

California Institute of Technology, Pasadena, California 91109 *(Received June 3, 1968)*

A double electrostatic analyzer electron-impact spectrometer capable of obtaining energy loss spectra of molecules as a function of scattering angle and impact energies has been constructed. It has been used to investigate the differential scattering cross sections for optically allowed and forbidden transitions in several atoms and molecules for electron-impact energies from 25 to 60 eV and scattering angles from 0 to 80°. The results obtained for helium, hydrogen, nitrogen, carbon monoxide, and acetylene are summarized. In general, the intensity of a spin-forbidden transition, relative to that of an optically allowed one, is enhanced by about two orders of magnitude as the scattering angle increases from 0 to 80°. This rule is useful in identifying unknown singlet → triplet transitions.

Introduction

The first measurements of energy losses suffered by electrons in collisions with atoms and molecules were made by Franck and Hertz[2a] in a multiple-collision experiment and were used to obtain information about the electronic energy levels of the target. A summary of the early work in this field can be found in the classical text of Massey and Burhop.[2b] However, the use of energy-loss measurements in electron–molecule collisions as a spectroscopic technique was quite limited due primarily to experimental difficulties. The last decade has seen a resurgence of interest in this field resulting in part from the more sophisticated electronic and electron-optical techniques which have since been developed. Lassettre and coworkers[3] did excellent pioneering work in obtaining electronic spectra in the impact-energy range from 400 to 600 eV, using electrostatic energy analyzers. Much of their work was aimed at testing the validity of the Born approximation at small scattering angles. At these relatively high impact energies, optically forbidden transitions are either detected as extremely weak ones or, as in the case of spin-forbidden transitions, usually not at all. In order to be able to investigate such transitions, we found that impact energies in the range from the excitation threshold to about 50 eV above threshold are required.

An elegant threshold technique, the trapped-electron method,[4] was developed by Schulz. In this technique, optically forbidden transitions are easily detected, but there are difficulties in marking valid state assignments simply on the basis of the resulting excitation spectra. For a given transition in the target, the impact energy cannot be varied by more than a few tenths of an electron volt above threshold (the depth of the potential well in which the electrons are trapped after causing the excitation) nor can measurements be made as a function of scattering angle. The energy resolution of this technique has recently been improved to about 0.05 eV by Brongersma and Oosterhoff,[5] Compton, *et al.*,[6] and Dowell and Sharp.[7]

A low-energy, large-angle electron-scattering spectrometer was developed by Kuppermann and Raff.[8] With this instrument, spin-forbidden transitions could be detected and identified in favorable cases by the dependence of the transition intensities on impact energy. However, the energy resolution of this instrument was rather low because of its wide angle of acceptance and the retarding potential method used for the energy analysis. Although the angular resolution can be improved,[9] this apparatus remains essentially one of low resolution and fixed scattering angle.

A very important step forward in developing low-energy impact spectrometry as a precise spectroscopic tool was taken by Simpson and Kuyatt,[10] who introduced spherical electrostatic analyzers for both the production of a monoenergetic electron beam and the measurement of the energy losses as a result of molecular excitations. One of their instruments has been devoted to studies at low impact energies and a fixed scattering angle of 0° and the other to higher impact energies and scattering angles up to about 20°. Re-

(1) (a) A. A. Noyes Laboratory of Chemical Physics. Contribution 3684. Work supported in part by the U. S. Atomic Energy Commission. Report Code No. CALT-532-31. (b) Work performed in partial fulfillment of the requirements for a Ph.D. degree in chemistry from the California Institute of Technology. (c) Jet Propulsion Laboratory. Work supported in part by the National Aeronautics and Space Administration under Contract No. NAS7-100.

(2) (a) J. Franck and G. Hertz, *Z. Phys.*, 20, 132 (1919); (b) H. S. W. Massey and E. H. S. Burhop, "Electronic and Ionic Impact Phenomena," 1st ed, Clarendon Press, Oxford, 1952.

(3) E. N. Lassettre and coworkers (a series of ten papers), *J. Chem. Phys.*, 40, 1208 (1964).

(4) G. J. Schulz, *Phys. Rev.*, 112, 150 (1958).

(5) H. H. Brongersma and L. J. Oosterhoff, *Chem. Phys. Lett.*, 1, 169 (1967).

(6) R. N. Compton, R. H. Huebner, P. W. Reinhardt, and L. G. Christophorou, *J. Chem. Phys.*, 48, 901 (1968).

(7) J. T. Dowell and T. E. Sharp, *ibid.*, 47, 5068 (1967).

(8) A. Kuppermann and L. M. Raff, *ibid.*, 37, 2497 (1962); 39, 1607 (1963); *Discussions Faraday Soc.*, 35, 30 (1963).

(9) P. S. P. Wei and A. Kuppermann, to be submitted for publication.

(10) (a) J. A. Simpson, *Rev. Sci. Instr.*, 35, 1698 (1964); (b) C. A. Kuyatt and J. A. Simpson, *ibid.*, 38, 103 (1967).

cently, Lassettre and coworkers[11] have used a double hemispherical electrostatic analyzer apparatus to investigate triplet states of molecules. They used impact energies as low as 35 eV and scattering angles as high as 20°. Doering[12] has reported the detection of triplet states with an apparatus using a double electrostatic analyzer system (one cylindrical and one spherical), low impact energies, and a fixed scattering angle of 90°. His resolution was about 0.2 eV.

Since essentially all of the information one can obtain about the excited states of the target from electron impact is contained in the differential scattering cross section, the measurement of this quantity as a function of angle as well as incident energy is desirable for the unambiguous identification of these excited states.

In 1963, Ehrhardt and coworkers[13] put into operation an impact spectrometer in which the target was a molecular beam. This apparatus was later modified to include double-energy analysis,[14] and although it has been used to investigate a few optically forbidden excitations at low impact energies and a wide range of angles (0–120°),[15,16] it is used mainly to study resonance scattering.

In this paper we briefly describe a high-resolution, variable-angle electron-impact spectrometer aimed specifically at the study of optically forbidden states and summarize some of the experimental results obtained so far.

Experimental Section

The spectrometer used in these experiments is of the same type as the one described by Simpson and Kuyatt.[10] Only minor modifications were introduced in the design. These modifications are, however, very important for experiments at high angles and low signal levels. The apparatus consists of an electron gun, two hemispherical electrostatic energy selectors (monochromator and analyzer), a scattering chamber, and a detector system. A schematic diagram of the spectrometer is shown in Figure 1.

The electron gun consists of a thermionic cathode and a two-stage lens system. It produces a well-collimated electron beam of about 2-eV kinetic energy at the entrance of the monochromator (beam intensity $\simeq 10^{-6}$ A; beam diameter $\simeq 0.5$ mm; beam divergence half angle $\simeq 0.5°$). The monochromator and analyzer are 180° spherical electrostatic energy selectors[17] with a mean radius of 25.4 mm. The electrons pass between the hemispheres and are dispersed according to their kinetic energy. Electrons emerging from the monochromator with kinetic energy within a narrow range are accelerated to the desired impact energy and focused into the scattering chamber. The energy width of this beam can be varied between 0.03 and 0.3 eV (full width at half-maximum, FWHM) by appropriately adjusting the monochromator potentials. Typical beam intensity into the scattering chamber is between 10^{-7} and 10^{-8} A. The electron gun, monochromator, and scattering chamber entrance optics are mounted on a gear wheel which can be rotated from outside the vacuum chamber. Rotation of this wheel permits scanning of the scattering angle.

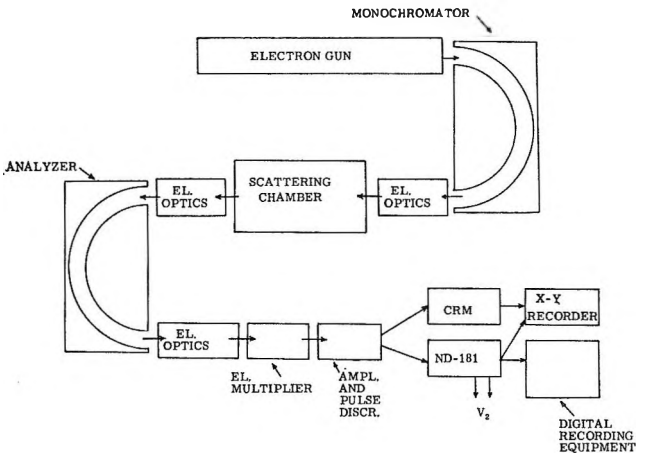

Figure 1. Schematic diagram of the electron-impact spectrometer.

The scattering chamber is made of two concentric bellows. The convolutions of the bellows have an S-shape cross section and are individually welded together to provide a very flexible structure which allows a variation of scattering angle from −30 to +90°. In addition, the small spaces between the convolutions form an electron trap along the inner surface of the scattering chamber. This feature is particularly important at large scattering angles where the intensity of the scattered signal is low and the background wall scattering could cause serious problems. The scattering chamber can be temperature controlled by introducing a heating or cooling fluid in the space between the two concentric bellows. The gas to be studied is admitted to the space enclosed by the inner bellows and kept at a pressure of about 10^{-3} torr, as measured by miniature ion and thermocouple gauges. A remotely actuated Faraday cup can be inserted into the scattering chamber to measure the intensity of the incident electron beam. The only vacuum connections between the scattering chamber and the surrounding main vacuum chamber are the two pinholes through which the electron beam enters and exits. The pressure in the main chamber can be kept in the 10^{-7} torr range, even with a sample pressure of 10^{-2} torr.

(11) A. Skerbele, M. A. Dillon, and E. N. Lassettre, *J. Chem. Phys.*, **46**, 4161, 4162 (1967).
(12) J. P. Doering and A. J. Williams, III, *ibid.*, **47**, 4180 (1967).
(13) H. Ehrhardt and U. Erbse, *Z. Phys.*, **172**, 210 (1963).
(14) D. Andrick and H. Ehrhardt, *ibid.*, **192**, 99 (1966).
(15) H. Ehrhardt and K. Willmann, *ibid.*, **203**, 1 (1967).
(16) H. Ehrhardt and K. Willmann, *ibid.*, **204**, 462 (1967).
(17) E. M. Purcell, *Phys. Rev.*, **54**, 818 (1938).

The components of the detector system are: electron multiplier, pulse amplifier and discriminator, count-rate meter (CRM), and multichannel scaler (ND-181). The discriminator is a single-channel pulse height analyzer and acts as a window. Pulses of low peak intensity (noise) and of high peak intensity (cosmic rays) can be eliminated. The scattered signal intensity is measured either with the CRM or with the ND-181 multichannel scaler.

The whole spectrometer is mounted on a 36-cm diameter flange. All mechanical and electrical connections are made through this flange and the whole assembly is attached to a stainless steel high-vacuum chamber. The apparatus and chamber are bakable up to about 400°. External fields are attenuated to the required degree by appropriate radiofrequency and magnetic shields.

The apparatus can function in several modes. When it is operated as a spectrometer, the scattered signal intensity is measured as a function of energy loss at a fixed impact energy (E_0) and scattering angle (θ). Electrons suffering collisions within a small volume which is defined by the intersection of the electron beam cone entering the scattering chamber and by the view cone of the exit electron optics of the scattering chamber are collected over a small solid angle ($\sim 10^{-3}$ steredian). The monochromator and analyzer are tuned to transmit electrons with the same kinetic energy. The lens potentials at the entrance and exit of the analyzer and the analyzer itself all ride on top of a sweep voltage (V_2) which is applied between these elements and the scattering chamber. When the sweep voltage is zero, electrons that did not lose any energy (elastic scattering) are transmitted to the detector. As the sweep voltage is increased from zero to V volts, electrons that have lost kinetic energy $\Delta E = eV$ electron volts can pass through the analyzer and are detected. The signal output of the detector system as a function of sweep voltage thus directly yields the energy-loss spectrum. When the ND-181 system is used, the memory channel number is decoded and transformed into an analog signal (V_2) which then is used for sweeping the energy loss. This analog voltage is proportional to the channel number into which the counts are being accumulated and can change by 1- to 100-mV step sizes as the memory advances from one channel to the next one. The channel dwell times can be varied from 50 μsec to 2 sec and the complete sweep (1024 channels) can be automatically repeated as many times as required to achieve a desired signal-to-noise ratio. After the experiment is finished, the contents of the memory can be dumped either in the form of an analog signal (X-Y recorder, oscilloscope) or in digital form (punched paper tape, typewriter). When the rate meter is used, the sweep voltage is generated either by a function generator in the form of a ramp or by the ND-181 system in the form of steps. It also drives the X axis of the X-Y recorder. The output of the rate meter corresponds to the Y axis.

The energy-loss scale is determined by an absolute-measurement technique. The origin of the energy-loss scale is placed at the center of the elastic peak. The sweep voltages corresponding to this peak center and to all inelastic features are measured by a calibrated five-place digital voltmeter (HP Model 2401A) and the readings are accurate to ± 0.001 V.

Measurements taken at different scattering angles correspond to different effective scattering volumes. If one wants to compare cross sections rather than cross section ratios at different angles, a normalization of all measurements to the same scattering volume is necessary. This correction was achieved by calculating the scattering volumes defined by the intersection of the electron beam cone and the view cone of the detector. The density distribution of the beam was taken as a truncated gaussian with the maximum density along the cone axis. Each volume element within the scattering volume was weighted for electron density and solid angle subtended at the entrance of the detector optics. These effective scattering volumes were then normalized at each angle to the 90° value. For studying the scattering angle dependence of the ratio of two cross sections this volume correction is not necessary, since it cancels out in numerator and denominator.

Results

Helium.[18] Regular grade tank helium was used without further purification. Figure 2 shows a spectrum of helium at an impact energy of 35 eV and a scattering angle of 25° obtained by the multichannel scaler. A single slow sweep lasting about 35 min was used. The resolution, defined as the full width at half-maximum of the elastic peak, was set at 0.1 eV which is sufficient for studying the four lowest excited states. The positions of the centers of the observed peaks in Figure 2 are given in electron volts by the numbers labeled "obs." Those labeled "opt." are obtained from tables of atomic energy levels.[19] As can be seen, the agreement between these values is 0.01 eV or better. The center of the largest peak, corresponding to excitation of the 2^1P state, could be determined more accurately than the others by locating the line of medians at several heights above the base line. The agreement between the optical and electron-impact value in this case is 0.001 eV, which corresponds to 1% of the peak width.

The first four peaks of Figure 2 correspond to transitions from the ground 1^1S state to the 2^3S, 2^1S, 2^3P,

(18) (a) J. K. Rice, A. Kuppermann, and S. Trajmar, to be submitted for publication; (b) J. K. Rice, A. Kuppermann, and S. Trajmar, *J. Chem. Phys.*, **48**, 945 (1968).

(19) C. E. Moore, "Atomic Energy Levels," Vol. I, National Bureau of Standards Circular No. 467, U. S. Government Printing Office, Washington, D. C., 1949.

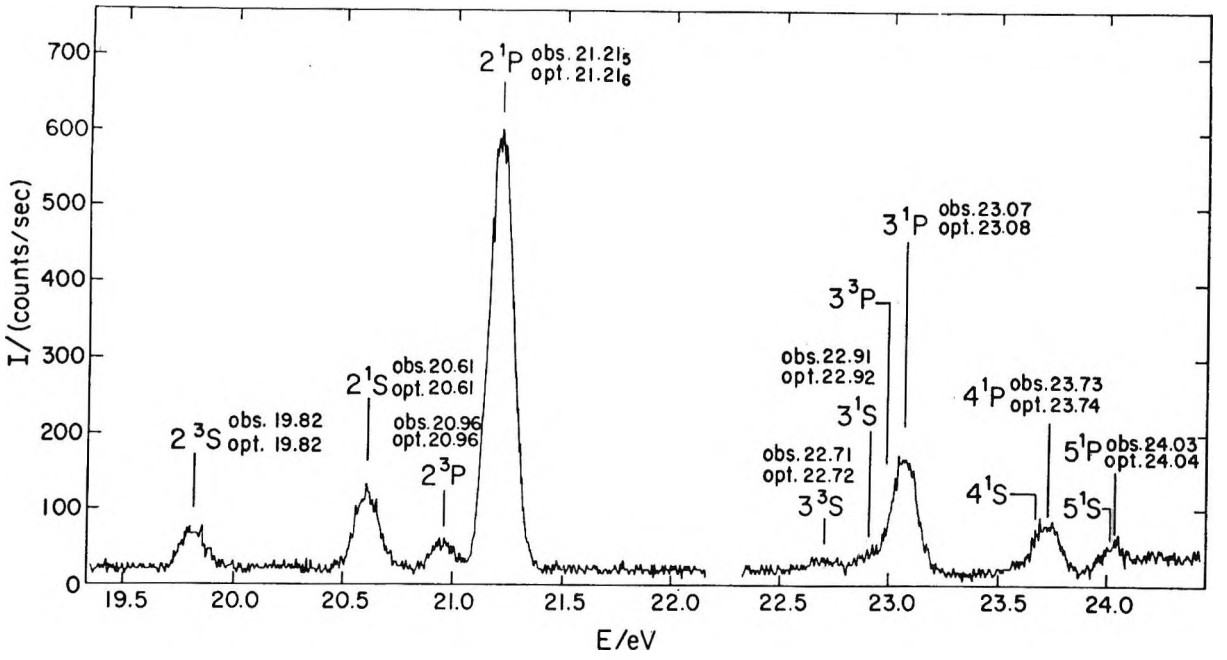

Figure 2. Electron energy-loss spectrum of helium; 35-eV incident electron energy; 25° scattering angle; 10^{-3} torr pressure gauge reading; 4×10^{-9} A incident beam current; 0.10-eV resolution (FWHM of the elastic peak); multichannel scaler mode—single sweep—with a voltage step of 5 mV/channel and a scan rate of 2 sec/channel.

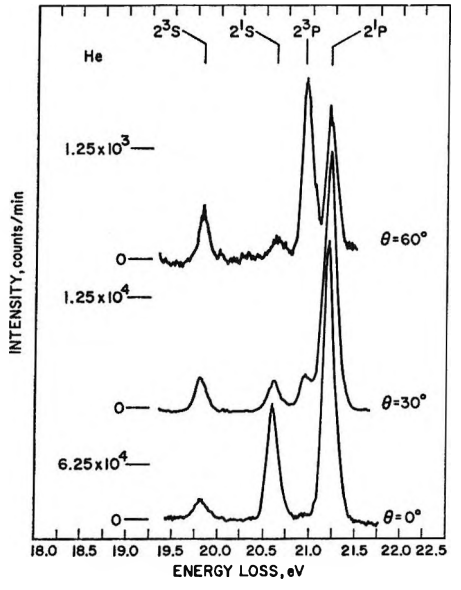

Figure 3. Electron energy-loss spectra of helium at scattering angles of 0, 30, and 60°; 34-eV incident electron energy; 1×10^{-8} A incident beam current; 10^{-3} torr pressure gauge reading; rate meter mode.

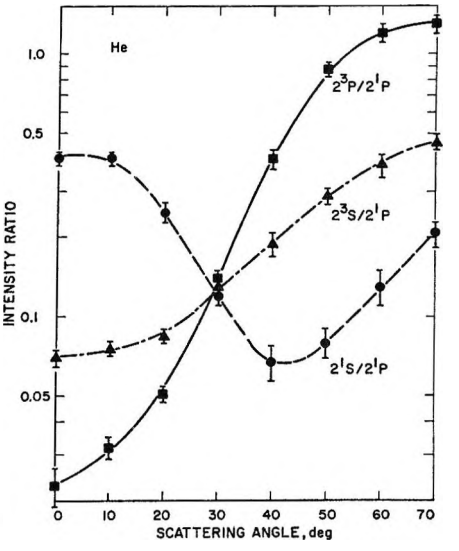

Figure 4. Peak intensity as a function of scattering angle for the three lowest transitions in helium with respect to that of the $1^1S \rightarrow 2^1P$ transition. Same conditions as Figure 3.

and 2^1P states, respectively. The first three of these are optically forbidden, while the last is optically allowed. Transitions to the 2^1S state are symmetry-forbidden (S → S), those to the 2^3P state are spin-forbidden, and those to the 2^3S state are both symmetry- and spin-forbidden. Figure 3 contains three impact spectra of helium, collected under identical conditions, except for different scattering angles of 0, 30, and 60°. A cursory glance indicates that these four transitions have very different angular dependencies. In Figures 4 and 5 we have plotted the ratio of the three optically forbidden peak intensities to the optically allowed 2^1P one as a function of scattering angle. The impact energies E_0 for these figures were 34 and 44 eV, respectively. As can be seen, the $2^3P/2^1P$ intensity ratio increases by about two orders of magnitude as the scattering angle increases from 0 to 70°. The $2^1S/2^1P$ intensity ratio has a local maximum at 0°, decreases to a minimum at about 40°, and increases thereafter. Finally, the behavior of $2^3S/2^1P$ intensity ratio is some-

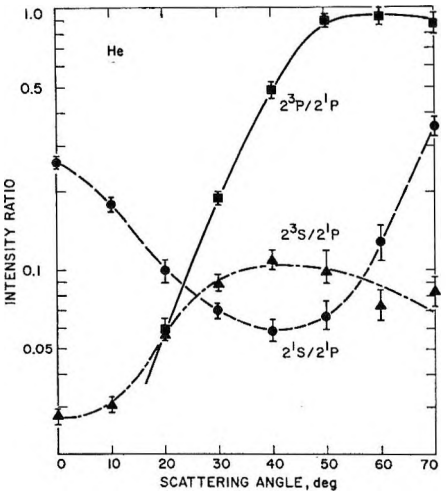

Figure 5. Peak intensity as a function of scattering angle for the three lowest transitions in helium with respect to that of the $1^1S \rightarrow 2^1P$ transition; 44-eV incident electron energy.

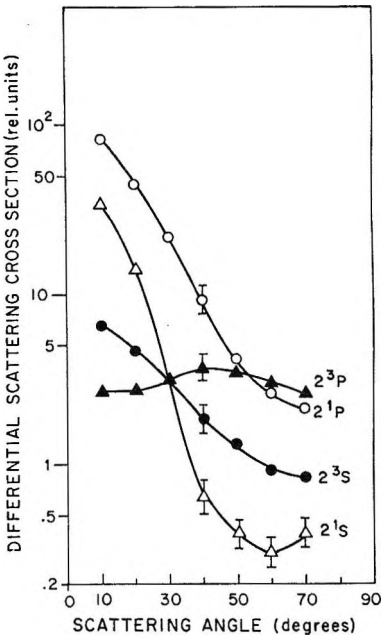

Figure 6. Differential scattering cross section as a function of scattering angle for excitation of the four lowest lying states in helium; 34-eV incident electron energy.

what similar to that of the $2^3P/2^1P$ one, except that the rate of its increase with scattering angle is not as large.

The differential cross sections corresponding to Figure 4 are plotted in Figure 6 in arbitrary units. Note that the differential cross section for the $1^1S \rightarrow 2^1P$ transition is sharply peaked in the forward direction, decreasing by a factor of about 50 as the scattering angle increases from 0 to 70°, whereas that for the $1^1S \rightarrow 2^3P$ transition is nearly isotropic in the same angular range, showing a flat maximum at about 40°.

It is interesting to ask why the angular dependencies of these two differential scattering cross sections are so different. No accurate calculations for them are available. Because of the low impact energies used (for the purpose of enhancing the intensity of spin-forbidden transitions), the first-order Born approximation for the direct-scattering transition amplitude and the Born–Oppenheimer approximation[20] for the exchange-scattering one are not expected to yield reliable results. An improved version[21] of the latter method has been used to calculate the differential cross sections for the $1^1S \rightarrow 2^3S$ and $1^1S \rightarrow 2^3P$ transitions,[22] but the results, although of the correct order of magnitude, do not show the correct angular dependence.

Nevertheless, a qualitative theoretical justification of the difference in the angular dependencies mentioned above can be given. The nature of the interaction giving rise to the $1^1S \rightarrow 2^1P$ transition (or any optically allowed transition) is the coulombic repulsion between the incoming electron and the atomic electrons. This is a relatively long-range force and as a consequence small angular deflections, corresponding to large impact parameters (in an approximate classical mechanical language), will contribute most to the differential cross section yielding a strongly forward-peaked distribution of scattered electrons. On the other hand, for a spin-exchange process such as that involved in the $1^1S \rightarrow 2^3P$ transition, the incident electron must approach the target with relatively small incident energies and impact parameters to allow the much shorter range exchange process to occur. Under these conditions, the scattered electron partly "forgets" where the incident electron came from and is emitted more isotropically than in the former case. This difference between angular distributions in the scattering of particles by long-range and short-range forces is well understood quantitatively for the quantum mechanical elastic scattering of a particle by a center of force.[23] It is based primarily on a partial wave expansion and an analysis of the number of partial waves which contribute significantly to the differential cross section. This argument can be extended to inelastic scattering processes by the use of a complex optical potential and is in principle qualitatively applicable to exchange phenomena. As a result, the relatively rapid increase with scattering angle of the intensity ratio of a spin-forbidden transition to an optically allowed transition is expected to be a general phenomenon, quite independent of the specific atom or molecule being excited. This expectation has indeed been verified for all such transitions we have studied, as indicated in the remainder of this paper.

Hydrogen.[24] High-purity tank hydrogen was used

(20) M. Born and R. Oppenheimer, *Ann. Phys.*, **84**, 457 (1927).

(21) (a) V. I. Ochkur, *Soviet Phys. JETP*, **18**, 503 (1964); (b) M. R. H. Rudge, *Proc. Phys. Soc.*, **85**, 607 (1965); **86**, 763 (1965).

(22) (a) D. C. Cartwright, Ph.D. Thesis, California Institute of Technology, 1967; (b) D. C. Cartwright and A. Kuppermann, forthcoming.

(23) H. S. W. Massey, "Encyclopedia of Physics," Vol. XXXVI, S. Flügge, Ed., Springer-Verlag, Berlin, 1956, p 233.

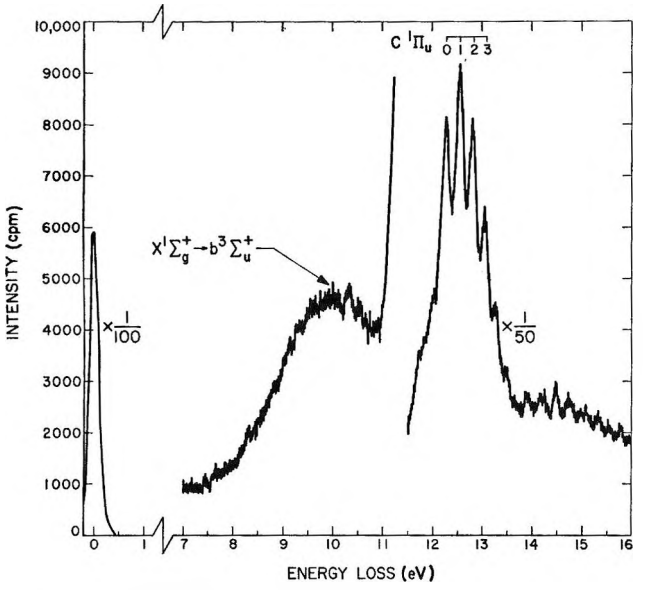

Figure 7. Electron energy-loss spectrum of molecular hydrogen; 50-eV incident electron energy; 40° scattering angle; 2×10^{-3} torr pressure; 2.8×10^{-8} A incident beam current; 0.20-eV resolution; rate meter mode.

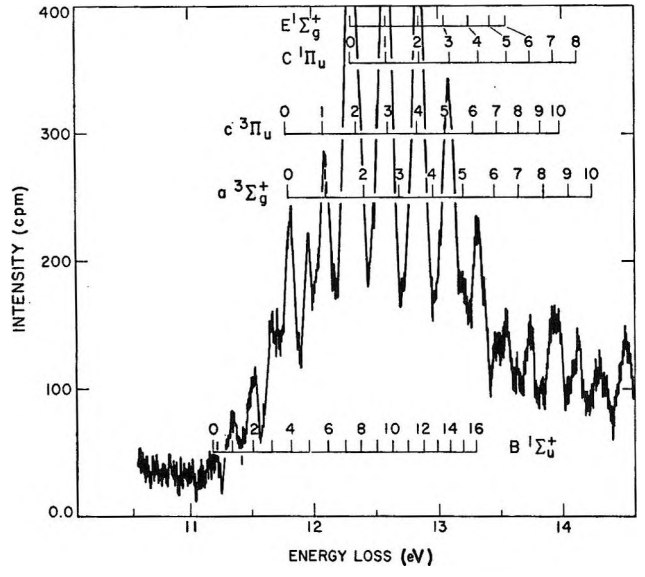

Figure 8. Electron energy-loss spectrum of molecular hydrogen in the region from 11 to 14 eV; 40-eV impact energy; 80° scattering angle; 1.5×10^{-3} torr pressure; 10^{-8} A incident current; 0.040-eV FWHM; rate meter mode.

without further purification. Figure 7 is a low-resolution (FWHM = 0.20 eV) energy-loss spectrum at an incident energy (E_0) of 50 eV and a 40° scattering angle (θ). The broad feature between 7.5 and 11 eV, peaking at about 10 eV, corresponds to the spin-forbidden transition from the $X^1\Sigma_g^+$ ground state[25] to the lowest triplet state $b^3\Sigma_u^+$. This triplet state is unstable with respect to dissociation. Under our experimental conditions, the collision time is short compared to a vibrational period, and, therefore, it is expected that the

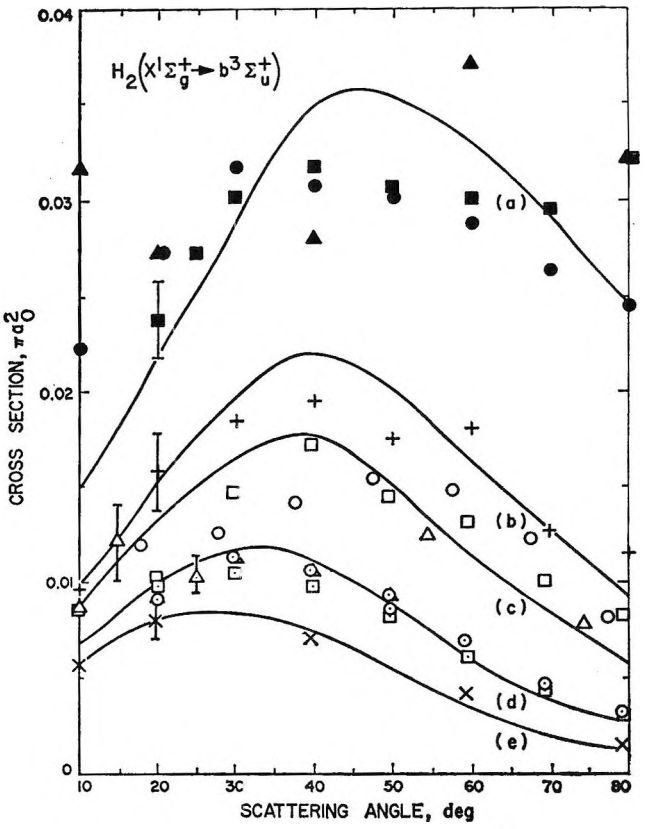

Figure 9. Differential scattering cross sections for the transition $X^1\Sigma_g^+ \rightarrow b^3\Sigma_u^+$ in molecular hydrogen as a function of angle at (a) 25-eV, (b) 35-eV, (c) 40-eV, (d) 50-eV, and (e) 60-eV impact energies. The solid curves are calculated values and the discrete points are experimentally determined under the conditions of Figure 7.

transitions should be vertical, according to the Franck–Condon principle. This explains the broad nature of this singlet–triplet band. Figure 8 is a higher resolution (FWHM = 0.04 eV) energy-loss spectrum, at $E_0 = 40$ eV and $\theta = 80°$, covering the energy-loss range from 11 to 14 eV. Contributions from the $v = 0$ and 1 positions of the $a^3\Sigma_g^+$ and/or $c^3\Pi_u$ states to the peaks located at the $v = 4$ and 6 positions of the $B^1\Sigma_u^+$ transition are indicated by the intensity alternation of the vibrational bands of this state.

Figure 9 depicts the differential cross sections for the $X^1\Sigma_g^+ \rightarrow b^3\Sigma_u^+$ transition as a function of scattering angle for several impact energies between 25 and 60 eV. The points are experimental and the curves were calculated according to the Ochkur–Rudge model.[24] The experimental points were scaled at each E_0 to the same average value as the theoretical results. Therefore, Figure 9 provides a comparison between the shapes of the angular distributions. As in the case for the $^1S \rightarrow$

(24) S. Trajmar, D. C. Cartwright, J. K. Rice, R. T. Brinkmann, and A. Kuppermann, *J. Chem. Phys.*, in press.

(25) All state assignments for the diatomic molecules discussed are from G. Herzberg, "Spectra of Diatomic Molecules," 2nd ed, D. Van Nostrand Co. Inc., Princeton, N. J., 1950, except as noted: H_2, p 530; N_2, p 551; CO, p 520.

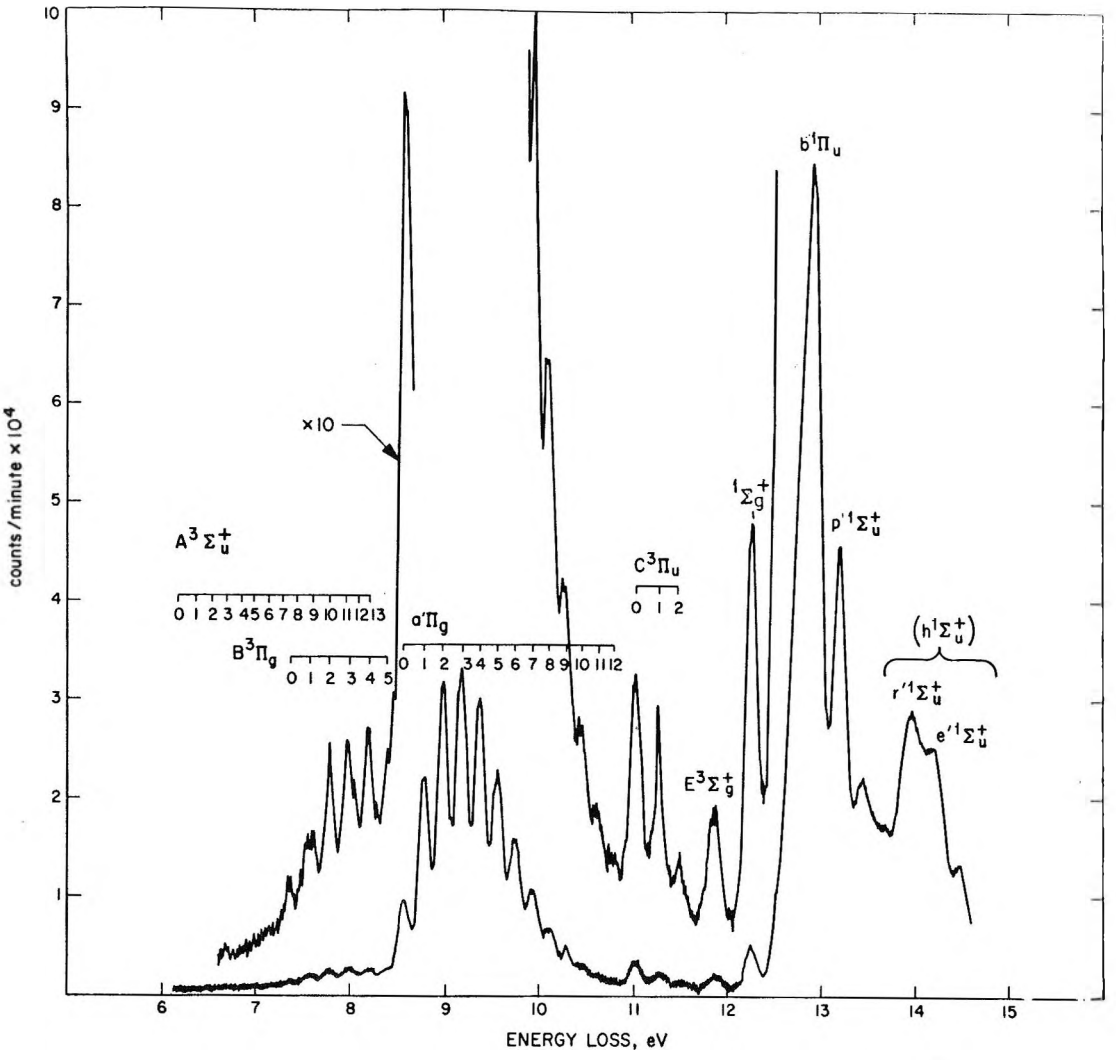

Figure 10. Electron energy-loss spectrum of nitrogen; 40-ev impact energy; 20° scattering angle; 10^{-3} torr pressure; rate meter mode.

2^3P transition in helium, the experimental angular distributions are nearly isotropic, showing a broad maximum around $\theta = 40°$ for $E_0 = 35$ and 40 eV. However, agreement between theory and experiment is much better than in the helium case[18a] and is quite satisfactory for E_0 between 35 and 60 eV. In any event, these angular distributions behave as expected from the qualitative theoretical discussion presented in the last section.

The overlap between transitions to the $B^1\Sigma_u^+$, $a^3\Sigma_g^+$, and $c^3\Pi_u$ states does not permit a study of the latter two states with a precision equivalent to that of the repulsive $b^3\Sigma_u^+$ one.

Nitrogen and Carbon Monoxide.[26] High-purity dry nitrogen and carbon monoxide were used without further purification. Figures 10 and 11 show energy-loss spectra of nitrogen at $E_0 = 40$ eV and $\theta = 20$ and 80°, respectively. The electric-dipole-forbidden $a^1\Pi_g$ (Lyman–Birge–Hopfield) and the spin-forbidden $B^3\Pi_g$, $C^3\Pi_u$, and $E^3\Sigma_g^+$ bands are clearly discernible. At $\theta = 20°$ the most intense transition is to the $b^1\Pi_u$ state, which is optically allowed and about 50 times more intense than any triplet peak in the spectrum. However, at $\theta = 80°$, optically forbidden transitions are in general as intense as the optically allowed ones.

Transition intensities from the $X^1\Sigma_g^+$ ground state to the $E^3\Sigma_g^+$ (11.87 eV), $^1\Sigma_g^+$ (12.28 eV), $p'^1\Sigma_u^+$ (13.21 eV), and $C^3\Pi_u$ (11.03 eV) states relative to that of the $b^1\Pi_u$ (12.93 eV) state are plotted in Figure 12. Since the vibrational levels of $p'^1\Sigma_u^+$ and $b^1\Pi_u$ are not resolved, the peak position does not correspond to the excitation of a particular vibration. The $p'^1\Sigma_u^+$ transition is optically allowed and the corresponding intensity ratio does not vary appreciably in the angular range studied. Dressler[27] has recently assigned the 12.28-eV energy-loss peak to the symmetry- (g → g) forbidden $X^1\Sigma_g^+ \rightarrow {}^1\Sigma_g^+$ transition. We find in sup-

(26) J. K. Rice, S. Trajmar, and A. Kuppermann, to be submitted for publication.

(27) K. Dressler and B. L. Lutz, *Phys. Rev. Lett.*, **19**, 1219 (1967).

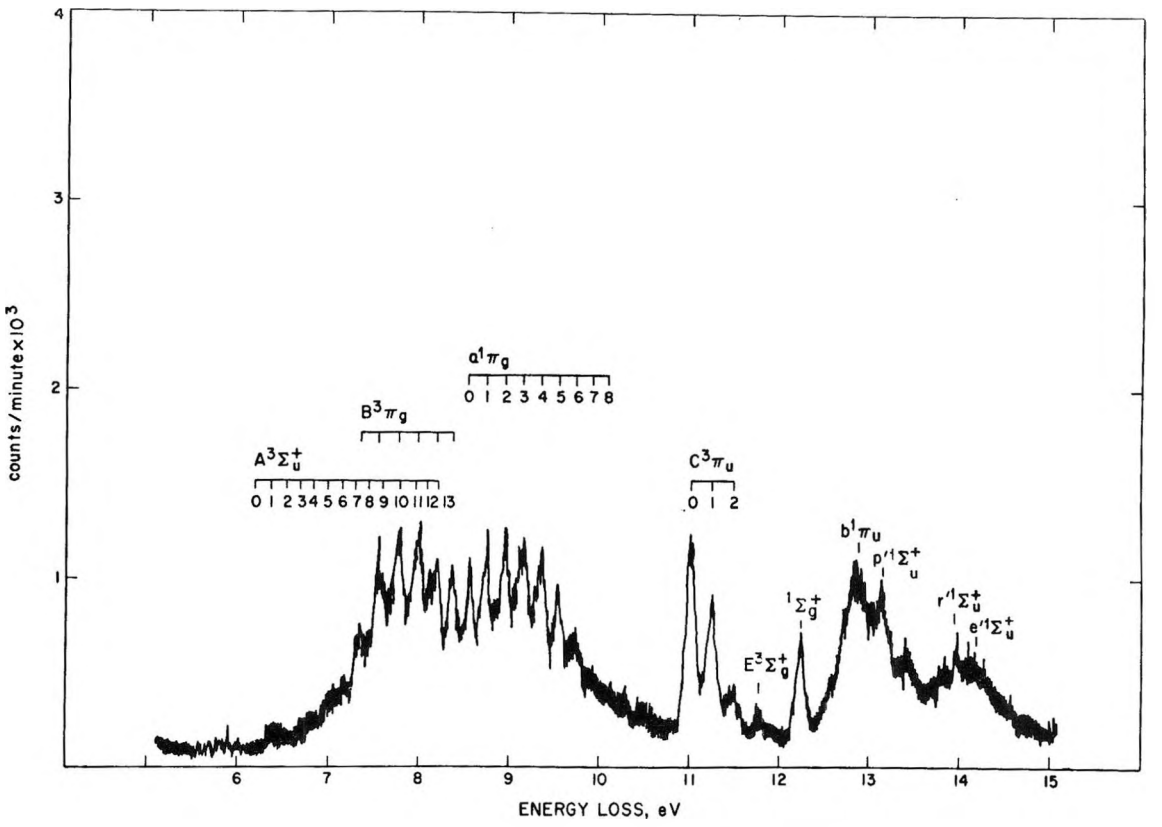

Figure 11. Electron energy-loss spectrum of nitrogen; 40-eV impact energy; 80° scattering angle; 10^{-3} torr pressure; rate meter mode.

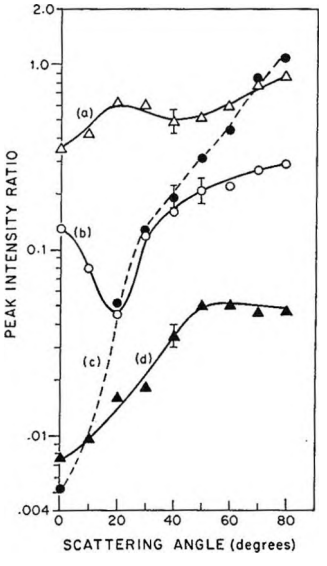

Figure 12. Intensity ratios for several transitions in nitrogen as a function of scattering angle: (a) $p'^1\Sigma_u^+$(peak)/$b^1\Pi_u$ (peak); (b) $^1\Sigma_g^+$ ($v' = 0$)/$b^1\Pi_u$; (c) $C^3\Pi_u$ ($v' = 0 + 1 + 2$)/$b^1\Pi_u$; (d) $E^3\Sigma_g^+$ ($v' = 0$)/$b^1\Pi_u$; 35-eV impact energy.

port of this assignment the intensity ratio has a behavior which resembles that of the 2^1S transition in helium. The $C^3\Pi_u$ transition is spin-forbidden and the corresponding intensity ratio changes by about two orders of magnitude between $\theta = 0°$ and $\theta = 80°$, in analogy to the $2^3P/2^1P$ ratio in helium. Finally, the $E^3\Sigma_g^+$ transition at 11.87 eV is both symmetry- ($g \rightarrow g$) and spin-forbidden and has a behavior somewhat analogous to the 2^3S transition in helium. Čermák[28] and Lassettre[29] have argued that this state is most likely a $^1\Sigma_g^+$ rather than a $^3\Sigma_g^+$ state, whereas Heideman, *et al.*,[30] argued in favor of the $^3\Sigma_g^+$ assignment. We see from Figure 12 that the state we have labeled as $E^3\Sigma_g^+$, in agreement with Heidemann,[30] has an angular distribution very different from that of the $^1\Sigma_g^+$ state, and quite characteristic of a triplet. The reason Čermák[28] observed this state as metastable is probably due to the fact that transitions from it to the $B^3\Pi_g$ state are symmetry- ($g \rightarrow g$) forbidden and those to the $A^3\Sigma_u^+$ state involve a double electron jump.[31]

Additional evidence to support the $E^3\Sigma_g^+$ state assignment can be obtained by comparing the N_2 cross section ratios with those of the isoelectronic molecule CO for which the states observed by electron impact below 12-eV energy loss are well known.[32] We have been able to observe transitions clearly from the $X^1\Sigma^+$ ($v = 0$) ground state to the optically allowed

(28) V. Čermák, *J. Chem. Phys.*, **44**, 1318 (1966).

(29) V. D. Meyer and E. N. Lassettre, *ibid.*, **44**, 2535 (1966).

(30) H. G. M. Heideman, C. E. Kuyatt, and G. E. Chamberlain, *ibid.*, **44**, 355 (1966).

(31) R. S. Mulliken, "The Threshold of Space," Pergamon Press, Inc., New York, N. Y., 1957, p 169.

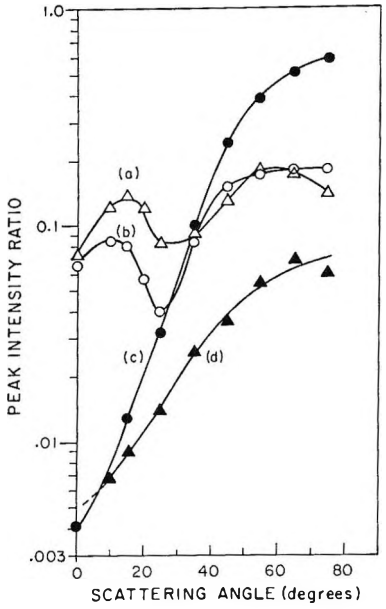

Figure 13. Intensity ratios for several transitions in carbon monoxide as a function of scattering angle: (a) $C^1\Sigma^+$ ($v' = 0$)/$A^1\Pi$ ($v' = 0 + 1 + 2$); (b) $B^1\Sigma^+$ ($v' = 0$)/$A^1\Pi$; (c) $a^3\Pi$ ($v' = 0 + 1 + 2$)/$A^1\Pi$; (d) $b^3\Sigma^+$ ($v' = 0$)/$A^1\Pi$; 25-eV impact energy.

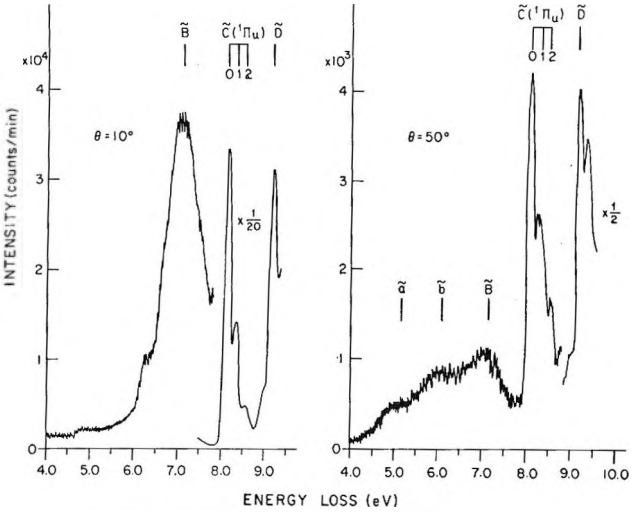

Figure 14. Electron energy-loss spectra of acetylene at scattering angles of 10 and 50°; 25-eV impact energy; 3×10^{-3} torr; 10^{-8} A incident beam current; rate meter mode.

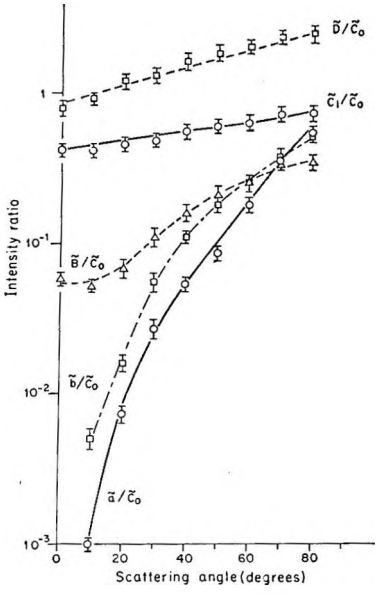

Figure 15. Peak intensity ratios for several transitions in acetylene as a function of scattering angle. $\tilde{C}_1$ is the $v' = 1$ vibrational level of the $\tilde{C}(^1\Pi_u)$ state and $\tilde{C}_0$ is the $v' = 0$ level; same conditions as Figure 14.

$A^1\Pi$ ($v' = 0$ through 6), $B^1\Sigma^+$ ($v' = 0, 1$), and $C^1\Sigma^+$ ($v' = 0$) states as well as to the spin-forbidden $a^3\Pi$ ($v' = 0$ through 4) and $b^3\Sigma^+$ ones. In Figure 13, intensity ratios of the differential excitation cross sections for these states with respect to that of the $A^1\Pi$ state are presented. These curves are remarkably similar in shape to the corresponding ones for nitrogen. The $a^3\Pi/A^1\Pi$ ratio behaves in a manner similar to its counterpart in N_2, $C^3\Pi_u/b^1\Pi_u$. The $B^1\Sigma^+/A^1\Pi$ and $C^1\Sigma^+/A^1\Pi$ ratios behave in a way that is intermediate between the $p'^1\Sigma_u^+/b^1\Pi_u$ (optically allowed) and $^1\Sigma_g^+/b^1\Pi_u$ (symmetry-forbidden) of N_2, showing minima near 20–30°. Finally, the $b^3\Sigma^+/A^1\Pi$ ratio bears a striking resemblance to the corresponding $E^3\Sigma_g^+/b^1\Pi_u$ one. The obvious similarity in shape between the corresponding carbon monoxide and nitrogen relative angular distributions provides a further justification for the assignment of the 11.87-eV transition in nitrogen to $E^3\Sigma_g^+$.

A detailed analysis of the peak intensities for the $v' = 0$ through 6 vibrational levels of the $A^1\Pi$ state and the $v' = 0$ through 4 levels of the $a^3\Pi$ state at $E_0 = 25$ and 35 eV shows that the relative intensities of these transitions (within a given electronic band) are independent of scattering angle and impact energy within experimental accuracy. This observation is consistent with the prediction that transitions caused by electron impact at these energies should be vertical and that Franck–Condon overlap integrals might determine these relative intensities.

More details about the spectra of these two molecules and their differential scattering cross sections will be published elsewhere.[26]

Acetylene.[33] Research grade acetylene was used without further purification. Figure 14 gives electron energy-loss spectra for this molecule at $E_0 = 25$ eV and $\theta = 10$ and 50°. Transitions from the $\tilde{X}^1\Sigma_g^+$ ground

(32) (a) V. D. Meyer, A. Skerbele, and E. N. Lassettre, *J. Chem. Phys.*, **43**, 805 (1965); (b) A. Skerbele, V. D. Meyer, and E. N. Lassettre, *ibid.*, **44**, 4069 (1966); (c) A. Skerbele, M. Dillon, and E. N. Lassettre, *ibid.*, **46**, 4162 (1967).

(33) S. Trajmar, J. K. Rice, P. S. P. Wei, and A. Kuppermann, *Chem. Phys. Lett.*, **1**, 703 (1968).

state to two low-lying states with maximum intensities at 5.2 eV ($\tilde{a}$) and 6.1 eV ($\tilde{b}$) are clearly seen, together with the spin-allowed transitions labeled $\tilde{B}$, $\tilde{C}(^1\Pi_u)$, and $\tilde{D}$.[34] The last two are Rydberg states, whereas $\tilde{B}$ is a complex series of diffuse bands that have not yet been analyzed.[35]

Figure 15 shows the intensity ratios for transitions to the $\tilde{a}$, $\tilde{b}$, $\tilde{B}$, $\tilde{D}$, and $\tilde{C}$ ($v' = 1$) states relative to the intensity of the transition to the $\tilde{C}$ ($v = 0$) state. The behavior of the $\tilde{a}$ and $\tilde{b}$ intensity ratios is characteristic exclusively of singlet → triplet transitions.

The uv absorption spectrum of acetylene begins at 5.23 eV with a weak absorption peaking at about 6 eV. Ingold and King[36] have shown that the upper state has A_u symmetry (*trans*-bent). Its singlet nature is suggested by the absence of Zeeman splitting.[37] The weakness of the absorption is due to the unfavorable Franck–Condon overlap between the linear ground-state configuration and the nonlinear excited-state one. Such Franck–Condon factor considerations seem to be valid for electron impact. Therefore, this transition is expected to be weaker at these low impact energies than the overlapping triplets, especially at large scattering angles.

Although there is evidently insufficient spin–orbit coupling to reveal the $\tilde{a}$ and $\tilde{b}$ triplet states by optical means, low-energy electron impact excitation, by means of electron exchange, is quite effective in causing transitions to these states.

Conclusions

These results have clearly indicated the usefulness of collecting energy-loss spectra over a wide range of angles for the detection and identification of triplet states in atoms and molecules. Although we have studied only a limited number of systems, an apparently general rule, compatible with our qualitative theoretical interpretation of electron-exchange phenomena, has emerged.

(1) Differential scattering cross sections for symmetry-allowed but spin-forbidden transitions relative to those for optically allowed ones increase by about two orders of magnitude with increasing scattering angle from 0 to 80° for impact energies within a few tens of electron volts of the excitation threshold. Two additional empirical "rules" whose explanation on theoretical grounds is yet to be formulated can also be given.

(2) Differential scattering cross sections for spin-allowed but symmetry-forbidden transitions relative to those of optically allowed ones seem to decrease with increasing angle, reach a minimum, and then increase under the same conditions as (1).

(3) Differential cross sections for transitions which are both spin- and symmetry-forbidden, relative to those of optically allowed ones, increase with increasing angle by approximately one order of magnitude under the same conditions as (1).

It is evident that further studies are needed, both experimental and theoretical, to characterize better these complex scattering processes.

(34) State assignments in C_2H_2 are from: G. Herzberg, "Electronic Spectra of Polyatomic Molecules," D. Van Nostrand Co., Inc., Princeton, N. J., 1966, p 611.

(35) T. Nakayama and K. Watanabe, *J. Chem. Phys.*, **40**, 558 (1964).

(36) C. K. Ingold and G. W. King, *J. Chem. Soc.*, 2702 (1953).

(37) A. E. Douglas, unpublished; see ref 34, p 517.

Gas-Phase Photolysis of Cyclohexane in the Photoionization Region[1]

by P. Ausloos, R. E. Rebbert, and S. G. Lias

National Bureau of Standards, Washington, D. C. 20234 *(Received May 7, 1968)*

The photolysis of cyclohexane (IP = 9.88 eV) has been studied in the gas phase using 1470-Å (8.4 eV), 1236-Å (10.03 eV), and 1067–1048-Å (11.6–11.8 eV) radiation. At the latter two wavelengths, ions and superexcited molecules are formed. Emphasis is placed on the measurement of accurate quantum yields at all three wavelengths through both chemical actinometry and saturation current measurements. The primary decomposition of the excited cyclohexane molecule, c-$C_6H_{12}^* \rightarrow C_6H_{10} + H_2$, reported earlier for the photolyses at 8.4 and 10.03 eV, is also seen to occur at 11.6–11.8 eV. In addition, evidence is presented for ring opening and rearrangement of the excited hexamethylene intermediate, followed by decomposition to form alkyl radicals. At 1470 Å, secondary decompositions of excited intermediates are readily quenched by an increase in pressure, the quenching being more effective for deuterated than for nondeuterated species. On the other hand, little or no pressure effect on product formation is observed in the photolysis at 1067–1048 Å. In the photolysis at 1067–1048 Å, the parent cyclohexane ions have sufficient energy to undergo fragmentation processes, but it is demonstrated that fragmentation is negligible at pressures above 1 torr. Using the photoionization results, it is also demonstrated that in the radiolysis, the ion pair yield of the cyclohexane parent ion is 0.3 at 13 torr and 0.34 at 90 torr. Assuming that the fragmentation of the excited cyclohexane molecule observed in the photolysis at 11.6–11.8 eV is roughly representative of the superexcited molecule dissociation which occurs in the radiolysis, the 1067–1048-Å photolysis product yields are used to derive a value for the ratio of neutral excited molecules to ion pairs formed in the radiolysis. This ratio is 0.1–0.3.

Introduction

The photolysis of cyclohexane has previously been investigated using 1470- and 1236-Å radiation in the gas[2,3] and liquid[4] phases. The 1236-Å (10.03 eV) radiation is only slightly higher in energy than the ionization energy of cyclohexane (9.88 eV);[5] at this energy, only 4.6% of the photons produce ions in gaseous c-C_6H_{12}. Therefore, the extension in this study to photolysis at higher energies (11.6–11.8 eV), where, as will be shown later, 50% of the photons produce ions, enables us to trace the ionic mechanism and to follow the fate of the parent ions more easily. Furthermore, the extension to these shorter wavelengths permits a derivation of the modes of decomposition of neutral cyclohexane molecules excited to states 1.7–1.9 eV above their ionization energy.

Needless to say, information gained from such studies can make a major contribution to our understanding of radiolysis systems. The mean energy of the superexcited[6] molecules formed in the radiolysis of cyclohexane, for example, is probably close to that of the excited molecules formed in the 11.6–11.8-eV photolysis, so knowledge of the modes of decomposition of the molecules excited in the photolytic system can be a useful interpretive aid for a radiolysis study. The major advantage of studying such phenomena in a photolytic system, however, is that the exact number of parent ions and neutral excited molecules can be derived from measured saturation ion currents and the photon flux; this means that the probabilities for the occurrence of the primary activation processes (excitation and ionization) can be exactly determined. In the radiolysis, one of the major interpretive difficulties[7] is that the role of neutral excited molecules cannot be determined on the basis of such measurements.

In the present study, emphasis is placed on the photolysis experiments carried out at photon energies above the ionization energy of cyclohexane. However, whenever appropriate, the photolytic results will be used to derive information from radiolytic observations on cyclohexane.

A special effort has been made in the course of this work to obtain accurate quantum yields, which are based on direct measurements of saturation ion currents in the course of the experiment rather than on *ex post facto* chemical actinometry.

Experimental Section

(*a*) *Irradiation and Actinometry.* The design and general operating procedure of the rare gas resonance lamps have been described previously.[8] The krypton

(1) This research was supported by the U. S. Atomic Energy Commission.

(2) R. D. Doepker and P. Ausloos, *J. Chem. Phys.*, **42**, 3746 (1965).

(3) R. R. Hentz and S. J. Rzad, *J. Phys. Chem.*, **71**, 4096 (1967).

(4) (a) R. A. Holroyd, J. Y. Yang, and F. M. Servedio, *J. Chem. Phys.*, **46**, 4540 (1967); (b) J. Y. Yang, F. M. Servedio, and R. A. Holroyd, *ibid.*, in press.

(5) K. Watanabe, T. Nakayama, and J. Mottl, *J. Quant. Spectrosc. Radiat. Transfer*, **2**, 369 (1962).

(6) The term "superexcited" state of a molecule was introduced by R. L. Platzman [*Radiat. Res.*, **17**, 419 (1962)] to indicate a molecule whose energy content is larger than the energy required for ionization.

(7) P. Ausloos and S. G. Lias, "Actions Chimiques et Biologiques des Radiations," Vol. 11, M. Haissinsky, Ed., Masson and Co., Paris, 1967, p 1.

resonance lamp was provided with a CaF_2 window in order to eliminate the 1165-Å line. The argon resonance lamp was fitted with a 0.3 mm thick LiF window, which transmits both 1048- and 1067-Å radiation. Because of the formation of F centers, the window had to be bleached after several hours of exposure to radiation from the discharge. None of the lamps needed cooling and no impurity lines could be detected; that is, total emission from impurities was less than 0.1% of the intensity of the rare gas resonance lines.

The lamps were fitted into a two-compartment cell.[9] The second compartment, which was filled with 5 torr of $(CH_3)_2NH$ or NO, received light from the first one through an LiF window. Both compartments were provided with parallel nickel-plated electrodes. By measuring a saturation current in the first compartment when it was filled with NO or $(CH_3)_2NH$ and by comparing the saturation currents in the two compartments, the fraction of the quanta passing through the evacuated first cell and entering the second cell could be established; knowledge of this factor made it possible to base actinometry on currents measured in the second cell. While the relative intensity factor between the cells remained fairly constant with time when 1470- or 1236-Å radiation was used, 1048–1067-Å radiation led to a gradual decrease in the fraction of quanta entering the second cell, because of the creation of F centers in the LiF window between the two compartments.

In order to obtain saturation currents, the intensity of the resonance lamps has to be kept quite low. Therefore, all experiments listed in Tables IV–VI were carried out at intensities in the range 10^{12} to 5×10^{13} photons/sec. Experiments lasted from 1 to 10 hr. The longer irradiation times were employed in experiments carried out at higher pressures. In any experiment, 0.005–0.05% of the starting material was decomposed. At these short conversions the drop in intensity during the course of an experiment due to deposition of polymer material on the window of the lamp was considerably less than noted in an earlier study.[3] The drop in transmission of the window was determined by measuring saturation currents at regular intervals. Typically, photolysis of pure cyclohexane at 1236 Å and a pressure of 20 torr led to a reduction in transmission of 12% by the end of the experiment (0.01% conversion). If a free-radical scavenger such as NO or O_2 was added to the system, the transmission of the window remained unchanged in the course of an experiment, even if the per cent conversion was extended to 0.05%. Similar observations were made at 1048–1067 Å.

Whenever isotopic analysis of products was required, the photolysis was generally carried out to much higher conversions (0.1–0.5%). The experimental procedure used to relate product yields to the number of quanta entering the cell was as follows.

(1) Prior to filling the front compartment with cyclohexane, the intensity of the lamp was adjusted by measuring the saturation current in the second compartment.

(2) The cyclohexane was introduced into the front cell and the value of the saturation current was determined immediately. Several such measurements were made at regular intervals during the course of an experiment. The potential difference between the two electrodes must be applied only long enough to measure the saturation current, since the electrons accelerated in the electric field can cause additional excitation of the sample molecules.

With the xenon resonance lines actinometry based on saturation current measurements is more complicated because only the minor (~2%) 1295.6-Å (9.56 eV) resonance line ionizes NO ($\eta_{NO} = 0.44$) while neither of the two resonance lines ionizes cyclohexane itself. Dimethylamine (IP = 8.24 eV) is ionized by both lines but the quantum yield of ionization is not known. Nevertheless, both NO and $(CH_3)_2NH$ can be used to monitor the intensity of the xenon resonance lamp. Approximate quantum yields can be determined by relating saturation currents in these gases to a chemical actinometer such as N_2O ($\Phi_{N_2} = 1.4$)[10] or ethylene ($\Phi_{C_2H_2} = 1$).[11] This procedure was used in this study with the understanding that the accuracy of any chemical actinometer is not as yet well established.[12]

(3) After irradiation, an aliquot was expanded into an evacuated loop attached to a gas chromatograph. Condensation of bulk material before the quantitative analysis was avoided because it was noted that the measured yield of the 1,3-butadiene product was drastically too low if the sample was condensed.

(4) In case isotopic analysis was required, the remaining irradiated material was condensed at 65°K to remove the hydrogen and methane fractions which were distilled off and measured in a gas buret prior to introduction into a mass spectrometer. The ethylene–ethane fraction was distilled off at 95°K and similarly analyzed by mass spectrometry. Isotopic analysis of higher boiling products was obtained by introducing the remainder of the sample onto a gas chromatograph from whose exit the products were trapped separately

(8) P. Ausloos and S. G. Lias, *Radiat. Res. Rev.*, **1**, 75 (1968).

(9) R. Gorden, R. Doepker, and P. Ausloos, *J. Chem. Phys.*, **44**, 3733 (1966).

(10) (a) M. Zelikoff and L. M. Aschenbrand, *ibid.*, **22**, 1680 (1954); (b) W. E. Groth and H. Schierholtz, *Planetary Space Sci.*, **1**, 333 (1959).

(11) R. Gorden, Jr., and P. Ausloos, to be submitted for publication.

(12) In essentially all studies dealing with chemical actinometry, the quantum yield of a particular product such as N_2 in N_2O or CO in CO_2 is based on another chemical actinometer as reference. Although at present there seems to be good internal agreement between some of these actinometers [see, for instance: J. Y. Yang and F. M. Servedio, *Can. J. Chem.*, **46**, 338 (1968)], there is a need to re-examine the quantum yields of the products formed in the chemical actinometers through actual physical measurements of the photon flux during photolysis.

and subsequently introduced into a high-resolution mass spectrometer.

(*b*) *Materials.* The cyclohexane was a standard sample obtained from the American Petroleum Institute. It contained no impurities which could be detected by gas chromatography. On the other hand, the cyclohexane-d_{12} and cyclohexane-1,1,2,2,3,3-d_6 contained several impurities with boiling points slightly above that of cyclohexane, the major one being methylcyclohexane (~0.1%). Because of the small differences in retention times on the gas chromatographic columns between these compounds and the parent compound, no attempt was made to purify the materials. Although the total percentage of impurities amounted to only 0.3%, their presence effectively prevented analysis of the cyclohexene product in the photolysis experiments carried out at conversions of less than 0.05%. The isotopic purity of the labeled materials has been described before.[2]

Results

(*a*) *Units.* In photoionization experiments, there is a problem of choosing meaningful units in which to express the yields of the product molecules. Obviously, when some quanta go to produce ions, a quantum yield no longer has the same meaning as it has in the subionization region. Upon consideration, it seems that two systems of units are appropriate for expressing yields in photoionization experiments. In discussing products which are formed in a process involving the ions produced in the system, it is useful to express the yields as "molecules, M, of species X formed per ion pair, N_i, produced in the system." Such a designation, $M(X)/N_i$, is essentially identical with the "ion pair yield" unit,[13] M/N, originally used by Lind[14] in early radiolysis studies (where all product formation was related to ionic processes) and currently used in gas-phase radiolysis studies concerned with ionic processes.[7] On the other hand, in expressing the yields of products resulting from nonionic processes, it is more meaningful to use the unit $M(X)/N_{ex}$, *i.e.*, molecules, M, of product X formed per superexcited molecule which does not autoionize or dissociate to form a positive and negative ion. For most gas-phase systems, N_{ex} can more simply be thought of as the excited molecules dissociating into neutral fragments. For photolysis in the subionization region, $M(X)/N_{ex}$ is simply the quantum yield.

Experimentally, an ion-pair yield, $M(X)/N_i$, is readily obtained, since N_i can be directly determined through saturation current measurements during the course of an experiment. $M(X)/N_{ex}$ can be obtained from the relationship

$$\frac{M(X)}{N_i} \times \eta \times \frac{1}{1-\eta} = \Phi \times \frac{1}{1-\eta} = \frac{M(X)}{N_{ex}}$$

where η is the ionization quantum yield and Φ is the over-all quantum yield

$$\Phi = \frac{M(X)}{N_i + N_{ex}}$$

(*b*) *Results Given in Tables I–VI.* The accuracy of the data compiled in the tables cannot be exactly evaluated. The saturation ion currents, on which most of the data are based, could be determined within 2%. Because the lamp output was very stable and practically invariant with time, the computation of the number of ions formed in the course of an experiment was no less accurate than the ion current measurement. When an absorbent gas is present in the cell, the photoelectric effect is negligible. On the other hand, at pressures above 1 torr corrections have to be applied to the saturation ion current measurements.[9]

Table I: Photoionization Quantum Yields

	1236 Å	1048–1067 Å
c-C_6H_{12}	0.045	0.49
c-C_6D_{12}	0.029	0.50
NO[a]	0.77	0.71[b]

[a] Based on values tabulated by K. Watanabe, F. M. Matsunaga, and H. Sakai, *J. Appl. Opt.*, **6**, 391 (1967). [b] Average value based on the intensities of the two argon resonance lines, taking 0.70 and 0.73 as the ionization quantum yields of NO at 1067 and 1048 Å, respectively.

The photoionization quantum yields given in Table I are as essentially accurate as the published values (referred to in the table) for the ionization quantum yield of NO.

The accuracy of the M/N_{ex} and M/N_i values given in the other tables depends mainly on the analytical procedure. The reproducibility is rather satisfactory. Ten photolysis experiments performed at a pressure of 5 torr and a wavelength of 1236 Å gave a value for $M(C_2H_4)/N_{ex}$ of 0.75 ± 0.03. These experiments were carried out at various intervals in the course of this investigation using intensities which ranged from 5×10^{12} to 5×10^{13} quanta/sec.

In Table II we present the per cent distributions of the hydrogen and ethylene fractions formed in the photolysis and radiolysis of c-C_6H_{12}–c-C_6D_{12}–NO mixtures. Statistical corrections have been made for the presence of 8.7% $C_6D_{11}H$ in the cyclohexane-d_{12}. 1,3-Butadiene in these experiments consisted of C_4D_6 and C_4H_6 at all

(13) We prefer to attach the subscript i to the symbol N (*e.g.*, M/N_i) in order to differentiate clearly between the number of molecules per *ion* pair (N_i) and the number of molecules per neutral excited molecule (N_{ex}). The symbol N_+ has also been used to designate the number of positive ions. For most purposes this is equivalent to N_i, but N_i is, of course, more general.

(14) S. C. Lind, "The Chemical Effects of Alpha Particles and Electrons," Reinhold Publishing Corp., New York, N. Y., 1928

Table II: Formation of Hydrogen and Ethylene

λ, Å	Pressure, torr	% distributions							
		D_2	HD	H_2	C_2D_4	C_2D_3H	$C_2D_2H_2$	C_2DH_3	C_2H_4
				c-C_6D_{12}–c-C_6H_{12}–NO					
1470	5.2	37.9	6.7	55.4	35.1				64.9
	61	39.4	6.1	54.4	25.8				74.2
1236	20.0	35.4	7.8	56.7	48.2				51.8
1067–1048	20.1	27.5	12.3	60.1	49.3				50.7
Radiolysis	20.0	25.3	29.7	45.0	46.8	1.2		1.5	50.5
				c-$C_6D_6H_6$–NO					
1470	20.0	18.9	12.2	68.8	41.0	5.6	28.7	4.7	20.0
1236	20.0	18.4	16.3	65.3	36.8	5.5	30.6	3.1	23.9
1067–1048	20.0	16.9	16.6	66.4	32.5	5.2	29.5	5.3	27.5

Table III: Photolysis of c-C_6D_{12}–H_2S

λ, Å	Total pressure, torr	% H_2S	D_2	HD	H_2	CD_4	CD_3H	C_2D_6	C_2D_5H	C_2D_4	C_2D_3H	C_3D_6 + C_3D_5H
			Photolysis; M/N_{ex}									
1470[a]	7.7	5.9	0.82	0.12	0.029	0.00	0.039	0.00	0.016	0.17		0.013
	7.4	9.1	0.82	0.15	0.053	0.00	0.040	0.00	0.018	0.17		0.012
1236	7.4	9.1	0.60	0.31	0.14	0.00	0.22	0.00	0.064	0.79	0.073	0.073
1067–1048	6.7	8.1	0.56	0.50	0.38	0.00	0.25	0.00	0.064	0.92	0.11	0.068
	8.5	16.5	0.54	0.58	0.54	0.00	0.27	0.00	0.056	0.92	0.11	0.062
			Radiolysis; M/N_i									
	58.0	2.0	0.42	0.62	0.14	0.025	0.12	0.015	0.075	0.44		0.11

[a] At 1470 Å, M/N_{ex} values are based on a chemical actinometer.

wavelengths. Partially deuterium-labeled butadienes and cyclohexenes were entirely absent. The isotopic analyses of the hydrogen and ethylene fractions formed in the photolysis of cyclohexane-1,1,2,2,3,3-d_6–NO mixtures are given in the same table. For the latter mixtures only approximate corrections have been made to account for the presence of about 10% cyclohexane-d_5. The recorded yields of C_2D_3H and C_2DH_3 may be due to the presence of about 2.5% cyclohexane-d_7 and possibly some cyclohexane-d_4 in the same material.

The yields of the isotopically labeled products formed in the photolysis and radiolysis of cyclohexane-d_{12}–H_2S mixtures (Table III) have also been corrected for the presence of 8.7% $C_6D_{11}H$ in the cyclohexane-d_{12}. The total yield of all hydrocarbon products containing more than one H atom was in all cases less than 2% of the total methane, ethane, or ethylene yield. The propylene formed in these experiments has not been analyzed isotopically. C_3D_7H was also formed in these experiments but its yield was in all experiments only about 10% of that of C_2D_5H. Yields of butadiene are abnormally low in these experiments and strongly dependent on the mole per cent of H_2S, the intensity, and length of stay of the irradiated mixture in the reaction vessel. The cause of the disappearance of butadiene after its apparent formation is not known.

All measured products formed in the photolysis and radiolysis of c-C_6H_{12} in the presence NO and O_2 are given in Table IV. Table V depicts the effect of pressure and isotopic labeling on some of the major products only. Finally, in Table VI the yields of propane and ethylene formed in the photoionization and radiolysis of the c-C_6H_{12}–C_3D_6 mixture are given. It is to be noted that when C_3D_6 is added to c-C_6H_{12} in the presence of a free-radical scavenger, the increment in the propane yield is entirely due to the formation of CD_3CDHCD_2H.

Discussion

A. Photoionization Quantum Yields. At 1236 Å and at 1048–1067 Å the following primary events should be considered

$$c\text{-}C_6H_{12} + h\nu \longrightarrow c\text{-}C_6H_{12}^* \quad (1)$$

$$\longrightarrow [c\text{-}C_6H_{12}^+]^* + e \quad (2)$$

c-$C_6H_{12}^*$ represents a superexcited molecule which can either dissociate

$$c\text{-}C_6H_{12}^* \longrightarrow \text{fragments} \quad (3)$$

or autoionize

$$c\text{-}C_6H_{12}^* \longrightarrow [c\text{-}C_6H_{12}^+]^* + e \quad (4)$$

The quantum yield of photoionization, η, of course, is

Table IV: Photolysis and Radiolysis of Cyclohexane; Product Distributions

λ, Å	Pressure, torr	Scavenger, 5%	CH_4	C_2H_2	C_2H_4	C_2H_6	CH_3CCH_3	C_3H_6	c-C_3H_6	C_4H_6	1,3-C_4H_6	trans-2-C_4H_8	cis-2-C_4H_8	1-C_4H_8	n-C_4H_{10}	c-C_6H_{10}
									Photolysis: M/N_{ex}							
1470	2	O_2	0.013	<0.0005	0.46	<0.0005	<0.0005	0.018	<0.0005	0.001	0.26	<0.0005	<0.0005	<0.0005	0.000	0.35
1236	2	O_2	0.012	0.004	0.84	0.002	0.011	0.065	0.001	0.0016	0.34	<0.0005	<0.0005	<0.0005	0.000	0.25
1067–1048	1	O_2	0.023	0.020	0.94	0.019	0.029	0.063	N.d.	0.024	0.33	~0.010	~0.005	<0.0005	0.012	0.21
	38	O_2	0.22	0.024	0.98	0.038	0.024	0.066	N.d.	0.029	0.28	<0.001	<0.001	<0.0005	<0.005	N.d.
	1	NO	0.016	0.026	0.92	0.006	0.029	0.057	0.014	0.007	0.33	0.032	~0.020	<0.0005	0.012	0.20
	20	NO	0.018	0.025	0.90	0.002	0.027	0.066	N.d.	0.005	0.33	<0.001	<0.001	<0.0005	<0.005	N.d.
									Radiolysis: M/N_i							
γ	20	O_2	0.012	0.059	0.42	0.017	0.014	0.13	0.0026	0.046	0.032	0.018	0.015	0.008	0.034	N.d.
	20	NO	0.012	0.049	0.41	0.015	0.012	0.12	0.0018	0.045	0.029	0.049	0.041	0.010	0.032	0.076

equivalent to the sum of the quantum yields of the ions formed by processes 1 and 4. Ion-pair formation which plays a minor role in the photoionization of n-alkanes[15] does not have to be considered as evidenced by the negligible yield of the $C_6H_{11}^+$ ion observed at photon energies up to 11.6 eV.[16]

It is generally seen that the ionization efficiency is somewhat greater for a deuterated species than for its nondeuterated analog.[17] Jesse and Platzman[18] have interpreted such isotope effects in terms of competition between fragmentation of the superexcited molecule (process 3) and autoionization (process 4). Because the rate of process 3 is probably some function of the reciprocal of the reduced mass, deuteration would tend to favor the autoionization process in any such competition, and hence a deuterated species might, according to this model, be expected to have a greater photoionization quantum yield.

The results given in Table I show that there is an inversion of the isotope effect on the photoionization quantum yield (ionization efficiency) of cyclohexane when the incident wavelength is lowered from 1048–1067 Å to 1236 Å. The higher than unity value observed for $\eta_{C_6H_{12}}/\eta_{C_6D_{12}}$ at 1236 Å is probably related to the fact that the incident wavelength 1236 Å (10.03 eV) is very close to the ionization potential of c-C_6H_{12} (IP = 9.88 eV). The ionization potential of a deuterated hydrocarbon is slightly higher than that of the perprotonated analog[19] and thus at 10 eV the irradiating energy must be very close to the onset of ionization for c-C_6D_{12}, while the formation of c-$C_6H_{12}^+$ has a wider energy margin here. Such a reversal of the isotope effect at energies near the onset of ionization has also been observed for ethane.[8] As indicated by the reversal of the isotope effect, a simple interpretation in terms of competition between processes 3 and 4 is not tenable in this energy range.

B. Fragmentation of c-C_6H_{12} and c-C_6D_{12}*.* In a previous study from this laboratory,[2] it has been shown that at 1470 and 1236 Å the major primary mode of decomposition of cyclohexane is the elimination of a hydrogen molecule

$$c\text{-}C_6H_{12}^* \longrightarrow C_6H_{10}\dagger + H_2 \qquad (5)$$

The internally excited[20] $C_6H_{10}\dagger$ species can either dissociate

(15) W. A. Chupka and J. Borkowitz, *J. Chem. Phys.*, **47**, 2921 (1967).

(16) P. Natalis, B. Steiner, and M. G. Inghram, unpublished results.

(17) W. P. Jesse, *J. Chem. Phys.*, **41**, 2060 (1964).

(18) W. P. Jesse and R. L. Platzman, *Nature*, **195**, 790 (1962).

(19) (a) P. G. Wilkinson, *Can. J. Phys.*, **34**, 643 (1956); (b) V. H. Dibeler, M. Krauss, R. M. Reese, and F. N. Harllee, *J. Chem. Phys.*, **42**, 3791 (1965); (c) C. Lifshitz and M. Shapiro, *ibid.*, **45**, 4242 (1966).

(20) In this discussion, an asterisk (*) will be used to denote electronic excitation caused by the absorption of a photon, while the symbol † will be used to indicate any excess internal energy contained in a fragmentation or rearrangement product.

Table V: Photolysis of Cyclohexane; Effect of Pressure and Isotopic Labeling

λ, Å	Pressure, torr	M/N_{ex} Cyclohexane[a]	Ethylene	Propylene	Butadiene	Cyclohexene
1470[b]	1.9	C_6H_{12}	0.46	0.018	0.26	0.35
	5.6	C_6H_{12}	0.34	0.018	0.20	0.41
	5.6	C_6D_{12}	0.25	0.011	0.085	N.d.
	10.0	C_6H_{12}	0.28	0.018	0.15	0.45
		$C_6D_6H_6$	0.18	0.021	0.14	0.50
		C_6D_{12}	0.14	0.0093	0.074	N.d.
	19.9	C_6H_{12}	0.22	0.015	0.12	0.49
1236	2.2	C_6H_{12}	0.82	0.063	0.33	0.20
	5.8	C_6H_{12}	0.75	0.054	0.30	0.23
		C_6D_{12}	0.75	0.055	0.28	0.23
	27.4	C_6H_{12}	0.70	0.056	0.27	0.25
1067–1048	1.9	C_6H_{12}	0.94	0.062	0.30	N.d.
	4.8	C_6H_{12}	0.92	0.057	0.29	0.18
	8.6	C_6H_{12}	0.9	0.056	0.30	N.d.
	8.6	C_6D_{12}	0.90	0.06	N.d.	N.d.

[a] 5% NO added. [b] At 1470 Å, M/N_{ex} values are based on a chemical actinometer.

$$C_6H_{10}\dagger \longrightarrow 1,3\text{-}C_4H_6 + C_2H_4 \qquad (6)$$

or dissipate its excess energy upon collision[2,3]

$$C_6H_{10}\dagger + M \longrightarrow C_6H_{10} + M \qquad (7)$$

The stabilized C_6H_{10} entity seems to consist mainly of cyclohexene. Apparently process 5 followed by process 6 also occurs at 1048–1067 Å, where 1,3-butadiene and cyclohexene are important products, (Table IV) and photolysis of a c-C_6H_{12}–c-C_6D_{12} (1:1) mixture in the presence of NO indicates that a considerable fraction of the hydrogen is formed in a unimolecular elimination process (Table II).

It will be shown later that if NO is present as a charge acceptor[21]

$$C_6H_{12}^+ + NO \longrightarrow C_6H_{12} + NO^+ \qquad (8)$$

then products are formed from the decomposition of superexcited molecules produced in the primary absorption process 1 rather than by neutralization of the $C_6H_{12}\dagger$ ion.

If we tentatively accept that the D_2 product in the photolysis of c-C_6H_{12}–H_2S experiments (Table III) is entirely formed by process 5 about 80, 60, and 55% of the excited c-C_6H_{12} molecules decompose by elimination of D_2 at 1470, 1236, and 1048–1067 Å, respectively. The elimination of D_2 from internally excited intermediates may, however, become more important at higher photon energies as is indicated by the increasing yields of unsaturated hydrocarbons such as acetylene and allene (Table IV). It is of interest that the $M(D_2)/N_{ex}$ yields at 1470 and 1236 Å agree rather well with the H_2 quantum yields of 0.74 and 0.57 reported by Hentz and Rzad at 1470 and 1236–1165 Å.[22] However, because the latter yields were obtained in an unscavenged system, an exact comparison cannot be made.

Table VI: Photoionization and Radiolysis of Cyclohexane–Propylene Mixtures[a]

Total pressure, torr	% propylene	M/N_i Ethylene	Propane
	Photolysis[b]		
1.9	...	0.98	0.00
1.8	5%	0.98	1.02
4.8	7%	0.96	1.04
9.0	1%	0.98	0.95
8.6	2%	0.92	1.02
9.0	5%	0.92	1.10
	Radiolysis		
13.0	...	0.43	0.04
13.0	5%	0.43	0.34
90.0	5%	0.42	0.38

[a] 5% O_2 was present in every experiment. [b] Wavelength, 1048–1067 Å; intensity, 10^{13} quanta/sec.

An isotopic analysis of the hydrogen formed in the photolysis of a cyclohexane-1,1,2,2,3,3-d_6–NO mixture confirms the conclusion reached in an earlier study[2] that the elimination of a hydrogen molecule from a single carbon atom does occur. Specifically, it is seen that the yields of H_2 and D_2 are both higher than that of HD at 1236 and 1470 Å. If hydrogen were removed from adjacent carbon atoms, then we would expect yield ratios such that: $H_2 > HD > D_2$, assuming the usual isotope effects were operative. Apparently at 1048–1067 Å, elimination of hydrogen from a single carbon atom also occurs but one cannot determine the probability of such a process in view of the larger contribu-

(21) P. Ausloos and S. G. Lias, *J. Chem. Phys.*, **43**, 127 (1965).

(22) Because at 1236–1165 Å the photoionization quantum yield of c-C_6H_{12} is ~0.1, a quantum yield of 0.54 reported in ref 3 corresponds to an M/N_{ex} value of 0.6.

tion of H (or D) atom reactions to the total hydrogen yield, as is indicated by the relatively large HD yield in the 1048–1067-Å photolysis of c-C_6H_{12}–c-C_6D_{12} mixtures. A larger percentage of NO or a more effective hydrogen atom scavenger would be needed to establish more clearly the detachment of a hydrogen molecule from a single carbon atom at 1048–1067 Å.

In view of the fact that especially at shorter wavelengths the M/N_{ex} values of D_2 in the c-C_6D_{12}–H_2S experiments are considerably less than unity (Table III), it follows that primary processes other than (5) must be considered. One of the plausible processes suggested earlier[2] was the elimination of an ethylene molecule

$$C_6H_{12}^* \longrightarrow CH_2CH_2CH_2CH_2\dagger + C_2H_4 \qquad (9)$$

followed by

$$CH_2CH_2CH_2CH_2\dagger \longrightarrow 2C_2H_4 \qquad (10)$$

The above sequence was suggested to account for the observation that the yield of C_2H_4 was larger than that of 1,3-C_4H_6. Although processes 9 and 10 may indeed occur, the presence of CD_3H and C_2D_5H in the photolysis of c-C_6D_{12}–H_2S mixtures requires the inclusion of other processes which may perhaps contribute to the relatively high M/N_{ex} values of ethylene at 1470, 1236, and 1048–1067 Å. It is of interest that the formation of methyl radicals was noted in earlier studies of the photolysis of cyclopropane,[23] cyclobutane,[24] and cyclopentane[25] as well as of cyclohexane[2] at 1470 and 1236 Å, although in the latter case no quantum yields were obtained. The most reasonable mode of formation of alkyl radicals can be written as

$$c\text{-}C_6H_{12}^* \longrightarrow CH_2CH_2CH_2CH_2CH_2CH_2\dagger \qquad (11)$$

$$CH_2CH_2CH_2CH_2CH_2CH_2\dagger \longrightarrow CH_3CH_2CH_2CH_2CH{=}CH_2\dagger \qquad (12)$$

$$CH_3CH_2CH_2CH_2CH{=}CH_2\dagger \longrightarrow CH_3 + CH_2CH_2CH_2CHCH_2 \qquad (13)$$

$$CH_3CH_2CH_2CH_2CH{=}CH_2\dagger \longrightarrow CH_3CH_2 + CH_2CHCH_2CH_2 \qquad (14)$$

The observation of 1-pentene in the solid-phase photolysis of cyclopentane[25] indicates the plausibility of such a sequence of events. Decomposition of the hexamethylene radicals through a reaction analogous to (9) probably competes with rearrangement to the excited 1-hexene intermediate (process 12). It may be expected that the higher the energy the more prevalent fragmentation of the diradical will be.

Process 9 would represent only one mode of decomposition of the hexamethylene diradical formed in process 11. The formation of propylene could be pictured in the same framework

$$CH_2CH_2CH_2CH_2CH_2CH_2\dagger \longrightarrow \dot{C}H_2CH_2\dot{C}H_2 + \dot{C}H_2CH_2\dot{C}H_2 \qquad (15)$$

$$\dot{C}H_2CH_2\dot{C}H_2 \longrightarrow CH_3CHCH_2 \qquad (16)$$

$$\longrightarrow \Delta \qquad (17)$$

It is of interest that cyclopropane is a minor product in the photolysis of cyclohexane just as it is in the gas- and solid-phase photolyses of cyclopentane. While the trimethylene species may be expected to form stable C_3H_6 products, the tetramethylene if formed in process 9 would rapidly decompose into two stable ethylene molecules (process 10). Decomposition of the tetramethylene diradical is exothermic[26] by 37 kcal (E_{act} = 4 kcal) while decomposition of trimethylene into CH_2 and C_2H_4 or C_3H_5 and H is endothermic by about 35 and 25 kcal, respectively. Decomposition of tetramethylene was questionned by Hentz and Rzad[3] on the basis of material balance considerations. However, certain discrepancies between product yields in that study and this one, as well as the omission by Hentz and Rzad of the primary process leading to propylene, methyl radicals, and allyl radicals, require a reconsideration of the argument put forward by these authors.

The fate of the C_4H_7 and C_5H_9 radicals formed in the unimolecular fragmentations (14) and (13) cannot be clearly established. Loss of a C_2H_4 from C_4H_7 or C_5H_9 to form a vinyl or allyl radical, respectively, is a likely reaction. The formation of vinyl radicals is indicated in the H_2S additive experiments (Table III) as has been noted before.

The c-C_6D_{12}–H_2S experiments indicate that HD is formed in low yields at 1470 Å, but $M(HD)/N_{ex}$ increases sharply at shorter wavelengths. If we assume[27] that most of the HD is formed by the abstraction reaction

$$D + H_2S \longrightarrow HD + HS \qquad (18)$$

then

$$M(HD)/N_{ex} = M(D)/N_{ex} \qquad (19)$$

The formation of some HD by a mechanism such as

$$H_2S^* \longrightarrow H\dagger + HS \qquad (20)$$

$$H\dagger + c\text{-}C_6D_{12} \longrightarrow HD + C_6D_{11} \qquad (21)$$

(where H† is an excited H atom) cannot be excluded. However, the fact that an increase in the H_2S percentage by a factor of 2 increases $M(HD)/N_{ex}$ by only about 20% indicates that reaction 21 is not of major importance. The increased importance of H (or D) atom

(23) A. A. Scala and P. Ausloos, *J. Chem. Phys.*, in press.

(24) R. D. Doepker and P. Ausloos, *ibid.*, **43**, 3814 (1965).

(25) R. D. Doepker, S. G. Lias, and P. Ausloos, *ibid.*, **46**, 4340 (1967).

(26) S. Benson, *ibid.*, **34**, 521 (1961).

(27) P. Ausloos and S. G. Lias, *ibid.*, **44**, 521 (1966).

formation at shorter wavelengths is, of course, also indicated by the isotopic composition of the hydrogen in the c-C_6H_{12}–c-C_6D_{12}–NO experiments.

It seems rather pointless at the present time to speculate as to the modes of formation of the hydrogen atoms. Detachments from C_6H_{12}* before or after ring opening and from any of the internally excited C_2–C_5 fragments have to be considered as definite possibilities.

The polymerization which was originally observed by Hentz and Rzad[3] in the photolysis of cyclohexane and which is confirmed in the present study by the reduction in the saturation current when pure cyclohexane is photolyzed (see Results) can be due to reaction of any of the reactive radicals formed by the fragmentation processes described above. The fact that oxygen or nitric oxide effectively prevents polymer formation (see Results) indicates, however, that the radical (or radicals) which contribute(s) to polymer formation is (are) intercepted by the free-radical scavengers used in this study. Prevention of polymer formation by oxygen has also been recently noted in the vacuum ultraviolet photolysis[23] and in the mercury-sensitized photolysis[28] of cyclopropane, where polymer formation was ascribed to reaction of radicals with the propylene product. Secondary reaction of radicals with product molecules may also be responsible for polymer formation at the window of the resonance lamp. The fact that polymer formation is more pronounced at shorter wavelengths may be related to a higher yield of free radicals produced at these energies.

If we accept the results obtained by chemical actinometry, $M(C_2H_4 + C_3H_6 + C_6H_{12})/N_{ex}$ is less than unity at 1470 Å. This seems to confirm the suggestion[3] that certain reactive carbon-containing species remain unaccounted for. It should, however, be pointed out that no attempt was made to analyze C_6 products other than cyclohexene. The formation of other isomers of C_6H_{10}, of cyclohexadiene, and stable C_6H_{11} radicals may conceivably bring the total carbon product yield up to unity. On the other hand, at 1236 and 1048–1067 Å, C_2H_2, C_2H_4, C_3H_4, C_3H_6, C_4H_6, and c-C_6H_{10} as well as the radicals evidenced by the H_2S experiments can be made to fit into a fragmentation mechanism such as the one proposed in this discussion.

Effect of Pressure. In earlier studies, conclusive evidence has been presented for the occurrence of deactivation step 7. In the present investigation, additional information on the deactivation of intermediates formed in the photolysis of cyclohexane can be derived from the results given in Tables II and V. As noted before,[3] the M/N_{ex} values of ethylene and butadiene products formed at 1470 Å decrease rapidly with an increase in pressure. The results given in Table V show, however, that over the pressure range 1.9–19.9 torr, the decrease in $M(C_2H_4)/N_{ex}$ (0.24) is much greater than the decrease in $M(C_3H_6)/N_{ex}$ (0.14). This would indicate that quenching of some other ethylene-forming decomposition besides the dissociation of C_6H_{10}† (process 6) is occurring; deactivation of C_4H_7 or C_5H_9 formed in processes 13 and 14 is a possibility.

The results given in Table V also show that in the 1470-Å photolysis at a given pressure, the M/N_{ex} yields of ethylene, propylene, and butadiene are considerably lower for c-C_6H_{12} than for c-C_6D_{12}. The yields of these products in the photolysis of c-$C_6D_6H_6$ are intermediate between those for the fully deuterated and nondeuterated cyclohexanes. That this effect can be attributed to a more effective quenching of the deuterated intermediate is clearly confirmed by the isotopic analysis of the ethylene formed in the 1470-Å photolysis of the equimolar c-C_6H_{12}–c-C_6H_{12} mixtures (Table II). Here it can be seen that an increase in pressure from 5.2 to 61 torr causes the C_2D_4/C_2H_4 ratio to go from 0.54 to 0.35, while the D_2/H_2 ratio (which mainly reflects the yields of the primary hydrogen-elimination process 5) remains unchanged. These observations are consistent with a longer dissociative lifetime of the deuterated intermediate species.

In strong contrast to the results obtained at 1470 Å are the results obtained in the 1236- and 1067–1048-Å photolyses where there is very little change in the yields of products with increase in pressure (especially at 1067–1048 Å (Table V)), and the C_2H_4/C_2D_4 ratio in the photolysis of c-C_6H_{12}–c-C_6D_{12} mixtures is close to unity (Table II). It is obvious that the smaller pressure effects at these higher energies are related to the higher energy content of the various intermediate species formed in the photolysis of cyclohexane.

As noted in an earlier study,[2] there is a decrease in the importance of intramolecular isotope effects in cyclohexane as the photolyzing energy is increased. This is again demonstrated in Table II by the isotopic distribution of the ethylene product formed in the photolysis of cyclohexane-1,1,2,2,3,3-d_6 at 1470, 1236, and 1067–1048 Å. The pronounced isotope effect favoring the formation of C_2D_4 (and to a lesser extent, $C_2D_2H_2$) seen at 1470 Å is progressively diminished as the photolyzing energy is increased until at 1067–1048 Å the yields of C_2D_4 and $C_2D_2H_2$ are nearly the same as that of C_2H_4.

From the pressure effects observed in this study, one would predict that in the liquid-phase photolysis of cyclohexane at 1470 Å, ethylene, propylene, and butadiene would not be formed. In the liquid-phase photolysis at shorter wavelengths, however, decomposition of excited intermediates to form these products cannot be excluded. Yang, *et al.*,[4b] in studying the photolysis of cyclohexane in the liquid phase, did in fact note yields of ethylene and butadiene at 1236 Å ($\Phi_{C_2H_4}$ = 0.02)

(28) O. P. Strausz, P. J. Kozak, G. N. C. Woodall, A. G. Sherwood, and H. E. Gunning, *Can. J. Chem.*, 46, 1317 (1968).

which, although small, were a factor of 20 higher than those observed at 1470 Å ($\Phi_{C_2H_4} = 0.001$).

C. Fragmentation of the Parent Ion. In the photolysis at 1236 Å (10.03 eV), the parent ions, which are formed by either direct ionization or autoionization, do not possess enough energy to decompose. Only at energies above 11.16 eV can the following fragmentation processes occur[16]

$$[C_6H_{12}^+] \longrightarrow C_2H_4 + C_4H_8^+ \quad (22)$$

$$\longrightarrow CH_3 + C_5H_9^+ \quad (23)$$

A photoionization mass spectrum obtained by Natalis, *et al.*,[16] showed that at 11.25 eV the unimolecular processes 22 and 23 accounted for 4.9 and 2.6% of the total ion abundance, respectively. The parent ion accounted for more than 90% of all ions produced. In the present investigation, photolysis with 11.6–11.8-eV photons would be expected to lead to more fragmentation, *i.e.*, a higher abundance of the $C_4H_8^+$ and $C_5H_9^+$ ions than were observed by Natalis, *et al.* However, at the pressures at which our experiments were carried out, the deactivation step

$$[C_6H_{12}^+]^* + M \longrightarrow C_6H_{12}^+ + M \quad (24)$$

may dissipate any excess energy contained in the parent ion, thus quenching decomposition processes 22 and 23. In the photolysis of cyclopentane[25] at 11.6–11.8 eV, it has been shown that the decomposition process

$$[C_5H_{10}^+]^* \longrightarrow C_2H_4 + C_3H_6^+ \quad (25)$$

can be quenched at pressures above 1 torr.

If process 22 occurs to form the 1-$C_4H_8^+$ ion, we can easily determine the importance of the fragmentation by measuring the butane yield, since the 1-$C_4H_8^+$ ion reacts with *c*-C_6H_{12}[21]

$$1\text{-}C_4H_8^+ + c\text{-}C_6H_{12} \longrightarrow n\text{-}C_4H_{10} + C_6H_{10}^+ \quad (26)$$

to form butane. However, as has been demonstrated before,[21] only 1-$C_4H_8^+$ ions undergo this reaction; 2-$C_4H_8^+$ ions do not. This has recently been confirmed in a mass spectrometric investigation[29] in which the different butene isomer ions were impacted onto cyclohexane. Thus, if a significant fraction of the $C_4H_8^+$ ions formed in process 22 are 2-butene ions, the yield of butane from reaction 26 will not directly give the extent of decomposition process 22. However, since the 2-$C_4H_8^+$ ions are relatively unreactive[29] toward *c*-C_6H_{12}, it is to be expected that the addition of a charge acceptor such as NO to the system will convert 2-$C_4H_8^+$ ions to 2-C_4H_8

$$2\text{-}C_4H_8^+ + NO \longrightarrow 2\text{-}C_4H_8 + NO^+ \quad (27)$$

This is actually confirmed by the radiolysis data given in Table IV which demonstrate that replacement of O_2 by NO raises the yields of the 2-butenes by approximately a factor of 3, while, as expected, the yield of 1-butene shows only a slight increase which is compensated by the small decrease in the yield of *n*-butane. Addition of a charge acceptor such as $(CH_3)_2NH$ to a cyclohexane–oxygen mixture led to similar changes in the yields of the C_4 products.

Returning now to the photoionization results, we see that the yield of *n*-butane at a pressure of 1 torr is quite low ($M(C_4H_{10})/N_i = 0.03$) and at pressures around 20 torr is entirely negligible ($M(C_4H_{10})/N_i < 0.01$) (where the ion-pair yields have been derived from the M/N_{ex} values given in Table IV). Because the yield of 2-butene in the photoionization of C_6H_{12}–NO experiments is also negligible, it follows that the fragmentation of $C_6H_{12}^+$ at these pressures can be ignored.

It is of interest that in the photoionization of cyclopentane[25] at 1048–1067 Å, process 25 occurs with much higher probability in this pressure region, even though the energy needed to ionize cyclopentane is 10.5 eV as compared to 9.88 eV for cyclohexane. Assuming that the activation energy of process 25 is about the same as that of process 22, a shorter dissociative lifetime of the cyclopentane ion must be invoked. This is not unreasonable in view of the greater strain in a five-membered ring structure as compared to a six-membered structure. The lower number of degrees of freedom in *c*-$C_5H_{10}^+$ may also shorten the lifetime of this ion compared to that of the *c*-$C_6H_{12}^+$ ion.

We may not consider the fate of the parent cyclohexane ion formed in the photoionization or radiolysis experiments. It has been shown earlier[21] that propylene reacts with cyclohexane ions by the H_2-transfer reaction

$$c\text{-}C_6H_{12}^+ + C_3H_6 \longrightarrow C_6H_{10}^+ + C_3H_8 \quad (28)$$

The fact that in the radiolysis only small quantities of C_3H_6 are required to intercept all cyclohexane ions indicates that *c*-$C_6H_{12}^+$ is relatively unreactive toward *c*-C_6H_{12}. The results shown in Table VI are in agreement with these earlier results. It is seen that in the photoionization of cyclohexane–C_3H_6 mixtures, $M(C_3H_8)/N_i$ shows little dependence on the percentage of propylene added to the sample.

It follows from the $M(C_3H_8)/N_i$ values given in Table VI that in the photoionization of *c*-C_6H_{12}–C_3H_6 mixtures approximately one propane molecule is formed per *c*-$C_6H_{12}^+$ ion. Because there is no reason to expect a different relationship in the gas-phase radiolysis, it follows from the data given in Table VI that the abundance of stable *c*-$C_6H_{12}^+$ ions in radiolysis is 30% at 13 torr and 34% at 90 torr. Comparison with the value of 0.15 for $M(c\text{-}C_6H_{12}^+)/N_i$ derived from the 70-eV mass spectral cracking pattern of cyclohexane indicates that fragmentation of the *c*-$C_6H_{12}^+$ ion is considerably less extensive in a closed radiolytic system at pressures of 13 torr or higher.

(29) F. P. Abramson and J. H. Futrell, *J. Phys. Chem.*, **71**, 3791 (1967).

Although it is not known what happens to $c\text{-}C_6H_{12}^+$ in the absence of C_3H_6, a few remarks can be made.

The fact that $M(C_3H_4)/N_i$ is the same in the presence or the absence of C_3H_6 indicates that neutralization of $C_6H_{12}^+$ or any other ion does not yield C_2H_4. This is also confirmed by the observation that $M(C_2H_4)/N_i$ is not reduced (Table IV) when a charge acceptor such as NO (IP = 9.25 eV) is replaced by O_2 (IP = 12.07 eV).

Oxygen scavenges radicals but does not readily react with $c\text{-}C_6H_{12}^+$. This is indicated by the observation that an increase of the O_2 concentration in the $c\text{-}C_6H_{12}$–C_3H_6–O_2 mixture from 5 to 25% leaves $M(C_3H_8)/N_i$ unaltered. There are several experimental observations which indicate that neutralization in the oxygen-containing mixtures yields products such as methane and ethane. The fact that those products have especially high yields at high pressures (see Table IV) seems to demonstrate that they are produced when neutralization occurs at the surface of the LiF window. The yields of methane and ethane were found to be independent of the percentage of oxygen added to $c\text{-}C_6H_{12}$ and were strongly reduced upon addition of a charge acceptor such as $(CH_3)_2NH$ (IP = 8.24 eV).

D. Neutral Excited Molecules in the Radiolysis. On the basis of the information which we now have concerning the modes of decomposition of superexcited cyclohexane, it should be possible to arrive at a reasonable estimate of N_{ex}/N_i (number of neutral excited molecules per ion pair formed in the system) in the gas-phase radiolysis of cyclohexane. Although the mean energy transferred to cyclohexane in the gas-phase radiolysis is not exactly known, we know from the optical approximation[30] that the probability for a given transition is proportional to the oscillator strength divided by the energy of the transition. Thus from the inelastic electron-scattering curve for cyclohexane (which essentially represents an excitation spectrum) determined by Lassettre and Francis,[31] we can roughly estimate that the mean energy transferred to cyclohexane in the radiolysis should be only a few electron volts above the energy absorbed in the photolysis at the argon line (11.6–11.8 eV). At any rate, in this energy range there is apparently little effect of energy on the M/N_{ex} values of products resulting from neutral excited molecule decomposition, as a comparison of the yields of products from the krypton (10 eV) photolysis with those of the argon (11.6–11.8 eV) photolysis (Table IV) will demonstrate.

From the mechanism for neutral excited molecule decomposition given above, it can be seen that there are essentially three species which can serve as the basis for the evaluation of N_{ex}/N_i; these are CH_3, C_2H_4, and $1,3\text{-}C_4H_6$.

Let us first estimate N_{ex}/N_i using the yields of ethylene in the cyclohexane–NO radiolysis and in the argon photolysis as a basis. In order to estimate the yield of ethylene resulting from neutral excited molecule decomposition in the radiolysis, we must subtract from the total ethylene yield (which according to the results given in Table II is entirely molecular) the contribution from ionic fragmentation process 22. This contribution, in the experiments containing NO, can be equated to the total yield of the butane (reaction 26) and the yields of the butenes. This leaves according to the results given in Table IV a residual M/N_i yield of ethylene of 0.278. In the argon photolysis, the M/N_{ex} value for ethylene which can be attributed to neutral excited molecule decomposition is about 0.92 (taking the high-pressure experiments with O_2 scavenger). Then the maximum value of N_{ex}/N_i in radiolysis at 20 torr is 0.30.

Making a similar derivation based on the formation of methyl radicals in the neutral excited cyclohexane decomposition, we see from Table III that $M(CH_3)/N_i$ in the radiolysis can be estimated to be about 0.12 (equating the yield of CD_3H in the H_2S additive experiment to the methyl radical yield).

From this we must subtract any methyl radical contributions from ionic processes. Some of the $C_4H_8^+$ ions formed in process 22 will contain sufficient excess energy to decompose further

$$[C_4H_8^+]^* \longrightarrow C_3H_5^+ + CH_3 \qquad (29)$$

Isotopic analysis of the propylene formed in the radiolysis of a scavenged $c\text{-}C_6H_{12}$–$c\text{-}C_6D_{12}$ (1:1) mixture indicates that 50% of the propylene is formed by reaction of the $C_3H_5^+$ ($C_3D_5^+$) ion. From the radiolysis experiments in Table IV, then we can derive an ion-pair yield of 0.055 for process 29. The maximum yield of methyl radicals originating in neutral excited molecule decomposition processes is then about 0.12 − 0.055 = 0.065. In the argon photolysis there is not sufficient energy for process 29 to occur, so we can simply take the $M(CD_3H)/N_{ex}$ value from Table III as being representative of the methyl radical yield resulting from neutral excited molecule decomposition. The value for N_{ex}/N_i which we derive on this basis is then $N_{ex}/N_i = 0.065/0.27 = 0.24$.

Finally, butadiene is probably the one product which can apparently be entirely attributed to the decomposition of neutral excited cyclohexane. From the yields of butadiene in the radiolysis and 1067–1048-Å photolysis given in Table IV, then, we can derive a value of $N_{ex}/N_i \approx 0.1$ in the radiolysis.

The low value for N_{ex}/N_i obtained from the butadiene yields indicates that we may be underestimating the contribution of ionic fragmentation processes to the

(30) For a discussion, see R. L. Platzman, "Proceedings of the Third International Congress of Radiation Research, 1966," G. Silini, Ed., John Wiley & Sons, Inc., New York, N. Y., 1967, p 20.

(31) E. N. Lassettre and S. A. Francis, *J. Chem. Phys.*, **44**, 4633 (1966).

ethylene and methyl radical yields in the radiolysis. For instance, process 23, which may account for an ion-pair yield of CH_3 radicals in the radiolysis as high as 0.045 (according to the 70-eV mass spectrum), has not been considered in the above derivation; if this process is indeed that important in the radiolysis, the value for N_{ex}/N_i derived from the CH_3 radical yields would be lowered to ~0.1.

The Photolysis of Ammonia at 2062 Å in the Presence of Propane

by W. E. Groth, U. Schurath, and R. N. Schindler

Institut für physikalische Chemie, Universität Bonn and Kernforschungsanlage Jülich, Jülich 1, Germany
(Received May 7, 1968)

Ammonia was photolyzed at 2062 Å in the presence of propane as a hydrogen atom scavenger. The only photo process at this wavelength is shown to be $NH_3 + h\nu(2062\ Å) \rightarrow NH_2(^2B_1) + H$ (a). H_2, N_2, N_2H_4, C_3H_6, C_6H_{14}, i-$C_3H_7NH_2$, n-$C_3H_7NH_2$, and small amounts of unidentified amines were produced in the photolyses. All products were determined quantitatively as functions of absorbed irradiation dose. A reaction mechanism is developed on the basis of the observed quantum yields. The ratio of disproportionation to addition reactions between amino and propyl radicals is obtained to be 0.21 ± 0.07.

Introduction

The absorption spectrum of ammonia in the region between 2200 Å and approximately 1660 Å[1] consists of a system of diffuse bands. The strong diffusiveness of the spectrum in this wavelength range is apparently produced by predissociation. Photolysis at 2062 Å, corresponding to an energy of 138 kcal/einstein, should thus lead to the dissociation of ammonia molecules with a quantum yield of unity. On energetic grounds only two primary processes need be discussed

$$NH_3 + h\nu(2062\ Å) \longrightarrow NH_2(^2B_1) + H \qquad 105\ \text{kcal/mol} \quad \text{(a)}$$

$$NH_3 + h\nu(2062\ Å) \longrightarrow NH(^1\Delta) + H_2 \qquad ca.\ 123\ \text{kcal/mol} \quad \text{(b)}$$

According to Herzberg,[2] process b should yield electronically excited $NH(^1\Delta)$ radicals, the excitation energy being in the order of 28 kcal/mol. Process a, however, yields ground-state $NH_2(^2B_1)$ radicals, as can be deduced from a potential diagram derived by Douglas.[3] Energetically, the formation of electronically excited $NH_2(^2A_1)$ radicals would also be possible. The excitation energy is 29.2 kcal/mol.

This investigation confirms that at a wavelength of 2062 Å photodissociation of ammonia proceeds exclusively *via* process a. Using propane as a hydrogen atom scavenger, reactions of $NH_2(^2B_1)$ radicals with propyl radicals and propane were investigated.

Experimental Section

Materials. Ammonia was dried on KNH_2 and degassed before use. Impurities were not detectable. HBr gas was prepared from 48% hydrobromic acid by reaction with P_2O_5. Molecular bromine was removed by repeated distillation over Hg. Phillips Research grade propane was used. The propane contained 3×10^{-3}% ethane and 8×10^{-3}% n-butane. ND_3 contained an unknown impurity which could be effectively removed by preirradiation of the sample before experimental use. SF_6 from the Matheson Co. was used without further purification.

Irradiations. A microwave-powered iodine lamp served as the light source. Argon (0.8 torr) and excess iodine were sealed off in a Pyrex flask with a quartz window. The iodine pressure could be kept constant by an ice-water bath. The lamp emits the iodine atom line at 2062 Å with high intensity. Emission lines at 1876 Å, 1844 Å, and shorter wavelengths were eliminated by insertion of a water-filled quartz cell of 1-cm path length into the light beam.

Photolyses were carried out in cylindrical quartz cells of 10-cm length and 5.5-cm diameter. Cell and lamp front windows were 5 cm apart. Irradiations were performed at ambient temperature. HBr gas

(1) K. Watanabe, *J. Chem. Phys.*, **22**, 1564 (1954).

(2) G. Herzberg, "Spectra of Polyatomic Molecules," D. Van Nostrand Co., Inc., Princeton, N. J., 1966.

(3) A. E. Douglas, *Discussions Faraday Soc.*, **35**, 158 (1963).

at a pressure of 60 torr was used as an actinometer. Light intensities were calculated from the amount of hydrogen evolved, assuming $\phi_{H_2} = 1.00$. In all experiments the ammonia pressure was at least 37.5 torr, providing for total absorption of the incident radiation. The absorption coefficients of HBr and NH_3 are 15 cm^{-1} [4] and 23.8 cm^{-1},[5] respectively. C_3H_8 and SF_6 are transparent at 2062 Å.

Analyses. The yields of the noncondensable gases were determined by pV measurement and subsequent mass spectrometric analysis. Hydrocarbons and amines were analyzed gas chromatographically. Products were identified by retention time. Separation of hydrocarbons was achieved on a temperature-programmed silica gel column. Ammonia and amines were retained quantitatively under working conditions. The amines were separated on chromosorb W, 45/60, treated with 15 wt % KOH and 15 wt % polyglycole 1000. A flame ionization detector was used. Because of its very low sensitivity for ammonia, the amines could be determined in spite of heavy tailing of the ammonia peak. The determination of hydrazine was carried out photometrically in solution.[6]

Results

(*a*) *Photolysis of Pure Ammonia.* Pure ammonia was photolyzed at a pressure of 37.5 torr. The yields of the permanent gases and of hydrazine as functions of quanta absorbed are given in Table I. The ammonia quantum yield was 0.325 after absorption of 3×10^{18} quanta. A pressure dependence has not been investigated. Hydrazine yields are plotted in Figure 1.

Table I: Product Quantum Yields as Functions of Quanta Absorbed in the Photolysis of Pure Ammonia (P_{NH_3} = 37.5 torr)[a]

Quanta absorbed × 10^{-17}	% N_2	ϕ_{N_2}	ϕ_{H_2}	$\phi_{N_2H_4}$
5.58	18.8	0.103	0.443	0.036
12.7	19.7	0.122	0.495	0.034
20.7	22.5	0.143	0.483	
32.4	24.5	0.157	0.485	0.003
103	25	0.163	0.490	0.0005
20.3				0.014
19.5				0.014
5.75				0.023
25.9				0.0066

[a] The hydrazine quantum yields are plotted in Figure 1.

(*b*) *Photolyses of NH_3–C_3H_8 Mixtures. Effect of Propane Pressure.* In a series of runs the quantum yields of permanent gases and of hydrazine were measured. The results are given in Figures 2 and 3. At light intensities of 5.5 to 8.8 × 10^{15} quanta/sec about 2×10^{18} quanta were absorbed per irradiation. The

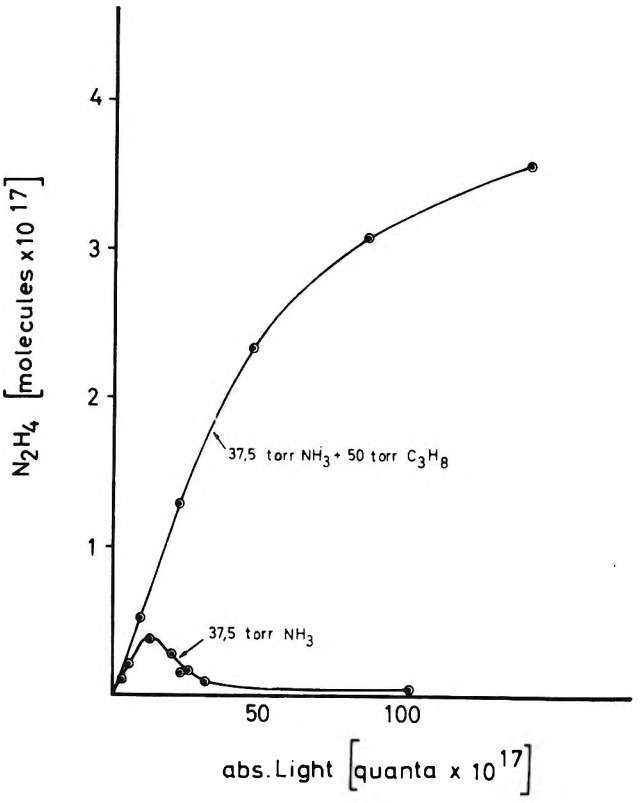

Figure 1. Hydrazine formation in the photolysis of pure ammonia and of ammonia–propane mixtures.

hydrogen yield rises from 0.49 in pure ammonia to 0.90 at a propane pressure of 700 torr. On the other hand, the nitrogen quantum yield is reduced by the addition of propane and reaches a limiting value of $\leq$0.01 at high propane pressures. The hydrazine quantum yield rises from *ca.* 0.01 in pure ammonia to a distinct maximum of 0.068 at 16 torr propane pressure and then falls off again.

To investigate the influence of total pressure on product formation, one irradiation was performed in the presence of 500 torr of SF_6. The results of this run are included in Figures 2 and 3. It is seen that the addition of 500 torr SF_6 does not influence the quantum yields measurably.

Effect of Radiation Dose. The following experiments were carried out at a propane pressure of 50 torr. Gas chromatographic analyses deteriorated when higher propane pressures were used.

Quantum yields of H_2 and N_2 are plotted in Figure 4 as functions of the number of quanta absorbed. Hydrogen quantum yields tend to fall off toward longer irradiation times. The limiting value of ϕ_{H_2} at short irradiation times is about 0.77. The nitrogen quantum

(4) E. Warburg, *Berl. Akad. Ber.*, 300 (1918); R. M. Martin and J. E. Willard, *J. Chem. Phys.*, **40**, 2999 (1964).

(5) P. Harteck, R. R. Reeves, and B. A. Thompson, *Z. Naturforsch.*, **19a**, 2 (1964).

(6) C. W. Watt and D. Chrisp, *Anal. Chem.*, **24**, 2006 (1952).

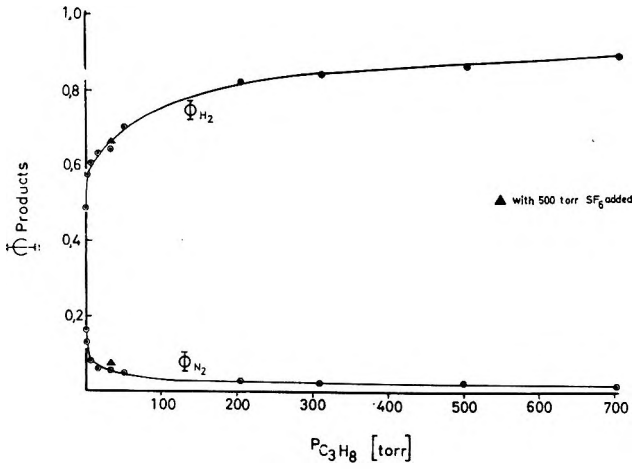

Figure 2. Quantum yields of noncondensable gases as functions of propane pressure. Absorbed dose, 1.5–2.5 × 10^{18} quanta.

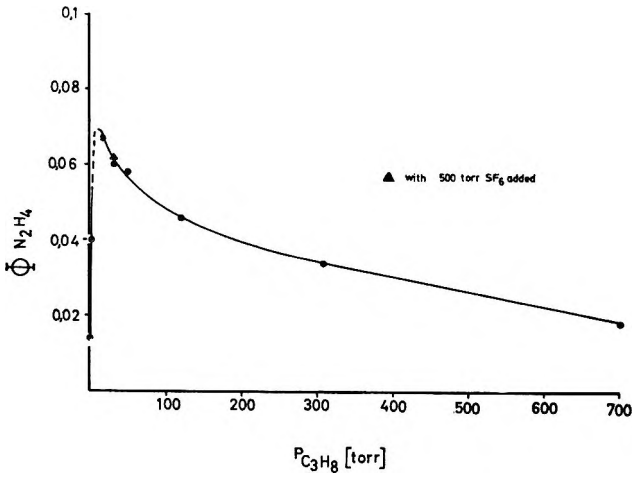

Figure 3. Hydrazine quantum yields as a function of propane pressure. Absorbed dose, 1.5–2.5 × 10^{18} quanta.

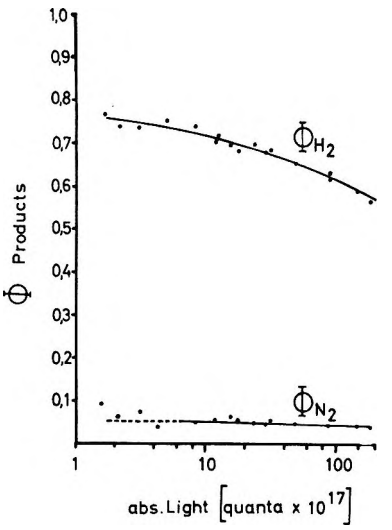

Figure 4. Quantum yields of noncondensable gases as a function of absorbed dose. p_{NH_3} = 37.5 torr; $p_{C_3H_8}$ = 50 torr.

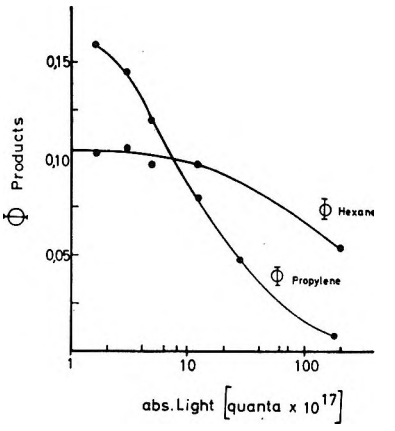

Figure 5. Propylene and hexane quantum yields as a function of absorbed dose. p_{NH_3} = 37.5 torr; $p_{C_3H_8}$ = 50 torr.

yield is within experimental error independent of irradiation time equal to 0.045 ± 0.01.

Quantum yields for propylene and 2.3-dimethylbutane formation are plotted in Figure 5. The limiting value $\phi_{C_3H_6}$ for short irradiation times is 0.16. Absorption of 5 × 10^{18} quanta yields a concentration of 1.5 × 10^{15} molecules of C_3H_6 within the reaction cell corresponding to a partial pressure of 2 × 10^{-2} torr.

The quantum yield of C_6H_{14} is 0.105 at low conversion. $\phi_{C_6H_{14}}$ decreases at longer irradiation times. Propylene, 2.3-dimethylbutane, and an isomer hexane were the only detectable hydrocarbon products when conversion was kept low. The isomer hexane yield was in the order of 5% of the 2.3-dimethylbutane.

Quantum yields for amine formation are plotted in Figure 6. A typical gas chromatogram of a sample after absorption of 5.95 × 10^{18} quanta is reproduced in Figure 7. It can be seen that in addition to iso- and *n*-propylamine, several further products are formed.[7] D is still not identified. E is assumed to be an isomer hexene diamine. Both retention times are shorter than that of isopropylhydrazine.

Hydrazine yields as a function of quanta absorbed are plotted in Figure 1. The quantum yield decreases with prolonged irradiation. After absorption of 1.5 × 10^{9} quanta the limiting hydrazine concentration had not yet been reached. A steady-state pressure of *ca.* 6 × 10^{-2} torr of N_2H_4 may be estimated from these data.

(*c*) *Photolysis of ND_3–C_3H_8 Mixtures.* Mixtures of 40 to 41 torr of ND_3 and 47 to 51 torr of C_3H_8 and a mixture of 41 torr of ND_3 and 620 torr of C_3H_8 were irradiated. Quantum yields for the formation of permanent gases may be taken from Table II. H_2 and D_2 are produced in negligible amounts only compared with HD. The ratio H_2:HD was (5.9 ± 0.4) × 10^{-2}

(7) Quantum yields of unidentified products were calculated on the basis of calibrations with isopropylamine. Thus for product D a quantum yield of 0.01 is found at ≲0.2% conversion. E and other unidentified products are 0.04 under the same conditions, E being the predominant species at higher conversion.

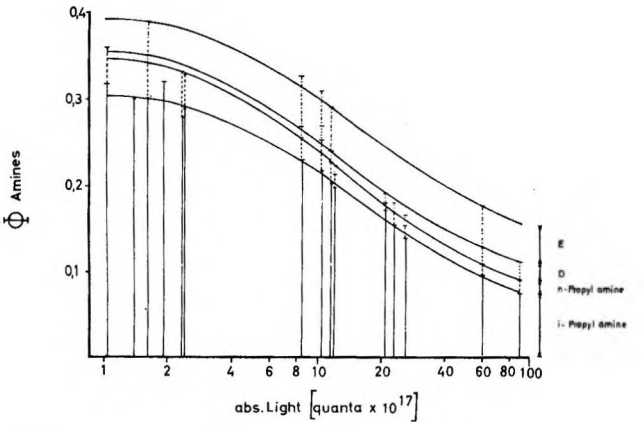

Figure 6. Amine quantum yields as a function of absorbed dose.

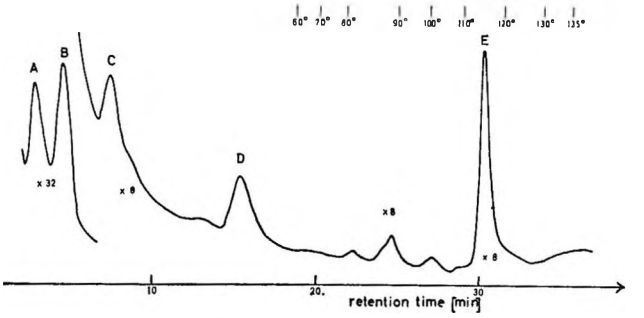

Figure 7. Gas chromatogram of an irradiated sample of 37.7 torr of ammonia and 50 torr of propane. Absorbed dose, 6×10^{18} quanta: A, ammonia; B, isopropylamine; C, *n*-propylamine; D and E, not identified.

practically independent of propane pressure, while the ratio D_2:HD fell off toward higher propane pressure. Hydrogen quantum yields were found to be somewhat higher, nitrogen yields somewhat lower than in NH_3 experiments at equal pressures. The irradiated samples were also analyzed by gas chromatography. The results were identical with those obtained with light ammonia. In one further run, 41 torr of ND_3 and 47.5 torr of C_3H_8 were irradiated in the presence of 640 torr of SF_6. Permanent gas yields were not significantly changed by the addition of SF_6. Moreover, H_2:HD and D_2:HD ratios remained unchanged within experimental error.

(*d*) *Photolysis of Ammonia in the Presence of Isopropylamine.* Mixtures of ammonia and isopropylamine 1000:4 and 1000:2 were irradiated. Under these conditions direct light absorption by the amine is negligible. The results are shown in Table III and Figure 8. Isopropylamine was nearly exclusively transferred into the species E which is assumed to be an isomer hexene diamine.

Discussion

The following discussion is based on the assumption that the photodecomposition of ammonia at 2062 Å occurs with a quantum yield of unity. Results from an investigation of the ammonia photolysis in the presence of ethylene at the same wavelength seem to support this assumption experimentally.[8]

When ND_3 is photolyzed in the presence of C_3H_8 as a D-atom scavenger, the D_2 quantum yield represents an upper limit for the relative probability of process b

$$ND_3 + h\nu(2062\ \text{Å}) \longrightarrow ND(^1\Delta) + D_2 \qquad (b)$$

From the fact that the photolysis of 41 torr of ND_3 and 620 torr of C_3H_8 produced D_2 at a quantum yield of $\phi_{D_2} \leq 0.003$ (*cf.* Table II), it can be concluded that the photodecomposition proceeds only *via*

$$ND_3 + h\nu(2062\ \text{Å}) \longrightarrow ND_2(^2B_1) + D(^2S) \qquad (a)$$

Reactions of hydrogen atoms with propane[9] as well as

Table II: Photolysis of ND_3–C_3H_8 Mixtures (640 torr of SF_6 Added in One Experiment)

Quanta absorbed × 10^{-17}	$\phi(HD+D_2)$[a]	ϕD_2	ϕN_2	H_2/HD × 10^2	D_2/HD × 10^2
	40 torr of ND_3 + 51 torr of C_3H_8				
6.2	0.763	0.01	0.04	5.6	1.5
5.9	0.742	0.01	0.04	5.5	1.6
	41 torr of ND_3 + 51 torr of C_3H_8				
3.25	0.813	0.01	0.035	5.7	1.6
10.4	0.791	0.01	0.04	5.5	1.6
	41 torr of ND_3 + 620 torr of C_3H_8				
4.35	>0.923	≤0.003	0.001	6.1	<0.3
17.2	≥0.941	0.003	0.004	6.3	0.35
16.8	≥0.934	0.006	0.0035	6.2	0.38
	41 torr of ND_3 + 47.5 torr of C_3H_8				
6.1	0.811	0.008	0.03	5.9	0.9
	Same Mixture + 640 torr of SF_6				
6.1	>0.70	0.008	>0.02	5.6	1.2

[a] The formation of some H_2 is due to isotopic impurities of ND_3. Photochemical production of H or H_2 from propane or any propane contamination can be ruled out since the ratio H_2/HD is independent of propane pressure.

Table III: Product Quantum Yields in the Photolysis of NH_3–Isopropylamine Mixtures

Quanta absorbed × 10^{-17}	p_{NH_3}, torr	$p_{i\text{-}C_3H_7NH_2}$ torr	ϕH_2	ϕN_2	$\phi_{i\text{-}C_3H_7NH_2}$	ϕE
18.3	41.4	0.16	0.60	0.03	−0.34 (?)	0.28
23.7	46.4	0.10	0.53	0.04	−0.22 (?)	0.28
			Mean value		−0.28	0.28

(8) U. Schurath, P. Tiedemann, and R. N. Schindler, *J. Phys. Chem.*, in press.

(9) K. Yang, *J. Amer. Chem. Soc.*, **84**, 719 (1962).

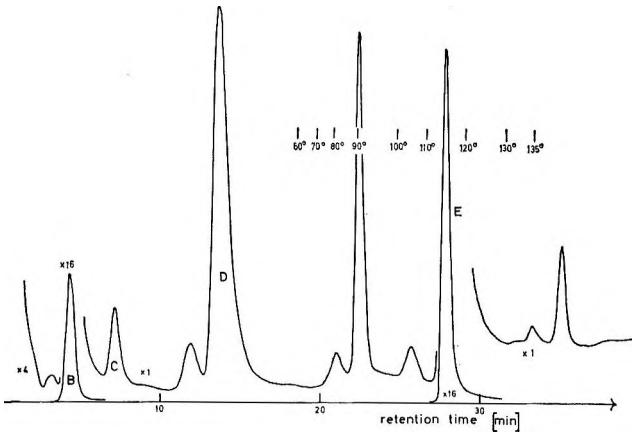

Figure 8. Gas chromatogram of an irradiated sample of 46.5 torr of ammonia and 0.1 torr of isopropylamine. Absorbed dose, 2.4×10^{18} quanta.

reactions between propyl radicals[10] are sufficiently well known. Considering the reaction products detected in our experiments, the following mechanism appears to be adequate to describe the photolysis of ammonia in the presence of propane.

$$NH_3 + h\nu \longrightarrow NH_2 + H; \quad \phi_{(1)} = 1.00 \qquad (1)$$

$$H + C_3H_8 \longrightarrow C_3H_7 + H_2 \qquad (2)$$

$$2C_3H_7 \longrightarrow C_6H_{14} \qquad (3)$$

$$2C_3H_7 \longrightarrow C_3H_6 + C_3H_8 \qquad (4)$$

$$NH_2 + C_3H_7 \longrightarrow C_3H_7NH_2 \qquad (5)$$

$$NH_2 + C_3H_7 \longrightarrow NH_3 + C_3H_6 \qquad (6)$$

$$2NH_2 \longrightarrow N_2H_4 \qquad (7)$$

However, hydrogen scavenging does not occur exclusively *via* step 2 in our system. Figure 2 shows that the hydrogen quantum yield is never unity and reaches a value of only 0.9 at a pressure of 700 torr. Consequently, addition reactions of hydrogen atoms must also be considered in our system.[11] The following steps will be discussed

$$H + NH_2 \longrightarrow NH_3 \qquad (8)$$

$$H + C_3H_7 \longrightarrow C_3H_8 \qquad (9)$$

Reaction 8 is postulated in the photolysis of pure ammonia to account for the low quantum yields of decomposition. It is generally assumed[12] that process 8 proceeds in termolecular collisions. This assumption is based on the observed pressure dependence of the quantum yields. As shown in Figures 2 and 3, however, addition of 500 torr of SF_6 does not change the product quantum yields in our experiments. Most significantly, the hydrazine quantum yield remains unchanged. Reaction 9 cannot be excluded in our system. It has been shown[10] to occur in the mercury-sensitized photolysis of isopropyl ketone in the presence of excess D_2.

Recombination of hydrogen atoms *via* triple collisions can be neglected in the presence of propane. The experiments with ND_3 indicate (*cf.* Table II) that molecular hydrogen is nearly exclusively formed by reaction 2. The low D_2 quantum yield remains unchanged when 640 torr of SF_6 is added to the mixture. This excludes triple collision recombination of D atoms as the main source of D_2.

The mechanism discussed so far holds only under the limiting condition of low conversion. As shown in Figures 5 to 7, several product quantum yields fall off after absorption of less than 6×10^{17} quanta corresponding to a conversion of about 0.2% ammonia. Direct light absorption by the products can be excluded under these conditions. Thus secondary attack of the products must be responsible for the reduction of quantum yields.

Propylene is known to be very sensitive to hydrogen atom attack.[9] The reduction of hydrogen quantum yields at higher irradiation times could result from this reaction.

Secondary decomposition of propylamines is not understood at present. As shown in Figures 7 and 8, the same products are formed in extended photolysis of NH_3–C_3H_8 mixtures and in the photolysis of ammonia in the presence of isopropylamine. Also, the products are formed in similar relative amounts. In the latter case an unknown substance E is produced in quantities approximately equal to the amount of isopropylamine consumed. When NH_3–C_3H_8 mixtures are submitted to prolonged irradiation, however, the yield of E does not compensate for the reduction of the yield of isopropylamine. Therefore, it is assumed that further secondary products are formed from isopropylamine which elude detection.

The dependence of hydrazine quantum yield on irradiation time is of interest in connection with the production of nitrogen. As shown in Figure 1, the hydrazine concentration is a linear function of irradiation dose up to about 2×10^{18} quanta absorbed. Deviation from linearity at higher conversion results from secondary decomposition of hydrazine and/or from a reduced rate of hydrazine production.

(10) C. A. Heller and A. S. Gordon, *J. Phys. Chem.*, **64**, 390 (1960).

(11) In the radiolysis of ammonia at atmospheric pressure, Johnson and Simic (*Nature*, **216**, 479 (1967)) found no detectable dependence of $G(H_2)$ on propane pressure in the region of 1.5–6 mol %. From this observation complete scavenging of H atoms was concluded.

In our system approximately 10^{16} H atoms/ml min are produced in the reaction zone as compared with about 1.6×10^{14} H atoms/ml min in the radiolysis experiments of Johnson and Simic. Since the completeness of H-atom scavenging depends mainly on the ratio of the partial pressures of H atoms and C_3H_8 molecules, considerably higher propane pressure would be necessary to achieve complete H atom scavenging in our system.

(12) W. Groth and J. Rommel, *Z. Phys. Chem.* (Frankfurt am Main), **45**, 96 (1965).

Table IV: Material Balance

Products observed	$\phi_{product}$	Reaction	$\phi_{intermediate}$ H consumed	$\phi_{intermediate}$ NH_2 consumed	$\phi_{intermediate}$ C_3H_7 formed	$\phi_{intermediate}$ C_3H_7 consumed
H_2	0.77	2	$0.77-\phi_{12}$	...	$0.77-\phi_{12}$	...
		12	<0.05	...	...	<0.05
C_6H_{14}	0.105	3	...	...	...	0.21
C_3H_6	0.164	4	...	...	...	0.13
		6	...	$0.10-\phi_{12}$	...	$0.10-\phi_{12}$
		12	See above	...	...	See above
$C_3H_7NH_2$	0.35	1	...	0.35	...	0.35
N_2H_4	0.06	7	...	0.12	...	...
N_2	0.04	...	...	~0.20	...	...
			0.77	$0.77-\phi_{12}$	$0.77-\phi_{12}$	0.79

Secondary decomposition of hydrazine leads to nitrogen formation.[13] Before absorption of at least 2×10^{18} quanta, however, this source cannot be responsible for the nitrogen produced. No conclusions can be drawn from our experiments concerning the mode of nitrogen formation at the lower doses absorbed where secondary decomposition of N_2H_4 is not yet detectable. To account for the quantum yield of nitrogen in the order of 0.04, other reaction sequences must be considered. NH_2 radicals which form hydrazine by recombination are also likely to form NH radicals by disproportionation

$$2NH_2 \longrightarrow NH_3 + NH \qquad (10)$$

Reaction 10 has been postulated in the flash photolysis and shock wave decomposition of hydrazine.[14] NH radicals may lead to nitrogen production, probably *via* intermediates like N_2H_3 or N_2H_2.

Apart from reactions 5–8 and 10, amino radicals may also be removed in process 11.

$$NH_2 + C_3H_8 \longrightarrow NH_3 + C_3H_7 \qquad (11)$$

Step 11 forms no characteristic products in our system. In this respect it may be compared with (8) and (9) which have been discussed previously. No information pertaining to the probability of reaction 11 is available from the literature. An abstraction reaction of this type had been proposed by Brash and Back[15] in the photolysis of HNCO vapor in the presence of paraffins. Also, the dependence of hydrazine yields on propane partial pressures (*cf.* Figure 3) cannot be explained easily if reaction 11 is omitted. Photolysis in the presence of SF_6 proved that the observed pressure dependence of hydrazine yields is specifically connected to propane partial pressure and cannot be brought about if the total pressure is increased by an inert additive. Increasing the propane partial pressure would decrease the stationary NH_2 radical concentration *via* step 11. Simultaneously, C_3H_7 radicals are formed, which consume further NH_2 radicals *via* reactions 5 and 6. Both effects result in a reduction of the hydrazine yield in agreement with the experimental results. The quantum yield for processes 8, 9, and 11 cannot exceed 0.2 (see below).

In the following section, propylene formation will be considered. The ratio of addition to disproportionation between isopropyl radicals is 1:0.64. For *n*-propyl radicals this ratio is 1:0.16.[16] Since reaction 5 yields 88% isopropylamine and 12% *n*-propylamine, the concentrations of iso- to *n*-propyl radicals will be in the order of 9:1 in our system. In this mixture the ratio of addition to disproportionation reactions may be assumed to be about 1:0.61. At low conversions the C_6H_{14} quantum yield is 0.105. Hexane production results from reaction 3. If propylene were only formed by disproportionation of two propyl radicals, $\phi(C_3H_6)$ should be approximately 0.064. However, the propylene quantum yield has been found to be 0.16 at very low conversion. Consequently, there must be further propylene-producing reactions to account for an additional quantum yield of 0.1. The following steps are considered

$$NH_2 + C_3H_7 \longrightarrow NH_3 + C_3H_6 \qquad (6)$$

$$H + C_3H_7 \longrightarrow H_2 + C_3H_6 \qquad (12)$$

The relative probability for the occurrence of reaction 12 can be estimated as follows. Hydrogen atoms are produced in the photoact with a quantum yield of unity; 77% are used up to form molecular hydrogen. The other atoms disappear through reactions 8, 9, and similar processes without forming detectable products. Therefore, the quantum yield of reaction 9 cannot exceed 0.23. Since $k_9:k_{12}$ is approximately 5,[10] the quantum yield of reaction 12 must be less than 0.05.

(13) F. T. Jones and T. J. Swerski, *Trans. Faraday Soc.*, **63**, 2411 (1967).

(14) D. Husain and R. G. W. Norrish, *Proc. Roy. Soc.*, **A273**, 145 (1963); R. W. Diesen, *J. Chem. Phys.*, **39**, 2121 (1963).

(15) J. L. Brash and R. A. Back, *Can. J. Chem.*, **43**, 1778 (1965).

(16) J. A. Kerr and F. A. Trotman-Dickenson, *Progr. Reaction Kinetics*, **1**, 105 (1961).

Thus, the ratio for the disproportionation to recombination reaction between amino and propyl radicals is obtained from these experiments to be $k_6:k_5 = 0.21 \pm 0.07$. A value of approximately 0.3 for the corresponding reactions between NH_2 and C_2H_5 radicals appeared to be in agreement with results in the photolysis of NH_3 in the presence of C_2H_4.[8] On the basis of the proposed mechanism the material balance shown in Table IV was obtained. The table lists quantum yields for the final products and attributes values for the consumption and production of the intermediates H, NH_2, and C_3H_7, respectively. H atoms and NH_2 radicals are assumed to be produced in the photoact with unity quantum yield. In view of the variety of reactions occuring in the system, the material balance is considered good. The largest uncertainty exists about the mode of nitrogen formation at low conversion. Production of this gas is not eliminated by 700 torr of propane. Even in the presence of excess ethylene the formation of N_2 cannot be suppressed completely.[8] Work is being continued on the reactions of the species N_2H_3, NH_2, and NH, respectively, in the presence of hydrocarbons.

A Pulsed-Radiolysis Study of Atomic Oxygen Reactions in the Gas Phase[1]

by G. M. Meaburn,[2] D. Perner,[3] J. LeCalvé, and M. Bourène

Service de Chimie Physique, Centre d'Etudes Nucleaires de Saclay, B.P. No 2, Gif-sur-Yvette, France *(Received May 7, 1968)*

The techniques of pulsed radiolysis, with spectroscopic detection of transients, have been used to study some gas-phase reactions of atomic oxygen produced in electron-irradiated CO_2, N_2O, and CO at pressures close to 1 atm. In the presence of small amounts of added O_2, oxygen atoms are removed from these systems mainly by the three-body reaction, O(triplet) + O_2 + M → O_3 + M. The formation of ozone is found to follow pseudo-first-order kinetics in all three cases with rate constants $k = 3.7$, 3.2, and 1.6×10^8 M^{-2} sec^{-1}, respectively, for M = CO_2, N_2O, and CO. Kinetic analysis of ozone formation in O_2 indicates the occurrence of two parallel reactions in this system: O(triplet) + O_2 + O_2 → O_3 + O_2, and O(singlet) + O_2 → O(triplet) + O_2. The rate constant for the deactivation reaction has been established to be 9.8×10^6 M^{-1} sec^{-1}. Mixtures of CO_2, O_2, and chloromethanes have also been studied and various transient spectra identified, including those of the radicals ClO and CCl. In particular, the relative concentrations of these intermediates have been determined in the three-component system CO_2–O_2–CCl_4. The experimental observations are explained in terms of competition between CCl_4 and O_2 for an undefined excited state of CO_2, with the resulting energy transfer processes yielding CCl and O(singlet), respectively. Reaction of O(singlet) with CCl_4 leads to the eventual formation of ClO in these mixtures.

Introduction

During recent years there have been numerous investigations of reactions involving atomic oxygen. Several methods have been employed to generate oxygen atoms in a variety of gaseous systems, *e.g.*, photolysis,[4] microwave discharge,[5] and titration of nitric oxide with nitrogen atoms.[6] Previous pulsed-radiolysis studies[7,8] have been concerned with the kinetics of ozone formation in oxygen and in gas mixtures containing oxygen as a minor component.

Direct observation of oxygen atoms by absorption spectroscopy is difficult. The transitions between different electronic states lie between 950 and 1400 Å, a spectral region which calls for the use of elaborate optical equipment and techniques. Their reactions can be followed indirectly, however, if one of the reaction products, stable or transient, itself has a conveniently located absorption band. The work of Sauer and Dorfman is a good example of the application of this method; the rate of ozone formation is readily determined by kinetic spectroscopy, thus allowing absolute rate constants to be obtained for the three-body reaction between ground-state oxygen atoms, O(^{3}P), and oxygen.

In the present study, particular attention is paid to

(1) Work performed under the auspices of the Commissariat a l'Energie Atomique, France.

(2) Armed Forces Radiobiology Research Institute, Bethesda, Md. 20014.

(3) Institut für Physikalische Chemie, K.F.A., Jülich, Western Germany.

(4) M. Clerc and F. Barat, *J. Chem. Phys.*, **46**, 107 (1967).

(5) A. A. Westenberg and N. de Haas, *ibid.*, **46**, 490 (1967).

(6) J. O. Sullivan and P. Warneck, *J. Phys. Chem.*, **69**, 1749 (1965).

(7) M. C. Sauer and L. M. Dorfman, *J. Amer. Chem. Soc.*, **87**, 3801 (1965).

(8) M. C. Sauer, *J. Phys. Chem.*, **71**, 3311 (1967).

the radiation-induced decomposition of CO_2, O_2, and mixtures of these two components at pressures of 1 atm or less. Using the indirect approach outlined above, it is possible to distinquish between the reactions of ground-state and electronically excited oxygen atoms generated by radiolysis of these gases.

Experimental Section

Standard techniques of pulsed radiolysis with optical detection of transients[9] have been used throughout this work. The experimental assembly will be described in detail in a future publication and only the main characteristics of the equipment will be outlined here.

Two different pulsed electron sources were employed. One was a 250-kV generator manufactured by CSF (France). This machine provided single pulses of ~130-nsec duration and delivered up to ~1 J of energy to a gas sample. The other was a Field Emission Corp. 600-kV, 30-nsec pulser with about five times this energy capability.

Cylindrical stainless steel irradiation cells were used with both sources. They were of similar design, although the 600-kV cell had the smaller capacity of the two, 4.0 l. against 4.6 l. for the 250-kV unit. Each was equipped with an internal multiple pass mirror system based on the White design[10] with the analyzing light beam traversing the cell coaxially to the electron beam. Typically 20 passes were used, giving a total optical path length of 9 m (mirror radii = 45 cm).

Transient spectra were photographed with aid of a Hilger medium quartz spectrograph using Ilford HP3 plates. The decay of a transient absorption was obtained from microdensitometer readings of optical density recorded at predetermined time intervals after the electron pulse. An analyzing light flash of about 1.5-μsec half-life was provided by a small argon-filled spectroflash lamp.

A photomultiplier detection system with oscilloscopic recording was adapted to the same spectrograph to follow the kinetics of ozone formation. A 450-W high-pressure xenon lamp was generally used as a continuous source of analyzing light. For some experiments this lamp was replaced by a suitably synchronized xenon flash lamp. A much improved signal-to-noise ratio was obtained at the detector output, an important factor when light fluxes across the photomultiplier window are low. This is particularly true in the ultraviolet region where both lamp intensities and mirror reflectivities are usually decreasing rapidly. The situation is further aggravated in the gas phase where monochromator entrance and exit slits must be kept narrow.

Dose rates were determined with the N_2O dosimeter assuming $G(N_2) = 10$.[11] The total dose received by a gas sample was not allowed to exceed ~10^{19} eV/g and was generally much lower than this.

Cylinder gases were further purified by vacuum line distillation. In particular, CO_2 was subjected to multiple freezing–sublimation cycles to remove trace impurities, mainly air. Carbon monoxide was distilled at 90°K to remove metal carbonyls.

The product gases, CO and O_2, were separated from irradiated CO_2 and analyzed by gas–solid chromatography. Ozone formation was followed by its optical absorption at 2550 Å, assuming a decimal extinction coefficient of 134 cm^{-1} at STP.[12]

Results

Ozone Formation in CO_2, CO, and N_2O Containing Small Amounts of Added Oxygen. In all three systems the reaction is first order with respect to ozone formation. Ozone yields and third-order rate constants derived from the kinetic data are given in Table I.

The variation of $G(O_3)$ as a function of O_2 concentrations in CO_2 is shown in Figure 1. The significance of the solid curve will be discussed in a later section. Ozone is not found in irradiated pure CO_2 even after 10 pulses. Oxygen is a product of radiolysis (see Table II), but its concentration in the reaction vessel after this dose amounts to only ~5×10^{-7} M, or ~0.002% of the total sample. It can be seen from Figure 1 that the ozone yield under these conditions would be much lower than our detection limit of $G(O_3) = 0.5$. The effect of SF_6 on the ozone yield in CO_2 containing 1.1% oxygen is shown in Figure 2.

The ozone formed in N_2O–O_2 mixtures disappears from the system within 0.1 to 1 sec. Its rate of disappearance does not follow a first-order law and the reaction half-life decreases with increasing number of pulses delivered to a given sample. This suggests that the ozone is reacting efficiently with a product of radiolysis, probably nitric oxide.

Ozone Formation in O_2. In this case a simple first-order kinetic law is not followed. The experimental data obtained for oxygen at 560 torr are plotted as a

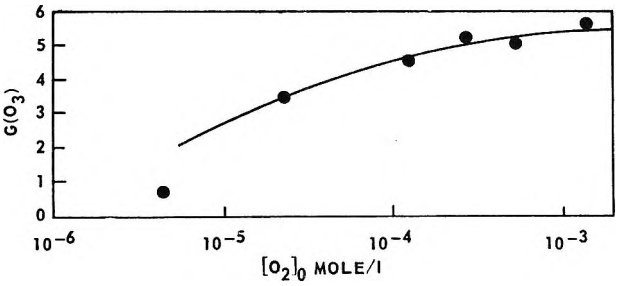

Figure 1. Ozone yield in irradiated CO_2 containing low concentrations of O_2: P_{CO_2} = 460 torr. For explanation of solid curve, see text.

(9) L. M. Dorfman and M. S. Matheson, *Progr. Reaction Kinetics*, **3**, 237 (1965).

(10) J. U. White, *J. Opt. Soc. Amer.*, **32**, 285 (1942).

(11) F. T. Jones and T. J. Sworski, *J. Phys. Chem.*, **70**, 1546 (1966).

(12) A. G. Hearn, *Proc. Phys. Soc.*, **78**, 932 (1961).

Table I: Third-Order Rate Constants for the Reaction of $O(^3P)$ Atoms with O_2 in Different Solvent Gases

Solvent gas, M	P_M at 295°K, torr	Energy absorbed, (eV/pulse) $\times 10^{-18}$	Mol % O_2 added	$G(O_3)$	k_{O+O_2+M} $(M^{-2}\ sec^{-1}) \times 10^{-8}$
CO_2	460	5.8	0	0	...
	460	5.8	0.018	0.70	*a*
	460	5.8	0.09	3.6	3.7
	460	5.8	0.50	4.6	3.6
	460	5.8	1.1	5.5	3.9
	460	5.8	2.2	5.3	3.0
	460	5.8	5.6	5.6	2.7
	110	2.2	4.5	5.3	4.3
N_2O	460	5.8	5.6	6.1	3.2
O_2	560	5.6	100	10.5	1.5[b]
CO	700	5.8	0.71	1.3	*a*
	700	5.8	3.7	2.0	1.6

[a] Rate constant not accurately determined. [b] See text for details.

Table II: Effect of Additives on the Yields of CO and O_2 from Irradiated CO_2[a]

Additive	Mol % added	$G(CO)$[b]	$G(O_2)$[b]
None	...	6.0 ± 0.3	2.6 ± 0.3
SF_6	0.04–5	4.2	2.0
O_2	up to 1	6.0	...
C_2H_4	0.1	~6	0.15

[a] CO_2 pressure = 460 torr. [b] Yields measured after a single pulse, dose rate $\sim 2 \times 10^{25}$ eV/g sec.

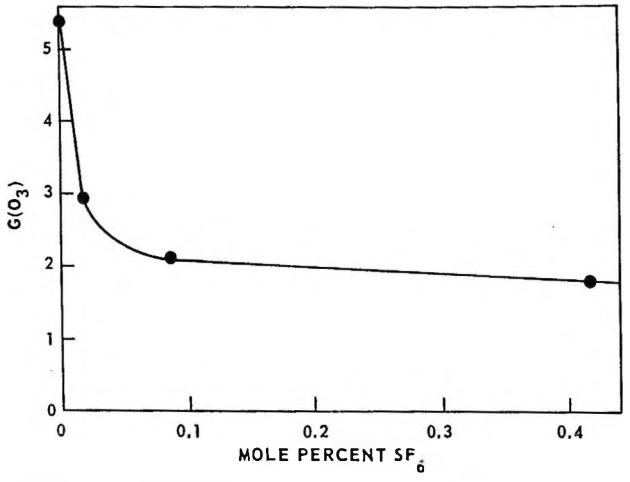

Figure 2. Effect of SF_6 on ozone yield in irradiated CO_2 containing 1.1% O_2: P_{CO_2} = 460 torr.

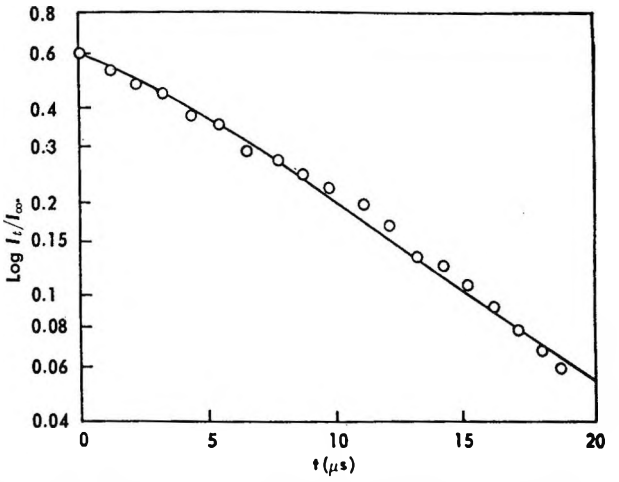

Figure 3. Kinetics of ozone formation in electron-irradiated oxygen. For explanation of solid curve, see text.

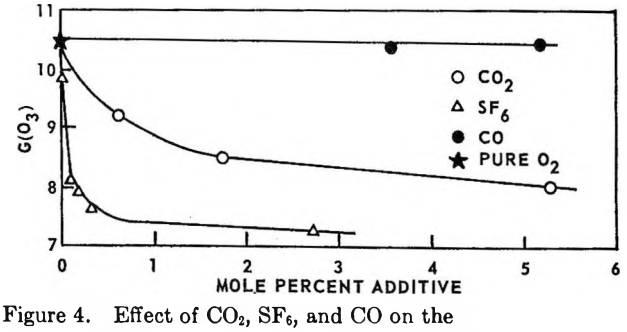

Figure 4. Effect of CO_2, SF_6, and CO on the ozone yield in irradiated oxygen: P_{O_2} = 560 torr.

first-order function in Figure 3. A small induction period is apparent during which the rate of ozone formation is actually increasing.

The ozone yield from pure oxygen is $G(O_3)$ = 10.5. The effect of added CO_2, SF_6, and CO on this yield is shown in Figure 4. Of particular interest is the marked influence of CO_2. The determination of $G(O_3)$ was extended over the complete range of O_2–CO_2 mixtures and the results, after correction for absorbed dose, are shown in Figure 5. The open circles represent relative ozone yields determined photographically and normalized to give the best fit to the absolute data previously described (solid circles). Considering the errors involved in plate work, the agreement between the two sets of data is satisfactory.

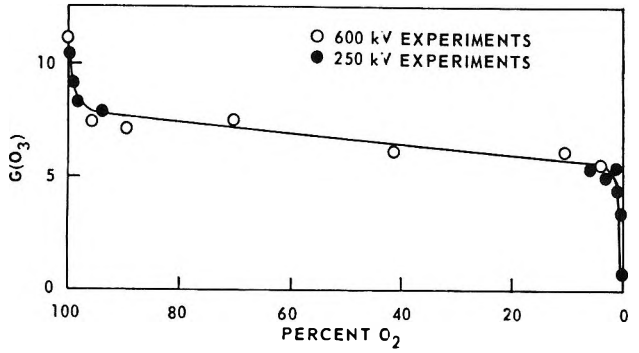

Figure 5. Ozone yield in irradiated CO_2–O_2 mixtures: total gas pressure = 1 atm.

Formation of Transients in CO_2–O_2–CCl_4 Mixtures. When oxygen containing a small quantity of a chloromethane is pulsed, the ClO radical is produced as a major intermediate product.[13] The radical is easily identified by its near uv absorption bands associated with the vibrational levels $n \leftarrow 0$ ($4 \leq n \leq 23$) of the $^2\pi \leftarrow {}^2\pi$ transition.[14,15] This spectrum is not observed in pulsed CO_2–chloromethane mixtures, but other strong absorption bands attributed to the $^2\Delta \leftarrow {}^2\pi$ transition of the CCl radical[16,17] are seen[13] in the region of 2780 Å.

Production of ClO and CCl in the three-component system CO_2–O_2–CCl_4 was examined in some detail. The relative concentrations of these radicals were determined over a wide range of CO_2–O_2 compositions, with the CCl_4 concentration fixed at 2%. The results are shown in Figures 6 and 7. The ClO absorption spectrum builds up by a pseudo-first-order reaction to reach a maximum ~30 μsec after the electron pulse. The radical is relatively stable under these experimental conditions, having a half-life of several hundred microseconds. Production of CCl is extremely rapid. The highest concentration of this radical is observed 0.3 μsec after the electron pulse. This delay represents the limit of resolution of the photomultiplier detection system. The absorption decays rapidly by what appears to be a second-order process with a half-life of ~10 μsec.

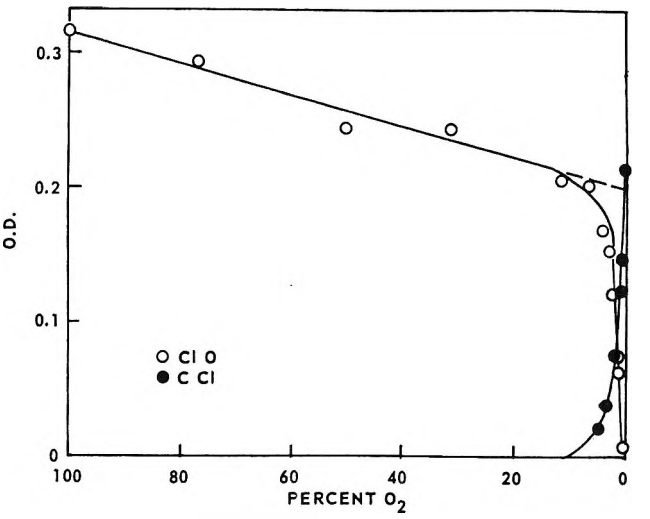

Figure 6. Yields of ClO and CCl radicals in irradiated CO_2–O_2 mixtures containing 2% CCl_4; total gas pressure = 1 atm; linear concentration scale.

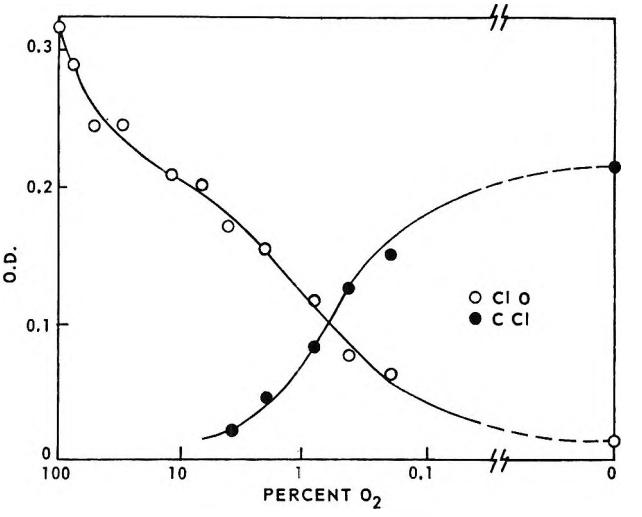

Figure 7. Yields of ClO and CCl radicals in irradiated CO_2–O_2 mixtures containing 2% CCl_4: total gas pressure = 1 atm; logarithmic concentration scale.

Discussion

In order to interpret the experimental data, one needs to make certain assumptions about the electronic state of the reacting oxygen atom. During radiolysis, oxygen atoms may be produced initially in higher (singlet) states as well as in the triplet ground state. The probability of deactivation of these excited atoms will depend upon the nature of the gases present and upon the residence time of an oxygen atom before reaction with an additive.

At gas pressures of several hundred torr, collisional deactivation of singlet oxygen atoms (^1D and ^1S) to the ground state (^3P) may occur readily. These processes have been the object of extensive study and discussion.[18–21]

(13) The formation of ClO and other transients in these systems will be described in detail in a later publication.

(14) R. W. B. Pearse and A. G. Gaydon, "The Identification of Molecular Spectra," 3rd ed, Chapman and Hall, Ltd., London, 1963, p 145.

(15) R. A. Durie and D. A. Ramsay, *Can. J. Phys.*, **36**, 35 (1958).

(16) R. D. Gordon and G. W. King, *ibid.*, **39**, 252 (1961).

(17) J. P. Simons and A. J. Yarwood, *Trans. Faraday Soc.*, **57**, 2167 (1961).

(18) D. L. Baulch and W. H. Breckenridge, *ibid.*, **62**, 2768 (1966).

(19) H. Yamazaki and R. J. Cvetanovic, *J. Chem. Phys.*, **39**, 1902 (1963).

(20) K. F. Preston and R. J. Cvetanovic, *ibid.*, **45**, 2888 (1966).

(21) W. D. McGrath and J. J. McGarvey, *Planet. Space Sci.*, **15**, 427 (1967).

In the radiolysis of oxygen, where both singlet and triplet oxygen atoms are initially present, the kinetics of ozone formation can be understood in terms of two parallel and consecutive pseudo-first-order reactions

$$O^1 + O_2 \longrightarrow O(^3P) + O_2 \quad (1)$$

$$O(^3P) + O_2 + O_2 \longrightarrow O_3 + O_2 \quad (2)$$

where O^1 may represent $O(^1D)$ or $O(^1S)$. Ozone concentration is expressed as a function of reaction time by

$$[O_3]_\infty - [O_3]_t = [O_3]_\infty e^{-k_2't} - \frac{[O^1]_0 k_2'}{k_2' - k_1'}(e^{-k_2't} - e^{-k_1't}) \quad (A)$$

where k_2' and k_1' are first-order rate constants, and $[O^1]_0$ represents the concentration of singlet oxygen atoms at $t = 0$.

The theoretical curve which best fits the experimental data is obtained when $k_1' = 3 \times 10^5$ sec^{-1}, $k_2' = 1.37 \times 10^5$ sec^{-1}, and $[O^1]_0 = [O(^3P)]_0$. The constant, k_2', is of course determined experimentally at high values of t. In accepting this mechanism it must be concluded that any contribution of reaction 3 to the ozone yield is negligible.

$$O^1 + O_2 + O_2 \longrightarrow O_3 + O_2 \quad (3)$$

Expressed in second-order terms, $k_1 = 9.8 \times 10^6\ M^{-1}$ sec^{-1}, which is in reasonable agreement with the deactivation rate constant of $2.4 \times 10^6\ M^{-1}$ sec^{-1} reported by Sullivan and Warneck,[22] but much lower than the minimum value of $6 \times 10^9\ M^{-1}$ sec^{-1} determined by Young and Black[23] for the deactivation of $O(^1D)$. The rate constant $k_2 = 1.47 \times 10^8\ M^{-2}$ sec^{-1} is in good agreement with values found by other authors.[24-27]

The pseudo-first-order plots of ozone formation in CO_2–O_2 mixtures are strictly linear and can be interpreted in terms of a single reaction

$$O(^3P) + O_2 + CO_2 \longrightarrow O_3 + CO_2 \quad (4)$$

This indicates that singlet oxygen atoms, if produced, are probably deactivated to the ground state at a rate much higher than that of ozone formation. Reaction 4, of course, proceeds slowly at the low oxygen concentrations used in these kinetic experiments. The third-order rate constant determined for reaction 4, $k_4 = 3.7 \times 10^8\ M^{-2}$ sec^{-1}, is in good agreement with the value obtained by Sauer.[8]

As shown in Figure 1, $G(O_3)$ decreases rapidly as the oxygen concentration falls below $\sim 10^{-4}\ M$. At these high dose rates, the recombination reaction

$$O(^3P) + O(^3P) + CO_2 \longrightarrow O_2 + CO_2 \quad (5)$$

is apparently competing effectively with reaction 4. This competition may be expressed in mathematical form by

$$\frac{k_5}{k_4} = \frac{xy}{2[O]_0[O_3]} \frac{1}{\ln x[O_2] - \ln y[O]_0([O_2] - [O_3])} \quad (B)$$

where $x = [O]_0 - [O_3]$ and $y = [O]_0 - [O_2]$ and where $[O]_0$ is the concentration of triplet oxygen atoms from any source.

The curve which best fits the experimental points is obtained for $k_5 = 2.1 \times 10^{10}\ M^{-2}$ sec^{-1}. This value is an order of magnitude higher than that reported by Morgan and Schiff.[28] It should be pointed out that the optical detection arrangement used in the present study was not designed for investigating true second-order reactions, and an error due to inhomogeneous distribution of oxygen atoms along the path of the electron beam is inevitable. A discrepancy of this magnitude cannot, however, be ascribed to such a geometrical factor.

A more likely source of error could arise from the possibility of energy transfer from CO_2 to O_2 leading to an instantaneous increase in oxygen atom concentration and a consequent overestimate of k_5. An energy transfer process undoubtedly occurs in these mixtures (see below) and any attempt to correlate the oxygen atom yield in pure CO_2 $\{=2G(O_2)\}$ with the ozone yield in CO_2–O_2, must be considered suspect. However, one valid observation can be made. The yield of carbon monoxide in pure CO_2 is not decreased by addition of O_2 to the system. This strongly suggests that, although O_2 is acting as a protective agent, the energy it accepts is not normally utilized to decompose CO_2, but is dissipated without effect in the absence of a suitable additive.

In N_2O–O_2 mixtures, any singlet atoms produced by radiolysis of N_2O react with[19,29] or are deactivated by[20] the solvent gas and only triplet atoms are finally available to produce ozone by reaction 6. The rate constant

$$O(^3P) + O_2 + N_2O \longrightarrow O_3 + N_2O \quad (6)$$

for this reaction, $k_6 = 3.2 \times 10^8\ M^{-2}$ sec^{-1} is in good agreement with previously published values.[8,30]

The production of ozone in CO–O_2 mixtures is entirely due to the occurrence of reaction 7, with a rate constant, $k_7 = 1.6 \times 10^8\ M^{-2}$ sec^{-1}.

$$O(^3P) + O_2 + CO \longrightarrow O_3 + CO \quad (7)$$

The fact that ozone is formed at all in this system indi-

(22) J. O. Sullivan and P. Warneck, *J. Chem. Phys.*, **46**, 953 (1967).

(23) R. A. Young and G. Black, *ibid.*, **47**, 2311 (1967).

(24) N. Basco, *Proc. Roy. Soc.*, **A283**, 302 (1965).

(25) S. W. Benson and A. E. Axworthy, *J. Chem. Phys.*, **42**, 2614 (1965).

(26) F. Kaufman and J. R. Kelso, *Discussions Faraday Soc.*, **37**, 26 (1964).

(27) J. A. Ghormley, C. J. Hochanadel, and J. W. Boyle, ORNL/4164 Report, 1967, p 35.

(28) J. E. Morgan and H. I. Schiff, *J. Chem. Phys.*, **38**, 1495 (1963).

(29) P. Warneck, *ibid.*, **43**, 1849 (1965).

(30) F. Kaufman and J. R. Kelso, *ibid.*, **46**, 4541 (1967).

cates that $O(^3P)$ reacts slowly with CO according to reaction 8. The rate constant estimated from the data

$$O(^3P) + CO \longrightarrow \text{product} \quad (8)$$

given in Table I is $k_8 \sim 2 \times 10^4\ M^{-1}\ \text{sec}^{-1}$, in reasonable agreement with the previously published value[31] of $1.2 \times 10^4\ M^{-1}\ \text{sec}^{-1}$.

There are several interesting features of the results obtained with gas mixtures containing CCl_4. The ClO radical is probably being produced by reaction 9. This

$$O^1 + CCl_4 \longrightarrow ClO + CCl_3 \quad (9)$$

reaction is endothermic by ~3 kcal/mol for ground-state oxygen atoms, but should occur readily for excited atoms. The fact that ClO is not formed in CO_2–CCl_4 mixtures again indicates that only $O(^3P)$ atoms are present at this stage.

From the shape of the ClO curve shown in Figure 6, it is evident that an energy transfer process of some kind is involved in the production of singlet oxygen atoms at high CO_2 concentrations. One such possibility is reaction 10 followed by dissociative recombination (11).

$$CO_2^+ + O_2 \longrightarrow O_2^+ + CO_2 \quad (10)$$

$$O_2^+ + e^- \text{ (or } O_2^-) \longrightarrow O^1 + O^3\ (+O_2) \quad (11)$$

As has been pointed out by Anderson and Best,[32] neutralization of CO_2^+ in these relatively high pressure systems does not necessarily result in the disruption of the molecule. The energy released may simply be used to break up ion–molecule clusters. In this respect, participation of reaction 10 would be consistent with the observation that $G(CO)$ in CO_2–O_2 mixtures is independent of O_2 concentration.

The singlet oxygen atoms being produced by reaction 11 are not rapidly deactivated as one might have suspected from the linear first-order plots of ozone formation in CO_2–O_2 mixtures, but go on to react according to reaction 9. This implies that, if in the radiolysis of pure CO_2 singlet oxygen atoms *are* formed, they must be in an electronic state different from that of the atoms produced by energy transfer to oxygen.

The CCl radical, observed only at high CO_2 concentrations, is produced very rapidly and is believed to arise from an energy transfer process in competition with reaction 10. Again assuming the CO_2^+ ion to be the energy donor, the reactions

$$CO_2^+ + CCl_4 \longrightarrow CCl_4^+ + CO_2 \quad (12)$$

$$CCl_4^+ + e^- \longrightarrow CCl + ? \quad (13)$$

may be written. The competition between reactions 10 and 12 may be expressed in terms of a rate constant ratio determined from the curves shown in Figure 7. This value is $k_{10}/k_{12} = 3.3 \pm 0.3$.

It is difficult to draw firm conclusions about the effect of electron scavengers in these systems. The decrease in $G(O_3)$ observed when SF_6 is added to CO_2–O_2 mixtures (Figure 2) could very well be the result of intervention in neutralization processes involving O_2^+ as well as CO_2^+. Carbon tetrachloride is also an efficient electron scavenger; account should be taken of this when attempting to correlate $G(ClO)$ with $G(O_3)$ in mixtures containing CCl_4. Approximately 30% of the ozone produced in the radiolysis of O_2 does appear to arise from ionic reactions susceptible to scavengers of this kind.

The marked effect of CO_2 on the ozone yield from O_2, shown in Figures 4 and 5, cannot be attributed to electron capture. At such high O_2 concentrations, the predominant negative ions are expected to be O_2^- and O^-. The observed decrease in $G(O_3)$ may well reflect the removal of these ions from the system by reaction with CO_2 to form CO_4^- and CO_3^-.[33,34]

It is rather surprising that the addition of CO has no effect on ozone formation in O_2, particularly in view of the high rate constant reported for reaction 14.[35] In

$$CO + O(^1D) \rightarrow CO_2 \quad (14)$$

accepting that singlet atoms, after deactivation, normally contribute to about one-half of the ozone production, one is led to the somewhat unlikely conclusion that $O(^1D)$ atoms are not produced in the radiolysis of oxygen. Direct observation of these excited atoms is clearly desirable.

Acknowledgment. The authors wish to express their appreciation to Dr. H. Heiing for his constant interest throughout the course of this work and for many useful discussions. D. P. gratefully acknowledges the the Commissariat a' l'Energie Atomique for support during his stay at Saclay.

(31) B. H. Mahan and R. B. Solo, *J. Chem. Phys.*, **37**, 2669 (1962).

(32) A. R. Anderson and J. V. F. Best, *Trans. Faraday Soc.*, **62**, 610 (1966).

(33) J. L. Moruzzi and A. V. Phelps, *J. Chem. Phys.*, **45**, 4617 (1966).

(34) J. M. Warman, *Nature*, **213**, 331 (1967).

(35) M. Clerc and F. Barat, *J. Chim. Phys.*, **63**, 1525 (1966).

The Point of Attack of a Chlorine Atom on Trichloroethylene

by L. Bertrand, J. A. Franklin, P. Goldfinger, and G. Huybrechts

Service de Chimie Physique I, Université Libre de Bruxelles, Brussels, Belgium *(Received May 7, 1968)*

The chlorine-photosensitized oxidations of C_2HCl_3, 1,1,1,2-$C_2H_2Cl_4$, and 1,1,2,2-$C_2H_2Cl_4$ have been studied at 357°K. From a comparison of the products of these long-chain reactions it can be concluded that the rate constant for the addition of a chlorine atom to the less chlorinated carbon atom in trichloroethylene is at least eight times greater than that for addition to the more chlorinated one.

Introduction

The photochlorination,[1-4] the oxygen-inhibited photochlorination,[5] and the chlorine-photosensitized oxidation[6] of trichloroethylene have been investigated earlier. All of these reactions involve the addition of a chlorine atom to trichloroethylene as a chain-propagation step. Both symmetric (R_S) and asymmetric (R_A) tetrachloroethyl radicals may be formed simultaneously

$$Cl + CCl_2{=}CHCl \xrightarrow{k_{2S}} \cdot CCl_2CHCl_2 \quad (R_S) \quad (1)$$

$$Cl + CCl_2{=}CHCl \xrightarrow{k_{2A}} CCl_3CHCl\cdot \quad (R_A) \quad (2)$$

If R_S and R_A give different products by long-chain reactions, the ratio of these products enables the ratio k_{2S}/k_{2A} of the rate constants for the formation of R_S and R_A to be calculated. Both radicals form C_2HCl_5 on reaction with Cl_2, but in the presence of oxygen they may yield different oxidation products, as is suggested by results on the chlorine-photosensitized oxidation of trichloroethylene.[6] The oxidation products of R_S and R_A separately may be determined by studying the chlorine-photosensitized oxidations of symmetric 1,1,2,2-$C_2H_2Cl_4$ (S) and asymmetric 1,1,1,2-$C_2H_2Cl_4$ (A). Each of these reactions involves only one type of tetrachloroethyl radical, formed in the chain-propagation steps

$$Cl + CHCl_2CHCl_2 \quad (S) \longrightarrow \cdot CCl_2CHCl_2 \quad (R_S) + HCl \quad (3)$$

$$Cl + CCl_3CH_2Cl \quad (A) \longrightarrow CCl_3CHCl\cdot \quad (R_A) + HCl \quad (4)$$

The oxidation products of S and A have been analyzed and compared with those of trichloroethylene. This leads to an estimate of k_{2S}/k_{2A}.

Experimental Section

Materials. Chlorine (Solvay) and C_2HCl_3 (Schuchardt, reinst) were purified as described previously.[5,7] 1,1,2,2-$C_2H_2Cl_4$ (Schuchardt, reinst) was distilled under atmospheric pressure and contained less than 0.3% impurities. 1,1,1,2-$C_2H_2Cl_4$ (Solvay) was purified by preparative gas chromatography, giving a purity of 99.9%. Oxygen (Société Belge de l'Air Liquide, 99.99%) was used without further purification. The purities of $CHCl_3$, CCl_4, C_2Cl_4, C_2Cl_6, C_2HCl_5, dichloroacetyl chloride, trichloroethylene epoxide, and chloral used as gas chromatographic standards were always greater than 98.5%.

Apparatus. The kinetic apparatus has been described in detail elsewhere.[8] Reactions were carried out at 357°K in a 136-ml Pyrex vessel and initiated by light of 4358 Å. The actinic light intensity was determined using the photochlorination of trichloroethylene as an actinometer.[3] The total pressure in the reaction cell was measured using a Pyrex Bourdon gauge capable of detecting pressure changes of 0.2 torr. The chlorine partial pressure was determined with an accuracy of 0.1 torr by light absorption at ~3600 Å using a logarithmic photometer.[9]

Product Analysis. After cutoff of the actinic light, the reaction mixture was evacuated from the reactor and the products condensable at −196° were recovered. They were then separated by distillation into three fractions: products condensable at −78° (fraction I), at −131° (fraction II), and at −196° (fraction III). Each of these fractions was transferred back into the reactor where its total pressure was measured; any chlorine present was measured photometrically.

Fraction I was analyzed gas chromatographically using a 4-m silicone grease column (Edwards Ltd. sili-

(1) K. L. Müller and H. J. Schumacher, *Z. Physik. Chem.*, **B35**, 455 (1937).

(2) F. S. Dainton, D. A. Lomax, and M. Weston, *Trans. Faraday Soc.*, **53**, 460 (1957).

(3) G. Chiltz, S. Dusoleil, P. Goldfinger, G. Huybrechts, A-M. Mahieu, and D. Van der Auwera, *Bull. Soc. Chim. Belges*, **68**, 5 (1959).

(4) G. Huybrechts, L. Meyers, and G. Verbeke, *Trans. Faraday Soc.*, **58**, 1128 (1962).

(5) G. Huybrechts, G. Martens, L. Meyers, J. Olbregts, and K. Thomas, *ibid.*, **61**, 1921 (1965).

(6) G. Huybrechts and L. Meyers, *ibid.*, **62**, 2191 (1966).

(7) P. Goldfinger, G. Huybrechts, G. Martens, L. Meyers, and J. Olbregts, *ibid.*, **61**, 1933 (1965).

(8) S. Dusoleil, P. Goldfinger, A-M. Mahieu-Van der Auwera, G. Martens, and D. Van der Auwera, *ibid.*, **57**, 2197 (1961).

(9) P. G. Ashmore, B. P. Levitt, and B. A. Thrush, *ibid.*, **52**, 830 (1956).

cone high-vacuum grease, 24% by weight on 30–50 Sil-O-Cel C-22 firebrick from Johns Manville, U.S.A.) and a katharometer as detector. Products were identified by their retention times and also by mass spectrometric analyses. Chromatographic peak areas were taken as a measure of the respective concentrations, taking into account the determined sensitivity of the katharometer for each compound.

Fraction II was passed over an antimony trisulfide column to remove chlorine, and the pressure of the remaining gas was measured: this was found to consist entirely of phosgene by the potassium iodide + acetone method.[10]

Fraction III consisted of Cl_2, HCl, and CO_2. Chlorine was removed by distillation, HCl was estimated by titration, and the pressure of CO_2 (identified by mass spectrometry) was obtained from $p(CO_2) = p(\text{fraction III}) - p(Cl_2) - p(HCl)$.

Results

1. Chlorine-Photosensitized Oxidation of 1,1,1,2-$C_2H_2Cl_4$. Figure 1 shows plots of total pressure and chlorine partial pressure against time for a reaction which was followed until the total pressure remained constant. The initial conditions were: $p(1,1,1,2\text{-}C_2H_2Cl_4) = 60$ torr; $p(O_2) = 250$ torr; $p(Cl_2) = 192$ torr; and $I_0 \simeq 2.3 \times 10^{-10}$ einstein cm^{-2} sec^{-1}. At the end of the reaction (~98% 1,1,1,2-$C_2H_2Cl_4$ consumption) the following products were found: $COCl_2$ (65 ± 2 torr); HCl (116 ± 1 torr), CO_2 (49 ± 1 torr), and 1,1,1,2-$C_2H_2Cl_4$ (1 ± 0.5 torr). Traces of $CHCl_3$, CCl_4, C_2HCl_3, C_2HCl_5, and CCl_3COH were also detected, but no $CHCl_2COCl$ was observed. The decrease in chlorine pressure was 4.5 ± 1.5 torr. These results can be explained by the overall reaction

$$CCl_3CH_2Cl + O_2 \longrightarrow COCl_2 + 2HCl + CO \quad (5)$$

followed by

$$CO + Cl_2 \longrightarrow COCl_2 \quad (6)$$

and

$$CO + {}^1/_2O_2 \longrightarrow CO_2 \quad (7)$$

Using these equations and the analytical results, the final increase in total pressure is calculated to be 87 ± 3 torr, which is in agreement with the observed value of 87 ± 1 torr. Experiments performed with the same initial conditions as above showed that after 10% 1,1,-1,2-$C_2H_2Cl_4$ consumption the products were the same as those observed after 98% consumption. The quantum yield for $COCl_2$ formation by reaction 5 was about 60.

2. Chlorine-Photosensitized Oxidation of C_2HCl_3. Figure 2 shows the variation of total pressure and chlorine partial pressure with time for a typical reaction in which the initial conditions were: $p(C_2HCl_3) = 59$ torr; $p(O_2) = 250$ torr; $p(Cl_2) = 200$ torr; $T =$ 357°K; and $I_0 \simeq 2.1 \times 10^{-10}$ einstein cm^{-2} sec^{-1}. The reaction was followed until the rate of change of total pressure was very small. The reaction products were $CHCl_2COCl$ (48 ± 1 torr), $COCl_2$ (10 ± 1 torr), HCl(10 ± 1.5 torr), and CO_2(10 ± 2 torr), together with traces of C_2HCl_3, C_2Cl_4, C_2HCl_5, C_2Cl_6, CCl_3COCl, trichloroethylene epoxide, $CHCl_3$, and CCl_4. From these analytical results, the observed decrease in chlorine pressure of 1 ± 0.5 torr and the overall reactions

$$C_2HCl_3 + {}^1/_2O_2 \longrightarrow CHCl_2COCl \quad (8)$$

and

$$C_2HCl_3 + {}^3/_2O_2 \longrightarrow COCl_2 + HCl + CO_2 \quad (9)$$

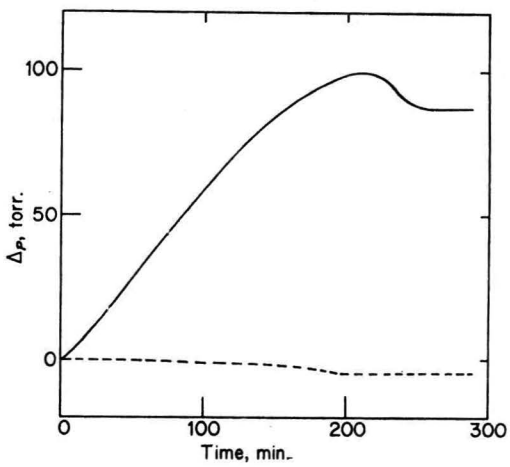

Figure 1. Chlorine-photosensitized oxidation of 1,1,1,2-$C_2H_2Cl_4$ at 357°K. Initial conditions: $p(1,1,1,2\text{-}C_2H_2Cl_4) = 60$ torr; $p(O_2) = 250$ torr; $p(Cl_2) = 192$ torr; and $I_0 \simeq 2.3 \times 10^{-10}$ einstein cm^{-2} sec^{-1}; ———, change in total pressure; – – – –, change in chlorine partial pressure.

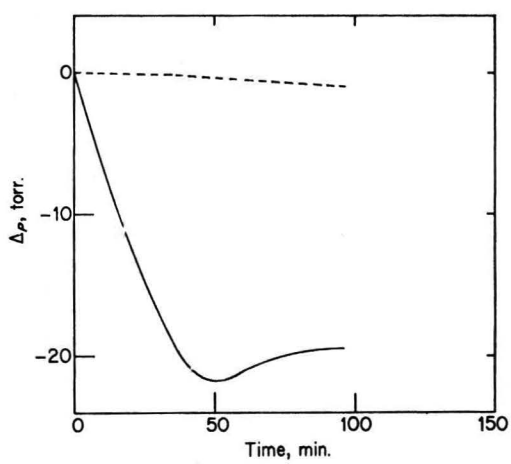

Figure 2. Chlorine-photosensitized oxidation of C_2HCl_3 at 357°K. Initial conditions: $p(C_2HCl_3) = 59$ torr; $p(O_2) = 250$ torr; $p(Cl_2) = 200$ torr; and $I_0 \simeq 2.1 \times 10^{-10}$ einstein cm^{-2} sec^{-1}; ———, change in total pressure; – – – –, change in chlorine partial pressure.

(10) J. C. Olsen, G. E. Ferguson, V. J. Sabetta, and L. Scheflan, *Ind. Eng. Chem.*, **3**, 189 (1931).

one can calculate the final decrease in total pressure. This is found to be 19 ± 2 torr, which is in agreement with the observed value of 19 ± 0.5 torr.

A series of experiments in which $p(C_2HCl_3)$ was varied from 60 to 100 torr, $p(O_2)$ from 20 to 250 torr, p(total) from 260 to 510 torr, and T from 357 to 403°K showed that in all cases after about 50% C_2HCl_3 consumption 88 ± 3% of the oxidized C_2HCl_3 appeared as $CHCl_2COCl$ and 12 ± 3% as $COCl_2$; after nearly 100% consumption these values were 83 ± 3% and 17 ± 3%, respectively. Quantum yields for $CHCl_2COCl$ formation were always greater than 100.

The fact that the percentage of C_2HCl_3 oxidized to phosgene increases slightly toward the end of the reaction suggests that the $CHCl_2COCl$ formed by reaction 8 may be oxidized slowly to $COCl_2$. This was shown to be the case in an experiment in which 60 torr of $CHCl_2COCl$ was illuminated with $I_0 \simeq 2 \times 10^{-10}$ einstein cm^{-2} sec^{-1} in the presence of 250 torr of O_2 and 200 torr of Cl_2 at 357°K. Phosgene and trichloroacetyl chloride were formed, each with a maximum quantum yield of about 5.

3. Chlorine-Photosensitized Oxidation of 1,1,2,2-$C_2H_2Cl_4$. This reaction was investigated with the following initial conditions: $p(1,1,2,2\text{-}C_2H_2Cl_4) = 60$ torr; $p(O_2) = 250$ torr; $p(Cl_2) = 200$ torr; and $I_0 \simeq 2.1 \times 10^{-10}$ einstein cm^{-2} sec^{-1}. Total pressure and chlorine pressure curves are shown in Figure 3. The reaction products after about 98% tetrachloroethane consumption were $CHCl_2COCl$ (39 ± 1 torr), $COCl_2$ (16.5 ± 1 torr), HCl + CO_2 (87 ± 2 torr), 1,1,2,2-$C_2H_2Cl_4$ (1 torr), CCl_3COCl (2 torr), and traces of C_2HCl_3 and C_2HCl_5. The decrease in chlorine pressure was 2.5 ± 1 torr. These results can be explained by the stoichiometric equations

$$CHCl_2CHCl_2 + {}^1/_2O_2 \longrightarrow CHCl_2COCl + HCl \quad (10)$$

$$CHCl_2CHCl_2 + {}^3/_2O_2 \longrightarrow COCl_2 + 2HCl + CO_2 \quad (11)$$

$$CHCl_2CHCl_2 + Cl_2 + {}^1/_2O_2 \longrightarrow CCl_3COCl + 2HCl \quad (12)$$

The calculated and observed values for the final increase in total pressure are 45 ± 2 torr and 42.5 ± 1 torr, respectively. The percentages of 1,1,2,2-$C_2H_2Cl_4$ oxidized to $CHCl_2COCl$, $COCl_2$, and CCl_3COCl were 66 ± 3, 28 ± 2, and 4 ± 1%, respectively. An analysis of the products of a reaction carried out up to about 50% tetrachloroethane consumption showed, on the other hand, that 85 ± 3% of the oxidized 1,1,2,2-$C_2H_2Cl_4$ appeared as $CHCl_2COCl$ (with a quantum yield of about 30) and 15 ± 3% as $COCl_2$; in this case only traces of CCl_3COCl were found. The increasing ratio of phosgene to dichloroacetyl chloride as the tetrachloroethane consumption increases can again be explained by oxidation of $CHCl_2COCl$ to $COCl_2$, as in the case of trichloroethylene.

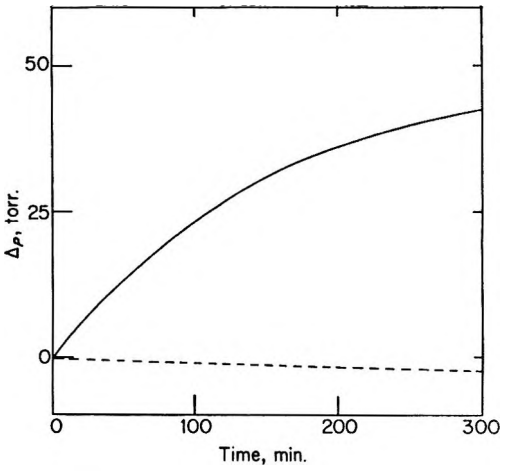

Figure 3. Chlorine-photosensitized oxidation of 1,1,2,2-$C_2H_2Cl_4$ at 357°K. Initial conditions: $p(1,1,2,2\text{-}C_2H_2Cl_4) = 60$ torr; $p(O_2) = 250$ torr; $p(Cl_2) = 200$ torr; and $I_0 \simeq 2.1 \times 10^{-10}$ einstein cm^{-2} sec^{-1}; ———, change in total pressure; - - - -, change in chlorine partial pressure.

Discussion

The long-chain chlorine-photosensitized oxidation of S leads to $CHCl_2COCl$ and $COCl_2$, while that of A yields only $COCl_2$. Dichloroacetyl chloride may therefore be considered to be a characteristic oxidation product of the R_S radical.

In the case of A, the long-chain $COCl_2$ formation must result from the oxidation of R_A radicals while for S it may be due to the following reactions: (i) direct oxidation of R_S to $COCl_2$; (ii) oxidation of $CHCl_2COCl$ formed from R_S; and (iii) isomerization of R_S to R_A, followed by oxidation of R_A. The oxidation of T may involve both R_S and R_A radicals, formed by reactions 1 and 2, and in this case $COCl_2$ formation may result both from the oxidation of R_A and from processes i–iii. It is found that in the oxidations of both T and S, the $COCl_2/CHCl_2COCl$ ratio increases as the reaction proceeds, suggesting that a considerable fraction of the $COCl_2$ is formed by process ii. This is supported by the experimental result that $CHCl_2COCl$ undergoes chlorine-photosensitized oxidation to $COCl_2$. In the oxidation of T the minimum percentage oxidized to $COCl_2$, corresponding to the shortest reaction time, was 12%. If all this phosgene is attributed to the oxidation of R_A radicals formed by reaction 2, an upper limit for the ratio $k_{2A}/(k_{2S} + k_{2A})$ is then 0.12; *i.e.*, $k_{2S} > 8k_{2A}$.

It can therefore be concluded that the rate constant for the addition of a chlorine atom to the less chlorinated carbon atom in trichloroethylene is at least 8 times greater than that for addition to the more chlorinated one.

Acknowledgments. The authors thank Dr. L. Exsteen-Meyers for valuable assistance. Thanks are also due to the Fonds de la Recherche Scientifique Fondamentale Collective for financial aid.

A Flash-Photolysis Study of Chromyl Chloride[1a]

by Rolf Halonbrenner,[1b] J. Robert Huber,[1c] Urs Wild,[1d] and Hans H. Günthard

Physical Chemistry Laboratory, Swiss Federal Institute of Technology, 8006 Zürich, Switzerland (*Received May 7, 1968*)

The photochemistry of chromyl chloride has been investigated in the gas phase by means of the flash-photolysis technique. Two transient absorptions have been found which are assigned to the CrO_2Cl radical and to the CrO_2 molecule, respectively. The evidence supports the view that the CrO_2 molecule arises from the photoexcited CrO_2Cl radical, *i.e.*, $CrO_2Cl_2 \xrightarrow{h\nu} CrO_2Cl_2^* \rightarrow CrO_2Cl \xrightarrow{h\nu} CrO_2Cl^* \rightarrow CrO_2$. Both transients reach their maximum concentration within the flash lifetime and decay independently of each other. Addition of inert gases lowers the initial concentrations of both intermediates, as well as the extent of the photolytic decomposition. The final products are gaseous chlorine and amorphous CrO_2.

Introduction

The photolysis of chromyl chloride has been studied by several workers using classical irradiation techniques. Kantzer[2] discovered the gas-phase photolytic decomposition by irradiation with photons of energy greater than 23,800 cm^{-1}. He found that the decomposition proceeds without pressure change at constant volume and temperature, and postulated the reaction

$$CrO_2Cl_2 \xrightarrow{h\nu} CrO_2 + Cl_2 \qquad (1)$$

The same reaction was assumed by de Kronig, *et al.*,[3] who first described fine structure near 18,000 cm^{-1} in the electronic absorption spectrum of chromyl chloride. This has also been observed by Shkapenko[4] in a study of the crystal spectrum of CrO_2Cl_2 at 20°K. This author inferred an upper state with a dissociation energy of only approximately 470 cm^{-1}. Recently, a new study of the crystal electronic absorption bands between 21,000 and 16,900 cm^{-1} has been published by Dunn and Francis.[5] These authors have shown that, in contradiction to Shkapenko's result, the upper state of this transition is strongly bonding. Schwab, *et al.*,[6] performed photolysis experiments with concentrated carbon tetrachloride solutions and obtained a quantum yield of 10^2 to 10^3 mol/einstein for the overall decomposition reaction (1). These workers postulated as a first step in the decomposition mechanism the dissociation process

$$CrO_2Cl_2 \xrightarrow{h\nu} CrO_2Cl + Cl \qquad (2)$$

which is followed by a chain reaction. This work has been extended by Pfoertner[7] to include dilute solutions and the gas phase. Helmholz, Brennan, and Wolfsberg[8] have examined the electronic spectrum of chromyl chloride with the aid of semiempirical MO methods. Good agreement with experimental results was obtained for the oscillator strengths and positions of the two electronic transitions in the long wavelength region of the absorption spectrum.

In this paper we report results of a flash-spectroscopic study of the kinetics of photodecomposition of chromyl chloride vapor both in the pure state and in inert gas mixtures, which was undertaken with the objective of formulating a detailed mechanism for the photodecomposition.

Experimental Section

Materials. Chromyl chloride was prepared by the method described by Sisler.[9] A solution of 150 g (1.5 mol) of CrO_3 in 100 ml of water slowly reacted at 0°, first with 330 ml of concentrated hydrochloric acid, and then with 450 ml of concentrated sulfuric acid. The chromyl chloride obtained from the reaction mixture was purified by distillation, under dry nitrogen, in a 50-cm Vigreux column at 120 mm pressure at 58–60°. All of these operations were carried out in the absence of light, and the compound was stored in the dark at −10° in sealed break-off ampoules. The overall yield was usually about 70%.

Flash-Photolysis Apparatus. The flash-photolysis experiments were performed with an instrument which has been described earlier.[10] Both photographic and photoelectric detection methods were employed. For photoelectric recording of transient spectra in the

(1) (a) This paper was abstracted, in part, from the dissertation submitted by R. Halonbrenner in partial fulfillment of the requirements for the degree of Dr.sc.nat. at the Swiss Federal Institute of Technology; (b) Hefti AG., Chemische Fabrik, 8048 Zürich, Switzerland; (c) Photochemistry and Spectroscopy Laboratory, Department of Chemistry, Northeastern University, Boston, Mass. 02115; (d) to whom correspondence should be addressed.

(2) M. Kantzer, *Compt. Rend.*, 196, 1882 (1933).

(3) R. L. de Kronig, A. Schaafsma, and P. K. Peerlkamp, *Z. Phys. Chem.*, B22, 323 (1933).

(4) G. Shkapenko, *J. Chim. Phys.*, 47, 21 (1950).

(5) T. M. Dunn and A. H. Francis, *J. Mol. Spectrosc.*, 25, 86 (1968).

(6) G. M. Schwab and S. Prakash, *Z. Phys. Chem.* (Frankfurt am Main), 6, 387 (1956).

(7) K. Pfoertner, Thesis, University of Munich, 1957.

(8) L. Helmholz, H. Brennan, and M. Wolfsberg, *J. Chem. Phys.*, 23, 853 (1955).

(9) W. C. Fernelius, *Inorg. Syn.*, 2, 205 (1946).

(10) U. Wild and Hs. H. Günthard, *Helv. Chim. Acta*, 48, 1061 (1965).

ultraviolet, visible, and near-infrared regions, the EMI 9552 B and DuMont K 2276 photomultiplier tubes, cooled to 77°K, were used. Flash energies from 100 to 625 J sufficed to produce substantial photochemical reaction. The flash tubes were filled with argon (10 mm) and, with a 400-J input energy, delivering 5×10^{18} photons at 33,000–25,000 cm^{-1} into the cells. The direct proportionality between the photon flux and the electrical energy was established by actinometric measurements.[11] For some experiments, solution filters were used in order to confine light absorption to specific wavelength regions.

Cylindrical Pyrex sample cells (10- and 20-cm length and 20- and 40-mm diameter) equipped with optical grade windows were used. The cells were directly joined to the break-off seal ampoules and were baked out for 12 hr at 200° under high vacuum prior to admitting the sample. In order to fill the cells to a predetermined partial pressure of chromyl chloride, the ampoules were thermostated at the appropriate temperature, which was chosen from the vapor pressure data of Kelley.[12]

Spectral Measurements. Spectra in the ultraviolet and visible range were recorded with a Beckman DK-2 spectrophotometer.

Continuous Photolysis Experiments. For determination of quantum yields, a number of continuous photolysis experiments were carried out with chromyl chloride in a sealed quartz cell, which was placed directly in the sample compartment of a Zeiss PMQ-II spectrophotometer. This instrument allows irradiation with light of 500 cm^{-1} band width. Absorption spectra were taken at 30- and 60-min intervals. The photon flux was determined by means of a ferrioxalate actinometer[11] placed in the photometer under exactly the same conditions as in the irradiation experiments.

Analysis of Kinetic Data. The output current $I(t)$ from the photomultiplier was displayed on a Tektronix 549 storage oscilloscope, and the trace was photographed with a Polaroid camera. The photographed records were measured with a modified Zeiss photometer which allows digital measurement of the cartesian coordinates of an arbitrary number of points and direct transfer to punched cards by means of a Hewlett-Packard DVM 3440 A–IBM 026 key punch combination. From the digital data, the change in transmission $T(t) = I(t)/I(\infty)$ of the sample was calculated as a function of time and analyzed by an iterative nonlinear regression procedure[13] to obtain a least-squares fit with one of the four following kinetic expressions: simple first-order process

$$\Delta D(t) = \Delta D(+0) \exp(-kt) \quad (3)$$

sum of two first-order processes

$$\Delta D(t) = \Delta D_{I}(+0) \exp(-k_{I}t) + \Delta D_{II}(+0) \exp(-k_{II}t) \quad (4)$$

simple second-order process

$$\Delta D(t) = \Delta D(+0)[1 + k\Delta D(+0)t]^{-1} \quad (5)$$

simultaneous first- and second-order processes

$$\Delta D(t) = \Delta D(+0)k'\{[k' + k''\Delta D(+0)] \exp(k't) - k''\Delta D(+0)\}^{-1} \quad (6)$$

In these expressions, $\Delta D(+0)$, $\Delta D_{I}(+0)$, and $\Delta D_{II}(+0)$ represent the initial changes in optical density immediately after the flash, and k, k_{I}, k_{II}, k', and k'' are the appropriate rate constants.

Results

(*a*) *Absorption Spectrum of Chromyl Chloride.* Figure 1 shows the absorption spectrum of chromyl chloride vapor between 50,000 and 15,000 cm^{-1} at room temperature. The most prominent bands are at 34,000 and 24,600 cm^{-1}, respectively, with a shoulder near 19,500 cm^{-1}. The latter has considerable fine structure[3-5] (not shown in Figure 1), which cannot be detected in the spectrum of the vapor at 200°, but which reversibly appears at room temperature. The fine structure may therefore be used for the measurement of the vapor temperature. For purposes of discussion, it is convenient to divide the spectrum of Figure 1 into the following regions: A, <17,000 cm^{-1}; B, 17,000–20,500 cm^{-1}; C, 20,500–22,000 cm^{-1}; D, 22,000–28,000 cm^{-1}; and E, >28,000 cm^{-1}.

(*b*) *Photolysis of Chromyl Chloride by Continuous Irradiation.* Measurements of the quantum yield of the photolytic decomposition of chromyl chloride vapor at room temperature have confirmed that irradiation into the long wavelength absorption shoulder

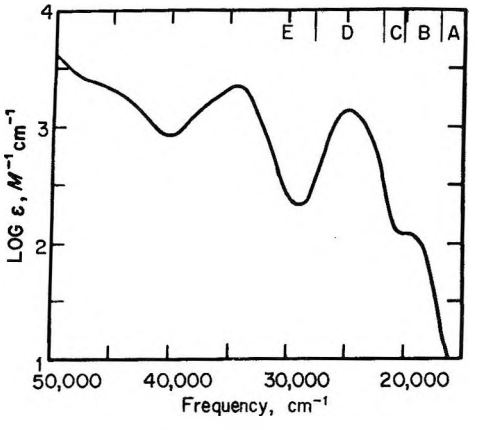

Figure 1. Absorption spectrum of chromyl chloride vapor at 298°K.

(11) C. G. Hatchard and C. A. Parker, *Proc. Roy. Soc.*, **A235**, 518 (1956).

(12) R. Kelley, U. S. Bureau of Mines Bulletin 383, U. S. Government Printing Office, Washington, D. C., 1935.

(13) U. Wild and Hs. H. Günthard, *Helv. Chim. Acta*, **48**, 1843 (1965).

shows no photodecomposition. The quantum yield rises near 23,800 ± 500 cm^{-1} from 0 to approximately 1. The photodecomposition can be followed visually by observing the formation of a suspension of particles (*i.e.*, fog) after starting the irradiation. The particles coagulate as a thin film on the cell walls. This film has been investigated by spectroscopy and by chemical analysis. The ultraviolet-visible spectrum is characterized by monotonically decreasing absorption between 50,000 and 15,000 cm^{-1}. The infrared spectrum between 4000 and 400 cm^{-1} shows only one prominent band at 1015 cm^{-1} (CrO stretching mode) and a weaker band at 660 cm^{-1}. The spectrum is characteristic for CrO_2.[14] In pressed potassium bromide disks, both the 1015- and 660-cm^{-1} bands are barely detectable. No distinct X-ray diffraction pattern could be obtained from the film material by the Debye–Scherrer technique, thereby proving the amorphous structure of the oxide. By chemical analysis, it was shown that at least 95% of the chromium contained in the film material is not in the Cr(VI) state. No chlorine was detected, and the solid decomposition product may therefore safely be considered to be amorphous CrO_2.

The gaseous photolysis products were analyzed by mass spectrometry and found to consist exclusively of chlorine. Consequently, the overall reaction given in eq 1 is confirmed insofar as gaseous chlorine and solid CrO_2 are the sole detectable photodecomposition products.

(*c*) *Flash-Photolysis Experiments.* To obtain transient spectra, experiments were conducted with partial pressures of chromyl chloride between 0.5 and 9.0 mm, and photographs were taken on Ilford HP-3 plates at 5-, 10-, 100-μsec, 1-, 10-, 100-msec, and 1- and 10-sec intervals after the photoflash. The Ilford HP-3 plate has low sensitivity below 17,000 cm^{-1} and consequently the observations in region A are not very reliable. In region B, (20,500–17,000 cm^{-1}) the fine structure[4-6] disappears at times below 2 sec and appears again afterward. This is obviously a consequence of heating the gas by the photoflash, which, a crude estimate shows, can generate temperatures up to 800°. At higher chromyl chloride concentrations, a transient with a lifetime of the order of milliseconds is observed in region C (22,000–20,500 cm^{-1}). Finally, in region D (28,000–22,000 cm^{-1}) a strong transient decrease of absorption is observed. Region E (>28,000 cm^{-1}) has not been studied.

From the continuous irradiation experiments it is known that light below 23,800 cm^{-1} is photochemically inactive. The same behavior was found in flash experiments with light filtered by passage through a saturated aqueous potassium nitrite solution. Neither transient absorption nor photochemical decomposition and practically no heating of the gas is observed under these irradiation conditions.

For quantitative investigation of the transient kinetics, spectrophotometric measurements were made at 500-cm^{-1} intervals in the region 28,000–10,000 cm^{-1} with pure chromyl chloride vapor and with mixtures containing inert gases.

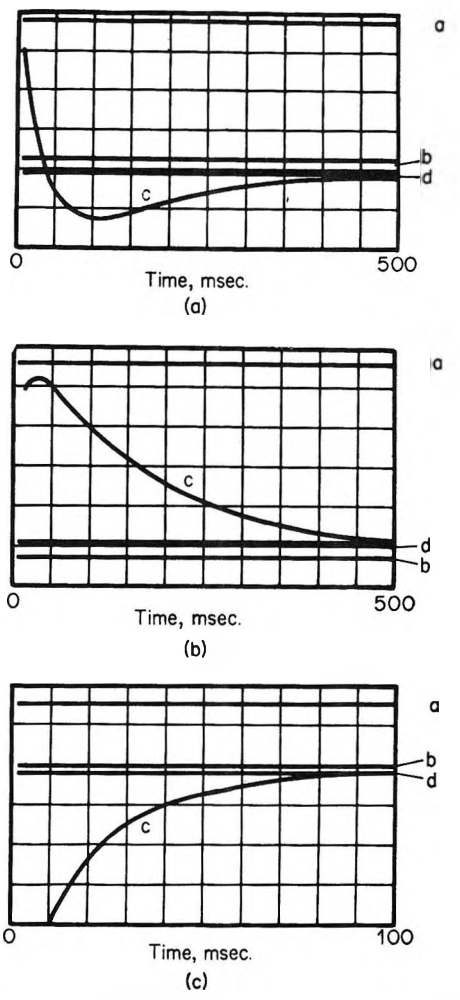

Figure 2. Oscilloscope traces representing the transient transmission changes. The zero line is represented by a, the 100% line before the flash by b, the transient curve by c, and the 100% line after complete decay by d. (a) region B (19,000 cm^{-1}); (b) region C (21,000 cm^{-1}); (c) region D (24,000 cm^{-1}).

It has already been pointed out that the photoflash excitation of pure chromyl chloride vapor is accompanied by substantial heating which may strongly influence the rates of particular steps in the photodecomposition mechanism. Although the heating has a considerable effect on the quantity of the transients produced, the decay behavior appears not to be strongly affected by the temperature increase.

1. Experiments with the Pure Vapor. The results with pure chromyl chloride vapor are illustrated in Figure 2, which shows the transient behavior in regions B, C, and D. Region A has been omitted since no transient is observed there.

(14) R. M. Chrenko and D. S. Rodbell, General Electric Information Series, Jan 1967.

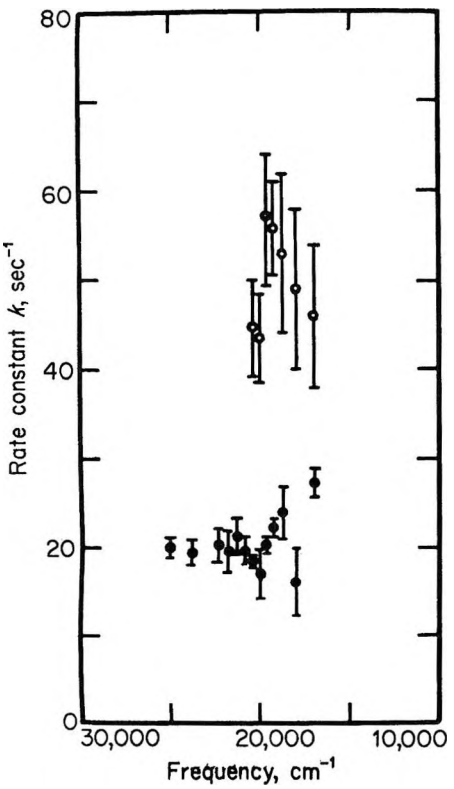

Figure 3. Frequency dependence of first-order rate constants k_I (transient T_I) and k_{II} (transient T_{II}). k_I is represented by ●, and k_{II} by ○.

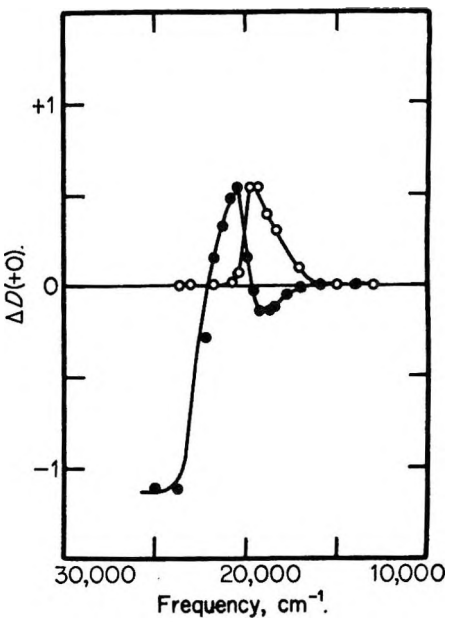

Figure 4. Initial change of optical densities $\Delta D_I(+0)$ and $\Delta D_{II}(+0)$ of the transients T_I and T_{II} *vs.* frequency. $\Delta D_I(+0)$ is represented by ● and ΔD_{II} (to) by ○.

In spite of the fact that the traces of Figure 2 represent nonisothermal conditions, they were analyzed in terms of first- and second-order kinetics (eq 3 to 6). It was found that, in most cases, the transient curves are satisfactorily represented by one or two exponential components. The corresponding rate constants and initial increases in optical densities are plotted in Figures 3 and 4, respectively, as functions of the frequency. The observations may be summarized as follows.

(*i*) *In Region B (20,500–17,000 cm⁻¹).* Figure 2a shows the transient behavior in this region. A fast transient absorption (T_{II}) is followed by an increase of transmission and a slower relaxation corresponding to the recovery of absorption. Analysis of the transient curve shows that it can be approximated by the sum of two exponential terms. Furthermore, the initial increase in optical density of T_{II} at 20,000 cm^{-1} ($\Delta D_{II}(+0)$, as obtained from curve fitting) is linearly related to the square of the flash energy. Thus the transient in region B appears to originate from a short-lived species whose initial concentration after flash excitation is proportional to the square of the flash energy. Therefore, a two-step excitation is considered to be involved in the formation of species T_{II}.

(*ii*) *In Region C (22,000–20,500 cm⁻¹).* The transient observed at 21,000 cm^{-1} (Figure 2b) is characterized by a very low optical transmission immediately after the flash and a rate constant which is approximately one-third as large as the fast decay constant measured in region B. The recovery of transmission is not complete. The initial change in optical density, $\Delta D_I(+0)$, is directly proportional to flash energy. This absorption is designated as due to a species T_I.

(*iii*) *In Region D (28,000–22,000 cm⁻¹).* As shown in Figure 2c, the flash produces an immediate substantial decrease in optical density (*i.e.*, $\Delta D_I(+0) < 0$), which then recovers to a value somewhat lower than before excitation. The permanent increase in transmission at this wavelength reflects the irreversible photodecomposition of chromyl chloride. However, most of the chromyl chloride which decomposes during the flash is regenerated within a few milliseconds. Analysis of the curve indicates that the transient behavior may reasonably be described by one exponential term. The rate constant is almost equal to the decay constant of transient species T_I.

2. Experiments with Inert Gas Mixtures. By the addition of a sufficient amount of an inert gas, nearly *iso*thermal conditions may be realized. Experiments were conducted with nitrogen, argon, and chlorine at partial pressures up to 1 atm. The results obtained may be summarized as follows. (i) All the gases investigated, including chlorine, show qualitatively the same effect, which is considered to be due to the heat capacity of the system. (ii) The effect of various partial pressures of nitrogen on the initial optical densities $\Delta D_I(+0)$ and $\Delta D_{II}(+0)$ is shown in Figure 5. (iii) The quantum yield of the formation of CrO_2 (corresponding to irreversible photodecomposition) is

reduced by the added gases. (iv) The dependence of the rate constant k_I on the nitrogen pressure shows the typical saturation behavior which is to be expected for a cooling gas. This is shown in Figure 6.

3. Dependence of the Transient Behavior on Spectral Range of Excitation. Further insight into the photodecomposition mechanism was obtained from experiments with filtered photoflash excitation. In these experiments, cobalt chloride solution filters[15] were employed, which pass particular spectral regions.

If the region 27,500–10,000 cm^{-1} is filtered out, the initial concentration of species T_{II} relative to species T_I is decreased by a factor of 6. This indicates that transient species T_{II} is produced by an absorption in the region 27,000–10,000 cm^{-1}. The absence of this spectral region in the exciting flash inhibits specifically the formation of species T_{II}.

Discussion

The results obtained may be rationalized in terms of the following mechanism, in which w denotes transition probability and ϕ photon flux.

Process	Reaction	Rate	
Excitation	$CrO_2Cl_2 \xrightarrow{h\nu} CrO_2Cl_2^*$	$w_1\phi[CrO_2Cl_2]$	(7.1)
	$CrO_2Cl \xrightarrow{h\nu} CrO_2Cl^*$	$w_2\Phi[CrO_2Cl]$	(7.2)
Deactivation	$CrO_2Cl_2^* \longrightarrow CrO_2Cl_2$	$k_3[CrO_2Cl_2^*]$	(7.3)
	$CrO_2Cl_2^* + M \longrightarrow CrO_2Cl_2 + M$	$k_4[CrO_2Cl_2^*][M]$	(7.4)
	$CrO_2Cl^* \longrightarrow CrO_2Cl$	$k_5[CrO_2Cl^*]$	(7.5)
	$CrO_2Cl^* + M \longrightarrow CrO_2Cl + M$	$k_6[CrO_2Cl^*][M]$	(7.6)
Decomposition	$CrO_2Cl_2^* \longrightarrow CrO_2Cl + Cl$	$k_7[CrO_2Cl_2^*]$	(7.7)
	$CrO_2Cl^* \longrightarrow CrO_2 + Cl$	$k_8[CrO_2Cl^*]$	(7.8)
	$CrO_2Cl \longrightarrow CrO_2 + Cl$	$k_9[CrO_2Cl]$	(7.9)
Chain reaction and	$CrO_2Cl + CrO_2Cl \longrightarrow (CrO_2Cl)_2$	$k_{10}[CrO_2Cl]^2$	(7.10)
termination	$CrO_2Cl + Cl \longrightarrow CrO_2Cl_2$	$k_{11}[CrO_2Cl][Cl]$	(7.11)
	$Cl + Cl \longrightarrow Cl_2$	$k_{12}[Cl]^2$	(7.12)
	$CrO_2Cl_2 + Cl \longrightarrow CrO_2Cl + Cl_2$	$k_{13}[CrO_2Cl_2][Cl]$	(7.13)
	$(CrO_2)_n + (CrO_2)_m \longrightarrow (CrO_2)_{n+m}$	$k_{14}^{n,m}[(CrO_2)_n][(CrO_2)_m]$	(7.14)

The reaction of eq 7.14 represents the polymerization of the gaseous CrO_2 molecule. In terms of the experimental results, the transients T_{II} and T_I may be identified as the species CrO_2 and CrO_2Cl, respectively. It is assumed that flash excitation produces an electronically excited state of chromyl chloride whose lifetime is compared to the flash duration, and which is either deactivated by emission, by collision, or by decomposition into the radical CrO_2Cl (transient species T_I) and a chlorine atom. The initial concentration of CrO_2Cl after flash was experimentally shown to be proportional to the flash energy. The transient radical CrO_2Cl may either be converted into the electronically excited state CrO_2Cl^* by further light absorption (eq 7.2), or it may decompose according to eq 7.9. The excited species CrO_2Cl^* may either be deactivated according to eq 7.5 and 7.6, or it may undergo dissociation to produce CrO_2 eq 7.8. The latter species is assumed to polymerize irreversibly into the solid Cr(IV) oxide; thus it represents the chain carrier for the irreversible photodecomposition of chromyl chloride. It was shown experimentally that monomolecular CrO_2 is produced by a two-stage excitation from chromyl chloride.

The reaction of eq 7.10 may be unimportant, since the compound $(CrO_2Cl)_2$ could not be identified under flash conditions. The formation of this compound has been postulated earlier[7] in order to explain the production of complex compounds containing the Cr–O–Cl linkage under constant irradiation conditions.

It is assumed that the process represented by eq 7.3 to 7.8 is fast in comparison with the other reactions, and that, consequently, the observed kinetics are dominated by the reactions of eq 7.9 and 7.11 to 7.14.

Furthermore, literature data for the chlorine–chlorine recombination reaction indicate that this reaction is unimportant under the conditions of our experiments. The chlorine abstraction reaction (eq 7.13) is more difficult to discuss. If this rate constant is computed from collision theory using an activation energy in the range 20–40 kcal/mol, the importance of this reaction in the decay process may be quantitatively determined.

Under conditions of continuous irradiation, the

(15) W. W. Wladimiroff, *Photochem. Photobiol.*, 5, 243 (1966).

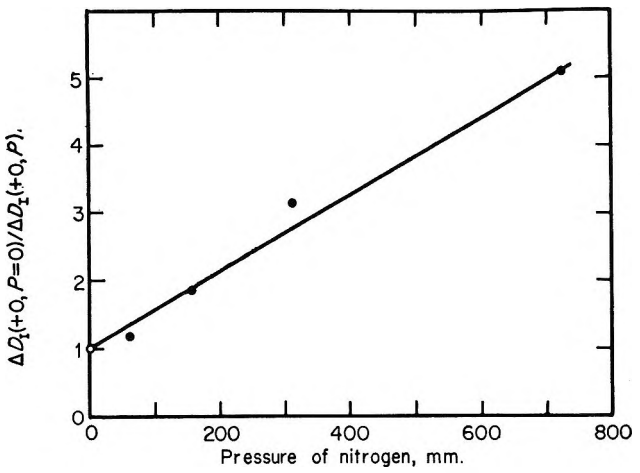

Figure 5. Relative change of the initial optical densities at 21,000 cm^{-1} as a function of partial pressure of nitrogen. The flash energy was 400 J.

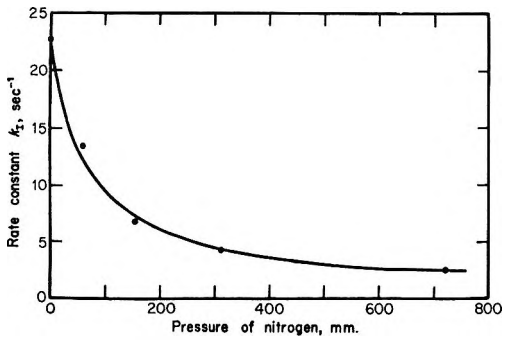

Figure 6. Plot of first-order rate constant k_I *vs.* nitrogen pressure measured at 21,000 cm^{-1}. The flash energy was 400 J.

steady-state concentration of CrO_2Cl is sufficiently low so that only the processes (7.1), (7.3), (7.7), (7.9), and (7.12) are of importance.

No attempt was made to solve the set of equations representing the rates of the individual processes (eq 7.1–7.4) analytically. Instead, extensive computations of numerical solutions by the Runge-Kutta procedure were carried out, starting with plausible values for rate constants and restricting the integration to isothermal conditions.[16] Consequently, the integrals cannot be rigorously compared with the observed kinetics; they are, however, useful to confirm relevant observations such as: (i) the determination of range of applicability of the rate constants; (ii) the dependence of the initial concentrations of transients $T_{II}(CrO_2)$ and $T_I(CrO_2Cl)$ on the flash energy; (iii) providing confirmation that the observed kinetics for the transient species CrO_2Cl and CrO_2 may be approximated by exponential terms, although the true kinetic behavior is expected to be non-exponential.

The following empirical expressions for the time-dependent variation of the concentration of pertinent species may be written

$$[CrO_2Cl_2(t)] = [CrO_2Cl_2(-0)] - [CrO_2(+0)] - [CrO_2Cl(+0)]e^{-k_I t} \quad (8)$$

$$[CrO_2Cl(t)] = [CrO_2Cl(+0)]e^{-k_I t} \quad (9)$$

$$[CrO_2(t)] = [CrO_2(+0)]e^{-k_{II} t} \quad (10)$$

where $[CrO_2Cl_2(-0)]$, $[CrO_2Cl(+0)]$, and $[CrO_2(+0)]$ denote the concentrations before and after flash excitation, respectively. By the suitable choice of the rate constants, the observed results may be satisfactorily reproduced. This treatment brings out a number of important points. These are: (i) $k_9/k_8 \ll 1$; *i.e.*, the reaction of eq 7.8 is responsible for the formation of CrO_2. (ii) $k_6[M] \approx k_8 \approx 10^6\ sec^{-1}$. In other words, under the condition of flash experiments, the excited radical CrO_2Cl^* is not observable. This also explains why the addition of a foreign gas so efficiently lowers the formation of CrO_2. Furthermore, the decay constant for the ground-state radical CrO_2Cl is $k_9 \lesssim 10^3\ sec^{-1}$. (iii) The polymerization rate constant k_{14} is of the order of $10^8\ M^{-1}\ sec^{-1}$, which is consistent with the lifetime of CrO_2 in the millisecond range.

The optical density (D) at a given frequency may be expressed as

$$D = \{\epsilon_{CrO_2Cl_2}[CrO_2Cl_2] + \epsilon_{CrO_2Cl}[CrO_2Cl] + \epsilon_{CrO_2}[CrO_2]\}l \quad (11)$$

where ϵ represents the extinction coefficients and l is the path length. Since the concentrations of all other species in the system are negligibly small, the time dependence of the change of optical density (ΔD) is, according to eq 8 to 10

$$\Delta D(t) = D(t) - D(\infty) = \Delta D_I(+0)e^{-k_I t} + \Delta D_{II}(+0)e^{-k_{II} t} \quad (12)$$

where

$$\Delta D_I(+0) = \{\epsilon_{CrO_2Cl} - \epsilon_{CrO_2Cl_2}\}[CrO_2Cl(+0)]l \quad (13)$$

and

$$\Delta D_{II}(+0) = \epsilon_{CrO_2}[CrO_2(+0)]l \quad (14)$$

If $\Delta D_I\ (+0)$ values are used to calculate the ratio

$$\Delta D_I(+0)/l\epsilon_{CrO_2Cl_2} = \left\{\frac{\epsilon_{CrO_2Cl}}{\epsilon_{CrO_2Cl_2}} - 1\right\}[CrO_2Cl(+0)] \quad (15)$$

as a function of analyzing light frequency, Figure 7 may be constructed. The right-hand side of (15) assumes as absolute minimum for $\epsilon_{CrO_2Cl} = 0$, the minimal value being $-[CrO_2Cl(+0)]$. According to Figure 7, the left-hand side of eq 15 assumes a maximum value near 20,500 cm^{-1}, which is flanked both below and above this frequency by equal minima. It is, therefore, plausible to assume that $\epsilon_{CrO_2Cl} \approx 0$ in these minimum regions. Consequently, eq 15 can be used to calculate the

(16) For details, *cf.* R. Halonbrenner, Doctoral Dissertation, Swiss Federal Institute of Technology, 1968.

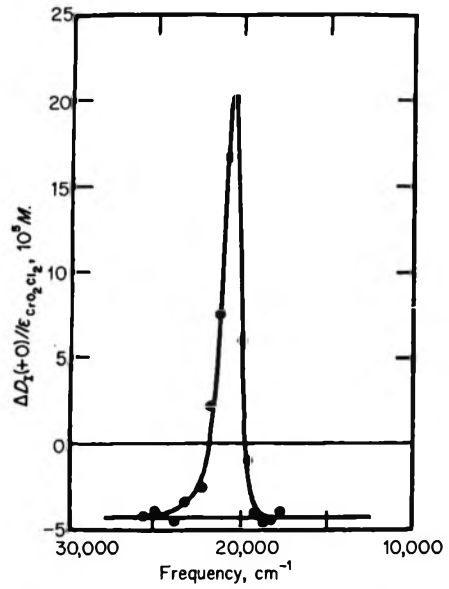

Figure 7. Plot of the ratio $\Delta D_I(+0)/l\epsilon_{CrO_2Cl_2}$ from eq 15 *vs.* frequency for pure chromyl chloride vapor.

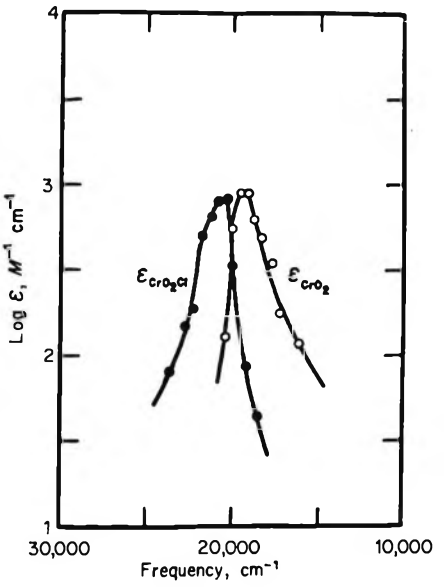

Figure 8. Electronic absorption band of $CrO_2Cl(g)$ (T_I) and $CrO_2(g)$ (T_{II}).

initial concentration $[CrO_2Cl(+0)]$ of the radical CrO_2Cl, which then serves to determine the extinction coefficient of this species. The results of these calculations are plotted in Figure 8, in which the solid circles represent one absorption band of the CrO_2Cl radical. Also shown in Figure 8 is one absorption band of the gaseous CrO_2 molecule. The extinction coefficients were calculated from values of $[CrO_2(+0)]$, which were obtained with the aid of eq 8 to 10, *i.e.*, $[CrO_2Cl_2(-0)] - [CrO_2Cl_2(\infty)] = [CrO_2(+0)]$. The initial CrO_2 concentration is given by the amount of chromyl chloride which has decomposed irreversibly.

Acknowledgments. We wish to express our gratitude to the Foundation of "Rare Metals" (President, Dr. O. H. C. Messner) for generous support of this work. We are indebted to Professor Karl Weiss, Northeastern University, for helpful discussions. Furthermore, we wish to thank Mr. W. Kummer for many suggestions, Mr. J. Keller (SANDOZ AG.) for assistance with the computations, and Dr. R. Bühler for performing the spectral measurements.